Universidade de Brasília
Departamento de Geografia

Relatório de Pós doutorado

Estudos da taxa de erosão e desnudação natural e antrópica no cerrado brasileiro utilizando ferramentas clássicas (monitoramento hidrossedimentológico), e geoquímica isotópicas (isótopos estáveis e nuclídeos cosmogênicos)

Prof.Dr Rogerio Uagoda

5 de dezembro de 2022

Indice

Patrick LACHASSAGNE
Directeur
Courriel : patrick.lachassagne@ird.fr

Montpellier, le 25 novembre,

A l'attention du Prof. Rogerio UAGODA

Objet : Accueil au laboratoire HydroSciences Montpellier (France) du Prof. Rogerio UAGODA
Ref. : HSM/DU/L034/21_PL

Je soussigné Patrick LACHASSAGNE, Directeur de l'UMR HydroSciences Montpellier, atteste que le Professeur Rogerio Uagoda de l'Université de Brasilia a été accueilli dans mon laboratoire dans le cadre du projet CAPES PRINT « IMPACTOS CLIMÁTICOS E ANTRÓPICOS NA FUNCIONALIDADE DE SISTEMAS HIDROLÓGICOS FLUVIAIS E CÁRSTICOS » an à compter du 29 novembre 2021 et pendant 1 an.

Durant son séjour au Laboratoire, le Professeur Rogerio Uagoda a eu l'opportunité d'utiliser l'infrastructure du Laboratoire HSM pour l'analyse des éléments chimiques par spectrométrie de masse à générateur de plasma ICPMS) sur les échantillons de son site de recherche au Brésil, de participer à et de donner des séminaires sur les recherches réalisées sur les milieux karstiques, de collaborer avec les chercheurs des équipes PEnSTer (Pollutions Environnement Santé Territoires) et HYTAKE (Hydrogéologie et Transferts dans les aquifères karstiques et hétérogènes).

Au cours de son séjour, Mr. Uagoda a bénéficié d'une bourse IRD (8 mois octroyés en 2021), ainsi que d'une bourse de 4 mois du gouvernement brésilien.

En foi de quoi la présente attestation lui est délivrée pour servir et valoir ce que de droit.

Patrick LACHASSAGNE
Directeur
HydroSciences Montpellier
IRD UR 050

1 Treinamento, preparação e processamento de amostras na plataforma AETE-ISSO no HSM.

Esse relatório de Pós Doutorado pretende demonstrar as atividades desenvolvidas no âmbito do Projeto “Études du taux d'érosion et de dénudation naturelle et sous pression anthropique dans la savane brésilienne (Cerrado) à l'aide d'outils classiques (surveillance hydrosédimentologique) et de la géochimie isotopique (isotopes stables et nucléides cosmogéniques)” ou em português “Estudos da taxa de erosão e desnudação natural e antrópica no cerrado brasileiro utilizando ferramentas clássicas (monitoramento hidrossedimentológico) e geoquímica isotópicas (isótopos estáveis e nuclídeos cosmogênicos), que fora realizado entre novembro de 2021 e novembro de 2022 no Hydrosciences Montpellier (HSM). Houve também um período intercalado de 4 meses no Centre Européen de Recherche et D'enseignement Des Géosciences De L'environnement (CEREGE) localizado em Aix-em-Provence. O projeto de Pós Doutorado foi financiado pelo IRD - Institut de Recherche pour le Développement/France.

No Relatório serão demonstrados o treinamento, preparação e processamento de amostras na plataforma AETE-ISSO no HSM; os resultados Preliminares dos traçadores geoquímicos; o treinamento, preparação e processamento de amostras no LN2C-CEREGE Laboratoire National des Nucleides Cosmogeniques; os resultados preliminares das datações por nuclídeos cosmogênicos; os treinamentos – HSM (em anexo); os treinamentos – CEREGE (em anexo); as apresentações que foram feitas do projeto; a participação em eventos no período na França e as publicações submetidas e publicadas durante o período na França.

A chegada ao HSM se deu no dia 29 de novembro de 2022. E, foram iniciadas as atividades de laboratório. Centrando-se no treinamento para uso dos equipamentos. A base que se está utilizando é a “AETE-ISO platform”, acrônimo de "Plataforma de análise de Elementos traços ambientais e Isótopos”;

No ano de 2021 foram realizadas diversas campanhas para coleta de água, sedimentos transportados, sedimentos contidos no interior de cavernas, solos externos e rochas fontes na bacia do rio Vermelho em Mambaí/GO (figura 1d, c, b e a).

As coletas se deram com uma estratégia de amostragem de campo para investigar a variabilidade espacial em concentrações de metais traço, partição e assinaturas isotópicas. A estratégia de amostragem de campo também considerou o conhecimento de circulação de água nas cavernas para a formação de terraços fluviais logo abaixo de áreas de plantio.

Sendo assim, foram escolhidas entre as amostras coletadas; 09 amostras de rocha para traçar origem; 32 amostras de solo para traçar origem; 260 amostras de terraços sedimentares recentes (<500 anos AP); 24 amostras de sedimentos transportados em fundo de rio; e, 16 amostras de água em fase líquida e sólida.

Em laboratório, os sedimentos superficiais foram secos ao ar, triturados, homogeneizados e peneirado na fração de 63 µm. Esta fração de tamanho de grão fino foi usada para todos os procedimentos (extração elementar, mineralógica, isotópica e sequencial). Todas as amostras sólidas foram trituradas e pulverizadas em uma moinho de ágata (figura 3a).

A água da superfície foi coletada a cerca de 1m de profundidade com uma garrafa de Van Dorn e armazenado em garrafas de polietileno de baixa densidade (LDPE) pré-limpas de 1 L. No laboratório, um volume preciso de amostra de água foi filtrado usando uma membrana de celulose Millipore® previamente limpa e pesada (figura 3b).

As membranas foram secas a 40 ° C e pesado para calcular a massa de SPM. As amostras filtradas foram acidificadas a um pH b 2 com HNO3 bidestilado (Merck, Alemanha) earmazenado a 4 ° C até a análise.

Figura 1. a) coleta de amostra de rocha origem no interior da caverna da tarimba (nível calcítico de paleopiso); b) coleta de cambisssolo e laterita sotapostos na formação Urucuia; c) coleta de depósitos sedimentares recentes em níveis de terraços na caverna Pedras 1; d) procedimento de coleta de águas superficiais para filtragem na caverna penhasco.

Procedimentos analíticos

A plataforma AETE-ISO possui um MC-ICP-MS Mass esoectrinetres (Neptune +, Thermo Fisher Scientific) além de dois IRMS-type mass spectrometers (Delta V Plus, Kiel IV, + two elementary analyzers, Thermo Fisher Scientific) o que permite a análise de vários tipos elementos traços, sendo dedicada aos elementos: Cu, Fe, Hf, Nd, Pb, Sb, Sn, Sr, U, Zn, dentre os principais, operada em modo líquido.

Abaixo temos as fotografias da sala de preparação de amostras e da sala do ICP-MS da Plataforma AETE-ISO no HSM.

Figura 2. Plataforma AETE-ISO no HSM. A. Sala de preparação de amostras. B. sala do ICP-MS

Digestão total de amostras sólidas

As concentrações de metais foram determinadas em sedimentos, solo e rochas após o procedimento de digestão total. Aproximadamente 100 mg de material seco foi digerido em um reator Savillex® PFA em 4 etapas de 24 h em 130 ° C e evaporado até a secura entre cada etapa: (1) um HF 5: 2 mL Mistura (40%, v / v) -HNO3 (65%, v / v); (2) um HCl 3: 1 mL (6 M, v / v) -Mistura de HNO3 (65%, v / v); e (3) uma mistura 2: 1 mL de HNO3-H2O2 (35%, v / v). Em seguida, a solução foi seca, o material restante foi redissolvido em 10mL de HCl (2M, v / v), e a solução foi centrifugada para remover possíveis resíduos.

Todos os procedimentos, incluindo as etapas de digestão e evaporação, foram realizadas em uma sala limpa de 1000 classes. A digestão foi realizada usando ácidos ultrapuros bidestilados (Merck, Alemanha) em temperaturas de sub-ebulição em alambiques de Teflon. Diluição foi realizada usando água de alta pureza (N18,2 MΩ) produzida por um Milli-Q (Nanop System®). As soluções e amostras foram armazenadas em Teflon (FPA) ou garrafas de plástico LDPE que foram limpas com HCl 6 N, 2 NHNO3 e água Milli-Q, cada um dos quais foi permitido descansar no garrafas por 2 dias a 60 ° C.

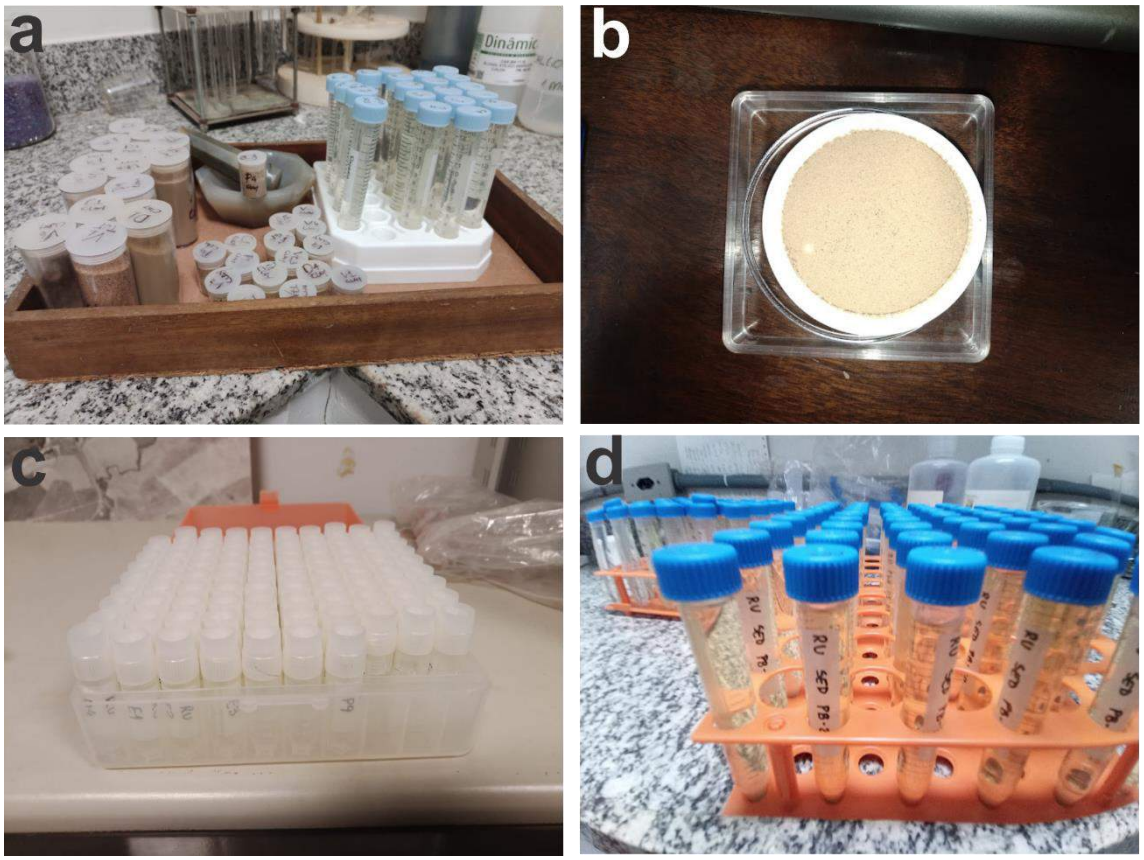

Figura 3. a) Amostras de sedimentos peneiradas (potes grandes), maceradas (potes pequenos) e digeridas (tubos de ensaio), com detalhe para o moinho de ágata; b) filtro contendo amostra particulada após filtragem da caverna penhasco; c) sequencia de amostras digeridas; d) sequencia de amostras digeridas e diluídas em 1:4000.

Extrações sequenciais

O protocolo sequencial de extração BCR ("Bureau Communautaire de Référence") foi realizado usando um procedimento modificado por Rauret et al. (1999). Todos os reagentes usados na extração de BCR foram adquirido da Sigma Aldrich (Canadá). O esquema de extração sequencial empregou uma série de soluções destinadas a metais alvo presente em fases sólidas operacionalmente definidas: solúvel em ácido (F1), redutível (F2), oxidável (F3) e residual (F4). O Zn extraído durante a extração F1 foi denominado originalmente como o ácido solúvel fração (Rauret et al., 1999) e foi definido operacionalmente como a fração trocável e carbonatada de partículas de sedimento (Larner et al., 2008). Esta etapa envolve a adição de 0,11 Macéticoácido (HAc) a 1 g de sedimento seco por 16 h. A fração F2 representa o Zn associado aos oxihidróxidos Fe-Mn e foi extraído com uma solução de cloridrato de hidroxilamina 0,5 M com um pH b2 por 16 h. A fração oxidável (F3) é composta principalmente de Zn associado com sulfetos reativos, piritas autigênicas e matéria orgânica (ácidos húmico e fúlvico, etc.) (Huerta-Diaz e Morse, 1992; Machado et al., 2008), e foi extraído com H2O2

puro e um 1 Solução de acetato de amônio M. Finalmente, a fração residual (F4) consiste em Zn associado ao material refratário proveniente do rocha parental, incluindo minerais de origem fluvial, biogênica ou autigênica de origem, e foi extraído usando o mesmo procedimento de digestão de metal total descrito na Seção 2.3.2.

O controle interno do método de extração sequencial, calculado como F% = 100 × (F1 + F2 + F3 + F4) / (digestão total), alcançou valores b10% para amostras desconhecidas, e materiais de referência (BCR 701) e material de referência internos (Csed6). Todas as extrações foram realizadas em três repetições independentes e brancos analíticos, tendo sido feitos de acordo com à recomendação de Rauret et al. (1999). As concentrações de Zn para os brancos do vaso, o branco do reagente e os brancos do procedimento foram todos inferiores ao limite de detecção (LD) da análise (LD = 0,015µg L − 1). Todas as amostras digeridas foram acomodadas em tubos de ensaio lacrados com parafilm (figura 2c). Cada amostra foi diluída separadamente na proporção 1:4000 para ser processada no ICP-MS (figura 2D).

A Concentrações de metais traço em todas as soluções derivadas das diferentes etapas de extrações (solúvel em ácido, redutível, oxidável e frações residuais), digestão total (sedimentos, solo e rochas) e águas superficiais foram encaminhadas para determinação com uso da base ICP-MS AETE-ISO platform do HSM Montpellier.

2 - Resultados Preliminares dos traçadores geoquímicos

A Concentrações de metais traço em todas as soluções derivadas das diferentes etapas de extrações (solúvel em ácido, redutível, oxidável e frações residuais), digestão total (sedimentos, solo e rochas) e águas superficiais foram processadas para determinação com uso da base ICP-MS AETE-ISO platform do HSM Montpellier. Foi processado um total de 187, sendo 09 amostras de rocha para traçar origem; 32 amostras de solo para traçar origem e 146 amostras sedimentares. Os íons-alvo resultantes da alanise, como podem ser consultados na tabela em anexo foram: ^{7}Li, ^{11}B, ^{23}Na, ^{24}Mg, ^{27}Al, ^{31}P, ^{34}S, ^{39}K, ^{44}Ca, ^{47}Ti, ^{51}V, ^{52}Cr, ^{55}Mn, ^{56}Fe, ^{59}Co, ^{60}Ni, ^{63}Cu, ^{66}Zn, ^{75}As, ^{85}Rb, ^{88}Sr, ^{89}Y, ^{95}Mo, ^{107}Ag, ^{111}Cd, ^{118}Sn, ^{121}Sb, ^{133}Cs, ^{137}Ba, ^{139}La, ^{140}Ce, ^{141}Pr, ^{146}Nd, ^{147}Sm, ^{151}Eu, ^{160}Gd, ^{59}Tb, ^{163}Dy, ^{165}Ho, ^{166}Er, ^{169}Tm, ^{72}Yb, ^{175}Lu, ^{205}Tl, ^{208}Pb, ^{232}Th, ^{238}U. Os resultados podem ser consultados ao final do documento e na tabela anexa.

As amostras foram processadas na base ICP-MS AETE-ISO platform do HSM Montpellier (figura 4). No MC-ICP-MS (figura 5), a amostra é introduzida na forma gasosa (via laser ablation) ou na forma líquida (via nebulizador). As pequenas partículas (gasosas ou aerossóis) passam por um eficiente processo de atomização e ionização térmica no plasma de alta temperatura (~10.000 °C), ainda sob pressão atmosférica. Entre o primeiro e o segundo setor deve haver uma interface, pois eles operam em pressões diferentes. De forma resumida, a interface é constituída por cones metálicos,

amostrador e skimmer, montados coaxialmente para aumentar o vácuo de forma gradual e eliminar componentes residuais.

Figura 4 – esquerda:vista frontal do sistema ICP-MS AETE-ISSO; direita: sistema automatizado de coleta de amostras.

Os íons gerados seguem para o segundo setor onde serão acelerados sob alto vácuo (~10- 11 bar) e alto potencial elétrico (> 10 kV), para, em seguida, serem focados eletronicamente para criar um discreto feixe de íons. Os íons seguem pelo setor ótico passando por estreitas fendas onde os diferentes isótopos são colimados e selecionados em função da sua massa. Em seguida, o feixe de íons passa por um discriminador eletrostático que reduz a distribuição energética dos íons de forma a criar um feixe quase que "monoenergético". Ainda no 2º setor, os íons passam por um forte campo magnético (quadrupolo) e têm seu trajeto modificado em função da razão massa e carga (m/z), de tal forma que os íons mais leves desviam mais e os íons mais pesados desviam menos.

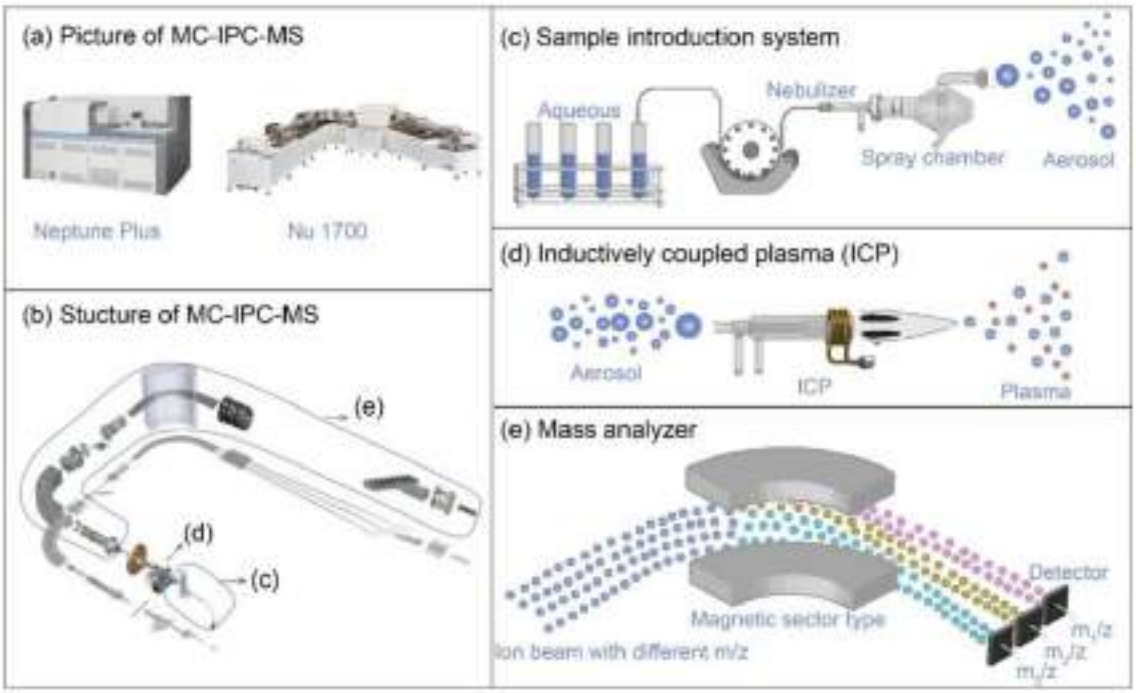

Figura 5 - Representação esquemática de um MC-ICP-MS. a) Fotografia de um MC-ICP-MS (Neptune Plus), b) Estrutura do MC-ICP-MS, subdividido em 4 partes principais; c) sistema de introdução de amostras; d) fonte de íons, plasma propriamente dito; e) analisador de massas (campo magnético).

GPTR AETE-ISO
OSU OREME, Université de Montpellier
– CC 22002, Place Eugène Bataillon
34095 MONTPELLIER CEDEX 5
hsm-aete-iso@umontpellier.fr
https://oreme.org/plateformes/aete-iso/

Rapport d'analyse Eléments Traces

Analysé avec ICAP TQ THERMO SCIENTIFIC le : 02/11/2021
Opérateur :Rémi Freydier
Expertise données: Rémi Freydier
Remarques: [Mo] un peu élevé dans SLRS-6, Problème échantillon FI-50 et S1B air aspiré, à repasser

	Sample List	7Li	11B	23Na	24Mg	27Al	31P	34S	39K
105	SLRS6-3	0,50363	7,53362	2738,90634	2112,08411	35,48722	4,84649	1725,17127	652,51810
105	SLRS6-3	1,26137	3,42429	0,74472	0,96164	2,07317	13,93232	2,13161	0,28168
156	SLRS6-4	0,53721	7,01557	2727,61346	2069,56254	34,01946	5,01895	1968,17289	651,27116
156	SLRS6-4	14,20713	7,26058	1,42828	1,14345	3,15113	15,95742	5,76264	0,85263
206	SLRS6-5	0,57872	7,30496	2787,82337	2179,74611	34,53329	5,05090	1919,27332	657,14245
206	SLRS6-5	15,52664	1,51979	1,86487	1,76885	4,05349	22,70402	5,72403	1,20484
	SLRS6	**0,53985**	**7,28472**	**2751,44772**	**2120,46425**	**34,67999**	**4,97211**	**1870,87249**	**653,64390**
	SLRS6	**0,03761**	**0,25962**	**32,00426**	**55,56775**	**0,74480**	**0,10996**	**128,52793**	**3,09331**
107	Px 1	0,16918	2,20283	11207,06083	711,52847	26,32091	3207,41009	3560,53765	3120,03260
108	Px2	0,16230	2,33864	11852,04436	717,60928	31,28798	3170,32879	3491,23063	3109,54561
109	Px3	0,04338	1,25015	2506,60003	372,46303	8,65747	3944,60471	4355,28051	3395,82086
110	Px4	0,04787	2,15857	2873,80529	501,64745	21,37601	4591,95638	5213,33531	4120,26293
111	Px5	0,05888	2,54687	1746,96945	518,35939	27,81263	3634,69844	2406,15955	5467,46390
112	Px6	0,05911	2,78324	2218,39012	615,70563	34,02035	4750,97889	3196,54939	7183,58563
113	Px7	0,08295	5,42730	2899,54832	608,75531	39,47511	4294,50066	3318,02689	6184,82969
114	Px8	0,06866	4,60424	2465,13118	511,11924	39,17278	3738,36836	2789,61733	5311,05444
115	Px9	0,07812	5,11709	129,11187	408,05305	220,04650	657,23503	153,38546	1526,78124
116	Px10	0,08763	5,36394	130,58631	455,50527	254,88214	723,05303	164,90923	1750,28373
117	Px11	0,02726	1,03762	82,31851	45,23348	19,28282	192,55898	**<LD**	71,67640
118	Sed58	49,45743	17,29478	6549,57386	6150,01052	35147,30655	366,15599	3171,79277	8051,70713
119	Sed118	53,72184	20,57988	8423,90026	6815,13886	37693,78132	354,02841	3848,81930	9172,70940
120	Sed120	62,41306	20,32175	7820,46200	7972,69184	42948,70456	328,95722	5089,17469	11710,47711
121	J4	0,15777	0,46927	14,91432	239,20021	1734,18324	584,25762	**<LD**	85,86393
122	L01 Pisolitos Jagua	0,94092	0,83813	39,22316	911,60160	7667,63977	399,44696	**<LD**	124,53040
123	RF14	0,24275	6,02068	6279,67707	1043,55760	79,83082	3729,11830	4124,03555	3870,25134
124	95	0,16304	5,44507	5614,56460	909,54779	43,94071	2946,45070	3910,35398	3623,33214
125	RF10	0,20911	7,12943	7168,32752	1148,69795	47,61593	4251,62258	5202,13560	4541,25727
126	J10	0,14463	5,72956	5272,24364	887,95710	99,31846	2974,86618	3459,29284	3738,55484
127	BIC	0,24245	7,11585	6884,47545	1159,51354	93,23782	2755,09536	6203,31277	3416,62553
128	107	0,59783	8,40040	8989,80372	1408,44474	244,27833	3154,38587	7010,88982	4056,55240
129	2	0,46960	6,86301	7973,98429	1268,28530	206,30010	2707,53272	5626,54116	3387,44236
130	RF5	0,44482	8,20223	8783,39326	1349,74192	174,98164	3096,02700	6542,33990	4084,54537
131	119	0,66714	8,63105	10570,21157	1634,92602	262,04628	3171,32821	6540,21620	3808,28732
132	CA	0,20424	7,25997	7765,79297	1193,33200	60,92944	3177,78315	6891,82510	4111,61478
133	CE	0,15809	6,45557	6645,67105	1017,00327	53,48155	2672,81443	6277,65768	3868,73386
134	CI	0,19388	7,07102	7235,52095	1172,43544	96,58756	3872,86220	6701,40080	4023,44635
135	LA	0,55657	7,53806	8134,62966	1340,44790	259,02433	3502,71030	7084,09688	4107,82602
136	LE	0,27391	7,92263	9467,51386	1433,97806	120,64134	3682,26057	6661,29476	4013,47302
137	LI	0,37853	10,12524	13373,78322	1906,16204	92,13706	3700,39556	8008,35516	4532,21861
138	LO	0,41314	7,97615	8892,98329	1410,60390	246,47105	3125,12265	7021,58862	3908,60528
139	J25	0,24248	8,11983	8510,24638	1260,04297	84,61991	3253,23261	7226,01255	4455,63402
140	RF2	0,36157	7,32618	7471,81643	1147,00942	138,56130	3512,17724	5511,52464	4058,28101
141	RF4	0,27027	6,14898	6482,84551	1007,56270	84,35665	2976,88620	5588,80423	3674,51331
142	J3	0,21335	7,38370	7587,66246	1139,75378	57,14754	2982,69252	6683,77036	4268,40422
143	RE	0,18537	7,27504	6932,02029	1078,82513	49,82783	2420,82439	6320,62936	3546,60164
144	88	0,11260	5,45983	6370,59921	940,81828	16,54132	1706,20676	4672,40660	2570,03074
145	86	0,18065	6,51622	6758,88203	1059,87985	39,44537	1926,15728	4950,79337	2800,84476
146	CO	0,23843	5,76155	5359,15559	895,98754	86,53686	2627,22240	5854,41039	3423,35111

147	J26	10,17810	9,84075	2315,37421	1433,15866	13563,56633	104,28068	2442,03578	2309,01087
158	AA	0,25686	8,64052	6776,96461	1048,34051	631,06318	2962,51607	5685,79548	3882,83613
159	RF13	0,23972	9,51727	10395,67052	1513,78852	53,36841	4272,94981	9023,21584	5523,98378
160	82	4,03628	91,79931	19473,85869	8098,16662	2303,16417	466,69982	14939,34278	13852,25671
161	129	21,58063	7,91427	2771,51461	2595,13246	15168,43901	160,52289	1518,70781	3413,86373
162	93	7,59011	2,86475	4105,43844	1323,02690	9561,66194	144,17716	12692,25520	2557,60951
163	RF3	5,35538	7,81130	11416,73928	2546,29039	4148,40692	64,01293	2895,57500	1782,85567
164	J19	6,04519	8,67288	11558,01649	2463,71254	4797,56536	70,13821	3421,04932	1930,58272
165	DA	14,75593	7,69610	1679,17606	1906,36458	11546,98430	136,82124	719,18967	2509,57579
166	60	15,65184	7,16345	2122,38659	1944,50065	11679,12892	176,53952	1190,37618	2768,53397
167	RASA	0,86149	1,33876	11,05915	10,96206	3086,00784	20,04677	**<LD**	30,88095
168	RAP	1,24403	2,45134	14,37716	19,03969	6501,20845	5,46660	**<LD**	43,27710
169	RP	20,85718	17,02899	970,68182	2994,83544	23720,84687	73,72159	**<LD**	8076,95570
170	RM	1,46739	2,27421	43,72369	164,31082	1034,62318	10,13301	**<LD**	437,24864
171	RC	17,03667	2,05769	33,48003	2828,11655	1187,35024	15,95909	212,14987	246,26302
172	LIM	1,04914	3,24748	71,01639	36285,36829	514,11755	6,04157	561,49227	273,49568
173	1646	5,35542	11,64360	2120,17508	1113,32478	6391,85575	83,84150	1051,99167	2531,65501
174	CRO	16,18944	9,72026	5603,93746	2640,97955	19244,95794	213,56676	**<LD**	11199,10237
175	E1	11,52505	11,07592	439,14922	1501,87520	14584,27153	71,97604	**<LD**	3383,46909
176	E2	13,21266	13,20795	468,05805	2195,39279	16040,16424	125,91792	**<LD**	5713,07276
177	PB-1	2,94708	10,06541	192,70650	476,22410	13315,19321	285,47621	**<LD**	2006,08781
178	PB-2	3,50303	9,51244	203,11201	597,90136	16989,22205	311,44080	75,86472	2200,06409
179	PB-3	3,82091	10,64903	217,41685	626,68429	17084,64800	324,02199	39,71819	2587,09126
180	PB-4	3,01769	9,78259	188,52824	504,83377	13094,67696	265,70790	55,45763	2339,37878
181	PB-5	3,49066	11,27095	218,96008	577,41915	14813,90349	299,11056	**<LD**	2752,96048
182	PB-6	3,39127	9,70161	195,99293	569,37950	14485,77475	273,79417	34,68008	2477,57066
183	PB-7	2,95207	9,06375	184,46000	506,84382	12962,08536	252,42299	**<LD**	2335,63816
184	PB-8	3,55862	8,78027	216,78438	597,49608	15488,28215	316,20072	**<LD**	2673,66514
185	PB-9	4,11685	9,71651	218,33118	733,31857	19055,00448	321,51448	**<LD**	2997,38082
186	PB-10	3,66654	10,43094	197,24766	648,89251	16748,73237	290,03003	**<LD**	2678,17294
187	PB-11	3,27810	10,48153	210,21404	590,92161	14895,78781	289,26086	**<LD**	2874,87506
188	PB-12	3,94000	10,04995	173,31983	709,10137	17569,10691	227,38446	**<LD**	3260,79599
189	PB-13	4,05870	10,22902	109,77467	742,19969	16858,19703	113,18819	34,40448	3378,80338
190	PB-14	4,08359	8,36855	114,47476	788,76283	17547,57366	110,86990	**<LD**	3741,12077
191	PB-15	4,27963	13,72200	157,66814	876,69088	20544,01715	123,94753	33,11456	5084,56584
192	PB-16	2,83257	9,84374	112,57378	600,93762	16867,34131	118,03075	39,21570	3470,47646
193	PB-17	3,40717	9,55543	135,94784	685,01791	16206,06914	142,12717	56,09063	3645,48597
194	PB-18	3,47343	10,42625	152,19409	703,46173	16944,77625	137,18972	154,98174	4027,89266
195	PB-19	2,97806	9,42672	150,34755	592,04218	14006,44467	153,41689	76,23564	3352,77195
196	PB-20	3,14750	10,74941	106,40389	619,14338	15133,95625	81,17743	133,19859	3213,27182
197	PB-21	3,55425	9,73055	113,52001	746,61027	18250,94527	86,77633	128,99545	3489,10689
208	PB-22	3,45831	10,78593	111,10075	772,72275	19862,36560	87,98879	171,60543	3442,73642
209	PB-23	3,39402	9,88911	115,58472	752,91160	18960,11464	80,56842	219,54501	3599,55749
210	PB-24	3,32335	8,81221	108,87988	765,14212	18839,71391	80,85218	196,12997	3453,58488
211	PB-25	3,79107	11,05533	120,21979	800,13110	19564,70853	86,89718	167,20241	3734,79951
212	PB-26	3,17275	8,54012	94,75724	675,59919	17919,85097	81,46329	**<LD**	2911,98523
213	PB-27	2,90248	11,26867	90,31127	552,06796	14358,02645	75,44761	**<LD**	2533,64481
214	PB-28	3,05888	11,19599	95,18414	504,79496	10533,06621	50,72346	**<LD**	2606,17500
215	PB-29	2,00293	17,66845	71,15141	265,48958	5335,65229	41,24309	**<LD**	1637,23965
216	PB-30	1,52002	15,26478	40,10019	133,20117	2043,98769	19,95632	**<LD**	660,17364
217	PB-31	2,21459	17,05145	60,37037	294,16406	4879,51486	37,68080	**<LD**	1243,65975
218	PB-32	2,52328	17,97003	71,16579	335,67500	5244,18455	37,07187	**<LD**	1398,88940
219	PB-33	1,71963	11,56321	45,54908	190,77302	2948,24523	18,12940	**<LD**	818,48315
220	PB-34	2,10444	15,42497	59,98078	248,96256	4171,62514	28,00750	**<LD**	1106,99995
221	PB-35	1,87631	20,89533	52,32156	229,32953	3433,55719	25,11595	**<LD**	887,26170
222	PB-36	2,04663	20,39577	202,65093	235,65867	4097,76919	36,96850	**<LD**	1164,40522
223	PB-37	2,04104	17,28204	73,09245	255,69316	4224,84912	29,32428	**<LD**	1604,13014
224	PB-38	1,96511	16,79925	70,12449	259,26230	3902,26293	23,64793	**<LD**	1516,30435
225	PB-39	2,00013	21,87341	63,41442	256,59856	3257,12533	32,82221	**<LD**	1298,11332
226	PB-40	2,79983	16,69177	81,31864	392,96861	5968,51529	31,91474	**<LD**	2034,90070
227	PB-41	2,28890	14,76618	73,51795	321,53051	5397,70603	28,42410	**<LD**	1778,64957
228	PB-42	1,93696	17,33752	64,88846	263,25476	4396,95117	26,19126	**<LD**	1457,77290

229	PB-43	2,94578	14,47215	81,26095	485,18804	9834,02119	62,13181	**<LD**	2134,02898
230	PB-44	1,68798	32,33532	63,72024	229,80573	2864,45619	36,42673	**<LD**	1149,65032
231	PB-45	2,66579	15,02577	77,36746	413,56489	6762,28286	46,25143	**<LD**	1944,63664
232	PB-46	2,63289	11,75422	74,62714	439,84074	9063,54607	52,39732	**<LD**	1976,13660
233	PB-47	3,51394	8,21056	89,64638	618,22947	13042,33455	70,44523	**<LD**	2515,49360
234	PB-48	3,93516	8,53138	90,87270	753,75881	17920,04467	93,11769	**<LD**	2948,15931
235	PB-49	3,71881	5,01069	86,22337	799,53144	19980,73408	97,37741	**<LD**	2910,95673
236	PB-50	3,72499	6,69533	77,83759	785,92287	19448,98391	93,65657	**<LD**	2744,62668
237	PB-51	3,93155	8,96722	86,79758	855,56527	20926,47136	98,49470	**<LD**	3043,43453
238	PB-52	4,36710	8,52779	97,84676	879,61634	20045,55691	96,71867	**<LD**	3364,67198
239	PB-53	4,17711	8,15941	92,54583	853,29217	18071,61341	92,26618	**<LD**	3215,78764
240	PB-54	5,10060	8,73243	107,15084	1067,91160	21693,45424	110,30532	**<LD**	3646,11335
241	PB-55	4,59064	8,76104	99,36587	959,31802	18691,24498	96,72187	**<LD**	3501,50047
242	PB-56	4,29075	7,90835	88,61271	909,63953	18413,94545	92,72668	**<LD**	3157,13831
243	PB-57	3,78612	5,79912	93,10592	779,33528	15549,57295	85,38501	**<LD**	2931,60541
244	PB-58	4,09928	7,26819	94,39773	862,84117	17356,46335	90,59612	**<LD**	3216,67005
245	PB-59	3,63045	8,51538	94,53558	734,85644	15166,55139	83,83493	**<LD**	2968,84128
246	E-3	11,87941	10,83765	586,54047	1344,41425	12257,35080	68,26117	**<LD**	3709,15335
247	**FI-50**	**<LD**	**<LD**	**<LD**	**<LD**	**<LD**	**<LD**	**<LD**	**<LD**
248	FII-50	12,21926	13,08963	405,58959	1825,35971	15262,52963	103,60018	**<LD**	4975,72104
249	FII-80	11,54512	12,15645	342,88286	1780,00601	16362,77579	112,23408	**<LD**	5181,30660
250	FII-110	11,98367	13,26291	339,17879	1830,61803	17076,32631	122,84903	**<LD**	5349,46159
251	S1A	15,48618	12,82244	79,51605	1610,57891	19166,25566	99,41918	**<LD**	4764,10508
252	**S1B**	**0,01786**	**<LD**	**<LD**	**<LD**	**<LD**	**<LD**	**<LD**	**<LD**
253	S2A	1,39199	9,83212	29,77607	177,28545	11582,43151	40,12178	**<LD**	396,96157
254	S2CR	1,37590	11,62788	27,21027	139,84746	9608,93275	22,77567	**<LD**	387,58033
255	S4A	0,61242	5,86519	16,13950	47,94178	41909,83542	98,26864	**<LD**	79,89151
256	S4BW	0,58476	7,05918	11,73271	36,55686	48892,58322	71,77843	**<LD**	53,50572
257	S8A	0,57361	4,65997	10,21126	33,97726	44873,12175	93,62148	**<LD**	53,00367
258	S8C3	0,68626	4,14134	11,98323	31,70111	43683,58841	72,10514	**<LD**	49,40268
259	S10A	10,20142	16,29201	118,90145	2596,37311	17829,15186	181,45881	**<LD**	6786,36928
260	S10Ca	8,78880	13,19731	85,04288	2584,62669	14980,89437	193,99991	**<LD**	5694,42794
261	S11AB	12,84002	10,93302	133,86131	1316,02715	19073,60614	68,00488	**<LD**	4359,13835
262	S11B	16,85758	12,86994	115,81724	1823,28129	26039,77141	63,00171	**<LD**	5042,05652
263	S9A	1,82806	5,25671	23,18307	224,84693	12797,50500	109,80286	**<LD**	315,48828
264	S9C3	2,22264	10,43141	19,87789	152,21690	9912,75708	28,26800	**<LD**	170,51976
265	P15	11,73570	19,58671	126,74733	3340,17613	21026,99928	114,06796	**<LD**	7846,63989
266	SP70	15,66973	22,94191	157,05985	5112,21483	26261,61181	135,78964	**<LD**	10323,41107

44Ca	47Ti	51V	52Cr	55Mn	56Fe	59Co	60Ni	63Cu	66Zn
9033,78415	0,60967	0,38055	0,26282	2,24943	87,39789	0,05296	0,62674	25,65790	1,76789
0,80724	4,02195	1,74663	0,41333	0,56250	0,98833	1,24038	0,58260	0,72669	0,90656
9007,08107	**0,57900**	0,37911	0,26554	2,26578	83,47431	0,06022	0,63464	25,71190	1,78274
1,24925	3,40000	0,33731	1,43099	0,68105	1,15270	4,19423	2,65136	1,24565	2,47925
9027,55344	**0,54300**	0,37759	0,26233	2,25256	86,56736	0,05684	0,63544	25,42158	1,74612
0,94465	0,20000	1,75073	2,14709	0,86053	1,68005	1,82651	1,42267	0,22006	0,40508
9022,80622	**0,57722**	**0,37908**	**0,26356**	**2,25592**	**85,81319**	**0,05667**	**0,63227**	**25,59713**	**1,76558**
13,97017	**0,03337**	**0,00148**	**0,00173**	**0,00868**	**2,06766**	**0,00364**	**0,00481**	**0,15441**	**0,01842**
2847,10560	1,84093	0,44701	0,86663	6,92459	65,77902	0,20578	0,81037	121,52978	52,73020
3023,65451	2,63095	0,49955	16,09503	7,42351	100,55021	0,21413	1,74028	124,11236	63,27834
322,63933	0,83397	0,14353	0,71018	3,20396	255,12660	0,16922	0,52616	7,46013	38,64874
1344,40817	0,84308	0,21592	5,22760	5,84789	344,20619	0,24840	5,09377	9,95407	103,55953
2815,38540	0,87997	0,27260	22,75342	7,10193	158,08845	0,38128	18,37810	4,50650	166,27150
3159,59462	0,96243	0,30436	27,45497	7,79419	181,19775	0,42122	21,14013	5,13845	157,43823
2596,11073	1,44868	0,21371	10,95717	5,07264	113,07340	0,27458	9,89824	4,75236	110,57029
2238,24882	1,38323	0,18336	9,70829	3,86524	92,45628	0,22242	7,68641	3,95176	88,36830
2089,20433	2,22718	0,18281	5,41165	170,05350	68,27974	0,24447	5,50717	2,62705	72,21138

2099,27596	2,59761	0,16875	4,72186	197,56910	64,27159	0,19753	5,01142	3,48407	68,77579
722,46293	0,36017	0,09544	2,91166	1,31000	29,38539	0,13445	2,74835	0,86920	33,85685
3849,78480	2309,02182	35,35177	32,93280	168,24996	18491,87463	4,86865	14,88541	30,23583	84,36591
4192,52513	2519,66653	38,27916	34,90424	164,22049	19401,82907	5,17383	14,82920	30,70855	79,65099
4903,41586	3042,03689	46,65367	40,25066	201,60431	22696,22434	6,30331	16,66793	21,89410	80,31478
103,88103	105,87385	100,84213	4,95333	39,93922	##########	30,79019	635,26840	103,97730	145,17750
480,40441	673,40235	65,88816	24,43643	37,02110	84357,94654	14,00133	299,77018	64,17809	100,16143
5614,03133	1,82856	0,23335	1,98642	19,85156	357,94956	3,04374	194,27076	11,93121	745,37299
3850,06031	1,55571	0,12170	0,37688	2,87407	217,37548	0,11178	0,29398	7,25990	576,41278
4496,79839	1,13264	0,10397	0,22921	2,79176	167,64338	0,10708	0,49461	8,98561	654,04040
5159,32550	0,82251	0,14460	4,94282	3,64210	246,11743	0,32746	8,87009	13,40137	509,15947
13640,05987	1,71197	0,53084	0,31670	3,92917	96,88840	0,08802	0,39609	41,96338	413,04245
9789,49029	7,83808	0,46438	5,78955	13,71411	261,10856	0,23615	4,38621	17,72837	806,26167
11843,50928	6,13039	0,36597	0,35318	7,47686	208,67132	0,16189	0,39786	20,31028	887,02464
8424,16758	5,35656	0,32373	0,38577	9,69399	175,59153	0,14598	0,37346	15,58873	571,38005
9122,29273	10,88342	0,55049	0,46379	9,04222	267,77135	0,21282	0,46413	9,97872	528,37230
3962,67672	2,07642	0,20301	0,28075	6,30292	78,88721	0,15229	0,41578	570,65586	2043,84682
6453,87009	1,43285	0,13302	0,20895	3,57535	53,34071	0,10889	0,18489	828,81106	2012,62136
8655,76770	1,42682	0,23191	0,24926	8,72120	88,81257	0,19608	0,25023	540,81252	1758,92074
5710,25363	9,55369	0,59735	0,54602	10,82709	262,82910	0,22206	0,56106	41,37623	751,75445
6313,54805	2,70313	0,32246	0,37959	5,14988	143,29165	0,15710	0,50074	370,84592	1292,67325
6129,26138	3,88038	0,41197	1,23812	5,52227	174,64422	0,21282	0,70016	492,14822	1425,61168
8176,11406	7,64288	0,50903	1,51104	4,95210	406,60703	0,24069	0,74803	629,53385	1591,05642
2870,99459	2,23909	0,20770	0,26229	7,49339	90,46804	0,14452	0,23766	662,40874	1624,42438
6135,02147	6,92606	0,32864	0,42170	5,49581	446,95769	0,14141	0,30564	32,98504	730,43438
4870,77887	3,29530	0,17652	0,40331	4,57279	84,56713	0,07238	0,18893	29,86735	638,45197
4222,62952	1,27414	0,16833	0,19015	3,24377	61,04332	0,10626	0,30758	448,84417	1485,22709
9570,48368	1,17978	0,48211	0,40221	2,26234	77,07399	0,07806	0,77345	46,38725	475,21894
4095,66392	0,39941	0,28166	0,14768	2,18666	44,81829	0,04861	0,33641	31,91095	373,96124
13471,76457	2,02324	0,37773	0,19318	2,61670	57,02564	0,04968	0,30436	33,51288	349,82793
8167,01803	3,16846	0,19639	0,24491	2,34957	85,88235	0,10320	0,19378	895,87316	1980,61035

712,65748	797,24741	14,26241	10,24186	40,26959	6432,75420	1,38860	3,37445	2,70635	18,72178
6382,02315	2,78384	0,22853	1,31607	4,60261	314,85888	0,29439	5,76030	449,30871	1388,19408
3689,47475	**<LD**	0,18229	0,19014	7,12467	70,51602	0,15108	0,26426	805,43913	1703,49990
15998,53213	152,45798	6,58817	2,25730	99,44294	1562,48601	0,73341	1,18665	25,90550	70,47493
1455,41712	1057,83487	15,22935	13,63806	69,97604	7900,34018	2,08216	5,74251	13,26472	28,88905
1603,55663	1166,93749	8,91389	3,02030	62,88113	13251,68578	1,15832	1,41487	2,01880	20,19501
1961,47810	474,95040	4,75113	4,28877	27,88859	2109,88115	0,50673	1,56313	1420,68242	306,85239
2010,10231	655,87283	5,23183	5,39475	31,90342	2293,83733	0,57041	1,94468	2791,53271	355,42289
1269,77614	800,06485	11,33231	9,68465	53,41398	5565,25520	1,49100	4,31413	7,78762	20,45226
1547,63341	807,91267	11,28796	9,99261	53,71981	5885,74277	1,58679	5,90602	16,27862	57,13951
57,77750	63,01076	2,52430	0,44732	11,32835	1158,61629	18,33549	1,58201	2,54364	2,31527
36,65885	562,43492	4,11295	6,14826	1,79558	457,41830	16,71148	1,03116	2,45683	1,02030
891,87091	1752,03530	32,84126	24,09784	160,16567	12069,70285	9,96849	11,89324	8,71145	24,74923
123,97188	91,78388	2,74530	2,48987	28,57903	1862,27942	82,76290	1,84092	2,92520	4,26642
###########	57,89557	1,80872	1,30381	33,25960	752,68968	3,90696	0,65163	0,59834	3,01660
68951,30177	34,54958	0,85080	0,86079	38,59680	610,47802	0,30319	1,01156	0,46924	2,81305
1868,13486	1506,52636	13,03058	13,27261	69,43896	5904,56368	1,36530	7,48838	3,51177	23,56403
4628,19318	856,89368	12,46410	22,31585	99,76640	5502,92794	2,12040	6,43750	3,12660	33,32740
1435,33508	1485,85236	21,56858	14,74358	108,28641	7487,70543	3,06677	7,69644	9,05330	18,44121
1071,78844	1508,91860	30,77118	19,14693	174,27562	11324,58086	9,91942	12,92667	12,32002	25,54542
698,96033	1627,25015	20,83581	7,85800	52,42347	5401,19854	1,13220	2,13331	4,26181	6,26187
930,44413	1581,95761	24,42769	9,54635	60,42265	6697,09753	1,49395	2,74268	5,32952	8,21021
901,80050	1825,55188	24,50273	9,96784	63,20187	6803,49803	1,46933	2,87394	5,11220	8,66978
760,94846	1530,00550	19,31539	8,08105	56,17612	5296,97497	1,15247	2,36735	4,32945	7,18866
798,74126	1763,17091	21,80610	8,80214	60,29898	5377,02757	1,29214	2,70233	4,75448	7,70925
783,23095	1566,63192	20,94418	8,80012	55,47086	5289,21824	1,19981	2,56790	4,58017	8,24284
669,86958	1444,89762	18,51820	7,65510	51,71503	4868,88101	1,05378	2,30794	4,19399	6,98495
745,33168	1452,80431	21,29150	10,73854	57,59899	6219,04056	1,20189	2,71442	12,41690	8,64843
863,24489	1679,50475	25,45573	11,11093	64,12826	7451,75441	1,54609	3,30800	5,94662	9,42402
827,12680	1524,06576	23,58638	9,72773	64,17460	6558,16132	1,34183	2,96206	5,51682	8,57765
707,39534	1470,83564	20,66811	8,33348	59,63443	6174,37609	1,32355	2,66740	4,89612	7,75524

768,44747	1562,98160	22,51243	9,70262	64,70023	7048,78671	1,40419	3,08381	5,35656	8,51824
734,10244	1539,68687	21,77330	9,26812	66,92829	6942,86304	1,41128	3,05522	5,59911	8,71592
737,51396	1472,44821	20,78044	10,15933	72,82539	7190,49286	1,58470	3,48126	4,96854	8,25556
807,65880	2153,15986	25,80228	10,70769	94,01683	7625,39764	1,66526	3,35660	5,79279	8,59965
666,53962	1672,29325	22,54868	9,06378	117,09433	8071,83044	1,37787	2,50135	4,70982	6,57795
733,46148	1511,45727	19,88065	8,17599	108,43677	7683,67009	1,54167	2,70313	4,65682	7,48981
772,05330	1775,83399	21,63233	9,03544	82,26308	7066,01475	1,93241	2,78207	5,05911	7,91220
595,67424	1542,33124	17,72396	7,28711	65,49631	5636,68890	1,36880	2,35920	4,16761	6,64029
584,78370	1541,76593	18,20039	7,84208	64,48136	5676,01852	1,40014	2,54168	7,42739	7,87533
684,43321	1597,46656	20,55540	8,37566	79,75095	6269,59537	1,54438	2,83699	5,16850	7,63811
677,24046	1568,01679	20,59129	8,88390	71,86494	5988,91171	1,55812	3,01132	5,22429	8,21387
684,13624	1477,85864	19,75981	8,41709	63,77063	5749,11826	1,52517	2,89069	5,73662	8,15835
720,01134	1367,48755	18,94950	8,69442	73,89614	5838,19790	1,52075	3,05007	6,92933	7,99484
854,98878	1583,65951	20,48941	9,78258	96,64140	6003,35785	1,76275	3,07124	5,36390	8,23783
813,38254	1428,31739	19,79904	8,09696	80,06073	5932,61679	1,52152	2,99143	4,90380	7,27388
674,66554	1534,43226	18,14645	7,57981	84,34535	5472,67203	1,53686	2,49171	4,32560	7,03347
610,16231	1663,96542	16,67632	6,93967	72,82459	4310,71651	1,29073	2,16100	3,97253	6,22540
312,38482	3465,38891	20,65813	9,98963	128,90189	5790,80571	1,34954	1,72003	3,81536	6,61509
154,47466	3383,03118	16,96866	18,39659	103,33720	4042,42650	0,96625	6,90392	2,89257	5,54581
452,86200	3070,33919	18,33110	8,29420	96,12066	4494,68630	1,18003	2,28954	3,94856	8,61922
338,91825	3292,99451	19,00936	8,57494	104,83603	4582,09435	1,18858	1,97556	3,38089	8,44009
211,24445	2355,80169	12,41685	5,95460	72,48216	2921,66754	0,78836	1,24617	3,56686	4,84223
292,34471	3436,16387	18,21624	13,99374	99,31752	4210,97333	1,24051	1,81113	3,10572	6,89892
166,67576	5037,98477	24,86081	10,72015	149,39742	5714,54864	1,41017	2,25767	4,45588	8,34902
311,99320	5968,13428	29,42505	11,81615	177,79182	6938,08343	1,46929	2,29568	6,08846	10,43980
259,94389	3373,77274	17,71423	8,05803	91,89080	4174,39345	0,97764	1,48355	2,74985	7,10624
208,57079	2973,97145	14,91433	6,38243	79,72152	3444,43972	0,88013	1,29179	2,42878	5,49224
175,42014	5839,88525	26,49382	13,22704	156,13975	5841,23385	1,36957	1,58833	3,41370	7,86472
315,87796	2313,60894	14,00789	6,65866	59,86705	3467,30491	0,89154	1,70752	2,61438	6,06477
253,30057	2341,76096	13,44902	6,07296	65,00557	3258,76981	0,87678	1,41015	2,56443	5,64430
233,25524	2584,34982	13,05043	6,45216	70,01065	3143,11311	0,82089	1,25471	2,24551	5,16469

375,23823	2507,53403	17,70232	8,29475	110,02969	5983,86297	1,38241	2,22909	3,97880	7,67271
154,73025	6468,12394	25,88967	10,66918	162,66038	5583,23858	1,32503	1,42928	3,65112	7,72922
341,16973	3328,38007	18,17474	8,43608	106,07341	5285,39166	1,18776	1,90068	3,18300	7,27693
341,65446	2350,86976	16,37190	6,91304	102,36890	5418,18561	1,26340	2,06067	4,04870	6,42460
492,05163	2088,71919	18,63326	10,16260	136,20686	6714,18015	1,71650	2,59928	4,32469	7,51159
646,18427	1685,01790	21,53934	9,16648	158,50689	8409,62277	2,14015	3,26355	5,42870	8,57433
670,32613	1356,14259	20,26791	8,76818	144,35958	7978,06690	1,97836	3,21576	5,15587	8,17345
639,52790	1185,47543	19,19909	7,68730	131,25661	7589,61024	1,83875	3,12958	4,89465	8,23172
683,17341	1344,41049	21,23040	8,58839	147,46063	8289,35358	2,04863	3,35873	5,99955	9,29450
682,78037	1475,47544	20,98686	9,30758	144,00929	8006,18547	2,04396	3,54803	5,40931	9,47320
634,60463	1347,27200	19,03239	9,05349	130,50799	7151,87322	1,91441	3,53497	5,01684	9,15486
810,87876	1420,07095	22,30799	11,05291	156,22796	8473,71594	2,37241	4,54290	5,97036	10,91206
738,16742	1344,06829	20,33672	9,45556	142,25651	7489,98461	2,12539	4,01816	5,36620	9,83704
697,62197	1260,40394	19,12352	8,95544	134,71894	7226,10232	2,01826	3,72771	5,53855	9,36091
709,77751	1165,81251	17,59148	9,16201	125,21587	6700,50384	1,85656	3,47007	4,73500	8,62438
800,72287	1284,26916	19,11614	8,62063	133,46060	7451,66257	1,97372	3,55602	5,42756	9,39140
801,05050	1460,07374	17,55816	9,14960	120,92221	6422,04235	1,76812	3,24057	5,18714	8,22530
1103,50740	1198,14447	19,86886	13,69219	151,39000	7697,06101	4,09091	7,64283	10,62822	16,87097
<LD	**<LD**	**<LD**	**0,00281**	**<LD**	**<LD**	**<LD**	**<LD**	**<LD**	**0,00747**
1353,89839	1541,70243	27,57591	20,35464	263,32825	10128,40917	7,78030	12,80212	9,33048	26,39882
1310,05961	1530,33427	27,68391	19,47416	181,60603	9622,08176	6,07602	11,39762	10,74660	23,16932
1627,86551	1543,96236	28,56026	20,07690	203,15688	9966,42540	6,54955	12,33841	10,66784	25,10805
886,79186	1572,18468	33,20061	20,90221	553,76785	14919,46379	5,14778	10,45364	6,63158	14,47587
<LD	**<LD**	**0,00059**	**0,00353**	**0,03140**	**<LD**	**<LD**	**<LD**	**<LD**	**0,00724**
420,60276	1600,97402	10,80640	7,34533	38,26132	2099,71528	0,55479	2,59710	2,26976	6,32739
89,28456	1897,60984	10,70254	6,05341	39,64336	1829,26149	0,60361	1,76368	2,38872	4,29220
72,46504	3122,51726	48,00609	27,27190	18,20626	16178,41396	0,26297	2,24962	1,37266	5,94838
66,33276	3567,19402	55,67137	30,32446	19,47586	18682,15545	0,29446	2,46403	1,59134	6,45139
142,69022	2379,06535	12,92110	30,66088	3,25149	1827,09725	0,25859	3,65014	5,97469	6,31504
110,70041	2369,40730	13,27200	29,20625	2,68881	1693,91723	0,25194	3,53092	6,11823	5,81657
926,20692	1725,17259	40,56543	21,99938	222,59555	10755,52262	5,59221	14,75197	10,32219	29,75090

450,06987	1029,78924	106,64213	36,54643	142,01034	26487,76862	17,44861	15,27672	13,83238	28,38435
994,19087	2074,43005	32,19127	25,78072	155,64606	10744,69876	4,68387	10,21660	11,02289	15,28148
1029,98279	1976,35859	41,43678	34,63401	160,76650	14756,42872	5,02201	13,96066	26,00201	18,87732
147,45984	2022,30558	13,02053	7,53729	25,77064	1627,03274	0,49620	3,20935	5,41602	5,06594
68,77306	2420,98857	11,67998	7,42115	27,32981	1148,35807	0,47835	2,39906	4,81261	3,84768
294,99320	1774,23348	46,63465	22,97185	73,74348	9419,53992	4,74020	12,32479	10,57665	33,42246
254,04817	1835,11231	47,85137	26,62326	301,50133	11126,39044	15,06152	14,75733	12,32780	35,37264

75As	85Rb	88Sr	89Y	95Mo	107Ag	111Cd	118Sn	121Sb	133Cs
0,52591	1,50304	42,38376	0,14423	0,32814	0,01391	0,00809	0,12362	0,34514	0,00803
2,88393	0,84513	1,19961	2,15491	15,71120	47,11508	7,93172	57,38211	3,19329	7,37610
0,55348	1,48184	42,02241	0,14044	0,26503	0,00984	0,00953	0,09237	0,33679	0,00798
1,54542	1,57251	1,57648	2,60977	N/A	67,81768	13,75912	72,98858	1,92434	26,45076
0,50610	1,48236	41,89212	0,13483	0,28083	0,01114	0,00734	0,08773	0,33642	0,00630
2,69290	0,66675	0,31181	3,11286	5,06243	47,71176	5,59876	66,54458	0,16973	28,50219
0,52850	**1,48908**	**42,09943**	**0,13983**	**0,29133**	**0,01163**	**0,00832**	**0,10124**	**0,33945**	**0,00743**
0,02379	**0,01209**	**0,25471**	**0,00473**	**0,03284**	**0,00208**	**0,00111**	**0,01952**	**0,00493**	**0,00098**
8,08334	1,44422	34,73323	0,49821	0,50300	3,96502	8,27337	25,26584	0,03894	0,00829
7,99534	1,23604	34,63419	0,50640	0,61775	3,98200	8,45229	24,90494	0,04194	0,00864
3,06448	1,54049	2,04477	0,00616	0,41307	0,49124	1,69119	28,38462	0,02478	0,02198
3,53388	1,88509	6,29384	0,00582	0,53360	0,55768	1,98415	26,00902	0,04607	0,02761
5,98313	2,30447	11,60206	0,00754	0,33040	0,11552	0,10317	23,29151	0,07715	0,09827
7,69956	2,89593	12,61242	0,00820	0,38490	0,11146	0,10362	26,06677	0,08821	0,12219
6,53069	2,72935	10,97540	0,00831	0,47601	0,13066	0,11251	27,03797	0,07034	0,05652
5,52119	2,33361	9,34643	0,00886	0,20690	0,13384	0,09720	21,87103	0,05845	0,04890
0,03109	6,28556	6,97278	0,01631	0,13653	0,05731	0,17538	25,85830	0,04382	0,10520

0,02986	7,75323	6,81118	0,01855	0,12502	0,04224	0,17438	24,00970	0,04228	0,12477
0,00649	0,48673	2,50640	0,00268	0,07500	0,02840	0,06216	20,00158	0,02996	0,00198
4,65670	59,23221	48,86379	7,27892	0,70427	0,06489	0,03855	4,29836	0,12430	3,66517
4,90688	65,31709	53,50028	7,79376	0,84312	0,08776	0,04363	3,91754	0,12189	3,90347
5,89404	82,55766	65,83356	10,07154	1,28684	0,07837	0,06196	4,32516	0,13535	4,79536
5,40769	0,58244	6,55302	4,58534	10,35410	0,04409	0,13588	1,25559	0,04436	0,01172
5,10787	1,13382	3,30520	5,65871	1,50131	0,10347	0,20075	1,26867	0,04650	0,03716
2,50946	2,75278	24,09566	0,14282	0,33469	0,05323	0,28878	0,65033	0,00814	0,01008
2,52449	2,11588	16,72375	0,11006	0,23190	0,04792	0,28489	0,52473	0,01026	0,00753
2,42402	2,29840	17,95944	0,11506	0,18242	0,08493	0,25150	0,40123	0,01263	0,00784
1,92686	2,17231	31,85362	0,08934	0,19727	0,06358	0,31934	0,29056	0,01053	0,00858
5,08555	1,74114	47,68564	0,11283	0,41312	0,66844	1,91406	0,22104	0,01189	0,01368
2,68882	2,25507	35,98460	0,17246	0,57205	0,08986	0,24141	0,20734	0,02009	0,02554
2,17031	1,79257	34,37622	0,24286	0,31870	0,08032	0,15612	0,19264	0,00899	0,02001
2,63061	2,20665	30,09560	0,16523	0,30230	0,05406	0,22419	0,19748	0,00992	0,01841
2,83949	2,11502	36,15345	0,21046	0,31678	0,05494	0,25402	0,16677	0,01246	0,03125
3,02403	2,24369	19,17798	0,18655	0,17222	0,01777	0,33359	0,20820	0,01097	0,01119
2,81986	2,06383	20,41116	0,16616	0,13421	0,01388	0,31290	0,21375	0,00860	0,00742
2,49831	2,10830	46,00555	0,08545	0,18039	0,01753	0,38281	0,23572	0,01061	0,00952
3,03311	2,46627	23,68891	0,28974	0,30634	0,04084	0,27569	0,23464	0,02552	0,03410
2,78534	2,01773	22,55249	0,18033	0,18556	0,03071	0,29739	0,22531	0,01576	0,01334
3,42663	2,25903	27,05548	0,21213	0,26218	0,03043	0,35560	0,25860	0,01450	0,01649
2,85336	2,17017	29,03128	0,31251	0,36173	0,08143	0,34355	0,44721	0,02221	0,02538
2,92122	2,22592	15,23856	0,21039	0,16764	0,01838	0,29804	0,34186	0,01011	0,01153
2,21739	2,11134	25,58584	0,13109	0,27159	0,05383	0,11800	0,18381	0,00947	0,02216
3,03180	1,89828	19,60323	0,08902	0,14315	0,17892	0,17953	0,12163	0,00856	0,01272
3,35983	2,06820	17,65625	0,17258	0,14330	0,02942	0,34355	0,15090	0,04114	0,00787
4,96766	1,76444	30,67394	0,08137	0,40477	0,57137	2,05798	0,15947	0,00998	0,00768
3,67714	1,26882	17,20091	0,04263	0,21156	0,38613	1,38842	0,06456	0,00540	0,00401
3,48197	1,36825	51,28179	0,08703	0,29545	0,46731	1,37199	0,08374	0,00557	0,00466
2,93755	1,74847	22,76087	0,35635	0,14276	0,04539	0,29522	0,20163	0,01118	0,01137

2,08658	15,91681	16,15661	4,07488	0,57680	0,01942	0,02763	0,71597	0,06593	1,11433
2,53985	2,40916	26,76881	0,31135	0,25335	0,11073	0,31687	0,69880	0,04835	0,01724
3,85122	2,55915	19,31016	0,13337	0,21181	0,03024	0,32759	0,33050	0,01047	0,01007
5,10207	9,04498	530,13097	0,79347	0,11167	0,01490	0,05774	0,38530	0,01663	0,29833
1,98431	22,88729	19,77480	3,11360	0,25656	0,02326	0,01996	1,26183	0,04854	1,51266
2,99014	9,71637	31,06316	4,57757	1,98090	0,01852	0,04471	4,36865	0,09516	0,20763
0,90363	7,02815	27,79572	1,88296	0,34441	0,03029	0,01154	0,82500	0,03067	0,32383
0,97122	7,85689	27,81347	2,56670	0,38002	0,06971	0,01687	1,57765	0,03925	0,35481
1,60384	16,12372	15,26355	2,77337	0,18967	0,01842	0,01253	0,75398	0,03205	1,01498
1,61200	17,38004	14,91029	2,77910	0,25382	0,08772	0,03257	2,29435	0,06769	1,05784
0,48151	0,25325	2,10630	0,46934	0,13022	0,03444	0,00169	0,30559	0,02743	0,01057
0,16320	0,28019	0,95268	0,80776	0,09474	0,03405	0,00251	2,17294	0,07026	0,01568
2,15266	43,14214	11,97684	7,28764	0,10409	0,01942	0,00724	1,36299	0,22919	2,13725
0,57793	2,86418	2,97426	0,43943	0,29164	0,13362	0,01227	0,29162	0,06796	0,19098
0,39115	1,66513	410,36453	0,86687	0,05816	0,01173	0,01361	2,37270	0,02614	0,26215
0,32668	1,19971	19,88576	2,49762	0,06770	0,00888	0,01654	0,44338	0,04348	0,04800
2,18948	10,83845	21,83292	3,61331	0,60897	0,03017	0,04703	0,79251	0,11142	0,38665
1,06315	70,67070	101,62994	6,05032	0,23006	0,01970	0,01069	2,06489	0,08565	3,60677
2,07620	21,35371	11,17660	7,17142	0,09935	0,67536	0,01689	5,85013	0,18492	1,25784
3,01694	31,33283	9,52332	8,02079	0,13916	0,07560	0,02405	4,43147	0,23720	1,67414
1,17194	9,24033	10,80555	6,51908	0,09340	0,12405	0,02236	5,85704	0,12342	0,44982
1,56268	10,38770	12,62982	7,42932	0,10742	0,12561	0,02513	6,05584	0,12943	0,55356
1,55751	11,80369	13,18415	7,84270	0,12859	0,13832	0,02470	6,39427	0,14171	0,58706
1,34412	10,65788	11,11436	6,94978	0,10460	0,12862	0,02232	5,63256	0,12662	0,49314
1,44360	12,10771	12,29758	7,36538	0,09973	0,12932	0,02562	6,15366	0,13295	0,56184
1,35895	11,26654	11,56427	7,08176	0,09712	0,12516	0,02006	5,73006	0,12130	0,55173
1,16128	10,80413	10,42044	7,21694	0,07696	0,12485	0,02164	5,17652	0,10724	0,50174
1,35374	12,18872	11,60997	7,59631	0,11214	0,14594	0,02195	6,53385	0,12404	0,59699
1,49339	14,00884	13,26518	8,67863	0,10743	0,13784	0,02408	6,16329	0,16232	0,72408
1,45482	12,63611	12,47167	7,98909	0,09103	0,14792	0,02436	5,60618	0,12839	0,63664
1,32713	13,04627	11,80707	8,18284	0,08858	0,12418	0,02272	5,85791	0,12148	0,59643

1,48844	15,03422	12,80127	9,23960	0,09319	0,16880	0,02441	3,61875	0,13425	0,73832
1,47231	15,94031	12,34373	8,86815	0,08686	0,07551	0,02336	0,75578	0,13069	0,77993
1,63614	17,25812	12,45142	9,83250	0,15782	0,07836	0,02092	0,75441	0,12671	0,81689
1,75753	21,34580	15,65521	13,12891	0,10514	0,10334	0,02814	0,92164	0,16253	0,90505
1,59796	14,65798	12,17853	10,63230	0,08419	0,07670	0,02111	0,72638	0,12884	0,60466
1,52776	15,84027	12,12229	9,90631	0,07907	0,07942	0,02227	1,69908	0,12744	0,69963
1,67475	17,16002	13,62145	11,10214	0,08520	0,09110	0,02608	1,67288	0,14069	0,71202
1,47046	14,48898	11,36779	9,32441	0,07864	0,09223	0,02124	2,49179	0,11911	0,61328
1,55995	14,17325	11,01056	10,11320	0,06743	0,06979	0,02157	0,76458	0,12238	0,63691
1,69231	15,72841	11,87979	11,43450	0,07938	0,06414	0,02126	0,74270	0,13820	0,75015
1,67547	14,49156	11,17765	11,78267	0,12044	0,11840	0,02247	0,78974	0,13799	0,75033
1,74537	15,46040	11,63425	11,69928	0,10025	0,08173	0,02153	0,76101	0,13454	0,74443
1,63435	15,26434	11,54701	10,79046	0,10551	0,08498	0,02039	0,79864	0,13345	0,75516
1,75836	16,24574	12,49061	11,86053	0,11058	0,09091	0,02276	0,78160	0,14763	0,79112
1,55247	12,97081	11,07848	10,60329	0,09048	0,06838	0,02405	0,69383	0,12763	0,65316
1,45216	11,81491	9,49013	9,70181	0,09466	0,07722	0,02523	0,72347	0,13188	0,60567
1,21091	11,97987	9,08309	8,29507	0,09257	0,07941	0,02391	0,68653	0,14162	0,54942
1,34330	6,93128	6,29664	12,48115	0,12917	0,16774	0,06679	1,33543	0,14652	0,24294
0,68619	2,79446	3,14293	10,51958	0,33245	0,16404	0,06378	1,43309	0,11286	0,09713
0,99472	5,56664	5,55495	10,00867	0,14866	0,13736	0,09586	1,79873	0,14586	0,23393
1,01574	6,34754	5,48333	11,15648	0,12249	0,12465	0,05459	1,13213	0,14976	0,27371
0,60402	3,65448	3,37999	7,22426	0,09856	0,10693	0,03629	0,86383	0,10963	0,14233
0,75548	4,92488	4,85109	10,70006	0,15113	0,13868	0,06009	1,02474	0,13920	0,19841
0,86421	3,95343	3,75483	16,10424	0,19046	0,23945	0,10226	1,67383	0,16139	0,15878
0,87082	5,07802	6,60002	18,00810	0,21890	0,28603	0,13412	1,52807	0,17012	0,15053
0,85480	6,69215	6,02702	13,67612	0,12309	0,16549	0,07351	0,91172	0,14863	0,22217
0,76303	6,27532	5,17744	10,94620	0,09168	0,14883	0,05799	0,75522	0,12675	0,21617
1,05239	5,47344	4,72461	21,43650	0,16053	0,28013	0,12400	1,08759	0,17430	0,18474
0,86839	8,98608	6,47875	8,25452	0,08975	0,08442	0,02887	0,72384	0,13240	0,33650
0,85421	7,77471	5,90041	8,89587	0,07796	0,09828	0,03903	0,70269	0,12956	0,28335
0,71836	6,17330	5,20931	8,31022	0,08459	0,10025	0,03726	0,67691	0,12603	0,21228

1,35299	9,50411	7,42481	11,31292	0,09847	0,11584	0,03720	0,80819	0,14733	0,39589
1,16214	4,81485	4,74194	20,97662	0,15784	0,22270	0,10087	1,17665	0,19687	0,14856
1,24187	8,53283	6,74386	12,78287	0,12081	0,10606	0,04791	3,15371	0,16459	0,33465
1,27683	8,82045	7,00064	10,13770	0,09134	0,09565	0,03243	0,67244	0,14123	0,36483
1,53294	11,16737	8,70160	9,70828	0,12805	0,08298	0,02797	2,34271	0,14254	0,49562
1,84938	12,15662	9,68092	9,72578	0,11968	0,08246	0,02493	0,97337	0,14468	0,61832
1,79734	13,04717	10,03128	9,71794	0,11810	0,05988	0,02081	3,38991	0,13764	0,64727
1,73116	12,67914	9,21241	8,87806	0,09489	0,03835	0,01854	0,61507	0,12583	0,64308
1,87948	13,52300	9,99699	9,67585	0,10124	0,06085	0,02055	0,73530	0,14532	0,68672
1,84507	15,23378	10,80571	10,03796	0,12997	0,05424	0,02338	0,70576	0,14373	0,73230
1,73503	14,61267	9,71286	8,79041	0,10617	0,07206	0,02084	0,65498	0,14073	0,71010
1,96791	17,47123	11,15148	9,87831	0,13447	0,07587	0,02638	1,76483	0,15242	0,90246
1,80054	16,89080	10,49765	8,94404	0,11222	0,07624	0,02118	0,76923	0,14341	0,84345
1,75632	14,89595	10,43307	8,79245	0,10814	0,06436	0,01947	0,68786	0,13159	0,75759
1,56732	14,05403	9,50440	7,90658	0,09409	0,05696	0,01943	1,20669	0,11984	0,71162
1,73094	15,48313	10,63432	9,01599	0,10371	0,07108	0,02106	0,74726	0,13249	0,77041
1,51430	13,81246	10,43639	8,71618	0,10906	0,07432	0,02305	0,66943	0,12599	0,65349
2,04933	22,80209	8,85024	6,17567	0,09553	0,04882	0,01478	3,43281	0,19153	1,28649
<LD	**-0,00908**	**<LD**	**<LD**	**<LD**	**<LD**	**<LD**	**<LD**	**<LD**	**<LD**
2,54436	28,92270	10,65905	9,14803	0,27652	0,04905	0,03146	1,02897	0,23499	1,54838
2,40346	30,11077	10,48913	9,71634	0,27880	0,06266	0,02709	2,45704	0,21956	1,68465
2,47282	31,34777	11,30066	10,03103	0,26195	0,03962	0,02624	1,16392	0,20858	1,78438
4,64845	34,64783	7,33041	9,12958	0,23060	0,08125	0,02734	1,19801	0,25329	1,93271
<LD	**-0,00545**	**<LD**	**<LD**	**<LD**	**<LD**	**<LD**	**<LD**	**<LD**	**<LD**
0,62983	2,89628	5,05668	5,21476	0,15014	0,05640	0,01746	0,59565	0,12405	0,31388
0,67542	2,53827	3,47674	6,71607	0,11090	0,08166	0,01857	0,68923	0,13633	0,26957
4,76857	0,42807	2,90577	3,45387	1,22603	0,05602	0,01236	1,90828	0,47646	0,04656
5,76007	0,26701	3,24804	3,89590	1,43413	0,05812	0,01131	2,29917	0,55219	0,03758
0,97928	0,26439	9,56754	2,99665	0,45607	0,07965	0,01096	1,46250	0,28829	0,04949
0,94278	0,23190	9,22921	2,91278	0,35844	0,08639	0,00999	1,49741	0,28457	0,04121
3,88375	36,85421	10,17746	9,68098	0,32644	0,04923	0,05826	1,57413	0,22287	2,11106

6,00208	28,67740	6,15660	8,06273	0,29284	0,06403	0,01826	2,20889	0,20675	1,69636
2,30414	32,32755	9,56164	9,32558	0,18140	0,04202	0,00961	0,94924	0,18497	1,69189
3,01755	38,97632	9,27853	9,43480	0,18088	0,06308	0,00982	1,12340	0,21933	2,30517
0,56476	3,15837	4,79816	3,14382	0,17666	0,06374	0,01815	1,81329	0,10497	0,52084
0,50746	1,52443	3,93171	4,23045	0,08730	0,04423	0,01405	0,66569	0,11839	0,27191
3,76178	41,98124	6,43110	9,17249	0,22989	0,05088	0,03056	1,59379	0,21142	2,85165
4,66101	51,90707	6,18628	10,20837	0,26647	0,03387	0,02837	1,75527	0,21774	3,92486

137Ba	139La	140Ce	141Pr	146Nd	147Sm	151Eu	160Gd	159Tb	163Dy
14,71996	0,27396	0,32415	0,06915	0,25515	0,04605	0,01290	0,03884	0,00807	0,02666
1,21236	1,47035	0,94770	4,68777	2,40668	5,35866	15,57453	4,74313	22,18009	8,43447
14,46531	0,26271	0,30727	0,06680	0,24031	0,04687	0,01191	0,03879	0,00876	0,02675
0,41471	2,26261	1,57371	7,89162	0,61811	6,25766	26,94671	9,17999	27,23409	7,66090
14,63506	0,25866	0,30648	0,06434	0,24137	0,04579	0,01097	0,03675	0,00685	0,02536
0,19595	2,14606	2,97124	3,48936	1,82737	8,00504	12,42289	6,05890	15,13476	5,37729
14,60678	**0,26511**	**0,31264**	**0,06676**	**0,24561**	**0,04624**	**0,01193**	**0,03813**	**0,00789**	**0,02626**
0,12966	**0,00793**	**0,00998**	**0,00241**	**0,00828**	**0,00057**	**0,00097**	**0,00119**	**0,00097**	**0,00078**
1,24615	1,61470	1,39767	0,20019	0,83792	0,11295	0,02351	0,11267	0,01240	0,06002
1,21260	1,65283	1,42972	0,20431	0,86154	0,11563	0,02270	0,11546	0,01281	0,05988
0,09464	0,03917	0,05043	0,00597	0,01973	0,00269	0,00100	0,00207	0,00073	0,00136
0,25812	0,02893	0,04219	0,00441	0,01306	0,00230	0,00109	0,00179	0,00060	0,00125
1,15338	0,01948	0,03274	0,00368	0,01141	0,00237	0,00100	0,00178	0,00052	0,00149
1,25832	0,02124	0,03582	0,00377	0,01292	0,00281	0,00088	0,00241	0,00066	0,00197
0,52255	0,02081	0,03639	0,00398	0,01354	0,00274	0,00084	0,00207	0,00054	0,00151
0,41894	0,02018	0,03695	0,00407	0,01345	0,00260	0,00082	0,00240	0,00046	0,00202
2,33772	0,03916	0,07303	0,00771	0,02608	0,00478	0,00093	0,00371	0,00067	0,00287

2,65922	0,04391	0,08323	0,00878	0,03107	0,00551	0,00100	0,00463	0,00080	0,00365
0,13051	0,01252	0,02262	0,00217	0,00674	0,00115	0,00032	0,00090	0,00019	0,00062
152,41644	18,57113	39,28826	4,08665	15,14226	2,81588	0,58752	2,21335	0,29501	1,63112
174,02184	18,88871	39,05292	4,08084	15,02445	2,83506	0,61434	2,24107	0,30356	1,71900
247,19038	28,83083	59,14448	6,38839	23,71622	4,37377	0,75690	3,36520	0,43151	2,29588
25,20597	5,95125	11,12233	1,60516	7,39579	1,43810	0,29815	1,09410	0,13838	0,91580
9,68931	6,74933	8,54409	1,58913	6,25441	1,20804	0,31423	1,16599	0,16354	1,05916
0,53449	0,21543	0,51102	0,04543	0,18283	0,03445	0,00711	0,02758	0,00377	0,02094
0,39218	0,47770	0,87142	0,07355	0,24820	0,03352	0,00633	0,02636	0,00344	0,01807
0,39895	0,36317	0,77236	0,06827	0,23270	0,03787	0,00675	0,02672	0,00350	0,01874
0,54187	0,28209	0,53831	0,04644	0,16062	0,02223	0,00438	0,01842	0,00252	0,01297
0,52466	0,29241	0,65905	0,07726	0,31015	0,05528	0,00998	0,04108	0,00536	0,02632
0,48781	0,29141	0,65491	0,05786	0,22389	0,04211	0,00883	0,03860	0,00529	0,02969
0,36121	0,38245	1,26283	0,10675	0,43080	0,08604	0,01981	0,07109	0,00903	0,05002
0,32820	0,28838	0,61522	0,05777	0,21176	0,04013	0,00745	0,03479	0,00477	0,02708
0,60198	0,35665	0,78027	0,07449	0,28068	0,05267	0,00960	0,04634	0,00632	0,03629
0,24257	0,30984	0,62357	0,06639	0,25756	0,04761	0,01105	0,04133	0,00584	0,03249
0,27615	0,17550	0,35945	0,04052	0,16344	0,03534	0,00892	0,03253	0,00482	0,02767
0,25591	0,16295	0,29531	0,03095	0,11532	0,01911	0,00440	0,01752	0,00254	0,01396
0,73660	1,42521	2,66315	0,23957	0,78761	0,10345	0,01878	0,07447	0,00963	0,05287
0,27214	0,43752	0,85981	0,07995	0,28523	0,04967	0,01023	0,04140	0,00565	0,03149
0,34556	0,32677	0,71546	0,06661	0,25467	0,05029	0,01046	0,04508	0,00629	0,03561
0,82046	0,92135	1,87192	0,17120	0,62608	0,10780	0,02243	0,08645	0,01136	0,06206
0,18158	0,27698	0,69028	0,07669	0,31284	0,06611	0,01544	0,05521	0,00771	0,04403
0,43162	0,21891	0,46666	0,04583	0,17850	0,03466	0,00729	0,03049	0,00394	0,02153
0,23673	0,19074	0,38943	0,03727	0,13475	0,02483	0,00516	0,02014	0,00285	0,01599
0,13359	0,23622	0,54795	0,06587	0,26741	0,05503	0,01259	0,04390	0,00576	0,03336
0,31793	0,37903	0,73624	0,07752	0,28100	0,04136	0,00754	0,03116	0,00375	0,01863
0,16488	0,17279	0,32819	0,03358	0,12180	0,01936	0,00376	0,01435	0,00171	0,00854
0,26801	0,35400	0,70411	0,07384	0,28120	0,04917	0,00944	0,03517	0,00441	0,02119
0,24033	0,70907	1,56304	0,17218	0,65687	0,12709	0,02545	0,10122	0,01405	0,07792

42,23389	9,82221	22,34960	2,19500	8,08441	1,42470	0,27773	1,14952	0,15298	0,85748
1,25981	1,63855	2,71296	0,25609	0,83650	0,11200	0,02157	0,08307	0,01213	0,05950
0,20035	0,19571	0,39932	0,04384	0,16984	0,03442	0,00852	0,03045	0,00506	0,02478
9,00094	2,22571	4,70878	0,49812	1,84961	0,32363	0,04791	0,24861	0,03296	0,17189
63,34612	7,18297	15,37845	1,65070	6,02980	1,12071	0,24006	0,89019	0,12180	0,67866
4,57082	11,64511	27,70320	2,79234	10,74671	1,78699	0,36987	1,36572	0,17625	0,98350
27,42435	6,13331	12,93180	1,41414	5,28597	0,97168	0,09821	0,72541	0,08804	0,44478
29,46745	9,65529	21,35738	2,31730	8,61928	1,57526	0,14019	1,16805	0,13999	0,64746
46,38627	8,27574	17,71696	1,83112	6,79255	1,19835	0,19470	0,91444	0,12000	0,63021
47,44440	9,44955	19,47996	1,98919	7,16530	1,25509	0,19709	0,96362	0,12312	0,63536
8,81808	2,26237	5,18550	0,81027	3,14779	0,44593	0,09153	0,24075	0,02980	0,14150
11,67178	3,59759	3,76118	0,30596	0,75945	0,10543	0,02469	0,09995	0,01879	0,13485
122,18997	14,62725	34,42716	3,34493	12,38611	2,21493	0,41970	1,73973	0,24680	1,46112
26,81072	0,57187	1,45562	0,13729	0,52893	0,10340	0,02077	0,09344	0,01523	0,09546
6,68862	0,97037	2,10285	0,23493	0,90633	0,19593	0,03694	0,19336	0,02888	0,17274
1,49649	1,54244	1,13246	0,24857	0,99177	0,15866	0,03732	0,19422	0,02769	0,19543
61,52042	5,76949	12,35043	1,42872	5,54242	1,05441	0,18327	0,89103	0,12223	0,70986
262,77253	18,63230	38,58654	4,05609	14,68860	2,42075	0,35575	1,60593	0,21053	1,17009
60,48454	8,27746	18,13067	2,03514	7,88991	1,59119	0,32832	1,43492	0,21067	1,32181
87,65225	8,94342	21,83979	2,15458	8,38206	1,69005	0,35619	1,59263	0,23609	1,48291
61,34145	9,66902	19,97709	2,26118	8,52079	1,62450	0,35285	1,33460	0,19774	1,20256
67,37617	12,12061	24,87492	2,81812	10,61266	2,00197	0,44465	1,62231	0,23336	1,42206
75,69496	11,89330	24,30847	2,76866	10,49242	1,99436	0,44190	1,63493	0,23703	1,46232
70,46880	9,93047	20,80536	2,33850	8,91981	1,71228	0,36960	1,43050	0,20941	1,28282
78,29076	11,16068	23,07876	2,59369	9,86356	1,88244	0,40981	1,54229	0,22524	1,37424
70,98404	10,75838	22,50790	2,51613	9,58587	1,84417	0,40574	1,54204	0,22143	1,33834
67,27201	9,83097	20,45745	2,32012	8,94859	1,75533	0,39071	1,48955	0,21836	1,34050
74,17332	10,40060	21,84800	2,47854	9,53201	1,92681	0,44372	1,61379	0,23567	1,44754
81,22056	13,13170	27,84170	3,13792	12,07207	2,37062	0,53669	1,96788	0,28227	1,68558
80,92626	12,14362	25,25168	2,87351	10,96024	2,12928	0,48046	1,77935	0,25450	1,54169
80,80197	11,11274	23,58372	2,67492	10,44575	2,08032	0,47532	1,78441	0,25814	1,56445

89,44077	12,86466	27,17167	3,09727	12,10317	2,43702	0,55243	2,05689	0,29458	1,76842
91,15031	11,39564	24,58375	2,75626	10,80231	2,21597	0,52198	1,93598	0,27648	1,68209
96,65451	11,70342	24,99153	2,88294	11,53980	2,42603	0,58894	2,16295	0,31237	1,88986
130,53041	15,06914	32,49851	3,73645	14,91213	3,14499	0,71961	2,76486	0,40318	2,48509
96,04557	12,09609	26,54595	3,00036	12,01403	2,53754	0,58967	2,26108	0,33084	1,99840
97,99051	11,56672	24,74398	2,87596	11,62899	2,45039	0,56966	2,17632	0,31286	1,89221
112,97816	12,17434	26,22668	3,02425	12,20195	2,56687	0,60108	2,32767	0,33888	2,07066
95,49860	10,86190	23,31151	2,67454	10,73270	2,25829	0,51125	1,99739	0,28984	1,75692
90,91613	11,21513	24,33179	2,78118	11,16339	2,39803	0,54911	2,14253	0,31020	1,89337
97,27686	12,95455	28,15841	3,23016	13,06757	2,83875	0,66961	2,51957	0,36589	2,21824
87,00173	12,22014	26,73642	3,08303	12,42789	2,72497	0,66462	2,50292	0,36261	2,24756
93,55950	12,55481	27,45564	3,16047	12,77227	2,80204	0,66950	2,55570	0,36888	2,23486
90,85995	10,99031	24,07696	2,81878	11,55237	2,57013	0,64537	2,34186	0,33993	2,08265
95,71305	12,85541	27,91669	3,20551	13,03168	2,84670	0,67588	2,58607	0,37417	2,29864
78,68057	11,32563	24,66968	2,86613	11,57006	2,52450	0,61340	2,29290	0,33124	2,03516
67,87310	10,06300	21,84959	2,50627	10,11372	2,13344	0,50401	1,97035	0,28840	1,79831
70,76241	8,03847	17,63238	1,97565	7,79155	1,64617	0,36714	1,51657	0,22840	1,48309
52,62402	9,33678	22,25683	2,22594	8,53949	1,71932	0,27830	1,61003	0,26196	1,86653
24,30819	4,61480	10,78949	1,07478	4,06480	0,86793	0,14932	0,93690	0,17909	1,45048
38,47637	6,06343	13,65096	1,46122	5,72113	1,22391	0,24106	1,19866	0,20117	1,47545
41,27436	8,75392	21,48522	2,10744	8,04018	1,65774	0,26272	1,54346	0,24519	1,71529
26,47303	4,44943	10,01263	0,97040	3,80728	0,82438	0,14843	0,82507	0,14339	1,07115
36,53139	7,05484	16,96063	1,64071	6,25915	1,27497	0,21050	1,25389	0,21140	1,56882
28,84387	6,89353	18,10884	1,62050	6,11032	1,33458	0,24461	1,46477	0,27365	2,18475
37,84834	7,06030	18,26825	1,69169	6,48354	1,41864	0,24065	1,52253	0,29033	2,34622
49,72119	7,70440	18,62951	1,84426	7,03520	1,46121	0,22993	1,45993	0,25554	1,94399
45,25884	7,50739	17,57114	1,76630	6,68434	1,34056	0,19562	1,29290	0,22076	1,61416
40,26732	12,00587	29,08796	2,78638	10,46848	2,16165	0,29118	2,16376	0,38484	2,95185
56,73024	6,60493	14,28379	1,56892	5,97315	1,21372	0,20152	1,13390	0,18390	1,28894
51,36381	7,71444	17,80940	1,84003	7,01136	1,40963	0,21009	1,29258	0,20371	1,39512
43,76914	6,11488	13,16017	1,40854	5,31804	1,07367	0,17666	1,03747	0,17529	1,27696

64,20386	12,54389	28,50783	3,01630	11,49796	2,23147	0,34957	1,97885	0,29443	1,91661
37,85871	15,64674	37,29256	3,68470	13,72932	2,72757	0,31444	2,52099	0,41803	3,05644
55,44629	12,42397	28,48002	2,91276	10,97062	2,12552	0,29979	1,89718	0,29413	2,01147
59,64244	10,86412	24,43651	2,56987	9,79409	1,93069	0,30674	1,70647	0,25788	1,70641
74,79938	11,52676	25,77752	2,79059	10,78514	2,18419	0,41241	1,88324	0,27807	1,74577
77,74447	11,36076	24,88351	2,80643	11,13958	2,35705	0,52251	2,06136	0,30021	1,83850
74,06523	11,18583	24,00238	2,77112	11,03888	2,32326	0,55687	2,09946	0,30127	1,85139
68,95233	10,90091	23,49572	2,70058	10,68533	2,26208	0,53284	1,98826	0,28498	1,73244
78,01282	11,15301	24,03576	2,80010	11,12579	2,37525	0,57810	2,12801	0,30498	1,86336
85,82570	11,65368	25,07767	2,86417	11,33421	2,39654	0,57644	2,14855	0,31062	1,91771
76,61285	10,40851	22,48279	2,55938	10,07609	2,13326	0,50080	1,90109	0,27494	1,68514
83,16787	11,85817	25,43281	2,94900	11,74669	2,48275	0,60923	2,22240	0,31734	1,91899
79,86930	10,73405	23,11937	2,63325	10,43146	2,21831	0,52818	1,97143	0,28434	1,74401
71,89384	10,24471	21,89705	2,53569	10,07104	2,15294	0,53575	1,93187	0,27936	1,70207
73,07675	9,75559	21,07489	2,38481	9,50305	1,96528	0,45999	1,75639	0,25178	1,52539
84,00248	9,98860	21,42380	2,47378	9,83274	2,09289	0,51516	1,93619	0,27985	1,71281
78,05816	9,95193	21,54456	2,42321	9,61244	2,01765	0,46370	1,82333	0,26304	1,63353
63,73930	6,93099	17,08843	1,64137	6,36883	1,28933	0,26713	1,21414	0,18061	1,13602
<LD	**<LD**	**<LD**	**<LD**	**<LD**	**<LD**	**<LD**	**<LD**	**<LD**	**<LD**
83,88133	9,32815	23,74051	2,23682	8,83932	1,84952	0,39620	1,79796	0,26778	1,68004
85,63433	9,43480	21,48258	2,29439	9,19030	1,99272	0,43321	1,94714	0,28835	1,79808
87,89656	10,02500	22,69574	2,46196	9,79990	2,12064	0,46292	2,08385	0,30289	1,88795
109,28347	10,82346	22,59474	2,56675	9,94413	1,99113	0,42442	1,85228	0,27354	1,70466
<LD	**<LD**	**<LD**	**<LD**	**<LD**	**<LD**	**<LD**	**<LD**	**<LD**	**<LD**
15,79995	5,49287	9,98278	1,25032	4,72237	0,97972	0,23379	0,87568	0,13413	0,89884
16,07135	6,14532	11,93493	1,48034	5,68551	1,23572	0,27956	1,11762	0,17363	1,16627
1,83984	3,12301	5,96751	0,59706	2,04580	0,38293	0,08015	0,36201	0,07060	0,54819
1,42617	3,55134	6,93363	0,67263	2,27529	0,42522	0,08859	0,40381	0,07882	0,61233
9,42661	13,71236	24,98118	2,43458	7,91660	1,32492	0,25345	0,89570	0,11945	0,66704
9,32839	13,39718	24,45082	2,37574	7,82155	1,31423	0,25127	0,89042	0,11946	0,65742
120,28963	10,02903	22,56866	2,39216	9,34027	1,97569	0,43454	1,92470	0,28845	1,78667

80,65940	7,48735	15,58171	1,82249	7,24472	1,59624	0,36913	1,68419	0,26695	1,70145
76,37434	10,17518	23,25721	2,53783	9,93969	2,08537	0,46922	1,96113	0,28335	1,74631
81,46271	9,86516	23,85213	2,51156	9,95861	2,14002	0,47910	1,97432	0,29045	1,80407
12,43142	4,78912	8,38861	1,15934	4,61151	0,88197	0,18842	0,62624	0,09019	0,57467
9,81864	4,29659	7,95253	1,08964	4,33161	0,87060	0,19079	0,66842	0,10627	0,71591
100,94475	9,69848	21,83173	2,33186	9,06765	1,89200	0,39728	1,78512	0,26692	1,67798
122,30019	11,88111	28,26857	2,81730	10,80161	2,15528	0,44053	2,00470	0,29771	1,88986

165Ho	166Er	169Tm	172Yb	175Lu	205Tl	208Pb	232Th	238U
0,00750	0,01590	0,00429	0,01442	0,00422	0,01303	0,18389	0,01554	0,07351
18,61079	5,02233	28,47878	5,35341	18,55919	16,70683	1,32294	14,49475	4,14495
0,00847	0,01727	0,00570	0,01555	0,00595	0,01497	0,17538	0,01701	0,07555
29,35517	9,99721	39,95495	12,83494	43,78940	22,66014	3,16226	8,27127	4,52252
0,00670	0,01461	0,00354	0,01306	0,00339	0,01140	0,17512	0,01428	0,06949
13,21751	6,22729	18,03696	7,01795	14,28447	17,85023	1,89165	18,33724	3,18246
0,00755	**0,01593**	**0,00451**	**0,01434**	**0,00452**	**0,01313**	**0,17813**	**0,01561**	**0,07285**
0,00089	**0,00133**	**0,00109**	**0,00124**	**0,00131**	**0,00179**	**0,00499**	**0,00136**	**0,00309**
0,01193	0,02724	0,00358	0,01370	0,00262	0,00492	3,53542	0,03662	0,03142
0,01164	0,02818	0,00371	0,01352	0,00271	0,00417	3,55556	0,02509	0,03277
0,00048	0,00074	0,00035	0,00049	0,00033	0,00561	0,88307	0,02330	0,01152
0,00051	0,00080	0,00034	0,00048	0,00031	0,00699	1,16481	0,02362	0,01482
0,00043	0,00081	0,00025	0,00061	0,00028	0,00408	0,86282	0,01183	0,00640
0,00062	0,00088	0,00036	0,00065	0,00031	0,00434	0,90745	0,01593	0,00666
0,00042	0,00097	0,00023	0,00082	0,00024	0,00373	0,83671	0,01431	0,00653
0,00046	0,00081	0,00024	0,00094	0,00018	0,00327	0,68577	0,01314	0,00530
0,00063	0,00147	0,00030	0,00164	0,00036	0,00839	0,72300	0,01391	0,00514

0,00069	0,00177	0,00035	0,00149	0,00029	0,00941	0,58741	0,01710	0,00530
0,00015	0,00028	0,00008	0,00019	0,00010	0,00092	0,45194	0,00324	0,00161
0,27763	0,77741	0,10335	0,69415	0,10231	0,35041	12,33735	4,57428	1,74902
0,29526	0,84436	0,11276	0,76011	0,11220	0,40885	12,77146	4,48706	1,85127
0,38507	1,07085	0,14164	0,96282	0,14363	0,51070	15,17283	8,07847	2,80486
0,18671	0,54848	0,06891	0,38352	0,05959	0,01626	4,82476	0,73140	1,68699
0,21024	0,62159	0,08198	0,50910	0,07435	0,00904	3,03001	0,65537	0,97362
0,00387	0,01143	0,00170	0,01106	0,00194	0,00280	0,10546	0,02608	0,23971
0,00340	0,00972	0,00143	0,00982	0,00160	0,00214	0,09421	0,02069	0,25348
0,00344	0,00960	0,00142	0,00895	0,00161	0,00178	0,07848	0,01806	0,13368
0,00257	0,00816	0,00116	0,00795	0,00146	0,00116	0,15642	0,01680	0,17891
0,00435	0,01031	0,00131	0,00735	0,00113	0,00173	0,12252	0,02529	0,11639
0,00548	0,01621	0,00222	0,01478	0,00235	0,00387	0,19698	0,01413	0,33186
0,00853	0,02197	0,00287	0,01771	0,00256	0,00280	0,18698	0,01874	0,23201
0,00506	0,01435	0,00210	0,01426	0,00229	0,00300	0,16704	0,01749	0,24397
0,00652	0,01976	0,00292	0,01838	0,00273	0,00364	0,19765	0,02021	0,49584
0,00605	0,01658	0,00211	0,01294	0,00201	0,00155	0,14546	0,00736	0,18031
0,00520	0,01463	0,00200	0,01265	0,00180	0,00119	0,09754	0,00666	0,12993
0,00271	0,00741	0,00101	0,00651	0,00103	0,00112	0,13859	0,00394	0,13600
0,00918	0,02683	0,00368	0,02338	0,00329	0,00401	0,39050	0,01564	0,45399
0,00559	0,01607	0,00211	0,01306	0,00215	0,00140	0,19468	0,00879	0,14384
0,00616	0,01768	0,00237	0,01541	0,00240	0,00166	0,17006	0,01386	0,17282
0,01024	0,02842	0,00355	0,02085	0,00311	0,00276	0,44969	0,01156	0,23345
0,00706	0,01978	0,00227	0,01368	0,00195	0,00120	0,17092	0,00850	0,10422
0,00392	0,01220	0,00156	0,01154	0,00186	0,00199	0,13689	0,01480	0,24246
0,00284	0,00829	0,00113	0,00718	0,00123	0,00168	0,09185	0,01225	0,09372
0,00556	0,01523	0,00187	0,01236	0,00189	0,00112	0,11130	0,01390	0,11395
0,00284	0,00801	0,00101	0,00579	0,00086	0,00102	0,12149	0,01294	0,13468
0,00162	0,00406	0,00051	0,00310	0,00048	0,00078	0,07076	0,00410	0,05440
0,00339	0,00782	0,00089	0,00504	0,00076	0,00070	0,09078	0,00586	0,10266
0,01249	0,03339	0,00391	0,02273	0,00292	0,00105	0,14353	0,01397	0,10051

0,15194	0,42956	0,05680	0,37279	0,05403	0,09188	5,18886	2,27143	0,67300
0,01154	0,02737	0,00448	0,02138	0,00372	0,00418	0,62773	0,06424	0,12982
0,00466	0,01221	0,00212	0,00977	0,00190	0,00217	0,15358	0,01767	0,09684
0,02990	0,07929	0,01048	0,06611	0,00944	0,02406	1,28707	0,45095	0,29561
0,12066	0,34113	0,04588	0,31156	0,04472	0,15248	5,08053	2,03100	0,75016
0,17665	0,49673	0,06380	0,40416	0,05899	0,10212	15,96478	1,49511	1,82000
0,07248	0,19241	0,02587	0,17406	0,02769	0,04402	1,96603	1,69104	0,66750
0,09953	0,25408	0,03326	0,22812	0,03500	0,04961	3,09899	2,91715	1,05800
0,10669	0,28880	0,03860	0,26251	0,03812	0,09415	4,00098	2,18786	0,68202
0,10770	0,29166	0,03811	0,25292	0,03679	0,11239	4,66726	2,28445	0,73904
0,02158	0,05710	0,00736	0,04920	0,00749	0,00967	1,01975	0,06926	0,09644
0,02970	0,10490	0,01781	0,13949	0,02189	0,00353	1,82096	0,93524	0,13490
0,28269	0,87184	0,12698	0,88709	0,13039	0,19163	6,00906	3,18465	0,81301
0,01852	0,05850	0,00858	0,05932	0,00853	0,05511	2,23886	0,42514	0,16479
0,03194	0,08601	0,01171	0,07141	0,01008	0,02291	0,94928	0,21502	0,10353
0,04445	0,13407	0,01714	0,10142	0,01451	0,01113	0,55908	0,13164	0,04045
0,13345	0,39445	0,05599	0,38825	0,05786	0,06050	3,49414	1,42450	0,55376
0,21256	0,62525	0,08829	0,59386	0,08703	0,40180	12,07220	7,81040	2,29262
0,26119	0,80752	0,11827	0,83508	0,12789	0,11890	6,29368	2,24042	0,66175
0,29075	0,87358	0,12357	0,84000	0,12562	0,15470	8,23482	2,45723	0,68572
0,23937	0,76594	0,11509	0,85297	0,13193	0,07840	7,67889	2,08717	0,72319
0,27627	0,85813	0,12834	0,91519	0,14225	0,09781	8,66316	2,29075	0,74063
0,28729	0,90365	0,13604	1,00274	0,15401	0,10301	8,95527	2,31519	0,79313
0,25649	0,81444	0,12412	0,91575	0,14202	0,08801	7,22254	2,20496	0,73450
0,27156	0,86100	0,12910	0,96223	0,14956	0,09476	7,87381	2,48897	0,78634
0,26094	0,81626	0,12257	0,88955	0,13782	0,08868	7,87653	2,38253	0,71933
0,26159	0,82296	0,12242	0,88406	0,13757	0,08510	7,04486	2,25155	0,68252
0,28123	0,86977	0,12911	0,90573	0,14128	0,09731	8,19440	2,13221	0,68296
0,32106	0,98311	0,14211	1,01387	0,15643	0,11760	9,79617	2,78676	0,80039
0,29604	0,91203	0,13446	0,94447	0,14539	0,10322	8,73223	2,47225	0,75186
0,30090	0,92936	0,13628	0,97032	0,14954	0,10204	8,30445	2,39916	0,72819

0,34171	1,05075	0,15301	1,07329	0,16273	0,11512	9,28046	2,82621	0,79263
0,32566	0,99416	0,14613	1,03528	0,15688	0,11709	8,97748	2,54657	0,77131
0,36721	1,11063	0,15846	1,10189	0,16748	0,12834	9,13155	2,80032	0,76322
0,49543	1,51224	0,22428	1,59640	0,24388	0,15441	11,21763	3,94989	1,10478
0,39373	1,19802	0,17706	1,24810	0,19093	0,11366	9,17879	3,08592	0,85784
0,36975	1,12055	0,16064	1,13324	0,17380	0,12110	8,83493	2,94656	0,80704
0,40581	1,25111	0,18538	1,31999	0,20229	0,13447	9,48110	3,28238	0,94494
0,34181	1,06381	0,15891	1,13429	0,17485	0,11022	7,88383	2,82391	0,82362
0,37190	1,14720	0,16736	1,18892	0,18449	0,10847	8,32031	2,81182	0,83561
0,42844	1,29778	0,18641	1,30277	0,19750	0,11667	9,51064	3,16221	0,85154
0,43321	1,33491	0,18848	1,33502	0,19992	0,10822	9,30159	3,02550	0,77199
0,43297	1,32190	0,18778	1,30003	0,19582	0,11219	9,26848	3,17301	0,76522
0,39969	1,21212	0,17392	1,18473	0,17527	0,11188	9,11769	2,64670	0,66112
0,44365	1,35363	0,19248	1,33723	0,20087	0,12468	9,57316	3,17751	0,78799
0,39427	1,20404	0,17356	1,20779	0,18387	0,10264	8,64809	2,79064	0,71392
0,35573	1,11929	0,16408	1,16927	0,17951	0,08852	7,84531	2,59310	0,73284
0,30088	0,97500	0,14718	1,07284	0,16659	0,08563	6,49546	2,37951	0,71692
0,42421	1,58018	0,27706	2,27490	0,38511	0,06371	5,18172	3,78549	1,95456
0,35037	1,37345	0,24607	2,06886	0,35065	0,02850	5,72251	2,50336	1,74878
0,33686	1,25206	0,21861	1,79446	0,30271	0,05200	6,17394	2,45193	1,51040
0,38267	1,41114	0,24316	1,99817	0,33350	0,05329	6,23841	3,62910	1,73508
0,24617	0,92639	0,16134	1,32689	0,22192	0,02999	4,08259	1,93206	1,14974
0,36524	1,37751	0,24477	1,99711	0,34224	0,04109	5,17526	3,21047	1,73245
0,53438	2,09260	0,38094	3,20112	0,55295	0,03604	7,14448	3,65772	2,76488
0,59276	2,36390	0,43762	3,72213	0,64352	0,04011	25,52916	4,74906	3,38845
0,46024	1,75188	0,31065	2,56026	0,43000	0,05162	4,33812	3,81855	2,12738
0,37133	1,39378	0,24147	1,98231	0,33680	0,04470	4,03384	3,34502	1,72200
0,70904	2,79016	0,50109	4,22939	0,72237	0,04469	4,84017	5,94680	3,62766
0,28572	1,02257	0,17286	1,38120	0,22455	0,06063	4,39526	2,71886	1,08837
0,30454	1,10307	0,18748	1,51003	0,24923	0,05423	4,57985	3,39438	1,24852
0,28457	1,04318	0,17854	1,42962	0,23612	0,04484	3,94849	2,59294	1,14508

0,39778	1,36210	0,21880	1,71503	0,27548	0,06874	5,86543	4,41532	1,35528
0,70359	2,65607	0,47235	3,90983	0,66209	0,04254	5,74963	7,89949	3,42380
0,43682	1,55629	0,26425	2,10582	0,34777	0,06005	5,21212	4,85181	1,72949
0,35321	1,22517	0,19993	1,55794	0,25232	0,06298	5,23014	3,83841	1,24631
0,35034	1,15236	0,17870	1,34201	0,21427	0,08247	6,79957	3,54394	1,05751
0,35955	1,13136	0,16640	1,19589	0,18350	0,10370	8,96667	2,84704	0,84056
0,35930	1,09600	0,15662	1,08570	0,16218	0,09765	8,89562	2,43214	0,65674
0,33093	0,99371	0,14000	0,98121	0,14344	0,09130	8,37018	2,36228	0,57761
0,35838	1,09276	0,15414	1,08765	0,16141	0,10062	9,12167	2,43926	0,63735
0,37187	1,14811	0,16500	1,15627	0,17627	0,10887	8,94767	2,71147	0,71076
0,32661	0,98738	0,14065	0,98942	0,14884	0,10180	8,14069	2,48793	0,63236
0,36890	1,10693	0,15637	1,08662	0,16294	0,12153	9,60738	2,69591	0,66744
0,33173	1,01268	0,14253	0,99878	0,15100	0,11466	8,40932	2,62660	0,62900
0,32824	0,98854	0,14122	0,97110	0,14694	0,10381	8,19896	2,39775	0,61111
0,29059	0,88812	0,12723	0,87940	0,13325	0,10083	7,14592	2,31884	0,57668
0,33056	1,01193	0,14525	1,00284	0,15306	0,11108	7,88984	2,34714	0,62381
0,31933	1,00328	0,14569	1,06967	0,16211	0,09882	7,24191	2,61413	0,74162
0,22403	0,68084	0,09731	0,67195	0,10340	0,11225	8,90095	2,10432	0,56482
<LD	<LD	<LD	<LD	<LD	<LD	<LD	<LD	<LD
0,32634	0,98927	0,13976	0,97754	0,14753	0,14378	6,80205	2,63279	0,71826
0,34811	1,05345	0,14585	0,99138	0,14835	0,15281	6,98357	2,61881	0,71929
0,36342	1,08789	0,14913	1,01770	0,15068	0,16072	5,82351	2,74069	0,73885
0,33264	1,00775	0,14116	0,99381	0,14727	0,27157	6,58396	3,33895	0,77660
<LD	<LD	<LD	<LD	<LD	<LD	<LD	<LD	<LD
0,18940	0,65573	0,10625	0,84210	0,13698	0,02340	5,25379	1,88081	0,64436
0,24625	0,84894	0,13779	1,08837	0,17873	0,02016	5,22355	2,92548	0,82959
0,12490	0,44088	0,07097	0,55368	0,08823	0,00996	2,25742	6,54885	0,64757
0,14029	0,49578	0,08089	0,62775	0,09955	0,00860	2,36176	7,80946	0,72040
0,12311	0,39894	0,06342	0,48476	0,07626	0,00469	10,75898	4,27347	0,44164
0,12014	0,39572	0,06260	0,47697	0,07796	0,00384	13,03612	4,32727	0,44903
0,34587	1,02649	0,14267	0,96774	0,14371	0,19763	5,98914	2,76166	0,70368

0,33067	1,01914	0,14750	1,04090	0,15311	0,14489	5,23691	2,15925	1,36401
0,33812	1,03009	0,14584	1,00263	0,15286	0,17326	5,75223	3,20457	0,70326
0,35165	1,08486	0,15441	1,08514	0,16433	0,22177	6,40863	3,54622	0,73546
0,11508	0,38638	0,06159	0,48420	0,07697	0,02611	4,75592	1,40878	0,43220
0,14917	0,51986	0,08669	0,68655	0,11100	0,01660	4,26858	1,83843	0,58416
0,32767	1,00040	0,14045	0,93918	0,14269	0,19658	6,01791	3,13564	0,79884
0,37285	1,13995	0,16295	1,10695	0,16581	0,25050	7,16656	4,34875	0,90647

3 - Treinamentos laboratoriais no HSM

Logo em anexo apresentamos os seguintes documentos relativos ao treinamento realizado no mês de novembro de 2021.

1- Working rules of the clean room HydroSciences laboratory
2- User Charter clean room HydroSciences Laboratory
3- Charte de l'utilisateur salle blanche
4- charte de l'utilisateur labo chimie
5- Quizz sécurité au labo chimie
6- Quizz hygiène-sécurité
7- Presentation Nouveaux Arrivants 100521
8- La sécurité au laboratoire de chimie

WORKING RULES OF THE CLEAN ROOM HYDROSCIENCES MONTPELLIER

What is a CLEAN ROOM?

"Room wherein the concentration of particles suspended in the air is controlled and which is constructed and used so as to minimize the introduction, production and retention of the particles within the room, and wherein other parameters, such as temperature, humidity and pressure are controlled as appropriate". (Definition derived from ISO 14644).

- Filtered ambient air so as to eliminate as much as possible from particles (HEPA filter)
- Filtration system city water producing MilliQ water (ultrapure water) at 18, 2 MΩ
- Controlled temperature and humidity
- Positive pressure relative to the outside

HydroSciences laboratory is equipped with a clean room of Class 10 000.

An environment is said to Class 10 000 where the atmosphere contains less than 10 0 00 particle size greater than 0.5 microns per cubic foot (335 000 particles larger than 0.5 size microns per m^3)

Schedule

The clean room is available for an **8:30 to 5:30 p.m. Monday through Friday** in the presence of at least one permanent staff of the chemical laboratory.
Permission is required outside of these hours.
It is imperative to prevent someone from your presence in clean room.

Access

The user must follow the rules. Any user not complying the rules of clean room and endangering its operation may be temporarily denied access to the clean room (or permanently in case of recurrence).

To access the clean room, you must:
• Have trained "manipulation in a chemistry lab" in first
• Have trained "manipulation cleanroom" by the manager
• Have submitted the "clean room charter" signed to manager

For use equipment in clean room, you must:
• Have trained beforehand on the equipment in question by a permanent staff
• Having obtained the permission of trainer equipment

HSM Staff is "at your service" (that means we are here to help you ... not to serve you!!)
If you need help with a project, training, equipment or anything else, plan beforehand. In other words, there is a minimum and reasonable time to consider before getting a response from the technical team!
You will have to adapt how you work with that of laboratory ... not the reverse.

Process input/output

The clean room entry is in two steps :
- The entry in the SAS (well go on the sensor dust carpet at the entry)
- The passage of SAS to clean room (well go on the adhesive dust carpet)

In the ICP room :

- Remove your shoes or Thread covers shoes
- Remove jewelry, watches, personal items (phone, keys ...) and store in the green drawer

In the SAS :

- Put the security glasses
- Put the white hair covers (for people with long hair)
- Put the special “clean room apron” (must put the hoodie that people not putting the hair covers) before entering in the clean room
- Put clog with socks
- Put "special clean room" nitrile gloves with the sleeves of the clean room apron inside gloves

Don’t forget :

- Changing the adhesive carpet sas soon as it is dirty
- Do not open both sas doors at the same time
- Verify the proper closing of a door before opening another
- Don’t get anything in a clean room without the agreement of the manager
- Remember to close the hood and turn off the lights when you get out of the clean room
- Remember turn off balances at the end of the day

The introduction of cleanroom equipment requires the agreement of the manager. This equipment should be cleaned with ethanol before being introduced into the clean room.

Permitted and prohibited items in clean room

In order to minimize the particles release and the contamination risk, it is forbidden to bring in clean room:

- foods, beverages, chewing-gum
- plain paper, wood or carton without a protective film : to take notes, use special paper or a book of clean room type
- pencil
- electronic equipment

Must minimize entry with:

- makeup, mascara, powders or perfumes
- jewelry
- fluffy clothes
- Short pants, shorts, skirt, dress too short (must wear clothing that covers as much skin as possible)

Drawer boxes are available on the console shoe before entering the sas to store your personal items.

Wait at least 30 min for rent in clean room after smoking.

All items (tools, instruments, boxes of samples, etc.) to be introduced in a clean room will be thoroughly cleaned beforehand. We will use all the means are necessary (ethanol and / or MilliQ water) to perform a thorough cleaning before entering in the sas.
If a sealed plastic bag to be opened, it will be done in the sas and not in the clean room, avoiding tearing the bag to prevent the emission of plastic particles.

Avoid working in a clean room if you are sick.

Clean room behavior and working methods

- Respect the work of other users
- Work quietly
- Be attentive to the presence of colleagues around you, especially when handling dangerous products
- Use only containers in teflon (PFA) for storing "clean" solutions
- Don't pipette directly into the wash bottles or dropper, or in mothers solutions and certified materials
- Don't decant surplus in a solution its original container
- Don't install automatic pipettes horizontally on the lab desk
- Clean the balance after use
- Change the MilliQ water in the wash bottle before use
- Put in order different lab notebooks, notepads and paper in the drawer

Reminder: Color = pigment = metals !!!

- Don't scatter his things and store all once your work completed
- Don't use the equipment with gloves plenty of acid

Reminder: Nitrile gloves are disposable gloves which become porous after 30 minutes of normal use and when they are in prolonged contact with a chemical product, doesn't scruple to change them often

- Leave a clean room in the condition where you would like to find yourself
- Report to the manager any malfunction and failure: not to make personal intervention on devices
- Indicate on the slate found in the small sas, missing consumables and think to replace it as soon as you exit the clean room
- Check the proper functioning of your hood before starting manipulations
- Write on laboratory notebook of all clean room handling and weighs made
- Don't store materials in hoods
- Check the level of the scales and the accuracy of pipettes before you use
- Out and replace the garbage cans and recovery when full
- Clean your workstation after use
- Rinse thoroughly with MilliQ water containers and test tubes after use (rinse at least 3 times during use acids or bases)
- Back in sas the tube racks as you exit
- Think to turn on the bellows (switch above evaporation boxes, Level 2 from the top) when using evaporation boxes
- Think to turn off the bellows (switch above the evaporation boxes) before opening the boxes evaporation
- When handling concentrated acid in the suction hood, check that the suction is turned on and turn off the bellows in evaporation boxes time handling
- To filtrations in clean room, don't forget to rinse the filter units with MilliQ water and use filters and clamps decontaminated

Decontamination of equipment

- **ICP polypropylene tubes and caps, tips:**

Presoak in a container filled with HNO_3 for analysis (PA) 10% (100 ml HNO_3 PA in 900ml MilliQ water, to be adapted to filling the pot) : put the container 24H in place, then 24H upside down, then rinse 3 times with MilliQ water and to dry with clean Kimtech paper.

- **Pillbox:**

Half fill with HNO_3 PA 10%. Leave 24H in place, then 24H upside down. Rinse 3 times with MilliQ water and let dry under the laminar flow hood with cap put on but not screwed over.

- **Savillex Teflon:**

After attack, clean with ethanol then three times with MilliQ water. Put Savillex in HNO_3 PA 20% and heat on hotplate (100-120° C) for at least 48 hours. Rinse 3 times with MilliQ water, let dry under the laminar flow hood or store with HNO_3 suprapur $1^o/_{oo}$.

- **Microwave equipment:**
  - Agitator: rinse well with MilliQ water and soak in a little Savillex in HNO_3 PA 20%. Heat on hotplate (100-120°C) for at least 48 hours. Rinse 3 times with MilliQ water, let dry under the laminar flow hood.
  - Caps (used 1 time): remove the collars on new caps, put heating in 10% HNO_3 PA on hotplate (100-120°C) for at least 48 hours. Rinse 3 times with MilliQ water, let dry under the laminar flow hood.
  - Pyrex tubes: If used with Teflon liner, rinse 3 times with MilliQ water. Otherwise rinse with MilliQ water, clean with ethanol and then rinse with MilliQ water. Put in HNO_3 PA 20% and heat on hotplate (100-120°C) for at least 48 hours. Rinse 3 times with MilliQ water, let dry under the laminar flow hood.
  - Teflon liners: Rinse with MilliQ water. With Kimtech paper and ethanol, clean the inside of the liner. Rinse again with MilliQ water. Presoak in a bath of HNO_3 PA 20% and heat at least 48 hours on hotplate (100-120°C). Rinse 3 times with MilliQ water, let dry under the laminar flow hood.

- Cleaning of **the** clean **room** with dilute decon90 or ethanol and MilliQ water quarterly
- Cleaning **"clean room aprons" and clogs** in the washing machine quarterly

Reminder: do not forget to fill the board on the door of the clean room with the date when you made one of those cleanings.

Use of chemical products

- Don't introduce new chemical products without the permission of the manager
- Grasp the bottles by the body and not by the cap
- Read safety data sheet (MSDS) of the product before use
- Always identify chemical products in a container
- Don't discard chemical product in the sink but use evictin tin (20L)
- Don't mix Solvent with acid or Base

"Acid in Water Well Done, Water in Acid Suicide"

Security

Reminder:

Don’t touch your face or skin with gloves.

In case of accident warn laboratory staff (Prevention Assistant: Sophie Delpoux, Lifeguard Rescue Lab: Rémi Freydier)

Phone number:

Rémi Freydier: (04 67 14) **90 93**

Sophie Delpoux: (04 67 14) **90 79**

Jean-Luc Seidel: (04 67 14) **36 61**

Chrystelle Bancon-Montigny: (04 67 14) **39 33**

Corinne Casiot: (04 67 14) **33 56**

Reception: (04 67 14) **90 90**

First Aid:

- Burns (acids, bases, solvents, flame, ...): Rinse in cold water for at least 15 min.
- Fluorhydric acid (HF) burns: Rinse with water for at least 5 min then apply of Calcium Gluconate 2.5% gel (available in the small sas). Go to a doctor urgently applying calcium gluconate regularly.
- Splashing in the eyes: Rinse thoroughly with water using eye-rinces located outside the clean room for at least 15 min.

Report the incident or accident to Prevention assistant.
Complete an incident or accident report.

User Charter "clean room" HydroSciences Montpellier Laboratory

Recall some important rules:

- Clean room available from **8:30 to 17:30 from Monday to Friday** in the presence of at least one permanent staff of the chemistry laboratory.
- All users must first be trained "manipulation clean room" and have read the document "working rules of the clean room HydroSciences laboratory".
- No visitor can enter in a clean room without the permission of the manager beforehand.
- If you need training on equipment, please contact the permanent staff. You have access to online booking equipment only after training and with the agreement of the person who trained you.
- It is forbidden to enter in the clean room without the proper dressing or with objects or makeup may generate particles. Any object from outside (box, sample, chemical product, ...) must be authorized beforehand by the manager and clean before introducing clean room.
- Any user not complying the rules of clean room and endangering its operation may be temporarily denied access to the clean room (or permanently in case of recurrence).

I have read the "working rules of the clean room HydroSciences Montpellier laboratory" and agree to comply with unrestricted work rules described therein and the terms of this Charter.

Name, First Name:

Date:

Signature:

Charte de l'utilisateur des infrastructures « salle blanche » du Laboratoire HydroSciences Montpellier

Rappel de quelques règles importantes :

- Salle blanche accessible de **8h30 à 17h30 du Lundi au Vendredi** en présence d'au moins un personnel permanent du laboratoire de chimie.

- Tout utilisateur devra au préalable avoir suivi une formation "manipulation en salle blanche" et avoir lu le document « Règles de fonctionnement de la salle blanche du laboratoire HydroSciences ».

- Aucun visiteur ne peut entrer en salle blanche sans l'autorisation au préalable du responsable.

- Si vous avez besoin d'une formation sur un équipement, veuillez-vous adresser au personnel permanent. Vous aurez accès à la réservation en ligne de ce dispositif seulement après cette formation et avec l'accord de la personne qui vous a formé.

- Il est interdit d'entrer dans la salle blanche sans l'habillage adéquat ou avec des objets ou maquillage susceptibles de générer des particules. Tout objet provenant de l'extérieur (boîte, échantillon, produit chimique, …) devra être autorisé au préalable par le responsable et nettoyer avant l'introduction en salle blanche.

- Tout utilisateur ne respectant pas le règlement de la salle blanche et mettant en péril son bon fonctionnement pourra se voir refuser temporairement l'accès à la salle blanche (voire définitivement en cas de récidive).

Je soussigné(e) certifie avoir lu les "Règles de fonctionnement de la salle blanche d'HydroSciences Montpellier" et m'engage à respecter sans restriction les règles de travail qui y sont décrites et les termes de la présente charte.

Nom, Prénom :

Date :

Signature :

Charte de l'utilisateur des infrastructures " laboratoires de chimie " de l'UMR HydroSciences Montpellier

Rappel de quelques règles importantes :

- Les laboratoires sont accessibles de **8h30 à 17h30 du Lundi au Vendredi** en présence d'au moins un personnel permanent du laboratoire de chimie.
- Tout utilisateur devra au préalable avoir suivi les formations "Hygiène et Sécurité" et "Manipulation au laboratoire" et avoir lu le document "Règles de fonctionnement des laboratoires de chimie d'HydroSciences Montpellier".
- Aucun visiteur ne peut entrer au laboratoire sans l'autorisation au préalable du responsable.
- Si vous avez besoin d'une formation sur un équipement, veuillez-vous adresser au personnel permanent.
- Il est interdit d'entrer dans les laboratoires sans blouse, lunettes de sécurité et gants.
- Il est interdit de manger et boire dans les laboratoires.
- Il est interdit d'utiliser des écouteurs dans les laboratoires.
- Le matériel utilisé doit être nettoyé et rangé après chaque utilisation. Les paillasses doivent être nettoyées après chaque utilisation.
- Tout utilisateur ne respectant pas le règlement du laboratoire et mettant en péril son bon fonctionnement pourra se voir refuser temporairement l'accès (voire définitivement en cas de récidive).

Je soussigné(e),
→ Certifie avoir lu les "Règles de fonctionnement des laboratoires de chimie d'HydroSciences Montpellier"
→ Avoir eu de la part de l'Assistant de Prévention, une visite des laboratoires. J'y ai pris connaissance :
- Des risques liés aux manipulations dans ces laboratoires.
- De la présence dans chaque laboratoire des Équipements de Protection Individuelles obligatoires : gants, blouse, lunettes de sécurité, masques (en fonction de la dangerosité des manipulations).
- Des conduites à tenir en cas d'urgence
- De la présence de trousses de secours, douches de sécurité et douches oculaires.
- De la présence de gluconate de calcium (pour les brûlures à l'HF) : l'utilisation de l'acide fluorhydrique est exclusivement réservée au personnel permanent et aux doctorants.
- Du règlement (travail isolé interdit…).

→ Avoir été formé par un personnel permanent aux techniques d'analyses que j'utiliserai au laboratoire.

Je m'engage à respecter sans restriction les règles de travail des laboratoires de chimie et les termes de la présente charte.

Nom, Prénom :
Bureau (Étage, N°) :
□ Personnel permanent de l'unité :
□ Thésard
□ Stagiaire du au
Préciser le type de stage (master, licence, autre…) :
Sous la responsabilité de :

Date :

Signature :

Quizz sécurité au labo chimie :

1. **Sur quelle plage horaire peut-on manipuler au laboratoire ?**

-8h/18h -7h30/17h -8h30/17h30

2. **Qui est le responsable du laboratoire de Chimie ?**

-Mylène -Sophie -Rémi

3. **Quels sont les EPI obligatoires pour pouvoir entrer dans une salle de laboratoire ?**

4. **Au bout de combien de temps est-il important de changer de gant ?**

-1h 30min -2h

5. **Pour l'identification d'un échantillon, qu'est-il important de marquer sur le flacon ?**

6. **Je mélange de l'acide chlorhydrique à 40% avec de l'eau, à quel endroit faut-il jeter la solution ?**

-À l'évier -bidon déchets acide -bidon solvant organique

7. **Pour une petite brûlure, il est important de rincer ?**

-10min -15min -30min

8. **Si je me verse des produits chimiques sur la peau,**

-Je rince et je mets un pansement si nécessaire

-Je rince, je le signale et je me soigne

- ?

9. **Si je souhaite utiliser de l'acide chlorhydrique concentré, je manipule ?**

-Sur la paillasse -Sous la hotte -Dans mon bureau

10. **Si je manipule une micropipette et que je la fais tomber involontairement, (plusieurs réponses sont possibles)**

-Je la ramasse et je la repose

-Je regarde si elle n'a rien

-Je la mets de côté

-Je le signale à un technicien permanent

11. **Avant de commencer toute manipulation, qu'est-il important de faire ?**

-Regarder l'heure

-Préparer les flacons

-Changer l'eau des pissettes

-Vérifier les hottes

12. **À quel endroit dois-je noter des observations sur une manipulation ?**

-Une feuille volante -Un fichier Word -Un cahier de laboratoire

13. **Après toutes les manipulations, qu'est-il important de faire ? (citez 2 actions)**

14. **Les sacs poubelles noirs correspondent ?**

-aux déchets souillés -aux déchets ménagers -aux produits infectieux

15. **Doit-on étiqueter chaque sac poubelle avant de les jeter ?**

-oui -non

16. **Quand j'ai fini d'utiliser une micropipette, je la pose ?**

-Verticalement -Horizontalement

17. **Avant d'utiliser de l'eau Milli Q, je regarde ?**

-Le niveau (barres bleues)

-La température

-La conductivité

18. **Pour l'utilisation de l'eau Milli Q, je laisse obligatoirement ?**

-une barre bleue -2 barres bleue -une barre rouge

19. **Qui est la responsable de la salle blanche ?**

-Sophie -Mylène -Rémi

20. **Est-ce que j'ai le droit de rentrer en salle blanche après avoir fumer ?**

-oui -non

21. **Pour la décontamination des flacons, combien de fois est-il nécessaire de le rincer à l'eau MilliQ ?**

-1 fois -2fois -3 fois

22. **Quel jour de la semaine sont évacués les déchets ?**

-lundi -mardi -mercredi -jeudi -vendredi

23. **Qu'est-il interdit d'amener en salle blanche ?**

24. **En cas de projection d'un produit chimique sur la peau ou dans l'œil, je dois :**

-Rincer abondamment à l'eau pendant 5 minutes

-Rincer abondamment à l'eau pendant 30 minutes

-Rincer abondamment à l'eau pendant 15 minutes

25. **Quelle est la consigne de sécurité incorrecte ?**

-Porter des lunettes de protection

-Porter une blouse blanche en polyester

-Manipuler debout

Quizz Hygiène/Sécurité

1. **Sur combien de sites est réparti HSM ?**

- 1 - 2 - 3

2. **Dans quel bâtiment sommes-nous ?**

- 32 - 29 - 39

3. **À partir de quelle heure il est important de fermer toutes les portes du bâtiment ?**

- 17h - 18h - 19h

4. **De quelle couleur est l'étiquette des déchets souillés ?**

- bleu -jaune - rouge

5. **De quelle couleur est l'étiquette des déchets biologiques ?**

- jaune -orange - rouge

6. **Quel document doit être obligatoirement rempli avant de partir sur le terrain ?**

7. **Pour qui est accessible la formation sécurité/Habilitation/Secourisme ? (entourer la ou les bonnes réponses)**

-Permanents -Stagiaires -CDD -Doctorants

8. **Quelles est la première chose à faire lors d'un petit départ incendie ?**

-Partir en courant -Utiliser un extincteur -Avertir

9. **L'extincteur AB est un extincteur à :**

-poudre -eau -Feu électrique

10. **Selon vous, une personne qui découvre un feu doit : (remettre dans l'ordre avec des numéros)**

- Prévenir (pompiers, gardien du site, le service hygiène et sécurité)
- Lancer l'alarme à l'aide des déclencheurs manuels
- Agir vite sans affolement et utiliser si possible les moyens d'extinction à disposition
- Assurer l'accueil des secours pour les guides
- Faire évacuer le bâtiment

11. **Quelle est la première chose à faire lors d'une évacuation ?**

- Fermer les fenêtres
- Partir chercher son téléphone
- Cesser le travail

12. **L’ascenseur est-il autorisé en cas d’évacuation ?**

- oui -non

13. **Ou peut-on trouver une boite à pharmacie ? (citez un endroit)**

14. **Que peut-on trouver dans une boite à pharmacie ? (citer 3 items)**

15. **Où se situe le défibrillateur automatique sur le site ?**

-Salle café - Hall d’accueil -Couloir du laboratoire

16. **Où se situe la sortie de secours la plus proche de vous ?**

HydroSciences Montpellier

http://www.hydrosciences.org/

Présentation d'Accueil Hygiène & Sécurité

Unité répartie sur deux sites

Maison des Sciences de l'Eau - MSE
Bâtiment 39 Université de Montpellier
300 Avenue du Professeur Emile Jeanbrau
34095 Montpellier

Faculté de Pharmacie
Département Sciences de l'Environnement et Santé Publique
Bâtiment C, 1er étage et 2ème étage
15, avenue Charles Flahault à Montpellier
34093 Montpellier cedex 05

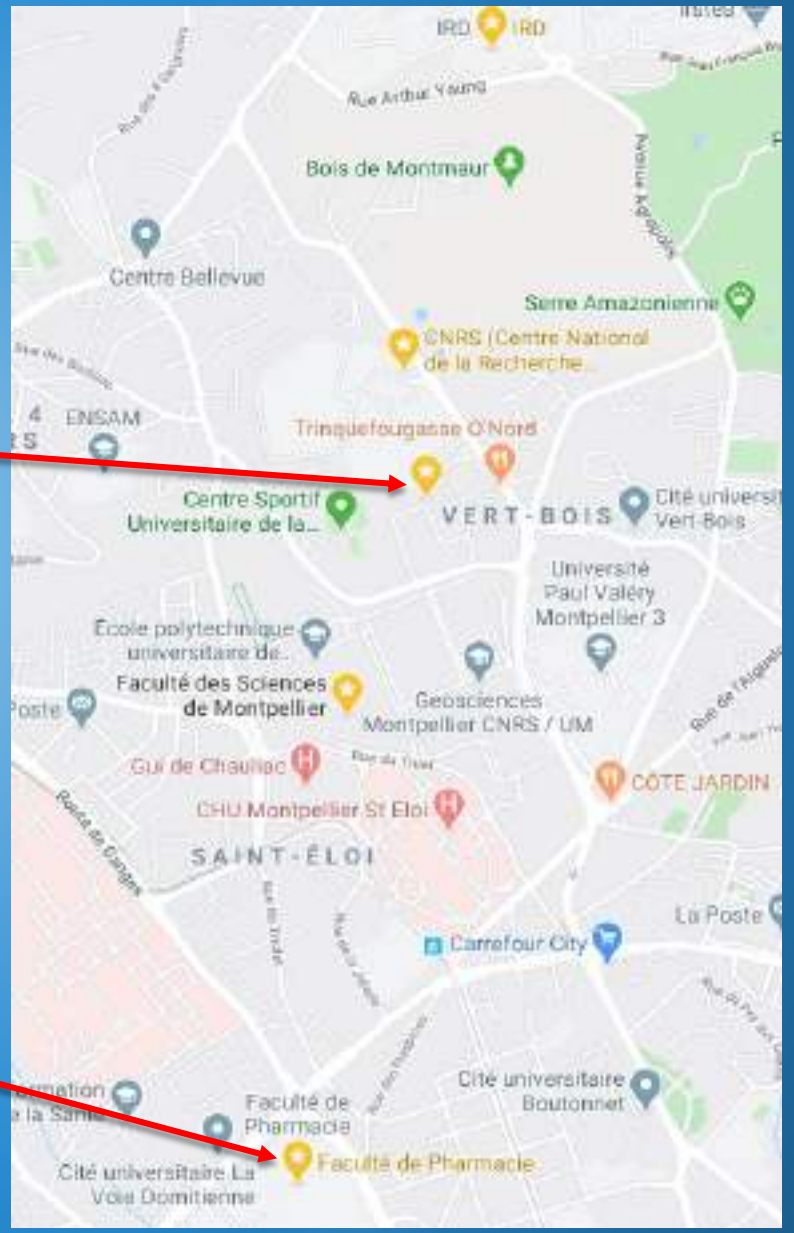

Cliquer sur l'image pour lancer la vidéo

Prévention des risques à l'UM

La sécurité est l'affaire de tous
et la responsabilité de chacun

Droits et devoirs

Tutelle/Institut d'accueil :

- garantit la sécurité des personnels (matérielle et RPS),
- offre de bonnes conditions de travail, donne accès aux formations/informations essentielles,
- met en place une politique appropriée de gestion des données personnelles.

Agent/Stagiaire :

- obligation de respecter les règlements et consignes,
- acceptation de facto de la politique de traitement des données personnelles,
- peut user du droit de retrait s'il/elle l'estime justifié (mène à une enquête).

La responsabilité des acteurs de la prévention

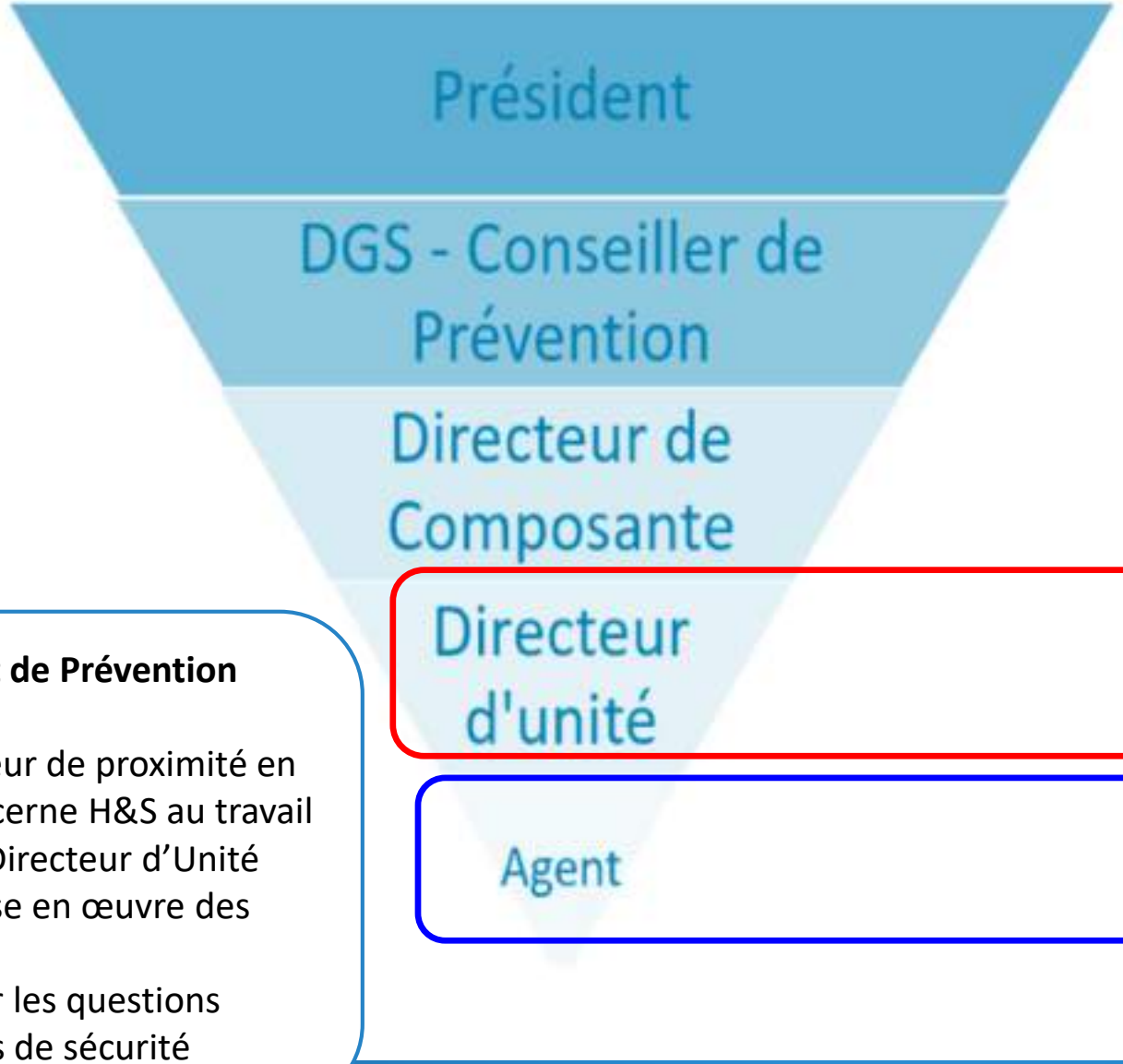

Le Président est responsable de la Sécurité des agents sur l'ensemble de l'Université de Montpellier.

Le DGS conduit au côté du Président la Politique de Prévention de l'Université de Montpellier avec l'aide du Conseiller de Prévention.

Si le Directeur de Composante a une délégation de pouvoir dans le domaine de la Santé Sécurité au Travail, il est responsable de la Sécurité des agents sur l'ensemble de sa composante.

Le Directeur d'Unité a la responsabilité de garantir la Santé/Sécurité de ses agents.

L'agent est responsable de sa propre sécurité mais également de celle de son entourage (collègues, usagers).

Assistant de Prévention

- Interlocuteur de proximité en ce qui concerne H&S au travail
- Assiste le Directeur d'Unité dans la mise en œuvre des règles H&S
- Relais pour les questions spécifiques de sécurité

Assistants de Prévention à HSM

- interlocuteurs de proximité en ce qui concerne H&S au travail,
- assistent le Directeur d'Unité dans la mise en œuvre des règles H&S,
- relais pour les questions spécifiques de sécurité,
- pas un Ingénieur Sécurité ➔ Référents et titulaires d'habilitations,
- rédigent le Document Unique d'Evaluation des Risques.

- Site MSE : 2 AP (Nicolas Patris, Sophie Delpoux)
- Site Pharma : 3 AP (David Rosain, Fabien Aujoulat, Sylvie Manguin)

Assistants de Prévention à la MSE

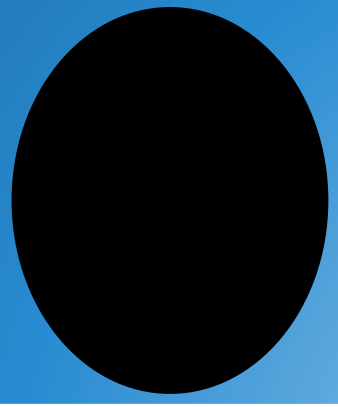

Nicolas PATRIS
Ingénieur de Recherche IRD
nicolas.patris@umontpellier.fr
04 67 14 90 31
Bureau 019 RDC

Responsable du LAMA (Isotopes stables)
Assistant de Prévention

Sophie DELPOUX
Assistant Ingénieur CNRS
sophie.delpoux@umontpellier.fr
04 67 14 90 79
Bureau 011 RDC

Responsable labo chimie
Assistant de Prévention

Référents pour questions spécifiques de sécurité :

- Laboratoire de chimie : Sophie Delpoux
- Laboratoire de microbiologie : Angélique Désœuvre (bureau 126)
- Terrain/Atelier : Pierre Marchand (bureau 101B) ou encadrant terrain

Sauveteurs Secouriste du travail à la MSE

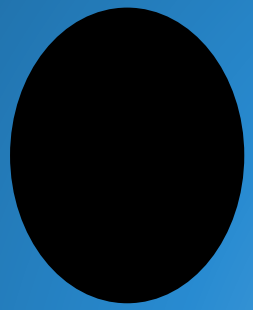

Nicolas PATRIS
Ingénieur de Recherche
IRD
nicolas.patris@umontpellier.fr
04 67 14 90 31
Bureau 019 - RDC
Sauveteur Secouriste du Travail

Rémi FREYDIER
Ingénieur de Recherche
CNRS
remi.freydier@umontpellier.fr
04 67 14 90 93
Bureau 016 - RDC
Sauveteur Secouriste du Travail
(Recyclage à faire)

Jean Denis Taupin
Chargé de Recherche IRD
jean-denis.taupin@umontpellier.fr
04 67 14 90 37
Bureau 123 - 1er étage
Sauveteur Secouriste du Travail

Pascal Brunet
Ingénieur d'étude CNRS
Pascal.brunet@umontpellier.fr
04 67 14 90 39
Bureau 119 - 1er étage
Sauveteur Secouriste du Travail
(Recyclage à faire)

Patrick Lachassagne
IRD
patrick.lachassagne@umontpellier.fr
06 03 85 15 71
Bureau 141 - 1er étage
Sauveteur Secouriste du Travail
(Recyclage à faire)

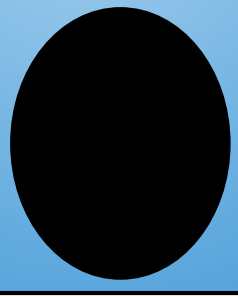

Marine Rousseau
PRAG UM
marine.rousseau@umontpellier.fr
04 67 14 .. ..
Bureau 116B - +1/2
Sauveteur Secouriste du Travail

Jacques Gardon
Directeur de Recherche
IRD
jacques.gardon@umontpellier.fr
04 67 14 90 32
Bureau 110 - 1er étage
Médecin épidémiologiste

Registre Santé & Sécurité

Le Registre Santé Sécurité au Travail

Le Registre Santé Sécurité au Travail est un registre permettant aux agents de faire remonter à la direction, des observations ainsi que des suggestions en matière de prévention des risques professionnels afin de tendre vers une démarche d'amélioration continue des conditions de travail.

Le Registre Santé Sécurité au Travail est également utilisé pour y consigner les accidents et incidents du travail. Cependant, il ne remplace pas la déclaration officielle d'Accident du Travail (document *cerfa*).

De la même façon, dans le cadre d'un Etablissement recevant du public, les usagers peuvent consigner dans ce registre leurs observations et suggestions.

Le Registre Santé Sécurité au Travail est situé dans chaque service. Son emplacement doit être accessible et porté à la connaissance de l'ensemble des agents du service et des usagers à l'aide d'un affichage.


SITE : .....

Registre Santé et Sécurité au Travail

Direction / Service / Laboratoire:

.....

Nom de l'assistant de prévention chargé de la tenue du registre :

.....

Responsable de l'unité : ....

N° du registre : ...

Contact : conseil-prevention@umontpellier.fr

- document officiel,
- accessible à tous à l'écriture et à la lecture (sur la banque d'accueil),
- recueil de tous incidents/accidents ou observations concernant H&S sur le lieu de travail.

Cliquer sur l'image pour lancer la vidéo

Horaires de travail

Lundi – Vendredi ouvrés : 07h30 – 21h00

Locaux techniques (Labos, atelier) : 08h30 – 17h30
Uniquement accessibles selon les consignes du référent !

APRES 17H30 :

FERMER TOUTES LES PORTES !!

Travail isolé

SITUATION DE TRAVAIL ISOLE :

Travailler de façon isolée, c'est réaliser seul une tâche dans un environnement de travail où l'on ne peut être vu ou entendu directement par d'autres personnes, et où la probabilité de visite est faible.

A éviter autant que possible, et à éviter absolument de façon habituelle/prolongée.

Interdiction sur le lieu de travail hors horaires ouvrés.

Autorisation à soumettre à la direction en binôme avec au moins un permanent de l'UMR.

Interdiction sur le terrain.

Cliquer sur l'image pour lancer la vidéo

Tri des déchets

- Poubelles de bureau :
  - déchets bureautiques/ménagers,
  - recyclage papier (propre et non froissé).

- Collecte pour Recyclage (bureau K. Gujda, 1er étage) :
  - piles,
  - cartouches imprimante/toner.

- Encombrants (à l'extérieur, devant la soûte à produit chimique) :
  - cartons vides,
  - mobiliers et matériels informatique hors d'usage.

- Verre (alimentaire/bureaux) :
  - pas de collecte sur le lieu de travail !

- Autres déchets (toxiques/souillés/électroniques…) :
  - se référer à la réglementation.

LE TRI SELECTIF DES DÉCHETS

Déchets Spéciaux

Déchets Souillés (par produits chimiques)

Déchets Biologiques (DASRI)

Déchets Papier et Carton

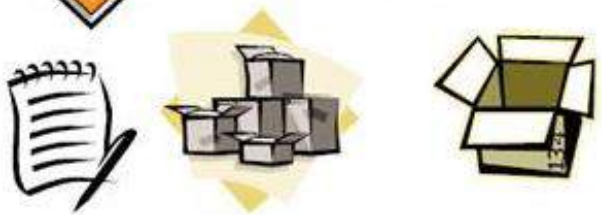

Déchets de type ménagers

Encombrants Remises aux domaines

RAPPEL SUR LE TRI DES DECHETS DANGEREUX ET SON ETIQUETAGE

Déchets Spéciaux
(Etiquette bleue)

Service GDD de la DLO : 31.26 → Centre de Services

B.E.T

Déchets Souillés
(Etiquette rouge)
Tous contenants vides souillés par produits chimiques, Papiers absorbants…

Service GDD de la DLO : 31.26 → Centre de Services

Déchets Biologiques
D.A.S.R.I (Déchets d'Activités de Soins à Risques Infectieux)
Conditionnés en cartons/containers
Coupants/Tranchants sécurisés

Service GDD de la DLO : 31.26 → Centre de Services

Exemples : Boites de pétri, gants, papiers absorbants, flacons de culture, litières, anses d'ensemencement jetables, tubes divers, plaques de titration, corps de seringue, …

Etiquette de refus

Placé par les agents du service GDD en cas de non-conformité du déchet

Service GDD de la DLO : 31.26 → Centre de Services

Pour toute question, contacter le service Gestion des Déchets Dangereux de l'UM via le centre de service ou l'adresse dhs-envt@umontpellier.fr

Missions

PAS DE SORTIE TERRAIN

SANS ORDRE DE MISSION

Ordre de Mission :

- correspondant à votre tutelle (UM, CNRS ou IRD),
- renseigne les dates, le(s) lieu(x), la nature des activités,
- OM sans frais permanents pour courtes distances,
- ne pas oublier de respecter les délais de traitement administratif !

Utilisation des véhicules de service :

- dossier complet à monter (permis de conduire, assurance, attestation de conduite signé par le DU, …),
- réservation en ligne : http://resa.msem.univ-montp2.fr/index.php .

Formation permanente

- formations Sécurité/Habilitations/Secourisme organisées régulièrement par les tutelles,

- formations accessibles aux :
  - Permanents
  - CDD / Post Docs
  - ATER
  - Doctorants

- Correspondante Formation CNRS et UM :
  - Angélique Désœuvre : angelique.desoeuvre@umontpellier.fr

- Correspondante formation IRD :
  - Catherine Marchand : catherine.marchand@umontpellier.fr

Incendie

Le triangle du feu

Solide : papier, bois, tissus, PVC

Liquide : essence, solvants

Gazeux : Butane, Propane...

Air (O_2 = 21%)

Produits chimiques riches en O_2 :

Peroxydes

Flammes, étincelles,
surfaces chaudes

Consignes incendie

1. Agir vite sur le départ <u>si possible,</u>

2. Utiliser les moyens à disposition :

- <u>extincteurs :</u>

AB : à eau (papiers, cartons, liquides org.)

ABC : à poudre (solides, liquides, gaz)

CO_2 : feux électriques

- <u>coupure de l'électricité :</u>

Une personne qui découvre un feu doit	
	- Agir vite sans affolement sur un départ de feu - Utiliser si possible les moyens d'extinction à disposition
	- Lancer l'alarme à l'aide des déclencheurs manuels
	- Prévenir : Les pompiers 18 Le gardien du site Le service hygiène et sécurité : 04.67.14.49.54
	- Faire évacuer le bâtiment jusqu'au point de rassemblement
	- Assurer l'accueil des secours pour les guider

Consignes incendie

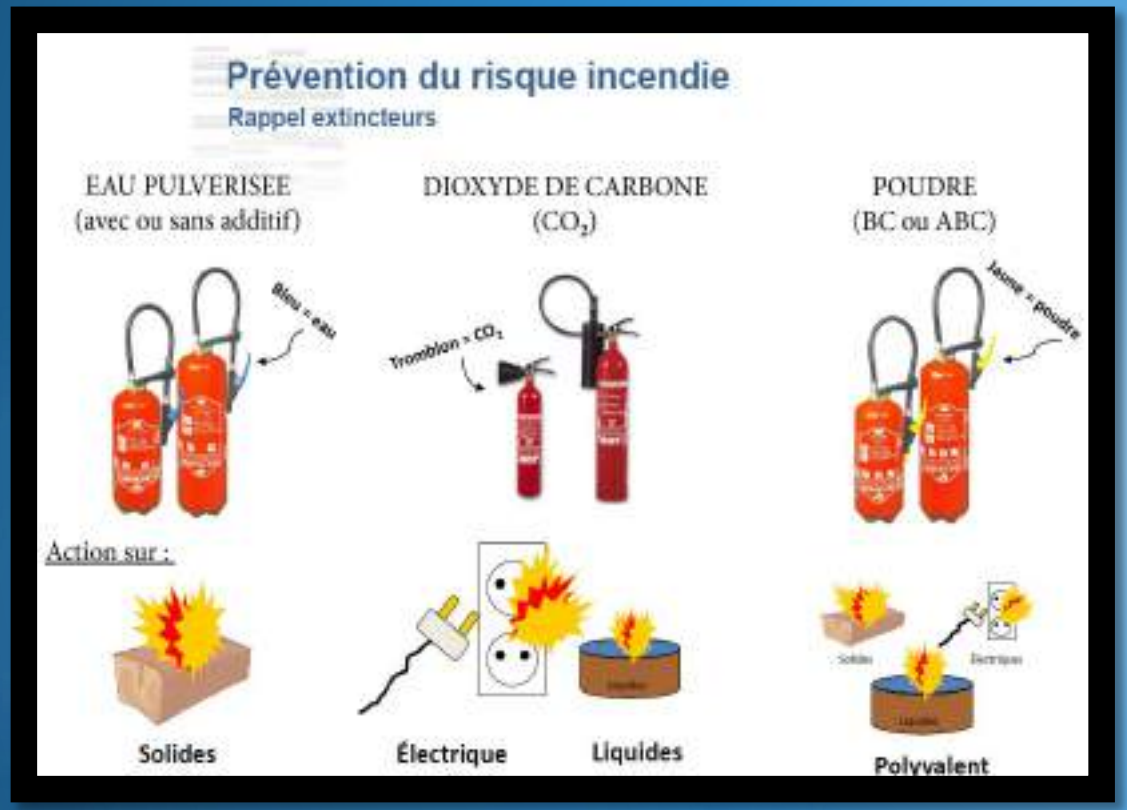

Cliquer sur l'image pour lancer la vidéo

Consignes incendie

3. Avertir :

- Déclenchement de l'alarme,
- Prévenir les secours :

Ligne fixe UM

- **0-18** Pompiers
- **3000** Poste de Garde

Tel portable

- **112** Pompiers
- **04 67 14 3000** Poste de Garde

4. Évacuation,

5. Guider l'arrivée des secours.

Une personne qui découvre un feu doit	
	- Agir vite sans affolement sur un départ de feu - Utiliser si possible les moyens d'extinction à disposition
	- Lancer l'alarme à l'aide des déclencheurs manuels
	- Prévenir : Les pompiers 18 Le gardien du site Le service hygiène et sécurité : 04.67.14.49.54
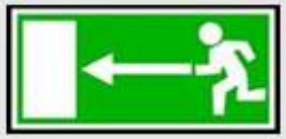	- Faire évacuer le bâtiment jusqu'au point de rassemblement
	- Assurer l'accueil des secours pour les guider

Evacuation

1. Cesser le travail,
2. Mettre en sécurité les équipements,
3. Fermer les fenêtres,
4. Évacuer en fermant les portes **par la sortie la plus proche,**
5. S'assurer que **tout le monde** évacue ! (Et porter assistance si besoin),
6. Escaliers obligatoires (ascenseurs et monte-charges interdits),
7. Ne jamais revenir en arrière,
8. Point de Rassemblement devant IEM.

Consignes Malaises/Blessés

1. Mettre la victime en sécurité sans créer de sur-incident,
2. Avertir des Secouristes présents dans le bâtiment,
3. Avertir les secours et le PC sécurité de l'UM,
4. Guider l'arrivée des secours.

MALAISE / ACCIDENT	
	- Prévenir le secouriste
	- **ALERTER LES SECOURS 18 – 15- 112** Communiquer * l'adresse exacte et complète de l'établissement (site, bâtiment, étage, salle) * un numéro de téléphone où vous joindre * le type d'accident * l'état de la victime, le nombre de victime, les soins pratiqués * les risques éventuels **NE JAMAIS RACCROCHER LE PREMIER**
	- Prévenir L'infirmerie Le poste de sécurité
	- Assurer l'accueil des secours pour les guider

Appel extérieur à partir d'une ligne fixe UM : faire le **0** avant le numéro de téléphone

POLICE	17
SAPEURS POMPIERS	18
NUMERO D'URGENCE EUROPÉEN	112
SAMU	15
NUMERO D'URGENCE PERSONNES SOURDES ET MALENTENDANTES	114
Centre antipoison (Toulouse)	05.61.77.74.47

Urgences	04.67.33.95.00
Urgences ophtalmologiques	04.67.33.77.90
Service des maladies infectieuses Et tropicales (Gui de Chauliac)	04.67.33.77.16
Service des Grands Brûlés	04.67.33.82.28

Numéro du PC Sécurité de l'Université de Montpellier
(04 67 14) 30 00

LE MESSAGE D'ALERTE:

- Numéro de téléphone de l'appelant
- Lieu de l'accident précis:
  - Site Universitaire: _____
  - Bâtiment + étage: _____
  - Adresse précise: _____
- Nature de l'accident et risques éventuels
- Nombre de personnes concernées
- État des victimes (appréciation de la gravité)
- Premières mesures prises et gestes effectués
- Point de rendez-vous de l'accueil des secours: _____

Ne jamais raccrocher avant que les services de secours ne vous en aient donné l'autorisation

Boîtes à pharmacie

Boîtes à pharmacie disposées dans l'Unité et les véhicules pour pallier aux petites blessures :

	Localisation		Numéro	Contact
HSM - site MSE	RDC	Dans laboratoire de microbiologie (004)	1	
	RDC	Dans laboratoire de chimie (005)	2	
	RDC	HALL de la MSE (Près du distributeur de boissons)	3	
	1er étage-ZONE A	Bureau de Kristine GUJDA (109)	4	Kristine GUJDA : gujda@msem.univ-montp2.fr
	1er étage-ZONE B	Sur colonne face bureau 141	5	
	1er étage-ZONE C	Mur coté bureau 126	6	
	-1/2	Mur à l'entrée du labo technique 009b	7	
	RDC	Bureau 011	8	Sophie Delpoux : sophie.delpoux@umontpellier.fr
Véhicules HSM	Toyota 4X4	Pochette papiers véhicule	9	
	Dacia Duster	Pochette papiers véhicule	10	
	Renault Scénic	Pochette papiers véhicule	11	
	Renault Trafic	Pochette papiers véhicule	12	
HSM - site pharmacie	EQUIPE PHYSE		13	Fabien AUJOULAT : fabien.aujoulat@univ-montp1.fr
	EQUIPE CONTEM		14	David ROSAIN : drosain@univ-montp1.fr

Boîtes à pharmacie

Contenu des trousses de secours :

- une paire de ciseaux à bouts ronds,
- une paire de gants à usage unique,
- protection pour bouche à bouche,
- une pince à écharde (type pince à épiler),
- une boite de pansements individuels hypoallergéniques prédécoupés auto-adhésifs,
- une couverture de survie,
- des compresses de gaze stériles en emballage individuel,
- un rouleau de sparadrap hypoallergénique,
- des bandages extensibles (type bande velpeau),
- un spray désinfectant,
- un gel hydroalcoolique,
- un tube de pommade contre des brûlures (type osmosoft),
- un tube de pommade contre les piqures d'insectes (type apaisyl),
- un tube de pommade contre les coups et bosses (type Arnica),
- des unidoses de sérum physiologique.

Défibrillateur automatique

- Localisé dans le hall d'accueil du bâtiment 39.

Plans des locaux

Vérifier placement extincteur, changer le plan

Issues de secours

Défibrillateur automatique

Armoire à pharmacie

Extincteur

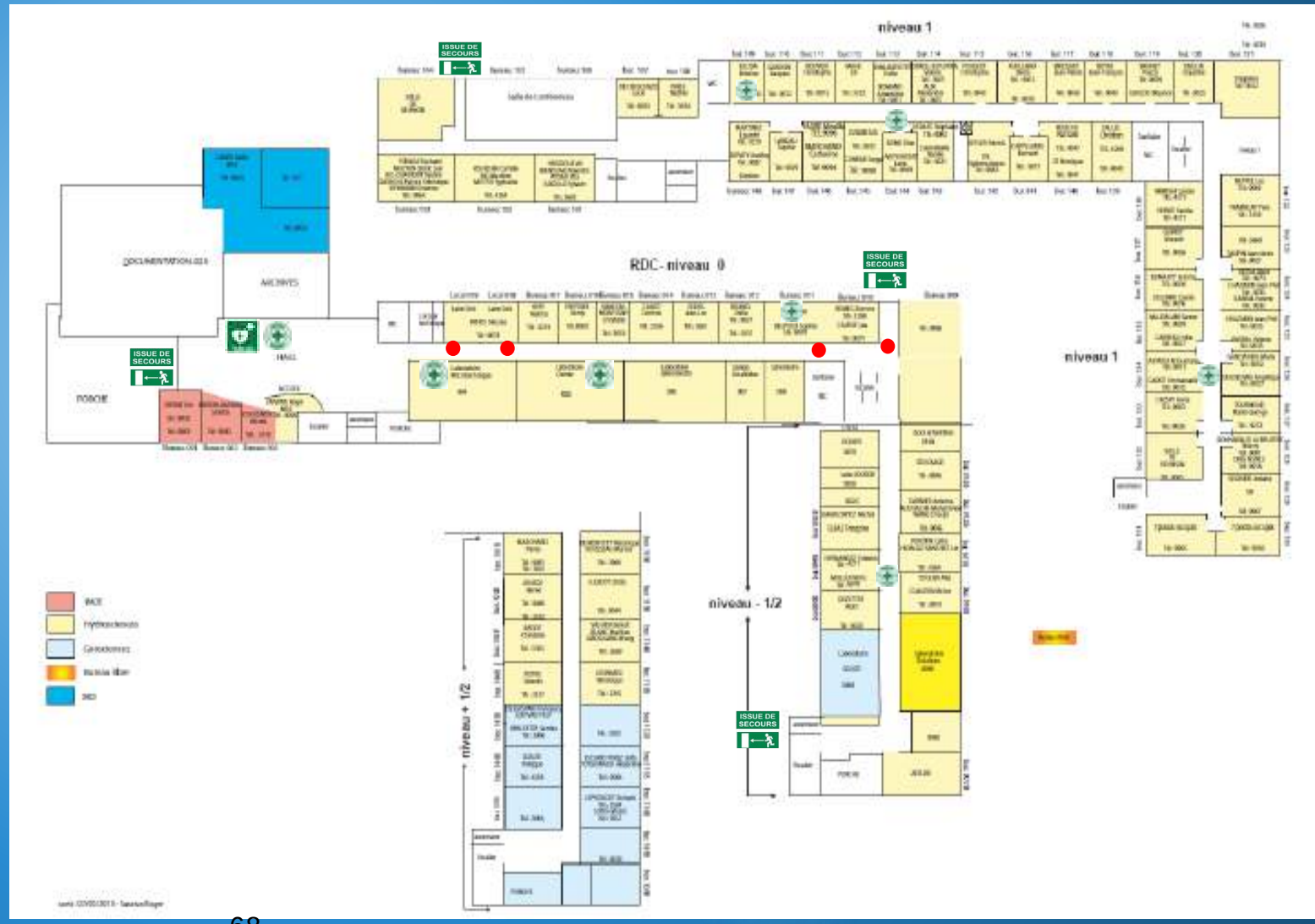

Risques Psycho-Sociaux

Cliquer sur l'image pour lancer la vidéo

Bon séjour parmi nous !

La sécurité au sein des laboratoires de chimie et de la salle blanche d'HydroSciences Montpellier

Localisation

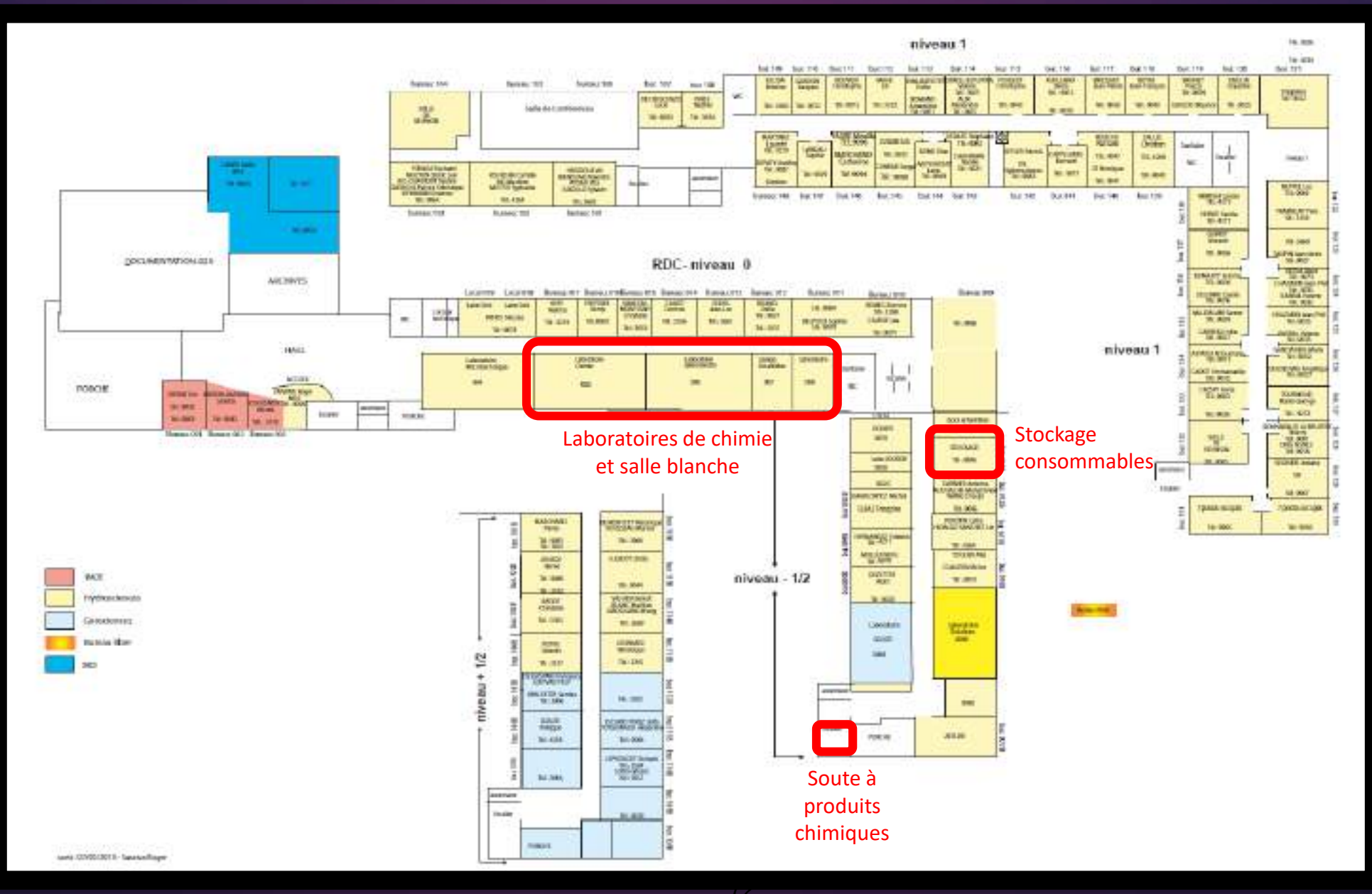

Droit d'accès

- Pour accéder aux laboratoires concernés :
  - avoir validé la formation "Hygiène et Sécurité",
  - avoir validé la formation "Laboratoires de chimie et salle blanche",
  - avoir remis la "Charte laboratoire de chimie" signée au responsable du laboratoire de chimie,
  - avoir remis la "Charte salle blanche" signée au responsable de la salle blanche.

- Pour utiliser un équipement des laboratoires, il faut :
  - avoir suivi une formation au préalable sur l'équipement par un personnel permanent,
  - avoir obtenu l'autorisation du formateur sur l'équipement.

- Tout utilisateur ne respectant pas les règles et mettant en péril le bon fonctionnement des laboratoires de chimie pourra se voir refuser temporairement l'accès (voire définitivement en cas de récidive).

- Le personnel de HSM est là pour vous aider … pas pour vous servir !!!

Horaires d'accès

Responsable Laboratoires de Chimie : Sophie Delpoux

Suppléants (en cas d'absence) : Mylène Marie, Rémi Freydier

08h30 – 17h30

Uniquement accessibles selon les consignes du référent et en présence d'au moins un permanent des labos !

Le travail isolé est interdit!!!

Après 17H30 :

Fermeture des laboratoires que les manips soient finies ou pas

Contact des laboratoires

Rémi FREYDIER
remi.freydier@umontpellier.fr
04 67 14 90 93
SST

Sophie DELPOUX
sophie.delpoux@umontpellier.fr
04 67 14 90 79
Responsable labo chimie
Assistant de Prévention

Mylène MARIE
mylene.marie@umontpellier.fr
Responsable Salle Blanche

Chrystelle BANCON-MONTIGNY
chrystelle.bancon-montigny@umontpellier.fr
04 67 14 39 33

Eléonore RESONGLES
eleonore.resongles@umontpellier.fr
04 67 14 90 84

Corinne CASIOT-MAROUANI
corinne.casiot-marouani@umontpellier.fr
04 67 14 33 56

Hygiène et sécurité

Formation "Laboratoires de chimie et salle blanche"

- Bien écouter et prendre des notes lors de la formation "Laboratoires de chimie et salle blanche" et lors des formations à l'utilisation des différents équipements.

Cliquer sur l'image pour lancer la vidéo

H&S dans les laboratoires

- Ne jamais pipeter un produit chimique à la bouche,
- ne pas manger, boire, fumer et utiliser des écouteurs dans les laboratoires,
- ne pas stocker de nourriture/boisson dans les réfrigérateurs/congélateurs des laboratoires,
- ne pas stocker d'échantillons ou produits chimiques dans les réfrigérateurs communs des "coins café" RDC et 1er étage,
- se laver les mains et ôter les EPI (Equipements de Protection Individuelle) au moment de quitter les laboratoires,
- repérer les douches de sécurité et les couvertures anti-feu,
- Repérer la trousse à pharmacie présente dans le labo central (laboratoire 005),
- ne pas se toucher le visage ou la peau avec les gants.

H&S dans les laboratoires

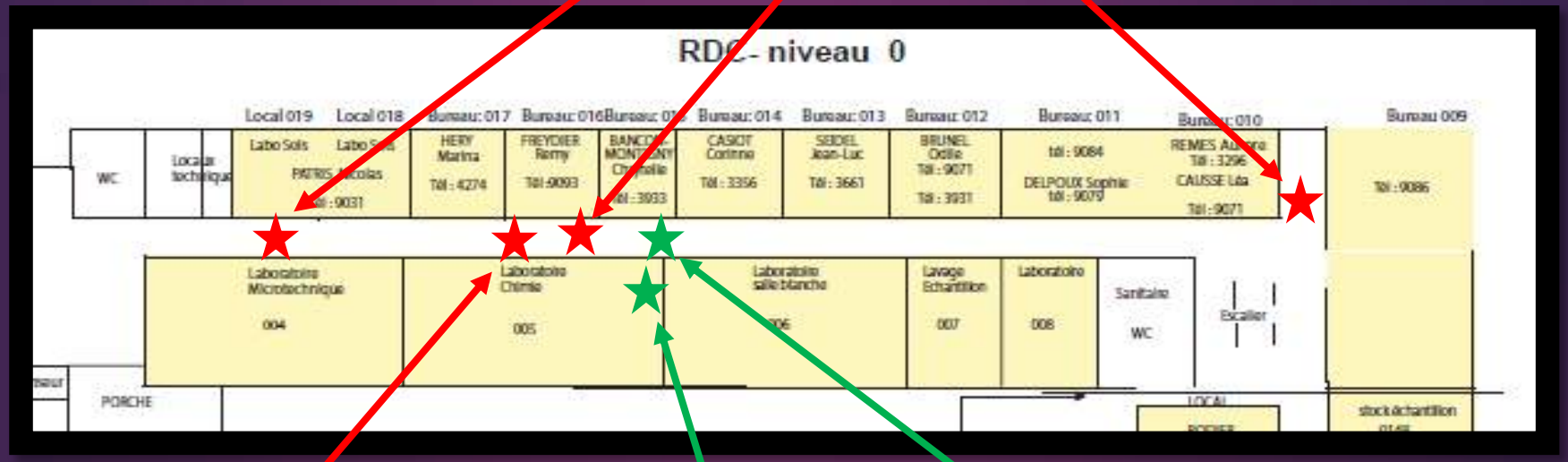

Protections individuelles EPI

- **Le port des EPI est obligatoire dès l'entrée dans les laboratoires et permet de protéger l'utilisateur et les échantillons manipulés :**
  - une blouse antiacide fermée à manches longues,
  - des lunettes de sécurité ou des sur-lunettes de sécurité,

  - → La blouse et les lunettes sont prêtées par l'UMR pour la durée du séjour et doivent être restituées avant le départ.

  - des gants en nitrile ajustés et adaptés à la manipulation des différents produits chimiques,
    - → des gants en nitrile de différentes tailles sont à disposition dans le premier tiroir de chaque laboratoire,
    - → ne pas utiliser le matériel avec des gants souillés par l'acide.

Les gants en nitrile sont des gants à usage unique qui deviennent poreux au bout de 30 min d'utilisation normale et dès qu'ils sont en contact prolongé avec un produit chimique, n'hésitez pas à les changer souvent.

  - porter un masque à poussière lors de l'utilisation de produits solides finement divisés

    ou un masque à cartouche adaptée ou isolant pour la manipulation de produits volatils très toxiques.

Les masques disponibles se trouvent dans le placard blanc coulissant du laboratoire central.

Masques de protection

- Masques anti aérosols (anti poussières) de couleur blanche :
  - P1 ou FFP1 : pour protéger des aérosols solides et/ou liquides sans toxicité spécifique,
  - P2 ou FFP2 : pour protéger des aérosols solides et/ou liquides dangereux ou irritants,
  - P3 ou FFP3 : pour protéger des aérosols solides et/ou liquides toxiques,
  - au fur et à mesure de leur utilisation, ces masques se colmatent :
    - si ils sont marqués R, ils sont réutilisables,
    - si ils sont marqués NR ils sont non réutilisables après un poste de travail.

Masques de protection

- Masques anti gaz (adsorption du gaz sur charbon actif) :
  - classe 1 : faible capacité de piégeage,
  - classe 2 : moyenne capacité de piégeage,
  - Classe 3 : grande capacité de piégeage,
  - à saturation, le masque laisse passer la totalité du gaz polluant.

Type	Couleur	Domaine d'utilisation
A	marron	gaz et vapeurs organiques dont le point d'ébullition est supérieur à 65 °C
B	gris	gaz et vapeurs inorganiques sauf le monoxyde de carbone (ex. Cl2, Br2, H2S, HCN...).
E	jaune	dioxyde de soufre (SO2) et autres gaz et vapeurs acides (ex. HCl...)
K	vert	ammoniac et dérivés organiques aminés
HgP3	rouge + blanc	vapeurs de mercure
NOP3	bleu + blanc	oxydes d'azote
AX	marron	produits organiques à point d'ébullition inférieur à 65 °C
SX	violet	composés organiques spécifiques désignés par le fabricant

Protections individuelles EPI

Cliquer sur l'image pour lancer la vidéo

Manipulation d'objets piquants et tranchants

Consignes de sécurité :

- utiliser un récipient adéquat résistant au percement pour éliminer les déchets piquants/tranchants,
- utiliser des gants résistants à la perforation,
- utiliser une pincette, une brosse et une pelle pour manipuler des débris de verre ou des aiguilles,
- ne jamais replacer la protection sur une aiguille usagée,
- éliminer les objets piquants immédiatement d'une seule main et sans manipulation dans les collecteurs adaptés.

Cliquer sur l'image pour lancer la vidéo

Les risques de l'Azote

Consignes de sécurité :

- ne jamais manipuler l'azote liquide sans protection,
  - ✓ utiliser des cryogants,
  - ✓ porter un écran facial ou un masque de protection adapté.
- n'utiliser que des matériaux et récipients cryogéniques,
- manipuler l'azote liquide dans un local bien ventilé pour éviter les risques d'asphyxie par anoxie.

Cliquer sur l'image pour lancer la vidéo

Le risque biologique

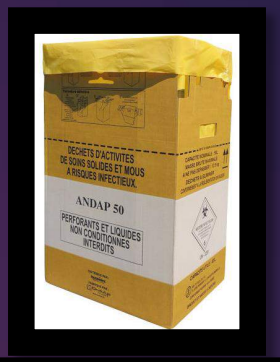

Consignes de sécurité :

- utiliser des gants à usage unique, une blouse et des lunettes de sécurité,
- protéger toute plaie avec un pansement imperméable,
- manipuler les échantillons à risque biologique uniquement sous PSM,
- ne pas porter les mains ou un objet à la bouche,
- jeter tous les déchets en contact avec ses échantillons dans des cartons DASRI,
- désinfecter le PSM après chaque utilisation,
- ranger la blouse séparément des vêtements de ville,
- bien se laver et désinfecter les mains après avoir retirés les EPI.

Cliquer sur l'image pour lancer la vidéo

Utilisation des produits chimiques

Cliquer sur l'image pour lancer la vidéo

Utilisation des produits chimiques

- saisir les bouteilles par le corps et non par le bouchon,
- lire la fiche signalétique (MSDS) d'un produit avant de l'utiliser,
- toujours identifier les produits chimiques dans un contenant avec le nom et les logos associés,
- ne pas mélanger Solvant avec Acide ou Base.

"Acide dans l'Eau Bravo, Eau dans l'Acide Suicide"

En cas d'accident

- stopper immédiatement l'activité en cours et avertir la personne la plus proche :
  - petites Brûlures (acides, bases, solvants, flammes, …) :
    - Rincer au robinet pendant au moins 15 min. Si doute ou soucis, voir un médecin rapidement.
  - grosses Brûlures (acides, bases, solvants, flammes, …) :
    - Rincer sous la douche du couloir RDC pendant au moins 15 min. Voir un médecin rapidement.
  - projections dans les yeux :
    - Rincer abondamment à l'eau à l'aide des rinces-œil situés dans le couloir pendant 15 min minimum. Si doute ou soucis, voir un médecin rapidement.
- signaler au plus vite l'incident ou l'accident aux Assistants de Prévention,
- remplir un rapport d'incident ou d'accident,
- en cas de doute sur la procédure à suivre en cas d'exposition à un produit chimique, contacter le centre antipoison (Centre Toulouse : 05 61 77 74 47).

Manipulation d'acide fluorhydrique

LA MANIPULATION DE L'ACIDE FLUORHYDRIQUE (HF) EST INTERDITE AUX ETUDIANTS (SAUF DOCTORANTS).

- PORT DES EPI OBLIGATOIRE : blouse, lunettes de protection, gants + Ajout d'une deuxième paire de gants,
- rincer ou emballer les consommables mis au contact d'HF avant de les jeter,
- indiquer au marqueur sur le bidon d'effluents la présence d'HF.

CONSIGNES EN CAS DE CONTACT :

- prévenir une personne du laboratoire qui se chargera d'appeler les secours,
- rincer abondamment la zone à l'eau pendant 15 minutes,
- en cas de contact cutané, appliquer (ou faire appliquer) ensuite du gluconate de calcium sur la zone touchée jusqu'à l'arrivée des secours.

Le gluconate de calcium est disponible dans le passe-plat de la salle blanche et dans la boîte à pharmacie du laboratoire (Laboratoire 005 - RDC).

Règles d'utilisation des laboratoires

Comportement dans les laboratoires

- respecter le travail des autres utilisateurs,
- travailler calmement,
- être attentif à la présence des collègues autour de vous, surtout lors de manipulation de produits dangereux,
- ne pas éparpiller ses affaires et tout ranger une fois votre travail terminé,
- ne pas poser ses lunettes de sécurité et son téléphone sur les paillasses,

- laisser les laboratoires dans l'état où vous aimeriez les trouver vous-même,
- nettoyer son poste de travail après utilisation,

- signaler à la personne responsable tout défaut de fonctionnement et panne : ne pas faire d'intervention personnelle sur les appareils,
- ne pas sortir de matériel du laboratoire (pipettes, verrerie, pissettes…) sans en informer les personnels permanents.

Comportement dans les laboratoires

- vérifier le bon fonctionnement des hottes avant de débuter vos manipulations,
- utiliser les hottes aspirantes pour toute manipulation de produits dangereux et pour toute manipulation avec risques de projections oculaires ou dégagement de vapeurs,
- ne pas entreposer de matériel sous les hottes,

- changer l'eau de la pissette MilliQ avant utilisation,
- ne pas pipeter directement dans les pissettes ou compte-gouttes, ni dans les solutions mères et matériaux certifiés,
- ne pas retransvaser le surplus d'une solution/poudre dans son récipient d'origine,

- écrire sur votre cahier de laboratoire toutes les manipulations et pesées effectuées,

- bien rincer avec de l’eau MilliQ les récipients et les éprouvettes après usage (rincer au moins 3 fois lors de l’utilisation d’acides ou de bases).

Gestion des stocks

- réapprovisionner les laboratoires avec les consommables que vous avez utilisés et finis (sopalin, gants, cônes…). Le matériel en stock se trouve en salle 13B,
- indiquer sur le tableau blanc à l'entrée du laboratoire central les consommables et produits chimiques que vous avez sorti du magasin ainsi que si vous avez pris la dernière boîte/bouteille,
- remplir les bonbonnes d'eau MilliQ et d’acide nitrique 20%.

Décontamination et nettoyage des laboratoires

- nettoyage des laboratoires avec des produits ménagers tous les trimestres,

- nettoyage des **blouses** à la machine à laver tous les trimestres.

- **Flacons HDPE < 250 mL :**
  - faire tremper dans un des deux bacs blancs en polypropylène (sous la dernière hotte du labo central) rempli avec HNO_3 pour analyse (PA) 20% pendant 24 heures minimum,
  - rincer 3 fois avec de l'eau MilliQ et remplir avec de l'eau MilliQ et acidifier à $1^{o}/_{oo}$ HNO_3 Suprapur.

- **Flacons HDPE ≥ 250 mL :**
  - remplir les flacons avec HNO_3 pour analyse (PA) 20% et laisser l'acide durant minimum 24 heures,
  - rincer 3 fois avec de l'eau MilliQ et remplir avec de l'eau MilliQ et acidifier à $1^{o}/_{oo}$ HNO_3 Suprapur.

Décontamination et nettoyage des laboratoires

- **Flacons en verre pour Carbone organique :**
  - faire tremper dans un des bacs blancs en polypropylène (sous la hotte en lavage flacon, à droite) rempli avec HNO_3 pour analyse (PA) 20% pendant 24 heures minimum,
  - rincer 3 fois avec de l'eau MilliQ et faire tremper dans les grands béchers en verre (sous la hotte en lavage flacon, à gauche) remplis avec de l'eau milliQ pendant 24 heures minimum,
  - faire griller les flacons dans le four à 500 °C (laboratoire 008).

- **Flacons en verre pour OSn :**
  - si utilisation d'isooctane, rincer les flacons à l'eau chaude (robinet du fond salle lavage flacon) puis mettre à tremper 24 heures dans du détergent (RBS) dilué. Rincer à l'eau chaude les flacons puis les mettre à tremper dans un des bacs en plastique avec couvercle bleu (sous la dernière hotte du labo central) rempli avec HNO_3 pour analyse (PA) 20% pendant 24 heures minimum. Rincer 3 fois avec de l'eau MilliQ et mettre à sécher dans l'étuve rouge sous la paillasse au laboratoire central à 60 °C ;
  - sinon, rincer directement 3 fois les flacons à l'eau MilliQ en lavage flacon faire tremper dans un des bacs en plastique avec couvercle bleu (sous la dernière hotte du labo central) rempli avec HNO_3 pour analyse (PA) 20% pendant 24 heures minimum. Rincer 3 fois avec de l'eau MilliQ et mettre à sécher dans l'étuve rouge sous la paillasse au laboratoire central à 60 °C.

Les déchets de laboratoire

Tri des déchets

Cliquer sur l'image pour lancer la vidéo

Tri des déchets

RAPPEL SUR LE TRI DES DECHETS DANGEREUX ET SON ETIQUETAGE

Déchets Spéciaux
(Etiquette bleue)

Service GDD de la DLO : 31.26

Centre de Services

B.E.T

Déchets Souillés
(Etiquette rouge)
Tous contenants vides souillés par produits chimiques, Papiers absorbants…

Service GDD de la DLO : 31.26

Centre de Services

Déchets Biologiques
D.A.S.R.I (Déchets d'Activités de Soins à Risques Infectieux)
Conditionnés en cartons/containers
Coupants/Tranchants sécurisés

Service GDD de la DLO : 31.26

Centre de Services

Exemples : Boites de pétri, gants, papiers absorbants, flacons de culture, litières, anses d'ensemencement jetables, tubes divers, plaques de titration, corps de seringue, …

Etiquette de refus

Placé par les agents du service GDD en cas de non-conformité du déchet

Service GDD de la DLO : 31.26

Centre de Services

Gestion des déchets

- sortir et remplacer les poubelles et bidons de récupération lorsqu'ils sont pleins,
- les déchets doivent être amenés dans le local "poubelle" en parpaing (parking arrière HSM) afin d'être évacués par l'UM tous les jeudis matin,
- pour l'évacuation de produits chimiques spécifiques, il faut demander des caisses spécifiques en plastique numérotées à l'UM :
  - faire la demande via le centre de service de l'ENT,
  - faire l'inventaire des produits chimiques à l'intérieur et le coller sur le couvercle,
  - les caisses ne peuvent être conservées qu'une semaine.

Gestion des déchets

- Déchets liquides :
  - **ne rien jeter dans l'évier** mais utiliser les différents bidons de récupération (déchets acides, déchets basiques, déchets solvants, déchets produits chimiques spécifiques) :
    - bidon de 20L avec bouchons rouges pour les solvants,
    - bidon de 20L avec bouchons noirs pour les acides ou bases.
  - ne pas remplir le bidon au-dessus du trait,
  - indiquer la composition exacte des effluents liquides,
  - coller une étiquette blanche avec :
    - l'adresse d'HydroSciences Montpellier,
    - la date de sortie du déchet,
    - l'identité du producteur de déchet (labo chimie, salle blanche).

Gestion des déchets

- Déchets souillés :
  - à jeter dans les poubelles avec les sacs noirs (on considère comme souillé tout contenant vide et matériau ayant été en contact avec des produits chimiques et échantillons),
  - aucun déchet de laboratoire (tube/gant/papiers) ne doit être jeté dans les poubelles de bureau et poubelles avec sacs transparents,
  - les gants utilisés dans les laboratoires doivent être jetés dans les déchets souillés (sauf si manipulation d'échantillons à risques infectieux),
  - le verre souillé est jeté dans les poubelles à verre vertes des laboratoires (labo central et lavage flacon), lorsque les poubelles verres souillés sont pleines, il faut transférer le sac dans un carton avant évacuation,
  - une étiquette rouge doit être apposée sur les déchets souillés (solides et verre),
  - une étiquette blanche doit être apposée avec :
    - L'adresse d'HydroSciences Montpellier,
    - La date de sortie du déchet,
    - L'identité du producteur de déchet (labo chimie, salle blanche).

Gestion des déchets

- Déchets infectieux :
  - les produits infectieux doivent être jetés dans les cartons jaunes (DASRI),
  - une étiquette blanche doit être apposée avec :
    - l'adresse d'HydroSciences Montpellier,
    - la date de fermeture du carton,
    - l'identité du producteur de déchet (labo chimie, salle blanche).

Utilisation du matériel de laboratoire

Utilisation des pipettes automatiques

- ne pas poser les pipettes automatiques à l'horizontale sur les paillasses et ne pas retourner les pipettes,
- vérifier la justesse des pipettes avant de vous en servir,
- réglage du volume :
  - pipettes de marques THERMO SCIENTIFIC et EPPENDORF : Tournez la bague de réglage du volume pour modifier le volume. Les chiffres de l'affichage du volume se lisent de haut en bas. Les positions après la virgule se trouvent sous le tiret. Le volume est affiché en µl.
  - pipettes de marque STARLAB : Tirer la bague de réglage vers le haut. Tournez la bague de réglage du volume pour modifier le volume. Pousser la bague de réglage vers le bas pour bloquer le volume. Les chiffres de l'affichage du volume se lisent de haut en bas. Les positions après la virgule se trouvent sous le tiret. Le volume est affiché en µl.

Utilisation des pipettes automatiques

Cliquer sur l'image pour lancer la vidéo

Utilisation des pipettes automatiques

- **utilisation des pointes de pipette :**
  - la pipette ne fonctionne qu'avec une pointe de pipette que l'on peut glisser à la main ou collecter directement dans son emballage.

- **prélèvement du liquide :**
  - pressez le bouton de dosage jusqu'à la première butée,
  - plongez la pointe de pipette verticalement dans le liquide,
  - prélevez le liquide en relevant lentement le bouton de dosage.
  - conservez la profondeur d'immersion pour empêcher l'aspiration d'air par inadvertance,
  - retirez lentement la pointe du liquide,
  - effleurez lentement le bord du tube de la pointe afin d'éliminer tout reste de liquide sur la pointe.

- **distribution de liquide :**
  - posez la pointe de manière inclinée sur le récipient,
  - appuyez sur le bouton de dosage lentement jusqu'au premier arrêt et attendez jusqu'à ce qu'il ne s'écoule plus de liquide,
  - appuyez sur le bouton de dosage pour vider complétement la pointe jusqu'au deuxième arrêt,
  - maintenez le bouton de dosage appuyé et glissez la pointe sur la paroi du récipient,
  - faites remonter le bouton de dosage à l'extérieur du récipient,
  - Pour éjecter la pointe, appuyez sur l'éjecteur.

Utilisation des balances

- vérifier que la balance est bien positionnée sur une surface plane,
- vérifier que la balance est bien de niveau (bulle centrée dans le rond). Si ce n'est pas le cas, tourner les différentes roulettes (pieds) de la balance pour centrer la bulle dans le rond,
- vérifier la propreté de la balance avant utilisation. Si nécessaire la nettoyer à l'aide du pinceau puis d'un papier KIMTECH humide,
- nettoyer les balances après chaque utilisation à l'aide du pinceau puis d'un papier KIMTECH humide,
- pour les balances PRECISA, effectuer une calibration interne tous les matins :
  - en appuyant sur T jusqu'à ce que CAL clignote sur l'écran.

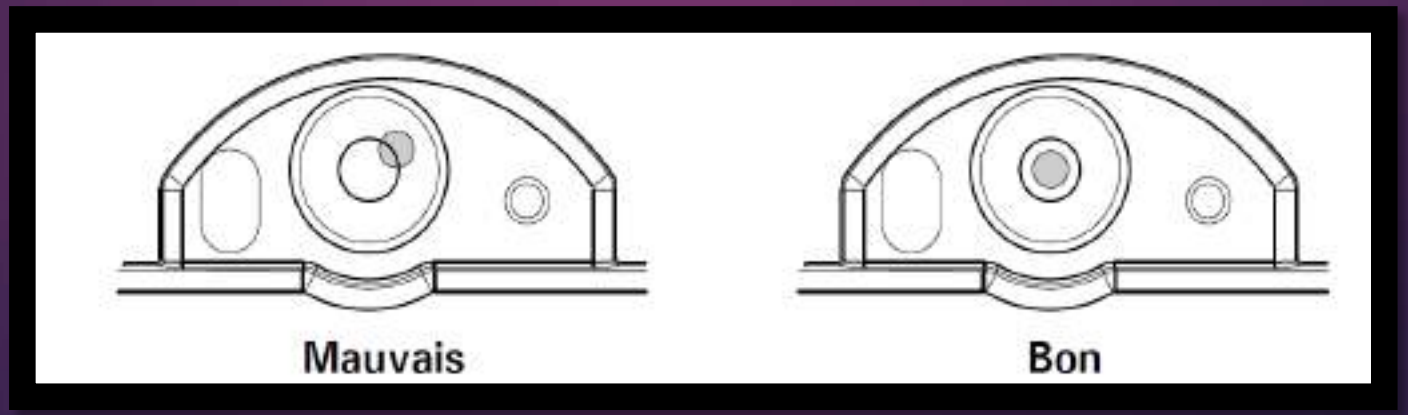

Utilisation de l'eau MilliQ

- avant toute utilisation, vérifier la qualité de l'eau ultrapure (18,2 mΩ/cm) et le niveau de remplissage de la cuve grise (barres bleue pleines sur l'afficheur du pistolet) :
- vérifier qu'aucun message d'alerte ou d'alarme n'apparaît,
- vérifier que personne n'utilise l'appareil d'eau MilliQ dans la salle blanche,
- laisser couler l'eau durant quelques minutes le matin avant la première utilisation,
- soutirer de l'eau en utilisant soit le bouton poussoir au-dessus du pistolet soit la pédale de soutirage par terre,
- **toujours laisser au minimum une barre bleue remplie,**
- pour utiliser le compteur : programmer le volume souhaité avec les + et le – sur l'affichage du pistolet puis appuyer sur la touche "éprouvette".

Consignes spéciales Salle Blanche

Définition Salle Blanche

"Salle dans laquelle la concentration des particules en suspension dans l'air est maîtrisée et qui est construite et utilisée de façon à minimiser l'introduction, la production et la rétention de particules à l'intérieur de la pièce, et dans laquelle d'autres paramètres pertinents, tels que la température, l'humidité et la pression sont maîtrisés comme il convient". (Définition extraite de l'ISO 14644).

- air ambiant filtré de façon à éliminer le plus possible de particules (Filtre HEPA),
- système de filtration de l'eau de ville produisant de l'eau milliQ (eau ultrapure) à 18,2 MΩ,
- température et humidité contrôlées,
- pression positive par rapport à l'extérieur.

Le laboratoire HydroSciences est équipé d'une salle blanche de Classe 10 000 (ISO 7).

Un environnement est dit de classe 10 000 si l'air ambiant contient moins de 10 000 particules de taille supérieure à 0.5 µm par pied cube (335 000 particules de taille supérieure à 0.5 µm par m^3).

Horaires d'accès

Responsable Salle Blanche : Mylène Marie

Suppléants (en cas d'absence) : Rémi Freydier, Sophie Delpoux

08h30 – 17h30

Uniquement accessible selon les consignes du référent et en présence d'au moins un permanent des labos!

Le travail isolé est interdit !!!

Après 17H30 :

Fermeture de la salle blanche que les manips soient finies ou pas*

* Pour certaines manips extrêmement longues, possibilité de rester plus tard si la manip était prévue à l'avance et qu'un des encadrants est présent jusqu'à la fin.

Conditions d'accès

- attendre au moins 30 min après avoir fumé pour rentrer en salle blanche,
- éviter de travailler en salle blanche si vous êtes malade,
- l'introduction de matériel en salle blanche nécessite l'accord du responsable. Ce matériel devra être nettoyé à l'éthanol avant d'être introduit dans la salle blanche :
  - tout objet (outils, appareils, boîtes d'échantillons, etc.) devant être introduit en salle blanche sera soigneusement nettoyé au préalable. On utilisera tous les moyens nécessaires (éthanol et/ou eau MQ) pour effectuer un nettoyage en profondeur avant d'entrer dans le SAS,
  - si un sac de plastique scellé doit être ouvert, cette opération sera effectuée dans le SAS et non pas dans la salle blanche, en évitant de déchirer le sac afin d'éviter l'émission de particules de plastique.

Rappel : Couleur = pigment = métaux !!!

Objets permis et interdits en salle blanche

- dans le but de limiter le dégagement de particules et les risques de contamination, il est interdit d'amener en salle blanche :
  - nourritures, boissons, chewing-gums,
  - papier ordinaire, bois ou carton non recouvert d'une pellicule de protection,
  - crayon à papier,
  - matériel électronique (y compris téléphone portable),
  - matériel métallique.

- il faut limiter au maximum d'entrer avec :
  - maquillage, mascara, poudres ou parfums,
  - bijoux, montres,
  - vêtements pelucheux,
  - pantacourt, short, jupe, robe (il faut porter des vêtements qui couvrent le plus de peau possible).

Entrée et Sortie de salle blanche

- l'entrée en salle blanche se fait en deux étapes :
  - l'entrée dans le SAS (bien passer sur le tapis capteur de poussière à l'entrée),
  - le passage du SAS en salle blanche (bien passer sur le tapis adhésif capteur de poussière).

- ne pas oublier de :
  - **ne pas ouvrir les deux portes du SAS en même temps,**
  - vérifier la bonne fermeture d'une porte avant l'ouverture de l'autre,
  - changer le tapis adhésif du SAS dès que celui-ci est sale,
  - ne rien rentrer en salle blanche sans l'accord du responsable,
  - penser à refermer les hottes et à éteindre les lumières lorsque vous sortez de la salle blanche.

Entrée et Sortie de salle blanche

- dans la salle ICP :
  - enlever vos chaussures (possibilité d'enfiler des sur-chaussures si pas de chaussettes),
  - enlever les bijoux, montres, objets personnels (téléphone, clefs…) et les entreposer dans le meuble à tiroir vert.

- dans le SAS :
  - mettre les **lunettes** ou les **sur-lunettes de sécurité,**

  - mettre la **blouse spéciale salle blanche** et les **sabots** (avec des chaussettes ou sur-chaussures),

  - mettre le **couvre cheveux blanc** (si vous avez les cheveux longs) ou/et la **capuche,**

  - mettre les **gants nitrile "spécial salle blanche"** en mettant les manches de la blouse à l'intérieur des gants.

Méthode de travail Salle Blanche

- laisser la salle blanche dans l'état où vous aimeriez la trouver vous-même,
- signaler à la personne responsable tout défaut de fonctionnement et panne : ne pas faire d'intervention personnelle sur les appareils,
- indiquer sur l'ardoise se trouvant dans le passe-plat, le matériel manquant et penser à le remplacer dès votre sortie de la salle blanche,
- remettre dans le passe-plat les portoirs de tube que vous sortez,
- ne pas éparpiller ses affaires et tout ranger une fois votre travail terminé,
- ne pas entreposer de matériel sous les hottes,
- nettoyer son poste de travail avant et après utilisation,
- sortir et remplacer les poubelles et bidons de récupération lorsqu'ils sont pleins,
- écrire sur le cahier de laboratoire de la salle blanche toutes les manipulations et pesées effectuées,
- ranger les différents cahiers de labo, blocs notes et papiers dans le tiroir.

Méthode de travail Salle Blanche

- utiliser uniquement des récipients téflonnés (PFA) pour conserver des solutions "propres",
- ne pas pipeter directement dans les pissettes ou compte-gouttes, ni dans les solutions mères et matériaux certifiés,
- ne pas retransvaser le surplus d'une solution/poudre dans son récipient d'origine,
- changer l'eau de la pissette MilliQ avant utilisation,
- bien rincer avec de l'eau MilliQ les récipients et les éprouvettes après usage (rincer au moins 3 fois lors d'utilisation d'acides ou de bases),
- pour les filtrations en salle blanche, ne pas oublier de bien rincer les unités de filtration à l'eau MilliQ et utiliser des filtres et pinces décontaminés,

Attention : ne pas utiliser l'unité de filtration dédiée au $NaBH_4$ pour la filtration d'échantillons.

- ne pas utiliser le matériel avec les gants souillés par l'acide.

Méthode de travail Salle Blanche

- vérifier le bon fonctionnement des hottes avant de débuter vos manipulations,
- lors de la manipulation d'acides concentrés sous la hotte d'aspiration, vérifier que l'aspiration est en marche.

- Utilisation des boîtes à évaporation :
  - **penser à allumer la soufflerie (interrupteur au-dessus des boîtes à évaporation, niveau 2 en partant du haut) lors de l'utilisation des boîtes à évaporation,**
  - **penser à éteindre la soufflerie (interrupteur au-dessus des boîtes à évaporation) avant d'ouvrir les boîtes à évaporation.**

L'allumage de la soufflerie va permettre d'éviter :

- la recondensation de l'acide évaporé dans les boîtes,
- la contamination croisée des échantillons,
- d'abimer et de corroder les plaques chauffantes et le revêtement des boîtes d'évaporation.

Décontamination du matériel en Salle Blanche

- **Consommables neufs à usage unique :**
  - **tubes ICP en polypropylène et bouchons, cônes :**
    - faire tremper dans un pot rempli avec HNO_3 pour analyse (PA) 10% (100mL HNO_3 PA dans 900mL d'eau MilliQ, à adapter en fonction du remplissage du pot) : mettre le pot 24h à l'endroit, puis 24h à l'envers puis bien rincer 3 fois avec de l'eau MilliQ et mettre à sécher avec du papier Kimtech propre dans une boite en plastique.
  - **piluliers et bouteilles :**
    - remplir un peu plus que la moitié avec HNO_3 PA 10%. Laisser les piluliers 24h à l'endroit, puis 24h à l'envers. Bien rincer 3 fois avec de l'eau MilliQ et mettre à sécher avec du papier Kimtech propre dans une boite en plastique.
  - l'acide de lavage (HNO_3 PA 10%) utilisé pour le consommable neuf est réutilisé une fois avant d'être jeté,
  - pensez à noter votre nom, la date et le contenu du pot (HNO_3 10%, 1ère ou 2ème utilisation) sur le couvercle de celui-ci.

Décontamination du matériel en Salle Blanche

- **Matériel de digestion en téflon (tubes micro-onde et Savillex) :**
  - rincer 3 fois les tubes et les bouchons à l'eau MilliQ,
  - inspecter visuellement, si résidus visibles : passage d'un papier Kimtech imbibé d'éthanol et nouveau rinçage 3 fois à l'eau MilliQ,
  - placer les tubes (ouverture vers le haut) dans un Savillex de 500 mL, placer les bouchons sur le dessus,
  - couvrir les tubes avec HNO_3 PA 20% et chauffer sur plaque (100-120°C) pendant minimum 48h,
  - rincer 3 fois à l'eau MilliQ,
  - mettre à sécher avec du papier Kimtech propre dans une boite en plastique.

Nettoyage de la Salle Blanche

- Le nettoyage de la salle blanche doit être réalisé **tous les mois**. Il garantit à chacun un travail dans des conditions propres, limitant les risques de contamination des échantillons.
- Les utilisateurs sont **responsables** du nettoyage de la salle blanche, sur la base du volontariat. Pensez à noter votre nom dans le tableau sur la porte de la salle blanche pour réserver votre tour de ménage puis à indiquer la date à laquelle vous l'avez fait !
  - en cas d'absence de volontaire, un « volontaire » sera désigné d'office ☺.
- Procédure de nettoyage :
  - ne pas intervenir dans une hotte si une manip est en cours ou si du matériel sèche,
  - nettoyer toutes les surfaces planes à l'aide d'un sopalin humidifié avec de l'eau MilliQ + éthanol (paillasses, boîtes d'évaporation (si vide), hottes, dessus et côtés de tous les meubles dessous et à côté des paillasses,…),
  - nettoyage du sol (y compris sous les paillasses) avec de l'eau + éthanol,
  - changer le tapis collant dans le SAS (sauf si changé récemment),
  - passer l'aspirateur sur le tapis à l'entrée du SAS de la Salle Blanche (salle ICP)
- Nettoyage des **blouses et des sabots** à la machine à laver tous les trimestres.
- Nettoyage intégral de la salle blanche **une fois par an**.

Bon séjour parmi nous !

4- Preparação e processamento de amostras no LN2C-CEREGE Laboratoire National des Nucleides Cosmogeniques

A chegada à Aix em Provence para trabalhar no Laboratório CEGERE (Centre Européen De Recherche Et D'enseignement Des Géosciences De L'environnement) em Aix-en-Provence/France se deu no dia 11 de Dezembro de 2021 (após isso seguiram-se agendas até novembro de 2022, trabalhando no HSM e no CEREGE de maneira intermitente), quando foram iniciadas atividades de treinamento no laboratório. Os treinamentos centraram-se em segurança e uso do ácido Fluorídrico (HF) o qual é classificado como muito Tóxico e corrosivo, o que justifica o treinamento para sua utilização. O Ácido fluorídrico é utilizado para corroer a superfície dos grãos de quartzo-alvo a fim de estudar a meia vida do nuclídeo 10Be apenas em seus núcleos não contaminados por Be atmosférico.

Os campos para coletas de amostras para datação de nuclídeos cosmogênicos foram realizados pelo proponente em 2021, resultando em 28 amostras de sedimentos quartzosos em rios (n=22) e cavernas fluviais (n=6), possuindo ~6kg cada. As coletas foram feitas no canal principal do rio Vermelho (n=6) e nos principais tributários: Pedras (n=9); Ventura (n=5); Extrema (n=3); Dores (n=4) e Chumbada (n=1). As amostras foram peneiradas, tendo sido divididas as frações: <0,063mm (para análises de isótopos estáveis); 0,125–0,25 mm e 0,25–1,0 mm (para análises cosmogênicas).

A caracterização das amostras, incluindo tamanho de partícula, forma dos grãos, mineralogia (DRX), teor de MO, composição química, datação por 14C e OSL (solos e sedimentos) está sendo realizada em cooperação com o IG/UnB. As taxas de erosão atuais estão sendo obtidas com runoff plots e monitoramento de carga sólida fluvial pelo grupo de pesquisas. Com o acesso à plataforma tecnológica AETE-ISO (ICP-MS X série 2 Thermo Scientific ICP-MS ICAP) no polo de água meio ambiente e saúde do HSM/Montpellier, garantida pelo Projeto CapesPrint, estão sendo realizados estudos de acúmulo de metais pesados nos sedimentos, com análises de isótopos estáveis Pb, Sr e Nd para investigar a influência do uso agrícola, além de permitir estimar a origem dos sedimentos que atravessam o carste.

A bacia hidrográfica do rio Vermelho (Figura 6) é tributária do rio Corrente e este do Tocantins, possuindo 693,65km2 e um rico sistema fluviocárstico que captura todos os rios a montante. Para o mapeamento geomorfológico, nós utilizamos o Topografical Position Index (TPI) em um grid MDT ALOS PALSAR de 12,5m com utilização de ArcGis 10.6, como descrito por Hussain & Uagoda (2020). A bacia foi dividida em quatro unidades geomorfológicas, sendo duas ligadas ao arenito Urucuia (Terras Altas e Talus) e duas ligadas aos carbonatos do Bambuí (Terrenos Cársticos e Terras Baixas).

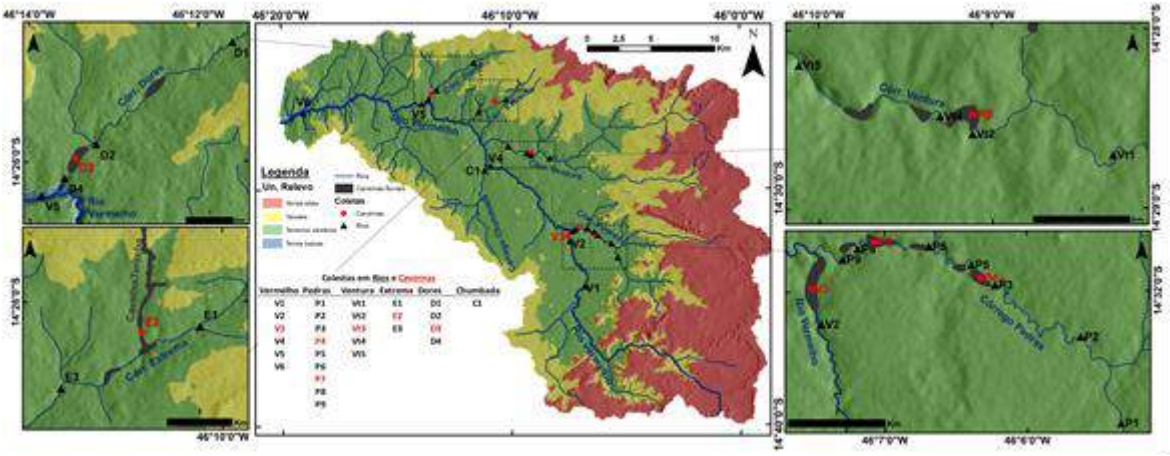

Figura 6. Localização das 28 coletas de sedimentos fluviais em canais abertos e no interior de cavernas fluviocársticas realizadas na bacia do rio Vermelho para essa pesquisa. Amostras da cor preta são em canais e da cor vermelha em cavernas. Os polígonos da cor chumbo mostram a topografia aproximada das cavernas fluviais. As cavernas vadosas nas zonas de recarga (n=132) não são apresentadas nesse mapa.

As amostras começaram a ser preparadas no Laboratório Nacional de Nuclíceos Cosmogênicos, havendo fazes de ataque ácido, dissolução total e cromatografia. Após esses passos as amostras são encaminhadas para o ASTER um acelerador de partículas de fonte 5MV com o objetivo de analisar nuclídeos cosmogênicos radioativos

A base utilizada é o LN2C – Laboratório Nacional de Nuclídeos Cosmogênicos para a preparação das amostras e o laboratório ASTER um acelerador de partículas de fonte 5MV com o objetivo de analisar nuclídeos cosmogênicos radioativos.

Figura 7. Acelerador de Partícula ASTER 5MV.

A preparação das amostras e datações da produção de 10Be in situ em sedimentos transportados em rios e cavernas está sendo realizada em conjunto com a equipe do acelerador de partículas ASTER, no Laboratório Nacional de Nuclídeos Cosmogênicos (LN2C), CEREGE/Marseille, sob supervisão do pesquisador Lionel Siame. A preparação de alvos para a medição de 10Be e 26Al produzidos in situ, em AMS (espectrometria de massas acelerada) segue procedimentos químicos adaptados de Brown et al. (1991) e Merchel e Herpers (1999).

Foi realizada a descontaminação do 10Be atmosférico nos grãos de quartzo carbonatados das cavernas, utilizando uma série de três lixiviações sucessivas em HF concentrado. Cada lixiviação removendo 10% da massa restante da amostra.

Os grãos de quartzo limpos sofrem digestão completa em HF concentrado, depois da adição de 100g de um veículo com (3.025±9)x10-3 g/g de 9Be, extraído de fenaquita minerada em profundidade (MERCHEL et al., 2008). Fumaça fluorídrica e clorídrica está sendo usada para remover fluoretos e acromatografia de troca catiônica e aniônica é utilizada para finalmente isolar Be e Al. Antes das medições 10Be e 26Al AMS no ASTER, óxidos de berílio e alumínio são misturados a nióbio de 325 mesh e pós de prata, respectivamente.

As medições de 10Be são calibradas em relação ao padrão interno STD-11 (10Be/9Be=(1.191±0.013)x10-11), segundo Braucher et al (2015). A razão isotópica 26Al/27Al é medida segundo o padrão interno SM-Al-11, cujo valor de (7.401±0.064)x10-12 tem sido calibrada em relação padrões primários de um escalonamento Round-robin, segundo Merchel & Bremser (2004).

A passagem de sedimentos através do extenso sistema fluviocárstico pode mitigar o acúmulo de NCs. Sendo assim, a amostragem foi orientada a esse problema e as análises estão sendo feitas de forma a estimar se a passagem dos sedimentos pelas cavernas está levando ao esvaziamento da razão 26Al/10Be durante o soterramento dos

5 – Resultados preliminares CEGERE

As amostras foram preparadas quimicamente no Laboratório Nacional de Nuclíceos Cosmogênicos, como já relatado. Após a oxidação dos alvos de 26Al e 10Be pode-se dar entrada no Laboratório ASTER (Foto 1), que contem um acelerador de partículas de fonte 5MV com o objetivo de analisar nuclídeos cosmogênicos radioativos.

Figura 8. Composição do Acelarado ASTER, 5MV

Para poder analisar as amostras no acelerador de partículas foi necessário o passo da "catodagem" onde se coloca cada alvo em um catodo metálico. Essa fase é realizada em laboratório limpo e capela fechada (Figura 9).

Figura 9. Capela limpa para realização da catodagem

As medições de 10Be serão calibradas em relação ao padrão interno STD-11 (10Be/9Be=(1.191±0.013)x10-11), segundo Braucher et al (2015). A razão isotópica 26Al/27Al é medida segundo o padrão interno SM-Al-11, cujo valor de (7.401±0.064)x10-12 tem sido calibrada em relação padrões primários de um escalonamento Round-robin, segundo Merchel & Bremser (2004).

O 10Beatm é produzido a partir de precipitações secas e húmidas sobre as superfícies, na mesma escala temporal do 10Be in situ, migrando no regolito em profundidades que dependem de características do solo como textura e pH (Dixon & Riebe, 2014). Nos solos, essa variedade também dura o bastante para ser medida mesmo que haja retirada de alguns metros de material da superfície, tornando-se um poderoso traçador para processos pedológicos.

Apesar de os nuclídeos cosmogênicos serem usados há duas décadas para medir a erosão de rochas em um período de 103-106 anos, foi só nos últimos anos que a razão 26Al/10Be começou a ser utilizada para medir modificações de longo termo nas paisagens (KNUDSEN & EGHOLM, 2018; STRUCK et al., 2018).

Logo em anexo apresentamos a tabela contendo os dados resultantes da leitura de 26Al e 10Be. Os resultados são preliminares, porém na figura 10 de síntese abaixo pode ser verificado que as taxas de erosão das amostras são determinadas pelas rochas fontes

de cada uma, e não pelo tempo de passagem nas cavernas, informação que está sendo corroborada com a análise de elementos-traço feita no HSM nas mesmas amostras.

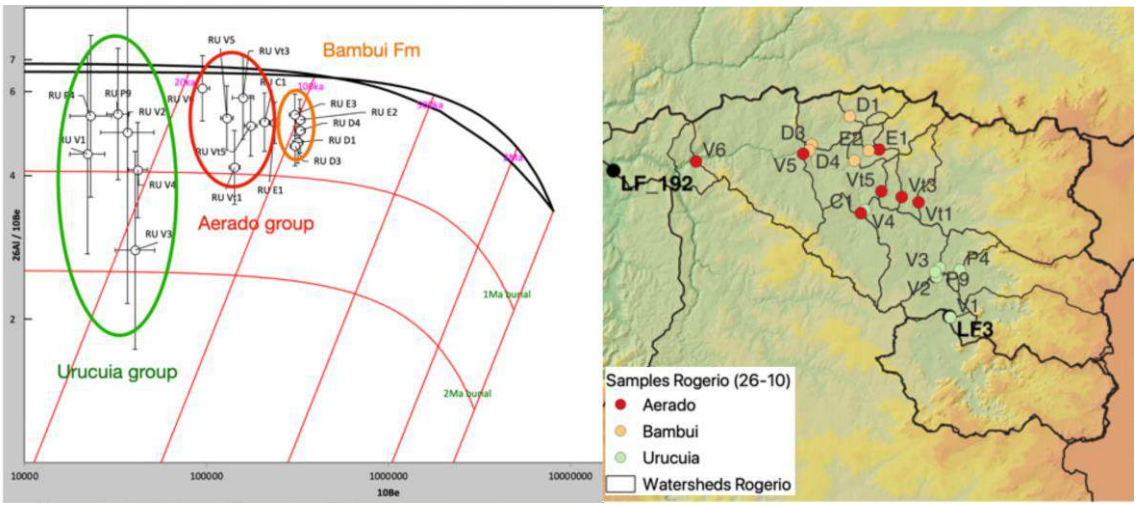

Figura 10. Diferença das taxas de erosão determinadas pela rocha fonte das amostras.

Sample name	Description	Al26/Al27	Total count Al26	Uncertainty Al26/Al27 (%)	N cath/ Ope	Dates	Position	Al26/Al27 machine
Al2O3_Blanc	-- Blanc machine #	**8,75709E-16**	3	57,7446	AKKB	* 15/03/2022 15:54:29 * 16/03/2022 15:21:01 * 17/03/2022 19:24:03	18	8,37726E-16
BK R1	RogerioUagoda_RioV --blanc	**1,87997E-15**	2	76,9137	IIRN	* 16/03/2022 08:37:25 * 17/03/2022 12:30:31 * 18/03/2022 13:22:40	116	1,79843E-15
RU V1	RogerioUagoda_RioV	**5,54033E-14**	27	20,8914	IIRO	* 16/03/2022 08:58:20 * 17/03/2022 12:51:26 * 18/03/2022 13:43:33	117	5,30002E-14
RU V2	RogerioUagoda_RioV	**1,07894E-13**	9	37,1960	IIRP	16/03/2022 09:19:13	118	1,03214E-13
RU V6	RogerioUagoda_RioV	**3,27610E-13**	267	6,2368	IIRQ	* 16/03/2022 09:40:04 * 17/03/2022 13:12:22 * 18/03/2022 14:04:28	119	3,13401E-13
RU Vt3	RogerioUagoda_RioV	**5,42725E-13**	204	7,0800	IIRR	* 16/03/2022 10:00:58 * 17/03/2022 13:33:16	120	5,19185E-13
RU Vt5	RogerioUagoda_RioV	**4,78480E-13**	467	5,9365	IIRS	* 16/03/2022 10:21:54 * 17/03/2022 13:48:31 * 18/03/2022 14:25:20	121	4,57726E-13
RU P1	RogerioUagoda_RioV	**5,16551E-14**	34	23,8453	IIRT	* 16/03/2022 10:42:47 * 17/03/2022 14:09:25 * 18/03/2022 14:46:14	122	4,94146E-14
RU P4	RogerioUagoda_RioV	**7,37801E-14**	89	13,9849	IIRU	* 16/03/2022 11:03:40 * 17/03/2022 14:30:18 * 18/03/2022 15:07:06	123	7,05799E-14
RU P9	RogerioUagoda_RioV	**9,83672E-14**	100	13,9069	IIRV	* 16/03/2022 11:24:34 * 17/03/2022 14:51:12 * 18/03/2022 15:27:57	124	9,41006E-14
RU E2	RogerioUagoda_RioV	**9,35355E-13**	1161	3,6594	IIRW	* 16/03/2022 11:45:30 * 17/03/2022 15:12:06 * 18/03/2022 15:48:49	125	8,94785E-13
RU C1	RogerioUagoda_RioV	**5,95735E-13**	503	6,1204	IIRX	* 16/03/2022 11:57:15 * 17/03/2022 15:27:01 * 18/03/2022 16:09:42	126	5,69895E-13
RU D1	RogerioUagoda_RioV	**8,49229E-13**	1052	3,6101	IIRY	* 16/03/2022 12:18:13 * 17/03/2022 15:47:55 * 18/03/2022 16:30:37	127	8,12394E-13
RU D3	RogerioUagoda_RioV	**7,91061E-13**	1061	3,3381	IIRZ	* 16/03/2022 12:28:23 * 17/03/2022 16:04:20 * 18/03/2022 16:51:30	128	7,56749E-13
RU D4	RogerioUagoda_RioV	**8,49406E-13**	896	4,0848	IISA	* 16/03/2022 12:39:36 * 17/03/2022 16:21:47 * 18/03/2022 17:12:30	129	8,12564E-13
RU E1	RogerioUagoda_RioV	**7,18341E-13**	861	3,5666	IISB	* 16/03/2022 12:52:25 * 17/03/2022 16:42:45 * 18/03/2022 17:33:24	130	6,87184E-13
RU E3	RogerioUagoda_RioV	**9,08708E-13**	1189	3,3430	IISC	* 16/03/2022 13:05:11 * 17/03/2022 17:03:46 * 18/03/2022 17:54:15	131	8,69294E-13
RU V3	RogerioUagoda_RioV	**4,25303E-14**	35	19,6903	IISD	* 16/03/2022 13:14:22 * 17/03/2022 17:17:36 * 18/03/2022 18:15:14	132	4,06856E-14
RU V4	RogerioUagoda_RioV	**7,78785E-14**	112	9,5075	IISE	* 16/03/2022 13:35:18 * 17/03/2022 17:38:32 * 18/03/2022 18:36:07	133	7,45006E-14
RU V5	RogerioUagoda_RioV	**3,76499E-13**	315	6,5162	IISF	* 16/03/2022 13:56:13 * 17/03/2022 17:59:23 * 18/03/2022 18:56:58	134	3,60168E-13
RU Vt1	RogerioUagoda_RioV	**3,43951E-13**	157	8,0716	IISG	* 16/03/2022 14:17:09 * 17/03/2022 18:20:18	135	3,29033E-13
BKR2	RogerioUagoda_RioV --blanc	**0,00000E+00**	0	∞	IISH	* 16/03/2022 14:38:02 * 17/03/2022 18:41:10 * 18/03/2022 19:17:51	136	0,00000E+00

6 Treinamentos laboratoriais no CEREGE

Logo em anexo apresentamos os seguintes documentos relativos ao treinamento realizado no mês de Dezembro de 2021.

1- Capa dos tres cursos de segurança atendidos.
2- Comprovante de finalização dos cursos de segurança
3- Livret d'accueil des visiteurs – LN2C
4- Sensibilisation à l'utilisation d'acide fluorhydrique
5- protocolo de preparação de amostras

NEO : Course ended

Administrateur NEO (via neo.cnrs.fr) <noreply@neo.cnrs.fr>

Ter, 04/01/2022 18:35

Para: Rogerio Elias Soares Uagoda <rogeriouagoda@unb.br>

Hi,

Congratulations, you have successfully completed your training programme on the NEO platform. Your NEO administrator has also received this email so that they can send you your training certificate.

Best regards,

Your NEO administrator.

SENSIBILISATION À L'UTILISATION D'ACIDE FLUORHYDRIQUE

Jean-Marie BERNARD – Responsable DHSE Campus Etoile

Cathy COXE – Fédération Sciences Chimiques de Marseille

Dr Amélie CHAMPARNAUD – Médecin de prévention AMU

SOMMAIRE

Présentation

Exemples accidents

Règlementation générale et spécifique

Prévention

Premiers soins et secours

Stockage / transport

Présentation

Principales utilisations de l'acide fluorhydrique:

- La fabrication de composés organiques fluorés ;
- La fabrication de fluorures inorganiques ;
- L'industrie pétrolière (catalyseur d'alkylation).

L'acide fluorhydrique, par rapport aux principaux acides, est un cas particulier car les brûlures occasionnées imposent des mesures thérapeutiques immédiates et adaptées

Quelques accidents en France et dans le monde

- **Plusieurs cas d'accidents avec du HF dans l'industrie**

COREE DU SUD – GUMI – 2012 :
Rejet de 8 T d'HF dans l'atmosphère :

- 5 morts / plus de 4000 intoxiqués
- 3 900 têtes de bétail abattus
- Dégâts estimés à 15 millions d'euros

- **Des accidents avec du HF dans la Recherche en France :**

Toulouse 2011 dans un laboratoire de recherche en biologie :
Perçage d'un circuit fermé réfrigéré avec déversement 2 L HF 50% au 1er étage

- Une flaque de 2m² a été neutralisé par les pompiers au niveau du RDC (pas de victime)

Montlucon 2002 :
Explosion d'un bouteille de 10L HF en TP Chimie

- Une dizaine de personnes sérieusement intoxiqués

Règles générales de prévention

Les règles de prévention du risque chimique se répartissent en plusieurs sections regroupant :

- les **règles générales de prévention** des risques dus aux **agents chimiques dangereux** (articles R. 4412-1 à R. 4412-57),
- les règles particulières aux **agents chimiques dangereux** définis réglementairement comme **cancérogènes, mutagènes ou toxiques pour la reproduction** (CMR) (articles R. 4412-59 à R. 4412-93),
- les règles spécifiques aux **activités pouvant exposer à l'amiante** (articles R. 4412-97 à R. 4412-148),
- les **valeurs limites d'exposition professionnelle** (VLEP) et des valeurs limites biologiques pour certains agents chimiques (articles R. 4412-149 à R. 4412-152),
- les règles visant la **silice cristalline** et le **plomb** et ses composés (articles R. 4412-149 à R. 4412-160).

Règles générales de prévention

- **Évaluation des risques**

(articles R. 4412-5 à R. 4412-10 du Code du travail)

- **Risque évalué comme faible**

(article R. 4412-13)

- **Mesures techniques et organisationnelles**

(articles R. 4412-11 à R. 4412-22 du Code du travail)

- **Information et formation des travailleurs**

(article R. 4412-38 et R. 4412-39 du Code du travail)

- **Mesures en cas d'accident ou d'incident**

(articles R. 4412-33 à R. 4412-37 du Code du travail)

- **Mesures d'hygiène**

(article R. 4412-20 du Code du travail)

- **Vérification des installations**

(articles R. 4412-27 à R. 4412-32 du Code du travail)

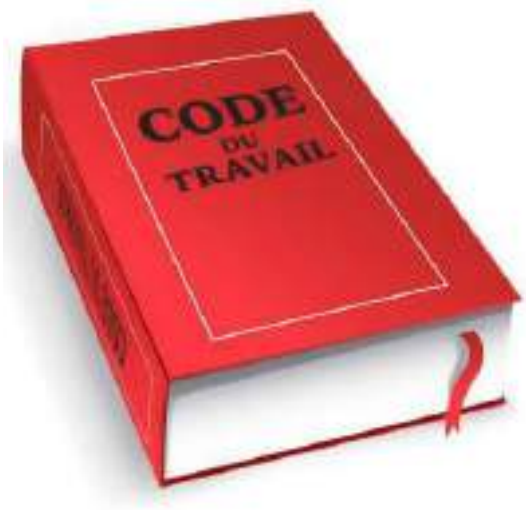

Quelques données sur le HF

- **<u>Interdiction de manipuler cette acide :</u>**
  - les mineurs, les travailleurs en travail temporaire, les travailleurs en CDD et pour des personnes ayant des contre-indications médicales particulières

- **Classement et étiquetage :**

Il est classé très toxique et corrosif.

H300+H310+H330 Mortel par ingestion, par contact cutané ou par inhalation
H314 Provoque des brûlures de la peau et de graves lésions des yeux

- **Valeurs limites d'exposition**

Des **valeurs limites d'exposition professionnelle contraignantes dans l'air** des locaux de travail ont été établies en France pour le fluorure d'hydrogène (art. R. 4412-149 du Code du travail) (voir tableau ci-dessous).

VLEP / PAYS	Moyenne pondérée sur 8 heures		Court terme (15 minutes au maximum)	
	ppm	mg/m³	ppm	mg/m³
France (VLEP contraignante - 2007)	1,8	1,5	3	2,5
Union européenne (2000)	1,8	1,5	3	2,5
États-Unis (ACGIH - 2005)	0,5	–	2(*)	–
Allemagne	1	0,83	–	–

(*) TLV-C = valeur limite plafond

Principe de prévention appliqué à l'HF

- Connaître le produit que l'on manipule
- Consulter la fiche de données sécurité **FDS** (le risque n'est pas le même en fonction de la concentration…)
- Connaître son environnement de travail

Evaluation des Risques

- Principe de substitution (le remplacer si possible)
- Locaux de manipulation ventilés (travail sous sorbonne)
- Stockage en faible quantité (prévoir les besoins en amont) dans des locaux ventilés à l'abri de l'humidité et de la chaleur et dans contenant inerte (pas de verre)
- Etiquetage obligatoire sur le produit, affichage à l'entrée de la salle et au poste de travail
- Le matériel électrique conforme à la règlementation en vigueur etrésistant à la corrosion.

Principe de prévention médicale

- Elle est définit par le **médecin de prévention / médecin du travail**

- Formation de Secouristes Sauveteur au Travail **SST**
  - Liste avec coordonnées bien visible dans les différents services du laboratoire

- Affichage clair des numéros de téléphone indispensables: SAMU, pompiers, centre antipoison, …

- Trousse de secours spécifique au risque HF

(voir liste plus loin dans la présentation – diapo 25)

Equipements de Protections Collectives : la sorbonne

Schéma de fonctionnement

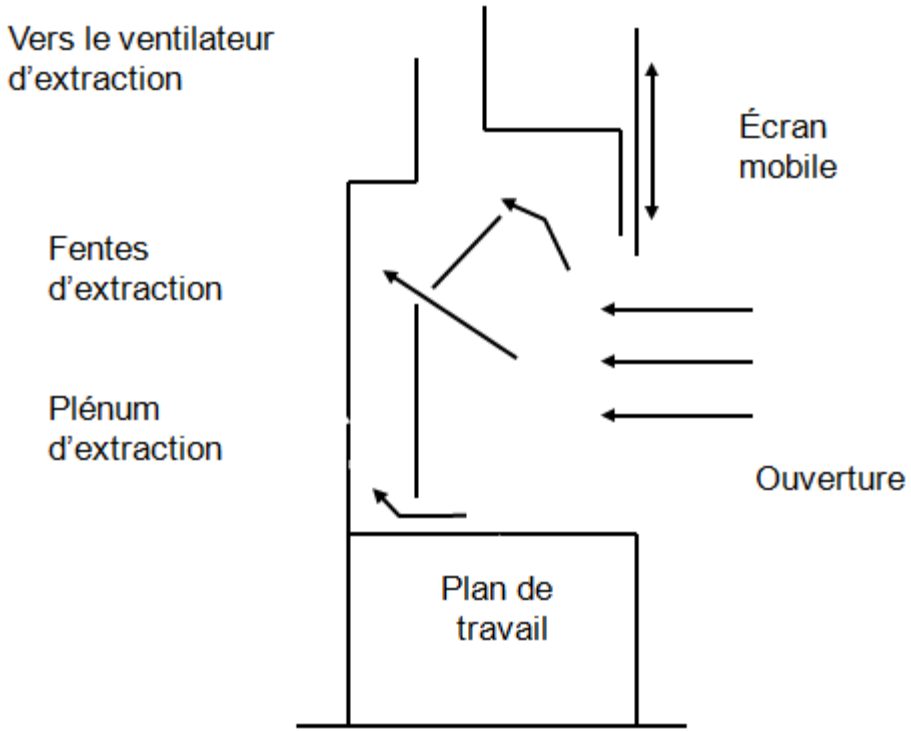

NF X 15-203 : spécifications
NF X 15-206 : méthodes d'essai de conformité

La sorbonne protège le manipulateur et l'environnement de travail

Vérifications périodiques obligatoires

Equipements de Protections Collectives : la sorbonne

Anticipation et organisation

- Préparer sa manipulation
- Limiter les quantités manipulées et les sources chaudes

Encombrement

- Travailler avec un encombrement du volume le plus faible possible

Zone de travail

- Ajuster la hauteur de la vitre en fonction de la manipulation avec une hauteur max de 40 cm
- Manipuler à une distance de 15-20 cm du plan d'ouverture
- En l'absence du manipulateur toujours baisser la vitre !

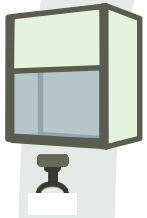

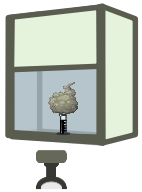

Dégagement de polluants

- Maintenir les contenants fermés
- En cas de dégagement de polluant maintenir la vitre fermée !

Posture

- Adopter une posture en adéquation avec la sécurité au poste de travail (gestes calmes, éviter les sorties et entrées de bras …….)

Environnement de travail

- Ne pas modifier la conception de la Sorbonne
- Ne pas obstruer les entrées de compensation d'air
- Respecter l'environnement aérologique de la pièce

GU-DHSE-7

Equipements de Protections Individuelles EPI

Marquage CE : apposé par le fabricant sur chaque exemplaire d'EPI, de manière distincte, lisible et indélébile et attestant de la conformité du produit aux dispositions de la directive qui lui sont applicables.

Marquage de conformité aux normes : EN et NF

- équipement de protection individuelle construit ou fabriqué conformément aux normes européennes harmonisées,
- équipement présumé répondre aux exigences relatives aux règles techniques applicables traitées par ces normes.

Dans les autres cas de normes homologuées ci-dessus, un décret peut rendre ces normes obligatoires.

Equipements de Protections Individuelles EPI

100% coton ou Mixte coton / polyester

Norme	Exemples	Performances requises
Type 6 NF EN 13034	Pétrochimie. Laboratoires. Industrie chimique. Milieux agricoles, risques phytosanitaires.	Protection limitée dans le temps contre les éclaboussures de produits chimiques liquides.
Type 5 NF EN 13982	Désamiantage. Milieux agricoles lors des opérations de poudrage.	Protection contre les produits chimiques solides, particules en suspension dans l'air. Équipement complètement étanche.
Type 4 NF EN 14605	Industrie chimique. Milieux agricoles, risques phytosanitaires lors des opérations de faibles pulvérisations.	Protection contre les produits chimiques liquides sous forme d'une pulvérisation. Le liquide ruisselle sur vêtement.
Type 3 NF EN 14605	Industrie chimique où les risques d'être en contact avec un produit chimique sont élevés.	Protection contre les produits chimiques liquides sous forme de jet. Projection violente de produit chimique liquide.
Type 2 NF EN 943-1	Industrie chimique : scaphandre chimique.	Protection complète du corps et des voix respiratoires contre les produits chimiques liquides et gazeux. Tenue non étanche aux gaz, à air respirable assurant une pression positive.
Type 1 NF EN 943-1 NF EN 943-2	Scaphandre chimique pour industrie chimique ou les équipes de secours. Intervention des premiers secours.	Protection complète du corps et des voix respiratoires contre les produits chimiques liquides et gazeux. Tenue étanche aux gaz.

Pictogramme :

Ces vêtements sont identifiés par le pictogramme suivant, associé au type de protection :

Type 3

Equipements de Protections Individuelles EPI

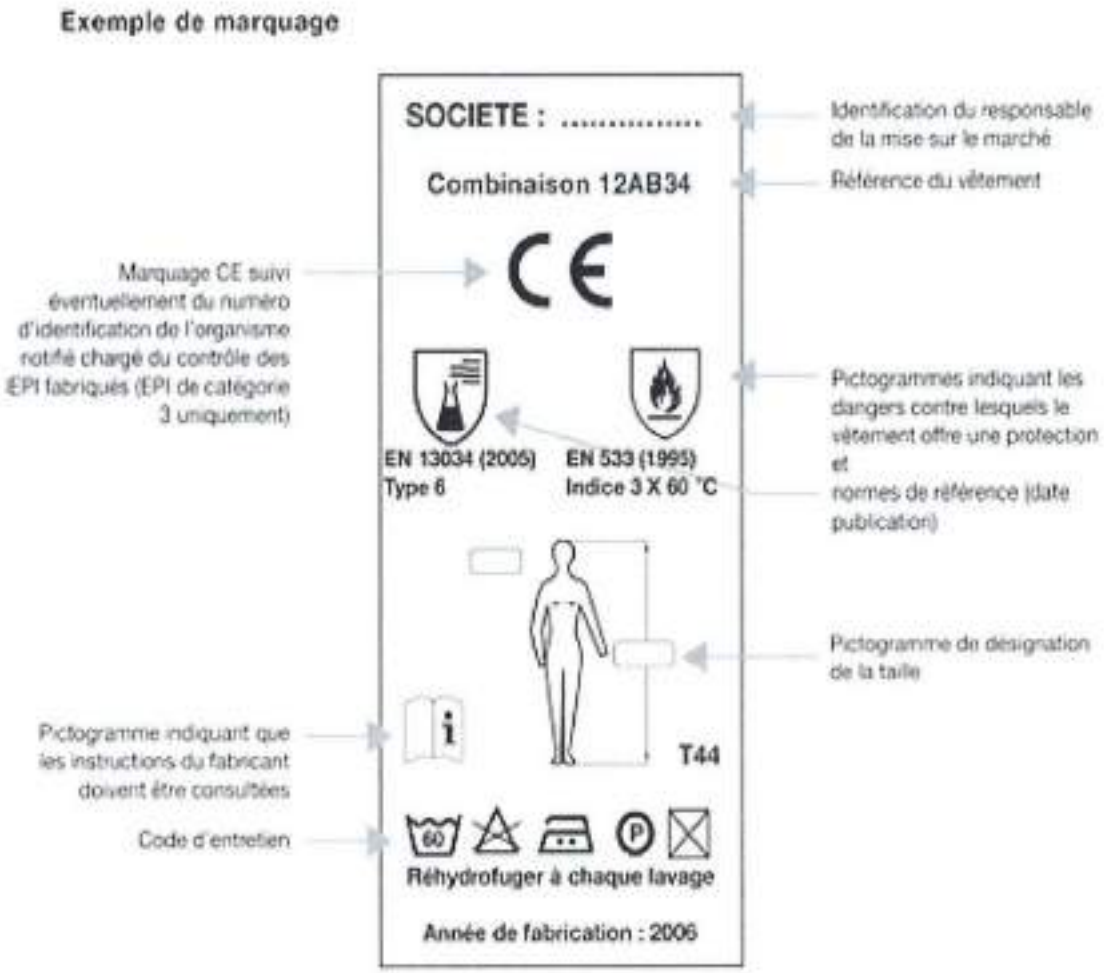

Equipements de Protections Individuelles EPI

- Gants de protection contre le risque chimique caractérisés par :
  - **EPAISSEUR :** jetables (< à 0,2 mm) et réutilisables
  - **FORME :** longueurs de manchette différentes
  - **MATIERE :** matière plastique, états de surface (lisses, reliefs…)

- Critères de résistance :
  - **La Dégradation :** transformation des propriétés physiques du gant (gonflement, durcissement, craquelure…)
  - **La Pénétration :** passage d'un produit chimique à travers les imperfections du matériau ou les porosités et les joints du gant.
  - **La Perméation :** diffusion à l'échelle moléculaire d'un produit chimique à travers le matériau qui constitue le gant.

Equipements de Protections Individuelles EPI

Protection chimique

EN ISO374-1/TYPE C

- Résistance à l'étanchéité
- Temps de perméation ≥ 10 min pour au moins 1 produit chimique de la nouvelle liste

EN ISO374-1/TYPE B

ABC

- Résistance à l'étanchéité
- Temps de perméation ≥ 30 min pour au moins 3 produits chimiques de la nouvelle liste

EN ISO374-1/TYPE A

ABCDEF

- Résistance à l'étanchéité
- Temps de perméation ≥ 30 min pour au moins 6 produits chimiques de la nouvelle liste

Peu résistant aux produits chimiques

Aucun matériau ne résiste de façon permanente à un produit !
Aucun matériau ne résiste à tous les produits !

Equipements de Protections Individuelles EPI

Latex naturel

Caoutchouc naturel (hévéa) : la plus élastique des substances connues

+ Bonne résistance à l'usure, aux déchirures ainsi qu'à tous les produits solubles dans l'eau et dilués

Existe aussi en gants jetables

- Mauvaise résistance aux produits huileux, graisseux et aux hydrocarbures

Peut être à l'origine de manifestations allergiques

Néoprène ®

Caoutchouc synthétique à base de polychloroprène

+ Résiste bien aux acides et bases forts

- Résistance mécanique moyenne

Ne résiste pas aux solvants aromatiques ou chlorés

Nitrile

Caoutchouc synthétique (copolymère acrylonitrile-butadiène ou NBR)

+ Bonne résistance mécanique ; résistance chimique large (huiles, graisses, alcools, produits pétroliers...)

Existe aussi en gants jetables

- Faible résistance aux cétones et produits halogénés (chlorés, fluorés...)

PVC

(Polychlorure de vinyle) Polymère synthétique à base de chlorure de vinyle Appelé aussi « Vinyle »

+ Résistance correcte aux acides, bases, alcools

Coût modéré

Existe aussi en gants jetables

- Faible résistance aux cétones, aldéhydes, hydrocarbures aromatiques ou halogénés

PVA

(Polyalcool de vinyle) Polymère synthétique à base d'alcool vinylique

+ Excellente résistance à de nombreux hydrocarbures (aliphatiques, aromatiques, chlorés...), aux esters et cétones

- Dégradation au contact de l'eau

Coût élevé

Matériaux fluorés

Matériaux synthétiques par exemple de marque Viton® ou Téflon®

+ Bonne résistance à de nombreux produits y compris au benzène et aux PCB

- Résistance réduite aux coupures et à l'abrasion

Coût élevé

Butyle

Caoutchouc synthétique (copolymère isobutylène-isoprène)

+ Résistance élevée aux acides forts, aux cétones, aux esters, aux éthers de glycol, amines, aldéhydes...

- Faible résistance aux hydrocarbures aliphatiques, aromatiques, halogénés...

Coût élevé

Matériaux multicouches

Laminé multicouches de polyéthylène et de copolymères éthylène-alcool vinylique, marques 4H®, Barrier®, Silver Shield®

+ Excellente résistance à la plupart des produits chimiques

- Manque de dextérité

Faible résistance mécanique

Equipements de Protections Individuelles EPI

Norme EN 166

Lunettes à branches et à coques latérale

Lunettes Masques

Écrans faciaux

Les bonnes pratiques de prévention

- Réaliser l'évaluation du risque et la consigner dans le document unique
- Consulter les FDS des produits utilisés
- Écrire les protocoles détaillés des manipulations, pour identifier tous les risques associés et les déchets
- Faire une analyse de risque pour toute nouvelle manipulation
- Remplir sa fiche individuelle d'exposition chaque année
- Tenir à jour une base de données répertoriant tous les produits détenus par le laboratoire (utiliser le numéro CAS)

Les mécanismes de pénétration

Mécanisme d'action des acides :

- déshydratation,
- coagulation des protéines,
- réaction exothermique.

La gravité dépend de :

- la nature,
- la quantité,
- la concentration,
- la durée du contact,
- l'étendue et la localisation.

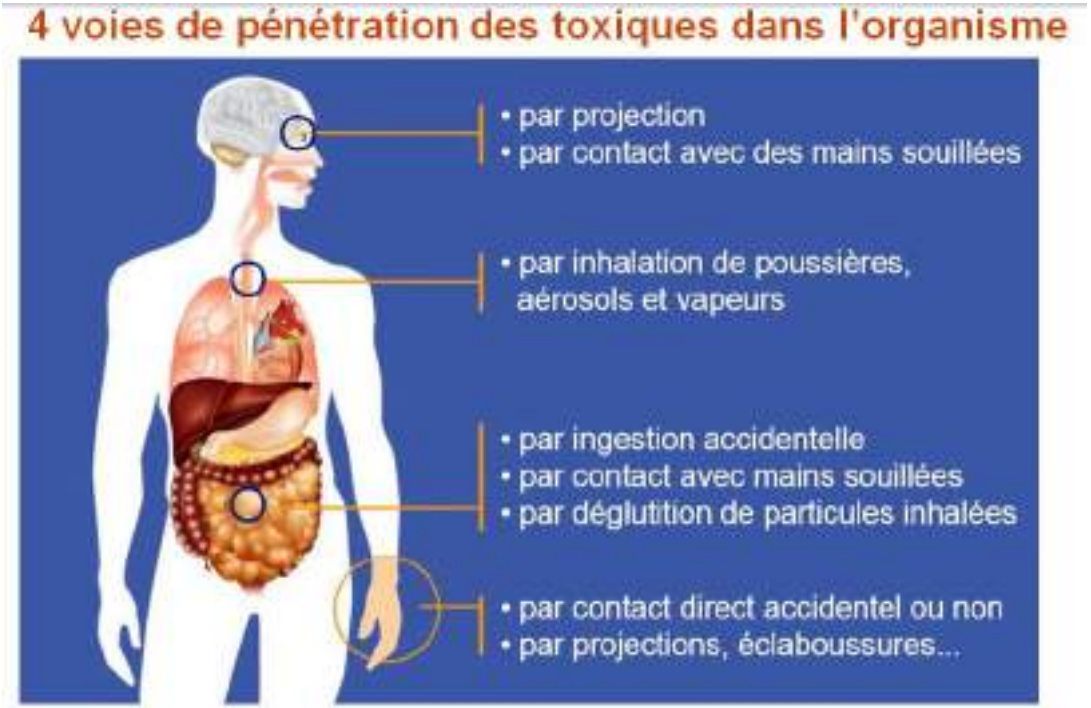

Brûlure chimique

Mécanisme spécifique de l'acide fluorhydrique ➔ Double action :

- corrosive,
- toxique : liée à l'ion Fluor qui se lie au Calcium

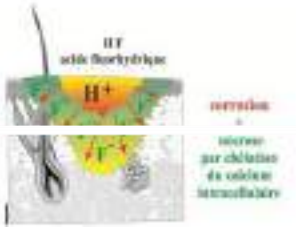

Brûlure par acide Fluorhydrique ➔ Evolution en 2 temps :

- période de latence indolore
- brûlure profonde ➔ douleur ++.

Projection sur la peau : pénétration rapide, surtout après franchissement de la peau : destruction des tissus et atteinte des os sous jacents.

Projection dans les yeux : brûlure grave et risque de cécité

Inhalation : détresse respiratoire avec œdème pulmonaire d'installation progressive ou retardée

Absorption digestive : brûlure grave et atteinte générale, en particulier cardiaque par baisse du calcium sanguin

Exemples de brulures

Cas n° 1 – Contact avec de l'acide fluorhydrique 70% (juste après contact)

Cas n° 1 - Acide fluorhydrique 70% à J+4 après excision et décharges.

Cas n° 2 - Manipulation robinet à mains nues - Initial

Premiers secours

Projection sur la peau

- Enlever les vêtements souillés, en portant des gants appropriés, sans contaminer d'autres parties du corps,
- laver à grande eau 15 mn. Le pronostic dépend de la précocité et de l'abondance du lavage,
- appliquer :
  - du gel de gluconate de calcium à 2,5% en couche épaisse,
  - OU
  - des compresses bien imprégnées de gluconate de calcium à 2,5 % en ampoule,
- facteur de gravité : surface corporelle contaminée supérieure à 3 % (1 % = surface de la main doigts compris).

Projection dans les yeux

- Laver immédiatement à l'eau, en écartant bien les paupières, au lave-œil ou à l'eau d'un robinet,
- veiller à ne pas contaminer l'œil non touché (à l'eau du robinet, positionner la tête pour placer l'œil à laver en bas),
- ne pas utiliser de collyre.

Inhalation

- Dégager la victime en se protégeant soi-même,
- appeler immédiatement le 15.

Ingestion

- Ne pas faire vomir ni manger ou boire,
- appeler immédiatement le 15

Premiers secours

DANS TOUS LES CAS PRENDRE UN AVIS SPÉCIALISÉ
AU CENTRE DES GRANDS BRÛLÉS – Hôpital de la Conception
En appelant le médecin de garde au 04 91 43 58 18

- Appeler le 15 pendant les premiers soins en cas de projection cutanée, même si la brûlure paraît minime ou indolore, et en cas de projection oculaire,
- Appeler immédiatement le 15 en cas d'inhalation, d'ingestion ou de projection cutanée sur une surface étendue (3 %) et faire intervenir immédiatement un sauveteur secouriste du travail,
- Fournir aux secours la FDS et/ou l'étiquette (elle renseigne sur la concentration) et cette fiche CAT.

CONNAÎTRE LE LIEU DE STOCKAGE DU GLUCONATE DE CALCIUM QUAND ON MANIPULE DE L'ACIDE FLUORHYDRIQUE

Composition de la trousse de premiers secours

- Gel de Gluconate de Calcium 2,5 %,
- Ampoule de Gluconate de Calcium 2,5 % buvable (arrêt de la commercialisation),
- Gants en néoprène : à utiliser pour aider la victime à enlever ses vêtements si besoin,
- Compresses :
  - Pour appliquer la solution de gluconate de calcium (plusieurs compresses bien imprégnées)
  - Pour couvrir après application du gel,
- Bande Nylex pour fixer les compresses.

A proximité de la trousse de secours : masque adapté pour intervention si atmosphère contaminée dans une pièce.

Premiers secours

En cas d'inhalation

Soustraire très rapidement la victime à l'atmosphère toxique avec la protection respiratoire adaptée

En cas de contact avec la peau ou les yeux

Se rincer abondamment pendant 15 min

De l’incident à l’accident grave

Des incidents sur le site doivent nous alerter sur les dangers du stockage et de transport de produits chimiques :

- Erreur d’identification des déchets
- Perte de confinement lors du transport jusqu’au magasin (cas du HF)

Les bonnes pratiques de stockage et de tri

Bidons et jerricans

- Résidus de manipulation,
- Code couleur différent selon les prestataires.

Seaux

- Produits chimiques de laboratoire (< 5 L),
- Echantillons d'analyse ou de synthèse.

Fûts pour emballages souillés

- Flaconnages en verre brun,
- Matériels de laboratoire souillés en verre blanc,
- Flaconnages en plastique ou métalliques.

Les bonnes pratiques de stockage et de tri

Les contenants de produits chimiques neufs ou les contenants non homologués ne doivent pas être réutilisés pour stocker vos déchets.

Il faut utiliser uniquement les bidons de déchets homologués pour le transport (mis à disposition par le prestataire en charge de l'enlèvement des déchets).

Stocker les bidons de déchets liquides sur des bacs de rétention et/ou dans des armoires ventilées.

Sécuriser les bouchons en attendant l'évacuation

Risque chimique : déchets et transport

Chariot pour petit flaconnage

Lors du transport intra-muros

- ✓ Consignes d'utilisation de l'ascenseur/monte-charge
- ✓ Utilisation d'un chariot sécurisé

Stockage temporaire

Lieux de stockage définitif

Attention aux protections à utiliser lors du remplissage

Risque chimique : déchets et transport

- Faire une procédure en cas de déversement de produits chimiques et l'affiche.
- Avoir un kit d'intervention en cas de déversement chimique lors du transport :
  - Un produit absorbant (feuilles absorbantes universelles…),
  - Des gants résistants aux produits chimiques,
  - Masque à cartouche (stocker à l'extérieur du laboratoire),
  - Seau pour récupérer les déchets.

Risque chimique : déchets et transport

Le producteur de déchets

- Responsabilité jusqu'à l'élimination au centre agréé
- Conformité de l'emballage
- Identification des déchets

Intermédiaire (ex : Magasin de produits chimiques, soutes)

- Stockage
- Vérification (dans la mesure du possible)

Le transporteur

- Chargement
- Vérification du contenu (produits chimiques)
- Document transport

Le centre d'élimination

- Déchargement
- Analyse des déchets
- Elimination des déchets

Les rubriques d'une fiche de données de sécurité

1. Identification du produit et de la société
2. Identification des dangers
3. Informations sur les composants
4. Description des premiers secours en cas d'urgence
5. Mesures de lutte contre l'incendie
6. Mesures à prendre en cas de dispersion accidentelle
7. Précautions de stockage, d'emploi, de manipulation
8. Contrôle de l'exposition, protection individuelle
9. Propriétés physico-chimiques
10. Stabilité et réactivité du produit
11. Renseignements toxicologiques
12. Renseignements éco toxicologiques
13. Informations sur l'élimination des déchets
14. Informations relatives au transport
15. Informations réglementaires
16. Informations particulières

Informations générales

Danger

Mesures de gestion du risque

MERCI DE VOTRE ATTENTION

Before you start :

This online training programme is equivalent to class-based training. It should therefore be completed during working hours.
The training courses contain both theoretical units ("Lessons") and interactive units ("It's your turn!") to consolidate learning.
You must work through each unit in its entirety before moving on to the next.
Validating a training course requires that you pass a final test (with a minimum of 70% correct answers). Your health and safety officer will issue you with a training certificate at the end of your training programme.

MY COURSES

Chemical risk

Fire risk

Prevention

LABORATOIRE NATIONAL DES NUCLEIDES COSMOGENIQUES

PLATEFORME TECHNOLOGIQUE AIX-MARSEILLE

RéGEF

Réseau Géochimique & Expérimental Français

cerege

CENTRE EUROPÉEN DE RECHERCHE ET D'ENSEIGNEMENT DES GÉOSCIENCES DE L'ENVIRONNEMENT

Livret d'accueil des visiteurs

Unités de préparation du LN2C

https://www.cerege.fr/fr/equipements/ln2c

Aix-Marseille université

cnrs

IRD Institut de Recherche pour le Développement

COLLÈGE DE FRANCE

INRAE

SOMMAIRE

Aspects pratiques

Hygiène et sécurité - Prévention

En cas d'incident

Consignes d'utilisation des espaces de travail et des instruments

Déchets de laboratoire

A MON ARRIVEE

- ❑ **Visiter les laboratoires**
- ❑ **Lire le livret d'accueil du LN2C**
- ❑ **Réaliser le QCM et le valider avec le « référent labo »**
- ❑ **Lire le protocole de préparation des échantillons**

Les visiteurs seront formés au protocole de préparation des échantillons et encadrés par l'encadrant référent durant les manipulations et ce, sur l'ensemble de leur séjour au LN2C.

Aucune manipulation ne sera réalisée sans formation préalable.

AVANT MON DEPART

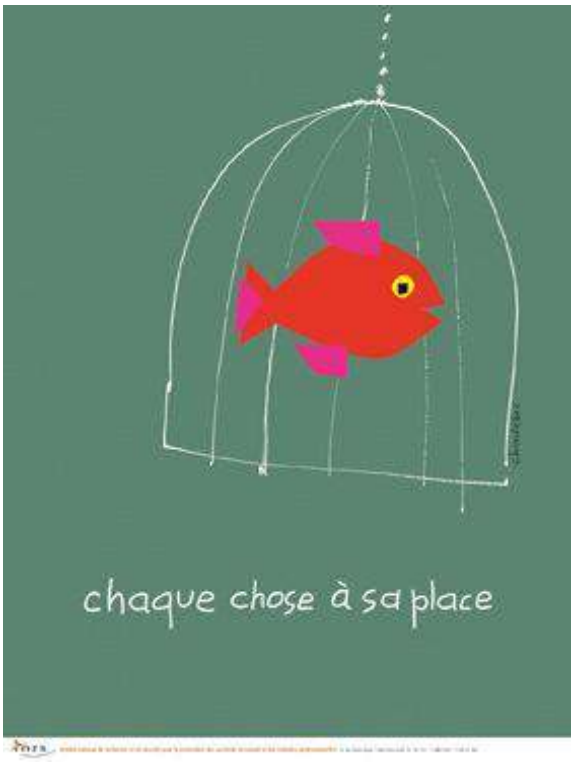

❑ Nettoyer le matériel selon le protocole approprié : béchers, éprouvettes, entonnoirs, colonnes,…

❑ Ranger le matériel à sa place après séchage naturel. <u>Le référent devra s'en charger si le matériel n'est pas encore sec.</u>

❑ Nettoyer : les sorbonnes, les portoirs de tubes, les portoirs de colonnes, les centrifugeuses, le vortex, les paillasses,…

❑ Labo séparation magnétique (Frantz) : aspirateur et dépoussiérage des paillasses et du sol (sous les meubles et autour).

PRESENTATION DU LN2C

Le laboratoire est composé de **10 unités de préparation**

- **Laboratoire « pré-traitements physiques et chimiques des roches»** : broyage, tamisage, décarbonatation, flottation, liqueurs denses. **Salle 116**
- **Laboratoire « séparation magnétique » Salle 303**
- **Laboratoire « extraction du nucléide cosmogénique d'origine atmosphérique ^{10}Be » Salle 404**
- **Laboratoire « extraction/purification/décontamination du quartz » ou « labo vert » Salle 406**
- **Laboratoires « extraction des nucléides cosmogéniques in-situ ^{10}Be et ^{26}Al » « labo jaune » - « labo bleu » Salle 406 – labo Salle 303**
- **Laboratoire « extraction du nucléide cosmogénique d'origine atmosphérique ^{36}Cl » Salle 408**
- **Laboratoire « extraction du nucléide cosmogénique in-situ ^{36}Cl » Salle 410**
- **Laboratoire de préparation des cibles pour la SMA Bâtiment ASTER**

Chaque laboratoire est destiné à une activité spécifique du fait des risques de contamination des échantillons par la nature et la qualité des produits chimiques utilisés. Par conséquent, aucune préparation destinée à l'extraction de ^{10}Be ne sera réalisée dans les laboratoires destinés à l'extraction du ^{36}Cl en raison de l'utilisation d'acide chlorhydrique.

Une attention particulière sera demandée aux encadrants pour l'utilisation de la salle 303 dont les moyens de protection collective en place (ETRAF) nécessitent une formation des utilisateurs par le personnel technique permanent du LN2C.

Chaque encadrant sera responsable du/des visiteurs qu'il accueille sur la durée de son/leur activité au sein des unités de préparation du LN2C et devra veiller au bon respect des règles de fonctionnement du laboratoire détaillées dans le présent document.

Une visite sera dispensée par « les référents labo » Laëtitia Léanni et Valéry Guillou dès l'arrivée du/des visiteurs avant toute activité au sein des unités de préparation.

SUPPORT TECHNIQUE DU LN2C

LN2C - ASTER

Spectromètre de Masse par Accélérateur – Unité de préparation des cibles

Karim KEDDADOUCHE (Ingénieur de Recherche) ☎ +33413949217

Georges AUMAITRE (Ingénieur d'Etude)☎+ 33413949171

LN2C - Idéfixe

Unités de préparation des échantillons

Frédéric CHAUVET (Ingénieur de Recherche)☎ 33413949189

Laëtitia LEANNI (Ingénieur d'Etude)☎ 33413949221

Valéry GUILLOU (Assistant Ingénieur)☎ 33413949212

Isabelle GIFFARD (Technicienne)☎

HORAIRES DE TRAVAIL AU LN2C

Les horaires de travail au sein des unités de préparation du LN2C : **8H – 17 H**

Les horaires seront ajustés avec l'encadrant.

Les visiteurs ne doivent pas travailler seuls dans les laboratoires – La présence d'au moins un agent ITA permanent ou chercheur du LN2C est obligatoire

Les jours de travail au sein des unités de préparation du LN2C : **lundi –mardi – mercredi – jeudi – vendredi** - hors jours fériés

Le travail le week-end est interdit.

LES BONNES PRATIQUES DE LABORATOIRE (BPL)


Pas de chaussures ouvertes


Pas de jupe ou de robe


Pas de short


Attacher les cheveux


Ne pas porter de bijoux risquant de perforer les gants


Proscrire le port de lentilles de contact.


Ne pas fumer dans le laboratoire


Ne pas manger ni boire dans le laboratoire


Se laver les mains à chaque fois qu'on quitte le laboratoire.


Ne pas toucher les poignées des portes avec des gants usagés.


Porter des lunettes de protection adaptée, également par-dessus les lunettes de vue.


Porter des gants lors de la manipulation de produits chimiques (vérifier la compatibilité des gants avec les substances manipulées).


Porter une blouse de laboratoire en coton avec fermeture par boutons pression (afin d'être retirée rapidement en cas d'accident).


Manipuler les produits chimiques et substances dangereuses sous la sorbonne


Si possible, ne jamais travailler seul ou au moins sans que quiconque ne soit au courant (en cas d'accident, une deuxième personne pourra vous porter secours).


Ne jamais pipeter à la bouche, utiliser une propipette.


Ne jamais tenter de reconnaître un produit à son odeur.


Examiner l'état de la verrerie avant de l'utiliser et si présence de brèche la jeter dans la poubelle à verre.


En cas de contact cutané ou oculaire avec un produit chimique rincer abondamment à l'eau froide (15 min).

LES EQUIPEMENT DE PROTECTION COLLECTIVE

ETRAF : hotte chimique à filtration

Consignes d'utilisation (salle 303)

MANIPULER UNIQUEMENT DE L'ACIDE CHLORHYDRIQUE SOUS LA HOTTE

Chaque utilisateur doit strictement respecter les consignes suivantes dans leur totalité pour une protection optimale des hottes et des usagers.

1. **Allumer la hotte 10 min avant les manipulations.**
2. **Compléter la fiche d'occupation des hottes.**
3. **Limiter les durées d'ouverture des flacons :**
   a. **Fermer les bidons de déchets acides et les bouteilles immédiatement après utilisation.**
   b. **Mettre du parafilm autour des béchers et des colonnes durant l'élution.**

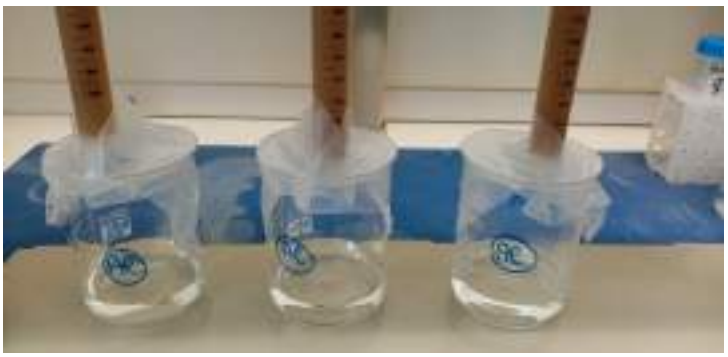

   c. **Poser un verre de montre au-dessus des entonnoirs.**

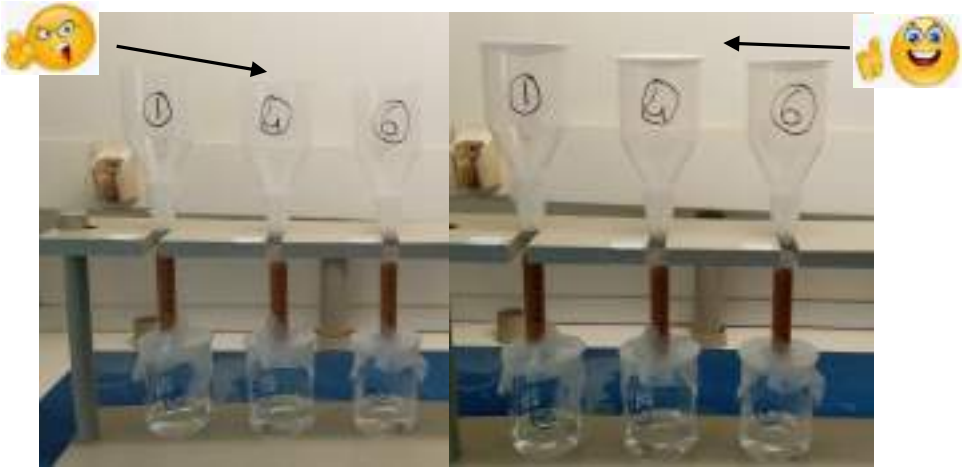

d. Ne pas préparer à l'avance les volumes d'acide chlorydrique à ajouter.

4. **Utiliser le matériel uniquement mis à disposition.**

5. **Respecter scrupuleusement le protocole de mise en œuvre.**

6. **Fin des manipulations = rien sous la hotte !**

7. **Ranger le matériel dans les rangements prévus à cet effet.**

8. **Nettoyer l'enceinte à l'eau savonneuse suivi d'un rinçage à l'eau claire et d'un séchage à l'aide d'un papier absorbant doux et non abrasif.**

9. **Attendre 15 minutes avant d'éteindre la hotte.**

10. **Aucun déchet souillé par de l'acide ne sera jeté dans les poubelles. Neutraliser ou rincer à l'eau de ville les pipettes ou papiers avant de les jeter à la poubelle.**

LES EQUIPEMENT DE PROTECTION COLLECTIVE

Sorbonne

Consignes d'utilisation

Aucune manipulation de produit chimique ne doit être réalisée en dehors de la sorbonne.

- La **vitesse d'aspiration** doit être **optimale** lorsque l'opérateur manipule. Se référer aux indications figurant sur chaque sorbonne.

- La **hauteur maximale d'ouverture** de la guillotine pour une sécurité individuelle et collective optimale est de **40 cm** et **ne DOIT pas être supérieure** (hauteur matérialisée soit par une butée ou soit par un repère : trait au marqueur, visses grises).

- Travail en position assise : régler la hauteur du tabouret pour travailler protégé !

- Travailler toujours avec un écran entre les produits chimiques et soi-même pour se protéger des projections.

- L'écran de la sorbonne doit être placé en position minimale lorsque l'opérateur ne manipule pas ou lors des étapes d'évaporation.

- **Limiter le travail sous sorbonne lors des étapes d'évaporation**, notamment lors de l'évaporation de la solution contenant de l'acide fluorhydrique (préférer l'évaporation de nuit).

EN CAS DE DOUTE L'OPERATEUR DOIT TOUJOURS SE REFERER A SON ENCADRANT OU LE PERSONNEL DU LABORATOIRE.

LES EQUIPEMENTS DE PROTECTION INDIVIDUELS (EPI)

LES GANTS : comment les utiliser ?

Les gants doivent être **jetés immédiatement après les avoir retirés**.

Seuls les gants bicolores (jaune et bleu) en néoprène peuvent être réutilisés. **Les gants doivent être cependant lavés et séchés avant d'être stockés à l'abri du soleil. (afin d'éviter leur dégradation)**

Comment retirer ses gants ?

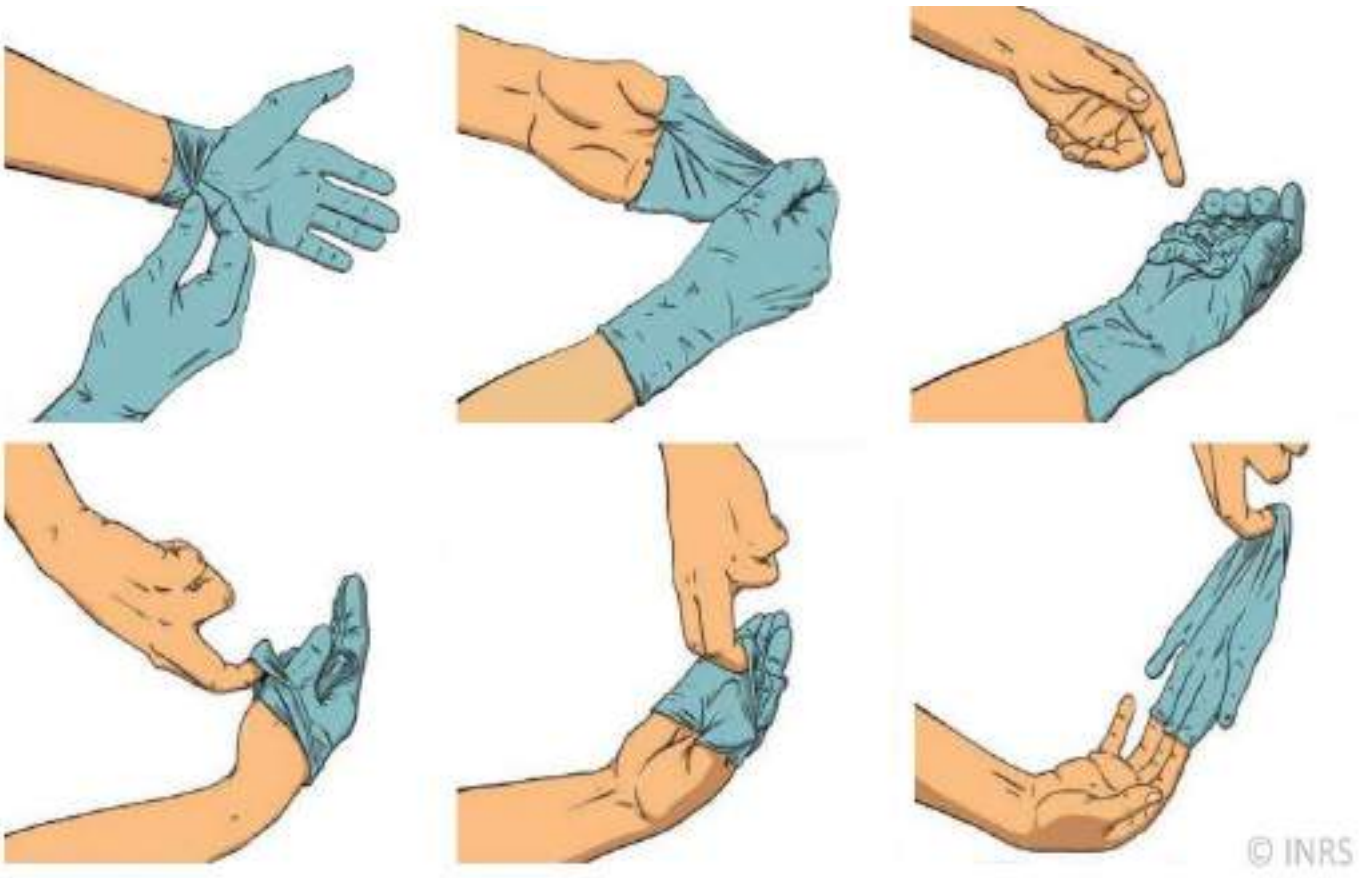

COMPATIBILITE DES GANTS

Source : www.protechnique.fr

Excellent	Bon	Moyen	Déconseillé
le gant peut être utilisé en **contact prolongé** avec le **produit chimique**, dans la **limite du temps de passage.**	le gant peut être utilisé en **contact prolongé** avec le **produit chimique**, dans la **limite du temps de passage.**	le gant peut être utilisé **contre des éclaboussures** du **produit chimique.**	**L'usage** de ce gant **est déconseillé.**

Désignation	Vinyle C.P.V.	Néoprène	Nitrile	Latex naturel
Acide acétique glacial	Excellent	Bon	Déconseillé	Bon
Acide chlorhydrique à 30 % & à 5 %	Excellent	Excellent	Excellent	Excellent
Acide fluorhydrique à 30 %	Excellent	Excellent	Bon	Bon
Acide nitrique à 20 %	Excellent	Excellent	Bon	Excellent
Acide perchlorique	Excellent	Moyen	Moyen	Moyen
Acide sulfurique jusqu'à 56 %	Bon	Bon	Bon	Bon
Acide sulfurique dilué (batterie)	Excellent	Excellent	Excellent	Excellent
Alcool éthylique (éthanol)	Bon	Bon	Bon	Bon
Ammoniaque concentrée	Excellent	Excellent	Bon	Excellent
Chlorure de calcium	Excellent	Excellent	Excellent	Excellent

L'ETIQUETTE D'UN PRODUIT CHIMIQUE (source INRS)

Attention les bouteilles de produits chimiques peuvent se ressembler, mais elles contiennent des produits différents associés à des dangers différents.

Je lis le nom inscrit sur l'étiquette avant d'utiliser le produit chimique.

Sur l'étiquette des produits chimiques figurent :

- **L'identité du fournisseur :** les étiquettes doivent comporter le nom, l'adresse et le numéro de téléphone du ou des responsables de la mise sur le marché du produit.

- **Le nom du produit.**

- **Les pictogrammes de danger :** ils symbolisent les dangers du produit pour la santé, la sécurité ou l'environnement.

- **Les mentions d'avertissement :** mot indiquant le degré relatif d'un danger : « DANGER » (utilisé pour les catégories de danger les plus sévères) ou « ATTENTION ».

- **Les mentions de dangers :** phrase qui, attribuée à une classe de danger ou à une catégorie de danger, décrit la nature du danger que constitue un produit chimique et, lorsqu'il y a lieu, le degré de ce danger.

- **Les conseils de prudence :** un nombre limité de conseils de prudence doit figurer sur l'étiquette et sont choisis, parmi ceux qui sont associés aux catégories de danger du produit, en tenant compte des utilisations de ce produit.

- **Des Informations supplémentaires :**

* informations additionnelles sur les dangers,
* éléments d'étiquetage additionnels concernant certains mélanges contenant une substance dangereuse,
* mention spécifique pour les produits phytopharmaceutiques.

TABLE DE COMPATIBILITE DES PRODUITS CHIMIQUES

									
	?	X	X	X	X	X	O	X	X
	X	O	X	X	X	X	O	X	X
	X	X	O	?	X	X	X	X	X
	X	X	?	O	?	X	X	X	X
	X	X	X	?	?	?	?	?	?
	X	X	X	X	?	O	O	O	O
	O	O	X	X	?	O	O	O	O
	X	X	X	X	?	O	O	O	O
	X	X	X	X	?	O	O	O	O

ORME CONSEIL - Management du risque chimique, 69006 LYON. Contact@orme-conseil.com

X Ne doivent pas être stockés ensemble O Peuvent être stockés ensemble

? Peuvent être stockés ensemble, sous conditions

NB : Cette table représente des principes généraux qui doivent être adaptés à votre analyse de risques.

LES PICTOGRAMMES DE DANGER

Dangers physiques

Je peux exploser, suivant le cas, au contact d'une flamme, d'une étincelle, d'électricité statique, sous l'effet de la chaleur, d'un choc, de frottements…

Je peux m'enflammer, suivant le cas, au contact d'une flamme, d'une étincelle, d'électricité statique, sous l'effet de la chaleur, de frottements, spontanément au contact de l'air, ou au contact de l'eau si je dégage des gaz inflammables. Je peux, dans certains cas, exploser même en l'absence d'air ou si la quantité d'agent désensibilisateur diminue.

Je peux provoquer ou aggraver un incendie, ou même provoquer une explosion en présence de produits inflammables.

* Je peux exploser sous l'effet de la chaleur (gaz comprimés, gaz liquéfiés, gaz dissous).

* Je peux causer des brûlures ou blessures liées au froid (gaz liquéfiés réfrigérés).

Dangers physiques et danger pour la santé

* Je peux attaquer ou détruire les métaux.

* Je ronge la peau et/ou les yeux en cas de contact ou de projection.

Danger pour la santé

J'empoisonne rapidement, même à faible dose.

* Je peux provoquer le cancer.
* Je peux modifier l'ADN.
* Je peux nuire à la fertilité ou au fœtus.
* Je peux altérer le fonctionnement de certains organes.
* Je peux être mortel en cas d'indigestion puis de pénétration dans les voies respiratoires.
*Je peux provoquer des allergies respiratoires (asthme par exemple).

Danger pour la santé et danger pour l'environnement

* J'empoisonne à forte dose.
* J'irrite la peau, les yeux et/ou les voies respiratoires.
* Je peux provoquer des allergies cutanées (eczéma par exemple).
* Je peux provoquer somnolence ou vertiges.
* Je détruis l'ozone dans la haute atmosphère.

Danger pour l'environnement

Je provoque des effets néfastes sur les organismes du milieu aquatique (poissons, crustacés, algues, autres plantes aquatiques…).

LA FICHE DE DONNEES DE SECURITE D'UN PRODUIT CHIMIQUE (FDS)

Avant d'utiliser un produit chimique, je lis la fiche de données de sécurité du produit. Elle apporte des informations importantes pour le manipulateur. On y trouve les rubriques suivantes :

- L'identification de la substance / du mélange et de la société / de l'entreprise.
- L'identification des dangers.
- La composition / les informations sur les composants.
- Les premiers secours.
- Les mesures de lutte contre l'incendie.
- Les mesures à prendre en cas de dispersion accidentelle.
- La manipulation et le stockage.
- Le contrôle de l'exposition / la protection individuelle.
- Les propriétés physiques et chimiques.
- La stabilité et la réactivité.
- Les informations toxicologiques.
- Les informations écologiques.
- Les informations relatives à l'élimination du produit.
- Les informations relatives au transport.
- Les informations réglementaires.
- Autres informations.

QUE FAIRE EN CAS DE PROJECTION DANS L'ŒIL

si c'est un produit chimique

rincez votre œil immédiatement.

- S'il n'y a pas de rince-œil, placez votre œil sous le jet du robinet le plus proche (eau tiède de préférence).
- Pendant le rinçage, maintenez les paupières ouvertes. Faites-vous aider si possible (on a tendance à fermer les yeux lorsque quelque chose y a pénétré).
- Rincez au moins pendant 15 minutes en attendant les secours.
- Indiquez au médecin la nature du produit projeté dans votre œil (huile de coupe, solvant, acide, etc.), afin qu'il adapte au mieux le traitement à suivre.

POURQUOI ? les produits chimiques créent des lésions dès les premières minutes.
En rinçant abondamment l'œil immédiatement après l'accident, on limite le risque de détérioration.

si c'est un corps étranger

n'essayez pas de le retirer vous-même

allez immédiatement à l'infirmerie
ou vers le sauveteur-secouriste le plus proche.

POURQUOI ? En utilisant des méthodes qui relèvent du « bricolage », vous risquez :
- d'infecter l'œil,
- d'enfoncer plus profondément le corps étranger fiché superficiellement.

S'il y a nécessité, vous serez orienté vers un spécialiste.

POURQUOI ? Seul un spécialiste pourra
- retirer rapidement et efficacement le corps étranger superficiel, évitant ainsi les risques de complication ;
- rechercher et retirer un corps étranger qui aura pénétré profondément et qui n'est souvent ni apparent, ni douloureux ;
- prescrire un traitement pour calmer la douleur, aider la cicatrisation et éviter toute infection.

Source : INRS

un truc dans l'œil QUE FAIRE ?

Pencher la tête légèrement sur le côté pour ne pas contaminer l'œil sain.

source : www.seton.fr

Je travaille avec HF (acide Fluorhydrique)

Jamais seul au labo avec HF !

Pourquoi me redouter ?

Parce que les premiers signes se font sentir lorsqu'il est trop tard !

Brûlure HF = période de latence indolore puis brûlure profonde avec douleur ++

Yeux : **irritation ou brûlure grave avec risque d'être aveugle.**

Peau : **brûlure très grave extensive avec destruction de la peau et de l'os.** La douleur peut-être retardée d'autant plus si la solution est diluée.

Poumons : **irritation avec risque de suffocation** grave progressive ou retardée (parfois après 24 heures).

Bouche : **brûlure digestive très grave avec risque général en particulier cardiaque** dû à la baisse du calcium dans le sang.

La gravité des lésions est fonction de la concentration, de la quantité, de la durée du contact, de la superficie et de la localisation de la brûlure.

Quels équipements de protection utilisés ?

Blouse en coton et boutons pression

Lunettes à coques latérales


Gants néoprène ou butyle

Manchons de protection à usage unique 

Conduite à tenir

- **Ne jamais toucher le mobilier du laboratoire**, robinets, poignées de porte, poignées de placard, interrupteur**,… avec des gants qui ont servi à la manipulation du HF.**
- **Après manipulation du HF laver les gants** avec de la poudre de carbonate de calcium **(CaCO3).** Rincer à l'eau.

⚠ **Ouverture de la sorbonne : maximum 40 cm**

Travail en position assise : régler la hauteur du tabouret pour travailler protégé !

Travailler toujours avec un écran entre l'échantillon et soi-même pour se protéger des projections

Déchets

- Les « restes d'acides » et les « eaux » de rinçages seront versés dans un bidon de déchets spécifique à l'HF : **« déchets acides HF ».**
- **Neutraliser l'acide résiduel avec une solution de carbonate de calcium $CaCO_3$** : pipettes, béchers, éprouvettes, papiers souillés,… **Contrôler le pH de la solution de rinçage** (pH=7-8). **Jeter la solution de rinçage à l'évier et jeter les déchets contaminés dans la poubelle de déchets contaminés de laboratoire**.

⚠ **NE PAS INTRODUIRE DE l'HF DANS LES AUTRES BIDONS DE DECHETS ACIDES !**

⚠⚠⚠ **NE PAS INTRODUIRE DE $CaCO_3$ DANS LES BIDONS DE DECHETS ACIDES ! = REACTION AVEC DEGAGEMENT GAZEUX = RISQUE d'EXPLOSION DU BIDON**

AUTRES PRECAUTIONS A PRENDRE LORS DE LA MANIPULATION DU HF

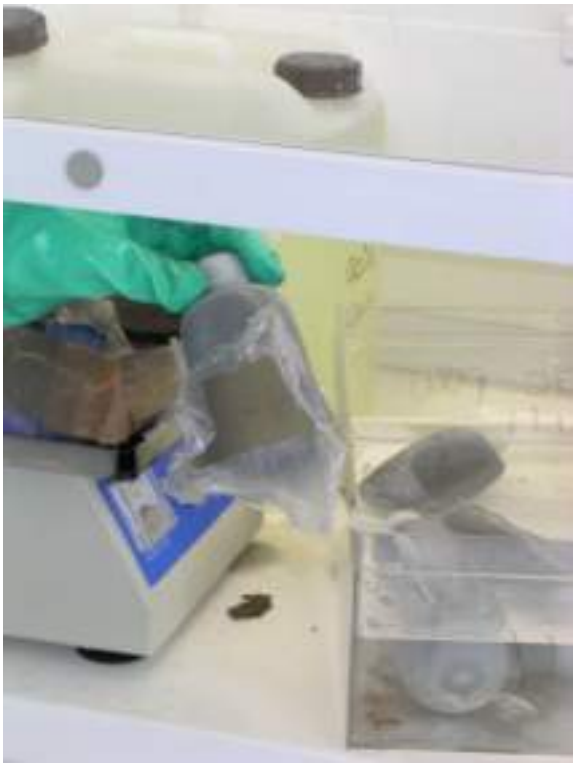

Accident HF : emballement de la réaction

DISSOLUTION TOTALE : après l'ajout du volume d'HF nécessaire pour la dissolution totale de l'échantillon, laisser reposer les bouteilles sous la sorbonne bouchons ouverts durant 4H minimum avant de les placer sur l'agitateur. Les bouteilles seront placées dans un sac puis le sac dans une boîte hermétiquement fermée.

Conduite à tenir en cas d'accident avec HF

(acide Fluorhydrique)

LES SYMPTOMES APARAISSENT TARDIVEMENT

AGIR TRES RAPIDEMENT

Que faire en cas de déversement accidentel ?

Sous la sorbonne :

1- Saupoudrer de Carbonate de Calcium ($CaCO_3$) jusqu'à ce qu'il n'y ait plus de réaction effervescente.
2- Attendre quelques minutes jusqu'à ce qu'il n'y ait plus de réaction.
3- Contrôler le pH =7-8.
4- Récupérer la poudre avec du papier absorbant.
5- Jeter la poudre et le papier souillé dans un sac en plastique.
6- Fermer hermétiquement le sac.
7- Jeter le sac dans la poubelle de déchets contaminés de laboratoire.

En dehors de la sorbonne :

1- Faire évacuer le laboratoire.
2- Désigner une deuxième personne qui empêche les autres d'entrer dans le laboratoire et veille sur la personne qui décontamine la zone.
3- Porter un masque à cartouche (Filtre E).
4- Aérer les locaux.
5- Verser de la poudre de Carbonate de Calcium (CaCO3) pour neutraliser l'acide.
6- Attendre quelques minutes.
7- Contrôler le pH =7-8.
8- Ramasser la poudre à l'aide de papier absorbant.
9- Jeter dans un sac plastique.
10- Fermer hermétiquement le sac.
11- Jeter le sac dans la poubelle de déchets contaminés de laboratoire.

Que faire en cas de projection sur la peau ?

- Enlever les vêtements souillés en portant des gants en **néoprène ou butyle**. Attention de ne pas contaminer d'autres parties du corps.
- Laver **immédiatement à grande eau 15 min**. Le pronostic dépend de la précocité et de l'abondance du lavage.
- Appliquer du **gel de gluconate de calcium à 2.5 % en couche épaisse** ou des compresses bien imprégnées de gluconate de calcium à 2.5 % en ampoule. Utiliser des bandes Nylex pour maintenir les compresses. L'application doit se faire tant que la douleur persiste (ou renouveler toutes les 3 heures).
- Facteur de gravité : surface corporelle contaminée supérieure à 3 % (1% = surface de la main doigts compris)

Que faire en cas de projection dans l'œil ?

- **Laver immédiatement à l'eau** en écartant bien les paupières, au lave-œil ou à l'eau du robinet pendant **15 min**.
- **Veiller à ne pas contaminer l'œil non touché** : placer l'œil contaminé vers le bas et faire couler l'eau de l'intérieur vers l'extérieur de l'œil.
- Ne pas utiliser de collyre.
- Ne pas utiliser du **gel de gluconate de calcium à 2.5 %**.
- **Contacter rapidement un service ophtalmologique hospitalier en contact avec le centre antipoison**.

Que faire en cas d'ingestion ?

- Ne pas faire vomir, ni manger ou boire.
- **Appeler immédiatement le 15**.

Que faire en cas d'inhalation ?

- Dégager la victime en se protégeant soi-même avec un **masque à cartouche (filtre E).**
- **Appeler immédiatement le 15.**

- ❖ Appeler le 15 pendant les premiers soins en cas de projection cutanée, même si la brûlure paraît minime ou indolore, et en cas de projection oculaire.
- ❖ Appeler **immédiatement** le 15 en cas d'inhalation, d'ingestion ou de projection cutanée sur une **surface étendue (3 %)** et faire intervenir immédiatement un sauveteur secouriste du travail.
- ❖ Fournir aux secours la FDS et/ou l'étiquette (elle renseigne sur la concentration) et cette fiche CAT (Conduite A Tenir).

DANS TOUS LES CAS PRENDRE UN AVIS SPÉCIALISE AU CENTRE DES GRANDS BRULES – **Hôpital de la Conception** - En appelant le médecin de garde au **04 91 43 58 18**. 147, boulevard Baille 13005 Marseille Téléphone

LES SECOURISTES DU CEREGE

AGENTS SECOURISTE CEREGE
(MAJ 06/2021)

NOM & PRENOM	*TELEPHONE BUREAU*	*PORTABLE*	*Bâtiment / étage / pièce*
ALEXANDRE Anne	+33 (0)4 13 94 91 66	+33 (0)6 25 55 85 52	Pasteur / 3° / 474
ANGELETTI Bernard	+33 (0)4 13 94 91 68		Pasteur / 1° / 261
BARBONI Doris	+33 (0)4 13 94 91 72	+33 (0)6 89 14 58 16	Pasteur / 3° / 409
DELANGHE Doriane	+33 (0)4 13 94 91 96	+33 (0)6 83 32 41 54	Villemin / rdc / labo sédim Pasteur / rdj / 153
DEMORY François	+33 (0)4 13 94 91 97	+33 (0)6 18 54 00 32	Pasteur / 1° / Chalet
DUVIVIER Adrien	+33 (0)4 13 94 93 10	+33 (0)6 67 66 72 87	Laennec / 1° / hall D
GATTACCECA Jérôme	+33 (0)4 13 94 92 08		Pasteur / 1° / 284
GUIHOU Abel	+33 (0)4 13 94 92 11	+33 (0)7 81 48 91 32	Pasteur / rdj / 155
LONGEREY Julien	+33 (0)4 13 94 92 27	+33 (0)6 09 25 62 92	Pasteur / 1° / 211
MAGNETTO Sandrine	+33 (0)4 13 94 92 28	+33 (0)6 08 66 98 85	Pasteur / 1° / 212
MICHE Hélène	+33 (0)4 13 94 92 34		Pasteur / 2° / 355
RIEU Patricia	+33 (0)4 13 94 92 44		Pasteur / 1° / 203
RINTERKNECHT Vincent	+33 (0)4 13 94 92 45		Laennec / 1° / hall D
ROSTEK Frauke	+33 (0)4 13 94 92 50	+33 (0)6 64 92 57 85	Pasteur / 2° / 359
SONZOGNI Corinne	+33 (0)4 13 94 92 57	+33 (0)6 15 69 15 13	Pasteur / 2° / 359

Numéro d'urgence / secours

☎ 112

Conduite à tenir en cas de déversement accidentel d'acide

Sous la sorbonne :

1. Saupoudrer de Carbonate de Calcium ($CaCO_3$) jusqu'à ce qu'il n'y ait plus de réaction effervescente.
2. Attendre quelques minutes jusqu'à ce qu'il n'y ait plus de réaction.
3. Récupérer la poudre avec du papier absorbant.
4. Jeter la poudre et le papier souillé dans un sac en plastique.
5. Fermer hermétiquement le sac.
6. Jeter le sac dans la poubelle de déchets chimiques de laboratoire.

En dehors de la sorbonne :

1. Faire évacuer le labo.
2. Désigner une deuxième personne qui empêche les autres d'entrer dans le labo et veille sur la personne qui décontamine la zone.
3. Porter un masque à cartouche (Filtre E).
4. Verser de la poudre de Carbonate de Calcium ($CaCO_3$) pour neutraliser l'acide.
5. Attendre quelques minutes.
6. Ramasser la poudre à l'aide de papier absorbant.
7. Jeter dans un sac plastique.
8. Fermer hermétiquement le sac.
9. Jeter le sac dans la poubelle de déchets chimiques de laboratoire.

Lequel en premier? L'eau? L'acide?

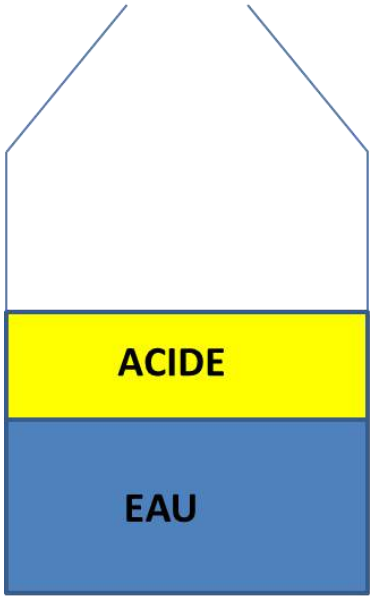

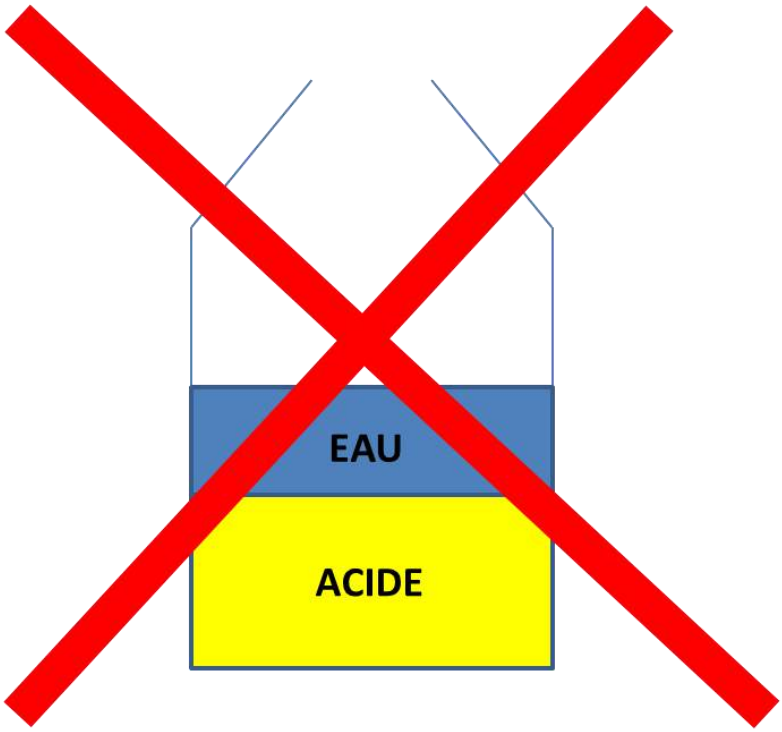

CONSIGNES DE TRAVAIL AU LABORATOIRE

- La pissette d'éthanol doit être placée à l'abri du soleil et de la chaleur, car le volume de gaz enfermé au-dessus du liquide se dilate sous l'effet thermique et pousse le liquide dans le conduit distributeur, pouvant entraîner ainsi l'éjection du liquide.

- **Le matériel de laboratoire** : bécher, éprouvette, micropipette, solution de produit chimique, pissette, … **ne doit pas entrer en contact avec l'échantillon** afin d'éviter tout risque de contamination du matériel.

- **Le matériel qui n'est pas à usage unique** (ex : bécher en téflon) **doit subir un protocole strict de nettoyage**.

- **Ne jamais verser le liquide ou le solide non utilisé dans son contenant d'origine !** Il doit être éliminé en tant que déchet selon la procédure appropriée.

- **Ne pas toucher avec des gants souillés les robinets ou les poignées de portes.**

- **Ne jamais sortir de récipients ouverts contenant des produits chimiques en dehors de la sorbonne,** même pour des courtes distances.

- Ne jamais sortir le matériel souillé par des produits chimiques en dehors de la sorbonne sans avoir pris soin au préalable de le rincer 2 à 3 fois à l'eau.

- **Ne jamais récupérer un échantillon qui s'est renversé sur la paillasse**. Un fois en contact avec cette dernière, il existe un risque de contamination : l'échantillon est perdu ! Appliquer le protocole approprié pour l'éliminer et nettoyer la paillasse. En cas de doute, toujours demander conseil.

- **Tout récipient placé dans l'étuve doit être au préalable rincé jusqu'à pH=7.**

UN DOUTE ? UNE QUESTION ? UNE PRECISION ? UNE CONFIRMATION ?

Vos interlocuteurs : votre référent et le personnel permanent du LN2C

PROTOCOLE DE NETTOYAGE DU MATERIEL DE LABORATOIRE

Béchers en téflon

1. Nettoyer le bécher à l'eau de ville.
2. Essuyer le bécher avec du papier pour éliminer les résidus.
3. Ajouter 2/3 d'eau ultra-pure.
4. Ajouter 1/3 d'acide chlorhydrique à 37 %. Attention laisser 0.5 cm entre le niveau de liquide et le haut du bécher.
5. Recouvrir le bécher avec un verre de montre en téflon.
6. Chauffer pendant 1 jour en réglant la plaque chauffante au minimum.

Matériel contaminé par de l'acide fluorhydrique HF

Bécher et éprouvette :

1. Préparer une solution de $CaCO_3$ dans une bouteille : ajouter de la poudre de $CaCO_3$ en excès et compléter avec de l'eau.
2. Remplir le bécher ou l'éprouvette de cette solution et attendre quelques minutes que la réaction soit terminée.
3. Contrôler le pH. S'il est acide rajouter de la poudre de $CaCO_3$ dans le bécher ou l'éprouvette. Si le pH est basique, la solution peut être jetée à l'évier. ⚠ **ATTENTION NE SURTOUT PAS JETER LA SOLUTION DE $CaCO_3$ DANS LE BIDON DE DECHETS ACIDES ! RISQUE D'EXPLOSIION DU BIDON !**

Pipette pasteur :

1. Prendre un bécher en plastique et verser 10 mL de solution de $CaCO_3$.
2. Prélever/ éjecter trois-quatre fois la solution avec la pipette en rejetant la solution dans le même bécher.
3. Pour finir prélever une quantité de solution de $CaCO_3$ contenue dans le bécher jusqu'au volume maximal de la pipette et attendre quelques minutes que la réaction soit terminée.
4. Contrôler le pH. S'il est acide rajouter de la poudre de $CaCO_3$ dans le bécher et recommencer les étapes 1 à 3. Si le pH est basique, la solution peut être jetée à l'évier et la pipette dans la poubelle de déchets de laboratoire. ⚠ **ATTENTION NE SURTOUT PAS JETER LA SOLUTION DE CaCO3 DANS LE BIDON DE DECHETS ACIDES ! RISQUE D'EXPLOSIION DU BIDON !**

Papier souillé :

1. Prendre un bécher contenant la solution de $CaCO_3$.
2. Introduire le papier dans la solution.
3. Laisser réagir quelques minutes.
4. Contrôler le pH. S'il est acide rajouter de la poudre de $CaCO_3$ dans le bécher. Si le pH est basique, la solution peut être jetée à l'évier. ⚠ **ATTENTION NE SURTOUT PAS JETER LA SOLUTION DE CaCO3 DANS LE BIDON DE DECHETS ACIDES ! RISQUE D'EXPLOSIION DU BIDON !**

CONSIGNES D'UTILISATION DU BROYEUR A MÂCHOIRES

FFP3

NE PAS UTILISER LE BROYEUR SANS AVOIR ETE FORME AU PREALABLE A SON UTILISATION

1. Fermer la porte du broyeur pour isoler du bruit le reste du laboratoire.
2. Mettre en marche l'extraction.
3. Vérifier l'état de propreté du broyeur. Eliminer la poussière résiduelle et d'éventuels grains à l'aide de l'air comprimé.
4. Positionner la mâchoire amovible. Pour se faire régler l'écartement des mâchoires en position 5.
5. Placer le bac de récupération de l'échantillon broyé sous les mâchoires.
6. Fermer la vitre de sécurité.
7. Mettre en route le broyeur (**NE JAMAIS INTRODUIRE D'ECHANTILLON LORSQUE LE BROYEUR EST ETTEINT**). Si le broyeur ne démarre pas, vérifier que la vitre soit bien enclenchée (mise en sécurité).
8. Introduire l'échantillon dans l'entonnoir d'alimentation. Ne pas introduire dans le broyeur des fragments de roche supérieurs à environ 7 cm. Si des morceaux de roche restent coincés dans le broyeur, arrêter le broyeur, retirer la mâchoire (position 5), récupérer les morceaux et les casser à la massette.
9. Arrêter le broyeur seulement lorsque la **totalité** de l'échantillon est passée.
10. Ouvrir la vitre.
11. Récupérer le bac échantillon.

Nettoyage entre chaque échantillon et à la fin du travail:

12. Retirer la mâchoire amovible.
13. Aspirer les grains.
14. Nettoyer à l'air comprimé l'ensemble des interstices et orifices dans lesquels de la matière aurait pu s'y accumuler. S'assurer qu'il ne reste plus de poussières dans les recoins du broyeur afin d'éviter de contaminer l'échantillon suivant.
15. Nettoyer avec un papier imbibé d'éthanol et sécher à l'air comprimé.
16. Nettoyer le bac de la même façon.
17. Ne pas oublier de retirer la mâchoire amovible pour nettoyer l'intérieur du broyeur.
18. Nettoyer les deux mâchoires à l'air comprimé et à l'éthanol.

Avant de partir :

- Aspirer les résidus d'échantillon et la poussière au sol, sur et sous les meubles.
- vider la poubelle.

CONSIGNES D'UTILISATION DU FRANTZ LB-1

FFP3

NE PAS UTILISER LE FRANTZ SANS AVOIR ETE FORME AU PREALABLE A SON UTILISATION

LES ECHANTILLONS DOIVENT ETRE LAVES A L'EAU ET SECHES AVANT D'ETRE SEPARES AU FRANTZ
NE PAS DEPASSER UNE INTENSITE DE 2A

1. Vérifier l'état de propreté du Frantz et si nécessaire utiliser l'aspirateur et l'air comprimé pour le nettoyer.
2. Monter le Frantz. Placer une rondelle entre l'écrou et la visse. Ne pas trop serrer !
3. Ne pas démonter la réglette de séparation de l'échantillon entre chaque échantillon.
4. Pour nettoyer entre chaque échantillon :
    a. Couper le champ magnétique (0 A).
    b. Mettre en route la vibration pour faire tomber les résidus d'échantillon.
    c. Retirer « le bloc » en partie basse de la réglette.
    d. Démonter l'entonnoir.
    e. Placer l'aspirateur sur la partie haute de la réglette et souffler de l'air comprimé de la partie basse de la réglette vers le haut (Attention de ne pas oublier d'aspirer an même temps que l'utilisation de l'air comprimé !).
    f. Contrôler qu'il n'y ait pas de grains coincés entre la réglette et la bande de plastique.
    g. Souffler à l'air comprimé les différentes pièces démontées et contrôler qu'il n'y ait pas de grains coincés.
    h. Nettoyer l'entonnoir et les béchers avec un papier imbibé d'éthanol et sécher à l'air comprimé.
5. A la fin du travail : réaliser la même procédure de nettoyage qu'au point 4. Démonter la réglette et la nettoyer avec un papier imbibé d'éthanol, sécher à l'air comprimé. Nettoyer la bande de plastique avec un papier imbibé d'éthanol.
6. Passer l'aspirateur sur la table du Frantz (y compris derrière le Frantz), évacuer les grains sous le Frantz à l'air comprimé et les aspirer.
7. Placer les visses et accessoires dans les tiroirs prévus à cet effet.
8. Passer l'aspirateur dans la pièce et sous les meubles.

LES DECHETS DE LABORATOIRE

Caisse palette

- **Matériaux pollués par des produits chimiques**
- **Sacs poubelle déchets de laboratoire (en cours d'organisation)**

Ex : *bouteilles vides en verre et en plastique ayant contenu des produits chimiques en dehors des produits comburants*

Fût bleu

Dans le local des produits chimiques

Déchets comburants

Ex : bouteilles d'acide nitrique

Poubelles roches et sédiments secs

Tonnelet

Inscrire « produits chimiques » + noms des produits

Ex : flaconnage plein, produits

Bidons de 5 L et 10 L

AUCUN DECHET DE LABORATOIRE DANS LES CONTENAIRS PREVUS POUR LES ORDURES MENAGERES !

Où jeter les cartouches de résines des systèmes de purification d'eau ? Tonnelet ou caisse palette « matériaux pollués » à l'extérieur du bâtiment.

Où jeter les bouteilles vides d'acide nitrique ? Fût bleu dans la salle de stockage des produits chimiques au rez-de-chaussée. Pas de stockage dans le laboratoire !

Où jeter les bouteilles vides d'acide fluorhydrique, acide chlorhydrique, acide hexafluorosilicique, ammoniaque ? Caisse palette « matériaux pollués » à l'extérieur du bâtiment. Pas de stockage dans le laboratoire !

Où jeter les bouteilles Nalgène® vides souillées par des produits chimiques ? Caisse palette « matériaux pollués » à l'extérieur du bâtiment.

Où jeter les petits flacons remplis (vials, tubes à centrifuger,…) ? Tonnelet blanc labellisé « produits chimiques ». Attention aux incompatibilités entre les produits chimiques. Préciser la nature des produits chimiques contenus dans les flacons.

Où jeter la résine souillés (DOWEX 50WX8 et 1X8) ? Bidon de 5 L labellisé « produits chimiques » + étiquette « déchets acides ». Solide uniquement ! Ne pas ajouter de liquide.

Où jeter les béchers en verre borosilicaté ? Caisse palette « matériaux pollués » à l'extérieur du bâtiment. ***Le verre de laboratoire n'est pas recyclé. En revanche, il peut être utilisé pour d'autres usages, demander à votre encadrant.*** **Pas de stockage dans le laboratoire !**

Où jeter les cartons ? Container de tri à l'extérieur du bâtiment. Différents points de collecte. Pas de stockage dans le laboratoire !

Où jeter les cartons souillés par des produits chimiques ? Caisse palette « matériaux pollués » à l'extérieur du bâtiment. ***Le carton souillé par des produits chimiques n'est pas recyclé et ne doit pas être mélangé aux cartons « sains ».*** **Pas de stockage dans le laboratoire !**

Où jeter les solutions d'acide fluorhydrique ? Bidon de 5 L labellisé HF + étiquette « déchets acides ». Stocker le bidon dans une armoire ventilée. Amener le bidon plein en salle de stockage des produits chimiques.

Où jeter les solutions d'acide nitrique ? Bidon de 5 L labellisé HNO_3 + étiquette « déchets acides ». ATTENION : ne pas mélanger avec de l'HCl. Stocker le bidon dans une armoire ventilée. Amener le bidon plein en salle de stockage des produits chimiques.

Où jeter les solutions d'acide chlorhydrique, acide hexafluorosilicique ? Bidon de 10 L labellisé HCl, H_2SiF_6 + étiquette « déchets acides ». Il est possible de jeter l'HF dans ce bidon ; dans ce cas noter : HF sur le bidon. Stocker le bidon dans une armoire ventilée. Amener le bidon plein en salle de stockage des produits chimiques.

Où jeter les solutions d'ammoniaque ? Bidon de 5 L labellisé ammoniaque + étiquette « déchets basiques ». Stocker le bidon dans une armoire ventilée. Amener le bidon plein en salle de stockage des produits chimique.

Où jeter le petit matériel souillé de laboratoire (gants, manchettes, papier essuie-tout, pipettes pasteur, embouts de pipettes, entonnoirs, filtres seringue, filtres papier,…) ? Dans la poubelle de laboratoire destinée à ce type de déchets. Jeter les sacs plein dans la caisse palette « matériaux pollués » à l'extérieur du bâtiment. (A venir…)

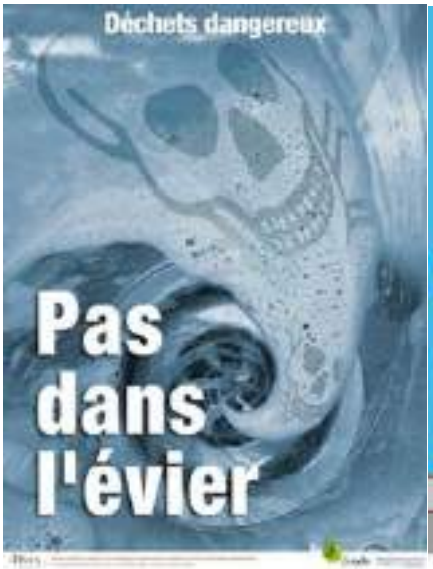

PAS DE PRODUITS CHIMIQUES DANGEREUX DANS L'EVIER

Les bidons pleins doivent être déposés dans la salle de stockage des produits chimiques au rez-de-chaussée (demander la clé à votre référent) en respectant les emplacements réservés aux acides et aux bases.

Target making protocol for ^{10}Be and ^{26}Al measurements by accelerator mass spectrometry (SMA)

6 units of preparation :

- **« Cold chemistry laboratory »** - ground floor – crushing, sieving, magnetic separation with Frantz LB-1, extraction and purification of Quartz.

- **« Meteoric ^{10}Be laboratory»** – third floor – samples preparation for meteoric ^{10}Be measurements.

- **« ^{10}Be/^{26}Al in-situ laboratory »** – third floor - samples preparation for ^{10}Be and ^{26}Al *in-situ* measurements.

- **« ^{36}Cl in-situ laboratory »** – third floor – samples preparation for ^{36}Cl *in-situ measurements.* **THE USING OF CHLORINE PRODUCTS IS FOBIDDEN IN THIS LABORATORY.**

- **« meteoric ^{36}Cl laboratory »** – third floor – development activities. **THE USING OF CHLORINE PRODUCTS IS FOBIDDEN IN THIS LABORATORY.**

- **Target manufacturing laboratory – ASTER bulding** (**A**ccélérateur pour les **S**ciences de la **T**erre l'**E**nvironnement et les **R**isques) – targets preparation for ^{10}Be/^{9}Be, ^{26}Al/^{27}Al, ^{36}Cl/^{35}Cl, ratio measurements with the accelerator mass spectrometer.

Each laboratory has a specific activity. This organisation must be respected to avaoid any risk of contamination. So, all material have to remain in its original laboratory and never be used for other manipulations.

CONTACTS :

CEREGE's prevention assistants : Frédéric Chauvet (Tél : +334 13 94 91 71 , office 492 at third floor)
Laëtitia LEANNI (Tél : +334 13 94 92 21 , office 462 at third floor)

Laboratory waste :

Plastic chemical product bottles : gray container for chemical watse, outside Pasteur's building (CEREGE). Don't rinse bottles before trashing.

Laboratory waste (pasteur pipettes, chemical soaked papers,…) : rinse them with tap water before trashing into the laboratory trash can. Trash water rinsing in the acid waste can. Work under the fume hood.


For pasteur pipettes with residus of HF  **, rinse them with a saturated solution of $CaCO_3$ before trashing in the laboratory trash can.**

Glass : gray container for chemical watse, outside Pasteur's building (CEREGE).

Accidental acid spilling : pour the $CaCO_3$ powder to neutralize acid (effervescent reaction). Wipe with a wet paper. When the acid is neutralized the paper can be thrown away the laboratory trash can.

Laboratory equipment :

- Clean with care the material and equipment laboratory after using.
- Tidy up and clean the laboratory before leaving (workplan + fume hood + centrifuge + material and equipment).
- Tidy up the equipments in their place.

In case of doubt, ask to your manager !!!!

***** Safety data sheet for the chemical products used: in the red book on wooden shelves in the laboratory corridor ^{10}Be / ^{26}Al *in-situ*.**

F - Facilement inflammable
• Brûle facilement ou très facilement !
Tenir éloigné de toute étincelle ou source de chaleur et des produits comburants.
E - Explosif
• Peut exploser !
Tenir éloigné de toute étincelle ou source de chaleur,
Attention aux chocs.
O - Comburant
• Fait brûler les autres substances !
Tenir éloigné de toute étincelle ou source de chaleur et des produits combustibles.
C - Corrosif
• Ronge les objets ou la peau !
Manipuler avec précautions, toujours porter des lunettes de sécurité.
T - Toxique
• Poison mortel !
Ne pas toucher sauf nécessité. Manipuler avec précautions, toujours porter des gants.
Xn - Nocif
• Dangereux en cas de contact !
Manipuler avec précautions, bien se laver les mains par la suite.
N - Dangereux pour l'environnement
• Tue les animaux et les plantes !
Ne pas jeter dans les éviers, récupérer dans un récipient spécial après utilisation.
• Récipient contenant un gaz sous pression !
Manipuler avec précautions.
• Dangereux pour la santé !
Manipuler avec précautions, bien se laver les mains par la suite.

The good laboratory practices

General rules :

- Follow the visitor training before starting your work in the laboratory.

- All manipulations are forbidden out of CEREGE opening hours (7 am-10pm). **Isolated work is forbidden**.

- Never working alone or inform other personns of your presence in the laboratory, of the nature and duration of the manipulations you have to do (in case of accident someone could save you).

- No eat, no drink in the laboratory.

- No food and drinks storage in the laboratory.

- No smoking on the balcony and at the laboratory's windows.

- Cleaning hands before going out the laboratory.

- No touching the door handles with used gloves.

- No storing the lab coat in the office.

- The Frantz using is forbidden for persons with pacemakers or metal implants.

Obligatory work clothes :

- Tieing long hair.

- Open shoes forbidden.

- Obligatory wearing pants to prevent risks of accidental spilling.

- No wearing jewells : necklace, bracelet, ring (risk of jamming or tearing up gloves).

- Wearing contact lenses is strongly no advised.

- Obligatory wearing a coton lab coat with push buttons (to undress in case of accident).

- Obligatory wearing adapted gloves (check the gloves compatibility with the chemical product used).

- Obligatory wearing arm protection for Hexafluorosilic and Fluorhydric acids handling.

- Obligatory wearing security glasses.

- Obligatory wearing ear protection when using the crusher and the Frantz.

- Obligatory wearing hair protection for personn with long hair during crusher using.

- Obligatory wearing FFP3 masks for cathod preparation.

Handling :

- Work under fume hood (check the fume hood is switched on and the ventilation is optimal).

- Knowing the risks of used chemical products for the samples preparation (safety data in the red book, hazard pictograms).

- In case of chemical product projection on the skin or on the eyes, rinse abundantly with water (10 minutes minimum).

- Respecting compatibility storage rules of chemical products (cf. table of incompatibilities between chemical products).

- Storing chemical products in the adapted ventilated cupboard for this.

- The ethanol bottles should be placed out of direct sunlight and heat.

- No mixing chemical products without potential reaction knowledge (risk of temperature increasing, release of toxic gas, creation of moss wich may overflow the container, ignition, explosion,…).

- Acid, base, and solvent should be stored separately.

- Check glassware before use.

- Identify always beackers and material used.

- No trying to smell a non-identified solution to determine its nature.

- No adding water in acid. Pour water first.

- Never pipette with mouth, use propipettes.

- Respect the recommendations regarding laboratory waste management.

Physical treatments of samples :

1. Crushing and sieving

Wearing ears protection and mask during crushing and sieving works. Turn on dust extraction.

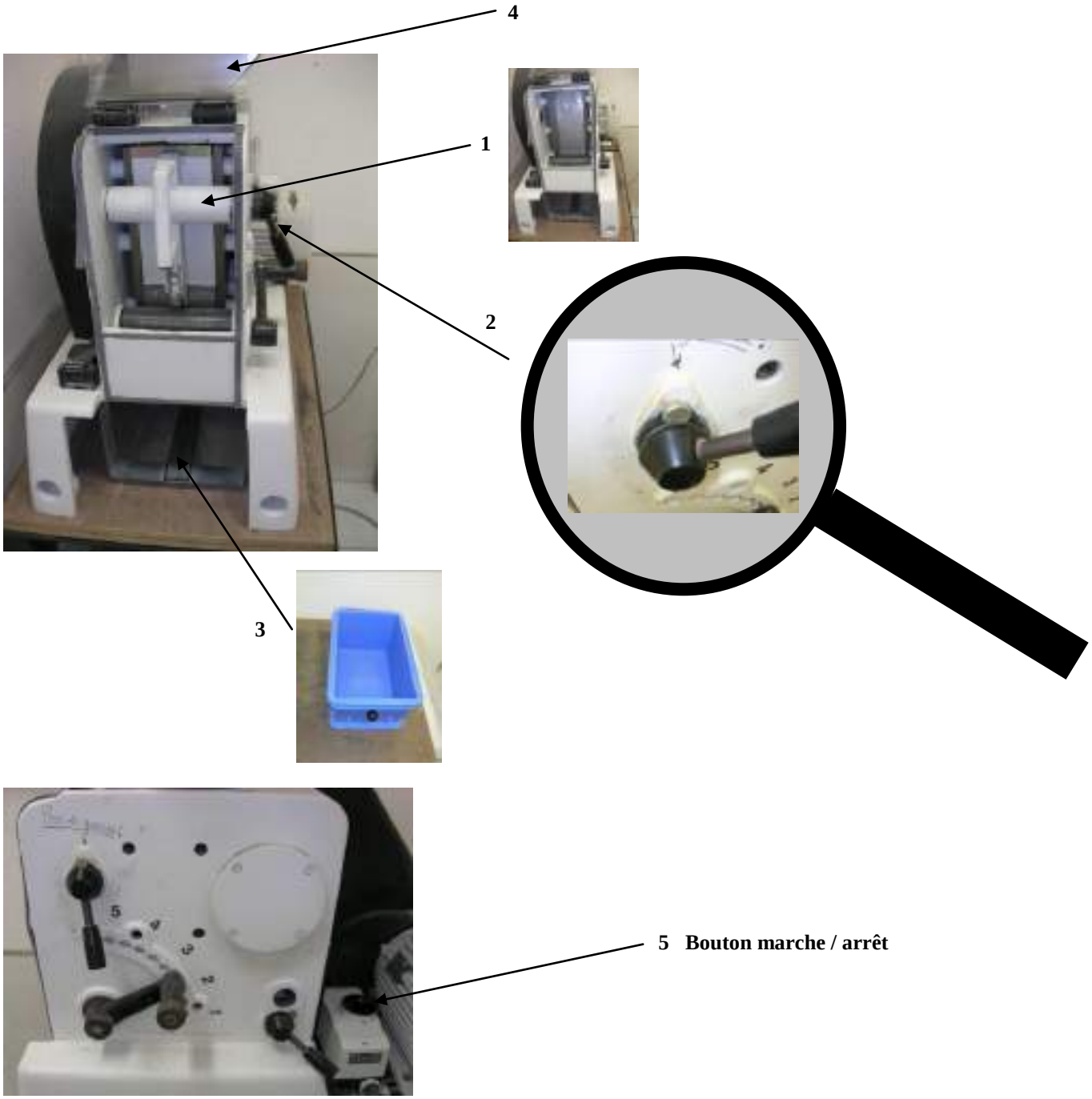

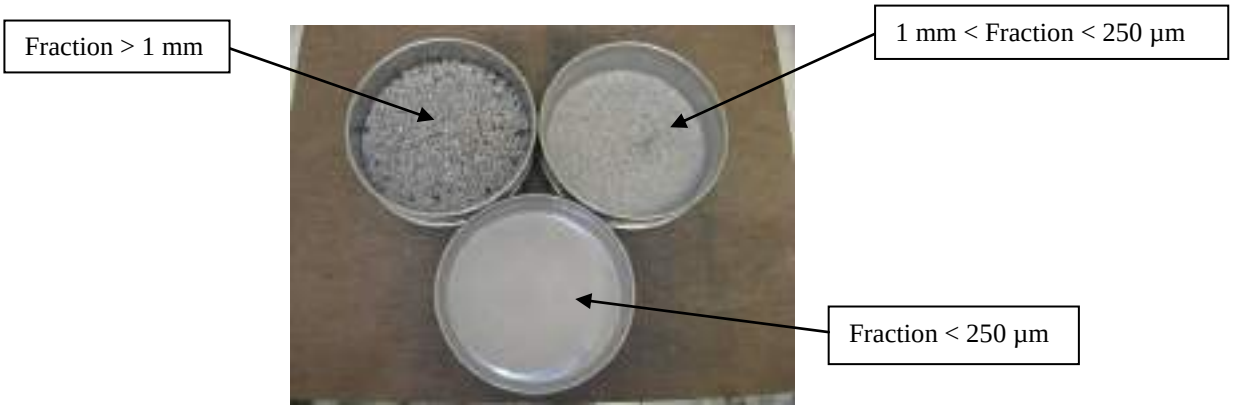

➔ Crushing / sieving :

- Before crushing, check if the crusher is clean (no grains and no dust). Set up the crusher in position 5 and remove the jaw from the crusher **(1)** to chek there is no dust and sample grains. Clean with the hoover, air compressed and ethanol if necessary.
- Set up again the jaw. Put the safety by inserting the screw in the notch. **(2)**
- Change the jaw position depending on pieces of rock to introduce in the crusher and the size of grains to obtain.

Don't feed the crusher with piece of rock more than 7 cm.

- Put the crushed sample box under the jaws. **(3)**
- Move down the plastic window **(4)**.
- Turn on the crusher **(5)**.
- Add the rock in the crusher and close the feeding.

NEVER ADD STONES IN THE CRUSHER WHEN IT IS TURNED OFF.

- Wait everything is crushed and turn off the crusher.

If pieces of rock is blocked in the crusher, stop the crusher, remove the jaw (position 5), take the piece of rock and break it with the mallet.

- Take the box of crushed sample.
- Sieve the crushed sample (between 0,25 mm and 1 mm). *This step allows to increase the specific surface of grains and so, the acid attack surface.*
- Trash fraction under 0,25 mm and keep the fraction of grains between 0,25 mm and 1 mm.

Note : sieving progressively the amount of crushed sample between each crushing step of the sample.

If the sample amount to sieve is too important, split the sample not to recover grains fraction under 0,25 mm.

- Repeat crushing / sieving as many times is necessary : reduce the gap between the jaws by lowering the position to obtain finner grains. Turn on the crusher. Add fraction > 1 mm in the crusher.

The goal is to recover about 200 g of material (fraction between 0.25 mm and 1 mm), adjustable according to the proportion of quartz in the crushed rock and the estimated amount of pure quartz to treat.

- Clean inner the crusher with compressed air, hoover and ethanol.

Check there is no dust in the corners of the crusher to avoid contamination of following sample.

Do not forget to remove the jaw to clean inner the crusher.

Clean the both jaws with compressed air and ethanol.

Clean correctly the sieve between each sample.

At the end of the work :

- Let the room clean for following user.

- Vacuum the sample residues under the cupboard and the crusher.

- Empty the waste bin.

2. Magnetic separation by Frantz.

First separation at 0,5 mA, then 1A and 1,5 A.

Note : these values are given as an indication, to adapt with the sample mineralogic composition and the proportion of magnetic mineral.

Clean the Frantz between each sample with the hoover, compressed air and ethanol.

At the end of the work :

Vacuum residues of sample around the Frantz, under the cupboard and the floor !

Extraction of quartz

Work in the « chimie froide » lab.

Turn on the fume hood's extraction.

Work is finished =

Close acid waste can.

Tidy up the chemical product bottles in the ventiled cabinet.

Clean beakers and test tubes following the appropriate cleaning protocol. Turn off the fume hood's extraction after an hour (to be sure to have evacuated all polutants). No storing of chemical product under the fume hood when it's turned off.

- ➔ Take a Nalgene® bottle of 250 mL, write the sample name on the cap and the bottle.
- ➔ Weight the empty bottle. Write the mass.
- ➔ Pour about 100 g in the Nalgene® sample bottle (the mass to add depend on quartz proportion of the sample and the necessary estimated pure quartz amount).
- ➔ Weight the bottle + sample. Write the mass.
- ➔ Rinse the sample several times with tap water to remove fine fraction and organic material (lichens…).

1. DECARBONATATION

READ BEFORE TO START DECARBONATATION

It is recommanded to carry out the decarbonatation in a big beaker for a safety and faster decarbonatation of the sample.

The reaction between hydrochlorid acid (HCl) and carbonates ($CaCO_3$) is exothermic and may be violente. The knowledge of lithology is necessary before to start this step of the protocol. In case of doubt make a sample test with few drops of hydrochlorid acid.

The temperature in the bottle will be increase and the mixture will start to foam : it's the normal reaction between HCl et $CaCO_3$. After HCl addition, wait reaction is finished before to continue acid addition. The reagent has to be totally consume to avoid reagent accumulation in the bottle which can induce a brutal release of accumulated energy. ***When reagent is totally consume, it is recommanded to discard the solution before adding a new amount of reagent to avoid dilution it.***

An exothermic reaction may be uncontrollable if this reagent addition is not made gradually, there may be a risk of overflow, a sudden release of gas or explosion of the container.

When the mixture starts to foam, grains of material go up with the foam and can form a film of material between the neck of the bottle and the cap. The accumulated gaz in the bottle during the raction can break brutaly this cap of material and cause projections. Then after each hydrochloric acid addition, the bottles'cap has to be removed.

In case of uncontrollable reaction, trash immediatly a part of liquid in the acid waste and put the bottle in a water bath.

In case of overflow in the glass beaker, add tap water with a pissette on the foam to break it and to dilute acid. The reaction will slow down.

➔  Add gradualy (about 5 mL) hydrochloric acide (HCl) 37%. **Take off the cap of the bottle to allow gaz evacuation during the reaction.** If the sample reacts, wait the reaction is finished. When the reaction is finished, shake and trash the acid in the acid waste. Repeat these steps until there is no more reaction.

OR

If there are a lot of carbonates, add the sample in a beaker of 3 L, add some water (tap water or ultra-pure water) and add HCl 37 %. In this case, the amount of acid added may be important BUT be careful to foam overflow ! Once the sample is completly decarbonated, tranfer it in the Nalgene® bottle using a funnel and a beaker of 250 mL.

2. ELLIMINATION OF MINERAL EXCEPTED QUARTZ BY ACID ATTAKS

Wearing thick Neopren gloves (bicolor : blue nad yellow)

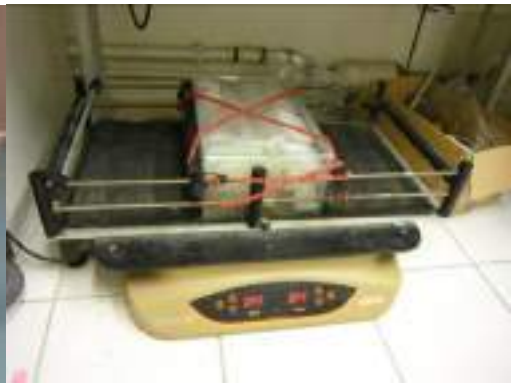

- ➔ Add 1/3 of hydrochloric acid (HCl) 37 %.
- ➔ Add 2/3 hexafluorosilic acid (H_2SiF_6) 34 %. Let 3-4 cm of free space between the level of the solution and the neck of the bottle.
- ➔ Shake during 48 H at 240 rpm on the shaker table.

For the first attacks if the reaction between the sample and the mixture is very efficient, repeat the previous steps after 24 hours of shaking.

- ➔ Discard the reacted solution in the acid waste. Rinse the sample one or two times with about 30 mL of tap water to remove the fine fraction and the foam produced. Discard the rinsings in the acid waste.
- ➔ Repeat these 4 steps as many times as necessary, until the attack efficiency is zero (solution clear and no fine fraction).
- ➔ When the sample no react anymore, discard the solution in the acid waste and rinse the sample 4 times with tap water. Discard the rinsings in the acide waste. Then, rinse the samples 4 times with tap water until pH = 7 and discard the rinsings into the sink. Rinse the neck of the bottle and the cap with tap water.

After working, rinse the sink with a lot of water.

- ➔ Dry the sample in the oven at 90°C (Doesn't forget to take off the bottle's cap !!!!)
- ➔ Let the sample cool.
- ➔ Weigh the bottle + sample. Write the mass

Elimination of meteoric ^{10}Be

Before working with hydrofluoric acid, read the user book and the Safety Data Sheet (SDS).

Obligatory wearing of following safety protections :

⚠ 2 paires of gloves : thin neoprene or nitrile gloves + thick neoprene gloves (yellow and blue).

⚠ Arm protections.

⚠ Safety glasses.

⚠ Put a water bath (cold tap water) under the fume hood.

⚠ Keep nearby a beaker with a saturated $CaCO_3$ solution to neutralize HF in case of accidental spilling or for waste contaminated by HF (paper, pipette, …) before to discard them in the laboratory trash.

⚠ Keep nearby a $CaCO_3$ bottle to neutralize HF in case of accidental spilling or leaks.

For an optimal protection, there is a neoprene lab coat (purple) on the lab's coat rack for users of HF.

Perform three partial dissolutions with HF 48 % (3,6 mL of HF 48 % per gram of quartz to dissolve). *These steps allow to remove all meteoric ^{10}Be diffused into the imperfections of quartz from the surface.*

Fluorhydric acid dissolve glass. Therefore, it's obligatory to cover the fume hood's table with absorbent paper in case of accidental spilling of HF.

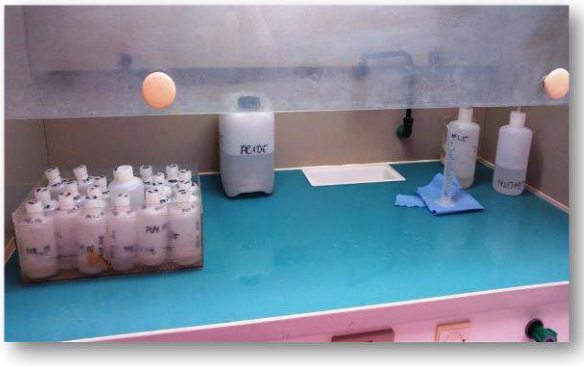

➔ Weigh bottle + sample. Write the mass of sample to decontaminate.

➔ Calculate the volume of HF (48 %) to add to dissolve 10 % of the mass of sample. A theoretical calculation is done for the two other partial dissolutions from the estimated remaining mass.

➔ Add ultra-pure water in the Nalgene® bottle until 0.5 cm – 1 cm above the sample grains. Shake to wet all grains.

➔ Pour the calculated amount of HF in the Nalgene® bottle.

For safety reasons :

- Pour an amount slightly above the calculated amount in a graduated plastic beaker. **CLOSE THE BOTLLE OF HF 48% IMMEDIATELY.**

- Adjust with precision the volume of HF to add with a graduated plastic tube. Pour gradually HF in the Nalgene® bottle with care to prevent violent reaction between the HF and the sample.

- ➔ Swirl sligtly the bottle and degaz (**becarefull risk of violent reaction**). In case of violent reaction, put the Nalgene® bottle in the water cold bath without loosen the cap to degaz (even if the whole wolume of HF has not been added). Wait until the bottle is cold, add the remaining volume of HF keeping the bottle in the water cold bath.
- ➔ Let the bottles in the cold water bath during ½ hour (the duration depend on the sample reaction). Let the caps loosen.
- ➔ \Take off the bottles from the bath, close them, shake them, loosen the caps to degaz and let them stand outside the bath for 1 hour.

  If the bottles are still warm, let them cool down until room temperature before to put them on the shaker. Ask to your manager.
- ➔ Put the bottles in a plastic bag. Put the bag in a plastic box : bottles in the lying position. Shake the bottles during 24 h at 240 rpm.
- ➔ Discard the solution in the acid waste. Rinse the sample one or two times with ultra-pure water and discard the rinsings in the acid waste. Make again the 6 prevoius steps 2 times. *If the mixture is milky add water before to discard the solution in the acid waste and rinse 2 or 3 times the sample with ultra-pure water before to add the calculated volume of HF.*
- ➔ **OPTIONAL** : if the solution is still milky or if somes feldspars are still inside the sample, a fourth attack must be carried out. The process must be repeated until perfect pure quartz is obtained !
- ➔ Discard the solution in the acid waste and rinse the sample 5 times with ultra-pure water. Discard the rinsings in the acid waste. Then, rinse the sample 5 times with ultra-pure water until pH = 6. Discard the rinsings into the sink.

After working, rinse the sink with a lot of water. 

- ➔ Dry the samples in the oven at 90°C.
- ➔ Let cooling samples.
- ➔ Weigh the bottle + sample. Write the mass. 

Checking the purity of quartz using a binocular lens

If the sample has a too large proportion of feldspars, the HF purifications must be continued by adjusting the amount of HF versus the proportion of impurities to eliminate.

If the impurities are in inclusion, stop the attacks with HF. In case of doubt, ask to your manager.


Weighing and back up of decontaminated pure Quartz

- ➔ Take a new Nalgene® bottle of 250 mL if the first is dommaged by the previous steps, write the sample name on the cap and the bottle.
- ➔ Weight the empty bottle. Write the mass.
- ➔ Pour 20 g of decontaminated pure quartz in the bottle. Weight the bottle + sample. Write the mass.

20g is usually amount of quartz used. It is strongly recommanded to estimate the amount of quartz to treat according to the GPS coordinates of the sample, the altitude, the depth of the sample and its estimated age or the geological period concerned. For this estimation, it is recommanded to take a $^{10}Be/^{9}Be$ and $^{26}Al/^{27}Al$ ratio values of 10^{-13}.

- ➔ Keep the pure decontaminated quartz in a plastic bag (write the name of the sample on the bag).

Adding of Spike ^{9}Be



The spike allow to handle a ponderable amount and to fix the $^{10}Be/^{9}Be$ ratio measured by Accelerator Mass Spectrometry.

Add ultra-pure water in the Nalgene® sample bottle to wet all grains inside.

Use the 10^{-5} g balance (SARTORIUS®) in the « yellow lab » to weight the spike.

With this balance, it is difficult to obtain a stable weigh by adding directly the spike in the Nalgene® bottle. Indeed, many electrostatic charges occur between the sample and the bottle, making the meausrement unstable even when using the « deionization » function. So, it is recommanded to weight the spike in a plastic vial of 1.5 mL with a conical bottom and to transfer it in the Nalgene® bottle.

The process is described below :

- ➔ To obtain the spike ask to these following persons : Laëtitia Léanni, Valéry Guillou, Régis Braucher. **Name of Spike : Phénakite, [^{9}Be]=3025±9 µg/g**
- ➔ Check the tara of the balance.
- ➔ Take a vial of 1.5 mL with a conical bottom, put it on the weighing pan, deionize (pushing on the « I » touch) and wait the balance is stable (« g » appears after the last digit). Make the tara.
- ➔ Collect 150 µL of spike and introduce them into the vial.
- ➔ Put the vial on the weighing pan, deionize (pushing on the « I » touch) and wait the balance is stable (« g » appears after the last digit). Write the mass.
- ➔ Pour the 150 µL of spike in the sample bottle.
- ➔ Rinse 3 times the vial with ultra-pure water. Pour directly the rinsings in the sample bottle. BECAREFUL : DON'T LOSE DROPS DURING THE RINSINGS !!!
- ➔ Discard the vial.

Take a vial for each sample.

Dissolution totale du quartz

Before working with hydrofluoric acid, read the user book and the Safety Data Sheet (SDS).

Obligatory wearing of following safety protections :

⚠ 2 paires of gloves : thin neoprene or nitrile gloves + thick neoprene gloves (yellow and blue).

⚠ Arm protections.

⚠ Safety glasses.

⚠ Put a water bath (cold tap water) under the fume hood.

⚠ Keep nearby a beaker with a saturated $CaCO_3$ solution to neutralize HF in case of accidental spilling or for waste contaminated by HF (paper, pipette, …) before to discard them in the laboratory trash.

⚠ **Keep nearby a $CaCO_3$ bottle to neutralize HF in case of accidental spilling or leaks.**

For an optimal protection, there is a neoprene lab coat (purple) on the lab's coat rack for users of HF.

THIS WORK MUST BE DONE ONLY UNDER THE ALCOPLAST® FUME HOOD !

➔ Add 3.6 mL of HF (48%) per gram of quartz to dissolve plus an excess of 30 mL.

$$SiO_2 + 6HF \longrightarrow H_2SiF_6 + 2H_2O$$

➔ In case of violent reaction, put the bottles with caps loosened, in a cold water bath during 1 or 2 hours.

➔ Take off the bottles from the cold water bath and let them with the caps loosened all the night.

➔ Put the bottles in a plastic bag. Put the bag in a plastic box : <u>bottles in the standing position</u> (to avoid leaks of HF during the shaking). Shake the bottles at 240 rpm during 48 hours.

Evaporation of the solution resulting of quartz dissolution

⚠ **Before working with hydrofluoric acid, read the user book and the Safety Data Sheet (SDS).**

Obligatory wearing of following safety protections :

⚠ **2 paires of gloves : thin neoprene or nitrile gloves + thick neoprene gloves (yellow and blue).**

⚠ **Arm protections.**

⚠ **Safety glasses.**

⚠ **Put a water bath (cold tap water) under the fume hood.**

⚠ Keep nearby a beaker with a saturated $CaCO_3$ solution to neutralize HF in case of accidental spilling or <u>for waste contaminated by HF (paper, pipette, …)</u> before to discard them in the laboratory trash.

⚠ Keep nearby a $CaCO_3$ bottle to neutralize HF in case of accidental spilling or leaks.

For an optimal protection, there is a neoprene lab coat (purple) on the lab's coat rack for users of HF.

DO THIS WORK <u>ONLY UNDER THE ALCOPLAST® FUME HOOD</u> !



➔ Clean with ultra-pure water one teflon beaker of 250 mL with a black bottom.

➔ Pour in the beaker the solution resulting of total dissolution of the sample.

➔ Rinse 3 times the sample bottle with 10 mL of HNO_3 at 65 %. Add the rinsings in the beaker.

➔ Let evaporate until dryness on the hotplate set to minium.

➔ If some residues remain in the Nalgene® bottle, don't add them in the teflon beaker. Rinse the bottle 4 times with tap water (fill half the bottle for the first rinsing), trash carefully the first rinsing in the acid waste not to lose residues and the other rinsings into the sink (for the the three other rinsings fill the botlle completly). Rinse the neck of the bottle and inside the cap and dry the residues in the oven at **<u>60°C</u>**.

Rinse the residues with care not to lose them because their mass will allow to correct the mass of quartz actually dissolved.

➔ Weigh the bottle + residues. Write the mass. ✍

Mass of dissolved quartz = (mass of quartz + bottle) – (mass of the bottle + residues)

➔ OPTIONAL : if the Nalgene® bottle have not be changed since the extraction steps of pure quartz, it will be necessary to weight the empty bottle without residue in order to take into account the loss of mass of the bottle (loss of mass after heating + abrasion during the several steps of shaking). Write the mass. ✍

➔ **Weight a centrifuge tube. Write the mass.** ✍

➔ Recover the sample at hot temperature, with **3 mL** of HCl at 7 mol.L^{-1} and transfer them in the centrifuge tube of 50 mL. If there are some indissolved residues, recover only the solution.

If the amount of residues in the bottom of the teflon beaker after evaporation until dryness is important, this means that the sample has not been correctly purified. Undisolved fluoride complexes are formed. In this case add few milliliters of more of HCl at 7 mol.$^{L-1}$.

➔ Rinse the beaker 3 times with **3 mL** of HCl at 7 mol.L^{-1} and transfer the rinsings in the tube.

If necessary adjust, at each rinsing, the volume of acid depending of the amount of residues in the bottom of the beaker.

➔ **Weight the tube + solution. Write the mass.**

These steps have to be done with care. Do not lose the Al because the Al content is not measured yet. The Al losses induce an error on the determination of the number of Al atoms in the raw sample.

If there is a negligible mass of residues in the centrifuge tube

If this step is necessary, the quartz is not correctly purified.

- Weight a new empty tube. Write the mass.
- Centrifuge 5 min at 4000 tr/min and transfer the solution in the new tube to separarte residues from the solution.
- Rinse the residues 3 times with **1.5 mL** of HCl at 7 mol.L^{-1}. After each adding of HCl : «vortex» to rinse efficiency the residues, centrifuge 5 min at 4000 tr/min and add the rinsings in the new tube.
- **Weight the tube + solution. Write the mass.**

Collect of a sample aliquot and measurement of Al content of the sample by ICP-OES

➔ **Weight an empty vial of 1.5 mL. Write the mass.**

➔ Centrifuge the sample tube during 1 min at 4000 tr/min.

➔ Vortex the solution at medium speed not to go up and stick sample drops in the cap.

➔ Collect an aliquot of 500 µL of the sample solution. Weight the vial + solution. Write the mass.

➔ **Weight the tube + solution – aliquot. Write the mass.**

Aliquot dilution for sample Al content measurement by ICP-OES

- ➔ Take a tube of 15 mL and make the tara.
- ➔ Vortex the vial of the sample aliquot.
- ➔ Collect 200 µL of aliquot and add them in the tube of 15 mL. Weight the solution. Write the mass.
- ➔ Add 9.8 mL of HNO_3 solution at 2 %. Weight the total solution (200µL of sample + 9.8 mL of HNO_3). Write the mass.

Adding of ^{27}Al spike

If the number of ^{27}Al atoms in the solution is inferior at 4.10^{19} atoms, a commercial solution of ^{27}Al (spike Al) is added to reach the number of atoms wanted.

- ➔ Make the tara of the sample tube.
- ➔ Add in the tube, the calculated volume of spike using an adjustable pipette. Weight and write the mass.
- ➔ Vortex and centrifuge during 1 min at 4000 tr/min.

Precipitation

This is a first step of purification, allowing to remove some elements in solution and to isolate Be end Al.

- ➔ Add ammonia 32 % drop by drop using a 3mL pasteur pipette, by shaking the mixture sometimes. Add ammonia until pH=8.

The pH should not exceed 8 because there is a risk of redissolution of part of the Al (10 % at pH=9 and 55% at pH = 10). The pH should not be inferior to 7 because a part of Be is redissolved.

If the pH is too high : add some drops of HCl, conversely : if the pH is too low : add some drops of ammonia.

- ➔ The reaction is exothermic. Let cool the tubes until room temperature.
- ➔ Vortex at maximum speed.
- ➔ Centrifuge during 5 min at 4000 tr/min.
- ➔ Check another time the pH is 8.
- ➔ Discard the supernatant and keep the precipitate.

Warning : check the precipitate is stuck well on the bottom of the tube. Otherwise centrifuge an other time or recover the supernatant with a pasteur pipette with care not to pipette a part of precipitate.

- ➔ Rinse the precipitate with 10 mL of water at pH 8 (add one drop of ammonia 32 % using 3 mL pasteur pipette, in about 240 mL of ultra-pure water – shake vigorously and check the pH – adjust if necessary the pH discarding a part of water and adding ultra-pure water).
- ➔ « Vortex » to break the precipitate and to rinse it.
- ➔ Centrifuge during 5 min at 4000 tr/min.
- ➔ Discard the supernatant.
- ➔ Add 1,5 mL of HCl at **10,2 mol.L^{-1}** using a pasteur pipette to dissolve the precipitate.
- ➔ Vortex.
- ➔ Centrifuge during 1 min. *This step allow to recover the sample drops from the wall of the tube.*

Anion exchange resin : elimination of Fe and Mn

The funnel <u>must not be in contact with the sample</u>.

Before starting, check that the equipments have been thoroughly cleaned by the previous user. If necessary clean them with ultra-pure water.


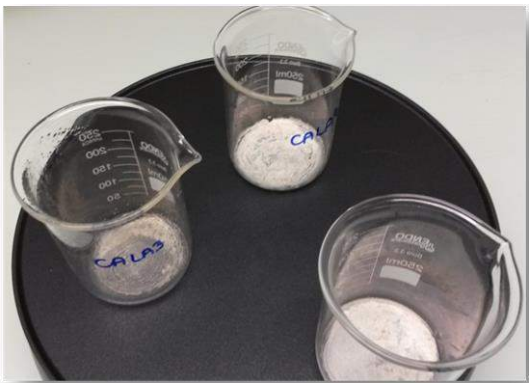


<u>Columns preprataion :</u>

- ➔ Check the white ring is correctly positionned. Adjust it if necessary with a plastic stick.
- ➔ Put the column on the rack.

- ➔ Put a « trash beaker » under the column.
- ➔ Pour the DOWEX 1*8 resin (100-200 mesh) mixed to ultra-pure water into a beaker.
- ➔ Pour the resin into the column until 9 cm. **WARNING :** the column must be always fulled with the same density to have an homogeneous distribution in the column. **If there are somes strats or bubbles inside the resin bed, the column MUST BE MADE AGAIN.**
- ➔ Let go down the water until 1 cm above the resin.

Resin cleaning :

- ➔ Insert a funnel above the column and add 50 mL of ultra-pure water.
- ➔ Let go down the water until 0.5 cm above the resin.
- ➔ Take off the funnel.
- ➔ Close the column : first the white cap and second the red cap. *This order allows all air bubbles trapped between the column tap and the white ring to be removed, so that they don't rise and be trapped inside the resin bed. The column can be stored like this for several days.*
- ➔ Discard water in the trash beaker.

Conditioning :

- ➔ Take off the caps.
- ➔ Let go down the water remaining in the column (above the resin bed).
- ➔ When the meniscus base reaches the level of the column, add 20 mL of HCl **10,2 mol.L^{-1}** using a pasteur pipette (10 mL drop by drop and along the wall of the column not to disturb the resin level and lift the resin, then add the remaining volume).
- ➔ Clean a new glass beaker with ultra-pure water to recover the sample eluted at column outlet.
- ➔ When 20 mL went across the resin column, put the sample beaker under the column and protect the beaker of splashing using parafilm®.

Sample injection :

- ➔ When the meniscus base reaches the top of the resin, inject the sample using a pasteur pipette. Wait total elution, then rinse the tube with 0.5 mL of HCl **10.2 mol.L^{-1}** and inject the rinsing in the column.

Sample elution :

- ➔ When the meniscus base reaches the top of the resin, insert the funnel above the column and add 18 mL of HCl **10.2 mol.L^{-1}** using a pasteur pipette (10 mL drop by drop and along the wall of the funnel not to disturb the resin level and lift the resin, then add the remaining volume).

RECOMMENDATIONS :

- Never let the resin until dryness.
- Never condition the resin in advance.
- Inject always the first milliliters of solution drop by drop along the column wall or the funnel not to disturb the resin level and lift the resin.
- During the conditioning the resin shrink and change color.
- When elution is finished :

  * Discard the resin in the « resin waste ».

  * Clean the column with tap water and to finish with ultra-pure water.

  * Adjust the white ring if necessary using a plastic stick.

  * Clean the funnel with tap water and to finish with ultra-pure water.

Evaporation of eluted fraction :

➔ Evaporate the eluted fraction until dryness at 200 °C.

➔ Recover the sample with 3 mL of HCl 7,1 mol.L^{-1} and transfer them in a centrifuge tube. Rinse the beaker 3 times with 3 mL of HCl 7,1 mol.L^{-1} and transfer the rinsings into the tube.

➔ **Immediately** cover the beakers with Parafim® (these beakers are used for recover Be fraction at following step).

Precipitation :

➔ Add ammonia 32 % drop by drop using a 3mL pasteur pipette, by shaking the mixture sometimes. Add ammonia until pH=8.

The pH should not exceed 8 because there is a risk of redissolution of part of the Al (10 % at pH=9 and 55% at pH = 10). The pH should not be inferior to 7 because a part of Be is redissolved.

If the pH is too high : add some drops of HCl, conversely : if the pH is too low : add some drops of ammonia.

➔ The reaction is exothermic. Let cool the tubes until room temperature.

➔ Vortex at maximum speed.

➔ Centrifuge during 5 min at 4000 tr/min.

➔ Check another time the pH is 8.

➔ Discard the supernatant and keep the precipitate.

Warning : check the precipitate is stuck well on the bottom of the tube. Otherwise centrifuge an other time or recover the supernatant with a pasteur pipette with care not to pipette a part of precipitate.

➔ Rinse the precipitate with 10 mL of water at pH 8 (add one drop of ammonia 32 % using 3 mL pasteur pipette, in about 240 mL of ultra-pure water – shake vigorously and

check the pH – adjust if necessary the pH discarding a part of water and adding ultra-pure water).

- ➔ « Vortex » to break the precipitate and to rinse it.
- ➔ Centrifuge during 5 min at 4000 tr/min.
- ➔ Discard the supernatant.
- ➔ Add 1,5 mL of HCl at **1 mol.L^{-1}** using a pasteur pipette to dissolve the precipitate.
- ➔ Vortex.
- ➔ Centrifuge during 1 min. *This step allow to recover the sample drops from the wall of the tube.*

Cation exchange resin : B, Be and Al separations

Columns prepratаion :

- ➔ Check the white ring is correctly positionned. Adjust it if necessary with a plastic stick.
- ➔ Put the column on the rack.
- ➔ Put a « trash beaker » under the column.
- ➔ Pour the DOWEX 50WX8 resin (100-200 mesh) mixed to ultra-pure water into a beaker.
- ➔ Pour the resin into the column until 9 cm. **WARNING :** the column must be always fulled with the same density to have an homogeneous distribution in the column. **If there are somes strats or bubbles inside the resin bed, the column MUST BE MADE AGAIN.**
- ➔ Let go down the water until 1 cm above the resin.

Resin cleaning :

- ➔ Insert a funnel above the column and add 50 mL of ultra-pure water.
- ➔ Let go down the water until 0.5 cm above the resin.
- ➔ Take off the funnel.
- ➔ Close the column : first the white cap and second the red cap. *This order allows all air bubbles trapped between the column tap and the white ring to be removed, so that they*

don't rise and be trapped inside the resin bed. The column can be stored like this for several days.

➔ Discard water in the trash beaker.

Conditioning :

➔ Take off the caps.

➔ Let go down the water remaining in the column (above the resin bed).

➔ When the meniscus base reaches the level of the column, insert the funnel add 30 mL of HCl **1 mol.L^{-1}** using a pasteur pipette (10 mL drop by drop and along the wall of the funnel not to disturb the resin level and lift the resin, then add the remaining volume).

➔ When 30 mL went across the resin column, take off the funnel.

Sample injection :

➔ When the meniscus base reaches the top of the resin, inject the sample using a pasteur pipette. Wait total elution, then rinse the tube with 0.5 mL of HCl **1 mol.L^{-1}** and inject the rinsing in the column.

Boron elution :

➔ Keep the « thrash beaker » under the column.

➔ When the meniscus base reaches the level of the column, insert the funnel add 40 mL of HCl **1 mol.L^{-1}** using a pasteur pipette (10 mL drop by drop and along the wall of the funnel not to disturb the resin level and lift the resin, then add the remaining volume).

This step removes boron whicht is eluted before beryllium.

➔ Clean a glass beaker with ultra-pure water to recover the eluted Be and write « Be » on it.

Beryllium elution :

➔ When the meniscus base reaches the top of the resin, put the « Be beaker » under the column and prtotect from splashes with parafilm®.

➔ Add into the funnel 115 mL of HCl **1 mol.L^{-1}** using a pasteur pipette (10 mL drop by drop and along the wall of the funnel not to disturb the resin level and lift the resin, then add the remaining volume).

➔ Clean a glass beaker with ultra-pure water to recover eluted Aluminium. Write « Al » on it.

Aluminium Elution :

➔ When the meniscus base reaches the top of the resin, put the « Al beaker » under the column and prtotect from splashes with parafilm®.

➔ Add into the funnel 50 mL of HCl **4.5 mol.L^{-1}** using a pasteur pipette (10 mL drop by drop and along the wall of the funnel not to disturb the resin level and lift the resin, then add the remaining volume).

RECOMMENDATIONS :

- Never let the resin until dryness.
- Never condition the resin in advance.
- Inject always the first milliliters of solution drop by drop along the column wall or the funnel not to disturb the resin level and lift the resin.
- Check the funnel is well inserted in the column and there is no liquid blocked between the funnel and the column, thus preventing the flow of eluent through the resin.
- During aluminium elution, the resin shrinks until 8 cm.
- When elution is finished :

  * Discard the resin in the « resin waste ».

  * Clean the column with tap water and to finish with ultra-pure water.

  * Adjust the white ring if necessary using a plastic stick.

  * Clean the funnel with tap water and to finish with ultra-pure water.

Evaporation of eluted fractions (Be, Al) :

➔ Evaporate the eluted fractions : « Be » and « Al » until dryness at 200 °C.

➔ Recover the sample with 3 mL of HCl 7,1 mol.L^{-1} and transfer them in a centrifuge tube. Rinse 3 times with 3 mL of HCl 7,1 mol.L^{-1} and add the rinsings in the tube.

Precipitation :

➔ Add ammonia 32 % drop by drop using a 3mL pasteur pipette, by shaking the mixture sometimes. Add ammonia until pH=8.

The pH should not exceed 8 because there is a risk of redissolution of part of the Al (10 % at pH=9 and 55% at pH = 10). The pH should not be inferior to 7 because a part of Be is redissolved.

If the pH is too high : add some drops of HCl, conversely : if the pH is too low : add some drops of ammonia.

➔ The reaction is exothermic. Let cool the tubes until room temperature.

➔ Vortex at maximum speed.

➔ Centrifuge during 5 min at 4000 tr/min.

➔ Check another time the pH is 8.

➔ Discard the supernatant and keep the precipitate.

Warning : check the precipitate is stuck well on the bottom of the tube. Otherwise centrifuge an other time or recover the supernatant with a pasteur pipette with care not to pipette a part of precipitate.

- ➔ Rinse the precipitate with 10 mL of water at pH 8 (add one drop of ammonia 32 % using 3 mL pasteur pipette, in about 240 mL of ultra-pure water – shake vigorously and check the pH – adjust if necessary the pH discarding a part of water and adding ultra-pure water).
- ➔ « Vortex » to break the precipitate and to rinse it.
- ➔ Centrifuge during 5 min at 4000 tr/min.
- ➔ Discard the supernatant.
- ➔ Rinse the precipitate with 10 mL of water at pH 8.
- ➔ « Vortex » to break the precipitate and to rinse it.
- ➔ Centrifuge during 5 min at 4000 tr/min.
- ➔ Discard the supernatant.
- ➔ Add 200 µL of HNO_3 à 65 % to dissolve the precipitate.
- ➔ « Vortex ».
- ➔ Centrifuge during 1 min. *This step allow to recover the sample drops from the wall of the tube.*

Oxydation

Wear a mask to load the cruccibles in the oven.

NEVER transport crucibles with BeO powder inside without cover them with parafilm® under the fume hood. Even for short trips, for example to load the oven.

- ➔ Add the sample in a crucible (clean it with ultra-pure water before) using a pasteur pipette of 1 mL.
- ➔ Rinse the tube and the pipette 3 times with 200 µL of ultra-pure water and add the rinsings in the crucible.

➔ Evaporate the solution until dryness at 200 °C. When it's dried increase the temperature until 400 °C during 15 minutes.

➔ Oxidize during 1 hour at 700 °C.

Be careful : at 700 °C the sample name written on the crucibles are erased. Note on your lab book the position of crucibles in the oven.

➔ Let cool and cover with parafilm®.

The samples are ready to prepare cathods for AMS.

Before your departure, please clean the laboratory (fume hoods, work tables, centrifuges, vortex, racks,…), do the dishes (beakers, graduated tubes,…) and put away the material in its dedicated cupboard once dried.

7 Apresentações do projeto

No dia 02/12/2021 ministrei uma palestra no programa de e-séminaires do HSM-Montpellier intitulado "*The hydro sedimentological studies in the fluvial karst of central Brazil*". O Conteúdo da apresentação segue abaixo.

Planning des séminaires HSM du jeudi des mois de nov, déc 2021, janvier 2022

Nathalie Rouche <nathalie.rouche@umontpellier.fr>

Sex, 22/10/2021 12:05

Para: hsm-personnels <hsm-personnels@umontpellier.fr>

Programme des e-séminaires internes HSM du jeudi

Mois de novembre* et décembre 2021, janvier 2022

Les séminaires ont lieu les jeudis de 13h15 à 14h sous forme de visioconférence sur Zoom, durée 45 minutes : présentation, discussion

18/11/2021 Malan Ellefsen, doctorante / Norwegian University of Science and Technology (NTNU), Norvège
Hydrogeology in the Faroe Islands.

25/11/2021 Sandra Bayonne, doctorante / HSM.
Hydrosédimento biogéochimique dans le bassin du Congo.

02/12/2021 Rogerio Elias Soares Uagoda, associate professor / University of Brasilia
The hydro sedimentological studies in the fluvial karst of central Brazil.

09/12/2021 Alain Laraque, potamologue / IRD
Comment un pays intertropical démuni peut-il maitriser (ou pas) ses ressources en eau ?.

16/12/2021 Stephane Debard, chef de projet science de la donnée et des modèles / HSM
Vision technique sur Data-Terra, les pôles de données et les services offerts aux scientifiques notamment en hydrologie.

06/01/2022 date disponible
lien d'inscription :https://framaforms.org/seminaires-internes-hsm-1629820575

13/01/2022 France Toma, chargée de productions audiovisuelles et multimédia / IRD
Présentation de la plateforme de ressources audiovisuelles IRD Multimédia.

20/01/2022 date disponible

27/01/2022 date disponible

Pour proposer un séminaire du jeudi en 2022 il suffit de s'inscrire par retour mail ou en suivant le lien d'inscription :
https://framaforms.org/seminaires-internes-hsm-1629820575

La programmation des séminaires se fait sur le principe du volontariat , dans les thématiques de l'UMR, à un ou plusieurs conférenciers.

Si les séminaires sont le plus souvent sur des thèmes scientifiques, d'autres sujets sont les bienvenus: sujets techniques, fonctions d'appui et/ou d'intérêt collectif, plateformes... Les présentations peuvent être données par des extérieurs, n'hésitez pas à solliciter vos visiteurs, voire à en inviter. Pour toute question, n'hésitez pas à contacter un membre de l'équipe d'organisation des séminaires.

Nous vous remercions de l''intérêt que vous portez à l'animation interne du laboratoire HydroSciences Montpellier.

novembre* : après les vacances de la Toussaint et le 11 novembre, jour férié.

--- L'équipe d'organisation des séminaires ---
Nathalie Rouché, Jacques Gardon, Carole Delenne, Christophe Peugeot, Emmanuelle Cadot

geoKarst - Research Group on Karst Geosystem

The hydro sedimentologial studies in the fluvial karst of central Brasil

Rogerio Uagoda
Associate Professor– University of Brasília/UnB
Fellow in Research Productivity –CNPq
Mobilité Sud-Nord IRD

Support:

geoKarst is a group hosted in University of Brasilia, focused in the studie of the karst in Central Brasil. These group involves 10 Researchers from 03 national and overseas Institutions , 01 Post doc fellow, 05 PhD, 02 master and 02 undergrad students.

We have currently funds from tree research projects and three Espeleological Compensation Terms.

The **Goal** of these presentation is to show the mean problems we are working since 2018 and the current project with IRD.

Support:

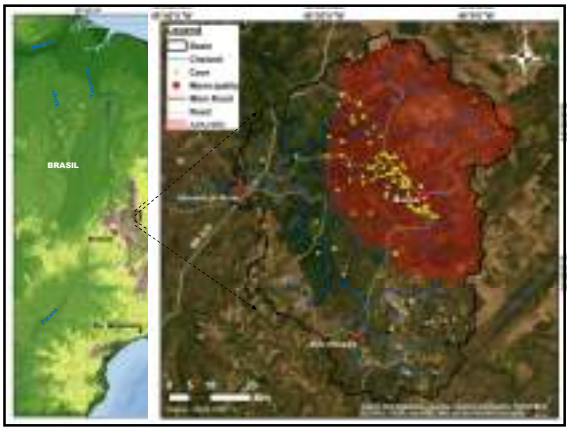

EXPLORATORY RESEARCH

GIS-Based Relief Compartment Mapping of Fluvio-Karst Landscape in Central Brazilian Highlands

Open Access

*Email:

INTERSECTION - LANDFORMS AND GEOLOGY

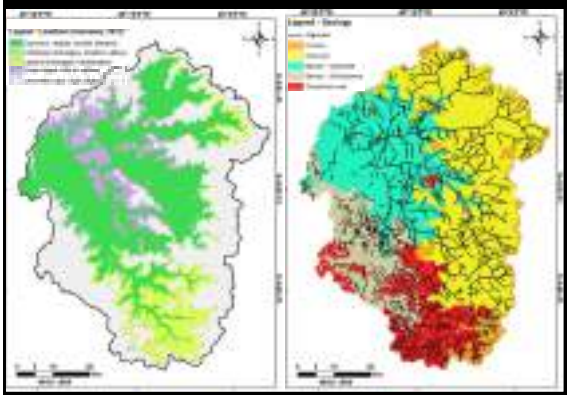

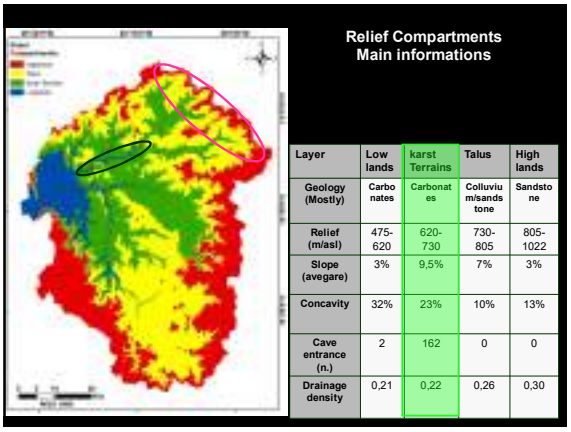

Relief Compartments Main informations

Layer	Low lands	karst Terrains	Talus	High lands
Geology (Mostly)	Carbonates	Carbonates	Colluvium/sandstone	Sandstone
Relief (m/asl)	475-620	620-730	730-805	805-1022
Slope (avegare)	3%	9,5%	7%	3%
Concavity	32%	23%	10%	13%
Cave entrance (n.)	2	162	0	0
Drainage density	0,21	0,22	0,26	0,30

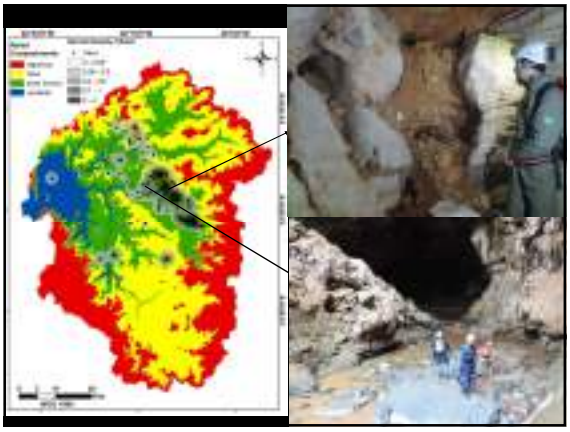

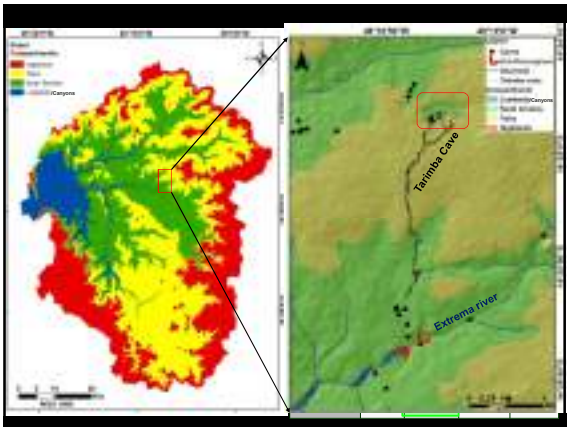

WATER AND SEDIMENT SOURCES IN A FLUVIAL KARST GEOSISTEM

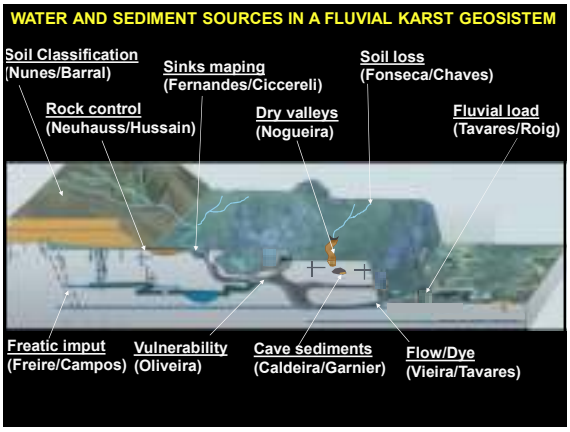

ROCK CONTROL STUDY

The Potential Use of Geophysical Methods to Identify Cavities, Sinkholes and Pathways for Water Infiltration

The potential use of geophysical methods to identify cavities, sinkholes and pathways for water

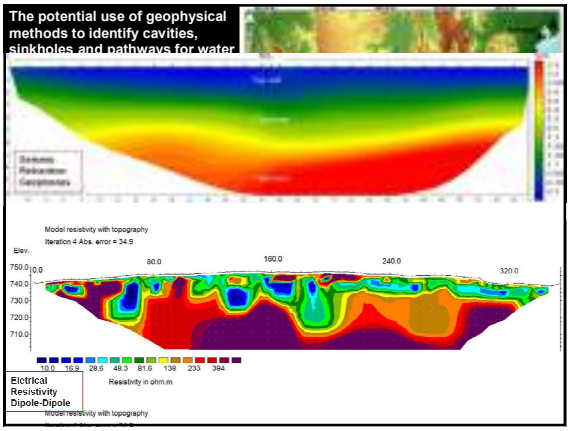

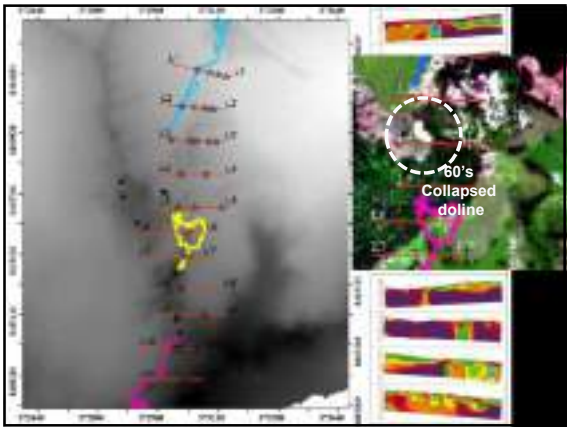

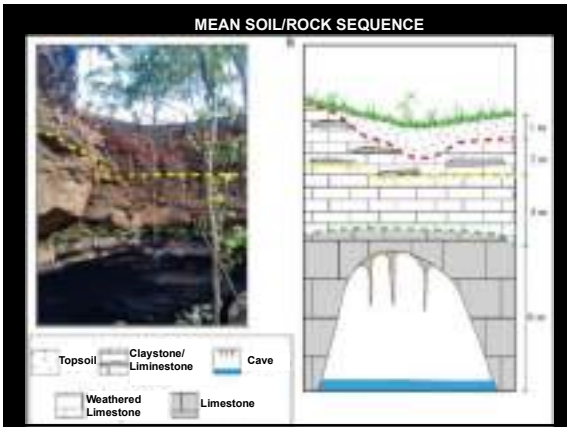

SOIL/
EPIKARST
STUDY

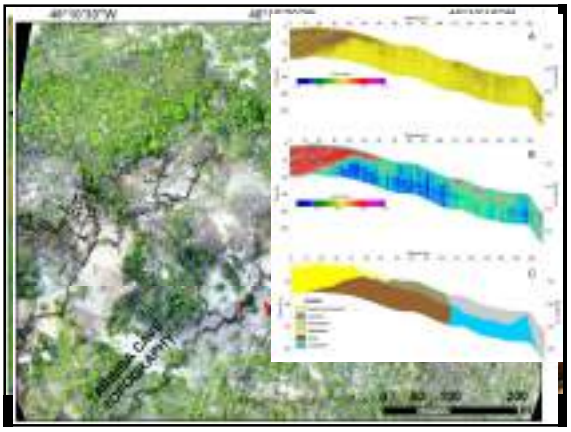

1:50.000 Escale
Soil Map

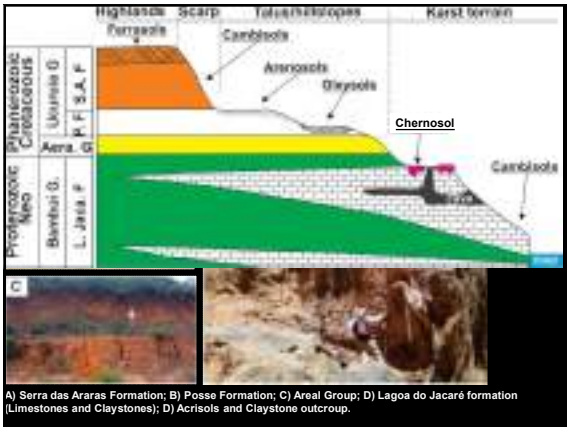

A) Serra das Araras Formation; B) Posse Formation; C) Areal Group; D) Lagoa do Jacaré formation (Limestones and Claystones); D) Acrisols and Claystone outcroup.

SEMI AUTOMATIC DOLINE MAPPING

THE USE OF UAV DERIVED DEM FOR MAPPING DOLINES IN THE ENVIRONMENTAL PROTECTION AREA OF "NASCENTES DO RIO VERMELHO", GOIÁS, BRAZIL

Dolines

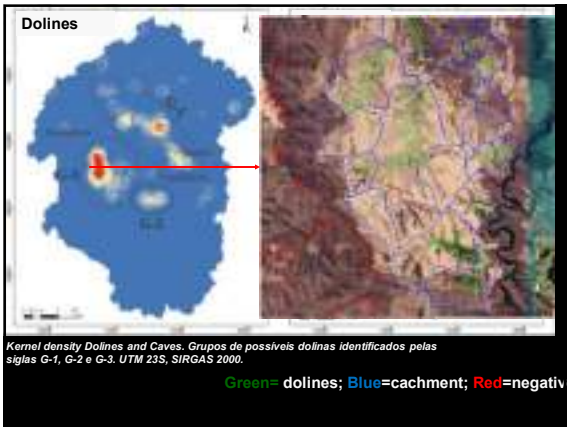

Kernel density Dolines and Caves. Grupos de possíveis dolinas identificados pelas siglas G-1, G-2 e G-3. UTM 23S, SIRGAS 2000.

Green= dolines; Blue=cachment; Red=negativ

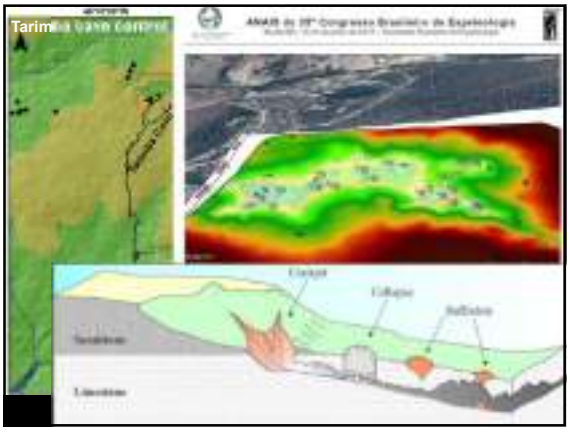

EROSION METHOD POTENTIAL (EPM) -INTENSITY OF EROSION AND OUTFLOW INTERO SPALEVIC, 2011

ANALYSIS OF THE EROSION POTENTIAL AND SEDIMENT YIELD USING THE INTERO MODEL IN AN EXPERIMENTAL WATERSHED MONITORED BY KARST IN BRAZIL

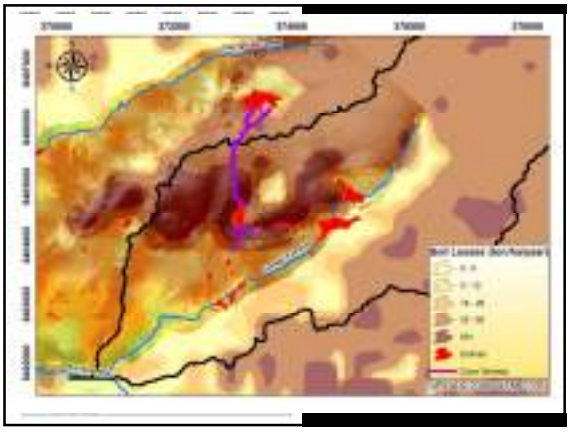

RUNOFF PLOT x LAND RECOVERY

Rates, factors, and tolerances of water erosion in the Cerrado biome (Brazil): A meta-analysis of runoff plot data


WISCHMEYER RUNOFF PLOT
L = 22,10 m; S = 11%
P0
P1
P2
P3
P4
P5
23 outubro 2018
23 outubro 2018

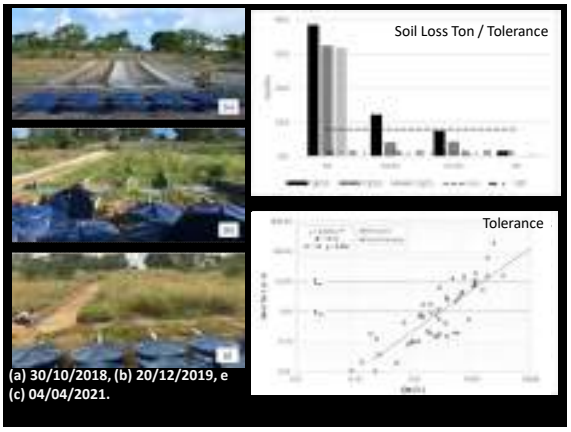
Soil Loss Ton / Tolerance
Tolerance
(a) 30/10/2018, (b) 20/12/2019, e
(c) 04/04/2021.

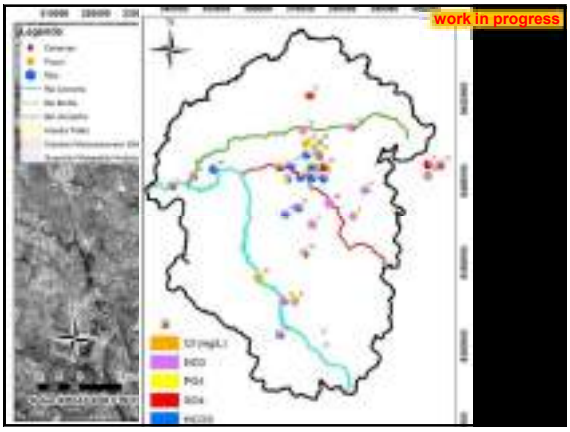
work in progress


Tarimba cave control site
work in progress
Tarimba Cave

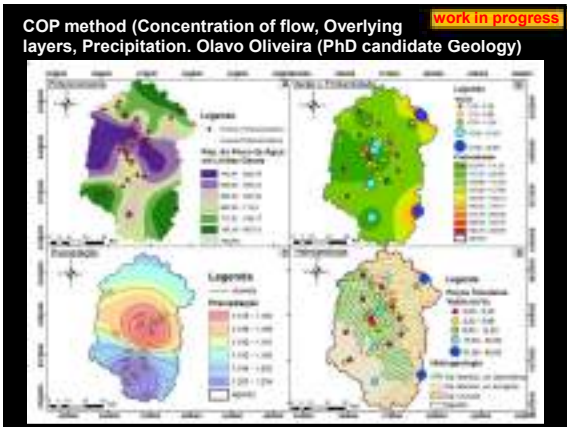
COP method (Concentration of flow, Overlying layers, Precipitation. Olavo Oliveira (PhD candidate Geology)
work in progress

CLASTIC SEDIMENTS IN CAVES

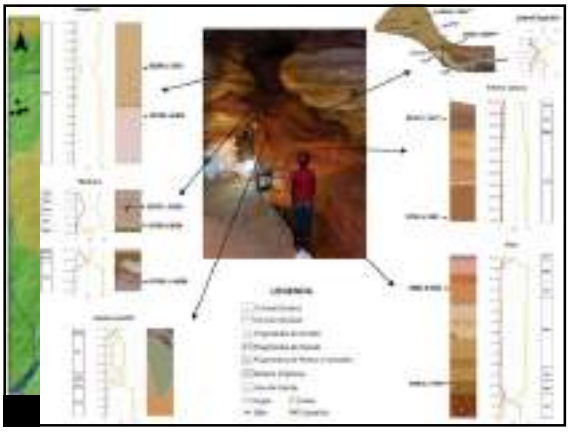

Adivane Nogueira (PhD candidate)
Quaternary sediments in dry valleys

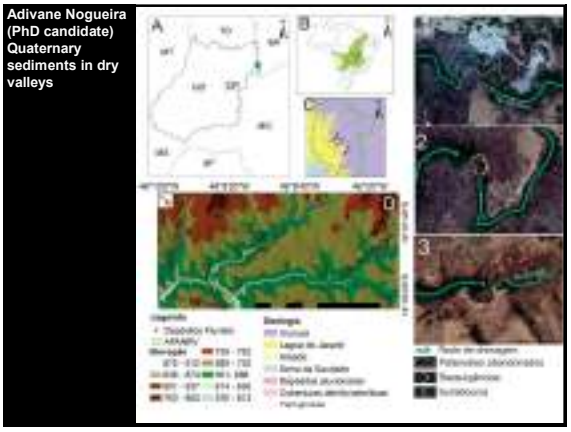

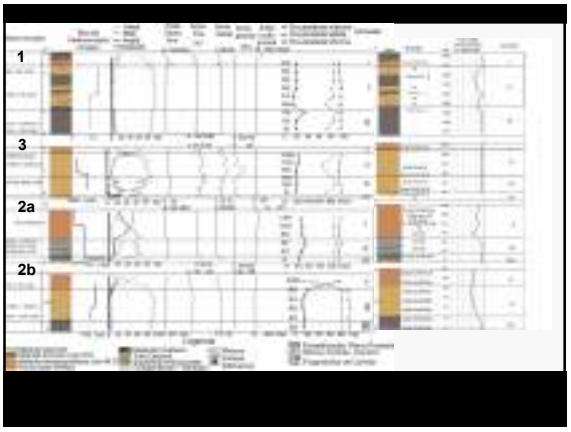

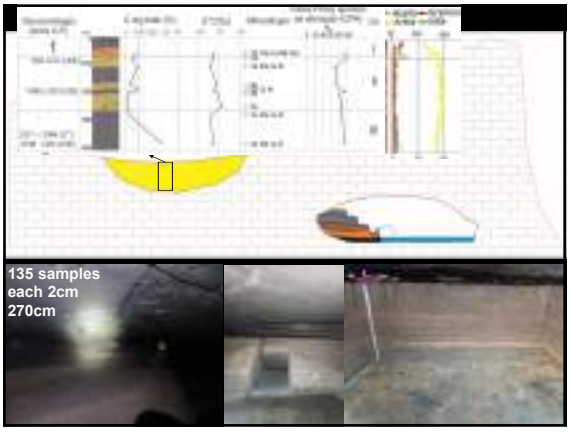

RESEARCH PROJECT IN FRANCE

HSM/Montpellier: Sediment source in caves and fingerprints.

CEREGE/Marseille: Erosion rates and study of the **"burial effect"** by caves in river sediments.

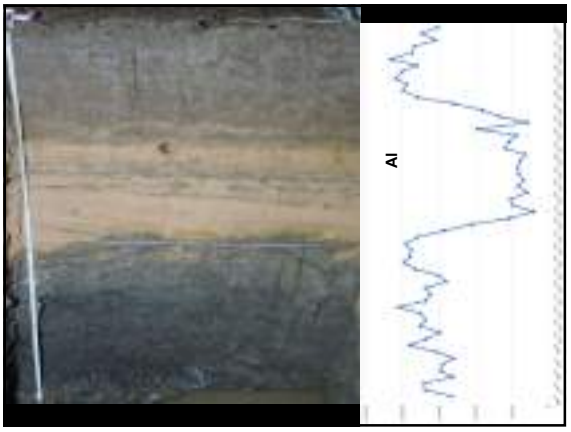

NOT ANSWERS BUT QUESTIONS

HOW THE LAND USE AFFECTS CAVES?
HOW THE CAVES AFFECTS PEOPLE?

MERCI BEAUCOUP!!

Contact:
rogeriouagoda@unb.br

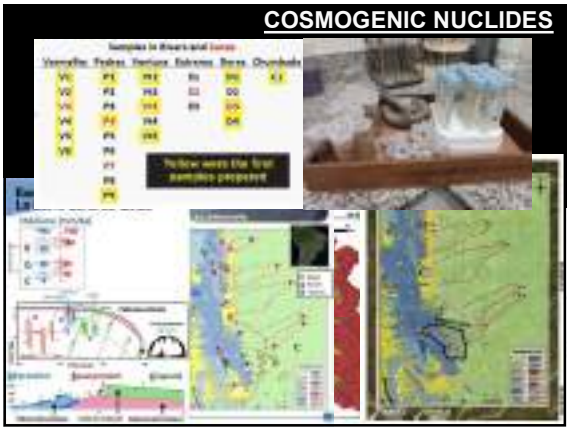
COSMOGENIC NUCLIDES

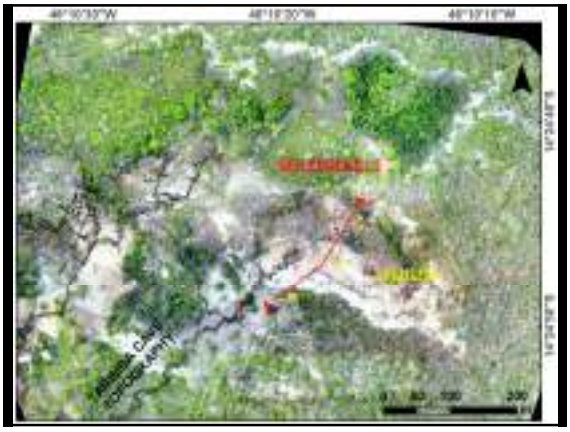

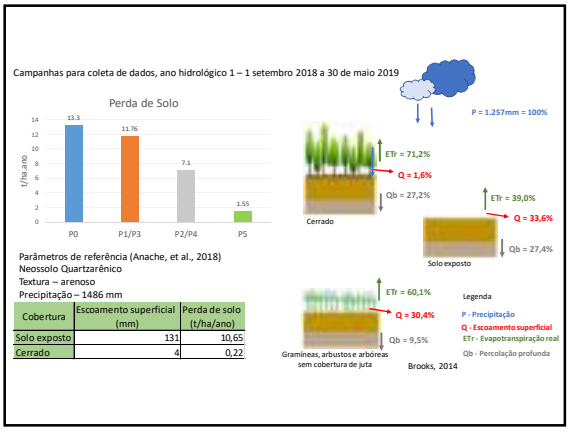

Cobertura	Escoamento superficial (mm)	Perda de solo (t/ha/ano)
Solo exposto	131	10,65
Cerrado	4	0,22

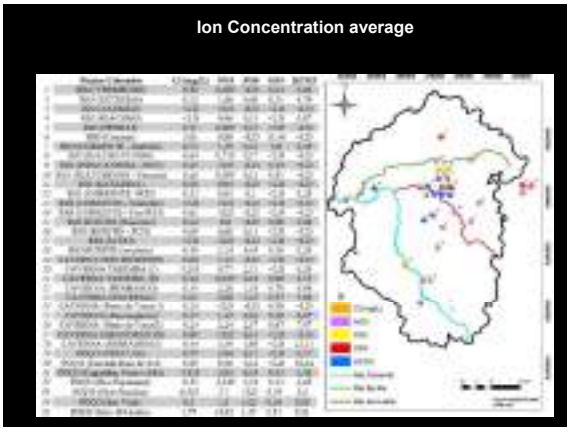

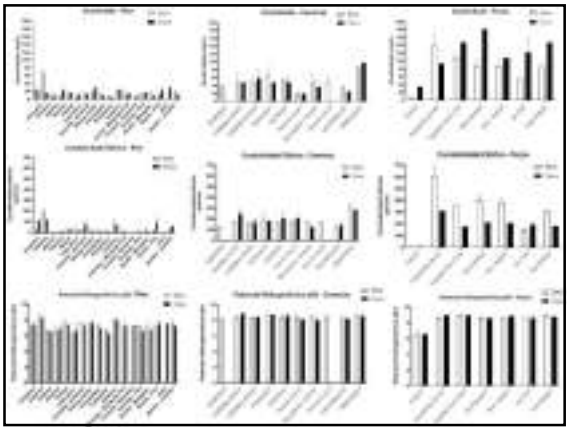

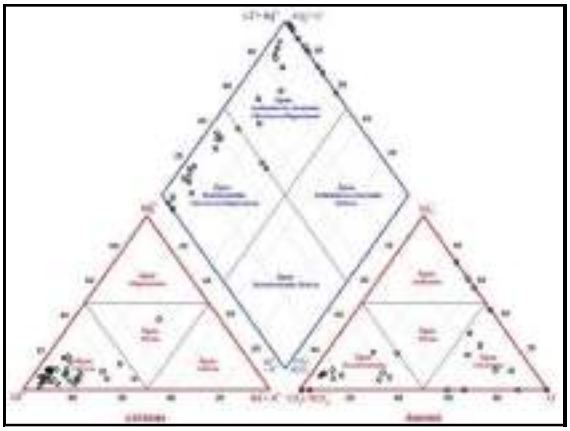


Estrutura para monitoramento no Sumidouro do córrego Extrema
Ponte para anexar equipamentos e medir vazão em cheias
Pluviômetro
Março de 2019
Vazão 0,16 m³/s (FlowTracker)
Sensor de nível e sonda multi
Estrutura para Amostrador Automático ISCO

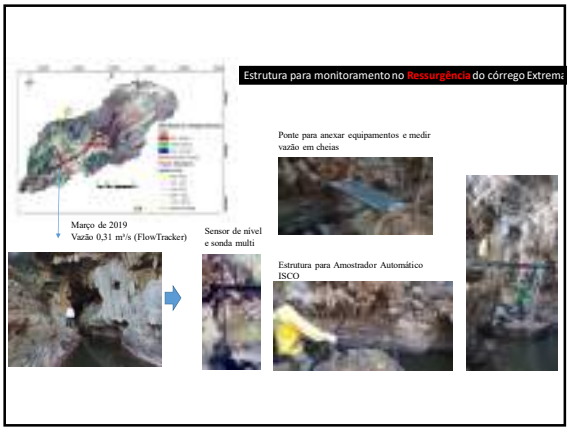
Estrutura para monitoramento no Ressurgência do córrego Extrema
Ponte para anexar equipamentos e medir vazão em cheias
Março de 2019
Vazão 0,31 m³/s (FlowTracker)
Sensor de nível e sonda multi
Estrutura para Amostrador Automático ISCO

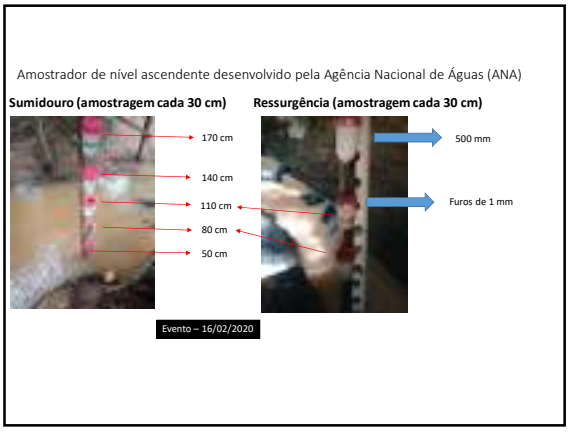
Amostrador de nível ascendente desenvolvido pela Agência Nacional de Águas (ANA)
Sumidouro (amostragem cada 30 cm)
Ressurgência (amostragem cada 30 cm)
170 cm
140 cm
110 cm
80 cm
50 cm
500 mm
Furos de 1 mm
Evento – 16/02/2020


Coleta de sedimentos Pós Evento de cheia
Sumidouro
- Turbidez = 820 NTU
- Condutividade = 80 Ms/cm
- pH = 8,8
- Vazão = 0,083 m³/s
Ressurgência
- Turbidez = 1.101 NTU
- Condutividade = 70 Ms/cm
- pH = 10,6
- Vazão = 0,13 m³/s

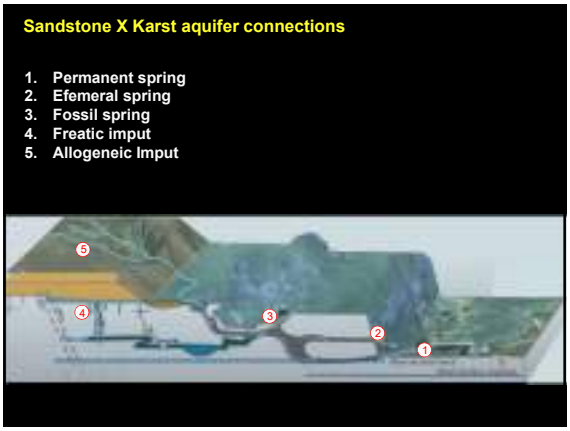
Sandstone X Karst aquifer connections
1. Permanent spring
2. Efemeral spring
3. Fossil spring
4. Freatic imput
5. Allogeneic Imput

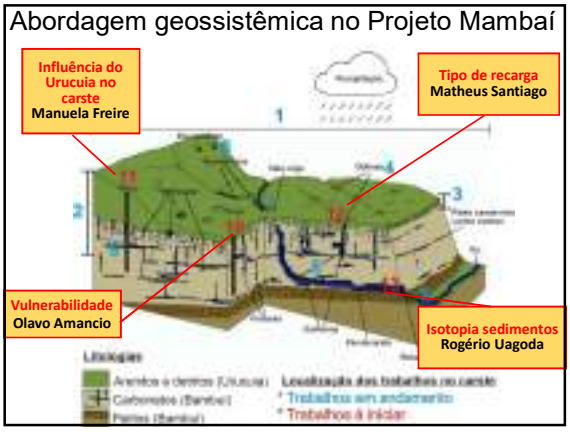
Abordagem geossistêmica no Projeto Mambaí
Influência do Urucuia no carste
Manuela Freire
Tipo de recarga
Matheus Santiago
Vulnerabilidade
Olavo Amancio
Isotopia sedimentos
Rogério Uagoda

COP method (Concentration of flow, Overlying layers, Precipitatio
Olavo Oliveira (PhD candidate Geology)

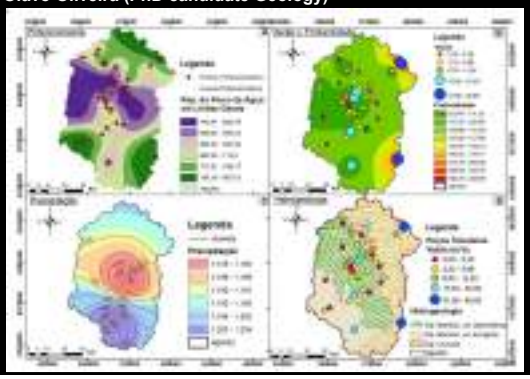

FREE AQUIFER INFLUENCE ON CAVES
Manuela Freire (Master Geology)

^{14}C, $d^{18}O$, ^{3}H, Geoquimistry

Dye tracing in runoff events
Matheus Santiago (Master Geology)

Diversas fontes de sedimentos no carste, com provável mistura para o sistema fluvial

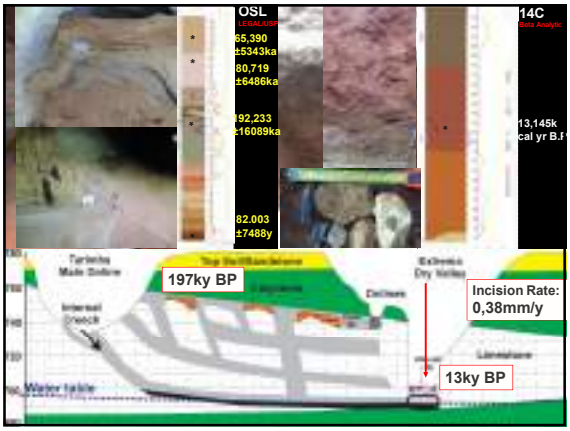

COSMOGENIC NUCLIDES

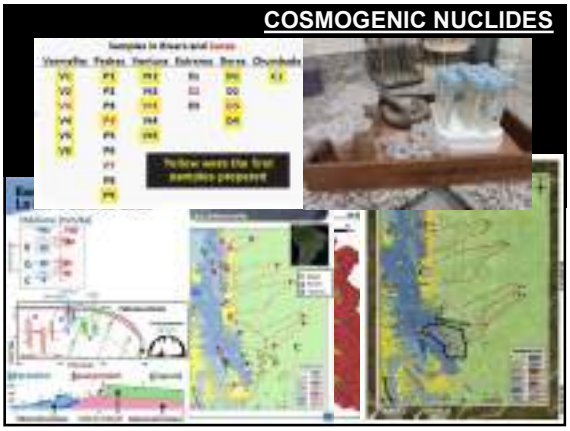

NOT ANSWERS BUT QUESTIONS

HOW THE LAND USE AFFECTS CAVES?
HOW THE CAVES AFFECTS PEOPLE?

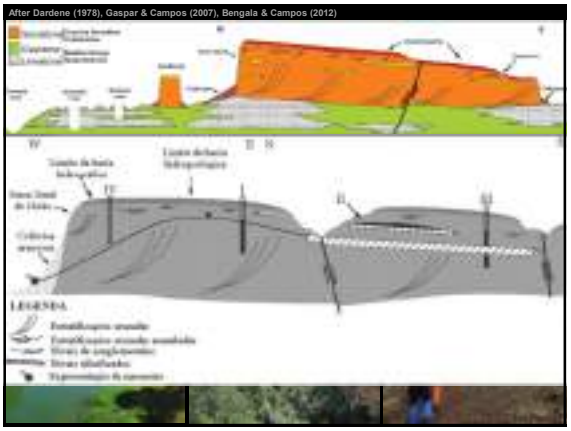

	Nome	Programa	Orientador	Objetivo	2018	2019	2020	2021
Dados Entrada	Cristiano Ferandes	Mestrado PPGea	Uagoda/ Ciccereli	Mapeamento sinks				
	José Gustavo	Mestrado PPGea	Uagoda/ Barral	Mapeamento solos				
Sedime. Quterniário	Dandara Caldeira	Mestrado PPGAG	Uagoda/ Garnier	Sedimentos Clásticos				
	Adivane Nogueira	Doutorado PPGea	Uagoda	Sedimentos Fluviais				
Água sedimentos	Maria Rita Fonseca	Doutorado PPGea	Uagoda Chaves	Monitor. de runoff				
	André Tavares	Doutorado PPGAG	Uagoda/ Roig	Monitor. de bacia				
	Matheus Vieira	Mestrado PPGea	Uagoda	Fontes de Agua/Traç.				
Aquífero Vulnerabi.	Manuele Freire	Mestrado PPGAG	Campos	Groundwater Isotopes				
	Olavo Amancio	Doutorado PPGea	Uagoda Hussain	Modelo Vulnerabili.				
Métodos Geofísicos	Yawar Hussain	Pós Doc	Uagoda	Métodos Geofísicos				
	Amanda Neuhauss	TCC Geofísica	Borges Ianniruberto	Resistividade Elétrica				
	Isabele Souza	Mestrado PPGAG	Ianniruberto Uagoda	Gravimetria				

Resultados

(a) Parcelas de enxurrada em 30/10/2018, (b) em 20/12/2019, e (c) em 04/04/2021.

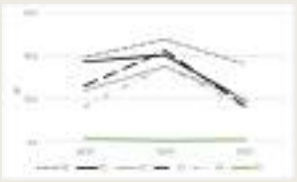

Escoamento superficial normalizado pela chuva

A média do coeficiente de escoamento superficial, nos três anos, nas parcelas restauradas com cobertura de juta foi 24,5% e sem cobertura de juta 30,4% e sem cobertura 41,2%.

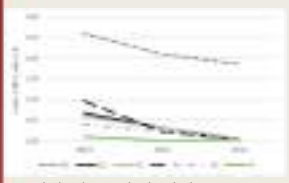

Perda de solo normalizado pela chuva

Coberturas P1/P3 e P2/P4	
Ano 1	a
Ano 2	ab
Ano 3	b

teste de intervalo múltiplo de Tukey (α = 0,05)

Erosão em pedestal, em 2020/05/23

Tolerância de Perda de Solo on e off site

Fonseca et al, 2020

Estrutura para monitoramento no Sumidouro do córrego Extrema

Março de 2019
Vazão 0,16 m³/s (FlowTracker)

Sensor de nível e sonda multi

Ponte para anexar equipamentos e medir vazão em cheias

Estrutura para Amostrador Automático ISCO

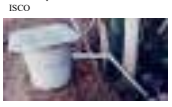

Pluviômetro

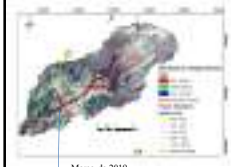

Estrutura para monitoramento no Ressurgência do córrego Extrema

Março de 2019
Vazão 0,31 m³/s (FlowTracker)

Sensor de nível e sonda multi

Ponte para anexar equipamentos e medir vazão em cheias

Estrutura para Amostrador Automático ISCO

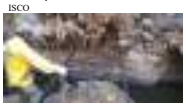

Dye tracing in runoff events
Matheus Santiago (Master Geology)

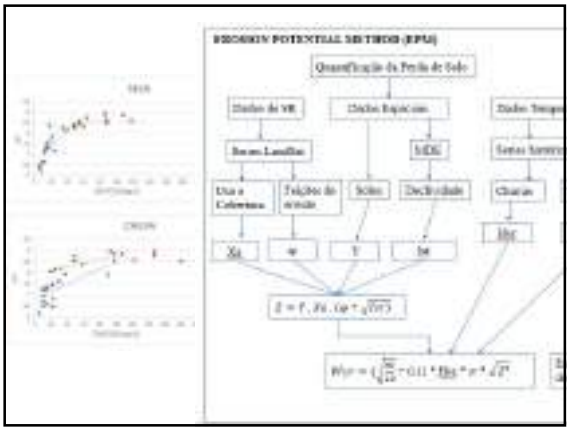

8 Participação em eventos no período

No período que estive na França tive trabalhos aceitos para três conferências internacionais, quais sejam: EGU General Assembly, 22-27/05/2022, em Vienna/Austria; 18th International Congress of Speleology – UIS, 24-31/07/2022, em Savoie/France; e, 10th IAG International conference on Geomorphology, 12-16/09/2022, em Coimbra/Portugal. Sendo que não pude comparecer ao último evento listado por problemas familiares.

Abaixo vai a lista de resumos aceitos nesses eventos, que também são anexados a esse relatório:

TAVARES, ANDRÉ SILVA ; Uagoda, Rogério. Assessment of Soil Losses by Erosion in a Karst Environment in the Cerrado Biome of Brazil. In: **18th International Congress of Speleology** - UIS 2022, 2022, Savoie Mont Blanc. 18th International Congress of Speleology - UIS 2022, 2022. v. 01. p. 01-01.

MENDES, Leonardo Chaves ; NOGUEIRA, ADIVANE MORAIS ; CALDEIRA, DANDARA ; R., UAGODA . Identification of calcareous tufa in northeast of the state of Goiás, Brazil. In: Conference**: 18th International Congress of Speleology**, **2022**, Savoie Mont Blanc. Conference: International Congress of Speleology, 2022. v. 01. p. 01-01

R., UAGODA; HUSSAIN, YAWAR ; ALMEIDA, A. ; MACIEL, SUSANNE ; BORGES, WELITOM ; KOIDE, S. ; NGUYEN, F. ; Nascimento, C., T. **EGU General Assembly 2022**, 2022, Vienna. EGU General Assembly 2022, 2022. v. 01. p. 01-01.

R., UAGODA; HUSSAIN, YAWAR ; CALDEIRA, D. M. V. S. ; NOGUEIRA, ADIVANE MORAIS ; FONSECA, MARIA RITA SOUZA ; TAVARES, ANDRÉ SILVA . Hydrosedimentological study of a covered fluviokarst in the Brazilian Cerrado. In: **10th International Conference on Geomorphology, 2022**, Coimbra. 10th International Conference on Geomorphology, 2022. v. 01. p. ICG2022-42-0.

AGUIAR, A. C. N. ; HUSSAIN, YAWAR ; BORGES, WELITOM ; R., UAGODA . Continuity among three-consecutive Brazilian caves established by a geophysical approach. In: 10th International Conference on Geomorphology, 2022, Coimbra. International Conference on Geomorphology, 2022. v. 01. p. ICG2022-424-00.

ZbpBB7A@DE@
Zbp b è S é B@BB
S 2 3B@BB9o é
U è U S é D9@g í 9

e u

m p è è[A]6 [B]6S è S è[C]6n è h èí [D]6b uè è í
S è [E]6b è l è è [F]6r T [E]6n f [C]6a í i [G]6è Uè oè
Uè è i è í [D]

[A]W è b è 6p T è è6T è è6T è 2 è èR é9é 3
[B]W è b 6p g 6g 6T 2 è è 9 R è 9 3
[C]U è Z è Z 6p T è è6T è è6T è 2 R é9é 3
[D]k è è è Uè 6p T è è6T è è6T è 2 è R é9é 3
[E]d b í í 6p T è è6T è è6T è 2 R é9é 3
[F]n è f gèé è n èí r è 6i è è n èí ní í U 6U Síè ní í 6T 6U è
2 è B@AFR AFC9 3
[G]ní Z 6p g 6g 6T 29 R 9é 3

o 7 è í í 6è è í é è è èí
è è 6 é èí è é èí í 9 o
í í è í è è í é í è í 2 íè 3è íè
í è è è í í èíí 9U è èí è í
èí í è è 6 é èí í í í è è
é íè è è èé í é è 9 d í 6
è 7è 7 è è è è í í
è è è è Uè è è 6T è è6
T è 9o í è S B@AE a é è B@AF9

b íè í í B@@h c è D@@h c è è è è
è D è l í 6í è è è è è B@@ [B]
í è 9Wè è èí è è è è è
Uè è è 9S íè 6 è è
è è í è 7 è í é í è é
í è í è è9o í è è í è èí è é èí è
è í è è 9

S 7è é è è 6 í í í 6 è è è è è
è è è í íè í é èí
í è è í 9S è 6è c é è è è è è è
èí é í 9

o è è 7è bkm è è è
èí íè è í è è í é èí í èí

è íè è è 7 è í í 9o è è
è í è è è è íè è è íè 9
uS é è è L 7 è Lc é è è L 7 è í

ICG2022-423
10th International Conference on Geomorphology

Hydrosedimentological study of a covered fluviokarst in the Brazilian Cerrado

Rogerio Uagoda[1], Yawar Hussain[2], Dandara Caldeira[3], Adivane Moraes Nogueira[1], Maria Rita Fonseca[1], and André da Silva Tavares[3]

[1]University of Brasilia, Departament of Geography, Brasília, Brazil (rogeriouagoda@unb.br)

[2]Department of Geology, University of Liege, Liege, Belgium

[3]Institute of Geosciences, University of Brasília, Brasília, Brazil

The studied region located in the Rio Vermelho watershed, situated at the foot of the *Serra Geral de Goiás* in the Brazilian Cerrado, hosts a covered fluviokarst system containing ~150 mapped caves that capture the rivers (sediment loads) upstream. The present study aims at developing a better understanding of the geomorphological controls, considering the impacts of climatic conditions and land use types on the production and transport of the sediments to the caves using an integrated approach (GIS mapping, hydrosedimentological monitoring, and geochronological analysis).

The preliminary results indicate the influence of two sites on sediment production: a) downstream, constituted by the karstic system developed in the Neoproterozoic carbonates (Bambuí group), where the soils are occupied by natural vegetation or pastures (family farming), and, b) upstream, on a plateau, which supplies water to the karstic system, with soils developed on Cretaceous sandstones (Urucuia group), the areas of growing mechanized agriculture. Models of the upper and lower fluviokarst systems are developed using the soil types and recharge zonation information. The chronology of the preserved sedimentary deposits, formed by the alternation of clayey and sandy facies, has been established, between 60ky and 200ky in the upper cavities and up to 20 ky in the fluviokarst blind valleys. Hydrosedimentological monitoring revealed the production of ~ 9 Mg ha-1yr-1 of sediments from degraded soils, while 2.0 Mg ha-1yr-1 are produced from soils having received the conservation protocol, a lower value than the geological rate as established in the literature. The sediments transported in the karst are poorly sorted compared to those in the rivers and an increase in the particulate load during floods (<7 against ~500 mg/L).

There is still a lack of evidence about the origin of the water and sediments circulating in this karst system. Further studies on fresh sedimentary deposits in the recent sinkholes may help to better quantify recent paleo-environmental modifications and the effects of anthropogenic activities upstream.

Keywords: GIS; Geochronology; Blind valleys; C14; Fluviokarst

ICG2022-424
10th International Conference on Geomorphology

Continuity among three-consecutive Brazilian caves established by a geophysical approach

Amanda Cecília Neuhauss Aguiar[1], Yawar Hussain[2], Welitom Rodrigues Borges[1], and **Rogerio Uagoda**[3]

[1]Institute of Geosciences, University of Brasília, Brasília, Brazil
[2]Department of Geology, University of Liege, Liege, Belgium
[3]University of Brasilia, Departament of Geography, Brasília, Brazil

For seldom investigated Brazilian caves, detailed non-invasive mapping is crucial for environmental, ecological, and geological investigations. However, the Cerrado region of Brazil hosts covered karst (underlain by a thick clayey layer) which makes its non-invasive mapping difficult using the readily available tools. In this study, we applied a geophysical technique to establish the linkage (continuity) among the three caves named *Trimba, Pasto de Vaca I*, and *Pasto de Vaca II* in the environmentally protected area of River *Vermelho,* Goias, Brazil.

Our analysis started with the optimization of the electrode array geometry and its depth of penetration in the area. A forward model was chosen based on the site where the river enters the cave and soil-clay-carbonate lithological contacts are exposed on the surface. As there are well-developed drainage networks and cave development is attributed to fluvial influences that still have subsurface water flows in most of the places. Therefore, buried streams were also considered in the numeral approximation study. Findings from the numerical simulation indicated that the best results could be obtained using either the dipole-dipole, pole-dipole, or Wenner-Schlumberger array configurations, with an inter-electrode spacing of 2.5 meters.

Hence, a dipole-dipole array of electrodes was selected to acquire the DC electrical resistivity data. Considering the objective of the study, the measurements were carried out using 72 electrodes were spaced 2.5 m apart and arranged in seven electrical resistivity tomography (ERT) profiles perpendicular to the one end of *Trimba cave*, covering the entire length of *Pasto de Vaca I* and the beginning of *Pasto de Vaca II* cave marked on existent caves topography.

In the first stage of resistivity data processing, a manual inspection and consequent removal of bad data points to improve the inversion results were conducted seeking a possible reduction in root mean square error. The inversion models, represented through 2D sections, indicated anomalous resistivity areas, interpreted as regions of subsurface cavity. Additionally, a geomodeling approach was used for improving the presentation of the inversion results (resistivity variables) in 3D. The latter revealed anomalous zones present on all profiles, attributed to the presence of a subsurface cavity.

The geophysical results made it possible to detect the continuity of the same cave from north to south, contrary to the previously held assumption about the existence of three individual caves. Results encourage the integrated application of geophysical techniques for further detailed investigations.

Keywords: Cerrado; Electrical Resistivity; Array optimization, Geomodeling

Assessment of Soil Losses by Erosion in a Karst Environment in the Cerrado Biome of Brazil

André Silva TAVARES (1), Rogério Soares UAGODA (2)

(1) University of Brasília, Darcy Ribeiro Campus, 70910-900 Brasília-DF, Brazil, andresttavares@gmail.com

(2) University of Brasília, Darcy Ribeiro Campus, 70910-900 Brasília-DF, Brazil, rogeriouagoda@unb.br (corresponding author)

Abstract

This work aimed to estimate the volume of soil losses due to water erosion in a watershed dominated by karst features, which results in the quantity of sediment directed to the caves in the region. The Corrente river watershed is located in the Northeast region of the State of Goiás, Brazil. Through the Potential Erosion Method (EPM) applied in the Geographic Information System, soil losses were quantified for the year 2021. The estimated average soil loss was 26.41 to/ha/year-1, with a maximum flow of 10,689,083.57 to/year-1 in the watershed outlet. The limits of the catchment, producing sediments to the caves were obtained, which allowed extracting an average estimate of transported sediments in these karst regions.

Résumé

Ce travail visait à estimer le volume des pertes de sol dues à l'érosion hydrique dans un bassin hydrographique dominé par des caractéristiques karstiques, ce qui se traduit par la quantité de sédiments dirigée vers les grottes de la région. Le bassin hydrographique de la rivière Corrente est situé dans la région nord-est de l'État de Goiás, au Brésil. Grâce à la méthode d'érosion potentielle (EPM) appliquée dans le système d'information géographique, les pertes de sol ont été quantifiées pour l'année 2021. La perte de sol moyenne estimée était de 26,41 to/ha/an^{-1}, avec un débit maximum de 10 689 083,57 to/an^{-1} en l'exutoire du bassin versant. A partir des limites des micro-bassins versants, ou zones productrices de sédiments, des zones de convergence vers les grottes ont été obtenues, ce qui a permis d'extraire une estimation moyenne des sédiments transportés dans ces régions karstiques.

Resumo

Esse trabalho visou estimar o volume das perdas de solo por erosão hídrica em uma bacia hidrográfica dominada por feições cársticas, que resulta no quantitativo de sedimentos direcionados para as cavernas da região. A bacia hidrográfica do rio Corrente está localizada na região Nordeste do Estado de Goiás, Brasil. Por meio do Método de Erosão Potencial (EPM) aplicado em Sistema de Informação Geográfica, foram quantificadas as perdas de solo para o ano de 2021. A perda de solo média estimada foi de 26,41 to/ha/year^{-1}, com vazão máxima de 10.689.083,57 to/year^{-1} no exutório da bacia. A partir dos limites das micro-watersheds, ou áreas produtoras de sedimentos, foram obtidas áreas de convergência para as cavernas, que permitiu extrair uma estimativa média de sedimentos transportados nessas regiões cársticas.

1. Introduction

In Brazil, karst makes up between 5 and 7% of the territory, and yet studies on hydrology and karst sedimentology are scarce (KARMANN, 2016). However, the karst evolution processes through superficial and underground flow networks carry relevant information about the type, quantity and quality of the transported material, revealing aspects of the functioning of the karst aquifer in the transport of sediments.

It is known that the degree of development of the karst relief forms varies according to the characteristics of the climate, vegetation and the type of source material. The characteristics of forms, surface and underground, have already been widely elucidated in the literature (PALMER, 1984, JENNINGS, 1985, FORD & WILLIAMS, 2007, HARDT, 2011).

In Brazil, the karst relief gains special importance in the Cerrado biome, where native vegetation is the most affected by suppression among other biomes in Brazil. Allied

to this, the deficiency of phosphorus and other nutrient minerals in some soils does not favor forest development and allows the origin of landscapes consisting mainly of pastures with sparse trees (BRECKLE, 2002). As a result, erosive processes become more and more intensified during rainfall, contributing to a large volume of sediment that is transported to underground channels and karst galleries.

The sources and types of dendritic sediments are varied, as the material is pedogenized on the surface, or alluvial sediments, or epiphreatic mud, or insoluble residues, or suspended solids and organic deposits. Deposition zones are seen in widened fractures, abysses, sinks, internal subsidence, flooded gallery networks and back-flooding (LAUREANO & KARMANN, 2013). These zones of autochthonous and allochthonous sediment transport can

imply high speeds and rise of the water table, which can promote rapid flooding above the vadose zone (CALDEIRA et al., 2019). Thus, the preservation of speleological heritage involves the need to delimit the areas that produce sediment, since inadequate land management and the replacement of native vegetation accelerate erosion processes, increasing the amount of sediment in rivers and caves.

2. Materials and methods

The Corrente River watershed (3,824 km2) belongs to the Tocantins River basin, located in the northeast of the State of Goiás, Brazil. The upper portion (Highlands) is formed by sandstones (Urucuia Group) that constitute unconsolidated siliciclastic sediments, while the lower portion (Karst Terrains) has pelitic rocks intercalated with carbonates (Bambuí Group). The area with densification of karstic features acts as recharge areas through fractures and large convections distributed in sinks and underground flows. About 47 cavities with perennial flows were identified (Fig. 1). The climate is tropical with dry winter (Aw), with an average of 1,165 mm/year-1 (CARDOSO et al., 2014).

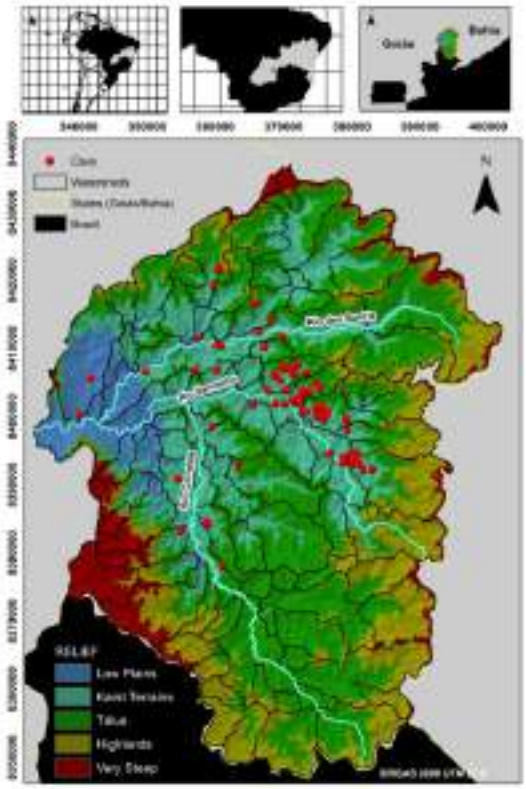

Figure 1: Stream river basin and mappe caves.

Between the domain of carbonates and siliciclastic sediments, karstic depressions occur with intensified erosive processes, from which there is capture of surface runoff by fractures or collapsed sinks, generating the accumulation of sediments in some caves above the base level.

Therefore, in order to assess soil loss and sediment production due to water erosion, this study used a watershed dominated by karst features in the Brazilian Cerrado biome, in which an extremely active process of underground karstification and relief dissection occurs. To quantify the sediments directed to the caves, the Potential Erosion Method (EPM) was used, which quantifies the loss of soil by erosion.

- Erosion Potential Method (EPM)

The EPM is an empirically-based model that estimates soil loss and the determinants of water erosion intensity, which directly affect soil loss rates at the scale of watersheds, such as soil slope, soil strength, erosive features , land use and management, air temperature and precipitation (GAVRILOVIC, 1988).
Soil loss (Wyr) in the EPM model is estimated by Equation 1.

$$W_{yr} = T * H_{yr} * \varphi * \sqrt[3]{Z^3} \qquad \text{Eq. 1}$$

Where: Wyr = total sediment production (m^3 yr^{-1}); T = temperature coefficient (dimensionless); Hyr = mean precipitation (mm $year^{-1}$); π = 3.14; Z = erosion coefficient (dimensionless).

The temperature coefficient (T) is calculated according to Equation 2.

$$T = \sqrt[3]{\frac{t_0}{10}} + 0{,}1 \qquad \text{Eq. 2}$$

Where: T = temperature coefficient (dimensionless); t_0 = mean air temperature (°C $year^{-1}$).

The erosion coefficient (Z) is obtained by Equation 3:

$$Z = Y * X_a * (\varphi + \sqrt[3]{I_{sr}}) \qquad \text{Eq. 3}$$

Where: Y = soil resistance to water erosion (dimensionless); Xa = land use and management (dimensionless); ϕ = degree of erosion features in the soil (dimensionless); Isr = mean slope of the watershed (%).
The Z coefficient values are classified according to the degree of erosion intensity (Figure 2).

Categories	Erosion intensity	Erosion Coefficient (Z)	Average of Z
I	Very severe	Z > 1.0	Z = 1.25
II	Severe	0.71 < Z < 1.00	Z = 0.85
III	Moderate	0.41 < Z < 0.70	Z = 0.55
IV	Weak	0.20 < Z < 0.40	Z = 0.30
V	Very weak	Z < 0.20	Z = 0.10

Figure 2: The degree of erosion intensity (Z)

In the ENVI 5.3 program, land use and land cover were classified using the OBIA (Object-Based Image Analysis) method. The method is based on the segmentation of matrix images, where samples are defined for training in supervised machine learning, based on the Support Vector

Machine model, a non-probabilistic linear binary algorithm (COHENCA & CARVALHO, 2015). LandSat 8 satellite images (OLI sensor) were used.

Through temporal series of rainfall stations, the average rainfall and temperature of the last 30 years was established, using the inverse distance weighting (IDW) method, which interpolates and gathers the areas of influence of each station from the polygons of Thiessen. Soils were classified based on the Brazilian Soil Classification System (EMBRAPA, 2018). Digital images from the Alos satellite (Palsar sensor) with 12.5 meters of spatial resolution were used for the relief classes. In addition to results obtained in the analyzes published by Nunes (2020).

3. Results

The predominant phytophysiognomy is field/pasture (56.67%), followed by Cerrado (21.40%), dense forest (10.98%), agricultural culture (7.60%), exposed soil (2.83%) and water bodies (0.49%). The dominant soils were Quartzarenic Neosols (38.51%), followed by Red-Yellow Latosols (29.47%), Chernosols (24.46%) and Cambisols (7.54%). The steepest slopes are located near the springs and dissected canyons. However, flat to smooth sloping areas (0-8%) are predominant, with an average slope of 5.6%. The average soil loss for the year 2021 in the Corrente River watershed was 26.41 to/ha/year^{-1}.

Figure 3 highlights the micro-watersheds that act as producers of sediments that converge to the caves. The caves with perennial courses are accumulated in the karst areas of the Vermelho River, more specifically, in the Extrema, Serragem and Ventura micro-watersheds, which contribute to a sediment production in the scale of 33.66, 19.45 and 35.22 to/ ha/year^{-1}, respectively.

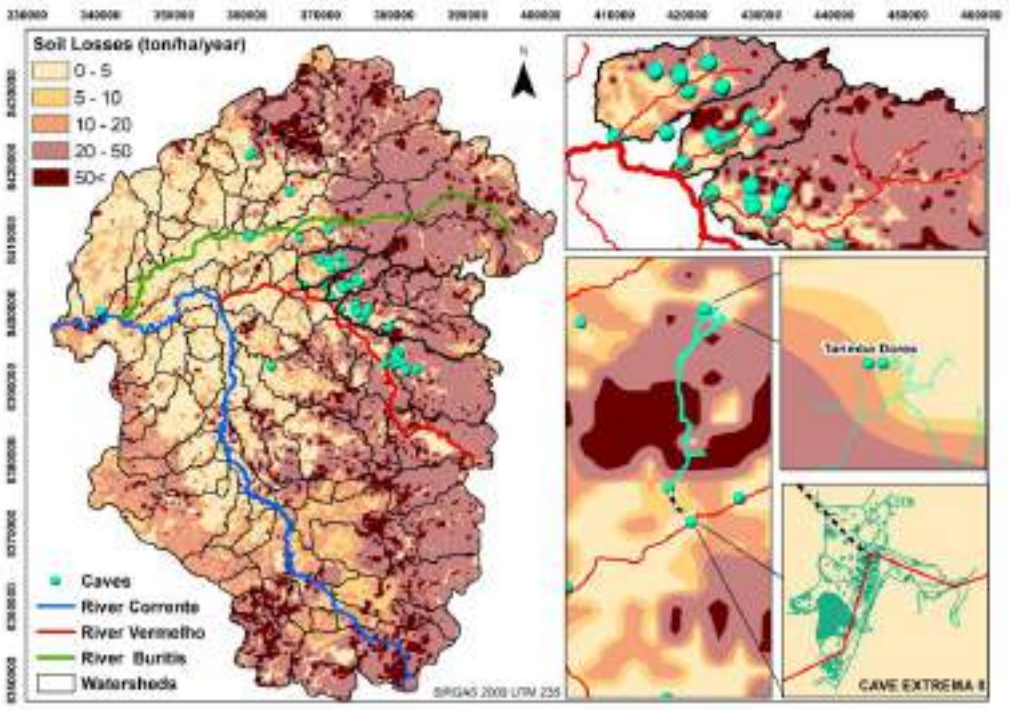

Figure 3 : Soil losses by erosion in the Corrente River watershed and in the karst areas

4. Discussions

In the watershed of the River Corrente, the cretaceous sediments of the Urucuia Group (upper), which would cover the Bambuí Group (lower), are found inside caves, guided by networks of conduits and fractures. The morphology of the transition from sandstones to carbonates occurs through abrupt breaks, in the form of steep slopes, with the presence of erosion in an advanced stage. Part of these structures are related to karstification, which in this situation is expressed externally in the form of sinkholes.

Cave Extrema III, for example, receives volumes of sediment in the scale of 33.12 to/ha/year^{-1}, originating from surface and underground flows associated with sinkholes and adjacent caves, such as coming from the Tarimba cave.

As the study is carried out in a covered karst, the hypothesis is that the underlying karst system works as an inducer of superficial erosion processes, that is, the opening of sinkholes or sinks leads to a rearrangement of the balance profile of rivers and, consequently, expands the erosive capacity of captured surfaces. The absence of

conservation practices in land use can increase this process, both with the increase in the sediment load in the suppression of native vegetation, and with the abstraction of water from aquifers, which tends to make karst systems more unstable.

In Figure 4, the estimated values of sediments transported in caves of perennial flows are highlighted, according to the related micro-watershed.

	Micro-Watershed			Soil loss average (to/ ha/ year^{-1})		
	Extrema	Serragem	Ventura	Extrema	Serragem	Ventura
Caves	Ponto de terra	Meândrica	Cachoeira do Funil	0,38	12,32	0,25
	Extrema I	Lapa I	Corredeiras	0,38	1,33	67,13
	Esperança	Ana Paula I	Posto	2,28	0,5	56,38
	Extrema II	Judite	Porcos	0,23	0,35	16,14
	Extrema III	Dores	Marimbondos	33,12	2,36	11,88
	Vila Nova	Tarimba	Associação II	0,43	2,36	1,27
		Serragem II	Desgosto		10,40	1,62
		Penhasco			10,34	

Figure 4: Average estimate of sediment transport to the caves.

5. Conclusion

Through the estimation of soil loss in the watershed scale, it was possible to evaluate the spatial dynamics of the sediment producing areas, allowing to highlight the transport potential of these materials in karstic micro-watersheds. From there, such units can be investigated and monitored to better assess the causes and effects that are still little known. The karst region in this research is managed by an important Conservation Unit for the preservation of the region's speleological heritage.

Acknowledgments

The authors thanks the Chico Mendes Institute for Biodiversity Conservation (ICMBio), National Water Agency (ANA), National Center for Research and Conservation of Caves (CECAV) and "Coordenação de Aperfeiçoamento de Pessoal de Nível Superior – Brasil" This study was financed in part by CAPES – Finance Code 001.

References

BRECKLE, S.W. (2002) Walter's Vegetation of the Earth : The Ecological Systems of the Geo-Biosphere, Springer Berlin Heidelberg, ed. 4, 527 p.

CALDEIRA, D.M.V.S.; Uagoda, R. and Nogueira, A.M. (2019) Dinâmica dos sedimentos clásticos cavernícolas: Potencialidade para estudo paleoambientes no Brasil. *Espaço & Geografia*, n°22 (1), 153-189.

CARDOSO, M.R.D.; Marcuzzo, F.F.N. and Barros, J.R. (2014) Classificação climática de Köppen-Geiger para o Estado de Goiás e o Distrito Federal. *Acta Geográfica*, 8(16), 40-55.

COHENCA D., CARVALHO, R. (2015) Comparação de métodos de classificação OBIA, Máxima Verossimilhança e Distância Mínima em imagem OLI/Landsat-8 em área de alta diversidade de uso do solo. *Anais* XVII Simpósio Brasileiro de Sensoriamento Remoto, João Pessoa-PB, Brasil, 1035-1042.

EMBRAPA - Empresa Brasileira de Pesquisa Agropecuária (2018) Sistema Brasileiro de Classificação de Solos. Brasília, 4. ed.356 p.

FORD, D.; WILLIAMS, P. (2007) Karst Hydrogeology and Geomorphology. Wiley: Chichester, 562 p.

GAVRILOVIC, Z. (1988). The use of empirical method (Erosion Potential Method) for calculating sediment production and transportation in unstudied or torrential streams. In: White, W.R. (ed.), International Conference on River Regime; Chichester, 411–422.

HARDT, R. Da Carstificação em Arenitos: Aproximação com o suporte de geotecnologias. Tese (doutorado). 224f. Universidade Estadual Paulista, Instituto de Geociências e Ciências Exatas. Rio Claro - SP, 2011.

JENNINGS, J.N. (1985) Karst Geomorphology. Oxford: Basil Blackwell, 293 p.

KARMANN, I. (2016) Carste e cavernas no Brasil: distribuição, dinâmica atual e registros sedimentares, breve histórico e análise crítica das pesquisas realizadas no âmbito do IGc USP. Livre Docência em Espeleologia. Instituto de Geociência. Universidade de São Paulo, 62 p.

LAUREANO, F. V. KARMANN, I. (2013) Sedimentos clásticos em sistemas de cavernas e suas contribuições em estudos geomorfológicos: uma revisão. *Revista Brasileira de Geomorfologia*, (14) 23-33.

NUNES, J.G.S. (2020) Mapeamento de solos através de técnicas diretas e indiretas na APA Nascentes Do Rio Vermelho, Mambaí-GO. Dissertação, Universidade de Brasília, 110 p.

PALMER, A.N. (1984) Geomorphic interpretation of karst features. In: Lafleur, R.G. Groundwater as a Geomorphic Agent. Boston: Allen and Unwin, 173-209

Identification of calcareous tufa in northeast of the state of Goiás, Brazil

Leonardo MENDES (1), Adivane NOGUEIRA (2), Dandara CALDEIRA (3) & Rogério UAGODA (4)

(1) Laboratório de Geografia Física, ICC Norte, Bloco 23, Campus Darcy Ribeiro, Brasília, Brazil, lchaves21@gmail.com (corresponding author)
(2) Laboratório de Geografia Física, ICC Norte, Bloco 23, Campus Darcy Ribeiro, Brasília, Brazil, adinogueira2010@hotmail.com
(3) Laboratório de Geografia Física, ICC Norte, Bloco 23, Campus Darcy Ribeiro, Brasília, Brazil, dandara.caldeira2014@gmail.com
(4) Laboratório de Geografia Física, ICC Norte, Bloco 23, Campus Darcy Ribeiro, Brasília, Brazil, rogeriouagoda@unb.br

Abstract

Studies in calcareous tufas are of great importance for the development of paleoenvironmental reconstructions and understanding of the landscape dynamics. As features originated from areas of occurrence of carbonate rocks, these concretions solidify in different forms and facies, due to the conditions provided by the environment in which they develop. This research seeks to map and describe the calcareous tufa formations in the northeastern portion of the state of Goiás, Brazil. Some areas of occurrence were identified through field work, involving description and extraction of outcrops. Thus, the carbonate deposits were spatialized with the registration of coordinates, inserting them in a Geographic Information System (GIS) environment, using the QGIS v.3.16.3 with GRASS v.7.8.5 software (v.10.6.1). In this sense, the faciological description of the testimonies was possible to be realized, associating them with depositional environments, identifying cascade, waterfall, dam and inter-dam pool tufas, correlated to the facies typology. In addition, cartographic materials of the spatial distribution of such features were generated, in which certain linearity of the occurrence of outcrops, including in areas without active drainage, was found.

1. Introduction

Over high porosity and solubility rocks, karstic terrains develop, known for being systems of constant interaction between water and the geological environment. The northeastern portion of the state of Goiás, Brazil, is encompassed by three main geological groups (Bambuí, Areado and Urucuia), associated with the Sanfranciscana Basin. The Lagoa do Jacaré formation, which belongs to the Bambuí, has pelite-carbonated outcrops linked to the regressive erosion of the Serra Geral do Goiás (W-E).

Thus, exuberant features such as caves, lapia, sinkholes, tufas and travertines, appears, generating rich and complex landscapes, which can be considered both open and closed systems (TRAVASSOS, 2019). Typical features of karst areas, such as tufas, occur near or in the bed of rivers that, at any moment, were in direct contact with carbonate rocks. Carbonate deposits are the result of the interaction between CO_2-rich waters and carbonate rocks. The supersaturation benefits the precipitation of calcite, a chemical precipitation mineral that constantly occurs in karstic areas (HILL; FORTI, 1997). The reprecipitation of calcite can be indicated by the equation:

$Ca^{+2}+2\ HCO^{-}_{3} \leftrightarrow CaCO_3\downarrow + H_2O + CO_2\ (g)\uparrow$
(Calcium carbonate precipitation equation)

A study by Ford & Pedley (1996) demonstrated that the formation of tufas is linked to climatic periods of great humidity and heat. However, other studies have recognized tufa formations in different environments, such as humid tropical (CARTHEW; TAYLOR; DRYSDALE, 2006) and semi-arid (MOEYERSONS et al., 2006, ORDÓÑEZ et al., 2005).

For interpretation about fossil tufas, environmental models are used, since weathering and burial complicate the stratigraphic and geomorphic characterization, influenced by biological and climatic aspects (CARTHEW; TAYLOR; DRYSDALE, 2006, PEDLEY, 2003). These environmental models are understood as conceptual representations, as they have the morphological characterization of the deposit, association of facies and sedimentation environments (PEDLEY, 1990). The need to use models related to regions with similar climatic factors is emphasized.

Calcareous tufas are extremely fragile, as their formation and conservation directly depend on the use of land throughout their area of influence. Thus, considering that the studied area stands out for agricultural production, the conservation of these features can be directly affected, even before they are properly studied to understand different perspectives (climatic, tectonic and anthropic) (FORD; WILLIAMS, 2007; CAPEZZUOLI; GANDIN; PEDLEY, 2014; MIRAGAYA, 2014, DABKOWSKI, 2020). Therefore, works containing mappings for the spatialization of these outcrops, as well as the development of scientific research on karst landscapes, are extremely important, as they foment conservation and greater understanding of the dynamics of such rich and vulnerable areas.

2. Materials and methods

This study sought to map and characterize the sedimentation environments of calcareous tufas in the northeastern portion of the state of Goiás, Brazil. In this way, a field visit was carried out during the first half of the second semester of 2021, aiming to verify the areas with occurrence of the features and the prior recognition of the characteristics of depositional environments. In order to verify the internal biological content as well as to carry out further analysis, it was necessary to extract samples from the cores.

In the field work, some testimonies were measured in terms of height and width, with coordinates recorded using the Avenza Maps application on an Android device. Photographs were also stored from available cameras. These cartographic and image data were inserted in a GIS environment (QGIS v.3.16.3 with GRASS v.7.8.5), generating the spatialization of the observed features. Other data, such as hydrography and contours (30 meters), were extracted, respectively, from the State Geoinformation System (SIEG) and the Alos PALSAR Digital Elevation Model. (DEM) of the Shuttle Radar Topography Mission (SRTM) project, both acquired from the United States Geological Survey (USGS). The satellite image applied comes from the Google Satellite Plug-in, available within the aforementioned GIS.

The characterization, both in field and in the observations of the samples in the laboratory, were based on the calcareous tufa model for tropical regions influenced by monsoonal systems (CARTHEW et al., 2006). In this way, aspects such as form, biological material, mineral and the place of deposition were considered in the context of the associated hydrography.

3. Results

The mapping procedure demonstrated the occurrence of fourteen points with tufa outcrops, being identified in the rivers and streams Ventura (area 1), Barreiro (area 2) Chumbada (area 3), and São Vidal (area 4). The highest concentration of occurrences, according to this survey, occurs in the pelite-carbonated Lagoa do Jacaré Formation, which belongs to the Bambuí Group (Figure 1ª A).

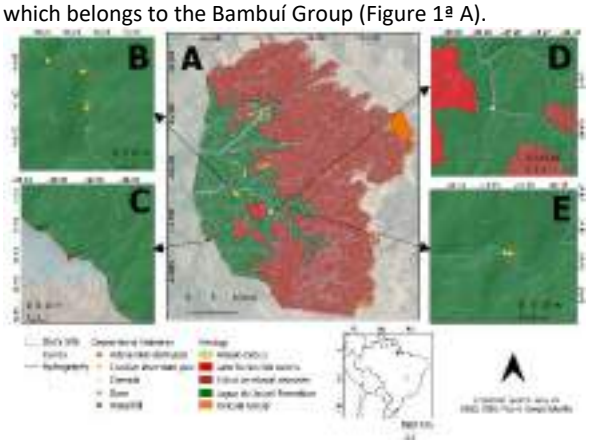

Figure 1ª: A) Spatialization of features; B) Barreiro tufa; C) São Vidal tufa; D) Chumbado tufa; E) Ventura tufa

Through the characterization, it is possible to establish a classification of the types of tufas, which are cascade, waterfall, inter-dam pool and dam. In addition, the classification also encompassed the presence or absence of water activity, as shown in Figure 1ª A, B, C, D, E. In relation to the different depositional environments related to the tufa genesis, in area 1, linked to Ventura, waterfall tufas were analyzed in areas of water spraying, where there was an association of the outcrops with bryophytes (Figure 2ª A) and inter-dam pool, in an area with undergrowth vegetation, such as ferns. Also, tufas with low or no activity were identified (Figure 2ª B, C) in an area associated with what was the drainage gutter in ancient times. Due the proximity to the inter-dam pool area, at a lower ground level, it is inferred that it is part of a system of small waterfalls/cascades. This characteristic is combined with dense laminations in the formation of tufas (Figure 2ª D). As observed in the field, there is a large transport of leaves by rivers, a fact that justifies the marking of incrustations of these in the deposits (Figure 2ª E).

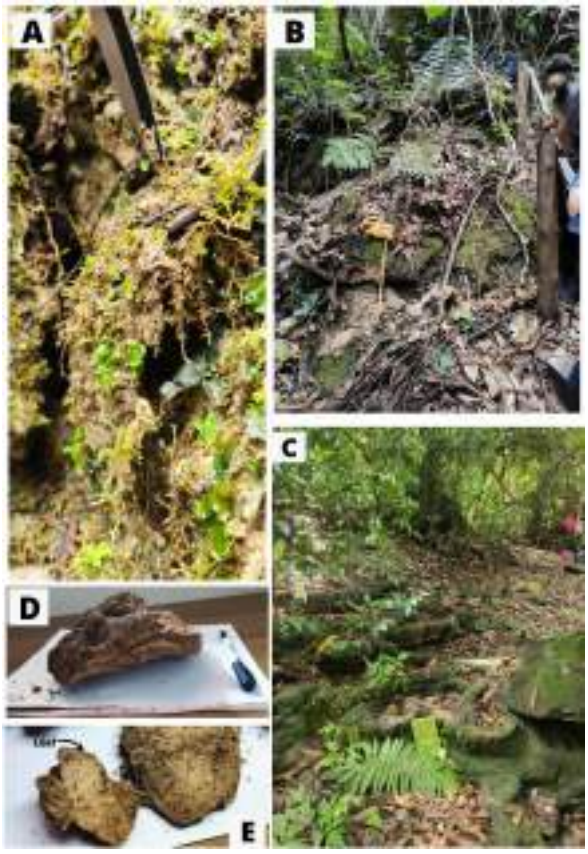

Figure 2ª: A) Funil Waterfall Tufa; B/C) Inter-dam pool tufa; D) Tufa with dense lamination; E) Leaf incrustation on calcareous tufa.

The area 2, linked to the Barreiro stream, presented dam tufas (Figure 3ª A) and an inter-dam pool with stromatolites at the bottom, in a 7-meter U shape, allowing the formation of two pool levels, one measuring 1.70m and the other, 2m wide (Figure 3ª B/D). Its structure shows leaf incrustations. A little further down the same river, there were inactive tufas (Figure 3ª C) of inter-dam pool, possibly forming a foregone large waterfall with a height of 1.93m.

Figure 3ª: A) Dam tufa; B/D) Active inter-dam pool tufa with stromatolites; C) Inactive inter-dam pool tufa formation, possibly an ancient cascade/waterfall.

The Chumbada stream area (area 4) has an environment of tufa formation related to cascades (Figure 4ª A, B). As in the previous cases, the transport of leaves through the river is intense, with the possibility that these plant structures may come to act as supports for calcite. However, no fossil records were found in the collected core. The dimension of the outcrop is 1.70m width by 2.20m height. It is evident that the forming river is in full activity.

Figure 4ª: A) Cascade tufa formation; B) Outcrop measured

Finally, in São Vidal stream (area 4), the outcrops occur originating an active waterfall of large dimensions (Figure 5ª A). Thus, the type of formation environment is predominantly waterfall. The outcrop of the specific extractions, which is 4.17 meters height, is located on the right bank of the waterfall and has a flow variation during the seasons of the year (Figure 5ª B, C).

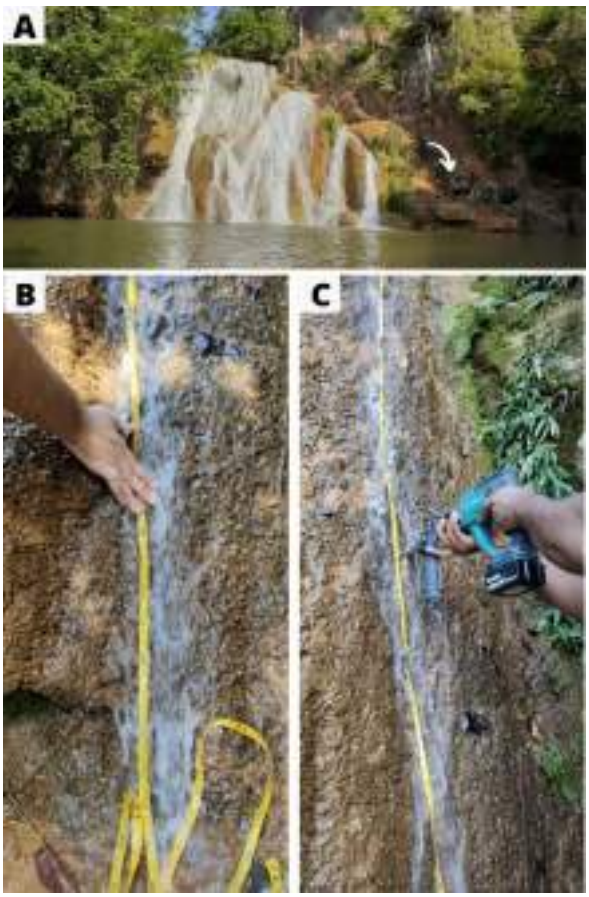

Figure 5ª A) Paraíso do Cerrado Waterfall tufa; B) Paraíso do Cerrado tufa outcrop; C) Tufa extraction process

4. Discussions

The calcareous tufas of northeastern Goiás in Brazil can be a source of information on climate history correlated by

monsoons. It is observed that there is a great variety of types of tufas in active and inactive places, however, well preserved.

The mapping of the tufas allows to observe their distribution in the study area, with a concentration of outcrops in the Barreiro stream, with morphology of altimetric variation along the hydrography, favoring the occurrence of tufa formation of waterfalls, as well as slower flows in flat terrain, with a predominance of dams. The concentration of abandoned outcrops on the edge of the river allows us to deduce that there was a time when the riverbed expanded due to an increase of water flow or that they are products of a river direction change.

Among the types of sedimentation environments, inter dam pool is the most prevalent type, occurring between two types of sedimentation ambients (dam and pool) observed in the field with frequency.

5. Conclusion

The study showed that the concentrations of calcareous tufa outcrops are associated with the Lagoa do Jacaré Formation, belonging to the Bambuí Group. There is a variation of types of environments in which they appear. This identification and the general characterization of the testimonies demonstrates the potential use for several environmental studies. For this reason, the importance of conserving these carbonate concretions is emphasized, regarding the anthropogenic pressure that directly affects their formation process.

Acknowledgments

The authors would like to thank the Postgraduate Program in Geography and the Postgraduate Program in Applied Geosciences, both at the University of Brasília (UnB). To CAPES, CNPq, the Postgraduate Deanship of UnB and also the funding obtained by TCCE 01/2018 Vale/ICMBio. We would like to thank Paulo Éder Gouveia e Adelaine Morais Nogueira for supporting in field works.

References

CAPEZZUOLI, E.; GANDIN, A.; PEDLEY, M. (2014) Decoding tufa and travertine (fresh water carbonates) in the sedimentary record: The state of the art. Sedimentology, v. 61, n. 1, p. 1–21.

CARTHEW, K. D.; TAYLOR, M. P.; DRYSDALE, R. N. (2006). An environmental model of fluvial tufas in the monsoonal tropics, Barkly karst, northern Australia. Geomorphology, v. 73, n. 1–2, p. 78–100.

DABKOWSKI, J. (2020). The late-Holocene tufa decline in Europe: Myth or reality? Quaternary Science Reviews, v. 230.

FORD, D; WILLIAMS, P. (2007). Karst Hydrogeology and Geomorphology. 2. ed. Chichester: Wiley.

FORD, T. D.; PEDLEY, H. M. (1996). A review of tufa and travertine deposits of the world. Earth-Science Reviews, v. 41, n. 3–4, p. 117–175.

HILL, C. A.; FORTI, P. (1997). Cave minerals of the world. National Speleological Society, p.463.

MIRAGAYA, J. F. G. (2014). O desempenho da economia na Região Centro-Oeste. Um olhar territorial para o desenvolvimento: Centro-Oeste, p. 424–453, 2014.

MOEYERSONS, J. et al. (2006). Age and backfill/overfill stratigraphy of two tufa dams, Tigray Highlands, Ethiopia: Evidence for Late Pleistocene and Holocene wet conditions. Palaeogeography, Palaeoclimatology, Palaeoecology, v. 230, n. 1–2, p. 165–181.

ORDÓÑEZ, S; GONZÁLEZ M, J. A.; GARCÍA DEL CURA, M. A.; PEDLEY, H. M. (2005). Temperate and semi-arid tufas in the Pleistocene to Recent fluvial barrage system in the Mediterranean area: The Ruidera Lakes Natural Park (Central Spain). Geomorphology, [S. l.], v. 69, n. 1–4, p. 332–350.

PEDLEY, H. M. (1990). Classification and environmental models of cool freshwater tufas. Sedimentary Geology, v. 68, n. 1–2, p. 143–154.

TRAVASSOS, L. E. P. (2019). Princípios de Carstologia e Geomorfologia Cárstica. Brasília: Instituto Chico Mendes de Conservação da Biodiversidade,

PEDLEY, M.; GONZÁLEZ MARTÍN, J. A; ORDÓNEZ DELGADO, S; GARCÍA DEL CURA, M. A. (2003) Sedimentology of quaternary perched springline and paludal tufas: Criteria for recognition, with examples from Guadalajara Province, Spain. Sedimentology, , v. 50, n. 1, p. 23–44.

9 Publicações submetidas e publicadas no período

O período em que estive na França foi frutífero para internacionalização do nosso grupo de pesquisas. Além da análises já mencionadas no projeto também pude desenvolver muitos trabalhos em parceria com pesquisadores estrangeiros que resultaram na submissão e publicação de 9 publicações em revistas internacionais conceituadas, ligadas a temática do projeto (os quais também são anexados a esse relatório):

FERREIRA, C. F. ; HUSSAIN, YAWAR ; Uagoda, Rogério . *A semi-automatic approach for doline mapping in Brazilian covered karst: way forward to the vulnerability assessm*ent. **ACTA CARSOLOGICA**, 2022.

HUSSAIN, YAWAR ; SEIVANE, H. ; QIANGSHAN, G. ; MACIEL, SUSANNE ; HAMZA, O. ; Uagoda, Rogério ; BORGES, WELITOM . *Seismic Signatures and Site Characterization of an Intermittent Stream in Dry and Flood Conditions: An Implication for Soil Losses and Landslide Triggering*. **Remote Sensing**, 2022.

HUSSAIN, YAWAR ; CAMPOS, JOSÉ ELOI GUIMARÃES ; BORGES, WELITOM RODRIGUES ; UAGODA, ROGÉRIO ELIAS SOARES ; HAMZA, OMAR ; HAVENITH, HANS-BALDER . *Hydrogeophysical Characterization of Fractured Aquifers for Groundwater Exploration in the Federal District of Brazil*. **Applied Sciences-Basel**, v. 12, p. 2509, 2022.

DA SILVA, ANA CAMILA ; RESENDE, ISABELA ; DA COSTA, RODRIGO CINTRA ; Uagoda, Rogério ; Avelar, André . *Geophysical for granitic joint patern and subsurface hydrology related to slope instability*. **JOURNAL OF APPLIED GEOPHYSICS**, v. 199, p. 104607, 2022.

VITALINA DA SILVA CALDEIRA, DANDARA MARIA ; Uagoda, Rogério ; NOGUEIRA, ADIVANE MORAIS ; GARNIER, JEREMIE ; SAWAKUCHI, ANDRÉ OLIVEIRA ; HUSSAIN, YAWAR . *Late quaternary episodes of clastic sediment deposition in the Tarimba Cave, Central Brazil*. **QUATERNARY INTERNATIONA**L, v. 01, p. 01-36, 2021.

HUSSAIN, YAWAR ; BORGES, WELITOM ; UAGODA, ROGERIO ; MOURA, CRISTIANE ; MACIEL, SUSANNE ; HAMZA, OMAR ; HAVENITH, HANS-BALDER . *Estimation of total groundwater reserves and delineation of weathered/fault zones for aquifer potential: A case study from the Federal District of Brazi*l. **Open Geosciences**, v. 13, p. 904-916, 2021.

TAVARES, A. ; R., UAGODA ; SPALEVIC, V. ; MINCATO, R. L. . *ANALYSIS OF THE EROSION POTENTIAL AND SEDIMENT YIELD USING THE INTERO MODEL IN AN EXPERIMENTAL WATERSHED DOMINATED BY KARST IN BRAZIL.* **THE JOURNAL AGRICULTURE AND FORESTRY**, v. 67, p. 153-162, 2021.

FONSECA, MARIA RITA SOUZA ; Uagoda, Rogério ; CHAVES, HENRIQUE MARINHO LEITE . *Rates, factors, and tolerances of water erosion in the Cerrado Biome (Brazil): A meta-analysis of runoff plot data***. EARTH SURFACE PROCESSES AND LANDFORMS**, v. 46, p. 01, 2021.

Uagoda, Rogério; HUSSAIN, YAWAR . *GIS-Based Relief Compartment Mapping of Fluvio-Karst Landscape in Central Brazilian Highlands*. **International Journal of Economic and Environmental Geology**, v. 11, p. 61-64, 2021.

A semi-automatic approach for doline mapping in Brazilian covered karst: the way forward to the vulnerability assessment

Cristiano F. FERREIRA[1 *], Yawar HUSSAIN[2] & Rogério UAGODA[3]

[1] Nacional Center for Research and Conservation of Caves – CECAV - Instituto Chico Mendes de Conservação da Biodiversidade – ICMBio. Brasília, 70635-800, Brazil, e-mail: cristiano.ferreira@icmbio.gov.br

[2] Georisk & Environment, Department of Geology, University of Liege, Liege, 4000, Belgium, e-mail: yhussain@uliege.be

[3] Department of Geography, University of Brasilia, Brasilia, 70910-900, Brazil, e-mail: rogeriouagoda@unb.br

16 **Abstract**

17 ***Cristiano F. Ferreira, Yawar Hussain & Rogério Uagoda: A semi-automatic***
18 ***approach for doline mapping in Brazilian covered karst: the way forward to the***
19 ***vulnerability assessment***

20 Doline mapping is paramount in the vulnerability and risk assessment of the
21 underground karst environment by identifying cave-ground connectivity points at the
22 surface. However, manual mapping, is labor-intensive, slow and subjective, especially
23 at large scales. Therefore, the present study adopted a GIS-based semi-automatic
24 approach for mapping large and medium-sized depressions/dolines in the Corrente river
25 basin in Brazil with a particular focus on the environmentally preserved areas of river
26 Vermelho (APANRV Portuguese abbreviation) using remote sensing (DEM and Google
27 Earth imagery) and field-based observations. Seven typical dolines forms (e.g., cockpit
28 with drain insertion, collapse, collapse with river capture, suffosion, solution, cover
29 collapse, and buried) are found from extensive field surveys. As an outcome of the
30 proposed approach, two hundred and thirty-two medium to large-sized dolines have
31 been identified and categorized into three main groups based on the cave density and
32 local geology G1, G2, and G3. The high density of identified dolines (164 known caves)
33 in G1 provides reconnaissance for future speleological works in the preserved areas.
34 Additionally, the presence of a considerable number of dolines in the adjoining areas
35 (G2 and G3) stresses the need to revise the existing boundaries of the APANRV.
36 Results correlate well with the dolines sites marked using field surveys and Google
37 Earth images. This doline mapping may help the researchers in the groundwater
38 vulnerability assessment and the protection of speleological heritage preserved in the
39 caves.
40

41 **Keywords:** cave-ground connectivity; preservation area; field surveying;
42 remote sensing.

1 INTRODUCTION

Dolines are natural depressions present at the surface, in different sizes (diameters ranging from meters to kilometers) and shapes (circular to sub-circular) (Ford & Williams, 2007). Dolines are characteristic of karstic environments that denote the predominance of subsurface solution processes as outcomes of the interaction of slightly acidic water with soluble rocks such as carbonates. Together with the epikarst, dolines serve as a reservoir for water for the underground environment (Williams, 2008) and a direct connection between surface morphology and underground environments (fauna and speleothems) making their detailed investigation an essential step in the cave vulnerability and hazard assessment (Hussain et al., 2020a, 2020b). The identification and mapping of dolines can also be used to obtain morphometric data for karstification rate estimation and to determine the evolution of karst landscapes (Williams, 1972; Day, 1976). Doline mapping can also play a role in geological hazard assessment by helping to identify areas prone to collapse (Hofierka et al., 2018; Salles et al., 2018).

Therefore, accurate identification and mapping of dolines is a way forward leading to the vulnerability assessment of cave environments to surficial contaminants. The task is expensive and requires many resources, mainly when performed through classical photo interpretation, or field mapping, especially in large areas. To reduce such high cost, several studies have been dedicated to doline detection and mapping by applying geoprocessing tools using automated approaches on satellite images, light detection and ranging (LiDAR), digital elevation models (DEMs), or other cartographic sources(Guimarães et al., 2005; Siart et al., 2009; Carvalho Júnior et al., 2014; Wu et al., 2016; Zhu & Pierskalla, 2016; Wall et al., 2017; Cahalan & Milewski, 2018; Hofierka et al., 2018; Mihevc & Mihevc, 2021). These automatic approaches of objects (doline) identification may lead to erroneous results, especially under limited data availability conditions.Therefore, Google Earth images and field survey-aided semi-automatic approaches are favored.

As in the case of Brazil where karst terrains are widespread, especially in the central and eastern regions of the country still, its study is in the infancy stage and requires further detailed analysis (Salles et al. 2018). The example can be taken off the Corrente river basin including APANRV, where there is still non-availability of detail databases required for the accurate identification of the dolines. An attempt has been

made in the past for such identification using different geophysical techniques by Hussain et al., (2020a, 2020b). However, the scale of the study was too small to be considered for the assessment on a large scale. Therefore, there is a dire need for such mapping at a large scale using freely available information.

In accordance with the needs, the present study aims to map the dolines present in the APANRV and the Corrente river basin (3,923.14 km²) in the northeastern Goiás state of Brazil. The ALOS-PALSAR and SRTM DEMs are evaluated in a semi-automated fashion together with Google Earth imagery and field surveys for a visual inspection based check on the proposed methodology. The present study's outcomes may help achieve dual objectives revising the existing boundary of the environmentally preserved areas and providing the GIS layer for the future vulnerability assessment of the underground environment. Comparison of doline mapping with known cave points may enhance the preservation of these areas and assist in speleological prospecting and plans for the sustainable exploitation of natural resources.

2 MATERIAL AND METHODS

2.1 Study area description

The study area covers the upper part of the Corrente river basin (Fig. 1), next to the Serra Geral de Goiás. The climate of the region is tropical, with dry (April to September) and rainy (October to March) seasons presenting a precipitation index of ~1260 mm/y (Caldeira et al., 2021). There is a well-developed drainage system constituting numerous rivers (e.g., Corrente, Vermelho and Buritis) and streams (e.g., Bezerra, Piracanjuba, Rizada, Chumbada, Ventura and Extrema). Some of the watercourses become subterranean in contact with the sink, which may again emerge as resurgences or springs on the surface, promoting the formation of caves. There are also numerous depressions commonly called 'grota', which contain water in the rainy season (Hussain et al., 2020a).

The northeastern region of Goias presents stratigraphic records of the Archean, Proterozoic, Mesozoic and Cenozoic ages, most of which are Proterozoic, including the following units: Ticunzal formation, sequence of volcanic-sedimentary rocks of Palmeirópolis and São Domingos, the Arai group, Serra Branca, Tonalito São Domingos, the Paranoá group and the Bambuí group (Gaspar & Campos, 2007). The

most extensive carbonate unit is the Bambuí group, which hosts the largest number of caves in Brazil. Below the sedimentary cover of the Urucuia Group, there are pelitic and carbonate rocks from the Bambuí Group (Gaspar & Campos, 2007).

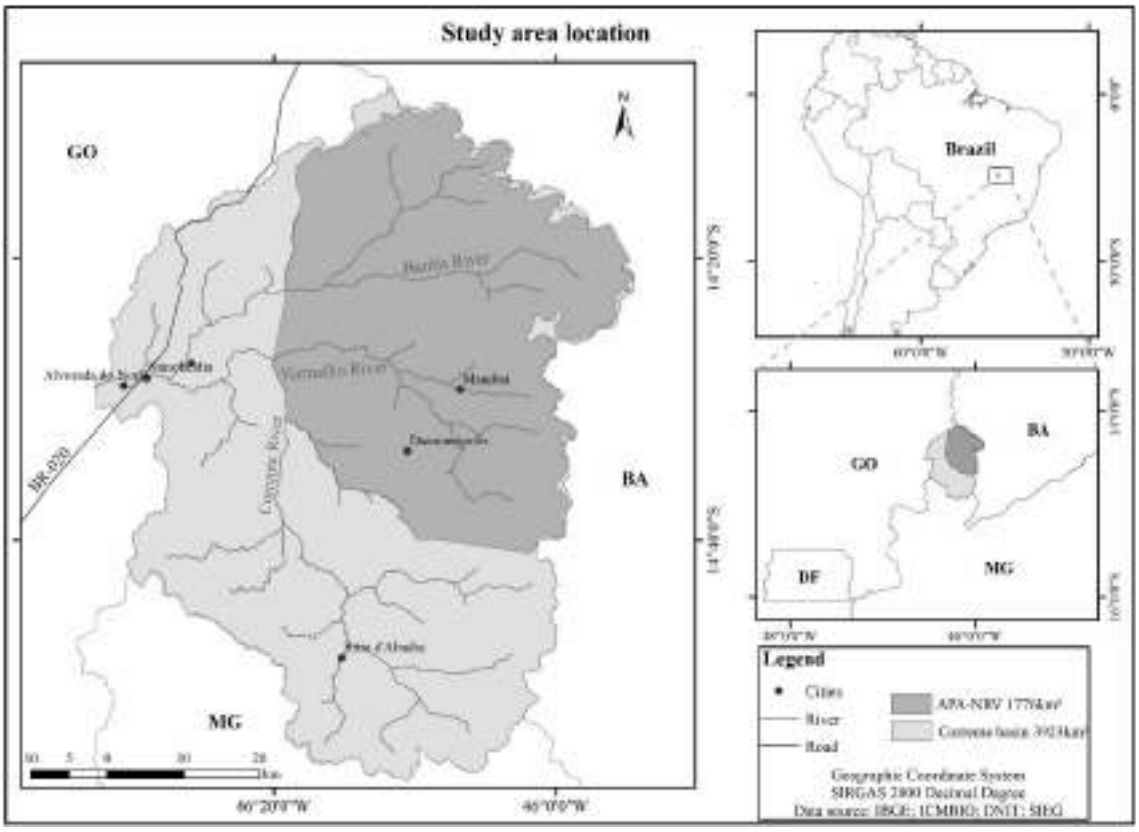

Fig. 1: Location of the study area on map of Brazil, zoomed location in reference to the neighboring states and the current boundaries of APANRV along with important rivers, streams, and settlements.

The following soil classes and sediments were found: oxisoils, podzolic, cambisols, plinthsol, gleysol, sands, hydromorphic quartz, organic soils, quartz sands, alluvial soils and petroplinthic soils. The general soil classification is driven by the local geology. The soil erodibility rate is higher and related to the presence of vegetation cover (Fonseca et al., 2021). The presence of clay and claystone (between sandstone and the epikarst) act as an impermeable layer, leading to the generation of a large amount of surface runoff and sediments. The runoff may infiltrate into the karst system at the places of geological contacts (sandstone and carbonate) and pathways to the caves (dolines/sinkholes) leading to contamination and causing a significant impact on the underground hydrological system.

123 The region integrates several geomorphological features: i) the escarpment; ii) the
124 very flat upper part of the sandstone; iii) the formation of oxisoil; iv) dolines opened in
125 convex-concave hill-slopes covered by claystone; v) canyons compartment formed as a
126 result of cave collapse; and vi) the lower basing part. Four landform units were
127 identified as canyons , deep valleys, local ridges, upland drainage, and mountain tops.
128 Details can be found in Hussain and Uagoda (2021).

129 The Urucuia aquifer system has a thick layer of siliciclastic sediments and stores
130 large groundwater volumes (Gaspar & Campos, 2007). This system covers a significant
131 part of the area. It recharges main rivers and their tributaries (Fig. 1). The presence of
132 soluble rocks, such as the carbonates (Lagoa do Jacaré formation) in the north-central
133 part of the area, drained by Buritis and Vermelho rivers, seems to stimulate regional
134 denudation as compared to the southern sector. This last one presents lateritic surfaces
135 that supported the relief during regressive erosion promoted by the Corrente river.

136 In the studied area, there are two types of cave systems have been proposed as
137 superior/vadose (top-bottom) that collect floods from hillslopes and sediments from the
138 nearby sandstone aquifer and deep epigene fluvial-karst (bottom-up) (Hussain &
139 Uagoda, 2021). The Tarimba (11 km in length) is considered one of the most important
140 (i.e., with a high level of biodiversity) and largest in the country (Hussain et al. 2020a).
141 The caves have connectivity with the superficial environment through weak spots (the
142 cave opening, dolines and geological contacts). In this way, land use at the surface can
143 definitely impact the subsurface in numerous ways (i.e., water, sediments, and
144 contaminants). So, the connectivity leads to the vulnerability of the underground
145 environment that affect the lives of fauna and flora there. Therefore, the identification
146 and mapping of these vulnerability-prone weak spots at the surface are crucial.

147 **2.2 Field surveying and imagery**

148 For the Google Earth imagery database download, the following simple criteria of
149 no cloud presence in the dry season and less vegetation had been adopted, which
150 enhanced the object detection threshold many fold. After that, a doline detection criteria
151 was adopted based on the features identification and their categorization into supportive
152 and non-supportive. The places or polygons where there are supportive features found
153 are considered as doline, while the opposite is true for the no doline. The places where
154 we encountered both supportive and non-supportive features are referred to as presumed

doline. The presumed and probable doline categories are, henceforth, referred to as "possible dolines". This approach is also helpful in separating karstic features from non-karstic ones as is the case with veredas (a riparian subsystem of the Cerrado biome). This image-based identification and categorization show clear advantages over the automatic approaches where there are higher chances of filtering out many features that can help in doline or depression identification. The salient features of the proposed criteria for visual inspection are presented in Table 1. Visual inspection using Google Earth imagery as a possible check on DEM-based automatic doline detection. The objects-based classification is ranked into probable dolines and no dolines. For example, the features of probable dolines are a change of vegetation in a circular shape, depression due to centripetal drainage, and depressions with evident sinkholes. The examples of the adopted inspection and marked objects on Google Earth images are presented in Fig. 2.

Tab. 1: The adopted criteria for visual classification of objects into probable, possible/presumed and no dolines in between them using Google Earth imagery.

Probable dolines		**No dolines**
Centripetal drainage		Open drainage
Drainage with apparent sinkhole		Dam
Change in vegetation		Homogeneous vegetation
Soluble rock		Slightly soluble rock
Circular pattern		Atypical formats
Plateau occurrence		Grand Canyons bottom
Large and deep depression		Veredas (shallow depressions)
Cave presence		Road
Known dolines	**Presumed**	Anthropic area

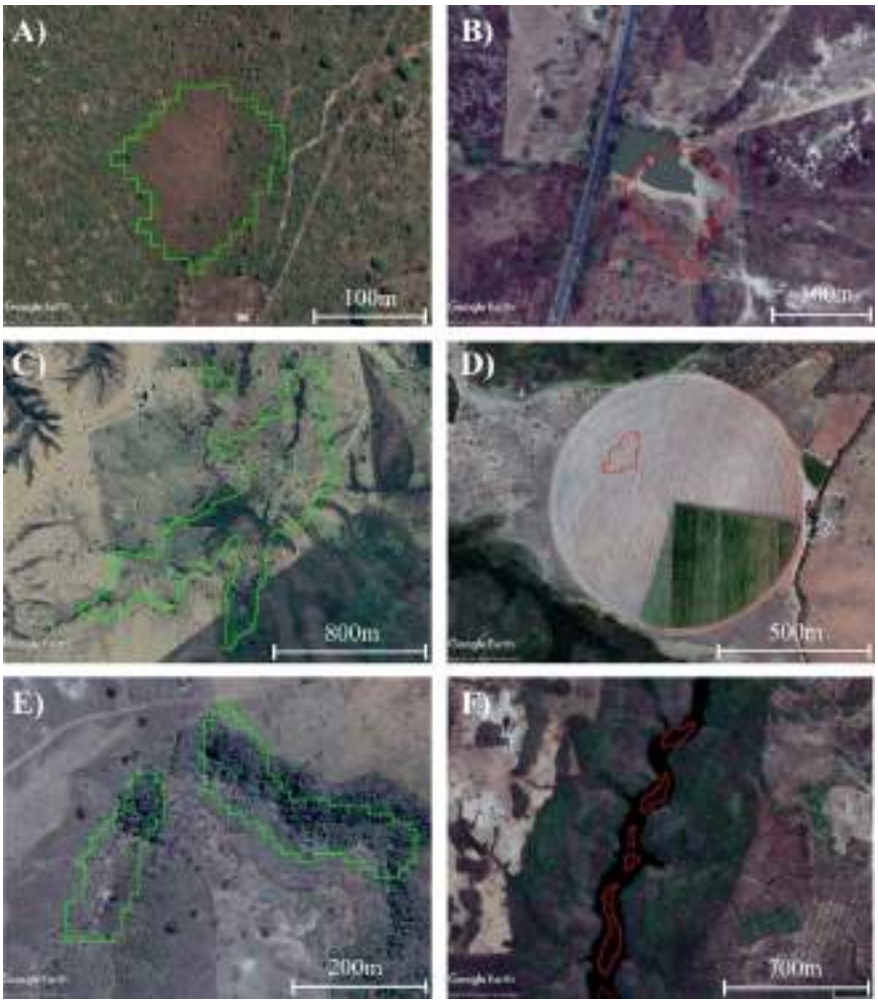

Fig. 2: *The visual classification results are color coded as green and red as probable and no-doline objects, respectively. A) change of vegetation in circular shape, B) depression related to road/dam, C) depression due to centripetal drainage, D) depression in anthropic areas, E) depressions with evident sinkholes and F) objects created on the canyon bottom, with open drainage. Source: Google Earth, 2020.*

2.3 DEM-based analysis

In order to check comparative performance evaluation, the DEM (12.5 m) from Advanced Land Observing Satellite Phased Arrayed type L-Band SAR (ALOS-PALSAR) and DEM (30 m) from Shuttle Radar Topography Mission (SRTM) are used (JAXA/METI, 2011; NASA, 2014). In the end, the specific object identification capabilities of these DEMs has been enhanced using Google Earth imagery and field survey results.

After obtaining these databases (DEMs and imagery), the next step is filling of DEM-ALOS-PALSAR based on the specific conditions of the studied area. This technique identifies depressions through the arithmetic subtraction of the DEM filled

188 from the original DEM (Bauer, 2015; Wall et al., 2017; Cahalan & Milewski, 2018;
189 Hofierka et al., 2018). The automatic filling of DEM resulted in erroneous features
190 especially near the watercourses and, in some cases, the formation of large "virtual
191 dams" in narrow gorges. This has been minimized (large depressions) after applying
192 gridding processing to the original DEM near erroneous points as recommended by
193 Doctor and Young (2013). This narrow leveling procedure, by images, eliminates large
194 depressions and can be applied to the erroneous points (Fig. 3). This has been executed
195 using "Serval" tool in QGIS software.
196

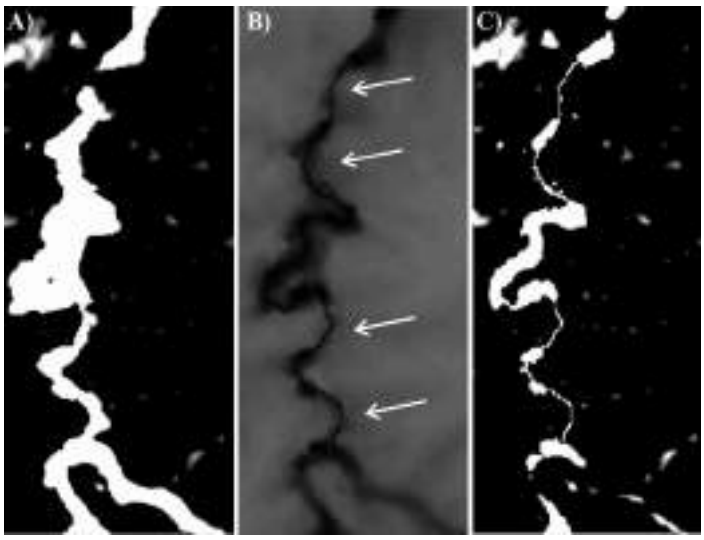

197

198 *Fig. 3: The grinding process of the DEM ALOS-PALSAR at narrow portions of*
199 *drainage: A) large dams above 500 m wide, B) arrows point to the linear rectification*
200 *performed in the original raster, and C) rectified DEM of width below 150 m.*

201 The filling is performed with the distinct altimetric filters with a Z limit value
202 using 'Fill' tool of ArcGIS software. The fills of different values as zero (Z0), three
203 (Z3), and ten meters (Z10) are tested. After the necessary visual inspection, we observed
204 that Z3 limit offers a more realistic distribution of objects while Z10 showed objects
205 only in the valley bottoms, and Z0 does not make any selection (Fig. 4). Next, occurred
206 the vectorization of the depression raster at a depth value greater than 3 m and created a
207 column containing the area information. At this stage, the depressions below 625 m^2
208 (four pixels) are eliminated from the analysis based on the field experience.

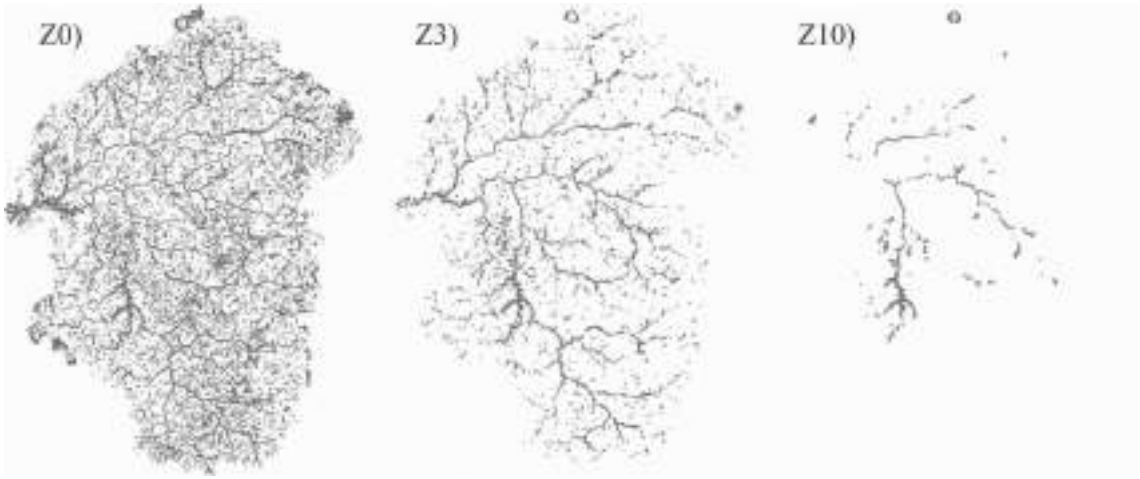

Fig. 4: Depth filter with increasing object depth from 0 m (Z0), 3 m (Z3) up to 10 m (Z10).

The subsequent cleaning is done based on the correlation of drainage with the objects that still remain. In the absence of hydrographic databases at the adopted scale, the drainage network has been obtained using DEM ALOS-PALSAR (Faulkner et al. 2013). A flow accumulation threshold of 500 pixels and rivers from 6th to 8th order is used (Strahler's hierarchy method) to eliminate false objects. The same aforementioned processing steps have been repeated for DEM SRTM, except for the use of a minimum area filter because of the pixel size greater than 625 m². After visual classification of the objects from the two bases (DEMs), we classified the dolines by morphometric characteristics such as: area, perimeter, depth, and minimum altitude. The deepest point is calculated using the unprocessed DEM ALOS-PALSAR. For the dolines distribution analysis, we converted the features into centroid points which were used for the density map preparation along with known cave location maps. A complete list of doline extraction processing steps is summarized in Fig. 5.

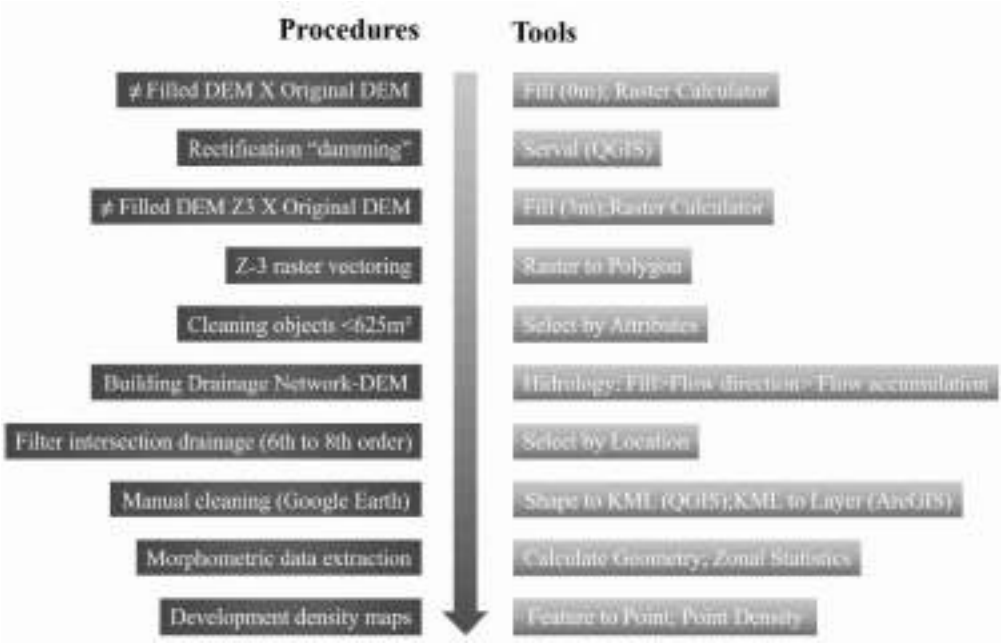

Fig. 5: List of processing workflow along with their execution in respective GIS tools.

3 RESULTS

3.1 Detection using DEM

The comparative evaluation of DEMs resulted in identification of three more probable dolines in SRTM base than ALOS-PALSAR base. There were 11 additional objects from the SRTM base as presumed dolines. We incorporated the added elements of the landscape as dolines, rivers and hills from those bases into the final database of features as potential dolines. The quantities of classified objects into presumed, probable and no dolines in the two analyzed databases (DEMs) indicate a substantial equivalence in their detectabilities (Tab. 2). In spite of having a lower resolution, the SRTM base can indicate nearly the same number of objects as of ALOS-PALSAR base. However, changes in the forms of objects from these databases are observed because of variable pixel sizes. Most of the objects from SRTM went through a form change during raster to polygon conversion. There is also some over ranking in the case where larger objects are found surrounded by smaller objects. Due to these drawbacks, the ALOS-PALSAR base is used for the extraction of objects for the analysis. Despite the large data volumes and extensive manual work requirement for the inspection of numerous elements (5,706 in all), the combined analysis of these two bases ensured redundancy and greater confidence in visual classification.

Tab. 2: Number of objects obtained using DEMs after applying filtering and classification procedures.

	ALOS	%	SRTM	%
Z0	26,410	100	25,479	100
Z3	3,377	12.79	3,430	13.46
Area < 625 m²	3,032	11.48	3,430	13.46
Drainage 6th-8th orders	2,686	10.17	3,020	11.85
Visual cleaning Google	218	0.83	213	0.84
Probable objects	99	0.37	97	0.38
Presumed objects	119	0.45	116	0.46
No dolines	2,510	9.5	2,807	11.02
Total ALOS/SRTM	232 possible dolines			

Considering the object parameters as area, perimeter, and depth (Tab. 3), we observe a greater extent (twice the perimeter and twice the area) in the probable dolines as compared to the presumed ones. This discrepancy shows the difficulty in discerning smaller features using DEM, even when checked with Google Earth imagery being classified as presumed. For the minimum altitude data, the most profound points varied between 680 and 700 m. Nevertheless, it presents an occurrence at the most varied altitudes, which is compatible with covered karst being exhumed. The lowest presumed depression identified was 2,812 m², indicating that only medium to large dolines can be delineated using DEM-based analysis.

Tab. 3: Morphometric parameters of the identified *depressions.*

Morphometry	**Probable Dolines (101)**			**Presumed Dolines (130)**		
	Max.	**Min.**	**Average**	**Max.**	**Min.**	**Average**
Area (m²)	851,875	3,750	76,807	404,063	2,812	22,126
Perimeter (Km)	10.6	0.275	1.63	9.025	0.225	0.795
Depth (m)	31	3	7.89	19	3	4.55
Lowest Point (m)	956	535	683.56	959	521	702.5
Total density (nº/km²)	0.059					

Among the identified dolines, one of much larger dimensions as 3.47 km² in the area and 20 m depth in the sandstone of the Urucuia Group, is considered as outlier and removed from the morphometric analyses (Tab. 3). This may possibly be created by the accommodation depression caused by underlying karst and may be referred to "sagging dolines" (Gutiérrez et al., 2008). Our methodology shows the potential of identifying

large dolines (compound depressions), not considering the smaller objects inside because of the coarser scale. There are concentrations of features (dolines) in certain areas, especially of carbonates rocks. In contrast, in non-carbonate rocks (siliciclastic, pelitic, and laterites) there are large empty extensions where only a few dolines occur. The occurrence and significance of these depressions lie out of the scope of the present study and deserve future detailed investigations.

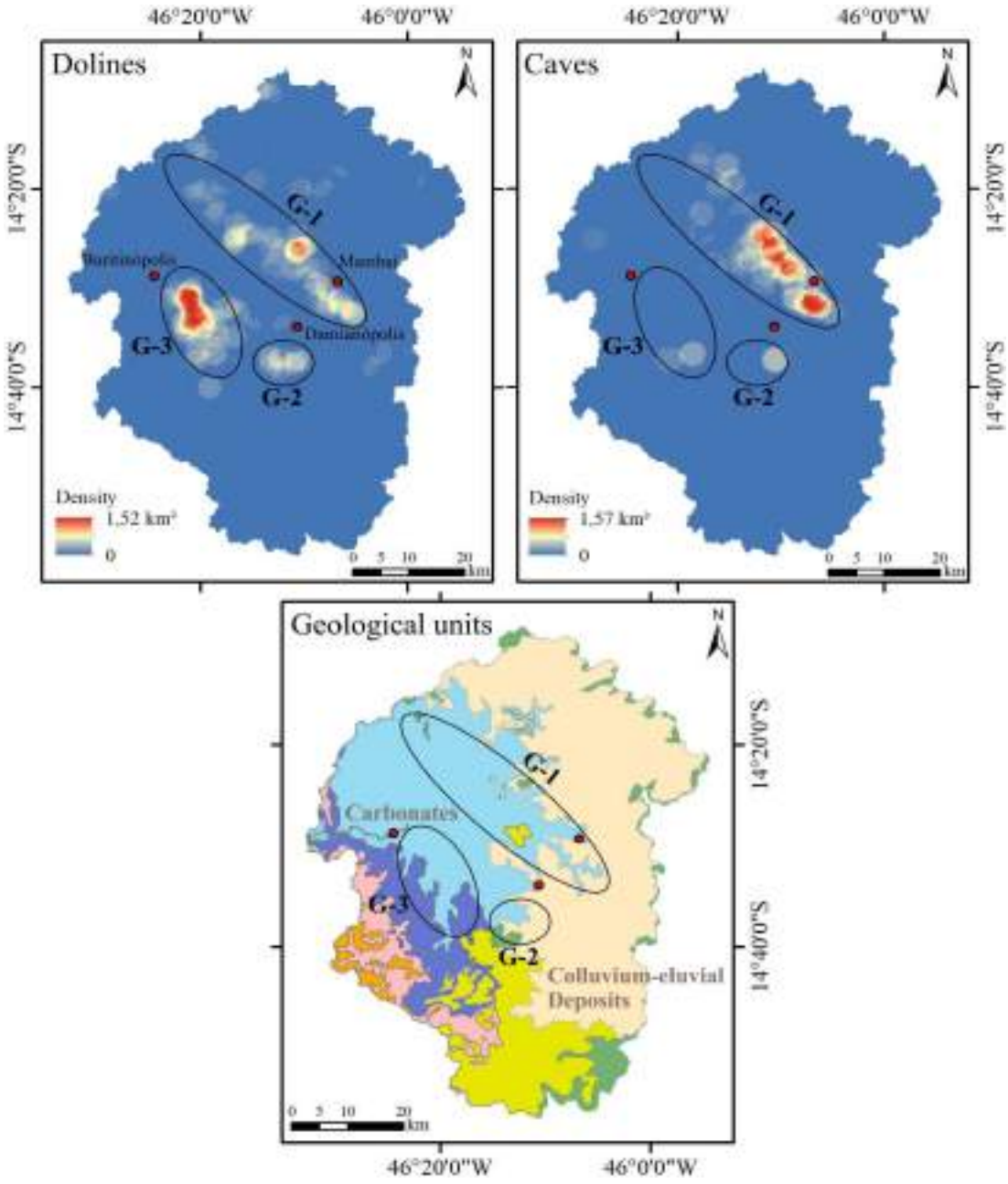

Fig. 6: The dolines versus caves densities in reference with the local geology. The groups are identified by the acronyms G-1, G-2, and G-3.

Regarding the spatial distribution, we elaborated a density map from the centroid points of all identified features and from the known cave points (Fig. 6). The total number of possible dolines is 232, packed in a low overall density (0.059/km²) because of the large extent of the study area (~ 3,923.14 km²). The doline density is found to correlate positively with the occurrence of carbonate rocks, such as the case with Lagoa do Jacaré formation, where 162 features are found with a density of more than double (0.155/km²) than the adjoining non-carbonated areas.

Fig. 7: Typical dolines forms found in the region which may serve as the connections points between surface and underground environments: A) cockpit with drain insertion,

B) collapse, C) collapse with river capture, D) suffosion; E) solution, F) cover collapse, and G) buried. Photos by Cristiano F. FERREIRA

3.2 Field survey and imagery

The local dolines, which represent the connection of surface and underground environments, are classified into various types (Fig. 2, 7). Larger composite depressions of the cockpit type, with the insertion of internal drains (channels), are quite common. Smaller collapse or suffusion features, can occur inside compound dolines and are often linked to large cave systems. Each identified typology has its own vulnerability potential and affects the underground environment accordingly.

The procedures resulted in approximately 26,000 features (Tab. 2). After automatic filtration, a visual analysis of only 10 to 12% of the original objects was conducted. After object inspection in DEMs as per established visual classification criteria, we obtained a total of 232 possible dolines, out of which 102 are classified as probable. The possible dolines represent less than one percent of the initial objects identified in each base (0.8%).

The dolines mapping provided an opportunity compare with the known dolines database developed as a result of successive visits in the study area, which identified smaller dolines (<1 m^2), beyond the capability of automated analysis. Out of 152 field-mapped dolines in the study area, only 69 show links with 23 objects (possible) created by the semi-automatic detection of used bases, and the rest did not generate any object and are considered as trivial or pseudo features (artifacts). These 23 objects have a single or more than one dolines per object (e.g., compound dolines). The mapping performed in this work focuses more on other features because it is challenging to confirm the large dimensions of these compound dolines in the field visually. In any case, it was possible to confirm substantial dolines densification in compound dolines (Tab. 4). This demonstrated the effectiveness of the adopted methodology as an indicator of karst areas, where isolated minor dolines can also occur. In this case, although 83 dolines do not have associated polygons, such features are precisely present in the areas with a consequent density of large objects (Fig. 8).

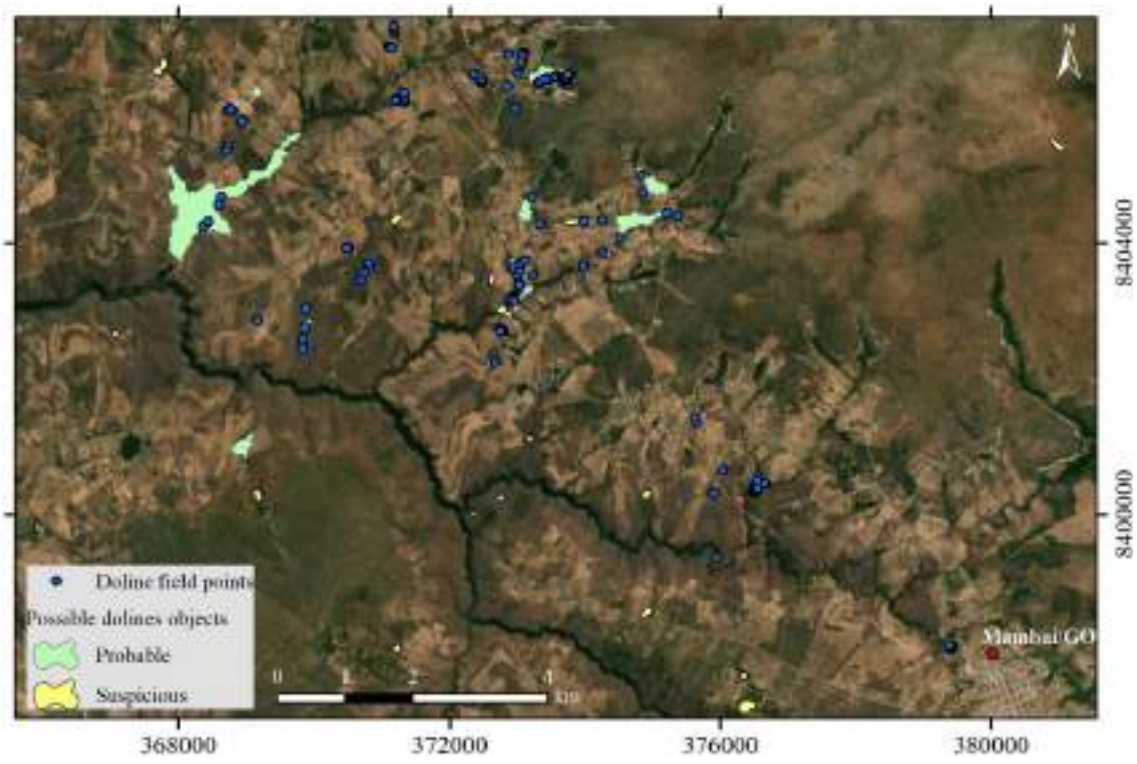

Fig. 8: Doline points checked in the field, and objects considered possible dolines in Group-1. Many doline points are referred as miniature features, which did not generate polygons at this scale (Esri et al.,2020).

The predominant typologies of dolines found in the study area were the suffosion one, followed by cockpits and collapsed ones (Tab. 4). Colmated types, solution, and coverage collapses had appear as expected. Group-1 presented more dolines because we studied it for longer than Group-3, which rightly drew attention after the mappings performed in this research. Both areas and all other objects generated in this work still require further confirmation. The results indicate areas prone to depression occurrence as a reconnaissance for further field activities in order to refine the mapping of undetected dolines and caves.

Tab. 4: Geologywise distribution of field-mapped dolines along with their typologies.

Type/area	Group-1	Group-3	Partials
Suffosion	54	16	70
Cockpit	37	2	39
Collapse	26	1	27
Colmated	7	0	7
Solution	5	0	5
Coverage collapse	4	0	4
Totals	**133**	**19**	**152**

4 DISCUSSION

The geologywise distribution of these possible dolines is mainly characterized in three groups: i) the first, a NW-SE trend near the sandstone-limestone contact at the north of Mambaí (Group-1); ii) the second of lesser prominence, south of Damianópolis (Group-2); and iii) the third and most dense, southeast of Buritinópolis (Fig. 6). Compared with the cave density map, we see an evident density convergence in these features with Group-1 dolines in the previous map. There is also a relationship between caves and Group-2 dolines. Group-3 has nearly no cave presence.

It is essential to highlight that the doline density map presents the result of an investigation based on remote sensing without field confirmation of all features. Thus, it may explain the occurrence of scattered sectors on the map with a substantial density, not included in any group mentioned, which may or may not contain dolines. On the other hand, the density in Group-3 and the convergence with the cave density of Groups 1 and 2 allow us to assume a greater possibility of features in such areas. The three identified groups converge at a greater or lesser degree with the occurrence of carbonates of the Lagoa do Jacaré formation as observed by overlapping the features with the geological map (Fig. 6). Scattered occurrences are associated with alluvial-colluvial clastic deposits from the Serra Geral de Goiás erosion. The carbonate occurrence under the clastic sediments, especially at the intersection of G-1 and G-2, indicates a process of exhumation in the karst.

No cave corresponding to group-3 may attribute to the fact that the area has not yet been the target of systematic speleological prospecting. Hence, we carried out a more accurate interpretative analysis by Google Earth images at the basin scale compared to the overflow level as documented in the literature (Telbisz et al. 2009; Bauer, 2015). Results show a polygonal typology for the local karst (Williams, 1972), something unexpected if considered the recurrent pattern of adjacent karst areas, with isolated dolines in the landscape (Fig. 9). Visual inspection also allowed the identification of other dolines, not pointed out in the automated process, and the subdivision of depressions during the filtration process (Z3). The semi-automated methodology could be applied for the initial detection of dolines but requires further

visual refinement for checking and delimitation, as recommended by Hiruma and Ferrari (2014).

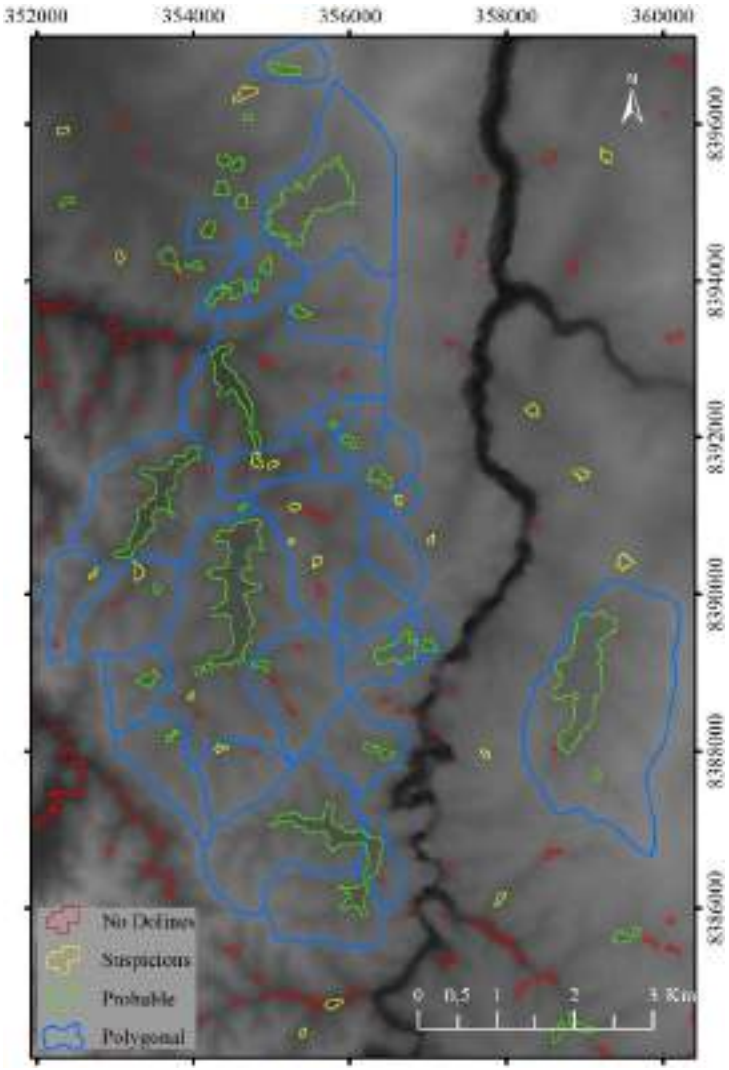

Fig. 9: Polygonal karst patterns (in blue), objects in green (probable dolines), yellow (presumed dolines), and red (no dolines) were identified by the automatic approach. Source: DEM ALOS-PALSAR (JAXA/METI, 2011).

Results obtained within in the boundaries of the APANRV show that large karst structures occur outside the current limits of the preservation area (Group-3) and in adjacent areas (Group-2), highlighting the need for quick actions (Fig. 10). Along with the isolated features, the polygonal or sagging depressions are also found outside the limits of the APANRV. These features indicate high capacities of surface water conduction to the underground environment, which increases the exposure of these areas to contamination of the karst aquifers.

Thus, in order to fulfill the local speleological conversion objective of the APANRV, it is necessary to expand the current boundaries of the preserved area to encompass these large karst structures in the adjoining areas. The location of the large, medium, and small dolines are areas of water recharge for karst systems. The preservation of the underground environment requires proper land use managerial plans, which prohibit the installation of large projects for agriculture, mining, highways, and other related incompatible activities.

If we consider the lack of other detailed databases and the existing doline maps, it is fair to affirm that the procedures we adopted have filled the existing knowledge gap regarding the identification of karst features. This new information can be added to the future planning of the APANRV through the reconnaissance of speleological prospection and mapping of small-scale dolines.

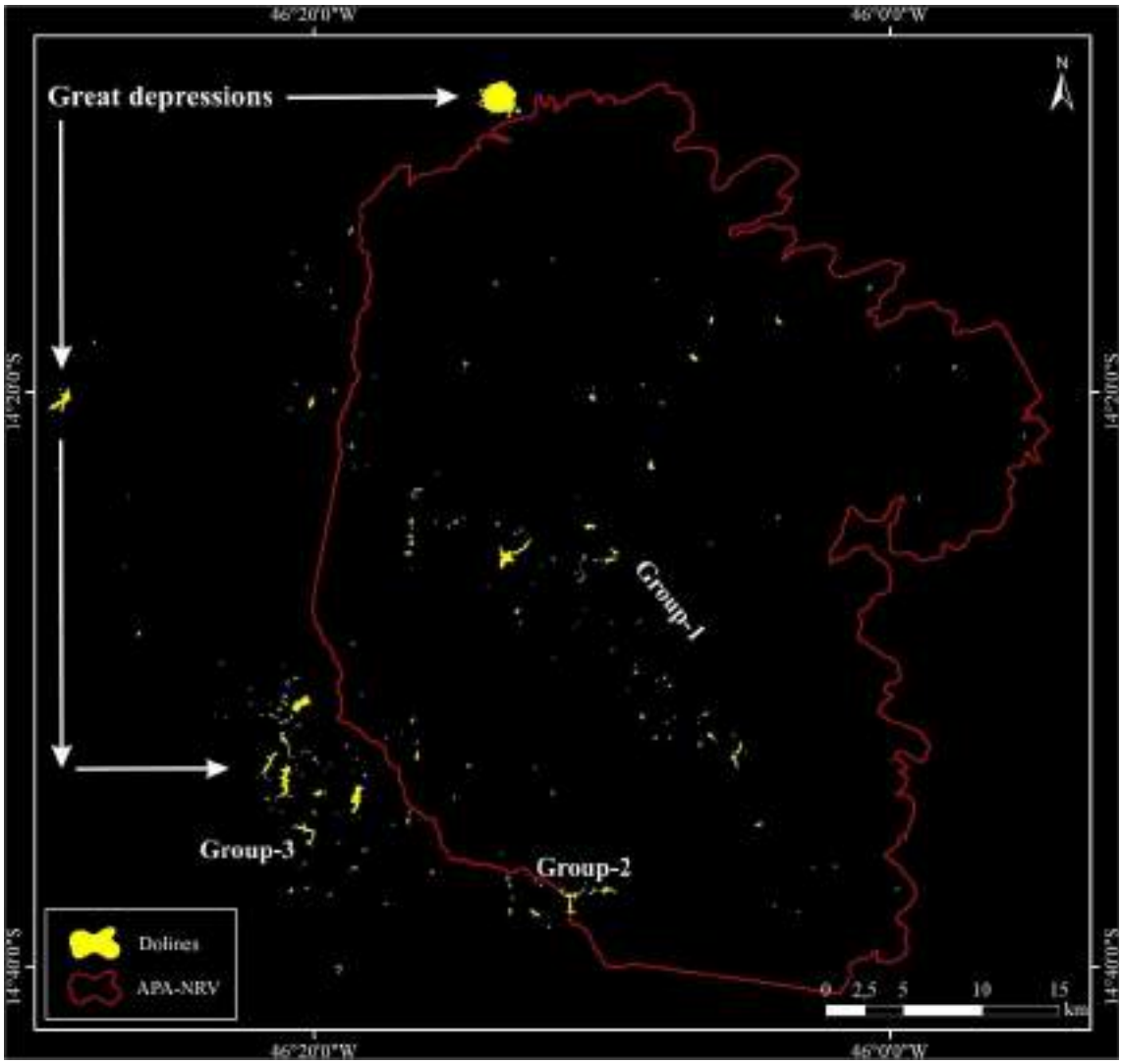

383 *Fig. 10: Spatial distribution of the possible dolines in the Corrente river basin*
384 *and the APA borders.*

385 # 5 CONCLUSIONS AND RECOMMENDATION

386 In areas of substantial territorial extension, doline mapping is a complex task that
387 becomes even harder using manual and non-automated techniques. The integrated use
388 of DEM, along with high-resolution images represents an additional source of
389 information that can be explored with geo-technological resources for doline mapping
390 and even beyond. We used the DEM ALOS-PALSAR and SRTM in this work, applying
391 series of automated procedures aimed at identification of medium to large karst
392 depressions. The results show that, although the digital models do not present
393 resolutions compatible with the detection of small dolines, they are essential for
394 identifying karstified areas, in which large and medium depressions occur, but also
395 small features. The analysis of two models in parallel ensured redundancy,
396 complementarity, and greater confidence in the classification of objects. Surprisingly,
397 the SRTM base, with lower spatial resolution, presented results equivalent to ALOS-
398 PALSAR, demonstrated its versatility.

399 Thus, from this research, we identified dominant density areas for possible
400 dolines, the presence of isolated dominant features, and structures of high hydrological
401 significance, such as polygonal karst zones. Such data will be available for the future
402 Planning Phase of the APANRV, directing detailed confirmations on the field. The
403 results also show areas of high speleological potential, indicating the methodology is
404 applicable to regions under investigation for cave occurrence as caves and dolines have
405 a significant evolutionary and environmental role. The observation of regional
406 karstification processes and indication points of higher water concentration and aquifers
407 vulnerability can be evaluated. For mapping the presence of features of different
408 dimensions and forms, high resolution drone-based photogrammetry and further
409 detailed field surveying are recommended.

410 The doline map can be considered a raster for the cave underground vulnerability
411 assessment using a suitable index-based karst vulnerability models, is recommended.
412 Around the identified dolines and caves, buffer zones of certain diameter based on the
413 field survey could be chosen. The afterword rating system could be signed to each
414 buffer zone based on its proximity to the vulnerability-prone features such as a river,
415 agricultural forms, industry, gas pumps etc.

REFERENCES

Bauer, C., 2015: Geomorphology Analysis of dolines using multiple methods applied to airborne laser scanning data.- Geomorphology, 250, 78–88. DOI: 10.1016/j.geomorph.2015.08.015

Cahalan, M.D. & A.M. Millewski, 2018: Sinkhole formation mechanisms and geostatistical-based prediction analysis in a mantled karst terrain.- Catena, 165, 333–344. DOI: 10.1016/j.catena.2018.02.010

Caldeira, D., Uagoda, R., Nogueira, A.M., Garnier, J., Sawakuchi, A.O. & Y. Hussain, 2021: Late Quaternary episodes of clastic sediment deposition in the Tarimba Cave, Central Brazil. *Quaternary International*, *580*, 22–37. DOI: 10.1016/j.quaint.2021.01.012

Carvalho Júnior, O.A., Guimarães, R.F., Montgomery, D.R., Gillespie, A.R., Gomes, R.A.T., Martins, E.S. & N.C. Silva, 2014: Karst depression detection using ASTER, ALOS/PRISM and SRTM-derived digital elevation models in the Bambuí Group, Brazil.- Remote Sensing, 6, 330–351. DOI: 10.3390/rs6010330

Day, M., 1976: The morphology and hydrology of some Jamaican karst depressions. Earth Surface Processes, 1, 111–129. DOI: 10.1002/esp.3290010203

Doctor, D.H. & J.A. Young, 2013: An evaluation of automated GIS tools for delineating karst sinkholes and closed depressions from 1-meter LiDAR-derived digital elevation data.- In: Land, L., Doctor, D.H. & J.B. Stephenson (Eds.) *Proceedings of the 13th Multidisciplinary Conference on Sinkholes and the Engineering and Environmental Impacts of Karst*, 13th, 2013, New Mexico, National Cave and Karst Research Institute, 449–458. DOI: 10.5038/9780979542275.1156

Esri, Maxar, Geo Eye, Earthstar Geographics, CNES/Airbus DS, USDA, USGS, AeroGrid, IGN, & GIS User Community, 2020. World Imagery. Available from: https://www.arcgis.com/home/item.html?id=10df2279f9684e4a9f6a7f08febac2a9 [Accessed 6rd January 2020].

Faulkner, M.G.S., Stafford, K.W. & A.W. Bryant, 2013: Delineation and classification of karst depressions Using LIDAR: Fort Hood Military Installation, Texas.- In: Land, L., Doctor, D.H. & J.B. Stephenson (Eds.) *Proceedings of the 13th Multidisciplinary Conference on Sinkholes and the Engineering and Environmental Impacts of Karst*, 13th, 2013, New Mexico, National Cave and Karst Research Institute, 459–467. DOI: 10.5038/9780979542275.1157

450 Fonseca, M.R.S., Uagoda, R. & H.M.L. Chaves, 2021: Rates, factors, and tolerances of
451 water erosion in the Cerrado biome (Brazil): A meta-analysis of runoff plot data.
452 *Earth Surface Processes and Landforms*, *47*(2), 582–595. DOI: 10.1002/esp.5273
453 Ford, D.C. & P.W. Williams, 2007: Karst Hydrogeology and Geomorphology.- Wiley,
454 pp. 562, Chichester.
455 Gaspar, M.T.P. & J.E.G. Campos, 2007: O sistema aqüífero Urucuia.- Revista
456 Brasileira de Geociências, 37, 4, 1068–1078. DOI: 10.25249/0375-
457 7536.200737S4216226
458 Google Earth, 2020: Google Earth Pro, version 7.3.4.8642 (64-bit). Available from:
459 http://www.google.com/earth/index.html
460 Guimarães, R.F., Carvalho Júnior, O.A., Martins, E.S., Carvalho, A.P.F. & R.A.T.
461 Gomes, 2005: Detection of karst depression by aster image in the Bambui Group,
462 Brazil.- SPIE, 5983, 328–339. DOI: 10.1117/12.627741
463 Gutiérrez, F., Guerrero, J. & P. Lucha, 2008: A genetic classification of sinkholes
464 illustrated from evaporite paleokarst exposures in Spain.- Environmental Geology,
465 53, 993–1006. DOI: 10.1007/s00254-007-0727-5
466 Hiruma, S.T. & J.A. Ferrari, 2014: Análise comparativa da extração automatizada de
467 dolinas a partir de modelos digitais de terreno.- Revista do Instituto Geológico, 34, 2,
468 1–11. DOI: 10.5935/0100-929X.20140006
469 Hofierka, J., Gallay, M., Bandura, P. & J. Šašak, 2018: Identification of karst sinkholes
470 in a forested karst landscape using airborne laser scanning data and water flow
471 analysis.- Geomorphology, 308, 265–277. DOI: 10.1016/j.geomorph.2018.02.004
472 Hussain, Y., & R. Uagoda, 2021: GIS-based relief compartment mapping of fluvio-karst
473 landscape in central Brazilian highlands.- International Journal of Economic and
474 Environmental Geology. DOI: 10.1002/essoar.10503441.2
475
476 Hussain, Y., Uagoda, R., Borges, W., Prado, R.L., Hamza, O., Cárdenas-Soto, M.,
477 Havenith, H-B. & J. Dou, 2020a: Detection of cover collapse doline and other
478 Epikarst features by multiple geophysical techniques, case study of Tarimba cave,
479 Brazil.- Water, 12(10), 2835. DOI: 10.3390/w12102835
480 Hussain, Y., Uagoda, R., Borges, W., Nunes, J., Hamza, O., Condori, C. Asslam, K.,
481 Dou, J. & M. Cárdenas-Soto, 2020b: The potential use of geophysical methods to
482 identify cavities, sinkholes and pathways for water infiltration. Water, 12(8), 2289.
483 DOI: 10.3390/w12082289

JAXA/METI, 2011: ALOS PALSAR ALPSRP267816890, ASF DAAC. Available from: https://asf.alaska.edu. DOI 10.5067/Z97HFCNKR6VA [Accessed 11rd July 2018].

Mihevc, A. & R. Mihevc, 2021: Morphological characteristics and distribution of dolines in Slovenia, a study of a lidar-based doline map of Slovenia.- Acta Carsologica 50/1, 11–36. DOI: 10.3986/ac.v50i1.9462

NASA, 2014: SRTM 1 Arc-Second Global, SRTM1S15W047V3, SRTM1S15W046V3. Available from: https://earthexplorer.usgs.gov/ [Accessed 22rd September 2018].

Salles, L.Q., Galvão, P., Leal, L.R.B., Pereira, R.G.F.A., Purificação, C.G.C. & F.V. Laureano, 2018: Evaluation of susceptibility for terrain collapse and subsidence in karst areas, municipality of Iraquara, Chapada Diamantina (BA), Brazil.- Environmental Earth Sciences, 77, 16, 593. DOI: 10.1007/s12665-018-7769-8

Siart, C., Bubenzer, O. & B. Eitel, 2009: Combining digital elevation data (SRTM/ASTER), high resolution satellite imagery (quickbird) and GIS for geomorphological mapping: A multi-component case study on Mediterranean karst in Central Crete.- Geomorphology, 112, 1-2, 106–121. DOI: 10.1016/j.geomorph.2009.05.010

Telbisz, T., Dragušica, H. & B. Nagy, 2009: Doline Morphometric analysis and karst morphology of Biokovo Mt (Croatia) based on field observations and digital terrain analysis.- Hrvatski geografski glasnik, 71, 2, 5–22. DOI: 10.21861/hgg.2009.71.02.01

Wall, J., Bohnenstiehl, D.R., Wegmann, K.W. & N.S. Levine, 2017: Morphometric comparisons between automated and manual karst depression inventories in Apalachicola National Forest, Florida, and Mammoth Cave National Park, Kentucky, USA.- Natural Hazards, 85, 2, 729–749. DOI: 10.1007/s11069-016-2600-x

Williams, P.W, 2008: The role of the epikarst in karst and cave hydrogeology: a review.- International Journal of Speleology, 37, 1, 1–10. DOI: 10.5038/1827-806X.37.1.1

Williams, P.W., 1972: Morphometric analysis of polygonal karst in New Guinea.- Geological Society of America Bulletin, 83, 3, 761–796. DOI: 10.1130/0016-

7606(1972)83[761:MAOPKI]2.0.CO;2

Wu, Q., Deng, C. & Z. Chen, 2016: Automated delineation of karst sinkholes from LiDAR-derived digital elevation models.- Geomorphology, 266, 1–10. DOI: 10.1016/j.geomorph.2016.05.006

Zhu, J. & W.P. Pierskalla, 2016: Applying a weighted random forests method to extract karst sinkholes from LiDAR data.- Journal of Hydrology, 533, 343–352. DOI: 10.1016/j.jhydrol.2015.12.012

Article

Seismic Signatures and Site Characterization of An Intermittent Stream in Dry and Flood Conditions: An Implication for Soil Losses and Landslide Triggering

Yawar Hussain[1*], Helena Seivane[2], Gao Qiangshan[3], Susanne Maciel[4], Omar Hamza[5], Rogério Uagoda[6], Welitom Borges[7]

[1]Georisk & Environment, Department of Geology, University of Liege, Liege, 4000, Belgium
[2]Andalusian Institute of Geophysics and Earthquake Disaster Prevention, University of Granada, Granada, Spain
[3]State Key Laboratory of Space Weather, National Space Science Center, Chinese Academy of Sciences, Beijing, China
[4] Planaltina Campus, University of Brasília, Brasília, Brazil
[5]School of Built and Natural Environment, University of Derby, Derby, UK
[6]Department of Geography, University of Brasilia, Brasilia, Brazil
[7]Institute of Geosciences, University of Brasilia, Brasilia, Brazil
* Correspondence: yhussain@uliege.be

Abstract

Identifying ambient noise-based (ANb) signatures of streams can help in the estimation of their erosive potential (EP) that promotes reverie landslides and soil losses in the fluvial valleys. This is particularly imperative on flooding or rainy days, leading to stronger erosion-prone conditions (colluvium and boulders) of the valley beds inferred from georadar attribute analysis. Developing such research direction can benefit the local communities, as is the case with the Cerrado region of Brazil, where these phenomena have high destructive potential with social, economic, and climatic implications. For the present study, a seasonal stream in the Federal District of Brazil was investigated by ANb monitoring supported by Ground Penetration Radar (GPR) for site characterization. The ANb monitoring was conducted (at a safe distance) with a seismometer over several durations of dry and rainy conditions. The power spectral density (PSDs) was computed as a function of several variables, including weather conditions (rainfall, wind speed, and pressure), time-frequency spectrograms, and ambient noise displacement root mean square (RMS). This analysis also considered the single station horizontal-to-vertical spectral ratio (HVSR), where rain, wind, pressure, river flow and anthropogenic signatures were evident (at selective frequency ranges). Multi-peaks that emerged on the HVSR curve were further analyzed to identify amplitude and frequency changes, and the three peaks shift on average to a lower position during the rainy period. The GPR amplitude and waveform variation features were attributed to the stratigraphy (i.e., the boundary between valid and invalid regions and coherence value) of the floodplain and regions susceptible to erosion (erosion-prone lithological spots). This approach provides the basis for non-destructive monitoring tools enabling the detection of 'seismic signatures' and weak spots of the fluvial channels for improving environmental management.

Keywords: weak spots; spectral analysis; ambient noise RMS; georadar attributes

1 Introduction

In recent years, floods and debris flow worldwide have increased riverbank and soil erosion and landslides, impacting the downstream communities and causing severe losses in lives, properties, and land functionality (Somos-Valenzuela et al. 2015; Zhang et al. 2022). Usually, local and small-scale erosions might not seem like serious instability problems. Still, in the long-term and extreme flood events, this situation often develops into landslides on riverbanks. It may also induce several issues, such as river blockage, a shift of river channel position, or flooding from rising riverbeds

 doi:10.20944/preprints202209.0447.v2

(Gu et al. 2020). Consequently, it may lead to the collapse of roads and bridges built along the river network (Chmiel et al. 2022).

With the effect of climate change, intermittent and ephemeral systems are expected to become increasingly common globally. However, these systems are understudied compared to perennial stream flows. These are of particular concern as they present a unique connection point at the terrestrial-aquatic interface, promoting soil erosion and landslide triggering. Moreover, complex spatial and temporal variations in hydrologic connectivity in non-perennial systems often require a unique interdisciplinary approach to advance the understanding of their function and response to global change. Therefore, monitoring riverbanks and erosive potential (EP) at an early stage is essential to inform the hazard evaluation and improve the risk management of erosion and landslide in such regions.

Fundamentally, EP is a function of various influencing factors, such as rainfall intensity (Rindraharisaona et al. 2022) and the nature of sediment transport and incision in the catchment area (Lawler 1993). In addition, the local site condition can play a vital role in this process. This condition may include the types and properties of soil, such as density (compaction), porosity, and permeability, and any variation in these properties that may represent potential shear plans (Hamza et al. 2020), soil thickness, the topography of bedrock, and the presence of rock fragments (Hussain et al. 2022). The EP assessment has a wide range of applications in landscape evolution, soil erosion, landslide, ecology, water quality, land use management, and civil and river engineering like dams and recreational reservoir silting (Giménez et al.; David et al. 2010; Oeurng et al. 2010; Graf et al. 2010; Araujo et al. 2012; Schmandt et al. 2013; Chao et al. 2015; Lai et al. 2018; Marchetti et al. 2019).

The accurate monitoring and prediction of EP of a river are challenging tasks. For such tasks, there are currently several adopted techniques, including (i) the stream hydrophones or geophones (Turowski et al. 2011), (ii) the identification of particles with a tracer or radiofrequency (Schneider et al. 2014), and (iii) calculation via empirical relationships calibrated in the laboratory (Wilcock and Crowe 2003). However, these techniques can be logistically challenging, particularly in significant flooding events, so their application becomes cost-prohibitive (Roth et al. 2016).

As river activity and site conditions of the valleys are coupled with physical properties, including the ambient noise and electromagnetic wavefields, among others, hence can be valuable sources for monitoring (time-variant) and characterization (time-invariant) using geophysical techniques. Thus, with the growing demands for remote monitoring of these signals from outside the river channel, geophysical methods are increasingly adopted for monitoring work.

For this remote monitoring of river flow, two types of seismic-based geophysical techniques are broadly emerging, where the generated seismic-based (GSb) and ambient noise-based (ANb) activities are measured. The seismic signals emitted by river dynamics can be monitored by non-invasive, cost-effective, long-term, and continuous methods with broad applications (Schmandt et al. 2013; Gimbert et al. 2014). Significant efforts have been made to quantify the spectral signature of bedload transportation water; however, it has been found that seismic power at low frequency is primarily generated by water discharges rather than bedload transportation (Burtin et al. 2008; Schmandt et al. 2013; Barrière et al. 2015). A theoretical model of PSD was calculated from the Rayleigh waves generated by saltating the bedload particles (Tsai et al. 2012). Another seismic activity produced by the turbulent river flow-based theoretical model was proposed by (Gimbert et al. 2014); it contributes to SPD variations in response to the seasonal hysteresis magnitude variations and has been reported in many other studies (e.g., Burtin et al. 2008, 2011; Schmandt et al. 2013; Chao et al. 2015; Barrière et al. 2015). These findings support the use of seismic for the high-resolution monitoring of river bedload and other flow attributes (Roth et al. 2016). From the previous studies, it can be concluded that for larger fluvial systems, high frequency (> 15 Hz) power excitation is created by high levels of bedload transportation (Schmandt et al. 2013; Roth et al. 2016;

Preprints (www.preprints.org) | NOT PEER-REVIEWED | Posted: 16 November 2022 doi:10.20944/preprints202209.0447.v2

Anthony et al. 2018). In contrast, turbulent flow and discharge modulate lower frequency seismic power (between ~1-10 Hz) (Burtin et al. 2011; Schmandt et al. 2013; Bartholomaus et al. 2015; Anthony et al. 2018).

Contrary, in ANb, the river-sponsored variations in the ambient noise wavefield are induced because of the impacts of the bedload on the riverbed and banks, flow noise generated by the water turbulence, and in response to the acoustic waves generated by the interaction of water and atmosphere (Díaz et al. 2014; Chao et al. 2015; Bakker et al. 2020; Lagarde et al. 2021). Monitoring such river-generated noise is consistently reported in hydrologic studies (Díaz et al. 2014). ANb monitoring techniques can provide high temporal and spatial resolutions of the landscapes, and their demands are increasing in bedload monitoring because of their low cost and non-invasiveness (Roth et al. 2016). In the past, an increasing number of contributions have been developed using the variations in ambient noise as the basis of the study of the river flow system (Burtin et al. 2008; Goodling et al. 2018; Anthony et al. 2018; Smith and Tape 2019; P.C and Sawazaki 2021). It was also found that the river discharge vs noise power followed a seasonal hysteresis trend consistent with the regional sediment transport rates in the river (Gabet et al. 2008).

To better decipher the EP of a river, particularly to better monitor the damage potential during floods episodes, the characterization of river beds and valleys can be achieved by GPR application (Arcone et al. 1998; Szuch et al. 2006; Weihermüller et al. 2007; Chalikakis et al. 2011; Fabregat et al. 2019). Overall, soil compaction affects soil dielectric constant and GPR EM signals, as reported in previous studies (Wang et al. 2016).

As in the case of the Cerrado region of Brazil, especially in active geomorphological valleys such as *Ribeirão Contagem valley,* erosion by water is a crucial soil threat and a significant cause of riverside landslides (Hussain et al. 2017; Gomes et al. 2019; Fonseca et al. 2022; Cunha et al. 2022). The present study considered an intermittent stream for the analysis that generates small seismic energies related to the sediments and water flows during rainy days in the Federal District of Brazil for the first time. In the first stage, an attempt has been made for the non-invasive detection of weak spots, susceptible to erosion and landslide, and subsurface layering based on geology (soil, boulder, bedrock) and degree of compaction (less compacted, more susceptible to erosion) by GPR attribute analysis. Afterwards, the contribution is focused on analyzing how the variations of water discharge in a small river can be observed and monitored using ambient noise analysis. We applied a new monitoring technique that calculates the displacement RMS amplitudes, PSD, spectrograms, and HVSR curves of ambient noise recorded during dry and rainy days. Additionally, HVSR peak attributes (i.e., amplitude and frequency) and their changes in relation to different meteorological factors are included in the analysis. The study offers insight into the approach applied, which can benefit the broader scientific community involved in the environment and geohazard management under future climate change extreme scenarios.

2 Material and Method

2.1 Study site description

The Ribeirão Contagem watershed is extended over 146 km^2 in the northern part of the Federal District of Brazil in the Sobradinho administrative unit (Figure 1). The study area has a translational landslide whose dynamism is controlled by river erosion (Hussain et al. 2019a). There are alluvial and colluvial materials weathered from the bedrock of the Paranoá group, though bedrock exposures within the channel itself are rare. Most of the Contagem catchment is located on a large erosion complex, where highly active hill slopes supply the channel during summer rainfalls (Ferreira and Uagoda 2015). The Maranhão river is the main tributary of the watershed that flows in the north and northeast directions. The drainage and channel densities of the watershed are 5.7 and 32.9 channels/km^2, respectively. The climate in the area is semi-humid tropical, with a rainy summer and dry winter. The mean annual precipitation in the area is 1,442.5 mm.

Preprints (www.preprints.org) | NOT PEER-REVIEWED | Posted: 16 November 2022 doi:10.20944/preprints202209.0447.v2

The soil analysis included granulometry, and geotechnical tests were performed on the samples collected with an auger and from trenches (Ferreira and Uagoda 2015). As a result, six soils types are identified in the Contagem basin, including deep and reddish oxisols on the hilltops, shallow inceptisols on the hillslopes, and ultisols because of the presence of clayey carbonate-rich rocks on valleys and plinthic oxisols on the border of hilltops. The erodibility (K factor) is larger for plinthic oxisols than the oxisols and ultissols, having an average value of 0.005790 ton.ha.h.MJ-1.ha-1.mm-1 and 0.004490 ton.ha.h.MJ1.ha-1.mm-1, respectively. The clayey soils in steep hillslopes (from 20° upper to 35° in hills and valleys) can control various linear erosional features such as gullies and landslides, e.g., creeps and translational, rotational movements. A significant proportion of these erosive features is found in inceptsoil in clay-rich rocks. About 63% of these features occur in close proximity to the river (~20 m), highlighting the active role of hydrological processes in erosion (Ferreira and Uagoda 2015).

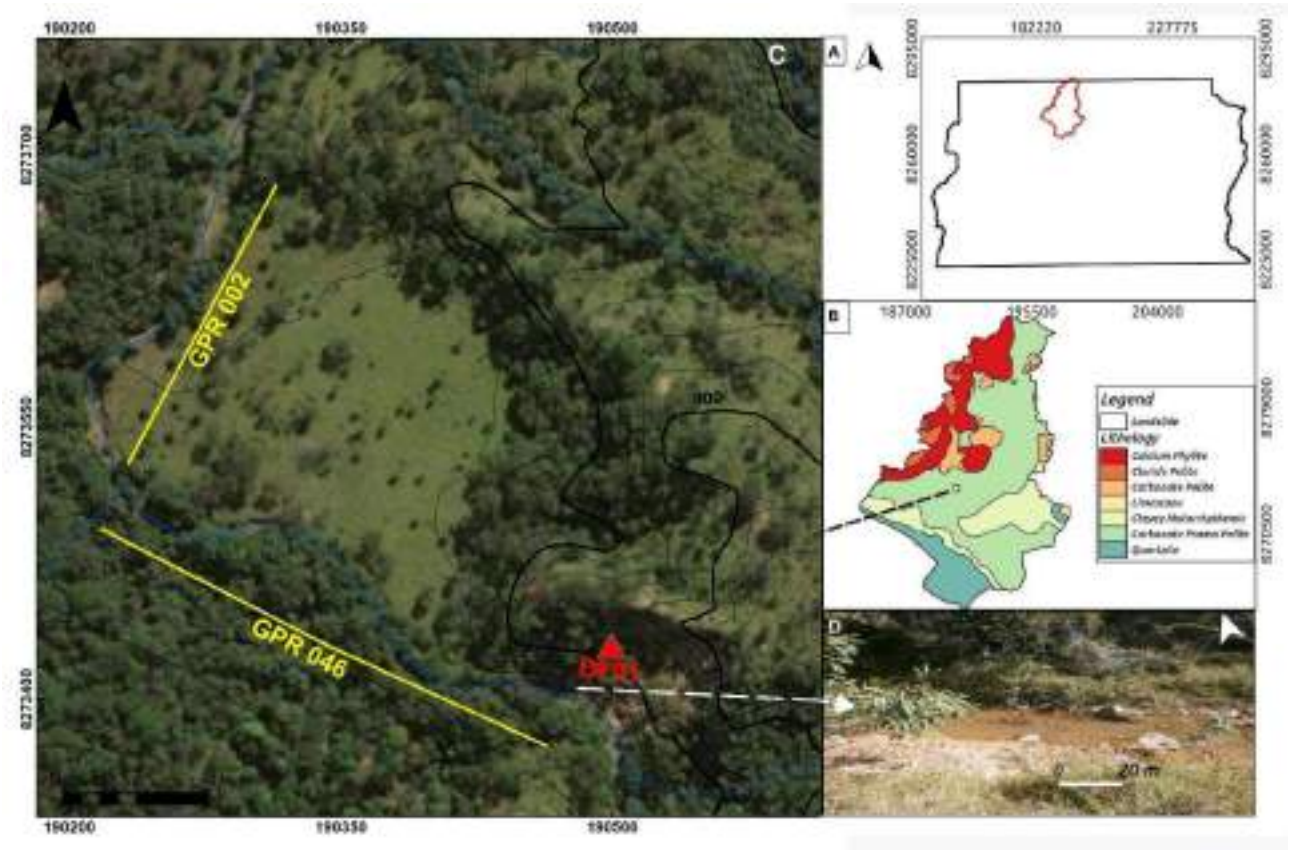

Figure 1. a) Geographic location of Ribeirão Contagem watershed on Federal District map, b) litho-technical units of the watershed c) red dashed ellipse is the Sobradinho landslide boundary and triangle is the position of seismometer (Hussain et al. 2019b) and D) the photograph of river floodplain in the dry season.

The Sobradinho Unit of Votorantim Cimentos Brazil is located in the Ribeirão Contagem Basin, where low-grade metamorphic sediments of the Paranoá and Canastra groups occur. The area is dominated by pelitic rocks such as gray slates and clayey metasiltites. The thickness of the unit varies between 120 m and 150 m, and the rocks that make up this unit are strongly influenced by the paleogeography of the bottom, marking the end of the deposition of the Paranoá Basin. Due to the composition of this unit, the primary minerals, when in contact with water or subjected to atmospheric conditions, are quickly weathered. The riverbank shows the connection between the colluvial-alluvial material and the alluvial material. The latter has a lateral continuity that varies between ~30 m and ~100 m long from the drainage bed (da

Preprints (www.preprints.org) | NOT PEER-REVIEWED | Posted: 16 November 2022 doi:10.20944/preprints202209.0447.v2

Silva Nunes et al. 2019). In the drainage bed, it was possible to observe that the finer-grained alluvial material (with well-selected grains, secondary minerals and low humidity) was superimposed on the colluvial material with poorly selected grains (varying from medium sand to gravel with decimetric boulders), composed of quartz with a high moisture content due to shallow water table. In general, the deposits in the Ribeirão Contagem channel are distributed as follows: soil masses moved by recent rotational landslides; river sediments deposited in recent river bars; sediments deposited in an alluvial fan; colluvial sediments; and alluvial sediments.

Figure 2. a) The former terraces eroding sites (b) photographs of various sizes of sediments from clay to pebbles and boulders in the riverbed, showing the transport capacity in river floods (c) the sediment sequence in terraces show clayey levels and on top with a clast supported layer on the base, showing events of high energy where recurrent (d) sites of undercutting of steep slopes inducing landslides by the river.

Ferreira and Uagoda 2015 proposed a classification for estimating EP based on hydrological units, slopes, and forms. Three classes were found in the Contagem basin as low, medium, and high EP. Concave hillslopes higher than 10° were classified as high potential due to subsurface flux and clayey material concentration. While on convex slopes, the critical to a movement was taken as 35°. The map showed the major proportion of known mass movements wherein high potential. So, the fluvial valleys and their steep hillslopes are dynamic areas composed of alluvium in the bottom, colluvium in the low and middle parts of the high slopes, shallow inceptsols in the elevated portion of the hillslopes, and oxisols in the hilltops. The concave hillslopes have a critical angle of up to 10°, being the most important trigger of rotational landslides on the border of deep valleys (Braga et al. 2018).

Preprints (www.preprints.org) | NOT PEER-REVIEWED | Posted: 16 November 2022 doi:10.20944/preprints202209.0447.v2

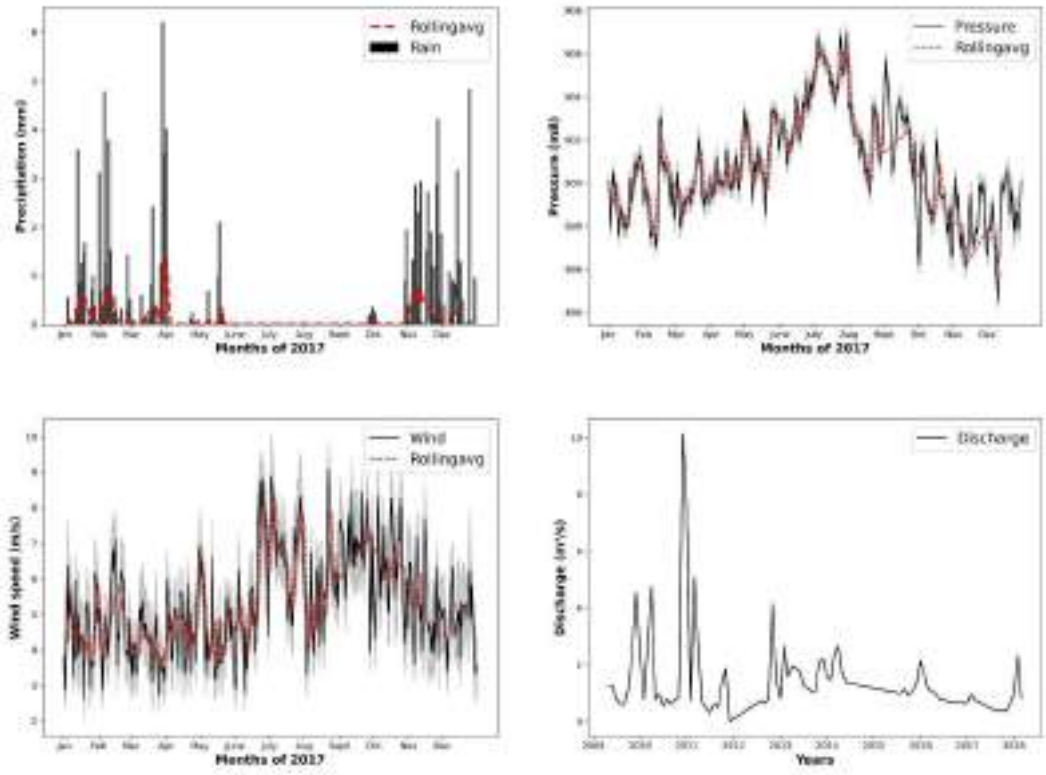

Figure 3 (a) Rainfall, (b) pressure, (c) wind speed and (d) river flow plots of the area.

2.2 Data Acquisition and Processing

2.2.1 Seismic Ambient Noise

For hydrodynamic analysis of the river, one Sorcel L-4A-3D short-period seismometer having a natural frequency response of 2 Hz was installed at the bank of the river at the '*Rua do Matto'* locality (Figure 1). The continuous data for the seasonal impact evaluation was divided into two acquisition campaigns (1) dry from Julian day 101 to 105 of 2017 and (2) rainy period from Julian day 344 to 350 of 2017. The records were performed in a continuous mode and at a sampling rate of 250 samples per second with a DAS-130 RefTEK data logger. Raw ambient noise record for the rainy days is presented in Figure 4.

The ambient noise wavefields of dry and rainy days were compared by applying spectral analysis of the ambient noise recorded two times, including power spectral density estimation, time-frequency analysis by spectrogram, and possible quantification effects on the site response by HVSR. After spectral analysis, the displacement RMS of ambient noise of two-time series was also calculated using a widely adopted approach (Lecocq et al. 2020). Details of this processing are provided below.

a) The fast Fourier transform (FFT) of each component is applied to check the response of fluvial mechanisms under the same geological conditions on the same station. This way, the signal's decomposition into a discrete spectrum is achieved. The waveform of dry and flooding conditions is selected, consisting of ground motion records of N-S, E-W and Z components. The steps include (i) subdivision of data into smaller windows of time length 50-60 s each with 10% overlap, (ii) each window is 5% cosine tapered and transformed into Fourier domain, and (iii) each spectrum smoothed

Preprints (www.preprints.org) | NOT PEER-REVIEWED | Posted: 16 November 2022 doi:10.20944/preprints202209.0447.v2

prior to the calculation of spectrum for a bandwidth coefficient 40, as the raw signal contained unusual spikes (Singh et al. 2019; Pandey et al. 2020).

b) The amplitude spectrum is obtained by applying a further transform to the FFT. Power is obtained as a square of the amplitude spectrum. PSDs are gathered by binning periods and powers. These power-period bins are normalized to obtain the probabilistic power spectral density (PPSD). The PSD and its aggregation provide ambient noise energy (power) variations, so the signal strength and distribution are a function of frequency (Díaz et al. 2014; Pandey et al. 2020). For the validation of spectral analysis, PSD is plotted as functions of rainfall, wind speed, and pressure from the nearby meteorological station. These data are useful in correlating the variation of amplitudes in seismic noise with the sudden changes brought by rainfall, wind speed and pressure. These meteorological data are divided into ranges, and the changes in PSD are observed accordingly.

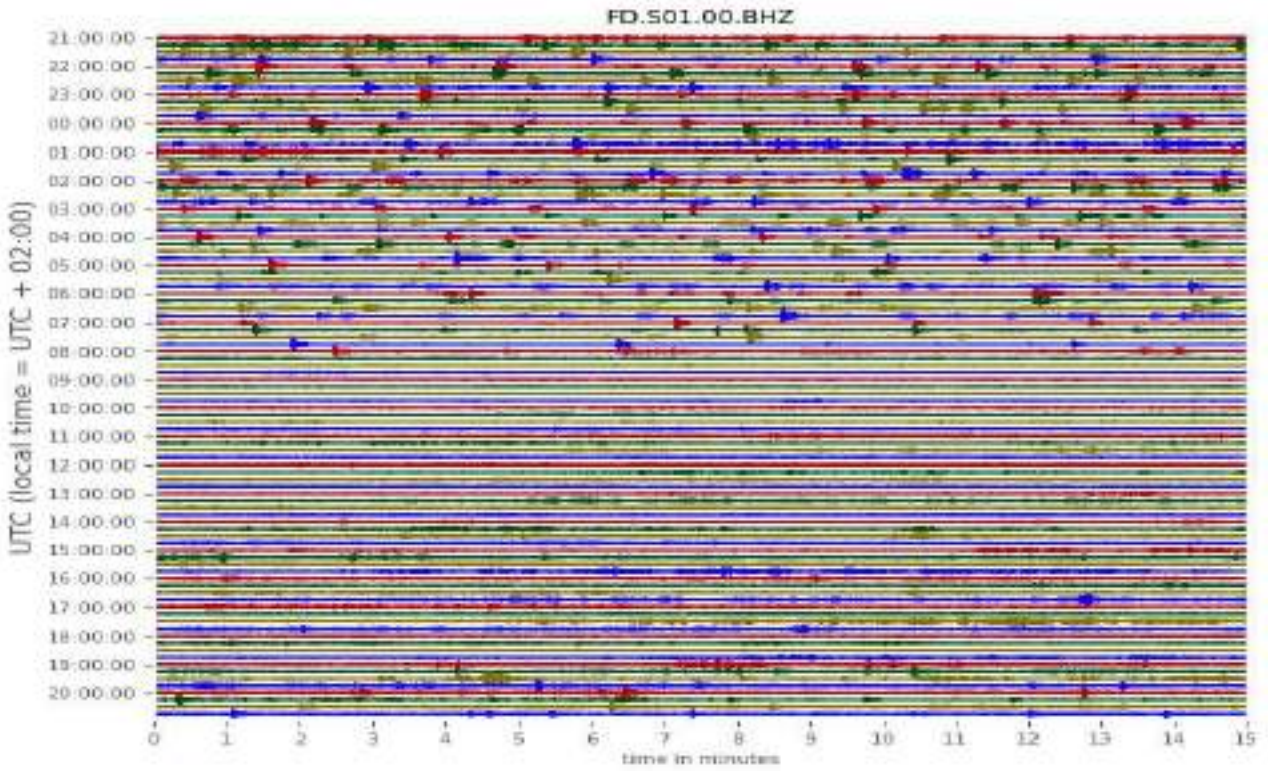

Figure 4. Seismograms recorded during rainy days. Periods of rainfall and river flow can be clearly seen in the plot.

c) As the seismic energy of a signal is proportional to the square of its amplitude; therefore, the root means square (RMS) analysis of a continuous record provides another way of highlighting the variations of seismic signals with time (Falanga et al. 2021). Displacement RMS of ambient noise records is calculated using a widely adopted methodology in "COVID Seismology" (Lecocq et al. 2020). It first calculates the PSD based on which the RMS displacement is derived. To access changes in RMS during hours of the day, clock plots are drawn at frequency bands of interest. In order to reduce the high energy ambient noise spikes, a time window of 0.1-7.0 hours is chosen. Similarly, to validate RMS results, change-point analysis (CPA), an approach for detecting the numerical value of change in two-time series, was adopted (Maciel et al. 2021). There are few case studies on the application of CPA in seismology as ambient noise interferometry (Sánchez-Pastor et al. 2018), landslide monitoring (Amorese et al. 2018), and seismic monitoring of COVID-19 (Maciel et al. 2021). An open-access python rupture library was used for the analysis (Truong et al. 2020). We choose Pruned Exact Linear Time (Pelt) algorithm, adopting a radial basis function model. It works on the assumption that the change point is unknown

Preprints (www.preprints.org) | NOT PEER-REVIEWED | Posted: 16 November 2022 doi:10.20944/preprints202209.0447.v2

and only a penalty parameter is required for the prediction. The choice of penalty is based on the iteration of a set of plenty values. We evaluated the precision and recall metrics for each segmentation for each value. The penalty value chosen was the one that optimized the precision-recall trade-off. This way, the change point is detected as a function of larger cost function intervals. In this study, we used the RBF cost function, a non-parametric approach based on a Gaussian kernel estimation. It can detect distribution changes rather than shifts in standard statistical measures, such as mean, mode, etc. A detailed explanation of the CPA approach and its application is explained by (Lykou et al. 2020; Maciel et al. 2021).

d) Time-frequency spectrograms are calculated using Obspy (a python library) inbuilt functions, which are expressed in units of energy as dB/(m^2/s^4) over different frequencies.

e) Changes in local site response can be an important contributor to soil erosion and landslide because detached soil blocks along the river bank have their natural period and are excited by the changes in Vs accordingly (Hussain et al. 2019a). Therefore, following (Goodling et al. 2018; Anthony et al. 2018), we applied the HVSR method (Nakamura 1989) to the three-component ambient noise records, which provide an ideal scenario for the estimation of site response due to changes in river flow. HVSR provides the response frequency of the loose sedimentary layer over the bedrock if there lies a considerable impedance contrast between them. Using this method, the natural period and the depth of the sedimentary layer are found using equation 1. The FFT of the vertical and horizontal ground motions is calculated after applying an energy normalization on each window following the diffuse approach for the HVSR methodology proposed by (Sánchez-Sesma et al. 2011). The spectra of both horizontal components are averaged following the vector summation described by (Albarello and Lunedei 2013) and divided by the spectral of the vertical component. In the end, results are smoothened by applying a smooth mean halfwidth 40, and results are plotted. More details about this process are provided elsewhere(Hussain et al. 2020a). Water infiltration and accumulation within unstable compartments may play a fundamental role in site stability. If the unstable compartment is susceptible to water retention, an increase in water content causes an increase in mass (M) and density (ρ). A decrease in both contact and bulk shear modulus (Gb) is simultaneously expected due to water seepage. A reduction in f1 and a negative dV/V are then expected. Lowering the water table and drying of the material generate the opposite effect (Colombero et al. 2021)

$$f_r = \frac{V_s}{4Z} \quad (1)$$

where Z is the depth, fr is the natural frequency, and Vs is the shear wave velocity.

2.2.2 Ground Penetrating Radar

The dielectric constant of the soil and the degree of its compaction (bulk density/penetration resistance) are somehow related, as documented in the literature (Wang et al. 2016). This relationship can be utilized in fluvial seismology for the stratification of soil based on the degree of compaction, as loose or unconsolidated soil susceptible to erosion and possible related hazards such as bank erosion. This can also change the river dynamics by increasing the amount of sediment loads and water viscosity, which impacts the seismic (both ANb and ESb).

In this regard, two GPR profiles of 180 m and 360 m long were taken along with the riverbank during dry days using a georadar device GPR GSSI SIR 3000 (Geophysical Services Systems, Nashua, NH, USA), with 400 MHz antenna, control unity, and rugged survey car. The authors used the GPR attributes (i.e., coherence, average amplitude and average energy) for the detailed stratigraphy of the river floodplain as well as marks the degree of compaction (weak spots) of different superficial material types and their susceptibility is discussed in terms of their erodibility.

Preprints (www.preprints.org) | NOT PEER-REVIEWED | Posted: 16 November 2022 doi:10.20944/preprints202209.0447.v2

We used Reflex-win software, version 9.0.5, to do GPR data processing which included: i) static correction for the time zero setting; ii) The "energy decay" module was used to compensate for the signal decay; iii) applying the "background removal" module to suppress or remove the coherent noise or stationary wave noise; iv) 1D type bandpass frequency filtering for removal of high and low-frequency random noise, cutting intervals were set subjectively according to the frequency spectrum of some traces; v) The "running average" module was applied to do data smoothing, the average traces was set as three. After the 5th step, the average amplitude, average energy, and coherence attributes were extracted using the C Language we coded. Finally, the attributes were displayed by the Reflex-win software. The average amplitude attribute is extracted from traditional GPR data by calculating the average of all positive values within a fixed time window, while negative amplitudes are discarded.

In the next stage, the coherence attributes that measure waveform similarity of neighboring traces are calculated to interpret the features of the river floodplain. There are numerous applications of coherence in GPR signal processing (Gao et al. 2020), after its first use for seismic signals by (Bahorich and Farmer 1995) and first applied to GPR data by (Young et al. 1997). This method achieves coherence using a classical mutual correlation algorithm with 0 and 1 values, and results can be applied to determine valid and invalid signal regions along the GPR profile. Details are provided by (Gao et al. 2020). In the end, the coherence image is color scaled as white high and black low values. The boundary of these two signal classes (valid and invalid) is interpreted as a lithological boundary or maximum penetrating depth limit. Valid signals are reflection or echo waves that can be attributed to stratigraphy, while invalid signals are the random noise generated by the radar system itself (Jol 2008).

3 Overview of the findings

3.1 Spectral analysis of seismic ambient noise recordings

PSDs

As described earlier, the spectral analysis includes PSDs, and spectrograms of two ambient noise time series recorded during dry and flooding days. Additionally, the PSDs were plotted as a function of wind speed and rainfall. The possible imprints of rainfall on the ambient noise may include the noise because of rainfall drop, river discharge, and properties of sediment loads and check on the urban activities in hours of rain. The details of the findings and discussion are documented below.

PSD, as a function of rainfall, wind speed and pressure, are plotted to delineate the effects of these meteorological factors on the power of noise at different frequencies. The wind speed in the considered time is divided into two ranges (Figure 5a). Discharge effects on PSD are clearly seen on horizontal and vertical components. The PSD at low frequency is found unaffected by the wind speed at all considered ranges. However, both time series are directly related at high frequency i.e. PSD is higher at high wind speed and vice versa. Similarly, the rainfall amount during rainy days is divided into two ranges: 0.00-2.47 and 2.47-4.93 mm. Then PSD is plotted as a function of these ranges. It is interesting to note that, similar to wind speed, the high rainfall affects the ambient noise PSD at higher frequencies (Figure 6b). The spectral peaks remained the same on all PSD plots.

On PSD plots, the identification of river flow and its sediment loads are discussed in terms of variations in power and peak shifting (Wenner et al. 2019). These variations are assumed to be excited by the discharge and other related phenomena on rainy days. The changes can also be seen on low-frequency power; this may be associated with the flow considerations of flood-induced changes in the riverbanks' roughness (Roth et al. 2016). The peaks at higher frequencies in rainy days (Figure 5d) are associated with variations in the ambient noise wavefields brought by river-related

phenomena and effects of other resonant structures such as landslides, local stratigraphy and the other riverine resonant structures related to the deposition of sediments in the floodplain. It may be associated with the same propagating source in the river floods, as explained by (Piantini et al. 2021). Another possible explanation for these peaks could be the sudden destabilization of debris deposits on slopes and cliffs, which usually result from mass wasting (Chmiel et al. 2022).

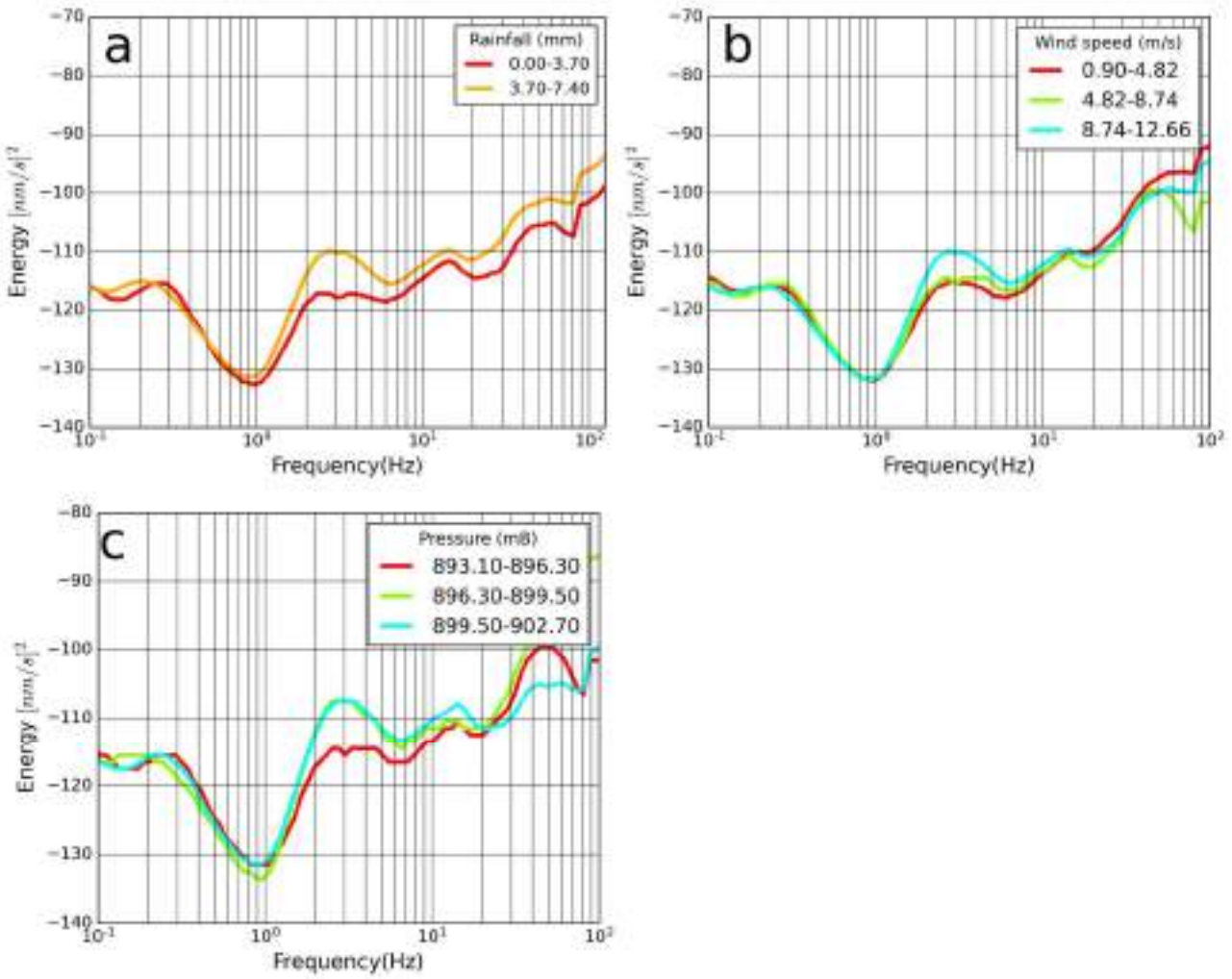

Figure 5. PSD as a function of a) rainfall, b) wind speed, and c) pressure during rainy days at the Z-component of the rainy record.

Figure 5a shows that with the increase in rainfall amount, there is an increase in PSD at a broad frequency range. Wind speed has different effects on the noise energy in rainy conditions; as the wind speed rises, there is an increase in PSD at a high frequency (2–20 Hz), while the lower frequency remains unaffected (Figure 5b). At a frequency range from 20-100 Hz, this trend does not hold. A similar trend of rising wind speed-increasing PSD during rainy days can be seen in Figure 5b. The fluvial effects on different frequency bands are documented in previous studies as 15–45 Hz (Schmandt et al. 2013), 5–15 Hz (Chao et al. 2015), 10-30 Hz (Schimmel et al. 2018) and ~0.1–45 Hz by (Anthony et al. 2018). The debris flow signature at the 5-10 Hz frequency band was observed by (Lai et al. 2018).

Spectograms

 doi:10.20944/preprints202209.0447.v2

The short-period spectrograms are shown in Figure 6, which present four different frequency bands (continuous or discontinuous). The spectrograms of two times show low-frequency ambient noise, query blats, and high-frequency noise. The significant energies induced by the river flow below 10 Hz and between 10-60 Hz can also be seen in Figure 6. These are combined effects of rainfall, river flow, and sediment loads. The sedimentary signals can be seen in Figure 6 as high-frequency events. The frequency band below 2 Hz is the instrumental noise; therefore, it was not possible to see the effects of high wind speed at low frequency. The other high-energy noise band is 2-12 Hz which can be seen on both dry and rainy plots to mark the effects of cultural noise. It also shows a diurnal pattern, another attribute that confirms the presence of cultural noise. The higher frequency band, 20–50 Hz, is only prominent on rainy days, showing river-related processes.

Interestingly, the quarry blast from the nearby mining can be observed on both spectrograms. The spectrograms of dry days don't show any energies at the frequency band where river influence emerged during rainy days. The quiet periods associated with lunch break hours (12-14) at frequencies below 10 Hz can be seen as small windows during rainy days. In literature, the river flow has been observed over different frequency ranges, which depend on the conditions of the river (discharge amount, roughness of river bed) and its site (soil conditions). (Polvi et al. 2020) reported stream flow and sediment transportation the frequency ranges as ~1–20 Hz and ~15–100 Hz, respectively. Very high energy peaks of the rainy spectrogram may be associated with the signatures of rain plus wind, as reported by (Rindraharisaona et al. 2022).

Preprints (www.preprints.org) | NOT PEER-REVIEWED | Posted: 16 November 2022 doi:10.20944/preprints202209.0447.v2

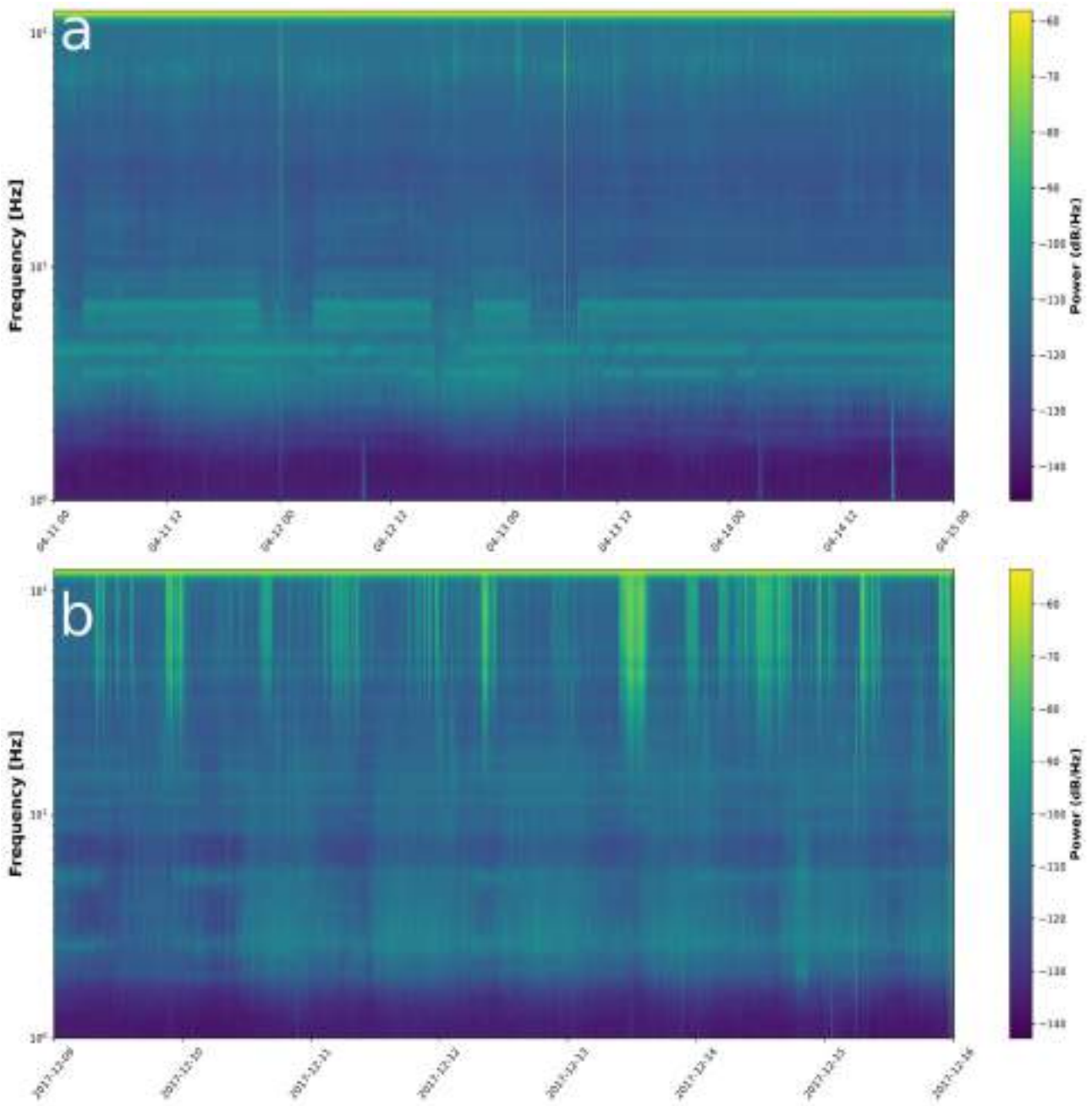

Figure 6. Spectrograms a) dry and b) rainy.

RMS amplitude and energy release

The ambient noise velocity RMS shows variations with hours of the day at different frequencies (2-5 Hz, 30-40 Hz, 50-70 Hz and 70-125 Hz) (Figure 7). It shows stability in ambient noise levels at low frequencies for both the considered time scales. At frequency bands of 30-40 Hz and 50-70 Hz, a decrease in RMS values is observed on rainy days, possibly associated with a break in anthropogenic activities because of rainfall. An increase in RMS is found at frequency ranges of 2-5 Hz and 70-125Hz. These are the possible frequency ranges where the combined effects (solid-fluid mixture) can be seen. However, the diurnal patterns can be seen in both series at higher frequencies. This may be associated with human activities and the influence of floods in the river at different frequencies; however, as the river is

Preprints (www.preprints.org) | NOT PEER-REVIEWED | Posted: 16 November 2022 doi:10.20944/preprints202209.0447.v2

small enough, the influences are less prominent on RMS plots. Under these limited data availability conditions, it is difficult to separate the urban noise and noise generated by the river.

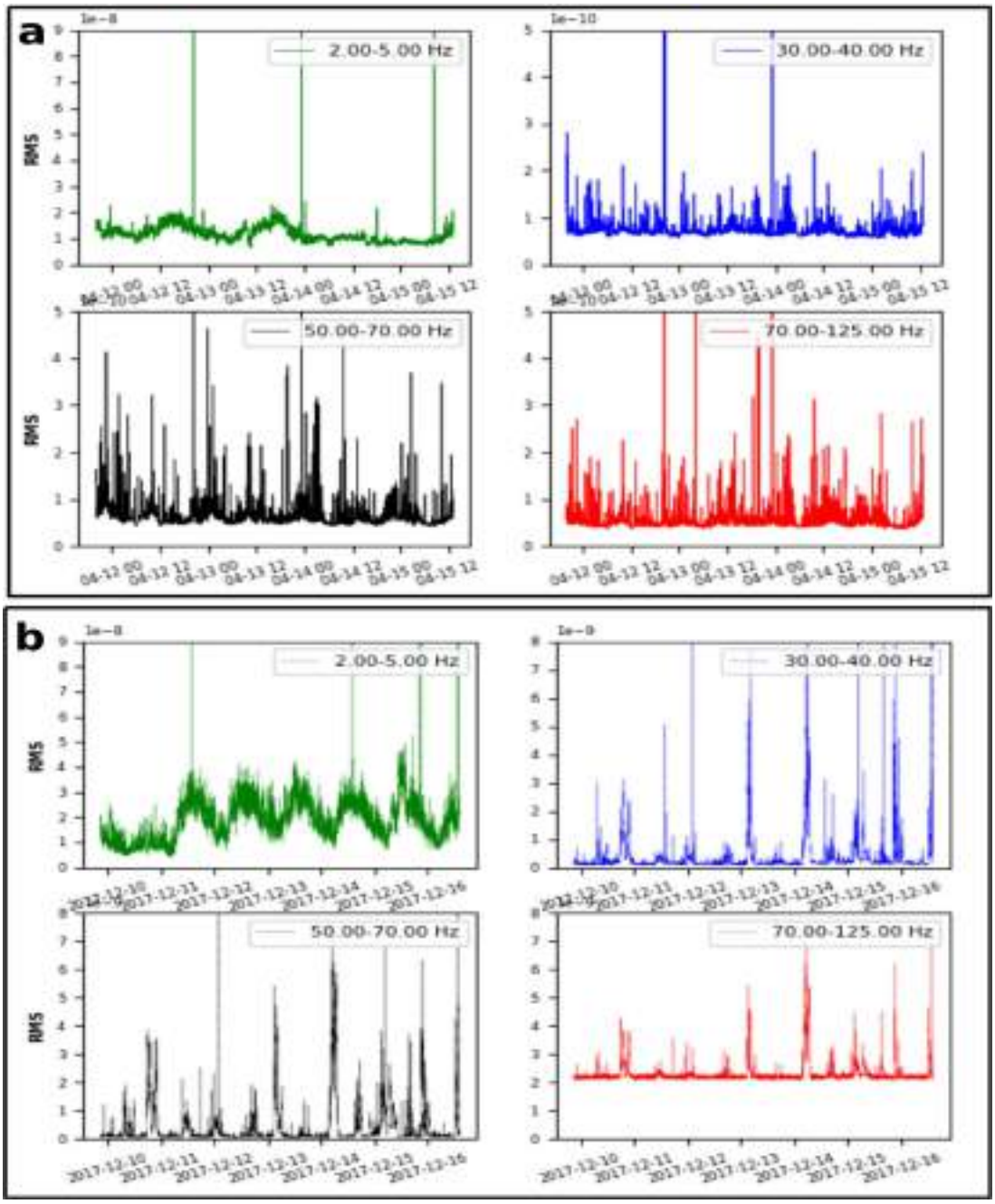

Figure 7. Displacement RMS amplitude of the ambient noise time-series average noise at 6h-16h hours of the day filtered at chosen frequency ranges (2-5 Hz, 30-40 Hz, 50-70 Hz and 70-125 Hz), a) dry and b) rainy days.

Change Point Analysis

Each changing point represents a change in the underlying distribution of the series. The correspondence between wind speed and seismic energy change points demonstrates that both phenomena are correlated somehow. In other words, there is an increase in ambient noise RMS with the wind speed and vice versa (Figure 8). The wind can have possible indirect effects by coupling with structures and vegetation on the ground as we buried the seismometer, so the direct impact of winds is negligible. These effects have also been highlighted in the literature. (Seivane et al. 2022), observed

Preprints (www.preprints.org) | NOT PEER-REVIEWED | Posted: 16 November 2022 doi:10.20944/preprints202209.0447.v2

the effects of wind speed on seismic records (HV curves), the ambient noise records and wind speed found well correlated in the Campo de Dalías basin in Spain. There is another study where the effects of windmills have been observed on ambient noise records (Saccorotti et al. 2011).

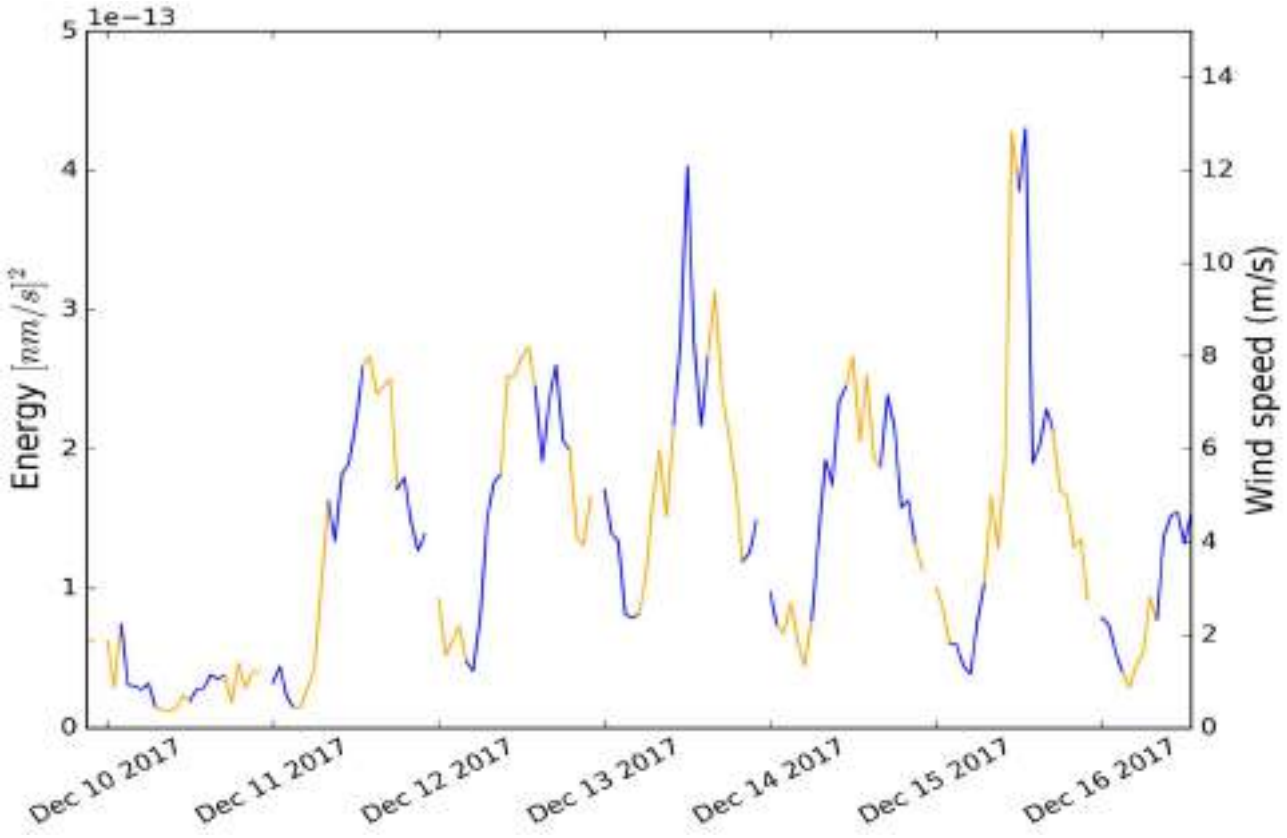

Figure 8. The change of color at each time series represents a change point automatically detected by a CPA algorithm.

HVSR curves

The HVSR curves obtained for the studied periods (rainy and dry) are characterized both by a condition of multiple-peak (Figure 9a). The fundamental HVSR peak identified by (Hussain et al. 2019a) as the contact between the low-velocity soft deposits and the Paranoá bedrock is also observed during both periods at 1.3 Hz. Moreover, the secondary peaks attributed to the landslide surface observed by (Hussain et al. 2019a) are also identified during the dry season at 4 and 9 Hz showing both significant HVSR amplitudes (SESAME 2004). This behavior agrees with the findings by (Hussain et al. 2019a) for these secondary peaks, which tend to decrease in amplitude or totally disappear during rainy days. On the other hand, the double peak found above 20 Hz is present in both periods (Figure 9b). It seems to slightly shift the frequency positions on average of each peak and vary the HVSR amplitude when comparing both periods.

In order to compare the differences between the two periods studied, Figure 10 gathers the HVSR variations, in terms of frequency and amplitude, for the two persistent peaks observed: the fundamental one at 1.3 Hz and the higher double peak between 20 and 100 Hz. During the rainy period, a wider variation is experienced in the two frequency bands, revealing a period of higher instability in the HVSR curves. Regarding frequency position, the three peaks shift on average to a lower position during the rainy period (Figure 10). Such observation agrees with the findings by (Stevens and James 2022), which revealed that the drops in f_0 coincide with sharp increases in water content. This is coherent with the overall soil moisture increase expected during heavy rainfalls in the study area. The daily variations show how a semi-diurnal

Preprints (www.preprints.org) | NOT PEER-REVIEWED | Posted: 16 November 2022 doi:10.20944/preprints202209.0447.v2

modulation on the HVSR amplitude exists for the highest secondary peaks, at 40 and 60 Hz, that is kept in both periods (Figure 11).

On the contrary, the amplitude variations of the fundamental peak have a daily modulation which loses clarity during the rainy period (Figure 11). While this daily modulation can be related to the well-known pattern of the cultural noise, the semi-diurnal behavior observed in the amplitude modulations of the highest peaks could show a tidal modulation likely induced by the river flow. This would support the hypothesis of the river origin behind these two peaks.

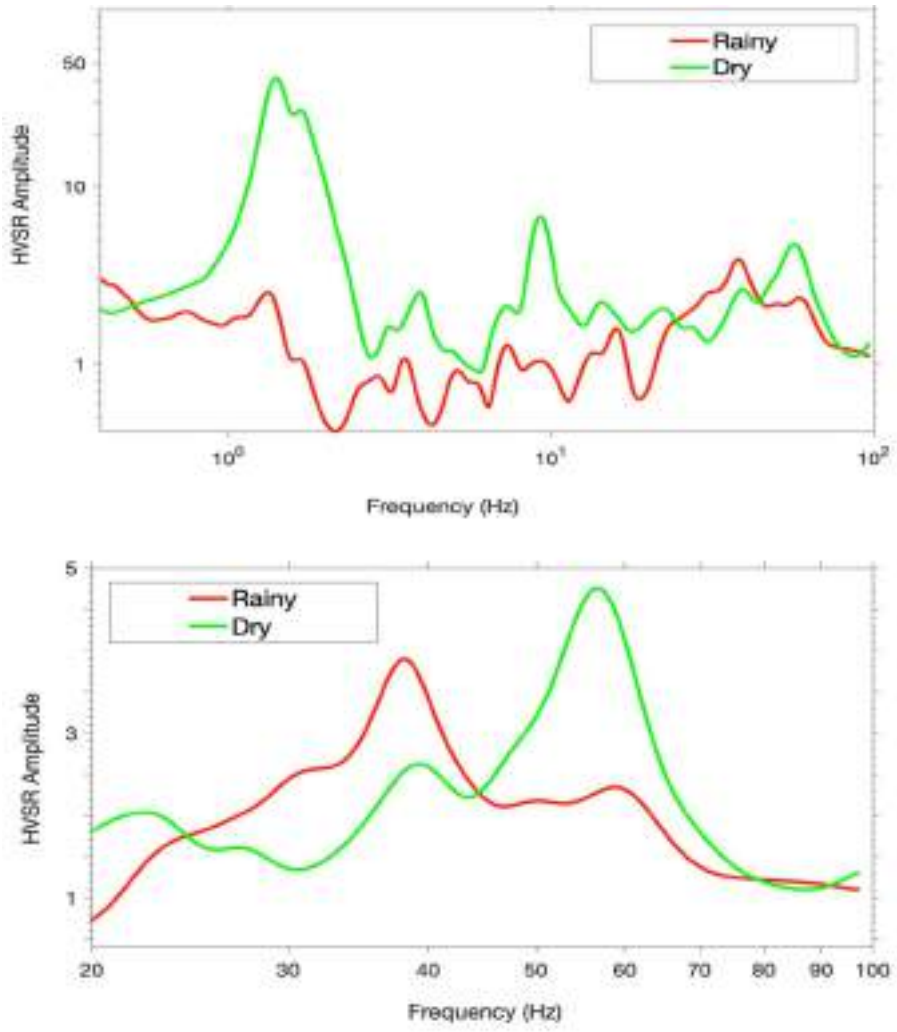

Figure 9 a) Averaged HVSR curves of dry (green curve) and rainy days (red curve). b) Zoom to the higher HVSR peaks found between 20 and 100 Hz.

Furthermore, when observing the frequency changes on a daily basis during the two periods (Figure 11), there is no evidence of daily modulations on any of the three HVSR peaks investigated. Comparison with atmospheric data does not show any evidence of a correlation between the non-periodic HVSR frequency fluctuations observed (Figure 11) and the windspeed and atmospheric pressure series for the two periods studied. We assume that they might have been excited by the river discharge and other related fluvial source mechanisms that can be delineated by detailed seismic studies together with UAV monitoring of the river. According to (Walsh et al. 2020), the frequency signature is a function of turbulence, velocity, viscosity, and density, collectively called a solid-fluid mixture. This relationship has also been

Preprints (www.preprints.org) | NOT PEER-REVIEWED | Posted: 16 November 2022 doi:10.20944/preprints202209.0447.v2

documented elsewhere (Coviello et al. 2019). If the flow velocity increases, the signal will emerge as low frequency while the viscosity damps the high-frequency signatures (Huang et al. 2004). The other factors that affect the frequency spectra by impacting the ground vibrations are the properties of the river bed (geometry, composition, and wetted perimeter) (Kean et al. 2015). There is an increase in the frequency of the seismic signal because of the smoothness and softness of bedrock compared to gravelly or fine sediment composed and dense bedrock, as observed by (Huang et al. 2007). Natural period as a function of changes in Vs can be a possible indicator of loose sediments subjected to detachment in response to EP of the river. The gravel bars in the river floodplain have their natural period and are a source of possible resonance peaks at the HVSR curve. This way, the river bank's compaction and material type can be linked with sediment quantification through natural frequency estimation. These similar features have been delineated based on subsurface stratification achieved by georadar; hence the results are comparable.

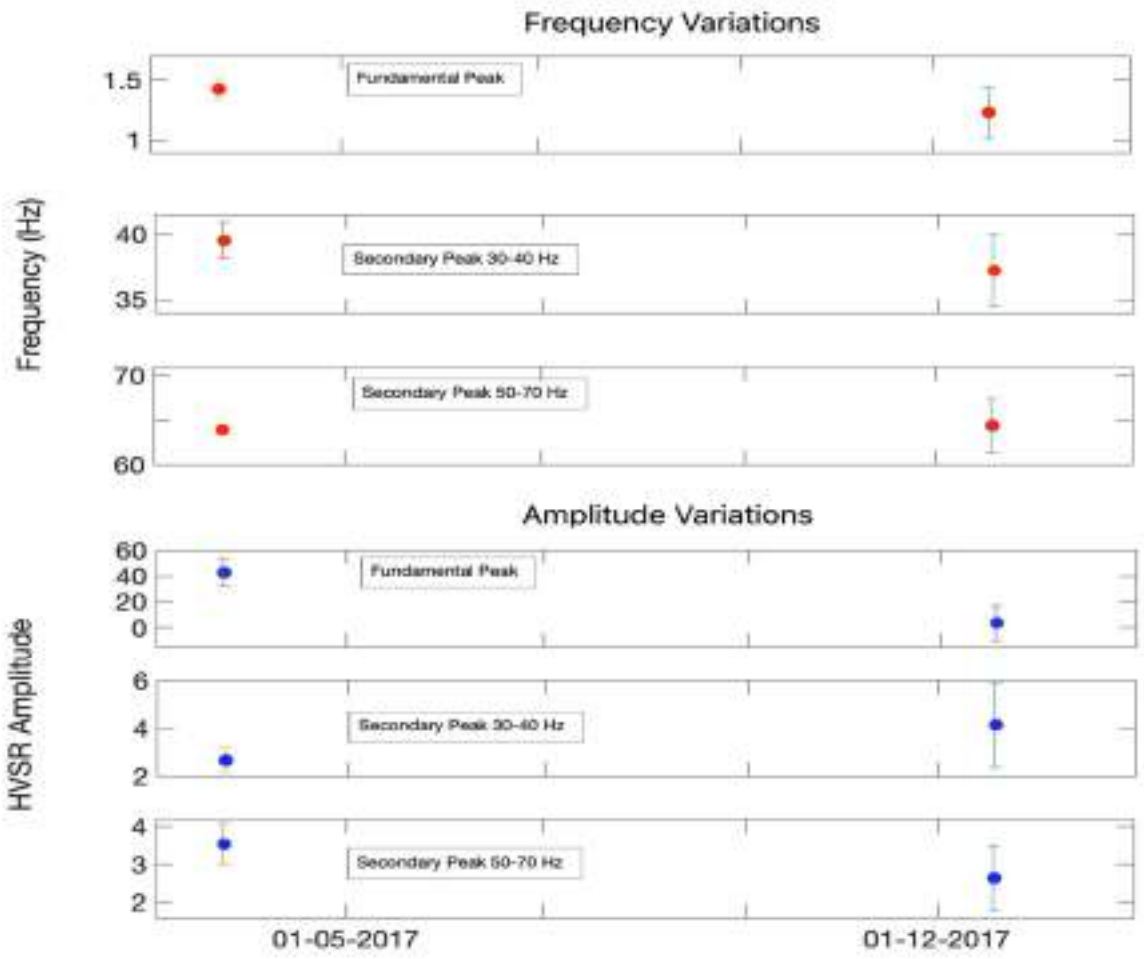

Figure 10. Averaged HVSR variations for the dry (April 2017) and rainy periods (December 2017) measured for the fundamental and secondary peaks observed. Error bars show the standard deviation.

Figure 11. HVSR amplitude variations sampled hourly for the a) fundamental and higher HVSR peaks at b) 40 Hz and c) 60 Hz for dry (April 2017) and rainy periods (December 2017).

Preprints (www.preprints.org) | NOT PEER-REVIEWED | Posted: 16 November 2022 doi:10.20944/preprints202209.0447.v2

Figure 12. HVSR frequency variations sampled hourly for the a) fundamental and higher HVSR peaks at b) 40 Hz and c) 60 Hz for dry (April 2017) and rainy periods (December 2017).

3.2 Site characterization by GPR

The GPR coherence attribute provides additional evidence on the subsurface characterization of the stream bed in the floodplain. Boulders, pebbles, and compacted soil have higher coherence values and more reflection interfaces, whereas unconsolidated or erodible soil shows lower coherence values and lower reflection interfaces. These material interferences are also delineated using coherence attributes where a clear boundary between the valid and invalid signals is found, which is associated with the bedrock interface. We used the "manual pick" mode of ReflexW software to plot the boundary according to the information reflected by the coherence attributes (see Figure 13). GPR images are naturally divided into valid and invalid signal regions, and the green line is also shown in other GPR images (Figures 13, 14 & 15). In the valid region of the GPR data profile, the reflection wave signals are dominated, while the invalid region, doesn't show reflection and can't be used to interpret geological units. There are two possible explanations for marking the depth boundary: electrical conductivity, the signal transmitted by GPR decayed to zero on reaching the depth marked by the green line in Figure 13. Another reason could be the presence of a compacted bedrock interface without a reflector (no reflection wave goes back), and GPR can only record random noise signals.

Figure 13. GPR coherence attribute a) profile 046 and b) profile 002. The green line is interpreted as the boundary between valid and invalid signals.

Contrasted with the traditional GPR image, where the boundary is considered the termination position or bottom of a dense, strong amplitude region (Al-fares et al. 2002), the coherence attribute can reduce the ambiguity and subjectivity of the boundary interpretation. The black dashed line in Figure 14 marks the different parts of the probable boundary interpreted by the traditional method, with the boundary (green line) interpreted using the coherence attribute. The traditional interpretation method can probably ignore the weak amplitude signals that contain effective reflection signals, such as the area between the black dashed line and the solid green line in Figure 14. The coherence attribute wipes off the amplitude information of signals and only reflects the signal waveforms, which reduces the ambiguities in the boundary interpretation.

We acquired the GPR data in the dry season, so the soil water content and conductivity are lower compared to the rainy season. In this way, the deeper penetration of GPR signals in the soil can be achieved as well as the invalid signal region corresponds to the highly compacted bedrock leading to a reduction in the emergence of the reflection interface. In the valid region, a low coherence value indicates the change in subsurface media or structure, such as the presence of rock fragments, pebbles, soil voids, small faults or other related discontinuities. The region corresponding to the high coherence value (white color) presents a higher degree of compaction relative to the corresponding low coherence value (black color) parts in the valid region. Therefore, we consider this position reflected by the black low coherence value in the valid region as the susceptible points to erosion. For instance, soil voids or discontinuity can provide permeable paths where rainwater can infiltrate into the subsurface and may cause instability by building pore water pressure (Hussain et al. 2020b).

Figure 14. Traditional GPR images a) profile 002and b) profile 046. The solid green and dashed black lines are interpreted by the traditional method and coherence attribute, respectively.

Preprints (www.preprints.org) | NOT PEER-REVIEWED | Posted: 16 November 2022 doi:10.20944/preprints202209.0447.v2

The average energy attribute can be used to delineate the presence and geometry of buried pebbles or boulders to the fact that the interface of rock and soil can reflect high energy waves with significant differences in electrical properties among them. Therefore, the places of high energy value may correspond to the positions of subsurface boulders. Information about their sizes can be inferred from the dimensions of the purple color regions on the energy attribute image (Figure 15).

Figure 15. GPR average energy attribute a) profile 002 and b) profile 046. The green line is the boundary of the valid and invalid signal regions. The purple color is high in average energy value, while white and gray are lower values. The blue circles marked out some possible boulders underground.

The traditional GPR images in Figure 15 contain purple and blue colors to display the strong positive and negative signals to observe the stratigraphy featured. Figure 16 clearly reflects that the subsurface layers generally are the distribution characteristics of approximately horizontal deposition. Some tilted deposit layers are also evident in the images, especially in Figure 16a. Only the valid signal region can be applied for the stratigraphy interpretation in the average amplitude attribute (Figure 16). The average amplitude attribute can be more convenient and visual for layer depth interpretation.

Figure 16. GPR amplitude attribute a) profile 002 and b) profile 046. The green line is the boundary of the valid and invalid signal regions. Purple is high value, and white and gray are low value.

ANb signatures of the streams on flooding days, along with erosion-prone conditions (colluvium and boulders) of stream beds inferred from georadar attribute analysis, can help in the estimation of stream EPs that promote reverie landslides and soil losses in the fluvial valleys. The higher EP, together with the presence of mechanically weak lithologies, lead to geological hazards (landslide and soil losses). As ambient noise level is sensitive to the changes in flood and sediment loads of the river, this can help in the quantification of force exerted by the flood on critical infrastructures (e.g., bridges, flood-resistant structures and many others) and hence assist in the estimation of their resilience and can be used as a precursor for the possible damage evaluations that river may cause during floods. The future climate change scenarios can also be predicted in this way. Such understanding may help minimize the damages and soil losses, as an important step in retaining agriculture in the Cerrado region of Brazil.

4 Conclusions

This study presents seismic monitoring and analysis of the river sediment carrying capacity in the *Ribeirão Contagem* watershed (of the Federal district of Brazil) on rainy and dry days. The GPR-based local site conditions and their possible impacts on the erosion and sediment load of the river are discussed. The ambient noise wavefields during dry and rainy days are measured and compared. This comparison was conducted by applying spectral analysis of the ambient noise (recorded two times), including power spectral density estimation, time-frequency analysis by spectrogram, and possible quantification effects on the site response by HVSR curves. Additionally, the GPR attributes are studied for the delineation of erosion-prone sites as a major source of geohazard and sediment quality in the river of the fluvial valley. Based on the findings, we may conclude the followings:

i) Ambient noise-based analysis showed variations in the PSD on rainy and dry days. An apparent change in the spectrogram of rainy days was identified, attributed to rainfall and river dynamics. PSD vs meteorological agent (rainfall and wind speed) plots showed changes in PSD during rainy days.

ii) Based on the spectrograms of the rainy days (the signals and their characteristics), it can be suggested that one of the signals dominantly results from bedload transport and the other two from fluid transport processes.

iii) The HVSR plots showed an increase in amplitude starting from 10 Hz. During rainy days, a shift to low frequency and a semi-diurnal modulation on the higher peaks are observed.

iv) Ambient noise RMS plots evidently showed variations in displacement during daytime. The correspondence between wind speed and seismic energy CPA demonstrates that both phenomena are somehow correlated.

Based on the variations and emergence of new typologies on different frequency bands, we assume that they might have been excited by the river discharge and other related fluvial source mechanisms that can be delineated by detailed seismic studies together with UAV monitoring of the river.

v) GPR average amplitude attribute profiles showed the detailed riverbank and floodplain stratigraphy, including depth and topography of bedrock. The presence of boulders of various sizes is identified by the GPR energy attributes. In contrast, the coherence attribute helped in evaluating the degree of compaction and a possible indication of the region as susceptible to erosion (weak spots). The invalid region corresponds to a high degree of compaction area in the subsurface because a little reflection surface can reflect waves, and GPR can only record random noise.

From our seismic noise analysis performed in Brasilia, it is evident that a seismometer can be an efficient tool to characterize the seismic signature of the river (at high frequency) to quantify better the river activity, particularly the bed load transport during floods. In addition, the presence of fluvial lithologies (boulder and colluvial sediments) and the slope steepness, characteristics of fluvial valleys such as Ribeirão Contagem, make it vulnerable to natural hazards (landslides and erosion). This is closely related to rainfall and lithologies, motivating a better understanding of the phenomena to help decipher such destructive environmental processes. This study is a preliminary step in integrating stream bed conditions and flood levels using remote, cheaper and non-invasive geophysical applications. The present study will allow further field investigation to improve the estimation of sediment transport during flood events by deploying seismometers along rivers in fluvial valleys.

Acknowledgment:

Statements and Declarations:

There is no competing interest among the authors.

Data Availability: Data are available by emailing the corresponding author.

References

Al-fares W, Bakalowicz M, Guérin R, Dukhan M (2002) Analysis of the karst aquifer structure of the Lamalou area (Hérault, France) with ground penetrating radar. J Appl Geophys 51:97–106. https://doi.org/10.1016/S0926-9851(02)00215-X

Albarello D, Lunedei E (2013) Combining horizontal ambient vibration components for H/V spectral ratio estimates. Geophys J Int 194:. https://doi.org/10.1093/gji/ggt130

Amorese D, Grasso J-R, Garambois S, Font M (2018) Change-point analysis of geophysical time-series: application to landslide displacement rate (Séchilienne rock avalanche, France). Geophys J Int 213:1231–1243. https://doi.org/10.1093/gji/ggy060

Anthony RE, Aster RC, Ryan S, et al (2018) Measuring Mountain River Discharge Using Seismographs Emplaced Within the Hyporheic Zone. J Geophys Res Earth Surf 123:210–228. https://doi.org/10.1002/2017JF004295

Araujo HA, Cooper AB, Hassan MA, Venditti J (2012) Estimating suspended sediment concentrations in areas with limited hydrological data using a mixed-effects model. Hydrol Process 26:3678–3688. https://doi.org/10.1002/hyp.8462

Arcone SA, Lawson DE, Delaney AJ, et al (1998) Ground-penetrating radar reflection profiling of groundwater and bedrock in an area of discontinuous permafrost. Geophysics 63:1573–1584. https://doi.org/10.1190/1.1444454

Bahorich M, Farmer S (1995) The coherence cube. Lead Edge

Bakker M, Gimbert F, Geay T, et al (2020) Field Application and Validation of a Seismic Bedload Transport Model. J Geophys Res Earth Surf 125:e2019JF005416. https://doi.org/10.1029/2019JF005416

Barrière J, Oth A, Hostache R, Krein A (2015) Bed load transport monitoring using seismic observations in a low-gradient rural gravel bed stream. Geophys Res Lett 42:2294–2301. https://doi.org/10.1002/2015GL063630

Bartholomaus TC, Amundson JM, Walter JI, et al (2015) Subglacial discharge at tidewater glaciers revealed by seismic tremor. Geophys Res Lett 42:6391–6398. https://doi.org/10.1002/2015GL064590

Braga LM, Caldeira D, da Silva Nunes JG, et al (2018) Geomorphological description and erosive-depositional dynamics of hillslopes on Ribeirão Contagen Fluvial Valley-DF, Brazil. Anu do Inst Geociencias 41:51–65. https://doi.org/10.11137/2018_2_51_65

Burtin A, Bollinger L, Vergne J, et al (2008) Spectral analysis of seismic noise induced by rivers: A new tool to monitor spatiotemporal changes in stream hydrodynamics. J Geophys Res 113:B05301. https://doi.org/10.1029/2007JB005034

Burtin A, Cattin R, Bollinger L, et al (2011) Towards the hydrologic and bed load monitoring from high-frequency seismic noise in a braided river: The “torrent de St Pierre”, French Alps. J Hydrol 408:43–53. https://doi.org/10.1016/j.jhydrol.2011.07.014

Chalikakis K, Plagnes V, Guerin R, et al (2011) Contribution of geophysical methods to karst-system exploration: An overview. Hydrogeol J 19:1169–1180. https://doi.org/10.1007/s10040-011-0746-x

Chao WA, Wu YM, Zhao L, et al (2015) Seismologically determined bedload flux during the typhoon season. Sci Rep 5:1–8. https://doi.org/10.1038/srep08261

Chmiel M, Godano M, Piantini M, et al (2022) Brief communication: Seismological analysis of flood dynamics and hydrologically triggered earthquake swarms associated with Storm Alex. Nat Hazards Earth Syst Sci 22:1541–1558. https://doi.org/10.5194/nhess-22-1541-2022

Colombero C, Jongmans D, Fiolleau S, et al (2021) Seismic Noise Parameters as Indicators of Reversible Modifications in Slope Stability: A Review. Surv. Geophys. 42

Coviello V, Arattano M, Comiti F, et al (2019) Seismic Characterization of Debris Flows: Insights into Energy Radiation and Implications for Warning. J Geophys Res Earth Surf 124:1440–1463. https://doi.org/10.1029/2018JF004683

Cunha ER da, Santos CAG, Silva RM da, et al (2022) Assessment of current and future land use/cover changes in soil erosion in the Rio da Prata basin (Brazil). Sci Total Environ 818:151811. https://doi.org/10.1016/j.scitotenv.2021.151811

da Silva Nunes JG, Uagoda R, Caldeira D, et al (2019) Application of GPR for the differentiation of alluvial and colluvial materials, based on direct observation in Contagem Valley – Distrito Federal (Brasil). Rev Bras Geomorfol 20:217–238. https://doi.org/10.20502/rbg.v20i2.1382

David MB, Drinkwater LE, McIsaac GF (2010) Sources of Nitrate Yields in the Mississippi River Basin. J Environ Qual 39:1657–1667. https://doi.org/10.2134/jeq2010.0115

Díaz J, Ruíz M, Crescentini L, et al (2014) Seismic monitoring of an Alpine mountain river. J Geophys Res Solid Earth 119:3276–3289. https://doi.org/10.1002/2014JB010955

Fabregat I, Gutiérrez F, Roqué C, et al (2019) Subsidence mechanisms and sedimentation in alluvial sinkholes inferred from trenching and ground penetrating radar (GPR). Implications for subsidence and flooding hazard assessment. Quat Int 525:1–15. https://doi.org/10.1016/j.quaint.2019.09.008

Falanga M, Cusano P, De Lauro E, Petrosino S (2021) Picking up the hydrothermal whisper at Ischia Island in the Covid-19 lockdown quiet. Sci Rep 11:. https://doi.org/10.1038/s41598-021-88266-9

Ferreira, R., Uagoda R (2015) Morphometric study of controls to erosional features and identification of areas susceptible to mass movement hazards in the contagem watershed, Distrito Federal. Rev Espaço e Geogr 18:187:216

Fonseca MRS, Uagoda R, Chaves HML (2022) Rates, factors, and tolerances of water erosion in the Cerrado biome (Brazil): A meta-analysis of runoff plot data. Earth Surf Process Landforms 47:582–595. https://doi.org/10.1002/esp.5273

Gabet EJ, Burbank DW, Pratt-Sitaula B, et al (2008) Modern erosion rates in the High Himalayas of Nepal. Earth Planet Sci Lett 267:482–494. https://doi.org/10.1016/j.epsl.2007.11.059

Gao Q, Wang S, Peng T, et al (2020) Evaluating the structure characteristics of epikarst at a typical peak cluster depression in Guizhou plateau area using ground penetrating radar attributes. Geomorphology 364:. https://doi.org/10.1016/j.geomorph.2019.107015

Gimbert F, Tsai V, Geophysical ML-J of, 2014 undefined (2014) A physical model for seismic noise generation by turbulent flow in rivers. Wiley Online Libr 119:2209–2238. https://doi.org/10.1002/2014JF003201

Giménez R, Casalí J, Grande I, et al Factors controlling sediment export in a small agricultural watershed in Navarre (Spain). Elsevier

Gomes L, Simões SJC, Dalla Nora EL, et al (2019) Agricultural expansion in the Brazilian Cerrado: Increased soil and nutrient losses and decreased agricultural productivity. Land 8:. https://doi.org/10.3390/land8010012

Goodling PJ, Lekic V, Prestegaard K (2018) Seismic signature of turbulence during the 2017 Oroville Dam spillway erosion crisis. Earth Surf Dyn 6:351–367. https://doi.org/10.5194/esurf-6-351-2018

Graf WL, Wohl E, Sinha T, Sabo JL (2010) Sedimentation and sustainability of western American reservoirs. Water Resour Res 46:. https://doi.org/10.1029/2009WR008836

Hamza O, De Vargas T, Boff FE, et al (2020) Geohazard Assessment of Landslides in South Brazil: Case Study. Geotech Geol Eng 38:971–984. https://doi.org/10.1007/s10706-019-01054-1

Huang C-J, Shieh C-L, Yin H-Y (2004) Laboratory study of the underground sound generated by debris flows. J Geophys Res Earth Surf 109:. https://doi.org/10.1029/2003jf000048

Huang C-J, Yin H-Y, Chen C-Y, et al (2007) Ground vibrations produced by rock motions and debris flows. J Geophys Res 112:F02014. https://doi.org/10.1029/2005JF000437

Hussain Y, Cardenas-Soto M, Martino S, et al (2019a) Multiple geophysical techniques for investigation and monitoring of Sobradinho Landslide, Brazil. Sustain 11:. https://doi.org/10.3390/su11236672

Hussain Y, Cardenas-Soto M, Moreira C, et al (2020a) Variation in rayleigh wave ellipticity as a possible indicator of earthflow mobility: A case study of sobradinho landslide compared with pile load testing. Earth Sci Res J 24:141–151. https://doi.org/10.15446/esrj.v24n2.81974

Hussain Y, Cardenas-Soto M, Uagoda R, et al (2019b) Monitoring of Sobradinho landslide (Brasília, Brazil) and a prototype vertical slope by time-lapse interferometry. Brazilian J Geol 49:. https://doi.org/10.1590/2317-4889201920180085

Hussain Y, Hamza O, Cárdenas-Soto M, et al (2020b) Characterization of sobradinho landslide in fluvial valley using masw and ert methods. REM - Int Eng Journal 73:. https://doi.org/10.1590/0370-44672019730109

Hussain Y, Schlögel R, Innocenti A, et al (2022) Review on the Geophysical and UAV-Based Methods Applied to Landslides. Remote Sens 14:4564. https://doi.org/10.3390/rs14184564

Jol H (2008) Ground penetrating radar theory and applications

Kean JW, Coe JA, Coviello V, et al (2015) Estimating rates of debris flow entrainment from ground vibrations. Geophys Res Lett 42:6365–6372. https://doi.org/10.1002/2015GL064811

Lagarde S, Dietze M, Gimbert F, et al (2021) Grain-Size Distribution and Propagation Effects on Seismic Signals Generated by Bedload Transport. Water Resour Res 57:. https://doi.org/10.1029/2020WR028700

Lai VH, Tsai VC, Lamb MP, et al (2018) The Seismic Signature of Debris Flows: Flow Mechanics and Early Warning at Montecito, California. Geophys Res Lett 45:5528–5535. https://doi.org/10.1029/2018GL077683

Lawler DM (1993) The measurement of river bank erosion and lateral channel change: A review. Earth Surf Process Landforms 18:777–821. https://doi.org/10.1002/esp.3290180905

Lecocq T, Hicks SP, van Noten K, et al (2020) Global quieting of high-frequency seismic noise due to COVID-19 pandemic lockdown measures. Science (80-) 369:1338–1343. https://doi.org/10.1126/science.abd2438

Lykou R, Tsaklidis G, Papadimitriou E (2020) Change point analysis on the Corinth Gulf (Greece) seismicity. Phys A Stat Mech its Appl 541:. https://doi.org/10.1016/j.physa.2019.123630

Maciel STR, Rocha MP, Schimmel M (2021) Urban seismic monitoring in Brasilia, Brazil. PLoS One 16:. https://doi.org/10.1371/journal.pone.0253610

Marchetti E, Walter F, Barfucci G, et al (2019) Infrasound Array Analysis of Debris Flow Activity and Implication for Early Warning. J Geophys Res Earth Surf 124:567–587. https://doi.org/10.1029/2018JF004785

Nakamura Y (1989) Method for dynamic characteristics estimation of subsurface using microtremor on the ground surface. Q Rep RTRI (railw Tech Res Institute) 30:

Oeurng C, Sauvage S, Sánchez-Pérez JM (2010) Dynamics of suspended sediment transport and yield in a large agricultural catchment, southwest France. Earth Surf Process Landforms 35:1289–1301. https://doi.org/10.1002/esp.1971

P.C S, Sawazaki K (2021) River discharge prediction for ungauged mountainous river basins during heavy rain events based on seismic noise data. Prog Earth Planet Sci 8:. https://doi.org/10.1186/s40645-021-00448-1

Pandey AP, Singh AP, Bansal BK, et al (2020) Appraisal of seismic noise scenario at national seismological network of India in COVID-19 lockdown situation. Geomatics, Nat Hazards Risk 11:2095–2122. https://doi.org/10.1080/19475705.2020.1830187

Piantini M, Gimbert F, Bellot H, Recking A (2021) Triggering and propagation of exogenous sediment pulses in mountain channels: Insights from flume experiments with seismic monitoring. Earth Surf Dyn 9:1423–1439. https://doi.org/10.5194/esurf-9-1423-2021

Polvi LE, Dietze M, Lotsari E, et al (2020) Seismic Monitoring of a Subarctic River: Seasonal Variations in Hydraulics, Sediment Transport, and Ice Dynamics. Wiley Online Libr 125:. https://doi.org/10.1029/2019JF005333

Rindraharisaona EJ, Réchou A, Fontaine FR, et al (2022) Seismic Signature of Rain and Wind Inferred From Seismic Data. Earth Sp Sci 9:295. https://doi.org/10.1029/2022EA002328

Roth DL, Brodsky EE, Finnegan NJ, et al (2016) Bed load sediment transport inferred from seismic signals near a river. Wiley Online Libr 121:725–747. https://doi.org/10.1002/2015JF003782

Saccorotti G, Piccinini D, Cauchie L, Fiori I (2011) Seismic noise by Wind Farms: A case study from the Virgo Gravitational Wave Observatory, Italy. Bull Seismol Soc Am 101:568–578. https://doi.org/10.1785/0120100203

Sánchez-Pastor P, Obermann A, Schimmel M (2018) Detecting and Locating Precursory Signals During the 2011 El Hierro, Canary Islands, Submarine Eruption. Geophys Res Lett 45:10,288-10,297. https://doi.org/10.1029/2018GL079550

Sánchez-Sesma FJ, Rodríguez M, Iturrarán-Viveros U, et al (2011) A theory for microtremor H/V spectral ratio: Application for a layered medium. Geophys J Int 186:. https://doi.org/10.1111/j.1365-246X.2011.05064.x

Schimmel A, Hübl J, McArdell BW, Walter F (2018) Automatic identification of alpine mass movements by a combination of seismic and infrasound sensors. Sensors (Switzerland) 18:. https://doi.org/10.3390/s18051658

Schmandt B, Aster RC, Scherler D, et al (2013) Multiple fluvial processes detected by riverside seismic and infrasound monitoring of a controlled flood in the Grand Canyon. Geophys Res Lett 40:4858–4863. https://doi.org/10.1002/grl.50953

Schneider JM, Turowski JM, Rickenmann D, et al (2014) Scaling relationships between bed load volumes, transport distances, and stream power in steep mountain channels. J Geophys Res Earth Surf 119:. https://doi.org/10.1002/2013JF002874

Seivane H, García-Jerez A, Navarro M, et al (2022) On the use of the microtremor HVSR for tracking velocity changes: a case study in Campo de Dalías basin (SE Spain). Geophys J Int 230:542–564. https://doi.org/10.1093/gji/ggac064

SESAME (2004) Guidelines for The Implementation of The H/V Spectral Ratio Technique on Ambient Vibrations-Measurements, Processing and Interpretations, SESAME European Research Project. SESAME Site Eff Assess using Ambient Excit 1–62

Singh AP, Kumar MR, Pandey A, Roy KS (2019) Investigation of spatial and temporal variability of site response in the Arunachal Himalaya using ambient seismic noise and earthquake waveforms. Near Surf Geophys 17:427–445. https://doi.org/10.1002/nsg.12053

Smith K, Tape C (2019) Seismic Noise in Central Alaska and Influences From Rivers, Wind, and Sedimentary Basins. J Geophys Res Solid Earth 124:11678–11704. https://doi.org/10.1029/2019JB017695

Somos-Valenzuela MA, Mckinney DC, Byers AC, et al (2015) Assessing downstream flood impacts due to a potential GLOF from Imja Tsho in Nepal. Hydrol Earth Syst Sci 19:1401–1412. https://doi.org/10.5194/hess-19-1401-2015

Stevens NT, James SR (2022) Capturing the Changing Cryosphere with Seismic Horizontal-Vertical Spectral Ratios. FastTIMES 26:

Szuch RP, White JG, Vepraskas MJ, Doolittle JA (2006) Application of ground penetrating radar to aid restoration planning for a drained carolina BAY. Wetlands 26:205–216

Truong C, Oudre L, Vayatis N (2020) Selective review of offline change point detection methods. Signal Processing 167

Tsai VC, Minchew B, Lamb MP, Ampuero J-P (2012) A physical model for seismic noise generation from sediment transport in rivers. Res Lett 39:2404. https://doi.org/10.1029/2011GL050255

Turowski JM, Badoux A, Rickenmann D (2011) Start and end of bedload transport in gravel-bed streams. Geophys Res Lett 38:. https://doi.org/10.1029/2010GL046558

Walsh B, Coviello V, Capra L, et al (2020) Insights Into the Internal Dynamics of Natural Lahars From Analysis of 3-Component Broadband Seismic Signals at Volcán de Colima, Mexico. Front Earth Sci 8:. https://doi.org/10.3389/feart.2020.542116

Wang P, Hu Z, Zhao Y, Li X (2016) Experimental study of soil compaction effects on GPR signals. J Appl Geophys 126:128–137. https://doi.org/10.1016/j.jappgeo.2016.01.019

Weihermüller L, Huisman JA, Lambot S, et al (2007) Mapping the spatial variation of soil water content at the field scale with different ground penetrating radar techniques. J Hydrol 340:205–216. https://doi.org/10.1016/j.jhydrol.2007.04.013

Wenner M, Walter F, McArdell B, Farinotti D (2019) Deciphering debris-flow seismograms at Illgraben, Switzerland. In: Debris-Flow Hazards Mitigation: Mechanics, Monitoring, Modeling, and Assessment - Proceedings of the 7th International Conference on Debris-Flow Hazards Mitigation. pp 222–229

Wilcock PR, Crowe JC (2003) Surface-based Transport Model for Mixed-Size Sediment. J Hydraul Eng 129:. https://doi.org/10.1061/(asce)0733-9429(2003)129:2(120)

Young RA, Deng Z, Marfurt KJ, Nissen SE (1997) 3-D dip filtering and coherence applied to GPR data: A study. Lead Edge 16:921. https://doi.org/10.1190/1.1437699

Zhang J, Zhou L, Huang D (2022) Development of rill erosion on bare sloping farmland under natural rainfall conditions. Environ Earth Sci 81:. https://doi.org/10.1007/s12665-022-10383-z

applied sciences

MDPI

Article

Hydrogeophysical Characterization of Fractured Aquifers for Groundwater Exploration in the Federal District of Brazil

Yawar Hussain [1,*], José Eloi Guimarães Campos [2], Welitom Rodrigues Borges [2], Rogério Elias Soares Uagoda [3], Omar Hamza [4] and Hans-Balder Havenith [1]

1 Georisk & Environment, Department of Geology, University of Liege, 4000 Liege, Belgium; hb.havenith@uliege.be
2 Institute of Geosciences, University of Brasilia, Brasilia 70910-900, Brazil; eloi@unb.br (J.E.G.C.); welitom@unb.br (W.R.B.)
3 Department of Geography, University of Brasilia, Brasilia 70910-900, Brazil; rogeriouagoda@unb.br
4 School of Natural and Built Environment, University of Derby, Derby DE22 3AW, UK; o.hamza@derby.ac.uk
* Correspondence: yhussain@uliege.be

Abstract: The present study applies a geophysical approach to the Federal district of Brazil, a challenging hydrogeologic setting that requires improved investigation to enhance groundwater prospecting to meet the rising water demand. The geophysical characterization of a complex hard-rock aquifer sub-system was conducted using direct current (DC) electrical resistivity tomography (ERT) integrated with surface geological information. With a total of twenty-seven ERT profiles, the resistivity acquisition was carried out using a dipole-dipole array of electrodes with an inter-electrode spacing of 10 m. Based on resistivity ranges, the interpretation of the inverted resistivity values indicated a ground profile consisting of upper dry soil, saprolite, weathered, and fresh bedrock. Along with this layered subsurface stratigraphy, the approach allowed us to map the presence of significant hydrogeological features sharp contrasting anomalies that may suggest structural controls separating high-resistivity (≥7000 Ω m) and low-resistivity (<7000 Ω m) conducting zones in the uppermost 10 m of the ground. The assumed impacts of these features on groundwater development are discussed in light of the Brasilia aquifer settings.

Keywords: dipole-dipole; fractures; saprolite; pumping well; Federal district of Brazil

Citation: Hussain, Y.; Campos, J.E.G.; Borges, W.R.; Uagoda, R.E.S.; Hamza, O.; Havenith, H.-B. Hydrogeophysical Characterization of Fractured Aquifers for Groundwater Exploration in the Federal District of Brazil. *Appl. Sci.* **2022**, *12*, 2509. https://doi.org/10.3390/app12052509

Academic Editors: Francisco Javier Alcalá, Maria Catarina Paz, Pedro Martínez-Pagán and Fernando Monteiro Santos

Received: 19 September 2021
Accepted: 29 November 2021
Published: 28 February 2022

1. Introduction

Most urban aquifers are increasingly stressed due to unplanned growths of the metropolitan areas. This situation applies to the Federal District (FD) of Brazil, where the surrounding areas and agricultural activities are growing. The ongoing expansion has directly affected the availability of water as the city will reach an estimated population of 3.4 million in 2025, resulting in rising water demands [1,2].

In the past, both surface and groundwater were used to supply the city. Since 1997, the Brasilia Environmental Sanitation Company (CAESB) has developed the supply system of São Sebastião city exclusively from groundwater abstraction from pumping wells. Until 2016, this system was mainly based on groundwater, with a small portion resourced from surface catchments. The aquifers are intensively used to supply water for rural areas (e.g., human supply and animal), industry (potting, beer and soft drink industries, refrigerators, among others), services (gas stations and workshops) and institutions (schools, universities, and sports clubs). A small portion (approximately 15%) of this supply comes from the *fractured* aquifer through pumping wells [3].

This water supply system underperforms in many regions (e.g., Sobradinho II, Condominiums of Greater Colorado, and São Sebastião) where aquifers are over-yielded as the extraction rate reaches the annual recharge rate. To promote the system sustainability,

there are other potential areas where groundwater can be explored. The use of groundwater has numerous advantages (regarding the surface water) including the provision of a smaller area of protection, shorter distance between water sources and consumption centers, the possibility of gradual implantation, lower cost of treatment, and smaller evaporation losses. On the other hand, there are some disadvantages as the irregularity in the spatial distribution of reservoirs, high energy expenditure, and very slow renewability.

The FD was planned on a hard-rock aquifer that has a complex groundwater flow system. Based on hydrogeological characteristics such as hydraulic conductivity (permeability), this aquifer is divided into domains, systems, and subsystems. Initially, groundwater prospecting seeks to locate suitable areas having groundwater reservoirs inferred by discontinuities, fractures, lineaments, and fissures, which are attributed to the presence of highly productive aquifers [4]. However, such natural geological settings represent challenging hydrological characteristics for groundwater prospecting. In particular, the presence of fractures as well as the intrinsic properties and physical environment of the site can play essential roles [5]. For such complex hydrogeological conditions, geophysical prospecting techniques, particularly DC-ERT, can be applied to deduce high-yielding weathered and fractured zones that may represent potential groundwater traps.

The ERT technique has been widely used to investigate many sites around the world for various purposes, including bedrock detection, geological mapping, and groundwater exploration [6–10]. Recent case studies of hard rock aquifers in Brazil have highlighted the significance of regional structures, hydrogeology, and petrophysical properties of the site in groundwater development [2,11–14]. Geological structures determine the aquifer geometry and the hydrogeological properties [15,16]. In addition, the groundwater compartmentalization inferred from the basement uplift or subsidence thought faults may increase or decrease the saturated thickness and therefore the groundwater reserves [14].

Although the previous research has advanced in geophysical techniques, their applicability in fine hydrogeological characterization of fractured aquifers may vary depending on the specifics field conditions. Therefore, further research to improve the understanding of fractured aquifers and optimize the geophysical investigation is required. The study aims to identify particular areas in which the groundwater use is viable to supplement public supply in the FD, considering the high risks of shortages as recently observed in the prolonged drought period of 2017. To achieve this goal, the paper presents a case study in the FD of Brazil, where ERT was utilized to identify the most suitable (productive) locations for drilling new pumping wells.

2. Materials and Methods

2.1. Study Area

Within the FD, the investigation was conducted in areas with the integrated supply system (Descoberto/Santa Maria—Torto system/Sobradinho Taguatinga) and in other areas located outside the integrated system (e.g., Descoberto and Santa Maria—Torto reservoirs) (Figure 1). According to the Köppen classification, the climate of the FD falls between the Tropical (Aw) and Tropical types of Altitude (Cwa and Cwb). Its striking feature is the existence of two well-established periods, defined as rainy in summer and dry in winter. The rainy period extends from October to April, while the dry period extends from May to September [17,18]. Water demand per capita varies—depending on the socioeconomic aspects of the administrative regions. In general, the demand as follows: (i) from 120 to 125 L per inhabitant and day (L/i·d) in rural areas with low human occupation density; (ii) from 126 to 140 (L/i·d): rural regions with small urban centers as headquarters of agricultural colonies; (iii) from 141 to 155 L/i·d in Planaltina and its expansion areas; (iv) from 156 to 180 L/i·d in Ceilândia; (v) from 181 to 220 L/i·d in Taguatinga and Águas Claras; (vi) from 121 to 275 L/i·d in Asas Sul and North of Brasília and (vii) from 276 to 472 L/i·d: Lago Sul de Brasília see details in Figure 1.

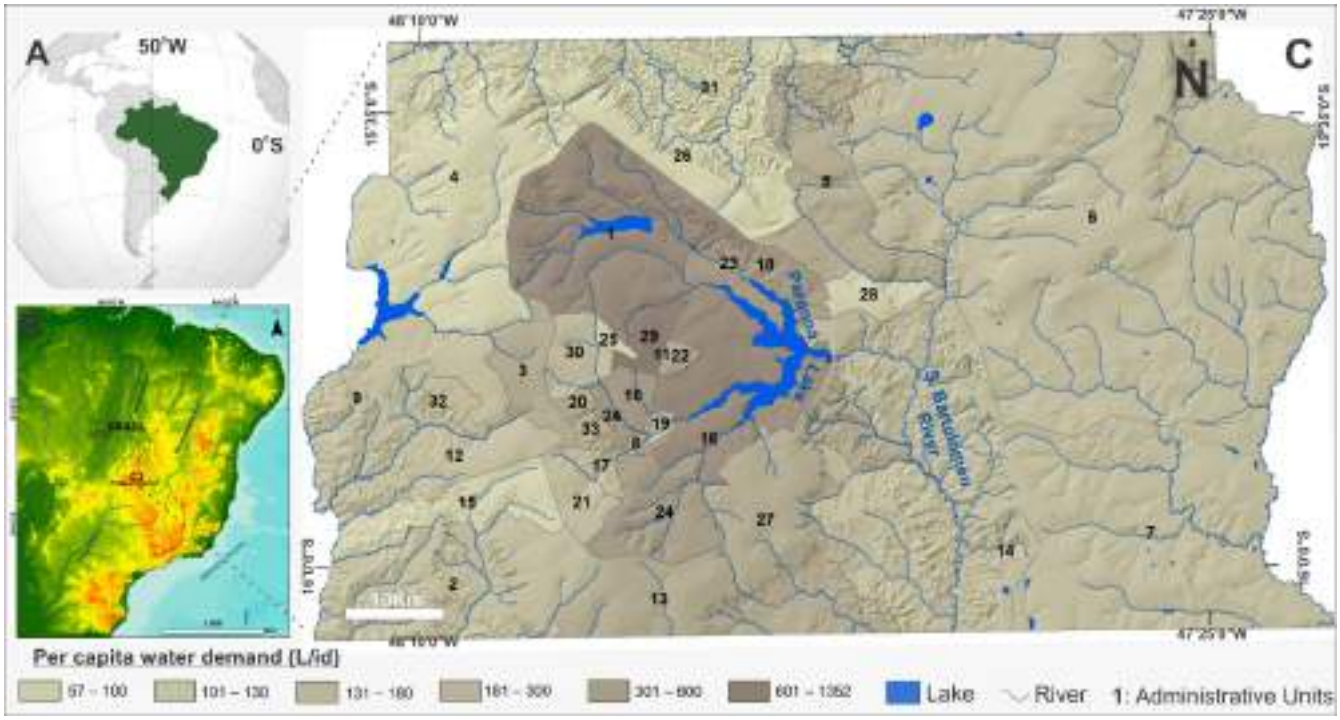

Figure 1. (**A**) Location of Brazil on South American map, (**B**) Location of Federal District (FD) on map of Brazil and (**C**) Administrative units of FD based on per capita water demand (source: [3]).

The geology of the FD is characterized by metamorphic rocks, covered by thick regolith. Within this geological setting, three large groups of aquifers are discriminated and classified as different groundwater domains, including the Intergranular (unconfined or porous) Domain, the Fractured Domain, and the Fissured-Karst Domain. The domains were subdivided into systems and subsystems by [17] and details can be assessed at [5]. This aquifer classification is presented in Figure 2, details are given in Tables 1 and 2. The flow rates from pumping wells range from zero (dry wells) to more than 100 m^3/h. The average flow in all aquifers (fractured and fissured-karst) is around 8000 L/h. This variability is a function of the different aquifer yielding, which depends on lithology and fracturing, soil type, and relief. In general, the more sand or quartzite content the rocks consist of, the greater is the potential of fractured and fissured-karst aquifers [17].

2.2. R3/Q3 Aquifer Sub-System

In the main water supply to the FD, some of these sub-systems have major contributions following further exploration for optimized productivity. Such aquifers are represented by the Canastra System F/Q/M sub-system and the Paranoá System R3/Q3 sub-system. The F/Q/M sub-system has intensively been used for water supply to São Sebastião, in which more than 90% comes from a battery of pumping wells located in the urban perimeter. Thus, the alternative option to supplement the water supply based on groundwater exploitation is limited to sub-system R3/Q3. This aquifer has the following characteristics that make it an attractive option for supplying urban areas: (i) it has an average flow (12,000 L/h) 0.5-fold higher than the average flow of the aquifers in the region; (ii) a low incidence of dry or very low flow rates wells; (iii) it occurs in a large area with a wide range of geographical distribution; (iv) it occupies the favorable localities suitable for the natural aquifer recharge as well as for aquifer artificial recharge projects and (v) it has good quality groundwater [3]. This aquifer sub-system has very high local relative hydrogeological importance, with a high occurrence of wells with flow rates that can be higher than 20,000 L/h. The distribution area of this sub-system is a factor that increases its local importance, occupying about 25% of the territory of the Federal District. Figure 3 presents the conceptual groundwater flow model and recharge mechanisms of the aquifer

sub-systems. This is important because groundwater flow paths in the fissured/pore aquifer widely vary over several depth magnitudes. These types of circulation conditions usually occur in fault zones and in such areas vertical groundwater flow is actually more important than lateral flow [19].

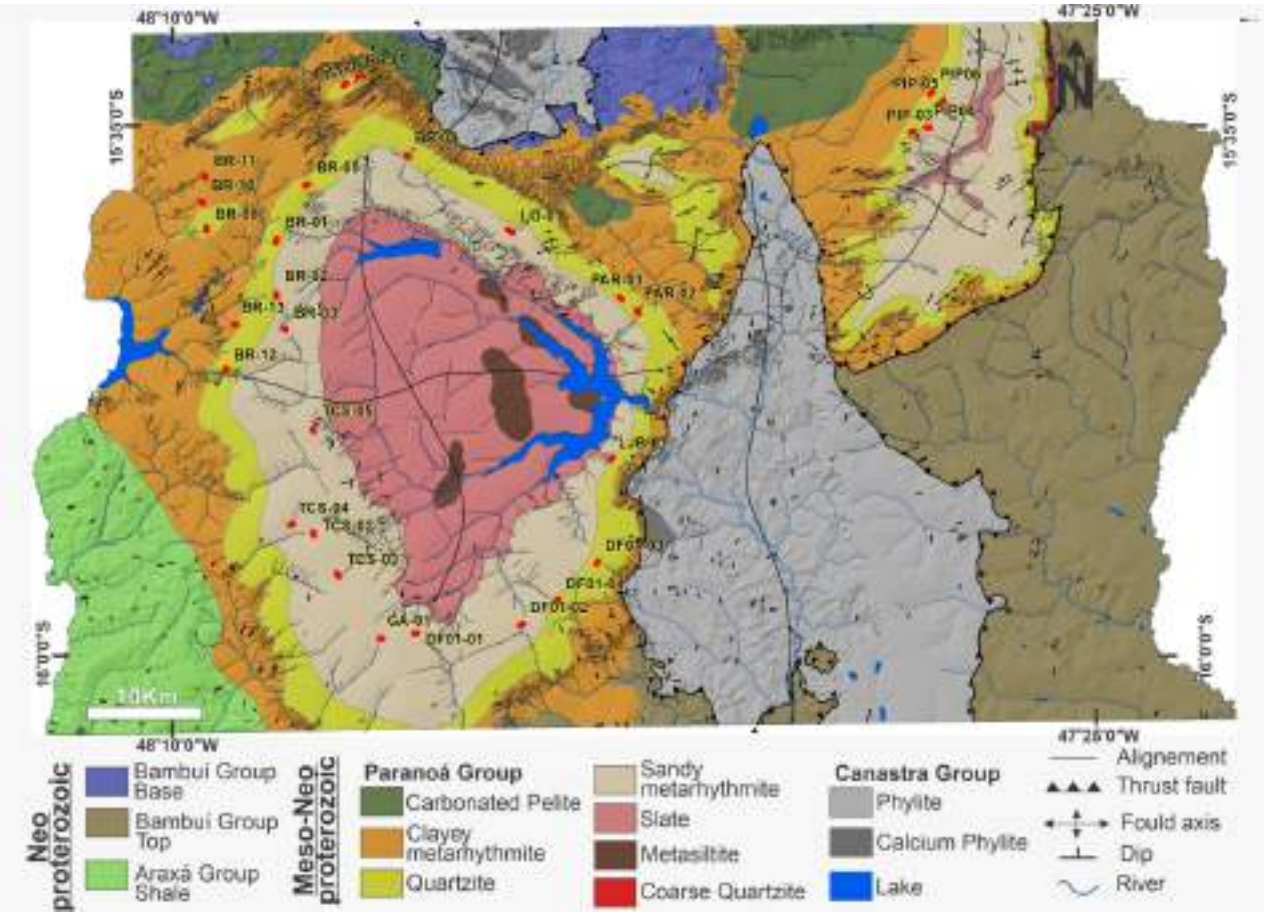

Figure 2. Geological units catalogued in Brasilia.

Table 1. Classification of the Federal District aquifers based on flow rates, lithology, and soil type [18].

Domain	System	Sub-System	Flow Rate (m^3/h)	Lithology/Soil Type
Unconfined	System P1		<0.8	Sandy latosols and Quartzarenic Neosols
	System P2 System P3		<0.5	Clayey oxisols Plinthic and argillaceous
	System P4		<0.3	Cambisol and Litholic Neosol
Fractured	Paranoa	S/A	12.5	Metasiltite
		A	4.5	Slates
		R3/Q3	12.0	Sandy quartzites and metarhythmites
		R4	6.5	Clayey meta-rhythmites
	Canastra	F	7.5	Micaceous phyllites
	Bambui	Topo	6.0	Silitos and Arcoses
	Araxa	-	3.5	Mica shales
Fissured-Karstic	Paranoa	PPC	9.0	Metasiltites and marble lenses
	Canastra	F/Q/M	33.0	Calciphyllites, quartzite and marbles
	Bumbui	Base	9.0	Silite and micritic limestone lenses

Table 2. Hydrogeological characteristics of the R3/Q3 aquifer sub-system. 24-h pumping test data of 27 deep pumping wells.

Units	R3			Q3		
	Maximum	**Minimum**	**Average**	**Maximum**	**Minimum**	**Average**
$T(m^2/s)$	7.8×10^{-4}	1.2×10^{-4}	4.9×10^{-4}	1.4×10^{-3}	1.4×10^{-4}	4.0×10^{-4}
$K(m/s)$	4.8×10^{-6}	5.3×10^{-7}	2.8×10^{-6}	1.6×10^{-3}	1.2×10^{-6}	4.6×10^{-6}
S	1.7×10^{-1}	2×10^{-2}	1.0×10^{-1}	1.6×10^{-1}	4.5×10^{-3}	1.5×10^{-1}
$Q(m^3/h)$	48	0.0	12.5	42	0.0	12.4

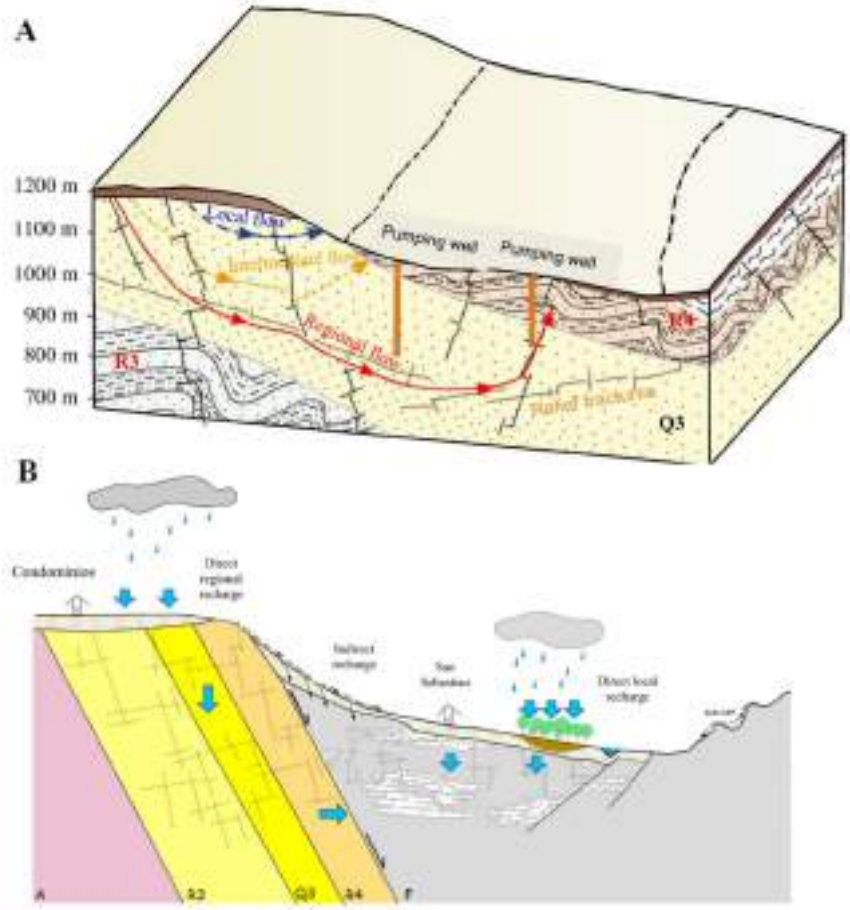

Figure 3. Conceptual groundwater flow model (**A**) recharge mechanism (**B**) of the aquifer sub-systems (A, R3, Q3, R4, F) of Brasilia.

The investigation was conducted on 27 different sites in the FD, which has initially been mapped with the aquifer sub-system-R3/Q3 of Brazil. The aquifer sub-system includes the Serra do Paranã (formerly Q2), Serra da Meia Noite (former R3) and Ribeirão Contagem (former Q3) of the Paranoá Group (Figure 4). The inclusion of three lithological units in a single aquifer sub-system is justified, as the types are dominantly sandy and have petrographic features that are quite similar in their hydrogeological characteristics, hydrodynamic parameters, the statistical distribution of average flow rates, and well typologies (Figure 4). The presence of quartzite makes the aquifer highly discontinuous, and it also keeps the fractures open because of the brittle behavior. In this way, the wells, that intercept rocks of different formations, would have a large number of water inlets, with fractures dispersed throughout the perforated section, in addition to significant inter-connectivity of the fractures [20].

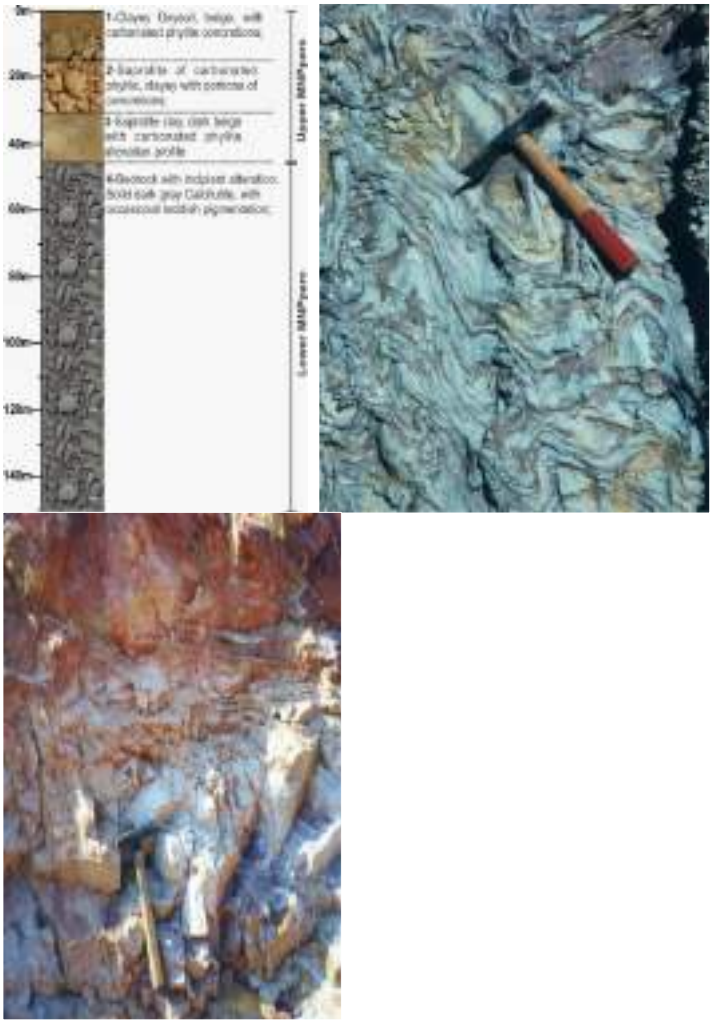

Figure 4. Synthesized lithological log of the area and photographs of the rock outcrops in the fractured aquifer system of Brasilia.

Hydrogeological conditions widely vary over the space, thus favoring the existence of unconfined or confined conditions and very anisotropic hydrodynamic characteristics. Table 2 shows the distribution of the values of transmissivity (T), hydraulic conductivity (K), and coefficient of storage (S), calculated from the pumping tests conducted on twenty-seven pumping wells pumped for a period of 24 h. Results obtained using the Moench method in the AquiferTest software for fractured aquifers [3]. The high-water potential of this aquifer sub-system is brought by the great flow of springs. In this way, the R3/Q3 sub-system is considered the only groundwater source that still has exploitable reserves or availability of water resources capable of contributing effectively to supplement public water supply in the event of extreme scarcities.

2.3. Electrical Resistivity Tomography (ERT)

The measurement of subsurface electrical resistivity of the geological material, using different electrode arrays, has generally been adopted to identify ground layers distributions or to identify features whose dimensions and depths vary between meters up to a few kilometers. Recently, automatic systems have emerged for data collection that can speed up measurement and interpretation processes. At the same time, a greater capacity for calculations by computers has allowed, in recent years, the obtaining of images in two or three dimensions of the real distribution of resistivity of the subsurface. The electrical resistivity measuring devices commonly consist of a system of four electrodes, two of which are used to send an electric current to the ground. Wenner arrangements, polo-polo, polo-

dipole, dipole-dipole, Wenner-Schlumberger, and gradients are typical electrode arrays whose selection depends on the research objective of the investigation. Each arrangement has a common characteristic such as resolution (dipole-dipole and pole-dipole), depth of investigation (pole-pole), and signal-to-noise ratio (Wenner and Wenner-Schlumberger).

For example, in groundwater prospecting applications, the dipole-dipole array is more effective among others [21]. In this array, transmitters are distanced from the receivers at a fixed distance for each investigation level, i.e., the depth and the investigated level, the distance between the transmitter and the receivers. The measurements are carried out at various levels of investigation (n), where n = 1, 2, 3, 4, 3, ... is the point of intersection between a line that starts from the center of the current electrodes and another part of the center of the potential electrodes. The result is an electrical resistivity data set obtained in n depths forming a section. This grid reflects the subsurface behavior in response to electrical currents inputs, which is a function of the mineralogical composition of the rock, pore water content, and pore-water electrical conductivity etc.

2.4. Data Acquisition and Processing

The SYSCAL System was used; it is sensitive to ambient noise during field acquisition. Two configurations prevented the high quality data acquisition itself: the presence of a wire fence barbed with concrete stakes and subsurface streetlights. In the first case, some electrodes showed very high contact resistance, and in the second, many electrodes appeared to be open. In some cases, when faced with a problem of ambient noise during acquisition, the penetration of the electrode into the soil can be increased where the volume of moisture with a saline solution would increase. However, in other cases, the problem cannot be avoided, and the section should be carried out in the most appropriate (alternative) place.

The software RES2DINV was used for the data processing workflow adopted after [5]. The data acquisition of the geophysical data was conducted along twenty-seven profiles (Figure 2); each one was approximately 350 m in length. In the field, the electrical resistivity data were collected with the electric roll-along technique, using the dipole-dipole (DD) arrangement, with a spacing of 10 m between the electrodes. The data acquisition protocol with the multi-electrode cables was elaborated in the software ELECTRE II, version 05.06.00, (IRIS Instruments) for acquisitions with 36 electrodes.

For better deployment of the geophysical prospecting, the field activities were carried out during the dry season and moisture in the soil was increased by pouring salt solution at each electrode, thus helping to minimize the absorption of electric current in the soil. The data were acquired with SYSCAL Pro 72 equipment (manufactured by IRIS Instruments), consisting of an interleaved acquisition module in multi-electrode cables. Thirty-six stainless steel electrodes were used to inject current and measure the electric potential generated by the current flow in the subsurface. ERT data were processed in a similar approach adopted by [22]. The filtering and topographical correction on the dataset were performed in the PROSYS II software (IRIS Instruments). In order to determine the effective depth, the pseudo-sections of electrical resistivity were inverted using the computer program RES2DINV (Geotomo Software). In our case, the resistivity values near the ground are high; therefore, narrower model cells were used in the RES2DINV program, where the width of model blocks was kept half of the electrode spacing for optimum result. The 2D model was then developed, which divides the subsurface into a series of blocks to determine the resistivity; its product is apparent resistivity pseudo-sections that fit with the field data, using an inversion process based on the variation of the least square method. The results obtained were presented in the form of 2D resistivity sections. The DC resistivity data processing workflow is shown in Figure 5.

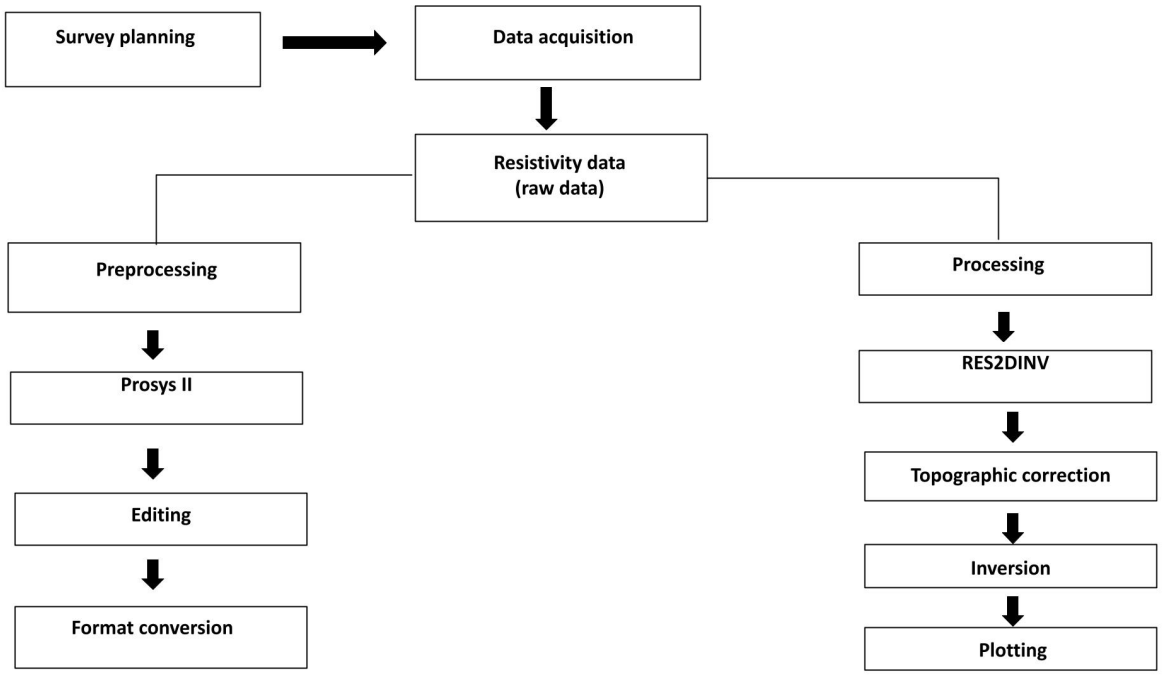

Figure 5. Processing workflow of DC resistivity data.

3. Results and Discussion

3.1. Analysis of ERT Data and Overview of the Findings

In the first stage of ERT data processing, the apparent and calculated resistivity along twenty-two profiles were analyzed. Linear regression is developed and the correction coefficient is calculated. In Figure 6 it can be seen that all the profiles show a value of 'r' greater than 0.9, which is acceptable accuracy. For some of the profiles, odd data points were trimmed to achieve this level of accuracy. However, five of the acquired profiles showed r-value < 0.9 and therefore these were removed from the analysis.

Following this initial stage, inverted ERT anomalies were correlated to the hydrogeological features inferred from the available information of the groundwater flow system R3/Q3. Then, the hydrogeological meaning of each feature with the groundwater development was highlighted. The correlation of inverted resistivity values with the lithological log of the nearby pumping wells reveals a three-layered subsurface stratigraphy as dry topsoil, saprolite, and quartzite (Q3) and at some places, Meta-rithmite clayey and sandy (R3) formations are also found. Along with layered stratigraphy, the numerous features of hydrogeological significance have been delineated on some of the inverted cross-sections as resistivity anomalies. These structures are recommended for future detailed investigations that may include the application of integrated geophysical techniques followed by geotechnical investigations and then finally the installation of pumping wells at the site. These features have been documented in numerous previous studies [8,10,23–30]. A common contour interval and respective color scale are chosen for all the resistivity inversion models. A detailed description of these features is provided below.

3.2. Resistivity Inversion Models and Geological Features

In the hard rock aquifers (plutonic and metamorphic), the groundwater development (presence and movement) is related to the secondary permeability in the rock matrix, created by weathering of the fresh bedrock. The tectonics of the region has nothing to do with the creation of this permeability [31]. These weathered portions of the bedrock can be detected on the inverted resistivity cross-section as a relatively low resistivity anomaly compared with the underlying fresh bedrock. Almost all ERT profiles mark the presence of this weathered profile with different thickness, degrees of weathering, and moisture contents (Figures 7–12). These sections are considered important features for groundwater development.

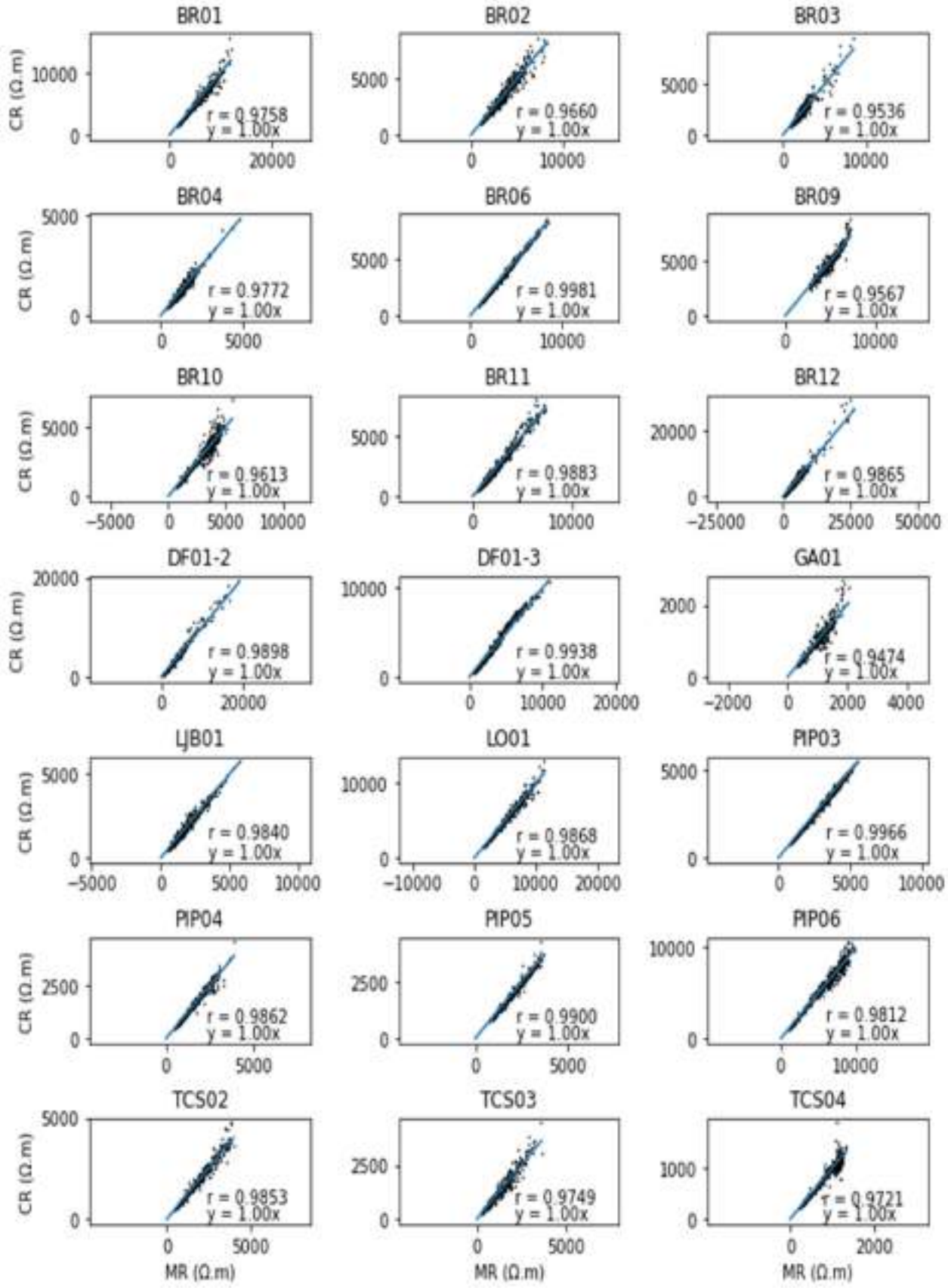

Figure 6. The relationship between calculated and measured resistivity at twenty-two ERT profiles. The abbreviations CR and MR stand for calculated and measured resistivities, respectively.

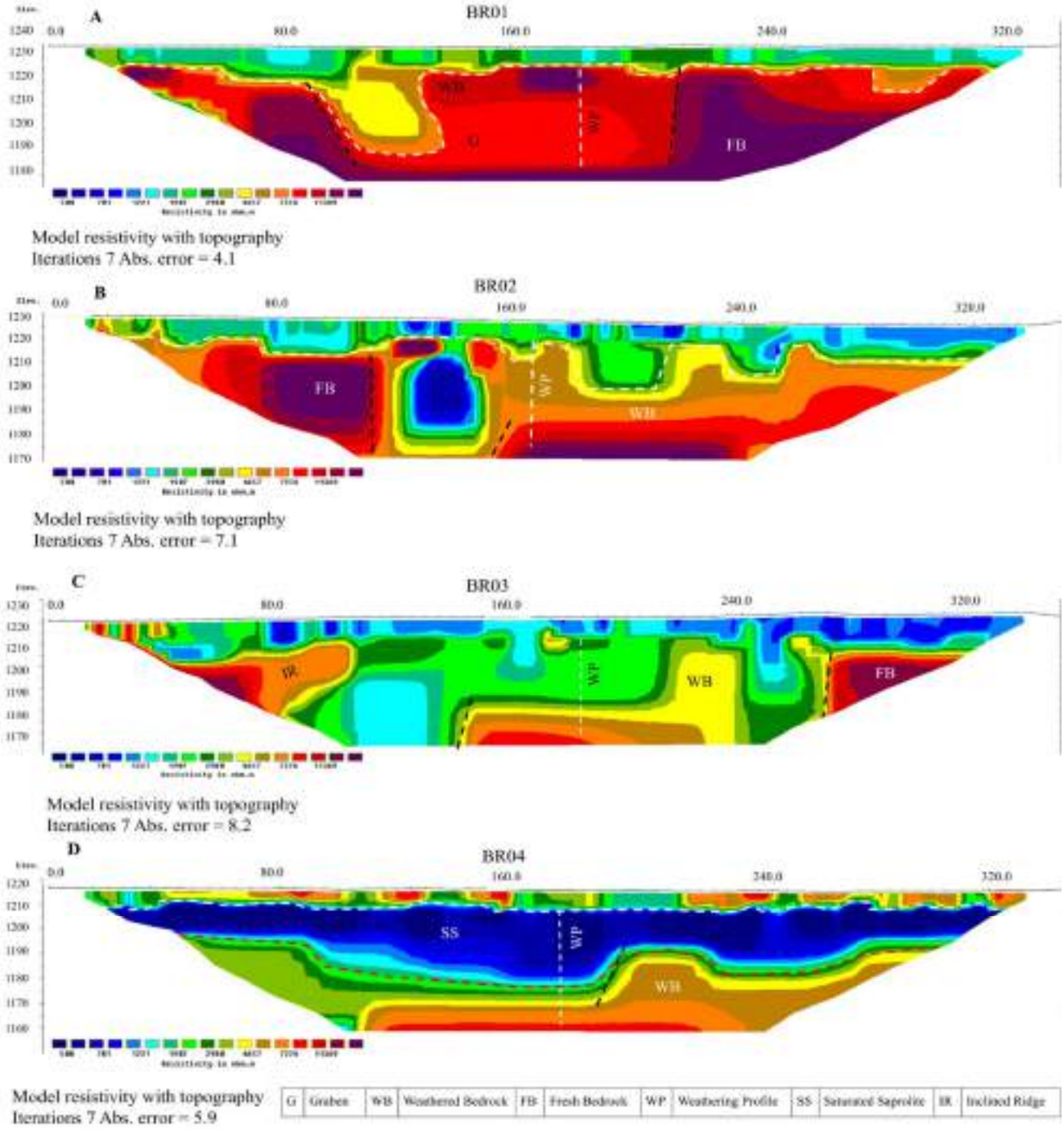

Figure 7. 2D resistivity models (**A**–**D**) in the region of Brasilia using a dipole-dipole array.

At the centers of the 2D profiles, as seen in Figure 8A–D, sharp contrasting anomalies may suggest structural features separating very high resistivity of the order of ≥7000 Ω m and low resistivity <7000 Ω m conducting zone from bottom depth ~10 m till close to the surface. It marks the position of the fault, high resistive material, and the recharge's pathway. It is interesting to note that on profiles shown in Figure 7A–D, increasing trends in the resistivity of the bedrock are observed. This may be associated with the rock breaking by fissuring and lineaments. Therefore, the center of this bedrock might have become boulders as described by [28]. This indicates highly weathered moisture saturated and quartzite of sub-system R3/Q3.

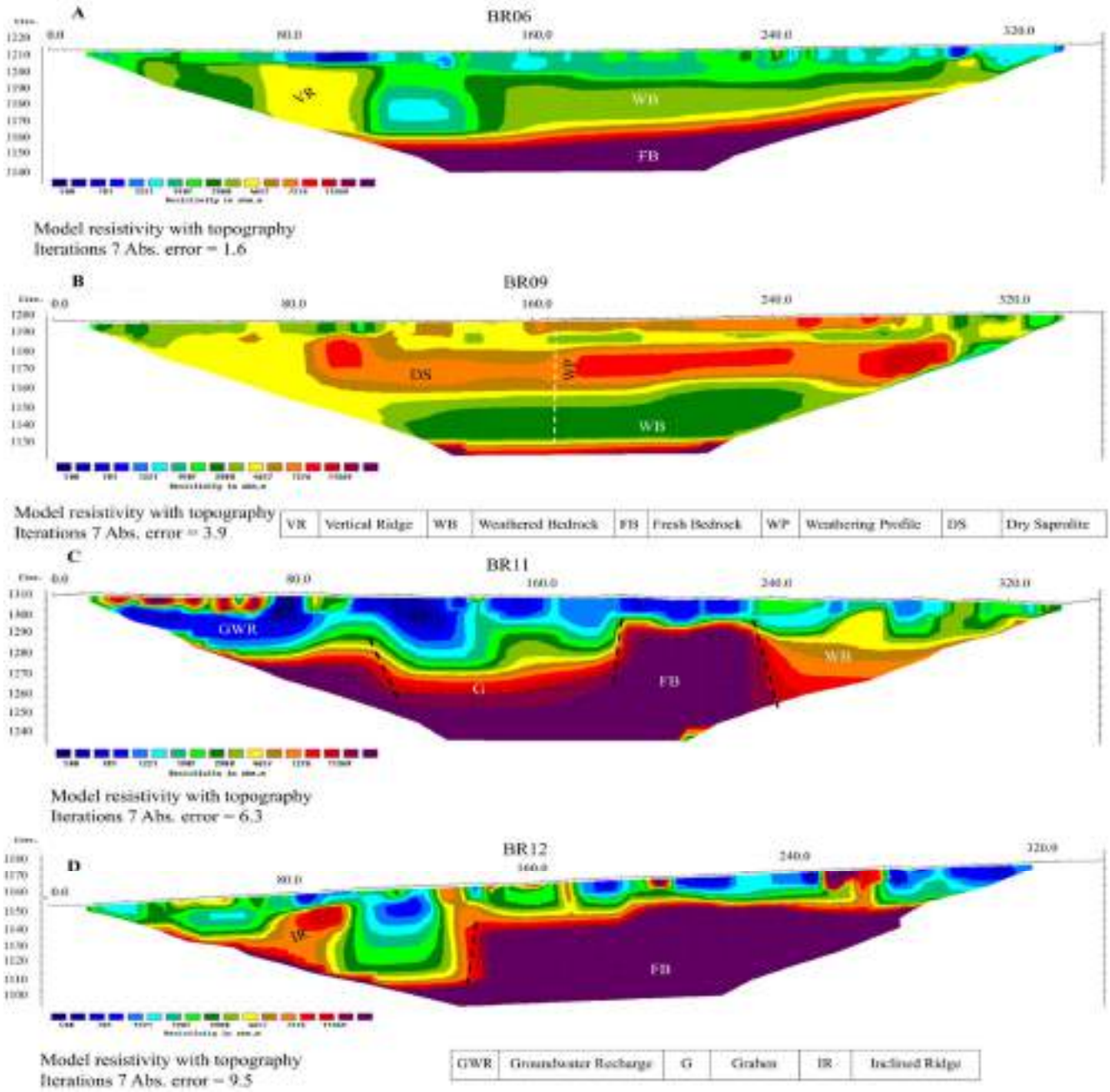

Figure 8. 2D resistivity models (**A**–**D**) in the region of Brasilia using the dipole-dipole array.

Fault mapping is key to understanding groundwater flow in hard-rock aquifers [32–34]. It is worth noting that faults can be seen in Figure 7A–D, Figure 8B,D, Figure 9A,D and Figure 10B,D. On ERT profiles, the faults are identified as sharp vertical boundaries found between two layers with distinct differences in resistivities. On some of the profiles (BR02, BR03, BR04), the strata above bedrock show resistivity ranging from <10 to >1000 Ω m as seen in Figure 7B–D. The prominent graben-like structures can be seen on some resistivity profiles, which were created by the faults (Figures 7A, 8B and 9D) in quartzite hard-rock. These structures have also been reported in previous studies on Brazilian aquifer systems [2,33,34]. A similar approach for delineation of faults has been adopted by [8].

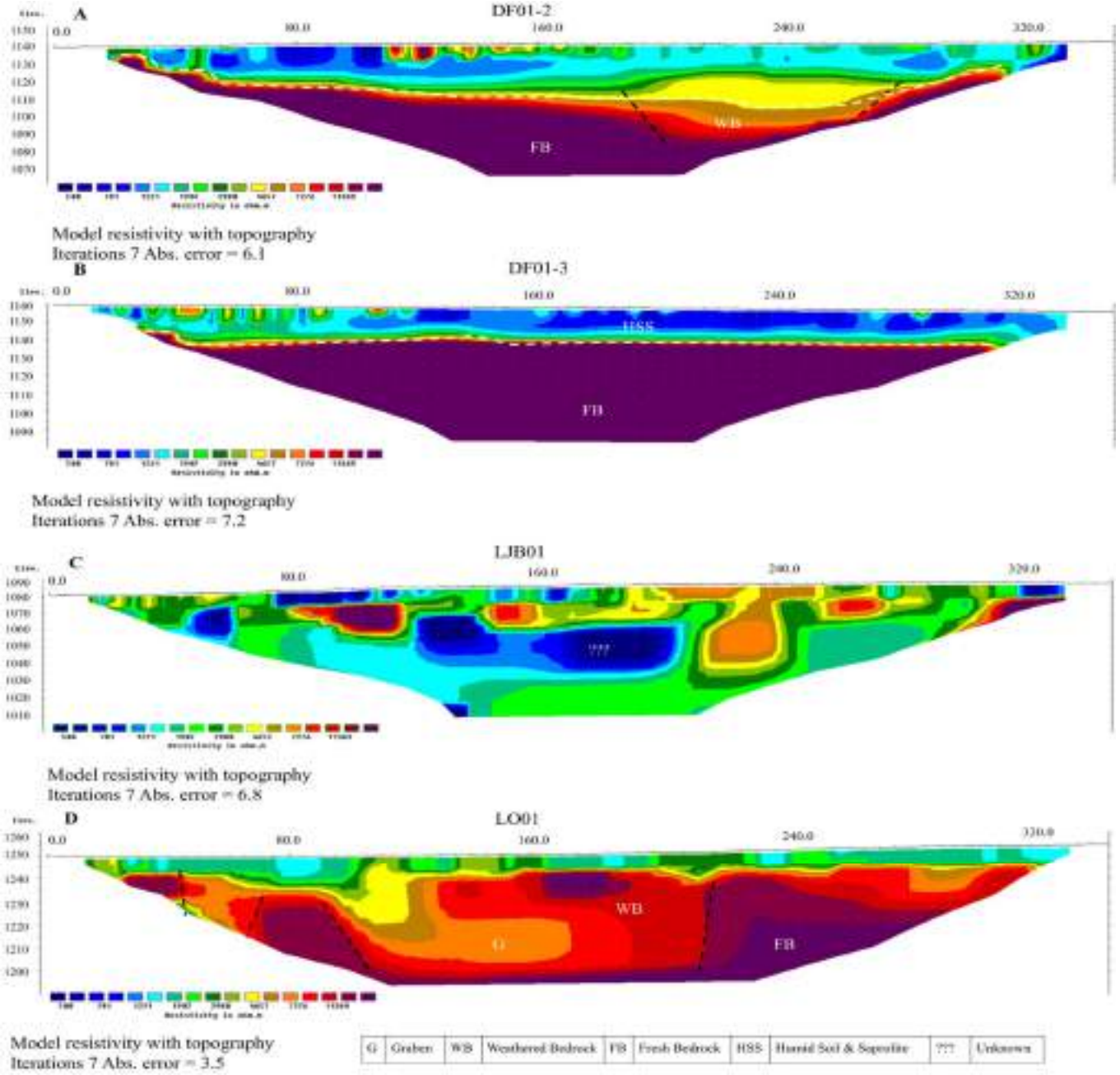

Figure 9. 2D resistivity models (**A**–**D**) in the region of Brasilia using the dipole-dipole array.

The fractured zone's shape and position in quartzite are delineated based on resistivity contrast on the 2D resistivity models as shown in Figures 7B and 8A,D. At the top, the fractured zones show variations in resistivity values related to the degree of weathering and thus are hydrologically potential sites for groundwater development in the areas. The comparatively low resistivity range (2000 to >10,000 Ω m) of ridge-like structures might be related to the coarse-grained material composition and having high permeability can favor rainfall infiltration and may act as aquifer recharge zones.

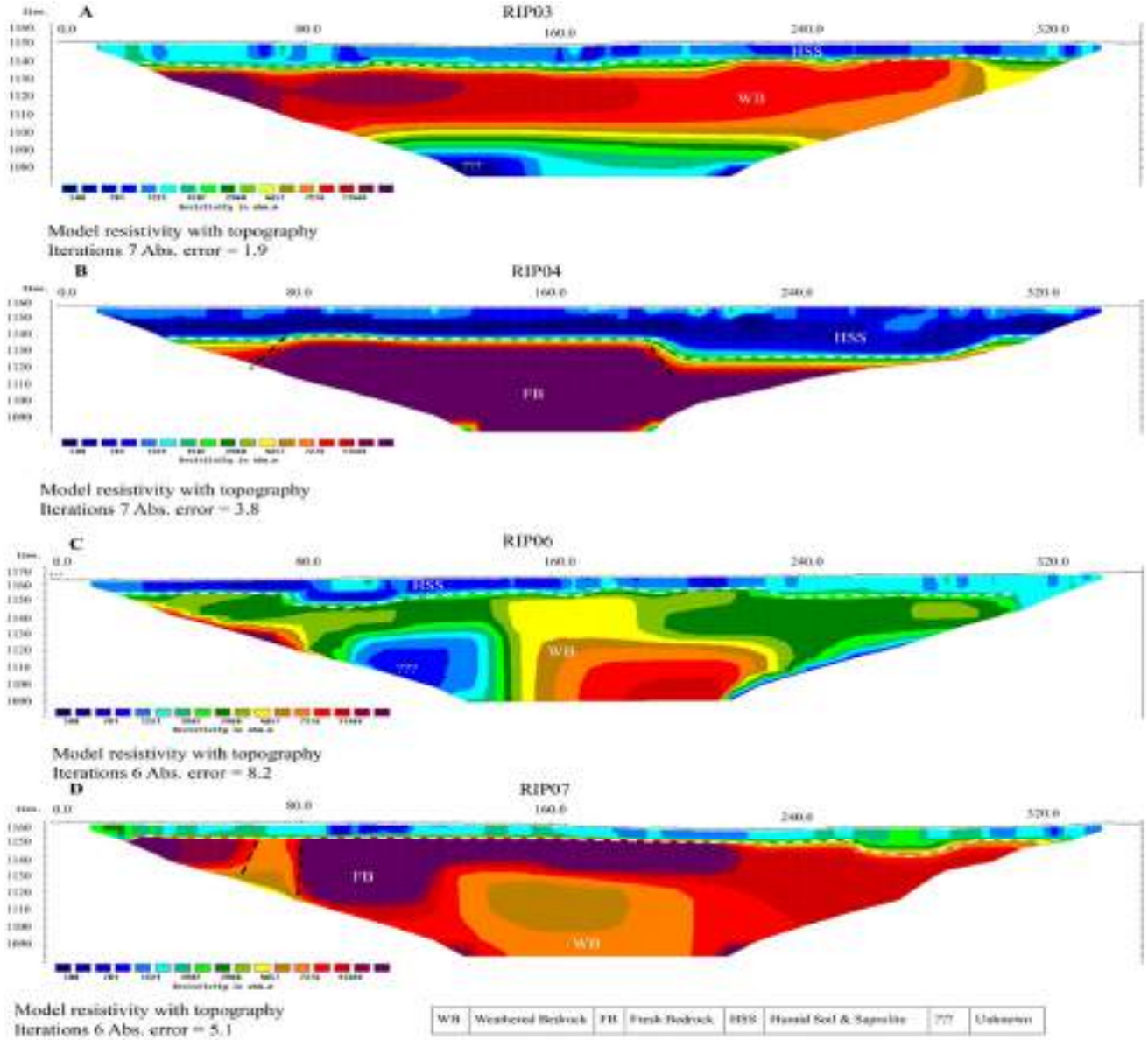

Figure 10. 2D resistivity models (**A**–**D**) in the region of Brasilia using the dipole-dipole array.

The depth and topography are important features for groundwater flow. In dual-porosity rocks, the base flow occurs primarily in fractures, while intergrain porosity plays an important role in water storage. The circulation of water in dual-porosity rocks is often very complex and is the subject of controversy in Groundwater Hydrology. This applies in particular to hydrogeochemistry and tracer study due to the possible diffusion exchange between the water flowing in the crevices and the stagnant water contained in the micropores of the rock matrix. More about the circulation of groundwater in double (or triple) porosity systems can be found, among others, in the previous works [33,34]. In comparison with the geological sequence of the studied area (comprising topsoil, saprolite and quartzite—Figure 4), the 2D resistivity cross-sections show the three-layered stratigraphy as well as the presence of soil contents in the strata as low resistivity anomalies (Figure 11B). The model shows the bedrock at shallow depth (20 m) and 350 m lateral distance along the profile. This information aids groundwater exploration in the area. With the available geological information, it is difficult to separate the geology of bedrock whether it is a quartzite of Q3 unit or sandy or clayey Metarrithmite of R3. However, onsite field investigations and communications with the experts working on the area are the sole

criteria for the attribution of these rock units. Another important aspect of the bedrock topographic variation is the development of compartmentalized aquifers and its effect on groundwater yielding. In this study, the formation of graben-like structures may indicate this compartmentalization (Figure 7).

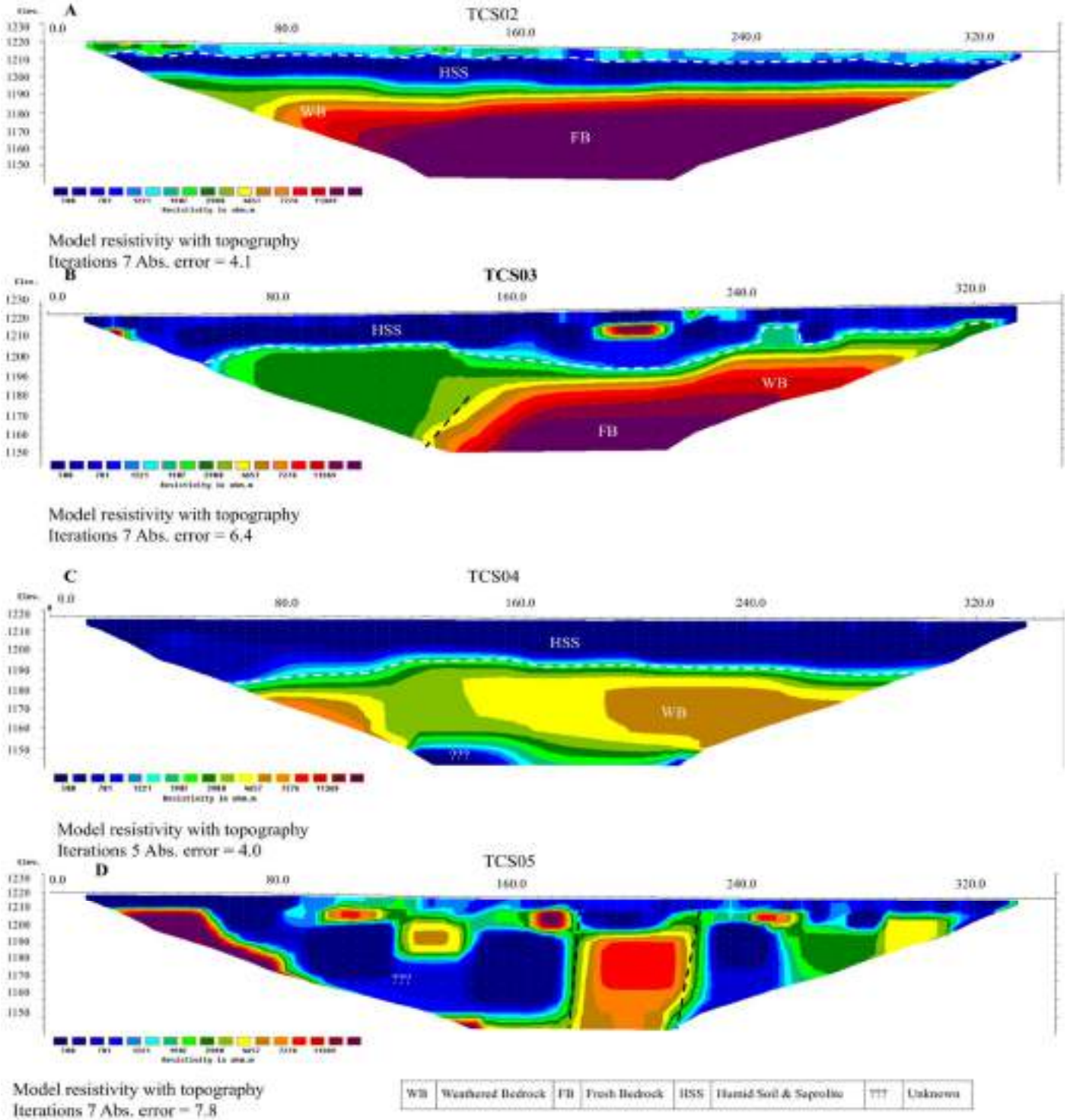

Figure 11. 2D resistivity models (**A**–**D**) in the region of Brasilia using the dipole-dipole array.

The secondary porosity created by the network of joints, fault planes, and bedding planes may form the aquifer system in the area in quartzite rocks [5]. This system may be identified on the inverted resistivity sections, where a relatively low resistivity zone (<100 Ω m) exists (Figures 9B, 10A,B and 11B,D). These deeper low resistivity anomalies may

present a potential site for groundwater development. Along with sufficient recharge, the exploitation of the groundwater from these deeper levels is important for the sustainability of the aquifer. Another possible explanation of this low resistivity deep anomaly would be the presence of a high clay proportion, which is created by the weathering of bedrock as explained above. Another possibility is the presence of sandy and clayey rocks of the R3 sub-system. However, in the present study, it is difficult to make this segregation because of the unavailability of the required information.

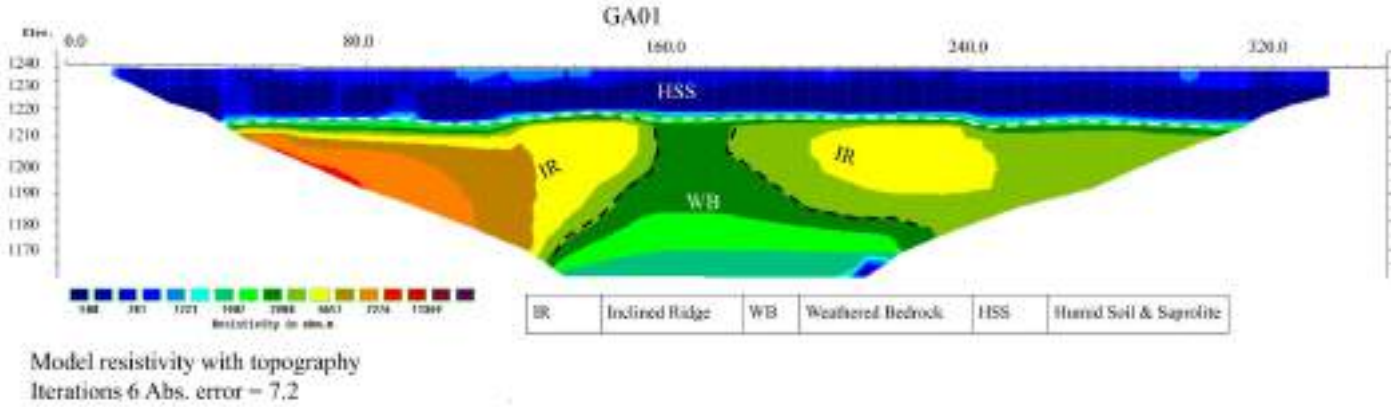

Figure 12. 2D resistivity models in the region of Brasilia using the dipole-dipole array.

4. Discussion

The results presented above generally agree with previous studies, which were carried out in different regions of Brazil, focusing on various groundwater regimes that highlight the role of litho-stratigraphy and hydrogeological features on the aquifer systems, which includes their geometries as well as hydrogeological characteristics [11–17]. The effects of porosity, permeability, and faults (acting as a barrier slowing water flow or connectors between aquifers) on the transmissivity are evaluated [35]. In addition to the role of faults causing structural aquifer compartmentalization, they may affect the volume of the aquifer by reducing or increasing its thickness as documented by [4,14]. Similarly, the significance of these hydrogeological features delineated on inverted resistivity cross-sections from an aquifer system of Brasilia is highlighted.

The geophysical results in Figures 7–12 shows overlapping layers (soil and rock), variations in soil and saprolite thickness, and a vertical anomaly position. Most of the profiles were taken in areas along the lineament, where significant geoelectric anomalies were found. The complexity of the hard rock aquifer is evident from the structural and spatial variability of its fracture networks and weathering [36]. The following are the detailed discussions on groundwater exploration features marked on the inverted resistivity sections.

The weathering processes have changed the properties of the bedrock, increasing the porosity and secondary permeability leading to the development of fractures. The fluid circulation is supported by the fractures prior to weathering. Another aspect is the precipitation, which may affect the structures of interest either positively or negatively [37]. The weathered profile is present on all profiles, which indicates the degree of weathering in the metamorphic basement aquifer. Along with groundwater development, the depth of weathered rocks has a prominent effect on many earth surface processes such as routing water and nutrients. The bedrock stored water can be used by plants in case of drought conditions through their roots penetration. The bedrock drainage can also influence the area's stream flows, their water quality, and also maintain base flow, especially in dry seasons. In this way, a direct nexus between the surface-groundwater can be seen. This connection is very important in any groundwater vulnerability assessment study. Another important influence is based on the extent of alteration in landscape evolution through the development of pore-water pressure related to the water circulation, which is an important trigger for shallow clayey landslides in the Federal District as documented by [5].

These aspects of weathering the bedrock are explained in detail by [38]. The presence of faults/discontinuities at the base of the weathering profile can also affect the hydraulic conductivity and have a major influence on the groundwater flow systems by affecting their hydraulic conductivity [36]. These fractures and fissures can also be developed by the expansion of minerals during the weathering process [39]. Depending on their form and material properties, these can be considered groundwater flow channels as conduits, barriers, or a combined conduit-barrier system and storage sites. The hydraulic fault behavior to transverse flow changed in case of acting as a barrier in the presence of clay-like materials (alteration of primary minerals) accumulation into fault cores. In contrast, the weathered or damaged zones improved the hydrodynamic properties of the aquifer rather than the fresh bedrocks, and they can also concentrate the water and improve its channelization along faults and fissures and improve discharge at the well [37,40]. On the one side, such a fault can provide a good source of groundwater where the source is connected to a deeper conducting zone with appreciable resistivity in contrast with the surrounding quartzite rock. On the other side, the fault can also act as a groundwater flow barrier as explained by [41]. The delineated graben-like structures created by faulting may be associated with the reservoir compartmentalization (fluid/pressure compartments created by sealed boundaries) as described by [2]. Therefore, these hydrogeological features are the potential site for groundwater development. These heterogeneous hydrogeological settings can also (i) influence the nitrate contamination transport and its fate by biogeochemical mechanisms [26], and (ii) increase the vulnerability of aquifers from surficial contaminates. These structures may outcrop at the ground and provide a pathway for contaminant transport. Therefore, the potential sites for groundwater can also increase the vulnerability of the underlying aquifer.

In the case of the existence of prominent geological discontinuities and fracture networks, the groundwater flow leads to the compartmentalization of the aquifer system. This geologic compartmentalization is further enhanced by the hydraulic containment created by the well's pumping. The hydrological models created from ERT inversion results show the three geological layers: the saprolite, which is mostly unsaturated during the dry season, the fissured layer, which provides most of the flow to the pumping wells, and the fresh bedrock. In the case of the depletion of the water table in the dry season created by intense pumping, the geological discontinuities may act as a barrier to flow and divide the aquifer into different compartments. As a result, the discharge at the nearby well decreases. It also causes variable groundwater chemistry [37].

In short, the delineated features can affect the hydrodynamics of the FD aquifer in various ways. The presence of quartzite bedrock topography and degree of weathering can affect the hydrodynamic characteristics of the site. One important feature is the brittle nature of the quartzite, which leads to opening of the fractures and thus creates a conducive environment for groundwater development. The open fractures can provide pathways for the aquifer recharge as well as increase the production of the installed wells. The presence of quartzite rocks is another peculiar hydrological feature of the FD aquifers and are delineated on ERT profiles. The presence of a thick soil layer and vegetation can hold the rainfall water, providing a conducive condition for the aquifer recharge. Almost all ERT profiles have a top-soil layer, however, its thickness and resistivity range significantly vary in the investigated areas. Like topsoil, the thick saprolite can also be seen on all profiles. This layer has quite variable resistivity values—mainly related to the degree of saturation or presence of high clayey proportions. On some of the profiles, the saprolite (high porosity, low permeability) layer is found to be very thick, which means it can store large volumes of groundwater and allows pumping the water from the underlain weathered zone (high permeability), which will significantly enhance the pumping life of the well. This thicker profile layer is also documented in a study conducted on nearby areas by [5]. Along with the role in groundwater prospecting, these structures of interest have a connection with the landslide hazards of the areas. The extremely heterogeneous geological conditions (with layers of various permeability) lead to the exfiltration of water

stored temporarily in the clayey formation, which may create perched aquifer conditions. Because of this permeability contrast, excessive pore-water pressure may develop, leading to slope instability in the region [22].

Based on the discussion above, the present study was able to highlight how key hydrologic processes are affected by the subsurface structures delineated on ERT cross-sections (e.g., depth to bedrock, weathered bedrock, and the topography of bedrock). As this field-work is based in a tropical Brazilian aquifer, the outcomes will inform current water resource management efforts accomplished by the local and regional authorities.

5. Conclusions and Recommendations

The main goal of the study is to investigate the hydrogeological characteristics of the aquifer sub-system-R3/Q3 of the Federal District of Brazil to improve groundwater extraction and pumping-well planning with the aid of ERT geophysical method. The study delineates the key hydrological drivers that modulate subsurface water storage and regulate groundwater development in the subsurface, which influences the hydrology in many ways. These include saprolite, fractured and fresh bedrocks, and their depths and topographies. On the inverted resistivity tomographs, site stratigraphy and other numerous structures are delineated, which have a direct influence on the hydrodynamics of the aquifer.

This study is significant because it provides a description of the aquifer sub-system of the area based on ERT profiles. The approach provides a promising framework for investigating and extracting groundwater in regions underlain by quartzite hard rock aquifers. Overall, the study strengthens the idea that geophysical methods can aid groundwater exploration in challenging geological settings. Therefore, this approach is recommended to be carried out on similar quartzite aquifers, which would ensure that the use of ERT inverted resistivity profiles accompanied with the geological information optimizes both position and productions of pumping wells. As this field-work is based in a tropical Brazilian aquifer, the outcomes will inform current water resource management efforts accomplished by the local and regional authorities.

In addition to groundwater prospecting, the use of ERT method also allowed us to identify geological structures and permeability contrast in connection with the landslide hazards of the area, which presents a further strength of our approach. For future work, coupled numerical modelling informed by geophysical, geological, hydrological, and meteorological data should be considered for a more accurate estimation of wells' production combined with landslide stability assessment.

Author Contributions: Conceptualization, Y.H. and J.E.G.C.; methodology, Y.H. and J.E.G.C.; software, W.R.B., Y.H. and R.E.S.U.; validation; (field) investigation, J.E.G.C.; writing—original draft preparation, Y.H.; writing—review Y.H. and O.H.; editing, O.H. and H.-B.H. All authors have read and agreed to the published version of the manuscript.

Funding: This research received no external funding.

Institutional Review Board Statement: Not applicable.

Informed Consent Statement: Not applicable.

Data Availability Statement: Data are available on request to the corresponding author.

Acknowledgments: The authors are most grateful to the University of Brasilia-UnB and Regulatory Agency for Water, Energy, and Basic Sanitation of the Federal District of Brazil (ADASA) for providing the resistivity data and other related information. The authors would like to thank the two anonymous reviewers and the editor for their constructive comments, which helped us to improve the manuscript.

Conflicts of Interest: The authors declare no conflict of interest.

References

1. Lorz, C.; Abbt-Braun, G.; Bakker, F.; Borges, P.; Börnick, H.; Fortes, L.; Frimmel, F.H.; Gaffron, A.; Hebben, N.; Höfer, R.; et al. Challenges of an integrated water resource management for the Distrito Federal, Western Central Brazil: Climate, land-use and water resources. *Environ. Earth Sci.* **2012**, *65*, 1575–1586. [CrossRef]
2. Nunes, L.M.G.; Lucena, L.R.F.D.; Silva, C.C.N.D. Reserve evaluation of a fault-conditioned aquifer: The Barreiras Aquifer in the coastal region of NE Brazil. *Braz. J. Geol.* **2020**, *50*. Available online: https://www.scielo.br/j/bjgeo/a/yyrTjbQSg3W5qkcMzqHfqQC/?lang=en (accessed on 19 September 2021). [CrossRef]
3. ADASA, Avaliação de aquíferos favoráveis para complementação ementação do abastecimento de água no distrito federal e locação de poços tubulares profundos: Profundos regiões atendidas e não atendidas pelo sistema integrado descoberto de—Santa Maria/torto. 2017. Available online: https://www.adasa.df.gov.br/ (accessed on 1 May 2021).
4. Kuznetsov, M.; Viero, A.P.; Sorek, S.; Roisenberg, A.; Ronen, D. Modeling the Flow Pattern at the Fractured Granites in Porto Alegre, Brazil. *Transp. Porous Media* **2014**, *101*, 413–436. [CrossRef]
5. Hussain, Y.; Uagoda, R.; Borges, W.; Susanne, M.; Hamza, O.; Havenith, H.-B. Estimation of total groundwater reserves and delineation of weathered/fault zones for aquifer potential: A case study of Federal District—Brazil. *Open Geosci.* **2021**, *13*, 1–13. [CrossRef]
6. Comte, J.-C.; Cassidy, R.; Nitsche, J.; Ofterdinger, U.; Pilatova, K.; Flynn, R. The typology of Irish hard-rock aquifers based on an integrated hydrogeological and geophysical approach. *Hydrogeol. J.* **2012**, *20*, 1569–1588. [CrossRef]
7. Zhou, Q.Y.; Matsui, H.; Shimada, J. Characterization of the unsaturated zone around a cavity in fractured rocks using electrical resistivity tomography. *J. Hydraul. Res.* **2004**, *42*, 25–31. [CrossRef]
8. Kumar, D.; Rao, V.A.; Sarma, V.S. Hydrogeological and geophysical study for deeper groundwater resource in quartzitic hard rock ridge region from 2D resistivity data. *J. Earth Syst. Sci.* **2014**, *123*, 531–543. [CrossRef]
9. Junaid, M.; Abdullah, R.A.; Saa'Ri, R.; Alel, M.; Ali, W.; Ullah, A. Recognition of boulder in granite deposit using integrated borehole and 2D electrical resistivity imaging for effective mine planning and development. *Bull. Geol. Soc. Malays.* **2019**, *67*, 99–104. [CrossRef]
10. Briški, M.; Stroj, A.; Kosović, I.; Borović, S. Characterization of Aquifers in Metamorphic Rocks by Combined Use of Electrical Resistivity Tomography and Monitoring of Spring Hydrodynamics. *Geosciences* **2020**, *10*, 137. [CrossRef]
11. De Lucena, L.R.F.; de Rosa Filho, E.F.; Hindi, E.C. O CONTROLE ESTRUTURAL NO AQÜÍFERO BARREIRAS—ÁREA DA BACIA DO RIO PIRANGI (RN). *Águas Subterrâneas* **2006**, *20*, 83–98. [CrossRef]
12. Soares, A.P.; Soares, P.C.; Bettú, D.F.; Holtz, M. VARIABILIDADE ESPACIAL NO SISTEMA AQÜÍFERO GUARANI: CONTROLES ESTRUTURAIS E ESTRATIGRÁFICOS. *Águas Subterrâneas* **2007**, *21*. [CrossRef]
13. Rodrigues, M.A.C.; Lucena, L.R.F.; Souza, I.V.F. Preliminary geometric model of the Barreiras Aquifer derived from hydrogeophysics data at the River Catu basin, NE Brazil. In Proceedings of the 12th International Congress of the Brazilian Geophysical Society, Rio de Janeiro, Brazil, 15–18 August 2011.
14. Lucena, L.R.F.; Oliveira, J.G., Jr.; Medeiros, W.E.; Queiroz, M.A. The potential of the Barreiras Aquifer in the lower course of the Doce River, Rio Grande do Norte State, Northeast Brazil—Integration of hydrogeologica land geophysical data. *Braz. J. Geophys.* **2013**, *31*, 43–57. [CrossRef]
15. Burazer, M.; Žitko, V.; Radaković, D.; Parezanović, M. Using geophysical methods to define the attitude and extension of water-bearing strata in the Miocene sediments of the Pannonian Basin. *J. Appl. Geophys.* **2010**, *72*, 242–253. [CrossRef]
16. Díaz, D.; Maksymowicz, A.; Vargas, G.; Vera, E.; Contreras-Reyes, E.; Rebolledo, S. Exploring the shallow structure of the San Ramón thrust fault in Santiago, Chile (~33.5° S), using active seismic and electric methods. *Solid Earth* **2014**, *5*, 837–849. [CrossRef]
17. Zoby, J.L.; Duarte, U. Caracterização hidrogeológica da bacia do Ribeirão Sobradinho-Brasília (DF). *Geologia USP Série Científica* **2001**, *1*, 79–99. [CrossRef]
18. Campos, J.E.G. Hidrogeologia do Distrito Federal: Bases para a gestão dos recursos hídricos subterrâneos. *Braz. J. Geol.* **2004**, *34*, 41–48. [CrossRef]
19. Kotowski, T.; Chudzik, L.; Najman, J. Application of dissolved gases concentration measurements, hydrochemical and isotopic data to determine the circulation conditions and age of groundwater in the Central Sudetes Mts. *J. Hydrol.* **2019**, *569*, 735–752. [CrossRef]
20. Campos, J.E.G.; Bogossian, J.; Carvalho, R.M. Sedimentology of the Psammo-pelitic-carbonate Unit, Paranoá Group, and Sete Lagoas Formation, Bambuí Group: Examples of mixed carbonate-siliciclastic sedimentation in the Proterozoic of the Brasília Fold Belt. *Rev. Bras. Geociências* **2012**, *42*, 513–522. [CrossRef]
21. Gallas, J.D.F.; Taioli, F.; Filho, W.M. Induced polarization, resistivity, and self-potential: A case history of contamination evaluation due to landfill leakage. *Environ. Earth Sci.* **2011**, *63*, 251–261. [CrossRef]
22. Hussain, Y.; Cardenas-Soto, M.; Martino, S.; Moreira, C.; Borges, W.; Hamza, O.; Prado, R.; Uagoda, R.; Rodríguez-Rebolledo, J.; Silva, R.C.; et al. Multiple Geophysical Techniques for Investigation and Monitoring of Sobradinho Landslide, Brazil. *Sustainability* **2019**, *11*, 6672. [CrossRef]
23. Comte, J.-C.; Ofterdinger, U.; Legchenko, A.; Caulfield, J.; Cassidy, R.; González, J.A.M. Catchment-scale heterogeneity of flow and storage properties in a weathered/fractured hard rock aquifer from resistivity and magnetic resonance surveys: Implications for groundwater flow paths and the distribution of residence times. *Geol. Soc. London Spec. Publ.* **2019**, *479*, 35–58. [CrossRef]

24. Cassidy, R.; Comte, J.-C.; Nitsche, J.; Wilson, C.; Flynn, R.; Ofterdinger, U. Combining multi-scale geophysical techniques for robust hydro-structural characterisation in catchments underlain by hard rock in post-glacial regions. *J. Hydrol.* **2014**, *517*, 715–731. [CrossRef]
25. Donohue, S.; McCarthy, V.; Rafferty, P.; Orr, A.; Flynn, R. Geophysical and hydrogeological characterisation of the impacts of on-site wastewater treatment discharge to groundwater in a poorly productive bedrock aquifer. *Sci. Total. Environ.* **2015**, *523*, 109–119. [CrossRef] [PubMed]
26. Orr, A.; Nitsche, J.; Archbold, M.; Deakin, J.; Ofterdinger, U.; Flynn, R. The influence of bedrock hydrogeology on catchment-scale nitrate fate and transport in fractured aquifers. *Sci. Total. Environ.* **2016**, *569–570*, 1040–1052. [CrossRef]
27. Alle, I.C.; Descloitres, M.; Vouillamoz, J.-M.; Yalo, N.; Lawson, F.M.A.; Adihou, A.C. Why 1D electrical resistivity techniques can result in inaccurate siting of boreholes in hard rock aquifers and why electrical resistivity tomography must be preferred: The example of Benin, West Africa. *J. Afr. Earth Sci.* **2018**, *139*, 341–353. [CrossRef]
28. Noorellimia, M.T.; Aimrun, W.; Azwan, M.M.Z.; Abdullah, A.F. Geoelectrical parameters for the estimation of hydrogeological properties. *Arab. J. Geosci.* **2019**, *12*, 62. [CrossRef]
29. Lee, S.C.H.; Noh, K.A.M.; Zakariah, M.N.A. High-resolution electrical resistivity tomography and seismic refraction for groundwater exploration in fracture hard rocks: A case study in Kanthan, Perak, Malaysia. *J. Asian Earth Sci.* **2021**, *218*, 104880. [CrossRef]
30. Pires, C.A.; Athayde, G.B.; de Souza Filho, O.A.; Ofterdinger, U. Litho-structural conditioning in the exploration of fractured aquifers: A case study in the Crystalline Basement Aquifer System of Brazil. *Hydrogeol. J.* **2021**, *29*, 1657–1678. [CrossRef]
31. Lachassagne, P.; Wyns, R.; Dewandel, B. The fracture permeability of Hard Rock Aquifers is due neither to tectonics, nor to unloading, but to weathering processes. *Terra Nova* **2011**, *23*, 145–161. [CrossRef]
32. Kumar, D. Efficacy of electrical resistivity tomography technique in mapping shallow subsurface anomaly. *J. Geol. Soc. India* **2012**, *80*, 304–307. [CrossRef]
33. Zuber, A.; Motyka, J. Hydraulic parameters and solute velocities in triple-porosity karstic-fissured-porous carbonate aquifers: Case studies in southern Poland. *Environ. Geol.* **1998**, *34*, 243–250. [CrossRef]
34. Motyka, J. A conceptual model of hydraulic networks in carbonate rocks, illustrated by examples from Poland. *Hydrogeol. J.* **1998**, *6*, 469–482. [CrossRef]
35. Pilli, A.; Sapigni, M.; Zuppi, G.M. Karstic and alluvial aquifers: Conceptual model for the plain—Prealps system (northeastern Italy). *J. of Hydrolo.* **2012**, *464–465*, 94–106. [CrossRef]
36. Adabanija, M.A.; Kolawole, L.L.; Afolabi, A.O.; Osinowo, O.O. Investigating aquifer structure in a low-latitude crystalline basement complex of southwestern Nigeria using radial vertical electrical sounding. *Arab. J. Geosci.* **2021**, *14*, 1–14. [CrossRef]
37. Perrin, J.; Ahmed, S.; Hunkeler, D. The effects of geological heterogeneities and piezometric fluctuations on groundwater flow and chemistry in a hard-rock aquifer, southern India. *Hydrogeol. J.* **2011**, *19*, 1189–1201. [CrossRef]
38. Pedrazas, M.A.; Hahm, W.J.; Dralle, D.; Nelson, M.D.; Breunig, R.E.; Fauria, K.E.; Bryk, A.B.; Dietrich, W.E.; Rempe, D.M. The relationship between topography, bedrock weathering, and water storage across a sequence of ridges and valleys. *J. Geophys. Res. Earth Surf.* **2021**, *126*, 217. [CrossRef]
39. Kouamé, I.K.; Douagui, A.G.; Bouatrin, D.K.; Kouadio, S.K.A.; Savané, I. Assessing the hydrodynamic properties of the fissured layer of granitoid aquifers in the Tchologo Region (Northern Côte d'Ivoire). *Heliyon* **2021**, *7*, 07620. [CrossRef]
40. Place, J.; Géraud, Y.; Diraison, M.; Herquel, G.; Edel, J.B.; Bano, M.; Le Garzic, E.; Walter, B. Structural control of weathering processes within exhumed granitoids: Compartmentalisation of geophysical properties by faults and fractures. *J. Struct. Geol.* **2016**, *84*, 102–119. [CrossRef]
41. Figueroa, R.; Viguier, B.; Taucare, M.; Yáñez, G.; Arancibia, G.; Sanhueza, J.; Daniele, L. Deciphering groundwater flow-paths in fault-controlled semiarid mountain front zones (Central Chile). *Sci. Total. Environ.* **2021**, *771*, 145456. [CrossRef]

Geophysical for granitic joint patern and subsurface hydrology related to slope instability

Ana Camila da Silva[a]; Isabela Resende[b]; Rodrigo Cintra da Costa[c]; Rogério Uagoda[d]; André Avelar[e]

[a] *Researcher associated with LIEG/ Department of Geography - Federal University of Rio de Janeiro. Av. Athos da Silveira Ramos, 274 - Cidade Universitária - Ilha do Fundão, Rio de Janeiro - RJ, 21941-916, Brazil.*

[b] *Bachelor in Geophysics from the University of Brasilia. Campus Universitário Darcy Ribeiro Universidade de Brasília- UnB Departamento de Geografia GEA ICC Norte 900 - Brasília, DF, Brazil.*

[c] *NUPEM/IGEO - Federal University of Rio de Janeiro.*

[d] *Department of Geography, University of Brasilia. Campus Universitário Darcy Ribeiro Universidade de Brasília- UnB Departamento de Geografia GEA ICC Norte 900 - Brasília, DF, Brazil.*

[e] *Department of Geography, Federal University of Rio de Janeiro. Av. Athos da Silveira Ramos, 274 - Cidade Universitária - Ilha do Fundão, Rio de Janeiro - RJ, 21941-916, Brazil.*

Abstract: The groundwater flow in fractured rock is an important process that allows to understand the hydrological dynamics at hillslope scales as well the increase of pore pressure at specific points in the soil-rock contact. Exfiltration from bedrock fractures on the failure surfaces and stability problems related to structural characteristics of rocks are common in the highland region of Rio de Janeiro, which were identified in a landslide scar resulting from a translational shallow landslide at the soil-bedrock interface triggered by the extreme rainfall events in January 2011. Considering the temporary springs from bedrock fractures in fresh landslide scars this research aims to analyze, through Ground Penetration Radar (GPR), the structure of the rock and the pattern of fractures in subsurface to understandand the hole the existence of a network of fractures in the slope hydrogeological dynamics and possible consequences for its stability. GPR results proved the existence of fissural suspended aquifers near the surface and sub-vertical tectonic fractures acting as geological barriers that create saturation zones inducing the formation of suspended discontinuous aquifers. It is possible that the fracture systems are determinant for the deflagration of mass movement in the region, mainly of translational shallow types, on slopes covered by saprolites overlying fractured rocks.

Keywords

fractured rock; landslide; GPR; slope stability

1. Introduction

The groundwater flow in fractured rock has been documented as an important process to understand the hydrological dynamics at hillslope scales (Haught and Tromp-van Meerveld, 2011). The formation of this flow is conditioned by the existence of a network of fractures, its connectivity and geometric characteristics (Gabrielli et al., 2012; Banks et al., 2009), acting as drainage of water infiltrated from the soil type (Van Asch et al., 1999; Montgomery et al., 1997), as well as for the increase of pore pressure at specific points on the slope (Gabrielli et al., 2012 and Brönnimann et al., 2013). The difference in permeability between lithologies or the non-connectivity of fractures form a barrier to infiltrated water which can accumulate and be stored temporarily, forming what we call a fissural suspended aquifer or a compartmentalized aquifers that, together with the occurrence of intense rainfall events, antecedent humidity and saturation of fracture rocks, drain the flow in an upward movement towards the overlying colluvium layer resulting in landslides (Montgomery et al., 1997; Montgomery et al., 2002; Dietrich et al., 2005; Matsushi and Matsukura, 2007; Brönnimann et al., 2013).

Prolonged and high-intensity precipitation are considered the main deflator of landslides in Brazil (Coelho Netto et al., 1999; Futai, 2014). These are concentrated in the mountainous regions that extend through the southeastern and southern regions of the Brazilian coast, especially in the Serra do Mar complex. The mountainous region of Rio de Janeiro state (RJ) registered in 2011 an accumulated rainfall volume, in almost 10 hours, close to the expected for the whole month, reaching 325mm in 48h (Coelho Netto et al., 2013). This event triggered approximately 3,600 landslides and as a consequence more than 1,000 people were killed, as well as severe damage to the rural and urban infrastructure of the municipalities of the region (Avelar et al., 2013; Coelho Netto et al., 2013). Although other characteristic events have already occurred in the RJ state (Lacerda, 1997, 2007), the January 2011 event was recorded as the most destructive natural disaster ever recorded in the Brazil.

Exfiltration from bedrock fractures on the failure surfaces and stability problems related to structural characteristics of rocks are common in the highland region of RJ (Avelar and Vinagre, 2009; Ehrlich, 2011). Such conditions were identified in a landslide scar resulting from a translational shallow landslide at the soil-bedrock interface triggered by the extreme rainfall events in January 2011.

Although the hydrogeological characteristics of the slope are relevant for the analysis of its stability, subsurface water flows in fractured rocks and in competent rocks researches remain restricted, mainly their behavior in relation to rainfall (e.g. Gabrielli et al., 2012 and Brönnimann et al., 2013). The limitations are usually justified by difficulties in accessing steep and unstable terrain. The analysis of subsurface features through electromagnetic high-resolution geophysical techniques such as the Soil Penetration Radar or GPR allows applicability for various purposes

such as identification and spatial distribution of lithologies and fractures, aquifers and groundwater in geological studies (Idi e Kamarudin, 2012), mechanisms of slope failure and containment investigating (Batayneh et al., 2014) and in archaeological investigations (Bonomo et al., 2009). It is common in Brazil to apply the GPR for ornamental rock (granite) mining purposes (Porsani et al., 2006); the identification of dissolution structures in carbonate rocks and caves (Botelho and Mufti, 1998), fractures in granite bodies (Souza Jr. and Porsani, 2002); and analysis of slopes stability, slopes rupture mechanisms and water table (Aranha et al., 2006; Silva, 2014).

Considering that temporary springs issuing from bedrock in fresh landslide scars are major indicators of flow through bedrock fractures (Johnson and Sitar, 1990; Calcaterra and Santo, 2004), this research aims to analyze through GPR the structure of the rock and the pattern of fractures in subsurface to help in understanding of the hydrogeological dynamics and the possible consequences for slopes stability, regarding geology, in the region.

The investigations start from the hypothesis that there is a shallow groundwater flow in fractured bedrock, being this flow associated to the exfiltration in the soil-rock contact in the investigated scar which contributed to the loss of stability and consequent rupture. In this way, this research aims to analyze through GPR the structure of the rock and the pattern of fractures in the subsurface to help understand the contribution of geology to the hydrological dynamics of the slope, more specifically, what is the slope fracture pattern and its contribution to subsurface water storage.

2. Methods

2.1 Study site

The landslide scar analyzed (UTM Zone 23K; 745500m W 7531932m S) is the result of a translational shallow landslide in the soil-rock contact caused by the extreme rainfall events of January 2011, in the mountainous region of Rio de Janeiro (Figure 1), which reached 325mm in 48 hours. The scar is located in the municipality of Nova Friburgo, specifically at a drainage head of the Dantas watershed (drainage area of the Paraíba do Sul river), severely affected by the series of catastrophic events, and approximately 1,350m altitude. This municipality is located in the region of the plateau and cliffs of Serra dos Órgãos (reverse of the escarpment of Serra do Mar), characterized, in sum, by funds of narrow valleys that develop along persistent tectonic fractures (Avelar et al. 2013). The annual average rainfall in the region exceeds 2,000mm/year (Coelho Netto et al., 2013), characterizing a very humid climate, conditioned by the physical barrier imposed by relief to the advance of frontal systems (orographic effect).

The landslide exposed a Granite outcrop (Figure 1a), characterized by a fine to medium xenomorphic/hipdiomorphic equigranular textured rock with gray coloration, sometimes pinkish

with a color index around 10-11%. The granite is an isotropic rock with a massive structure without any evidence of ductile deformation analyzed from its 130m extension, along its longitudinal axis and 50m, latitudinally. The outcropping also has a surface dipping approximately 40º to NW, being interpreted as a relief fracture (Avelar et al., 2016).

Water exfiltration points were observed in the scar (Figure 1b) located at the low and middle slope and in isolated points in the middle slope by tectonic fractures (Figure 1c). The tectonic fractures have basically a NE - SE strike line attitudes and high angle at the crest of the scar (Avelar et al., 2016). The weathering material remobilized by the shallow landslide refers to sandy saprolites and rounded blocks (Avelar et al., 2016; Borges, 2017).

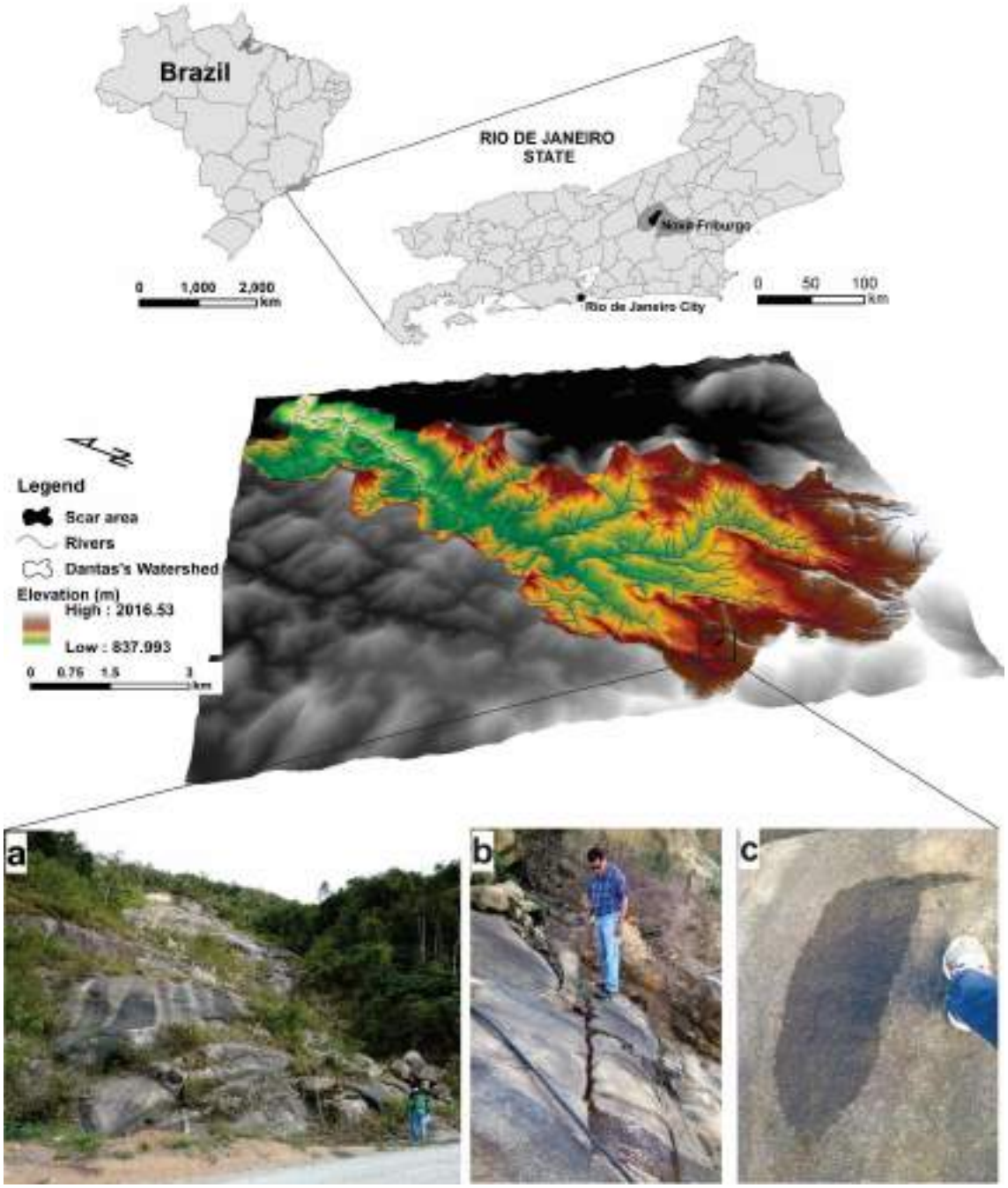

Figure 1: Location of the landslide in the southwestern portion of the Dantas watershed, in a first-order sub-basin at approximately 1,350 meters above sea level. The Dantas watershed is located in the municipality of Nova Friburgo, a mountain region in the state of Rio de Janeiro, approximately 150km from the city of Rio de Janeiro. The landslide exposed a Granite outcrop (a), with water exfiltration points along the fracture in the low and middle slope (b) and in isolated points by tectonic fractures (b).

2.2 *Physical characteristics of the slope*

2.2.1 Landslide scar topographic survey and mapping of fractures

The equipment Total Trimble S3 Autolock and the DGPS Ashtech Promark 2 were used in the topographic survey to generate hypsometric curves with interval of 1m to be used in the interpretation of data referring to the geophysical surveys, slope and topographic profile of the scar. The point demarcations were acquired by point-to-point survey using prism and surface scanning.

The mapping of fractures in the scar was elaborated simultaneously to the topographic survey and had as an intention to spatialize the most relevant fractures. Two points were marked for each of the most expressive fractures found along the surface of the outcrop, delimiting the beginning and end of the fractures, whenever it was possible to travel through the scar. Areas with water exfiltration were avoided because they were considered unsafe due to the slope of the terrain. Thus, approximations were made regarding their position, since they are less than 1m. The products generated by the mapping served as a basis for interpretation of the geophysical data, comparing with previous geological mapping performed in the Dantas watershed (Avelar et al., 2016).

2.2.2 Scar geophysics by Ground Penetrating Radar technique (GPR)

The acquisition of GPR scanning in the study area was done using the GSSI SIR 3000 equipment, coupled to a 400 MHz antenna. The basic acquisition parameters were the same for all profiles, except for the temporal window (range). The opening time of the time window is directly proportional to the depth of the scanning material and consequently the amount of data to be recorded (Daniels, 2004).

The depths reached were between 6 - 7.5m. The field parameters used in the GPR system were 1024 samples per trace and time window of 100ns (nanosecond). Three scans were performed for each of the three profiles traced on the scar investigated. All the acquisitions were made through reflection profiles with constant offset. The profiles were performed in continuous

mode, where the antennas are dragged over the surface under analysis. A string was used as a guide in the direction of the profile scan to be traversed.

The profiles traced on the scar were spatially located in the high and middle slope and near the crest of the scar. This area was purposely chosen to be free of rocky blocks which are deposited over the middle and low slope. The orientation, mean altitude, distance traveled and spatial location of the profiles are given in Table 1.

Profile	Orientation	Mean Altitude (m)	length
L1	Longitudinal	1.386	10 m
L2	Longitudinal	1.355	12 m
L3	Latitudinal	1.362	21 m

Table 1: Guidance, mean altitude and distance traveled for each GPR profile.

The data were processed in ReflexW Software, version 7.5 (Sandmeier, 2014). The raw data processing routine (figure 2) were made as a variation of the approach proposed by Xavier & Medeiros (2006), including: Static Correction for the Time-Zero adjustment; 1D Filter (Dewow), to the amplitude desaturation and to remove the noise related to electromagnetic induction (electronic noise), with a pulse period of 2.5ns (figure 2a); Gain filter (Energy Decay), to emphasize low amplitude ranges (figure 2b); Expectral Balance, to correct the attenuation caused by propagation effects (figure 2c); 1D filter (Bandpass Frequency), to remove random noises, mainly of high frequency with the cutting intervals of 93.3, 213.8, 575.2, 688 e 715.7 MHz (figure 2d); Migration routine (Diffraction Stack), to promote the diffraction collapse, using 10 traces and 0.1m/ns as the velocity (figure 2e); Time-Depth conversion (figure 2f); and, Static Correction, to insert topography on the resulting radargrams. The average electromagnetic wave velocity of propagation was determined by the method of hyperbolic adjustment, obtaining the velocity of 0.1m/ns, which was used in the conversion of the records from time to depth. The final process allow identifying a penetrative linear discontinuity (fracture) that intersects the surface. The fracteres were drawn in ReflexW with technical interpretation.

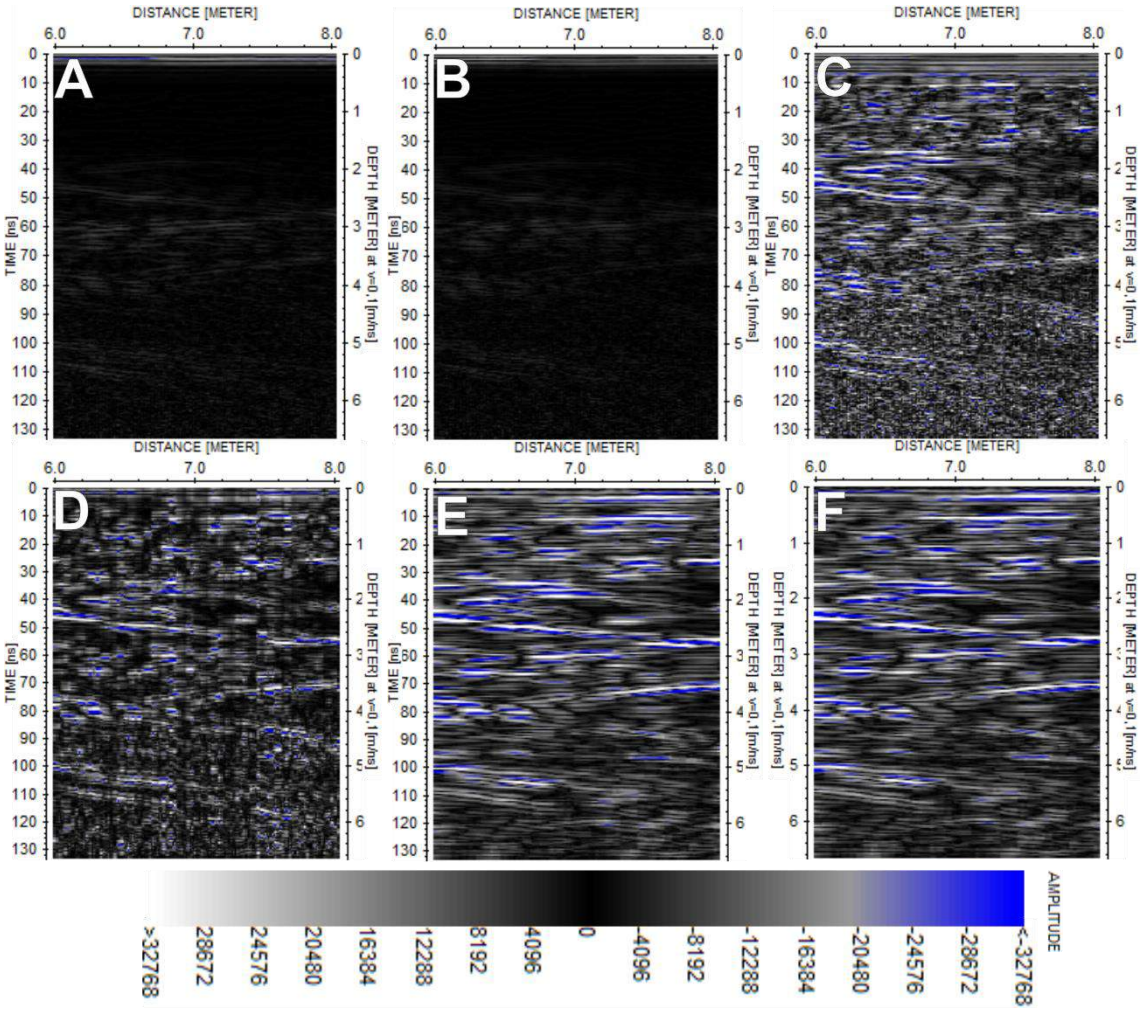

Figure 2: Process Work-Flow of the radargrams after Time-Zero adjustment and before Static Correction, with: a) Dewon; b) Energy Decay; c) Spectral Whitening; d) Bandpass Frequency; e) Diffraction Stack; and, f) Time-Depth Convertion.

2.2.3 Rotary drilling and rock structure description

The rotary drilling was performed to obtain two holes (SR01 and SR02) with 6m depth each for the installation of two wells and two piezometers. Rock samples were used to improve slope lithological interpretation, analysis of rock properties, qualitative characterization of rock and reconstruction of wells (in 2D profiles).

The rock samples were classified according to the percentage of recovery, degree of alteration and fracture using the standard ABNT NBR 6502. The Rock Quality Designation (RQD) parameter was classified according Deere (1989). In general, the degree of rock alteration allows the identification of the weathering stage considering the modification of mineral constituents. The degree of fracture of the rock is determined by the simple counting of fractures along a certain direction, using the number of fractures per meter in rock samples or counted directly on the surface of rock outcrops, discarding the fractures created by the drilling process.

In addition to the RQD classification, from the analysis of the degree of rock alteration and fracture, the samples were analyzed for discontinuity conditions (inclination, alteration and filling by other minerals). The depth of each fracture in the samples was recorded to determine their spatial position in the mass for making two-dimensional sketches. Since the rotary drilling rock samples were not performed according to a predefined orientation, the information about sub-vertical and sub-horizontal fractures position was shown in the sketches in an illustrative way.

3. Results and discussion

3.1 Topographic parameters and their implications on slope subsurface hydrology

The topographic map of the scar (Figure 3) shows that the altimetry range is 95m, being at 1.395m high point (crest of the slide scar) and 1.310m at the lowest point of the area studied (intersection with the road). Slope topographic profile (Figure 3b) shows that at the base, between the heights 1.320 and 1.340, the blocks mobilized by the landsliding are concentrated. Upstream, between 1.350 and 1.360, three points of water exfiltration by fractures in the rock were observed. Between the heights 1.310 and 1.320m, two tectonic fractures drain the water from the slope (also observed in Figure 1b-c).

With a 27.9° of declivity, the slope is characterized as strong undulated (Embrapa, 1979), being part of the group of hillsides with angles above 25° which can present gravitational movements faster than those with inferior angles. The slope analyzed is also included into the group of 52% of the scars mapped in the Córrego Dantas watershed after event of 2011 January, that occurred predominantly between slopes of 20º and 35º of declivity (Lima et al., 2014).

The most common types of landslides triggered by extreme rainfall events in January 2011 in the Córrego Dantas watershed were, according to Avelar et al. (2013), the shallow translational type, generally occur on steep slopes and often triggered by extreme rain (Dhakal and Sidle, 2004; Sidle et al., 2001; Iverson, 2000). Fernandes et al. (2001) also attest to the influence of declivity on landslides conditioning, suggesting critical limits through mathematical models which the increase of slope declivity angle leads to a potential increase in the occurrence of landslides. On the other hand, Palma et al. (2013) concludes that more than 90% of the 244 scars mapped in the Córrego Dantas watershed occurred in slopes below 45°, usually associated with the non-development of thick soils at slopes greater than 45°.

In this way, the use of slope declivity as the main or even only topographic parameter incorporated into the prediction and definition studies of unstable areas often generates distortions in the analysis of landslides susceptibility. In another hand, areas of lower slope, initially defined as low susceptibility, show in a certain frequency, the presence of landslides (Fernandes et al., 2001; Guimarães et al., 2008).

Besides the topographic factor, other geological-geomorphological conditions of the slope create the ideal condition to raise its instability. Judging by the literary consensus, straight or convex slopes in plants have infiltration rates balanced by the amount of water withdrawn from the interior by subsurface flows, not allowing excessive pore-positive pressure increase. The slopes of concave forms in plan and profile, as the study area is characterized, the water flows are directed to the interior of the concavity, favoring conditions of soil saturation, loss of cohesion and effective stresses, which become responsible by the generation of landslides (Avellar and Coelho Netto, 1992, among others).

It is also observed that the product of weathering on the slope, shallow saprolite with gray color, is low weathered and loamy-sandy (Avelar et al., 2016; Borges, 2017), with high infiltration rates in the first centimeters of the soil, analyzed on the slope by Borges (2017). The high infiltration rates are associated to the 30cm most active of the soil, depth where 90% of the root biomass is composed generally by grasses and herbaceous, in area of forests in succession stage (Genet et al., 2010). In the case of root architecture, the concentration of water flows and the increase of positive pore-presure are considered unfavorable to slope stability, especially when they occur on potential rupture surfaces (Ghestem et al., 2011).

In addition, as indicated by Marques (2016), analyzes of soil suction in secondary forest area in the Rio Grande basin, adjacent to the Córrego Dantas basin, show that rains above 40mm are responsible for the advance of the front wetting and maintenance of high soil moisture in depth. In extreme events, 100mm in 48h, the humidity remains in depth for approximately 11 days (Marques, 2016). The author also confirms that the maintenance of soil moisture and saturation in depth is directly associated to the thick tree roots and the ducts formed after their decomposition, concluding that grass roots, concentrated at the top of the soil, are responsible for the predominance of vertical flows. In forest area, where the roots reach up to 200cm in the soil, they are responsible for the predominance of lateral flows. In this way, from the results of Marques (2016) and Borges (2017), we can suggest the formation of lateral preferential paths in depth, or in the soil-rock contact on the slope, formed mainly by root activity, as pointed out by Uchida et al. (1999) and McDonnell et al. (2007). The existence of subsurface flows on the hillside suggests the high occurrence of landslides in secondary forest and grassland coverages in the extreme rain event in January 2011 in the mountainous region of Rio de Janeiro and specifically in the Córrego Dantas watershed.

The conditions of antecedent humidity have a strong influence on the probability of occurrence of landslides and when higher the rainfall intensities are, the higher the hazard level could be, especially when we attribute the low saprolite capacity to transmit water. In the region, the hydrological conductivity of the saprolites at different depths (2.4 to 14m) defined values of 10^{-5} cm/s for k_{sat} (Machado, 2016; Silva, 2014), considered as low to very low according to the classification of Klute and Dirksen (1986). The granulometric characteristics of saprolite

reinforce its greater permeability in the first centimeters of the soil, as verified in Borges (2017). While the permeability results characterized it as poorly permeable in depth, as suggested by Machado (2016) and Silva (2014). The decrease of the permeability with the increase of the depth, or due to the proximity with the contact of soil-rock was already supposed by Avelar and Coelho Neto (1992). So, the slope geomorphological conditions, which defined the instability of the slope and landslide triggering, would be related to the formation of a water table with an increase of pore pressures and consequently reduction of the effective stresses at the soil-rock interface.

The same behavior was observed by Brönnimann et al. (2013), in the subalpine region of central Switzerland (Rufiberg). The authors verified that soils low permeability in the contact with the rock forms a suspended water table with confined aquifer pressure conditions. Lacerda (1999) affirms that, in the mountain region of Rio de Janeiro, the formation of suspended water table with confined aquifer pressure conditions is associated with the presence of dikes that act as an obstacle to subsurface flow generating a potential rupture surface. Lanni et al. (2013) adds that rock microtopography and the presence of rock depressions play a key role in slope stability by inducing increased pore pressure in localized areas. These areas would be responsible for the rapid transition from stable to unstable conditions on the slope, generally observed for unpredictable and shallow landslides phenomena.

As for shear strength, shallow gray-colored saprolites were characterized as more resistant when compared to lateritic soils in the region, which is observed on slopes and valley bottoms classified as sandy clay or clayey sand (Machado, 2016; Avelar et al., 2016). In contrast, when introduced to complete submersion in laboratory simulations, they completely disaggregate, indicating zero effective cohesion (Lacerda, 2014; Avelar et al., 2013). The result of complete disaggregation behavior can be applied to submersion conditions of saprolite in the slope when the formation of suspended water table.

The precipitation conditions in January 2011, plus slope geomorphological characteristics and to the shear and hydraulic behavior of the soils, it is possible to consider that these components were sufficient for the sudden increase of pore-pressure. The fractured rock mass plays an active role in creating these saturation points in the saprolite when water exfiltration due to fractures occur, as is the case in the research area, to be analyzed below.

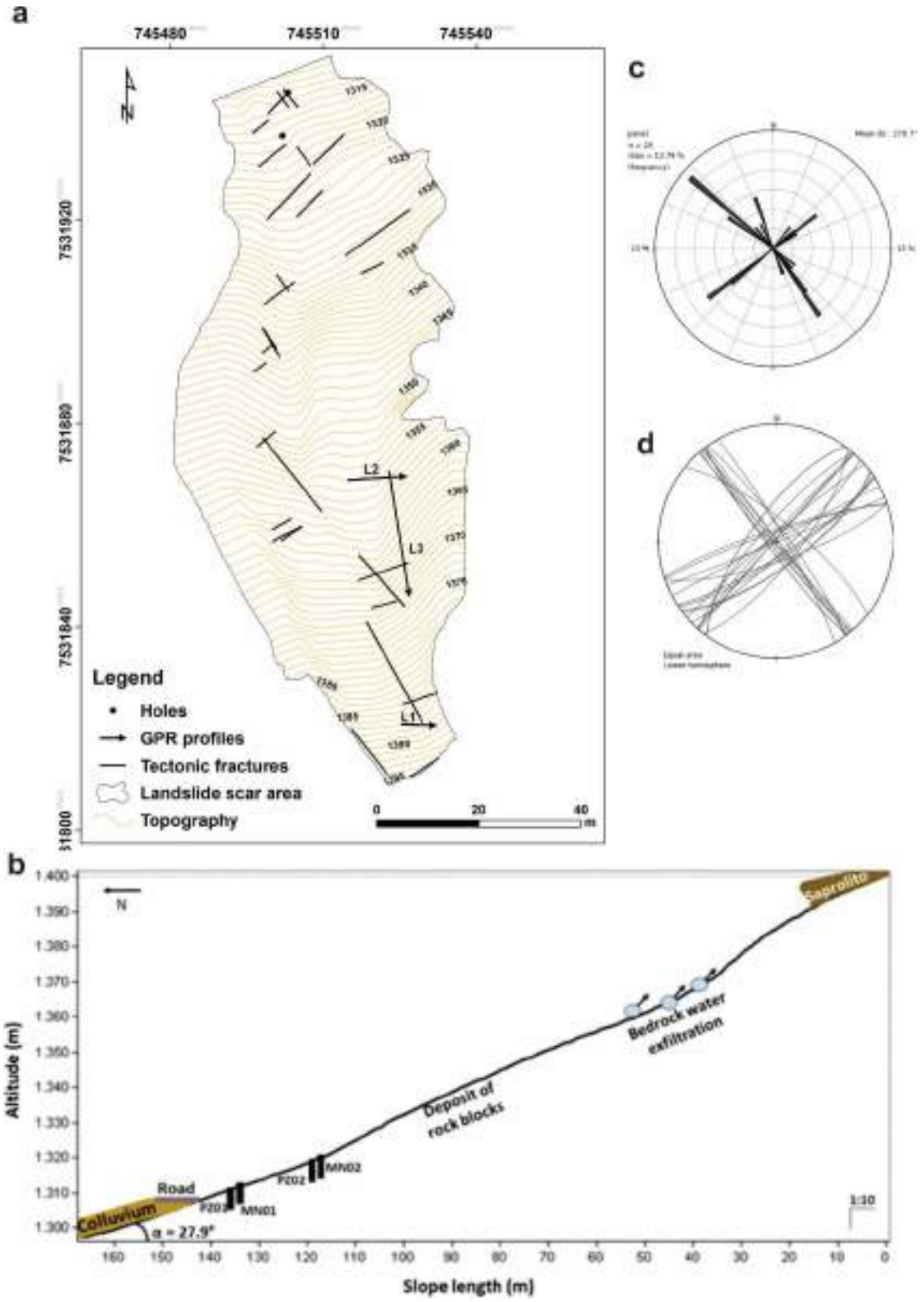

Figure 3: Landslide scar topographic survey and mapping of fractures. Topographic base of the scar with 1 m distant level curves. The black arrows show the spatial distribution of GPR profiles in the landslide and the scan direction when profiles were executed (a); Slope topographic profile with wells spatialization, bedrock water exfiltration points by fractures, deposit of rock blocks and angle of the slope (b); The stereogram (c) and rosette chart (d) shows the orientation of the fractures in the outcrop exposed by the landslide.

3.2 Rock fracture systems

Fracture orientations generally point to the existence of two distinct families of tectonic fractures. Their structural dips were usually SW, with angles between 70 and 80 degrees, and NW, between 70 and 90 degrees. The exposed by the landslide is characterized as a relief fracture which is part of NW fracture orientation (Figure 3c, d).

The dominant fracture strike observed in landslide scar is SW, which is the same for most other fractures mapped in Dantas river basin, which has its SW-NE longitudinal axis. The mapping of fractures results affirms the previous survey prepared by Avelar et al. (2016) for Dantas river basin. However, the authors identified, in addition to the SW and NW dominant strike fracture families, a third family of tectonic fractures with NW strike. Avelar et al. (2016) had 45 fractures as sample, having their attitudes measured through the tracing of circles in mesh by the scar. The higher number of fractures sampled justified the higher number of fracture families. The 29 fractures sampled in the study landslide scar were characterized by being the largest located in the outcrop and were mapped to be specialized, serving as support for the interpretations of the GPR scans.

3.2.1 Rotary drilling samples of rock analysis

The SR01 (Figure 4) and SR02 (Figure 5) rotary drilling holes' samples were organized by rock cuttings to facilitate the interpretation and visualization of fractures, cracks and fragments. For our purposes crack is a break (a brittle discontinuity) where the sides pull apart as the crack opens which forms a movement. These can be massive (the boundaries between the tectonic plates themselves) or very small. Fractures are simply cracks in the crust where there is no movement. A profile was elaborated for each hole to interpret the spatial distribution of fractures results, respecting in scale the dimensions (height and length, in cm) for each cutting. However, the profile of the hole does not accurately indicate the orientation and angulation of the fractures.

The first SR01 hole cutting had the lowest recovery percentage, with the quality of the rock classified as 57% RQD (Table 2). We also identified 1 sub-horizontal not expressive fracture. However, the rock has signs of incipient alteration of the primary minerals and slightly discolored but maintaining the same physical and mechanical properties of the basement, which characterizes it as few altered. In the second and third SR01 hole cutting, it is possible to observe a high angle fracture and a subvertical fracture (specifically in the second fragment of the third cutting, with greater color change). These rock sample also presents color change, more evident in the subvertical fracture, of darker coloration.

From the 4th cutting onwards, from 220 to 595cm, the number of fractures varied from 3 to 5, characterized in vertical and subvertical. Subvertical fractures and alteration of the color of

the primary minerals were detected, evidencing advanced stages of weathering and consequent water flow. The 4th cutting, specifically, shows the first 5 fragments of rocks resulting from high angle subvertical fracture and color change of minerals. The last fragment of this cutting maintains the coloration of the rock and, like 5th cutting, shows less contact with the water, in wich it is possible to identified 3 closed fractures with slight color change, more present in the second and third fragment.

The sixth and seventh cutting were identified 5 fractures in each one, with emphasis on two parallel vertical fractures. The vertical fracture is filled by chlorite. Insulating tapes were used to join the fragments of the subvertical fractures, facilitating the sample layout to proceed with the analysis. Throughout these two cuttings, the fractures intersect forming numerous fragments of rocks that were releasing with the execution of rotary drilling. The seventh rotary drilling cutting has greater alteration of color and oxidation, mainly along the subvertical fractures.

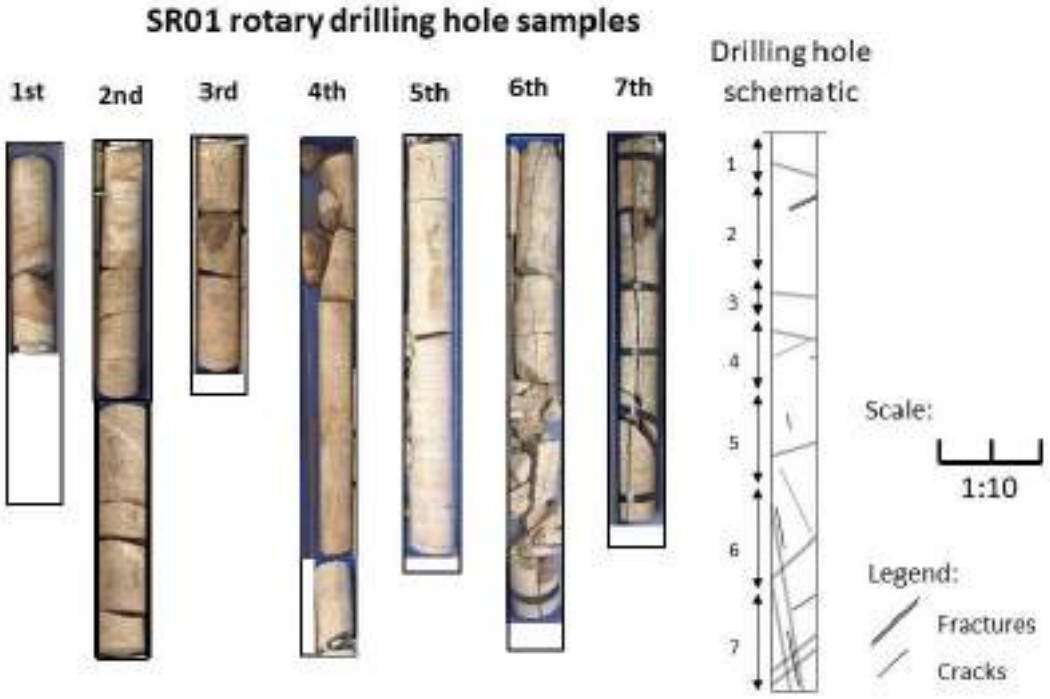

Figure 4: SR01 rotary drilling hole samples separated and organized for cuttings; schematic profile of the spatial distribution of fractures in the rotary drilling hole samples.

Cutting (cm)	Recovery (%)	RQD (%) and quality of rock mass	Number of fractures	Degree of fracture	Degree of rock alteration
1st : 0 – 70	57	57 - Moderate	1	Presence of fractures	with little change
2nd : 70 - 170	100	83 – Good	1	Presence of fractures	no change
3rd : 170 – 220	92	90 – Good	1	Presence of fractures	with little change
4th : 220 – 330	100	97 – Very good	3	Presence of fractures	with little change
5th : 330 - 415	97	97 – Very good	3	Presence of fractures	no change
6th : 415 - 515	95	62 – Moderate	5	Presence of fractures	moderately altered
7th : 515 - 595	95	94 – Very good	5	Presence of fractures	moderately altered

Table 2: SR01 samples analysis by rotary drilling cutting for: number and length of cutting, percentage of recovery by cutting, quality of rock mass, number of fractures, degree of fracture and alteration of rock.

The parameters analyzed in the SR02 rotary drilling hole samples (Figure 5, Table 3) presented characteristics closer to the bedrock, with no major physical and chemical changes in the main minerals. Parts of the rotary drilling cutting samples have minerals with color change along fractures, except for the 5th cutting. The degree of fracture varies from little altered to fractured with a number of fractures lower than that found in samples from SR01 rotary drilling hole samples. The quality of rock mass is predominantly good to very good. The fractures may be classified as high-angle subvertices (1st, 3rd, 4th and 6th cutting) and a sub-horizontal fracture (2nd cutting).

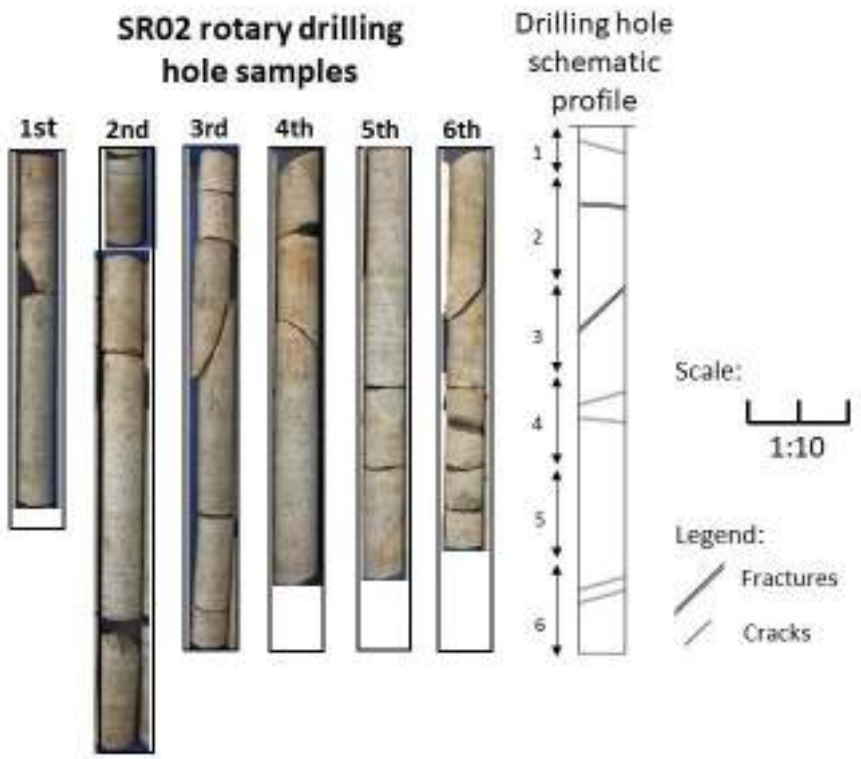

Figure 5: SR02 rotary drilling hole samples separated and organized for cuttings; schematic profile of the spatial distribution of fractures in the rotary drilling hole samples.

Cutting (cm)	Recovery (%)	RQD (%) and quality of rock mass	Number of fractures	Degree of fracture	Degree of rock alteration
1st: 0 – 75	96	94 – Very good	1	Presence of fractures	with little change
2nd: 75 – 195	100	100 – Very good	1	Presence of fractures	with little change
3rd: 195 – 295	100	86 – Bom	1	Presence of fractures	with little change
4th: 295 – 395	87	87 – Good	2	Presence of fractures	with little change
5th: 395 – 495	86	86 – Good	0	Few fractures	no change
6th: 495 – 595	80	50 - Poor	2	Presence of fractures	no change

Table 3: SR02 samples analysis by rotary drilling cutting for: number and length of cutting, percentage of recovery by cutting, quality of rock mass, number of fractures, degree of fracture and alteration of rock

3.3 Geophysical Analysis: Ground Penetration Radar (GPR)

Three reflection patterns were identified in the GPR radargrams, spatially distinguished in the figure 6. The reflection zones in the line of GPR 1 (L1), line 2 (L2) and line 3 (L3) spatially distributed in the landslide scar (Figure 3a) were interpreted according to the local geological mapping, field visits, fracture mapping and analysis of SR01 and SR02 rotary drilling samples. Figure 6 presents the patterns the radargrams presents after the application of the work-flow detailed in figure 2. The first pattern identified in the GPR radargrams is characterized by the absence of reflectance and/or presence of areas with low reflectance and low amplitude, classified as standard A; the second standard classified as B is distinguished by high reflectance, assuming straight and high amplitude forms; the third pattern, C, is characterized by the medium-amplitude reflectance and normally distributed around the A and B patterns, being the pattern that predominates in the three radargrams. Figure 6 also shows the pattern D, where interrupctions in the reflectors or enlargement zones, marqued by the yellow dashed line, presents structural fracures, as it was proposed by Silva et al (2004).

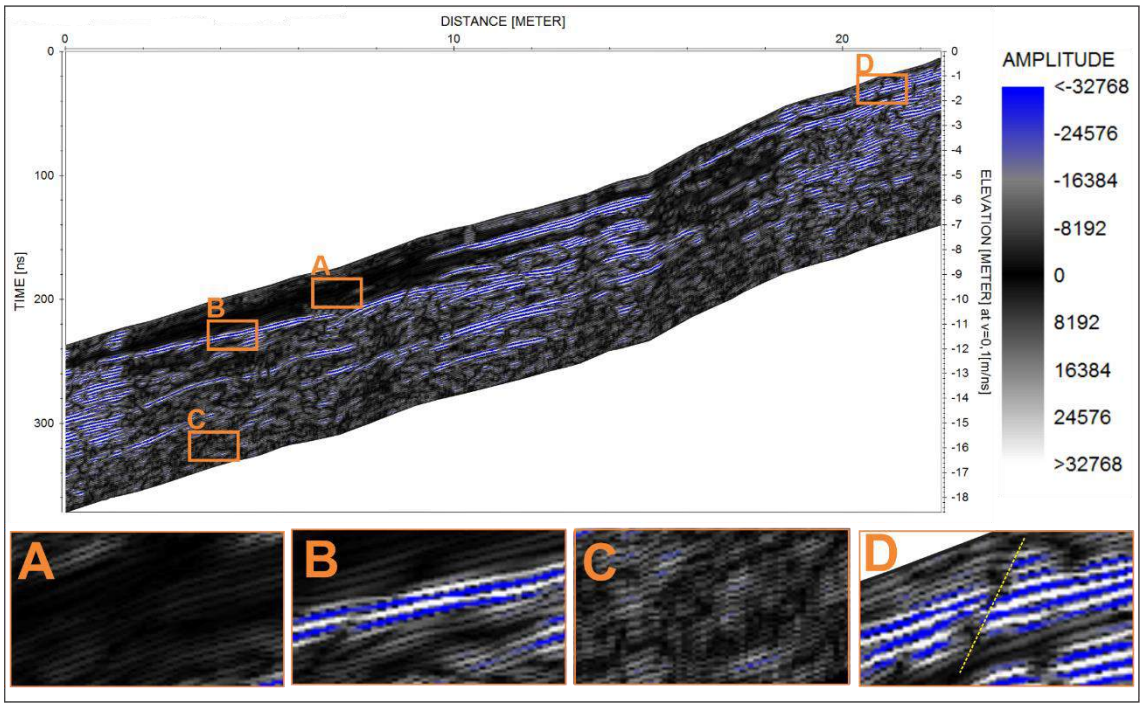

Figure 6: Interpretation of reflectance patterns according to analysis of slope geological characteristics: a) Pattern A, points of water exfiltration; b) Pattern B, showns the relief joints; c) patern C are the medium-amplitude reflectance areas of the rock; d) pattern D, presents the delimitation of tectonic fractures as interruptions in the reflectors.

Areas classified as pattern A were spatially related to water exfiltration points on the rock surface. The water has a very high dielectric constant relative to the rock constant, which makes the electromagnetic signal velocity smaller and more difficult to capture (Benson et al., 1995).

The absence of reflectors, and/or presence of low amplitude reflectors, allowed to associate these patterns as being areas of saturation in the granite and with possible formation of fissural aquifers suspended and compartmentalized by zones of competent rocks (Dietrich et al., 2005). This interpretation is supported by the authors' Montgomery et al. (1997), McDonnell (2003), Tromp-van Meerveld and Weiler (2008) and Gabrielli et al. (2012), in which they affirm that the rocky substratum is not completely impermeable, allowing the water to infiltrate, be driven and stored in the rock by the presence of fracture systems.

The geological mapping performed in the study area by Avelar et al. (2016) and the analysis of samples from rotary drilling indicate the presence of numerous sub-horizontal fractures, with different thicknesses, defined as relief joints. No lithology beyond the granite was identified on the slope, eliminating the possibility of areas characterized by rectilinear reflectors of high amplitude being associated to other types of rocks. Throughout the mapping of fractures and geophysical survey with GPR, loose layers of rock, characteristic of pressure relief, were recorded in the high and medium slope. High-amplitude reflections are also defined by Jol (2009) as fractures in rocks. In this way, the B pattern reflection zones, spatially distributed in L1, L2 and L3 in parallel alignments to the surface were defined as relief joints, or pressure relief fractures, based on the classification criteria suggested by Wyatt and Temples (1996).

As interpreted by Stevens et al. (1995) and Porsani et al. (2006), pressure relief fractures are manifested in the radargrams as interfaces or discontinuities in the dielectric constant of the granite forming zones of strong reflectance and laterally continuous. It is also observed in the radargrams, as observed by Silva et al (2004) that the relief joints are being crossed in depth by subvertical discontinuities or tectonic fractures, some more persistent (in depth) than others. These discontinuities have predominantly straight and relatively continuous tendencies of signal loss, being defined by Wyatt and Temples (1996) and interpreted in the scar as subvertical tectonic fractures.

Medium-amplitude reflectors occupy most of the radargrams and have a more homogeneous appearance in the C pattern. Sometimes, this reflection pattern is interrupted by signal discontinuities interpreted as high-angle sub-vertical tectonic fractures. Like SR02 samples analysis by rotary drilling weel prove, the rock was more homogeneous, less fractured and slightly altered, leading to the interpretation of the C pattern as intact (or not fractured) granite.

3.3.1 GPR profile L1

The pattern A zones of reflection do not appear in L1, representing the non-formation of saturated areas in the granite and the non-formation of fissural aquifers suspended near the crest of the scar. The B pattern reflection zones are spatially distributed in alignments parallel to the surface.

Three relief joints are observed in the L1 radargram (figure 7). The first one, starting at 1387.00m and extending in depth up to the 1384.00m height, between 0 and 7.5m SW-NE direction. The second joint is the largest in length, crossing the entire radargram in the SW-NE direction, it is located from altitude 1384.00m to 1383.00m. The third of greater prominence, is located from 0 to 7m SW-NE direction and between the 1382.00 and 1381.00m. Interpretation showed in Figure 7 can be visited in figures 2 and 5. Both family patterns of tectonic fractures were inferred in figure 7b as yellow lines.

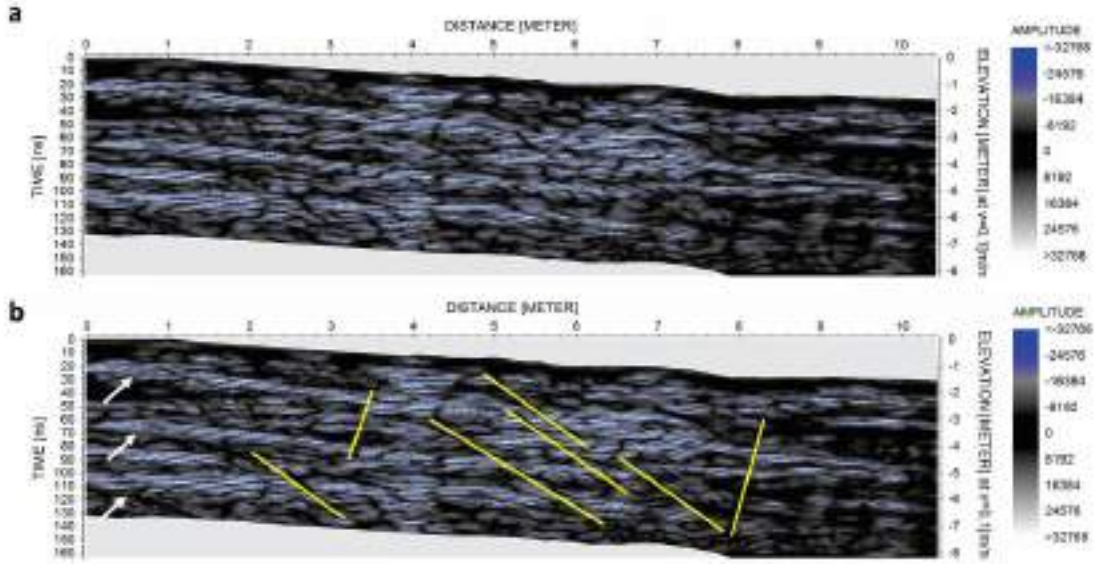

Figure 7: Radargram of L1 (longitudinal profile) executed on the high slope near the crest of the slide scar (a) and its interpretation (b). The white arrows indicate the B pattern classified as relief joints; the yellow lines indicate tectonic fractures, pattern D. The C pattern is normally distributed around the A and B patterns, and it is not highlighted with any symbol. Color should be used in print.

3.3.2 GPR profile L2

As explained in figures 2 and 5, the reflection zones characterized by the A pattern are evident in L2 (located in the middle slope). Two areas with no reflectors were identified and demarcated as fissural aquifers suspended between 6 and 12m east. Other two areas (with low reflection), interpreted as saturated granite (Figure 8 a and b), are located in depth between the heights 1356.00 to 1354.00m and in the first 6m of distance traveled, also east direction.

In the L2 profile a set of relief joints is concentrated in the western portion of the radargram and another one, highlighted, can be observed between 0 and 10m near the surface (between 1356.00 and 1355.00m). There is presence of tectonic fractures with predominance of fractures family which dominant fracture strike observed in the radargram is NE.

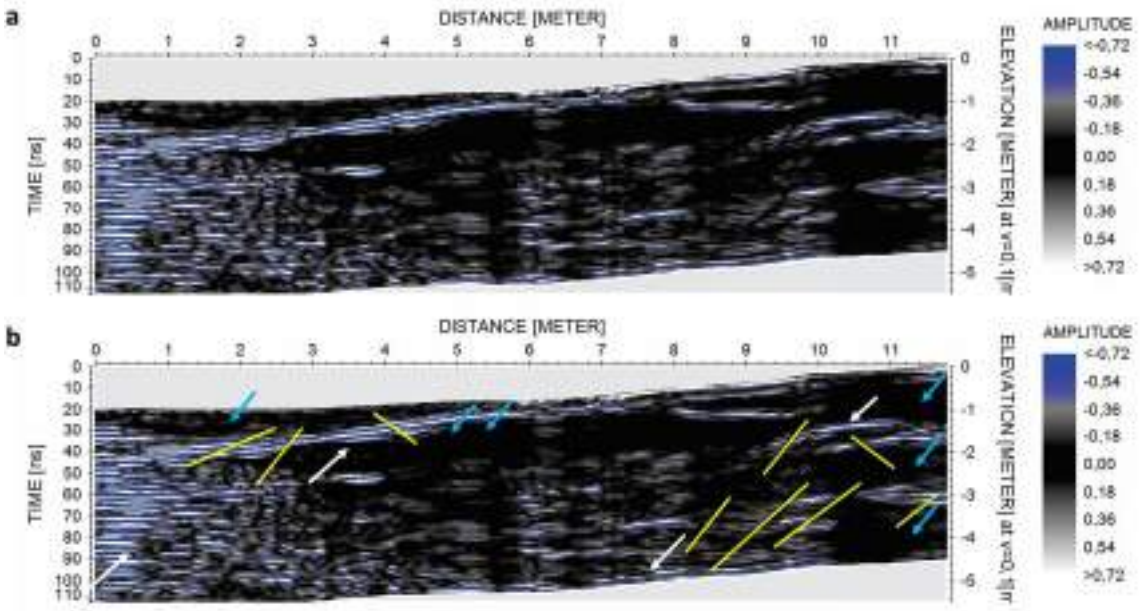

Figure 8: L2 Radargram (longitudinal profile) executed in the middle slope (a) and its interpretation (b). The white arrows indicate the pattern B classified as relief joints; yellow lines indicate tectonic fractures, pattern D; blue arrows indicate the pattern A, classified as saturated areas and possible formation of fissure aquifers. The C pattern is normally distributed around the A and B patterns, and it is not highlighted with any symbol. Color should be used in print.

3.3.3 GPR profile L3

Relief joints appears throughout the radargram in GPR profile L3 (Figure 9 a and b). Many rectilinear fractures are distributed through the GPR image and three of them of great interest for the interpretations in the landslide scar. The first one and closest to the surface, is located between the distances 10m to 15m NW-SE direction, approximately between the 1358.00m and 1360.00m. This most expressive relief joint appears between areas of saturation located at the upper limit of rock surface and just above the largest saturated area (A pattern) characterized as the largest fissural aquifer in radargram L3 (between 0 and 16m SE direction distance and 1362.00 to 1356.00m). Another relief joint is observed just below this suspended aquifer, and consequently would be acting for its compartmentation, located between distances 0m to 16m, approximately, in NW-SE direction, precisely between the heights 1354.00m to 1359.00m. A third relief joint is observed between distances 0m to 16m NW-SE direction and 1347.00m to 1357.00m heights. Fractures of smaller extent are distributed at different depths and parallel to the surface. Three families of tectonic fractures that were mapped on the slope (SE, NW and NE) are represented on GPR profile 3. The key to interpretation figure 9 can be visited in figures 2 and 6.

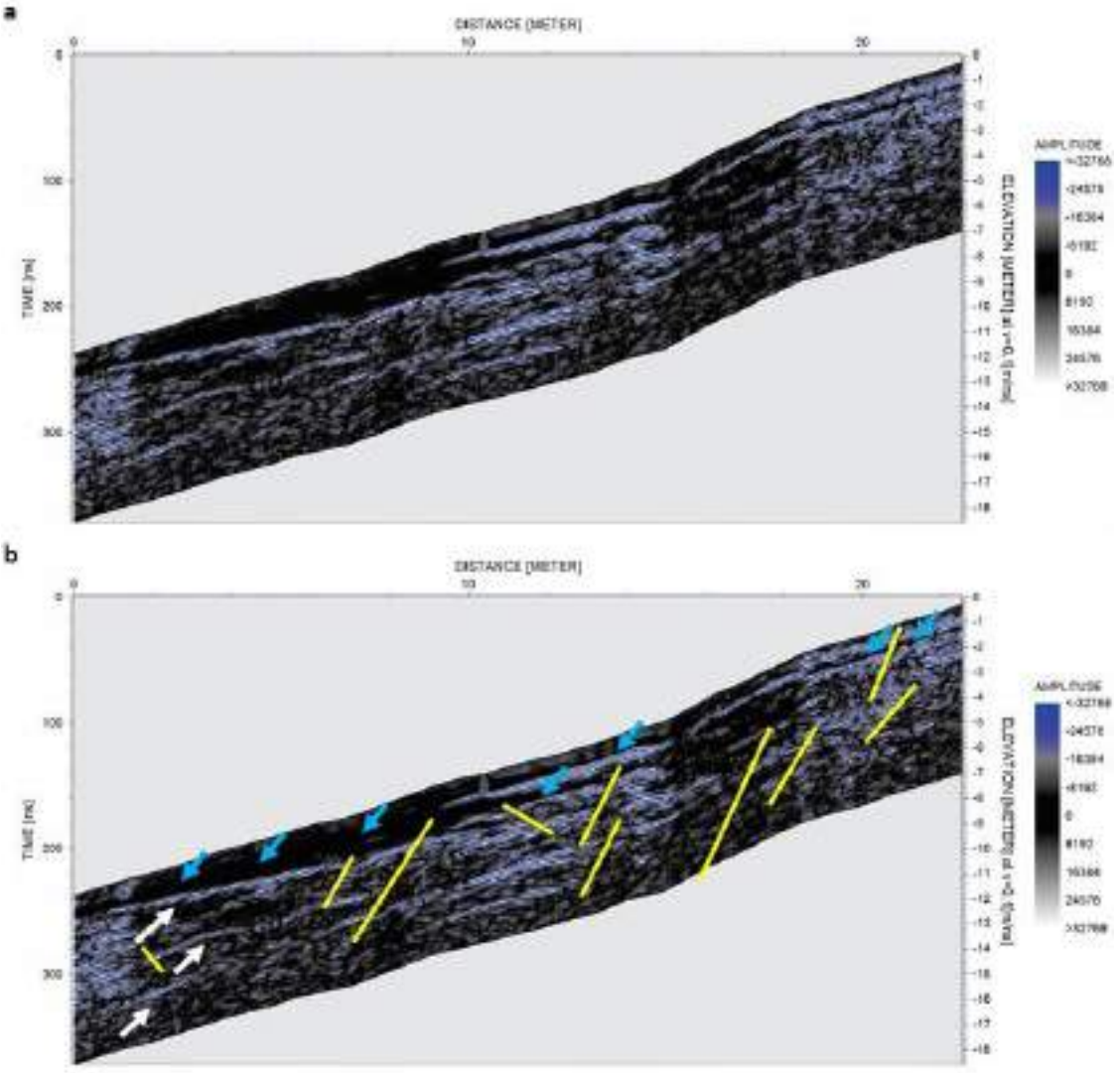

Figure 9: L3 radargram (latitudinal profile) performed in the middle slope (a) and its interpretation (b). The white arrows indicate the pattern B classified as relief joints; yellow lines indicate tectonic fractures, pattern D; blue arrows indicate saturated areas (A pattern). The C pattern is normally distributed around the A and B patterns, and it is not highlighted with any symbol. Color should be used in print.

In general, the wetlands identified in L2 and L3 are formed by hydraulic percolation through relief and tectonic fractures, which behave as a saturated zone, being connected and forming a preferential conductivity system within the rock (Paitan, 2013; Brönnimann et al., 2013). Other indications of the formation of these aquifers are related to the constant exfiltration of water, being more intense in humid periods, mainly in the medium and low slope.

The profile L3 have saturated areas located between parallel subvertical fractures and sound rock of very low hydraulic conductivity. Fractures behave like geological barriers and the contrasts of conductivity can force the water to a return movement by increasing pressure, exfiltrating through fractures to the soil-rock interface (Blöcher et al., 2010). These same conditions of exfiltration by difference in the hydraulic conductivity were identified by

Montgomery et al. (1997), and Montgomery et al. (2002), who point out that local conductivity variations in fractured rocks have a strong influence on positive pore pressure, contributing to the initiation of mass movements in slope sites where soils are thin and do not require a substantial flow to reach their saturation and consequent induction of instability.

The analysis of fractures through mapping, drilling holes' samples and GPR profiles showed that, although considered as little to medium fracture, they are sufficient to transmit and store water in the first meters of the fractured layer of the rock and, consequently, near the surface. The fracture pattern, its geometry and permeability contribute to the dynamics of the hydrological response to rainfall events.

4. Conclusion

The results obtained by analysis of the GPR profiles confirm the existence of many systems of fractures in the granite. The numerous sub-horizontal fractures are also confirmed by the analysis of samples from rotary drilling, which reveals the presence of rock minerals modificated by chemical weathering. The modification of rock minerals confirms the storage and passage of water at different depths of the rock mass.

The GPR profile L2 and L3 proved the existence of fissural suspended aquifers near the surface, in depths of up to 4m. The geometry of relief fractions spatially distributed in layers almost parallel to the surface and the tectonic fractures, in great majority of high angle and perpendicular to the fractures of relief, induce the formation of spatially suspended discontinuous aquifers. These aquifers are formed by the efficient permeability in stress relief fractures, which lead to subsurface infiltrated water. Sub-vertical tectonic fractures act as geological barriers and prevent the percolation of water creating spatial distribution zones only in the fractured portions of the rock. These saturation zones delimited by tectonic fractures and permeable relief form the water exfiltration points in the soil-rock contact when there is enough water to reach the surface.

It is possible that the fracture systems at the slope are determinant for the deflagration of mass movement in the region, mainly of translational shallow types, on slopes covered by saprolites overlying fractured rocks. Rock exfiltration points are frequently observed in the region and are often associated with loss of stability on the basin slopes. Although the slope system analyzed is representative in the Córrego Dantas basin, geological and geomorphological characteristics, as future stages, it is suggested to expand the hydrological monitoring network, spatially and temporally, in order to understand the role of geological control as a conditioning factor for the mass movements in the mountainous region of Rio de Janeiro due to extreme rainfall events.

Aknowledgement

We thank Dr. Willy Alvarenga and Dr. Ana Luiza Coelho Netto that made the installations and contracting services viable through the INCT-REAGEO project. We also thank Natália Silva for reviewing this manuscript and researchers from the LIEG/UFRJ laboratory for assistance in the lab and field.

References

1. ARANHA, P. R. A. et al. Aplicação do GPR na análise da estabilidade de taludes na região metropolitana de Belo Horizonte, MG. Revista de Geologia, Fortaleza, v. 18, n.2, p. 203-214, 2006. (in Portuguese)
2. AVELAR, A. S.; COELHO-NETTO, A. L. Fluxos d'água subsuperficiais associados à origem das formas côncavas do relevo. 1ª Conferência Brasileira sobre Estabilidade Encostas (1ª COBRAE), ABGE/ABMS, p. 709-720, Rio de Janeiro, 1992.
3. AVELAR, A. S.; VINAGRE, R. Relatório de investigação geológico-geotécnica: Rodovia BR-116, Rio- Teresópolis, km 90, 2009. (in Portuguese)
4. AVELAR, A. S.; COELHO NETTO, A. L.; LACERDA, W. A. *et al.* "Mechanism of the recent catastrophic lanslides in the mountainous range of Rio de Janeiro, Brazil". *In:* Landslide Science and Practice, Margottini, C.; Canuti, P.; Sassa, *K. (*Org*),* 1 ed., Springer- Verlag, v. 4, Global Environmental Change, p. 265-270, 2013.
5. AVELAR, A. S.; VINAGRE, R.; LACERDA, W. A. Influências Geológicas, Geomorfológicas e Geotecnicas nos Movimentos de Massa ocorridos nos dias 11 e 12 de janeiro de 2011, em Nova Friburgo, Rio de Janeiro, Brasil. In: Proceedings of 15CNG/8CLBG, Porto, Portugal, 2016. (in Portuguese)
6. BANKS, E. et al., 2009. Fractured bedrock and saprolite hydrogeologic controls on groundwater/surface-water interaction: a conceptual model (Australia). Hydrogeol. J. 17 (8), 1969–1989.
7. BATAYNEH, A.T., ZUMLOT, T., GHREFAT, H. et al. The use of ground penetrating radar for mapping rock stratigraphy and tectonics: Implications for geotechnical engineering. J. Earth Sci., v. 25, p. 895 - 900, 2014.
8. BENSON, A. Application of Ground Penetrating Radar in Assessing Some Geological Hazards: Examples of Groundwater Contamination, Faults, Cavities. Journal of Applied Geophysics, v. 33, p. 177–193, 1995.
9. BLÖCHER, M. G.; ZIMMERMANN, G.; MOECK, I. et al. 3D numerical modeling of hydrothermal processes during the lifetime of a deep geothermal reservoir. Geofluids, v. 10, p. 406-421, 2010.
10. BONOMO, N., CEDRINA, L., OSELLA, A., et al. GPR Prospecting in a Prehispanic Village, NW Argentina. Journal of Applied Geophysics, v. 67, p. 80–87, 2009.
11. BORGES, Giselle Ferreira. Infiltração e sucção dos solos: subsídios aos estudos dos movimentos de massa na bacia do Córrego Dantas, Nova Friburgo, RJ, 2016, 89 f. Dissertação (Mestrado em Geografia) – Universidade Federal do Rio de Janeiro, Instituto de Geociências, Programa de Pós- Graduação em Geografia, Rio de Janeiro, 2016. (in Portuguese)
12. BOTELHO, M.A.B.; MUFTI, I.R. Exploitation of limestone quarries in Brazil with depth migrated ground penetrating radar data. Proceedings of the 68th Annual International Meeting, Society of Exploration Geophysicists, Expanded Abstracts, vol. 2, p. 898–903, 1998.
13. BRÖNNIMANN, C.; STÄHLI, M.; SCHNEIDER, P. et al. Bedrock exfiltration as a triggering mechanism for shallow landslides. Water Resources Research, v. 49, p. 5155–5167, 2013.

14. CALCATERRA, D., and A. Santo (2004), The January 10, 1997 Pozzano landslide, Sorrento Peninsula, Italy, Eng. Geol., 75, 181–200, doi:10.1016/ j.enggeo.2004.05.009.
15. COELHO NETTO, A. L. Catastrophic landscape evolution in a humid region (SE Brazil): inheritances from tectonic, climatic and land use induced changes. Supplementi di Geografia Fisica e Dinamica Quaternaria, III, T.3: p. 21-48, 1999.
16. COELHO NETTO, A. L.; SATO, A. M.; AVELAR, A. S. et al. January 2011: The Extreme Landslide Disaster in Brazil. In: Claudio Margottini; Paolo Canuti; Kyoji Sassa. (Org.). Landslide Science and Practice. 1ed. Berlin: Springer Berlin Heidelberg, v. 6, p. 377-384, 2013.
17. DANIELS, D. J. Ground Penetrating Radar. London: The Institution of Electrical Engineers, 2004.
18. DEERE, D.U. Rock quality designation (RQD) after 20 years. U.S. Army Corps of Engineers Contract Report GL-89-1. Vicksburg, MS: Waterways Experimental Station, 1989.
19. DHAKAL, A. S.; SIDLE, R. C. Distributed simulations of landslides for different rainfall conditions. In: Hydrological Processes, v. 18, p. 757-776, 2004.
20. DIETRICH, W. E.; DUNNE, T. The channel head. In BEVEN, K. E KIRKBY, M. (Org.) Channel Network Hydrology. John Wiley, Chichester, p. 175-219, 1993.
21. DIETRICH, P.; HELMIG, R.; SAUTER, M.; HÖTZL, H.; KÖNGETER, J.; TEUTSCH, G. (EDS.). Flow and Transport in Fractured Porous Media. Springer-Verlag, Berlin, 2005.
22. EHRLICH, M. Parecer técnico sobre a drenagem subterrânea na BR-116/RJ km 90, 2011. (in Portuguese)
23. EMBRAPA. Manual de métodos de análise de solo. Ministério da Agricultura e do Abastecimento, Rio de Janeiro. 212 p, 1999. (in Portuguese)
24. FERNANDES, N. F.; GUIMARÃES R. F.; GOMES, R. A. T. et al. Condicionantes Geomorfológicos dos Deslizamentos nas Encostas: Avaliação de Metodologias e Aplicação de Modelo de Previsão de Áreas Susceptíveis. Revista Brasileira de Geomorfologia, v. 2, n 1, p. 51-71, 2001. (in Portuguese)
25. FUTAI, M. M. Landslides in unsaturated conditions caused by rainfall infiltration. In In: LACERDA, W.A. et al. (Org), Extreme rainfall induced landslides, 1 ed., p. 36–69, 2014.
26. GABRIELLI C. P.; MCDONNELL J. J; JARVIS, W.T. The role of bedrock groundwater in rainfall–runoff response at hillslope and catchment scales, Journal of Hydrology, v. 450, p. 117–133, 2012.
27. GENET, M., STOKES, A., FOURCAUD, T., NORRIS, J.E. The influence of plant diversity on slope stability in a moist evergreen deciduous forest. Ecological Engineering, v. 36, p. 265- 275, 2010.
28. GHESTEM, M., SIDLE, R. C., STOKES, A. The influence of plant root systems on subsurface flow: Implications for slope stability. BioScience, v. 61, n. 11, p. 869-879, 2011.
29. GUIMARÃES, R. F., CARVALHO JÚNIOR, O. A., GOMES, R. A. T., FERNANDES, N. F. Movimentos de Massa. In: FLORENZANO, T. G. (org). Geomorfologia: conceitos e tecnologias atuais. Oficina de Textos. Rio de Janeiro, RJ, Brasil, p. 159-184, 2008. (in Portuguese)
30. HAUGHT, D. R. W.; TROMP-VAN MEERVELD, H. J. Spatial variation in transient water table responses: Differences between an upper and lower hillslope zone, Hydrol. Processes, v. 25, n. 25, p. 3866–3877, 2011.
31. IDI, B. Y. e KAMARUDIN, M. N. Imaging stratigraphy of Pontian Peatland, Johor Malaysia with Ground Penetrating Radar. Asian Journal of Earth Sciences, n. 5, p. 36-49, 2012.
32. IVERSON, R. M. (2000), Landslide triggering by rain infiltration, Water Resource Research, 36 (7), 1897–1910.

33. JOHNSON, K. A., and N. Sitar (1990), Hydrologic conditions leading to debris-flow initiation, Can. Geotech. J., 27, 789–801.
34. JOL, H. M. Ground penetrating radar: Theory and Applications. Amsterdam: Elsevier, 2009, 545p.
35. KLUTE, A. e DIRKSEN, C. Hydraulic conductivity and diffusivity: Laboratory methods. In: Klute, A. Ed., Methods of Soil Analysis - Part 1 - Physical and Mineralogical Methods, American Society of Agronomy, Madison, 687-734, 1986.
36. LACERDA, W. A. Stability of natural slopes along the tropical coast of Brazil. In: Almeida, M. (ed.) Proceeding of the Internacional Symposium on Recent Developments in Soil and Pavement Mechanics. Balkema, Brookfield, p.7-39, 1997.
37. LACERDA, W. A. Local instability in saturated colluvial slopes in southern Brazil. In: International Symposium on Slope Stability Engineering, Shikoku, Japan. v.1, 199-204 p., 1999.
38. LACERDA, W. A. Landslide initiation in saprolite and colluvium in southern Brazil: Field and laboratory observations, Geomorphology, v. 87, n. 3, p. 104–119, 2007.
39. LACERDA, W. A. A Suggested Shallow Slide Mechanism of Accidents in the Região Serrana of the State of Rio de Janeiro. In: LACERDA, W.A. et al. (Org), Extreme rainfall induced landslides, 1 ed., p. 128–140, 2014.
40. LANNI, C.; MCDONNELL, J.; HOPP L.; RIGON R. Simulated effect of soil depth and bedrock topography on near-surface hydrologic response and slope stability. Earth Surf. Process. Landforms v. 38, p. 146–159, 2013.
41. LIMA, P.H.M.; COUTINHO, B.H.; GOMES, G.B.; et al. Parâmetros morfométricos relacionados às bacias de 1º ordem e a ocorrência de deslizamentos rasos na bacia do Córrego Dantas: Nova Friburgo - RJ. REVISTA GEONORTE, Edição Especial 4, v.10, n.1, p.165 – 170, 2014. (in Portuguese)
42. MACHADO, K. M. Estudo de um deslizamento de terra em Campo do Coelho, Nova Friburgo, RJ. Dissertação de Mestrado - COPPE, Universidade Federal do Rio de Janeiro, Rio de Janeiro, 2016. (in Portuguese)
43. MARQUES, M. C. O. Influência de vegetação florestal secundária e de gramínea na hidrologia de encostas: subsídios aos estudos dos movimentos gravitacionais de massa em Nova Friburgo (RJ). 123 f. Dissertação (mestrado) - Instituto de Geociências, Universidade Federal do Rio de Janeiro, Rio de Janeiro, 2016. (in Portuguese)
44. MATSUSHI, Y.; MATSUKURA, Y. Rainfall thresholds for shallow landsliding derived from pressure-head monitoring: Cases with permeable and impermeable bedrocks in Boso Peninsula, Japan, Earth Surf. Processes Landforms, v. 32, p. 1308–1322, 2007.
45. MCDONNELL, J. Where does water go when it rains? Moving beyond the variable source area concept of rainfall–runoff response. Hydrol. Process, v. 17, n. 9, p. 1869–1875, 2003.
46. MCDONNELL, J.; SIVAPALAN, M.; VACHÉ, K. et al. Moving beyond heterogenity and process complexity: A new vision for watershed hydrology. Water Resour. Res., V. 43, 2007.
47. MONTGOMERY D. R.; DIETRICH, W. E.; TORRES, R.; ANDERSON, S. P.; HEFFNER, J. T.; LOAGUE, K. HYDROLOGIC. Response of a steep, unchanneled valley to natural and applied rainfall. Water Resources Research, v. 33, n. 1, p. 91–109, 1997.
48. MONTGOMERY, D. R., DIETRICH, W.; HEFFNER, J. Piezometric response in shallow bedrock at CB1: Implications for runoff generation and landsliding, Water Resour. Res., v. 38, n. 12, p. 1274, 2002.
49. PAITAN, C. A.T. Modelagem Numérica de Fluxo em Meios Fraturados e Meios Porosos Fraturados. Dissertação de Mestrado. Departamento de Engenharia Civil, Pontifícia Universidade Católica do Rio de Janeiro, Rio de Janeiro, 2013. 107p.
50. PALMA, L. H.; COLEHO NETTO, A. L.; COUTINHO, B. H. Inventário e classificação topográfica de cicatrizes de movimentos de massa na bacia do córrego Dantas – Nova

Friburgo/RJ. In: XXXV Jornada Giulio Massarani de Iniciação Científica, Tecnológica, Artística e Cultural – UFRJ, 2013. (in Portuguese)
51. PORSANI, J. L.; WILLIAM, A. S.; ABAD O.S.J. GPR for mapping fractures and as a guide for the extraction of ornamental granite from a quarry: A case study from southern Brazil. Journal of Applied Geophysics, v. 58, n. 3, p. 177-187, 2006.
52. SANDMEIER, K.J. Program for the processing of seismic, acoustic or electromagnetic reflection, refraction and transmission data. Manual do Software 03, Karlsruhe, Germany, 2014.
53. SIDLE, R.C., NOGUCHI, S., TSUBOYAMA, Y., LAURSEN, K. A conceptual model of preferential flow systems in forested hillslopes: evidence of self organization. Hydrological Process. 15, 1675–1692, 2001.
54. SILVA, C., MEDEIROS, W., SÁ, E, XAVIER, P. Resistivity and ground-penetrating radar images of fractures in a crystalline aquifer: a case study in Caic¸ara farm—NE Brazil. Journal of Applied Geophysics, v. 56, p. 295-307, 2004.
55. SILVA, R. P. Comportamento hidrológico de encosta em substrato rochoso granítico sob influência de deslizamento raso - Nova Friburgo, Rio de Janeiro. Dissertação de Mestrado Universidade Federal do Rio de Janeiro, Instituto de Geociências, Programa de Pós-graduação em Geologia, UFRJ, 151 f., 2014. (in Portuguese)
56. SOUZA JR., A.O. e PORSANI, J.L. Localizacão de fraturas em rochas graníticas no município de Capãoo Bonito - SP, Brasil. Revista Brasileira de Geofísica, v. 20, n. 2, p. 123–128, 2002. (in Portuguese)
57. STEVENS, K.M.; LODHA, G.S.; HOLLOWAY, A.L.; SOONAWALA, N.M. The application of ground penetrating radar for mapping fractures in plutonic rocks within the Whiteshell Research Area, Pinawa, Manitoba, Canada. Journal of Applied Geophysics, v. 33, 1995.
58. TROMP-VAN MEERVELD, H.J.; WEILER, M. Hillslope dynamics modeled with increasing complexity, J. Hydrology, v. 361, n. 1–2, p. 24–40, 2008.
59. UCHIDA, T.; TROMP-VAN MEERVELD, I., MCDONNELL, J. J. Runoff characteristics of pipeflow and effects of pipeflow on rainfall-runoff phenomena in a mountainous watershed. J. Hydrol., v. 22, p. 18–36, 1999.
60. VAN ASCH, T.W.J., BUMA, J., VAN BEEK, L.P.H. A view on some hydrological triggering systems in landslides. Geomorphology, v. 30 (1–2), n. 25, 1999.
61. WYATT, D. E.; TEMPLES, T. J. Ground-penetrating radar detection of small-scale channels, joints and faults in the unconsolidated sediments of the Atlantic Coastal Plain. Environmental Geology, v. 27, p. 219 - 225, 1996.
62. Xavier Neto, P., Medeiros. W. A practical approach to correct attenuation effects in GPR data J. Appl. Geophys., 59 (2006), pp. 140-151.

Journal Pre-proof

Late quaternary episodes of clastic sediment deposition in the Tarimba Cave, Central Brazil

Dandara Maria Vitalina Da Silva Caldeira, Rogério Uagoda, Adivane Morais Nogueira, Jeremie Garnier, André Oliveira Sawakuchi, Yawar Hussain

PII: S1040-6182(21)00029-X

DOI: https://doi.org/10.1016/j.quaint.2021.01.012

Reference: JQI 8734

To appear in: *Quaternary International*

Received Date: 14 November 2020

Revised Date: 12 January 2021

Accepted Date: 15 January 2021

Please cite this article as: Vitalina Da Silva Caldeira, D.M., Uagoda, Rogé., Nogueira, A.M., Garnier, J., Sawakuchi, André.Oliveira., Hussain, Y., Late quaternary episodes of clastic sediment deposition in the Tarimba Cave, Central Brazil, *Quaternary International* (2021), doi: https://doi.org/10.1016/j.quaint.2021.01.012.

Late Quaternary episodes of clastic sediment deposition in the Tarimba Cave, Central Brazil

Dandara Maria Vitalina Da Silva Caldeira [a, *], Rogério Uagoda [a, b], Adivane Morais Nogueira [b], Jeremie Garnier [a,] André Oliveira Sawakuchi [c], Yawar Hussain[d]

[a] Institute of Geoscience, University of Brasilia, Brasilia 70910-900, Brazil

[b] Department of Geography, University of Brasilia, Brasilia 70910-900, Brazil

[c] Institute of Geosciences, University of São Paulo, São Paulo 05508-080, Brazil

[d] Environmental Engineering and Earth Science Department, Clemson University, Clemson, SC 29634, USA

*Corresponding author.

E-mail address: dandara.caldeira2014@gmail.com.

Abstract: The study presents three sedimentary profiles from Tarimba cave in central Brazil. The data allow constraining the late Quaternary sedimentary evolution of cave systems in the region. A multi-techniques approach was used to characterize sediment texture (grain size and circularity index), mineralogical composition (X-Ray Diffraction), chemical composition (ICP-OES) and deposition ages (Optically Stimulated Luminescence and radiocarbon). Eight sedimentary facies were identified, including a facies formed by autochthonous sediments (Guano) and seven facies formed by allochthonous siliciclastic sediments. The siliciclastic facies range from clayey to gravelly deposits that correspond to high-density gravity flows (Diamicton) and water laid traction process of varied deposition energy (Channel, Backswamp, and Slackwater). The studied deposits reflect an intense cave filing from the Middle to Late Pleistocene in the last 200 Ka. Subsequent depositional events formed three sedimentation phases: the first before 200 Ka corresponding to a larger granulometric interval, clay to gravel, identified through erosive surfaces; the second, after 197 Ka, is composed of sandy sediments and oscillations in the water flow energy. The third phase between 87 and 52 Ka (which covered the other stages) was responsible for the last fluvial deposition.

Keywords: Cave, Paleoenvironment, Sedimentation, Sedimentary facies

1 INTRODUCTION

Caves are fragile systems that may contain and preserve reliable sedimentary records of surface and subsurface paleoenvironmental conditions. The allochthonous (clastic) and autochthonous (chemical or biogenic) sediments deposited within caves, which provide a degree of resilience to physical and

chemical weathering process and erosion, providing unique paleoenvironmental records for the Quaternary deposits (Gillieson, 1996; Ballesteros et al., 2019; McAdams et al., 2019). Although the sedimentation processes inside a cave are analogous to the surface ones, they are poorly documented in comparison with surface systems and their complex depositional-erosive dynamics, often difficult their paleoenvironmental significance (Gillieson, 1996; White, 2007). Moreover, cave sedimentary systems are coupled to surface conditions and their understanding needs a comprehensive and diverse knowledge derived from geomorphologic, sedimentological, paleo-ecological, and geochronological studies compared to external records (Woodward and Goldberg, 2001).

Generally, the clastic sediments within caves are allochthonous and derived from adjacent rocks units under weathering, and their triggers mechanism depends on external regional factors such as climate, tectonics and surface geomorphology, thus representing the scenario of the surrounding environment/watershed (Farrant and Smart, 2011; Plotnick et al., 2015). Therefore, the deposited materials and deposition patterns reflect the scale of terrestrial processes caused by regional driving forces transmitted by climate and tectonics (Springer, 2005; Arriolabengoa et al., 2015).

The study of clastic sediments in caves is challenging since even with deposition processes similar to the superficial ones, the particular sedimentary dynamics in the cave can lead to deposits with complex stratigraphic configurations (Osborne, 1986; Gillieson, 1996; Ford and Williams, 2007), sometimes having older sediments overlapping the younger ones (Springer, 2005). Moreover, the deposition in the conduits is highly heterogeneous, generating temporal gaps and discontinuity into sediment records, reinforcing the need to gather several deposits to obtain a more comprehensive paleoenvironmental scenario (Gillieson, 1996; Plotnick et al., 2015). Thus, establishing a precise chronology of depositional and erosion phases is fundamental to shed light on the connections between underground and surface events (Osborne, 2005; White, 2007).

In this context, Brazil stands out for presenting expressive cave systems with more than 20,000 mapped caves and a growing potential for increase (ICMBio/CECAV, 2020). In the last decades, clastic sediments within caves have been consolidated as an important target to reconstruct paleoenvironmental conditions of both surface and subsurface landscapes since this is a crucial demand for extensive paleontological and/or archaeological studies performed so far (Roosevelt et al., 1996; Michab et al., 1998; Peyre et al., 1998; Faure et al., 1999; Santos et al., 2003; Piló et al., 2005; Auler et al., 2006; Fontugne, 2013; Kinoshita et al., 2014; Oliveira et al., 2014). Among the studies about Brazilian cave deposits (Auler et al., 2002; 2009; Hubbe et al., 2011; Jaqueto et al., 2016; Laureano et al., 2016; Haddad-Martim et al., 2017; Novello et al., 2019), few of them have been carried out in the central region of the country (Auler et al., 2002; Jaqueto et al., 2016) and so far there are no studies about sedimentary deposits within caves from on the western edge of the São Francisco Craton, which hosts a major Brazilian karst area.

The state of Goiás is the 5th largest in the number of mapped caves in Brazil, hosting approximately 1001 cavities, among them the Tarimba cave. Tarimba is the significant cave of Vermelho River Rising Environmental Protection Area (APARNRV), in central Brazil (Fig. 1), being the sixth largest cave in horizontal projection of the Brazilian territory with about 14 km mapped, but still little studied. It holds an endemic fauna and is currently threatened by anthropic activities. On all over the APARNRV there are anthropogenic activities with potential for environmental impacts, such as the use of cave waters for public supply, mining in karstic areas, severe soil degradation, sedimentation in recharging areas and accelerated pipeline clogging (ICMBio/CECAV, 2017). This work aims to understand the sedimentary dynamics within the Tarimba cave during the late Quaternary, including the association of the surrounding surface landscape's evolution dynamics. Also, it seeks to provide the first composition characterization and chronology of deposition of clastic sediments in the region that may serve as a basis for paleoenvironmental interpretations.

2 GEOLOGICAL/GEOMORPHOLOGICAL CONTEXT

The study area is located on the western edge of the São Francisco Craton, being composed of sediments of the São Francisco Basin (Fig. 1-A). The base, formed by a succession of carbonate and silicaceous rocks of the Neoproterozoic Bambuí Group, hosts one of Brazil's main karst provinces. The carbonated succession is covered by Phanerozoic sediments of the Sanfranciscan Basin (Areado Group, Urucuia Group, and Chapadão Formation) (Campos and Dardenne, 1997), Fig. 1-B.

The Bambuí Group occurs extensively in the area and is associated with sediment deposition on a stable epicontinental platform from transgressive-regressive mega-cycles in a basin with a very low bottom gradient and shallow waters (Dardenne et al., 1978; Dardenne, 1981; Araujo and Moreton, 2008). In the area, the total thickness of the complete stratigraphy is 1700 m (Cruz, 2012) include six lithostratigraphic formations, proposed by Dardenne et al. (1978), described from the base to the top as: Jequitaí Formation, Sete Lagoas Formation, Serra de Santa Helena Formation, Lagoa do Jacaré Formation, Serra da Saudade Formation, and Três Marias Formation. Locally, the Lagoa do Jacaré Formation is characterized by the intercalation of oolitic and pisolitic limestones, dark grey, foul, crystalline, lenticular with siltstones and marls. It constitutes the predominant lithology of the region and where the caves are developed, including Tarimba cave.

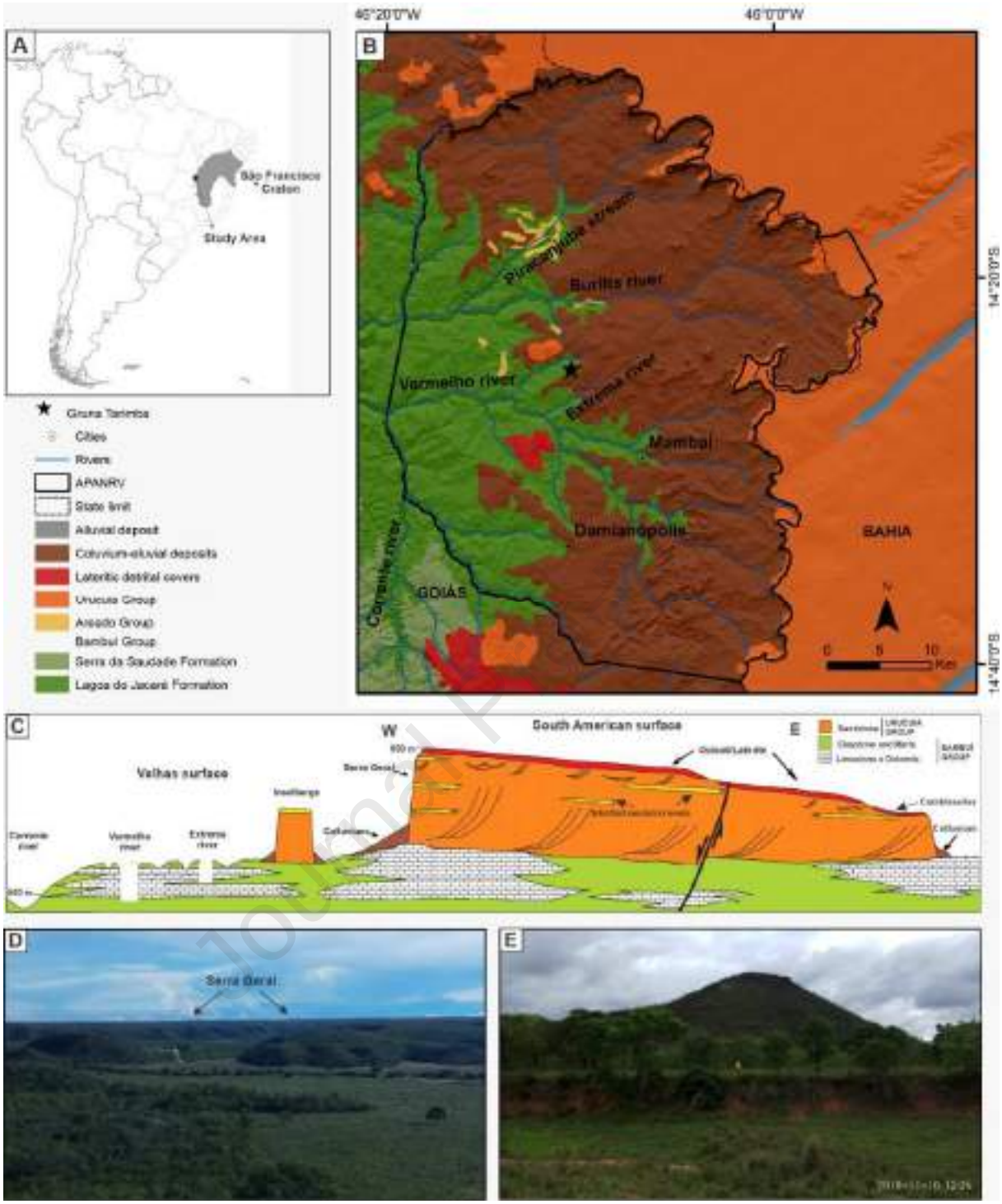

Fig. 1 Location of the study area in the São Francisco Craton. B- Geological map. Source: Serviço Geológico do Brasil (CPRM). Coordinate system, UTM. Zone, 23S. SIRGAS 2000. C - Geomorphological context (Gaspar and Campos, 2007) adapted by Uagoda et al. (2019). D - Serra Geral overview. E- Inserlberg near carbonates.

The Areado Group occurs only in the northern portion and corresponds to sediments of the Eocretaceous marked by lateral variations due to the various depositional environments (Campos and Dardenne, 1997). The Urucuia Group has Cretaceous ages and consists basically of sandstones in a system of fluvial/eolic deposition occurring in the eastern portion of the area, primarily in the state of

Bahia and in some inselbergs near the carbonates. The Urucuia Group is characterized by quartz sandstones, reddish and white, fine to medium grain, rounded and well-selected with rare occurrence of clay matrix (Iglesias and Uhlein, 2009). Locally the pink to reddish sandstones, thin to medium, develop in the form of isolated inselbergs (Cruz, 2012). The sandstone forms a reddish well developed oxisol and sometimes forms lateritics outcrops on the surface (Fig.1 A and B). The Chapadão Formation expressively occurs in the region corresponding to the Cenozoic colluvium/detritic covers, predominantly unconsolidated sandy. The formation results from intense processes of erosion and escarpment regression of Ucucuia group, forming Talus deposits and covering the formations from Bambuí group where the caves are located (Campos and Dardenne, 1997; Iglesias and Uhlein, 2009).

The geomorphological configuration is a cuesta landscape called Serra Geral de Goiás, generated mainly by regressive erosion (Cherem and Varajão, 2014), Fig. 1-C and Fig. 1-D. The mountain range has a north-south direction with about 400 km of extension is the divider of two important Brazilian watersheds, São Francisco (east) and Tocantins-Araguaia (west). In this scenario, the upper portion (Chapadão Central), remaining from the South American surface, makes up the sandstones of the Urucuia Group. The lower portion (Vão do Paranã) corresponds to the remnants of the Velhas surface installed in the rocks of the Bambui Group. In the intermediate portions are observed colluvium-eluvial deposits generated by the sandstone's erosion (Cherem and Varajão, 2014). The area is still observed inselberg hills that stand out in the middle of the landscape (Fig. 1– E).

Erosive processes involving the Chapadão Central retreat remove sediments and leave them available in hillslopes to later transportation to the underground karstic system located downstream.

Such dynamics favor a covered karstic system in which two types of caves stand out: those near the transition zone between karstic lands and talus (alluvial-colluvial deposits from the Urucuia Group) with vadose and meandering caves filled by sediments and signs of paragenesis; and those fluvial caves adjusted to the rivers inside canyons are transporting the fluvial load. (Hussain and Uagoda, Unpublished results).

The evolution of karst correlates with local rivers dynamics such as Vermelho, Buritis, Piracanjuba, and Prata was developed through the opening of fractures and faults by the process of dissolution forming dolines, canyons, karstic bridges, sinks and springs with sharp top shapes, strong drainage density and slopes of 20 to 45% (IBGE, 1995). The recharging system comes from the Urucuia aquifer

that feeds the rivers of the carbonate regions, locally represented by Vermelho e Buritis rivers. Typical features of karst, such as sinkholes, suffusion, and collapse types, are found on the surface (Ferreira and Uagoda, 2019) and also dry valleys, abandoned valleys, sinks, resurgence, and karrens where limestone are exposed (Motta, 2003).

The climate is tropical with seasonal characteristics, presenting a dry period (April to September) and a rainy one (October to March) with precipitation index of approximately 1260mm.y^{-1}. The average annual temperature is 24°C and the vegetation is typical of the Cerrado. Recent works (Nunes and Uagoda, Unpublished results) points out the main types of soils correspond to Quartz Neosols (43.1%) associated with plains, consisting basically of sand (>90%) with a mineralogical composition containing quartz and kaolinite; Chernossols (19.3%) in the middle slope mainly in carbonate areas having a hard and prismatic clay texture; and, Oxisols (13.3%) present in the plateaus. These later soils have a frank clay-sand texture, and identification was performed considering presence low activity clays (mainly kaolinite) and oxides (hematite and goethite). These soils types point out to weathering processes in humid and hot conditions in which the erosion is responsible for their removal and transportation under caves.

3 TARIMBA CAVE

The Tarimba cave is an important cave in the Brazil scenario because of its extension and also because of the occurrence of endemic species such as the fish *Ituglanis Boticário* (Rizzato and Bichuette, 2014). The Tarimba cave is located at the boundary between the Bambuí Group and alluvial/colluvial deposits of Chapadão Formation, characterized by a covered karst. The exposure of limestone on surfaces that are often covered by soil, often originated from the sandstone's weathering, is located in a peripheral depression of a cuesta in regression (Hussain and Uagoda, Unpublished results.; SBE et al., 2014). The main Tarimba entrance (14º24'42.84"S and 46º10'29.63"W) is located in a large sinkhole indicating drainage capture to the cave's interior, as is showed in the topography (Fig. 2 A) and UAV image (Fig. 2 B). The area suffers from anthropic activities typically represented by agricultural practices as pasture (Fig. 2 E), which result in degradation and formation of bare soils (Fig 2 C), increasing runoff and sediment production in the hilltops (Fig. 2D). This anthropogenic process can lead to karst desertification and a rise of the sediment amount entering the cave, which shows the correlation between sediment production and surface changes.

As a covered karst, near Tarimba cave, unconsolidated sediments of the Urucuia Group are observed on the top of the slope, lithic neosol on the medium slope and chernosols and limestone of the Lagoa do Jacaré Formation, Bambuí Group in the lower portions (Hussain et al., 2020). The patterns of surface runoff and aquifer recharge, connected to the different types of soil and rock and their characteristics, such as porosity and permeability (Hussain et al., 2020) are conditioning factors for removing and transport sediment under the cave.

The deposition of sediments at higher levels was controlled by the change of the hydraulic gradient of the mean Vermelho River, which consequently reflected in its tributary, Extrema River, which corresponds to the local base level. In the deep areas, a perennial flow is observed that, during the

rainy periods, receives an essential amount of water and load from runoff. The underground interconnections, still unknown, are in the mapping phase, but the landscape suggest a connection between the Tarimba cave and the sink in the Extrema River.

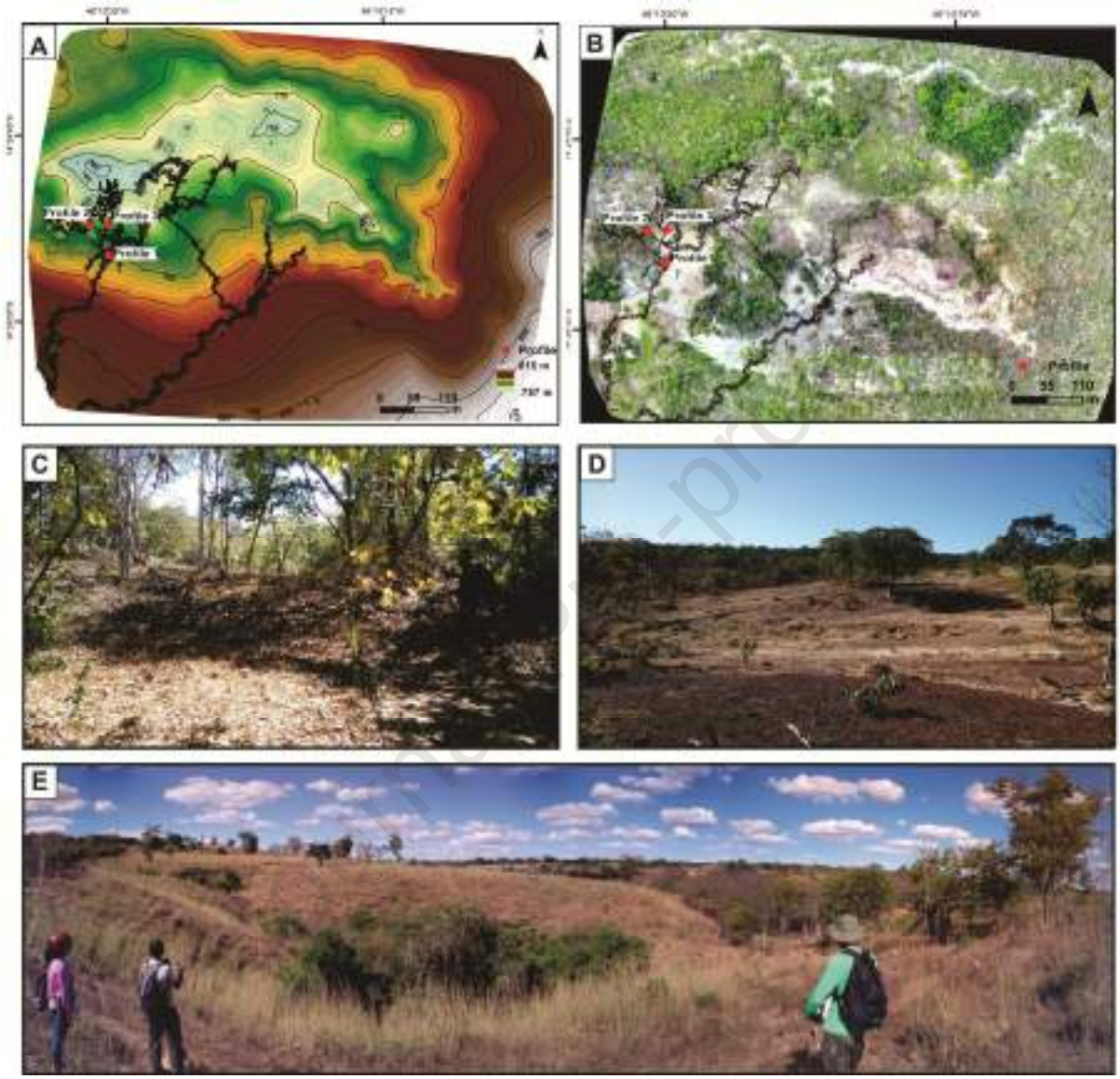

Fig. 2 Landscape surrounding Tarimba cave. A - Hypsometric map. B- High resolution image in which the whitish shades represent the unconsolidated sediments of the Urucuia Group sedimentary deposits at the top of the slopes. D - Main entrance of Tarimba cave. E - Soils with advanced degradation process in the cave adjacencies. F - Sinkhole in one of the entrances. Pictures: Dandara Caldeira, Renan Smith Penido Louzada and José Gustavo da Silva NuneS.

Tarimba is Classified as a vadose cave on the upper galleries, dendritic with a tendency to rectilinearity of the conduits being an anastomosed at the entrances, what is attributed to the existence of several collectors and sedimentary concentration that cause the entanglement of the passages (Motta, 2003), as can be seen on the total topography of the cave (Fig. 3-A) and in the studied detail (Fig. 3 B). The cave presents a diversified development exhibiting an average vertical amplitude of 17

191 m in the highest part and decreases drastically up to 2 m in some paths sheltering countless fossil
192 galleries (Motta, 2003). Currently, it does not receive visitation due to the narrow and deep pipelines
193 that make tourism dangerous, especially during rainy periods

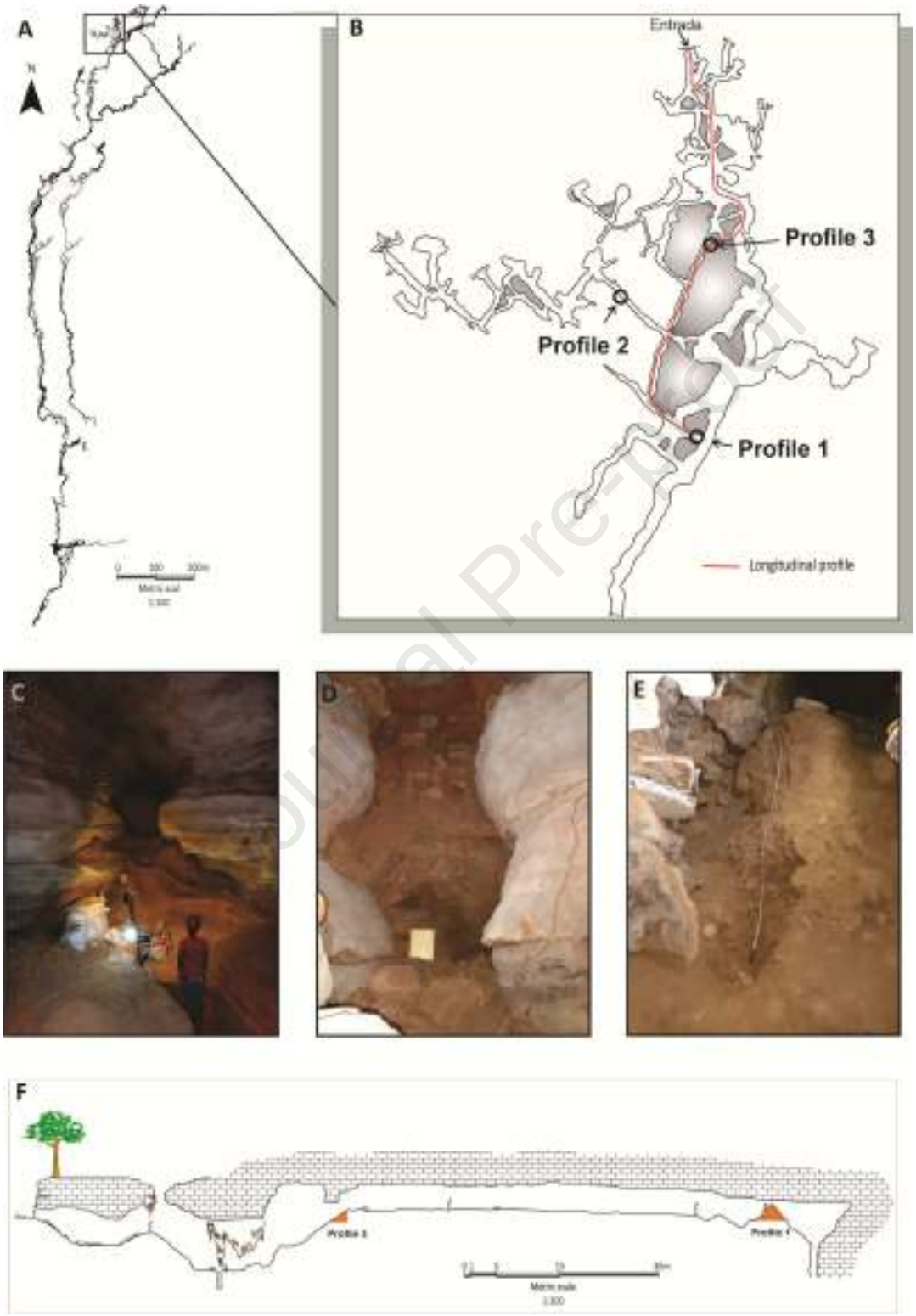

194

195 *Fig. 3 A - Tarimba cave Map. B - Location of the sedimentary deposits studied: C - Profile 1, D - Profile*
196 *2 and E - Profile 3. F- Longitudinal profile from the entrance to Profile 1.*

There are large quantity and variety of speleothems with well-decorated halls. The cave horizontal floor is composed of compacted sediments, with lateral continuity (Fig. 3F) confirmed through the profiles studied in this article (Fig. C, D and E). The cave ceiling is rectilinear with evidence of sedimentary deposition on the sides and paleo floors, indicating more than one phase of sedimentation/erosion.

The Tarimba cave was chosen due to: 1) the importance of the cave hydro sedimentology system; 2) several contemporary studies are being carried out to manage the Vermelho River Rising Environmental Protection Area (APARNRV); 3) sedimentary deposits are accessible near the main entrance of the cave.

4 METHOD

The method applied in this study comprises the choice of one main deposit (Profile 1) (Fig.3 C) and two others (Profiles 2 and 3) to allow the facies interpretation (Fig. 3-D and E). Those three profiles were chosen because they include extensive preserved sedimentary records, unlike other ones along the cave entrance. Furthermore, the path to the cave interior is difficult and dangerous due to its narrow configuration. The geometry on the chosen portion with plain floor and available deposits allows the survey work. This research consists of description and sampling based on accessibility, thickness, positioning in the cave, and the stratigraphic architecture of the deposit. The approach applied consists of several methodologies, combining grains size, roundness, facies analysis, geochemistry (IPC-OES), X-ray, and geochronology (Optically Stimulated Luminescence and Carbon 14), Fig. 4.

Profile 1 (P-1) shows the main deposit, which is located in the most distal portion of the cave entrance, with about 5 m of thickness and presenting a diverse sediment deposition compared with the other profiles, in which clast supported medium angle level truncated low angle laminations of sand sediments. Due to specific characteristics such as unconsolidated sediments presence and stratigraphic architecture, the sampling was performed in two sections, central and lateral (columns A and B, respectively), Fig. 4. Such a situation implied a study in several levels (Units I to VII), interspersed by sample collection interruption in the sedimentary sequence.

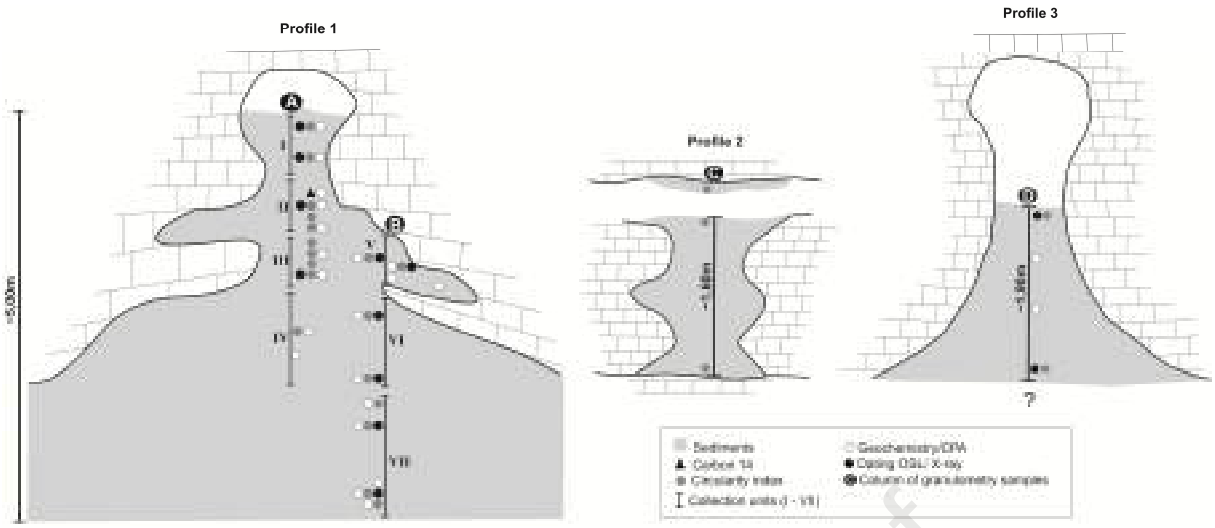

Fig. 4 Graphic synthesis showing the geometry of data collection in the profiles, with the collect level for each proxy. Location of Profiles 1, 2 and 3 in Tarimba cave can be seen in Fig. 3.

Profile 2 (P-2) is located in the intermediate portion between the cave entrance and the most distal duct (P-1), in a 1.60 m thick conduit near the main one, where clay-sand sediments are distributed in bands, probably filling up to the roof. Profile 3 (P-3), about 1.90 m thick, is located next to the Tarimba entrance and, because it is at a lower level, constitute a ladder that gives access to other deposits in which sand-clay sediments are distributed in decametric bands having on the top a horizontal calcitic floor that serves as access to the other profiles.

4.1 Grain size Analysis

The grain size analysis was performed at the Geochemistry and Water Laboratory – LAGEQ/ University of Brasília, using samples collected at 10 cm intervals (n=111 samples, where: 73 in P-1, 18 in P-2 and 20 in P-3),Fig. 4. The samples were air-dried, disaggregated, and sifted through the 2 mm and 1 mm sieve, and the larger fractions were weighted. To eliminate organic matter from sediments smaller than 1 mm, Hydrogen Peroxide (H_2O_2) was used, followed by chemical (Sodium Pyrophosphate – $Na_4P_2O_7$) and physical (30 minutes in 50W ultrasound) dispersants. The remaining fractions were analyzed using the Bettersize ST Granulometer, using the LALLS – Low Angle Laser Light Scattering method, which is based on the fact that the diffraction angle is inversely proportional to the particle size.

A smaller number of samples (n=23, where: 18 in P-1, 3 in P-2, and 2 in P-3) was selected, and its grain shape was determined by an automated analysis performed by the Bettersize S3 equipment in the ACIL & Weber Laboratory (São Paulo, Brazil), following an internal procedure (Fig. 4). Initially, the data were inserted, and a blank measurement was taken. Then, the samples were added directly to the

analytical well with agitation of 1600 rpp and ultrasound (50W), posteriorly added to the chambers (0.5x and 10x) for a wider analytical range, and then the analysis was performed. Data were analyzed using the model system with the data treatment and grain size calculation software of the equipment (Bettersize Laser Particle Size Analysis System V8.0), based on the *ISO standards 13320-1(1999)* and *9276-1(1998)*. The main parameter to be obtained is the Circularity Index (CI), which indicates particle rounding (Equation 1):

$$CI = \frac{4\pi x Area}{Perimeter^2}$$

Equation 1

4.2 Facies Analysis

Facies analysis was performed based on lithological and sedimentary features, relative to the concept of sedimentary units defined by Anderton (1985) and the classification for caves proposed by White, (2007). It was mainly observed features such as carbonate content, grain size and classification, and the presence of sedimentary structures. In order to determine correlations between the sedimentary environments, it was established an association of facies that consists of a cluster of spatially and genetically related facies (Martini, 2011). The delimitation of the facies allows understanding the sedimentation environment, concentrating on the origin of the sediments, and combined with geochronological methods, that corroborates the understanding of the evolution of the landscape (Hubbe et al., 2011).

4.3 Geochronology

Twelve samples were collected from the sandy units to be dated by Optically Stimulated Luminescence (OSL), with 10 samples from P-1 and 02 from P-3 profiles (Fig. 4). Opaque PVC pipes were inserted horizontally to retrieve sediment samples under dark conditions. Sediments from the edge of the tubes were discarded to avoid eventually light exposed sediments.

OSL dating was applied on quartz sediment grains isolated according to the procedures described by Aitken (1998): 1. Wet sieving to separate the 180μm-250μm fraction; 2. Hydrogen peroxide (H_2O_2) treatment to eliminate organic matter; 3. Hydrochloric acid (HCl, 10%) treatment to eliminate carbonates; 4. Separation of light from heavy minerals in lithium metatungstate (LMT) solution with a density of 2.75 g/cm³; 5. Separation of quartz from feldspar in an LMT solution with a density of 2.62 g/cm³; 6. Hydrofluoric acid (HF, 38%) etching for 40 minutes to eliminate remaining feldspar grains and the outer layer of quartz grains dosed by alpha radiation; 7. Wet-sieving to eliminate etched grains

finer than 180 μm . After these procedures, infrared (IR) stimulation was used to check for possible contamination by feldspar in quartz concentrates.

The luminescence measurements were performed on a Risø TL / OSL DA-20 reader from the Gamma Spectrometry and Luminescence Laboratory (LEGaL) of the Institute of Geosciences of the University of São Paulo (IGc-USP). The reader is equipped with blue LEDs (peak emission at 470 nm) and infrared LEDs (peak emission at 870 nm) for stimulation, beta irradiation source (90Sr/90Y) with a dose rate of 0.120 ± 0.004 Gy/s, and Hoya U-340 filters for light detection in the ultraviolet band. The equivalent dose (De) was estimated using the single-aliquot regenerative dose (SAR) protocol (Murray and Wintle, 2000) as described in Table 1. Dose recovery tests were performed to set up the measurements conditions for the dose range of the studied samples. Equivalent doses were calculated using the Central Age Model (CAM) (Galbraith et al., 1999). Only aliquots with recycling ratio within 0.9-1.1 range, recuperation less than 5% and negligible IR signal were used for equivalent dose calculations. The OSL signal was calculated, integrating the first 0.8 s of light emission and the last 10 s as background. Dose response curves were fitted using a single-saturating exponential function.

Table 1- OSL-SAR protocol used for equivalent dose estimation. Di: D1<D2<D3<D4; D5=0 Gy, D6=D1; D7=D6 (with IR stimulation before the OSL). Dose response curves were built using signals (Li/Ti) from D1 to D4. The signal of D5 was used to calculate recuperation. Recycling ratio was calculated through signals from D1 and D6. The relation between signals from D6 and D7 was used to appraise feldspar contamination

	Step
1	Dose (Di)
2	*Pre-heat* at 200º C for 10s
3	Blue light stimulation at 125º C for 40s (L_i)
4	Teste dose (D_t)
5	*Pre-heat* at 160° C
6	Blue light stimulation at 125º C for 40s (T_i)
7	*Blue bleach* a 280º C for 40s

The radiation doses rates were estimated from 238U, 232Th e 40K concentrations determined by high-resolution gamma-ray spectrometry using a High Purity Germanium (HPGe) detector (energy resolution of 2.1 keV and relative efficiency of 55%) encased in an ultralow background shield. The samples were dried and packed in sealed plastic containers for storage during a minimum period of 28 days for radon requilibration before gamma ray spectrometry. Water saturation was determined from

the ratio between water weight and dry sample weight. Radionuclide concentrations were converted into dose rates using conversion factors outlined by Guérin et al. (2011). Cosmic radiation contribution to the dose rate was calculated using longitude, latitude, altitude, and burial depth of each sample, according to the model proposed by Prescott and Stephan (1982).

One sample of organic matter in P-1 was dated using Accelerated Mass Spectrometry (AMS ^{14}C) in the Beta Analytic – Testing Laboratory (Miami, Florida, United States), following internal procedures (Fig. 4). To calibrate the ages, the software BetaCal3.21: HPD and the method SHCAL13 were used. The "conventional radiocarbon age" was calculated using Libby's half-life (5568 years), and the results were credited by ISO / IEC-17025: 2005. Total fractionation effects were corrected from the radiocarbon conventional ages, and the calibration was performed using calibration databases from 2013.

4.4 Geochemical and Mineralogical Analysis

The analysis of the major elements (SiO_2, Al_2O_3, Fe_2O_3, CaO, MgO, Na_2O, K_2O, TiO_2, MnO, P_2O_5, and Loss on ignition - LOI) was performed on twenty-two samples (Fig. 4). The samples were air-dried, crushed, and homogenized in an agate mill and digested by fusion of lithium borate. The solutions obtained were analyzed by Inductively Coupled Plasma Optical Emission Spectrometer (ICP/OES), Agilent 5100 model, in the Geochemistry and Water Laboratory (LAGEQ) of the University of Brasília (Brazil). To compile the data, a Principal Component Analysis (PCA) was used, which is based on the relationship between the original variables using the PAST software.

Sediment's qualitative mineralogical analysis (total fraction) were performed on a selection of twelve samples using X-ray diffraction at the Diffractometry Laboratory of the University of Brasília. The diffractometer RIGAKU, ULTIMA IV model, equipped with copper tube and nickel filter under 35 kV and 15 mA current at a scanning speed of 2 θ/min in a scanning interval from 2° to 60°, velocity of 5°/min and step of 0.05°. The resulting diffractogram was analyzed and the identification of the minerals was performed with the aid of the program Jade XRD 9.0 (Materials Data), Windows-based, with database ICDD pdf-2 and pdf-4 (Power Diffraction File – PDF to PC – ICDD).

4.5 CIA (Chemical Index of Alteration)

The intensity of the chemical weathering can be evaluated by several proxies estimated from compositional indices (WIP, CIA, CIW, PIA, CIX, eg.). These proxies are widely used to infer paleoclimate conditions and more especially the weathering intensity. Therefore, the value of the index increases with the intensity of the weathering (Dinis et al., 2020).

Although it is probably the most used, the CIA (Chemical Index of Alteration) is not appropriate in establishing CaO bound to carbonate since the mobility of Ca and Mg is predominantly controlled by the behavior of calcite and dolomite (Buggle et al., 2011; Garzanti and Resentini, 2016). Thus, it was decided to apply the Chemical Proxy of Alteration (CPA) $Al_2O_3/(Al_2O_3 + Na_2O)$ x 100.

5 RESULTS

5.1 Grain Size Analysis

The granulometric analysis yielded unconsolidated sand sediments, predominated by fine sand. Such sediments have continuous and sometimes extensive sand phases that are interspersed with finer sediments, mainly clay, indicating a change in hydraulic conditions of the deposition and/or variation in the source.

In Profile 1, the upper part of units I, VI, and VII converge to similar situations with deposition of essentially sandy sediments in horizontal layers (Fig. 5 and Fig. 6). Besides this pattern, lower central (Unit IV) and upper portions on the side of the profile (Unit V) stand out for the presence of silt-clay sediments and gravel. Also, units II and III present an irregular deposition with an adverse configuration related to the others, characterized by sandy levels with significant amounts of gravel.

From the base to the center of Profile 2, can be seen a change from greater amounts of sand to silt sediments (Fig. 7). The top, unlike the other sedimentary sequences, presents a prevalence of clay and silt with no sand, indicating an extremely slow flow. A sample from the ceiling reveals features like the lower strata and may indicate the resumption of a more intense flow that filed the conduit.

Grain size data of the Profile 3 showed a gradual decrease in silt quantity, in contrast with a gradual increase in the sand, and this trend is observed from the base to the middle of the profile (~1.0 m depth), Fig. 7. From the middle to the top, the levels are essentially sandy with only one inversion of values (~1.4 m). Such dynamics may indicate a progressive decrease in flow, followed by a considerable increase that culminates in a temporal gap with deposition of the paleofloor on the top.

361

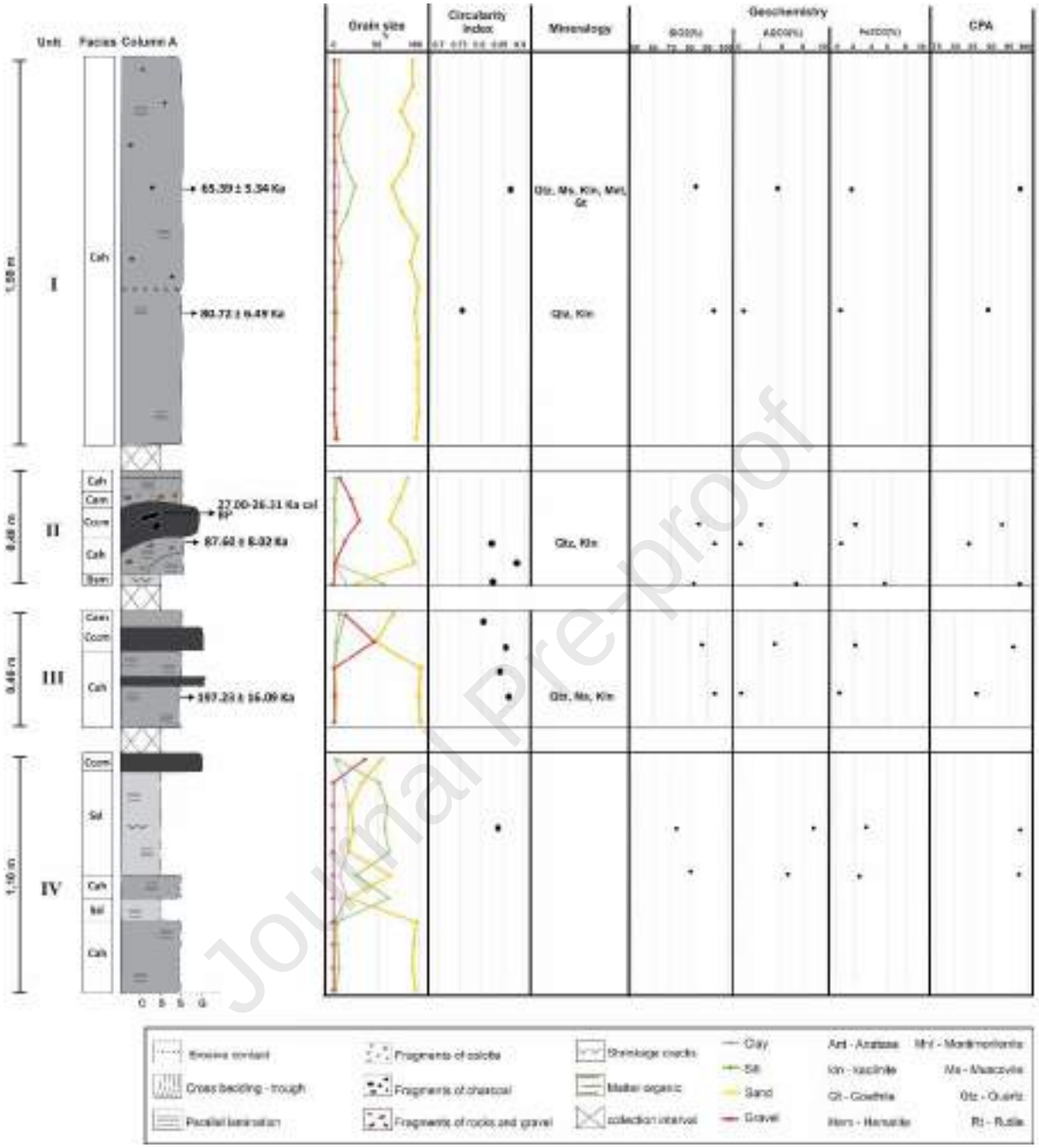

362

363 *Fig. 5 Sedimentary facies, ages, textural and compositional data obtained in Column A of Profile 1. The location*
364 *of the column is shown in Fig. 4..*

365

366

367

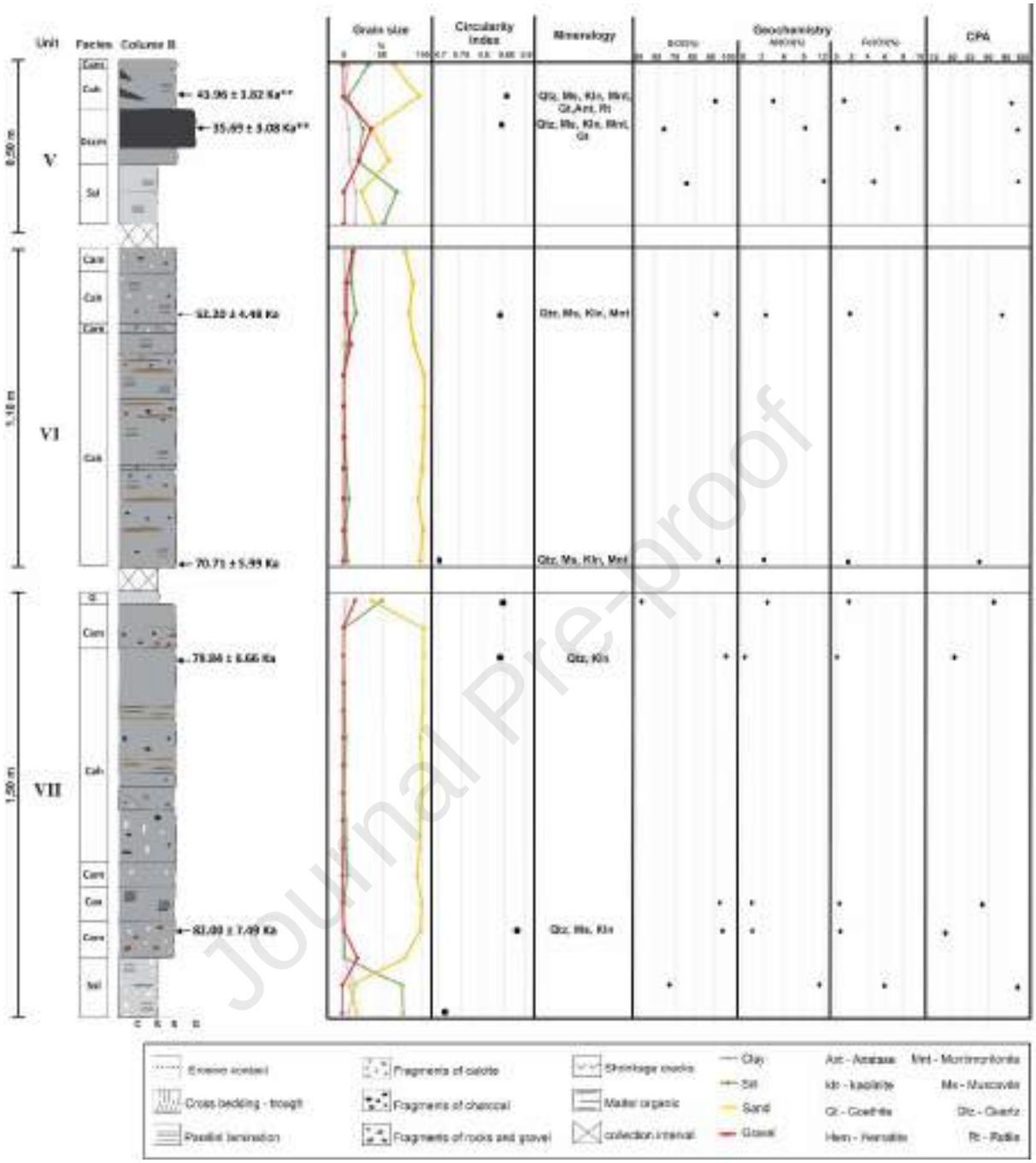

368

369 *Fig. 6 Sedimentary facies, ages, textural and compositional data obtained in Column B of Profile 1. The location*
370 *of the column is shown in Fig. 4.*

371

372

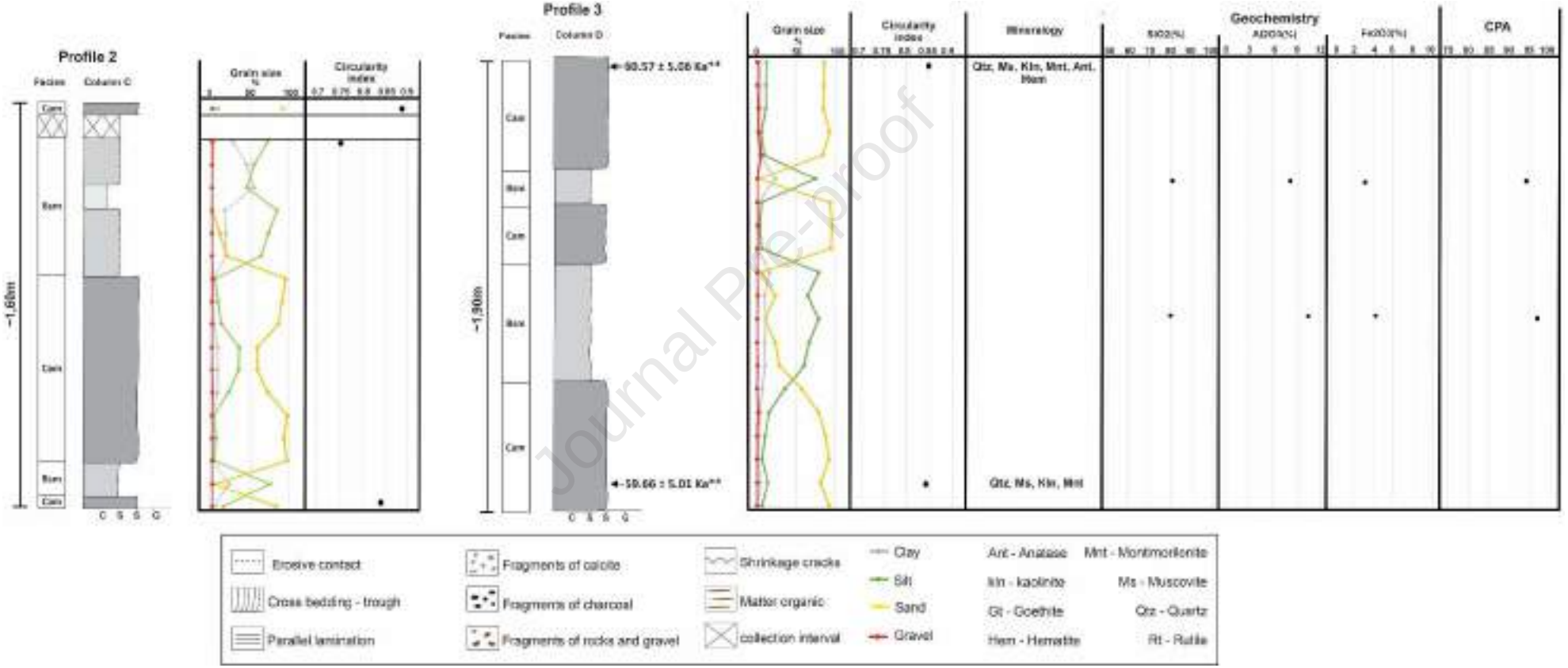

373

374 *Fig. 7 Sedimentary facies, ages, textural and compositional data obtained in Profiles 2 and 3. The location of the column is shown in Fig. 4.*

Circularity index data are homogeneous in both profiles, and no dominant pattern was found. The values with a mean of 0.829 are close to good roundness, around 1, with few levels in the order of 0.7, both in Profile 1 (Fig. 8). Such characteristics can be attributed to the aqueous sedimentary transport, in which grain borders are smoothed, as well as due to abrasive processes (Campaña et al., 2016). However, the high degree of roundness also found in the sediments of the Urucuia Group (Iglesias and Uhlein, 2009) indicates that such characteristics originate from the source area and not necessarily from processes inside the cave.

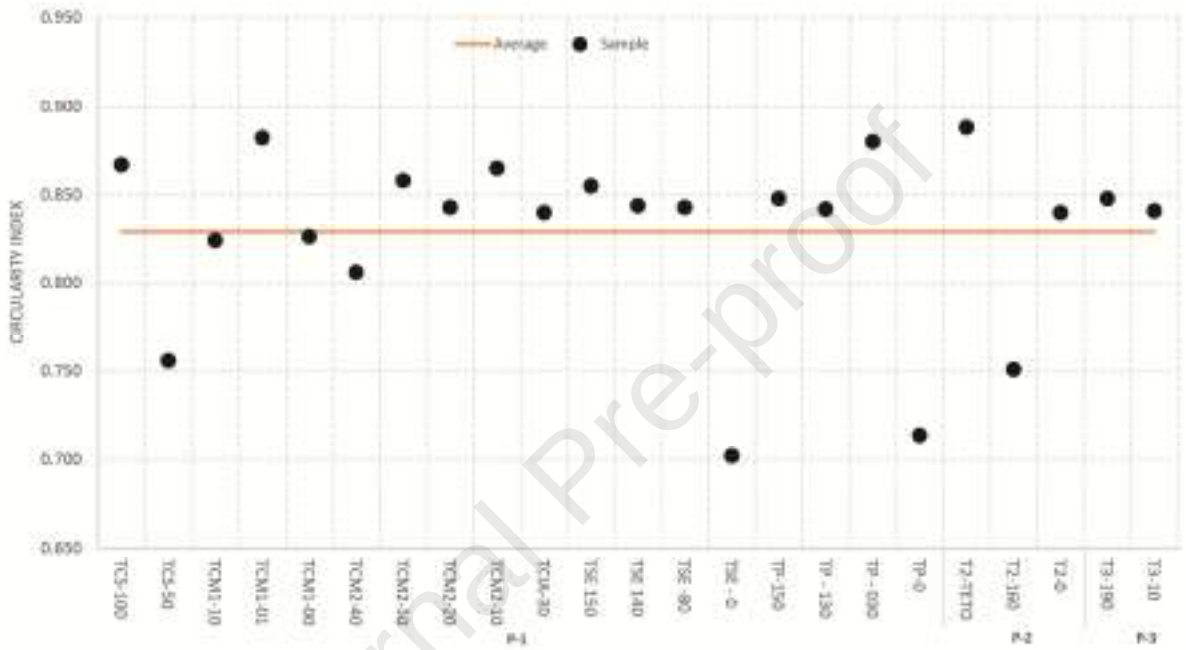

Fig. 8 Circularity Index results compared to the average Circularity Index (horizontal red line) from all samples.

5.2 Facies Description

In the Tarimba cave, the sedimentary deposits were grouped into eight different facies represented by autochthonous and allochthonous sediments (Table 2 and Fig. 9- A,B,C,D). The Guano deposits (facies) represent phosphate accumulation and are the only sediments of autochthonous origin, corresponding to fecal material of animals. They occur as black sediments with whitish portions at the top of the section. In the allochthonous deposits, fine-grained sediments (silt and clay) are predominant, but they can contain up to 35% of sand and 15% of gravel (Fig. 9 – E). Following the classification of White (2007), the allochthonous sediments were separated into two main groups comprising four facies (Diamictiton, Channel, Backswamp, and Slackwater). Following the classification of White (2007), the allochthonous sediments were separated into two main groups comprising four facies (Diamicton, Channel, Backswamp, and Slackwater).

397

398 *Table 2 Sedimentary facies described in the studied deposits*

399

Sediments Origin	Flow Type	Facies	Code	Description	Structure
Autochthonous	-	Guano	G	Guano	Structureless
Allocthonous	Debris flows	Conglomerate	Dccm	Clast-supported gravel	Structureless
	River flow	Channel	Caa	Fine to coarse sand that may contain gravel	Trough cross-bedding
			Cah	Fine to coarse sand that may contain gravel	Horizontal lamination
			Cam	Fine to coarse sand with occasional gravel	Structureless
			Cccm	Clast-supported gravel	Structureless
		Backswamp	Bsm	Silt, clay and sand	Massive and contraction cracks
		Slackwater	Ssl	Silt, clay and sand	Heterolithic lamination and contraction cracks

400

401 The Diamicton facies represents high density gravity flow and would results from extreme rainfall
402 events and sediment flux in high gradient cave passages yielding in a massive and poorly sorted
403 sedimentary deposit (White, 2007). In the Tarimba cave, they occur exclusively in the sides of Profile
404 1 and also in a configuration of lateral accretion and intercalated with the Channel facies (Fig. 9 – F,
405 G). This facies is formed by poorly-sorted sediments represented by clast-supported massive gravel,
406 with about 20-35% of gravel of varied roundness degree and sand-silt matrix composed of 34-55% of
407 sand, 15-25% of silt, and less than 10% of clay.

408 The alluvial deposition is the main sedimentary process responsible for sediment deposition inside the
409 cave. The alluvial deposits are represented by Channel, Backswamp, and Slackwater facies, ranging
410 from clay to gravel. Fractures and cracks in the surroundings, are absent and the water transport is
411 interpreted in association with the existence of an active watercourse with the surface at ~8 m below
412 the location of the deposit, in addition to lamination and cross-stratification pointing to water-laid
413 sediment transport.

414 The Channel facies occurs in all studied profiles and is the most common in Tarimba cave. Its deposits
415 can be stratified, showing layers with similar thicknesses, different shades, well-defined contacts, and
416 poor to moderately sorted sediments, which may also contain levels with organic matter besides
417 fragments of charcoal and calcite crusts (Fig. 9). The Channel deposits comprise sandy channel facies
418 and gravelly channel facies. The sandy facies have over 60% of very fine to coarse sand, with mean
419 values above 90%. The gravelly facies are found in minor proportions and can reach up to 20% of
420 gravel, with 35% of silt, and 7% of clay. The definition of these facies is essentially based on the
421 observed sedimentary structures (Fig. 9- H, I, J, K).

422 The Channel facies with gravel, defined as clast-supported structureless gravel – Cccm, is similar to
423 the Dccm facies due to the high amount of gravel (30 - 46 %) (Fig. 9– G, H). However, it is
424 differentiated by a matrix with 45 - 65% of sand and a low quantity of silt/clay (< 5%). Another
425 difference is that their sediments are moderately sorted, as opposed to those originated by flow debris
426 and always occur associated with the sandy channel facies. Sometimes, it presents low cohesion,
427 which would be characteristic of the minor amount of fine-grained sediments and lack of cementation.

428

429

430

431

432

433

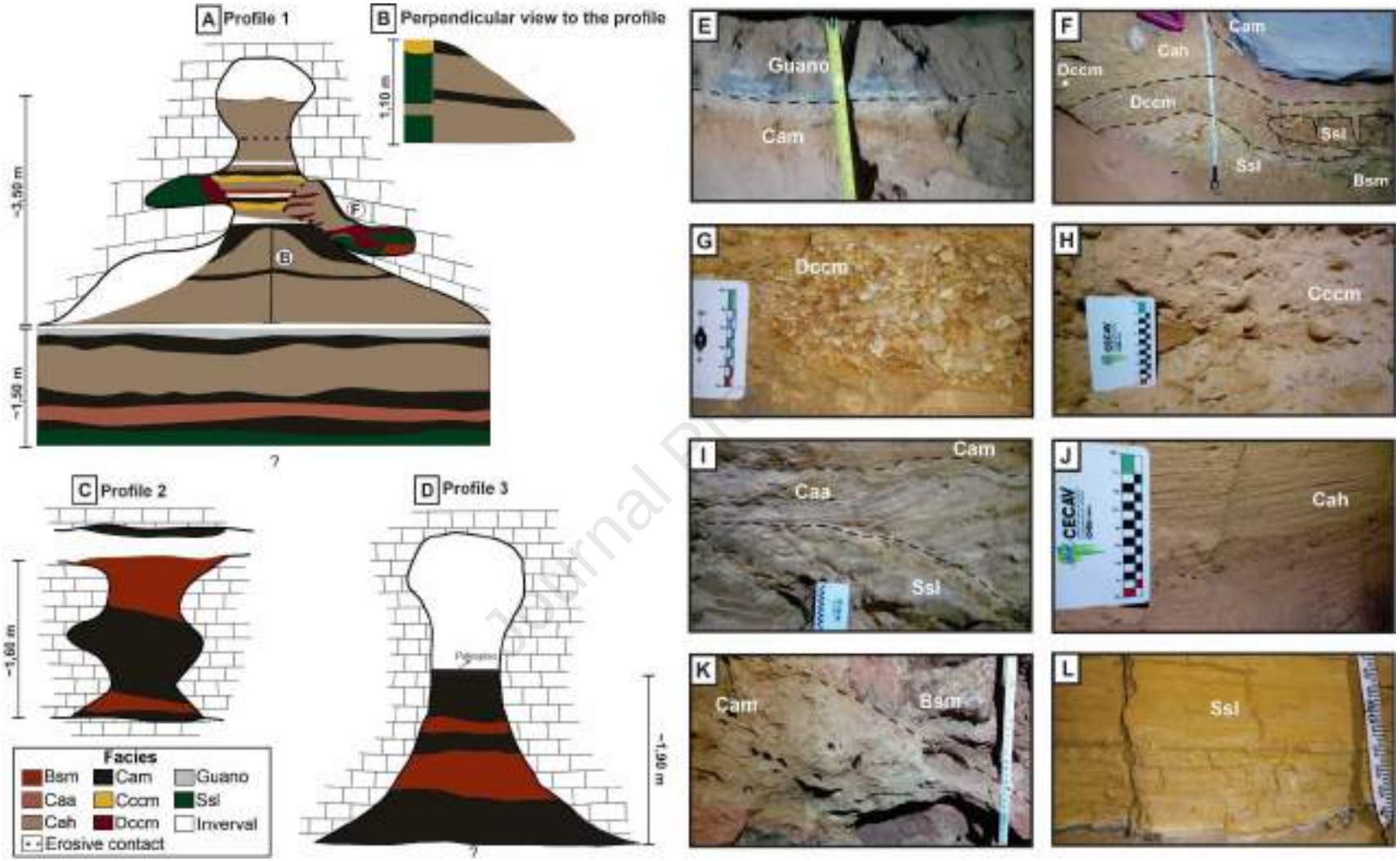

Fig. 9 Spatial distribution of sedimentary facies in profiles: A – Profile 1, B – Perpendicular view of the facies located on the base of Profile 1, C – Profile 2 and D – Profile 3. Pictures represent the facies found in the Tarimba cave (E, F, G, H, I, J, K, L).

The Backswamp facies is interpreted as suspended sediments transported by cave streams and fastly deposited by decantation in calm water settings (Campaña et al., 2017). It corresponds to Bsm facies with high content of very fine to fine silt that may reach more than 80% of the deposit, and above 50% of clay, with minor amount of gravel. Less than 30% of sand is found, although the average value is around 10% with a few levels above 20%. It is formed by ocher yellow, brown, and red sediments, often covered by a black coating pointing to oxidation. Sometimes, it is organized in the form of massive prismatic blocks with contraction cracks in some portions. It occurs predominantly in P-2 and P-3, usually associated with channel facies in an alternating deposition (Fig. 7 and Fig. 9- K).

The Slackwater facies is formed from the combined deposition of sediments by decantation and traction originating from flooding or pulsed flow (Ford and Williams, 2007; White, 2007), leading to the formation of heterolithic lamination. In the studied profiles, it corresponds to Ssl facies that resembles Bsm facies, but differs mainly for having laminations (Fig. 9– L). Sometimes, it presents contraction cracks, besides a smaller clay amount (maximum of 30%), and higher content of sand, with an average of 20% that may reach up to 37%. It shares the highest silt content (45-75%) and the lower amount of gravel. It occurs only in P-1, associated to the Diamicton or Channel facies as well as in the lower central portion of the cave (Unit IV).

5.3 Geochronology

The geochronological results are shown in Table 3 and Table 4. In P-1, the obtained ages range from 50 to 90 Ka (Units I, II and VII, Fig. 5 and Fig. 6). In their upper portion, two dates differ from the rest: the OSL age of 197 Ka (Unit III) represents the bottom of the succession, but it must be analyzed with caution and associated with other proxies and observations since incomplete bleaching of quartz grains can occur in cave environments, leading to age overestimation (Jacobs et al., 2011; Rhodes, 2011; Constantin et al., 2014). However, all samples presented equivalent dose distributions with overdispersion ranging from 10 to 25% (Table 2). These overdispersion values suggest sediments well bleached prior to deposition and absence of significant post-depositional mixing or dose rate heterogeneities. Some samples (two samples at P-3, and two samples at P-1, Unit V) have OSL signals in saturation. For these samples, minimum ages were calculated considering the double of the characteristic dose ($2D_0$) from dose response curves as a minimum equivalent dose. The saturated samples have higher dose rates, which would explain the signal saturation. All non-saturated samples have ages in stratigraphical order, which supports the reliability of the OSL ages to interpret the depositional history within the cave. It is also highlighted that the relatively low dose rate of non-saturated samples allowed a relatively extended age limit.

The second outlier age occur in Unit II, where the ^{14}C age (27.00 – 26.31 Ka cal BP) is significantly younger than the OSL ages (ages older than 50 Ka). One of the interpretations for the younger radiocarbon age may be due to the absorption of modern ^{14}C from HCO_3 in the flowing groundwater, resulting in age underestimation (Ford and Williams, 2007). Water containing humic acids that may have infiltrated in the deposited sediments is another possibility leading to radiocarbon age underestimation (Darrénougué et al., 2009). The other possible explanation would be the existence of long time lag between the entering of sediments in the cave (sunlight blocking and triggering of the OSL chronometer) and their final deposition in the studied profiles. However, the normal stratigraphic order of luminescence ages and equivalent dose distributions with low overdispersion, pointing to absence of post-depositional mixing, make this last explanation less plausible.

Table 3 Summary of OSL dating results.

	Unit	Facies	Lab. cod.	Sample cod.	Depth (m)	Acepted/ measured aliquots	Overdispersion (%)	Water sat.	U (ppm)	Th (ppm)	K%	Total Dose rate (Gy/Ka)	Equivalent dose (Gy)	OSL age (Ka)
Profile 1	I	Cah	L1228	TCS-100	6.40	23/24	10.7	0.012	0.668±0.042	3.292±0.173	0.145 ± 0.011	0.610±0.047	39.9 ± 1.0	65.39 ± 5.34
		Cah	L1227	TCS-50	6.90	23/24	17.7	0.002	0.428±0.024	0.857±0.059	0.024 ± 0.004	0.260±0.018	21.0 ± 0.8	80.72 ± 6.49
	II	Cah	L1225	TCM1-10	7.80	24/24	22.1	0.020	0.575±0.036	1.821±0.115	0.210 ± 0.012	0.539±0.042	47.2 ± 2.2	87.60 ± 8.02
	III	Cah	L1226	TCM2-10	8.15	23/24	18.9	0.003	0.321±0.020	0.695±0.053	0.015 ± 0.003	0.207±0.015	40.8 ± 1.7	197.23 ± 16.09
	V	Dccm	L1223	TSE-140	6.44	6/6	-	0.055	1.283±0.056	11.263±0.387	1.691 ± 0.072	2.740±0.228	97.8 ± 2.2	35.69 ± 3.08*
		Cah	L1224	TSE-150	6.22	6/6	-	0.026	0.930±0.042	7.344±0.265	1.080 ± 0.046	1.872±0.159	82.3 ± 1.6	43.96 ± 3.82*
	VI	Cah	L1221	TSE-0	7.29	24/24	18	0.017	0.500±0.027	1.551±0.088	0.160 ± 0.009	0.457±0.035	32.3 ± 1.2	70.71 ± 5.99
		Cah	L1222	TSE-80	6.69	22/24	10.9	0.018	1.626±0.072	2.741±0.158	0.242 ± 0.015	0.889±0.071	46.4 ± 1.4	52.20 ± 4.48
	VII	Cam	L1220	TP-30	7.20	24/24	26.2	0.011	0.268±0.020	1.200±0.072	0.124 ± 0.007	0.344±0.026	28.2 ± 1.5	82.00 ± 7.49
		Cah	L1219	TP-130	6.20	22/24	18.3	0.003	0.295±0.021	0.573±0.052	0.006 ± 0.004	0.194±0.014	15.5 ± 0.7	79.84 ± 6.66
Profile 3	-	Cam	L1360	T3-190	6.00	17/34	-	0.010	0.910±0.042	5.426±0.207	0.695± 0.030	1.400±0.116	84.8 ± 0.9	60.57 ± 5.06*
	-	Cam	L1361	T3-10	7.80	10/10	-	0.030	1.277±0.053	7.321±0.256	0.923 ±0.040	1.805±0.150	107.7±1.4	59.66 ± 5.01*

*Samples with signal in saturation - minimum age from $2D_0$

Table 4 ^{14}C dating.

	Unit	Lab code	Sample code	Depth (m)	Method	Material	Age (Ka ^{14}C BP)	Calibrated age (Ka cal BP)
Profile 1	II	Beta - 510831	TCM1-20	7.7	AMS	organic sediment	22.39 ± 0.07	27.00 – 26.31

5.4 Chemical and Mineralogical Analysis

The results of chemical analysis can be seen in Fig. 5, Fig. 6 and Fig. 7to for the main data. The PCA of sediment data breaches into two principal components (Fig. 10), with 79% of the total variance. The PC1 (57%) shows high factor loadings for Al2O3, TiO2, FeO3, MgO, K2O, clay, and silt, and are grouped with Ssl and Bsm facies. Additionally. It also includes the Dccm facies that despite having high gravel content, also presents high levels of clay and silt.

The positive values of PC2 (22 %) are related only to facies G, which may have values associated with animal feces (LOI and P_2O_5), and dissolution and precipitation processes on the surface (LOI and CaO). Finally, the negative values of PC1 and PC2, composed of SiO_2 and sand, delimitate the Channel facies (Cah, Cam, Caa, and Cccm).

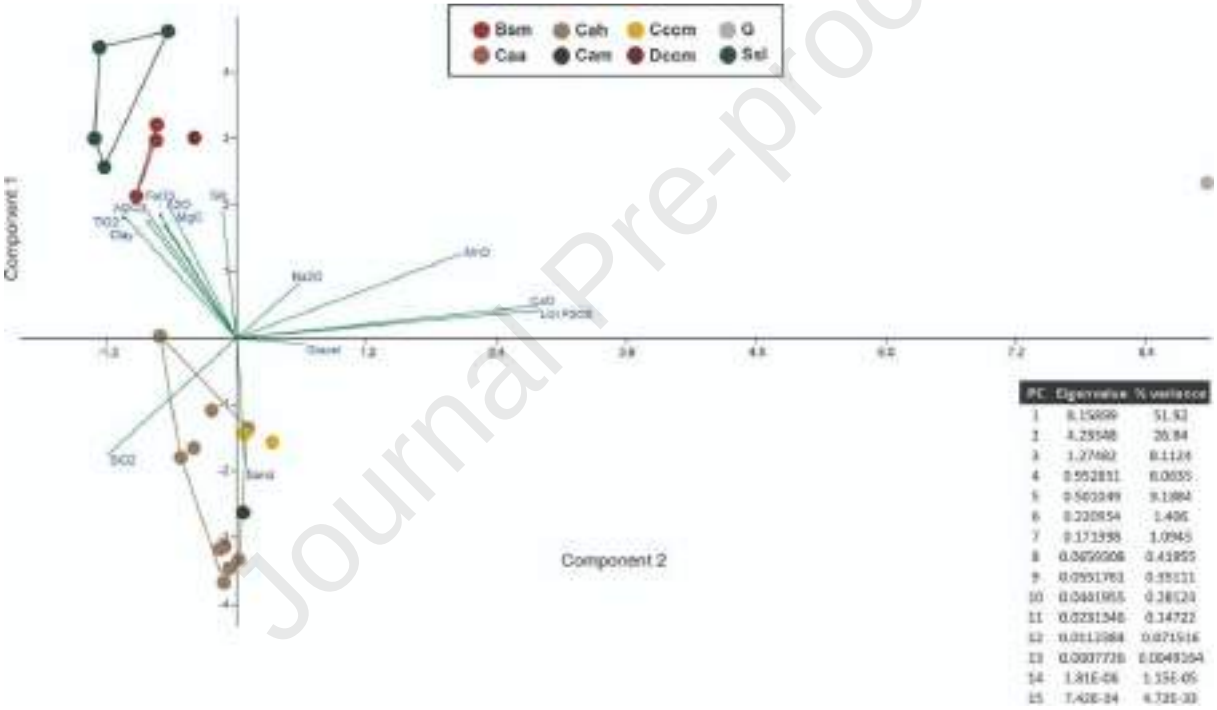

Fig. 10 Principal Component Analysis bi-plot for major elements in the sediments from Tarimba cave. The percentual of the component of each variance is in the right corner of the figure.

The high CPA values from 70 to 98% demonstrate high weathering rates for these. Notoriously, there is a tendency for superficial layers to have higher values compared to intermediate and base layers that assume comparatively lower rates.

The qualitative mineralogical analysis is presented in Table 5, showing a similar composition between the facies that correlate with the homogeneous chemical composition. In general, there is a predominance of quartz and kaolinite in all facies analyzed, as well as muscovite and montmorillonite

discontinuously along with the profile. Iron oxides and hydroxides such as hematite (Profile 3) and goethite (Profile 1 - Units I and V) occurred with lower recurrence, associated with the top of the sedimentary sequences. Minerals like anatase and rutile were exclusive to level of P-1 and P-3 (Fig. 5 to Fig. 7).

Table 5 Clay mineralogy result.

	Unit	Facies	Sample	Quartz	Muscovite	Kaolinite	Montmorilonite	Goethite	Rutile	Anatase	Hematite
Profile 1	I	Cah	TCS-100	x	x	x	x	x			
		Cah	TCS-50	x		x					
	II	Cah	TCM1-10	x		x					
	III	Cah	TCM2-10	x	x	x					
	V	Cah	TSE-150	x	x	x	x	x	x	x	
		Dccm	TSE-140	x	x	x	x	x			
	VI	Cah	TSE-80	x	x	x	x				
		Cah	TSE-0	x	x	x	x				
	VII	Cah	TP-130	x		x					
		Cam	TP-30	x	x	x					
Profile 3	-	Cam	T3-190	x	x	x	x			x	x
	-	Cam	T3-10	x	x	x	x				

6 DISCUSSION

6.1 Superficial Environment and sedimentary deposition phases

The sediment deposition within the Tarimba cave is related to the superficial environmental dynamics. The sediments are originated from rocks of the Urucuia and Bambuí Groups (Fig. 1and 2). This is supported by the compositional and grain size characteristics of the cave sediments, which present similarities with the soils mapped in the region. Three distinct compositional-textural groups of sediments are recognized: a) silt with high levels of P_2O_5 inside the cave; b) sandy sediments rich in SiO_2; c) fine sediments (clay and silt) containing a high percentage of Al_2O_3, TiO_2, FeO_3, MgO and K_2O. Such variations may indicate the existence of different sediment transport conditions and sources areas during the filling of the endokarst (Arriolabengoa et al., 2015). In the studied cave, the

sediments constituting the described facies would be sourced from local areas. Hence, they allow to interpret changes in the local landscape over the last 200 Ka.

The oldest sedimentary records indicate a discontinuous deposition that occurred from the Middle Pleistocene to the Late Pleistocene, comprising an interval of around 145 Ka. The upper ducts filled with sandy-clayey sediments of metric thicknes were abandoned due to the reestablishment of the regional base level, generating the current cave configuration (SBE et al., 2014). The sedimentary facies, textural, compositional and geochronological data permitted to constrain the sedimentary evolution of the Tarimba. These data allowed to track the major depositional events and interpret possible landscape scenarios during the Late Quaternary.

Three phases of sediment deposition with established chronological intervals were found in Profile-1 (P-1,Fig. 11). Phase 1 comprises the oldest sediments of Profile 1 with age older than 197 Ka in contact with sediments of Unit V from 35 to 45 Ka (minimum age). However, the stratigraphic sequence bounded by erosive contacts could indicate older deposition. The lower and upper limits of the unit representing this phase are unknown. The lower limit was not reached during excavation and the upper is uncertain for not having any trace of accumulation in the ceiling of conduit. At least three depositional events can be identified in this phase (Fig. 11- a, b, c): the first (Phase 1a) represented by the SSL facies (Unit IV and V) indicates low energy water flow with oscillations characteristic of flooding facies followed by a period of removal and sub-area exposure marked by contraction cracks (Phase 1b) (Fig. 5 and Fig. 6). This facies is truncated by an erosive phase and followed by a gravity flow depositional event (Phase 1c) with higher energy hydraulic conditions, capable of depositing massive gravel and fine sediments (Dccm facies) with progressive transition to Cah facies (Fig. 9 – F).

Phase 2 corresponds to Unity III and starts after an erosive event where the age with which part of the sediments of Phase 1 was removed from the central portion of the profile is unknown, leaving remaining material on the sides (Fig. 11– d, e). The lack of dating at the base makes the beginning of this event uncertain. However, it is known that around 197 Ka, a high energy flow deposited the sandy facies, which includes layers with plane parallel laminations inclined at an angle compatible with erosion also observed in other overlapping strata. At the top of the phase, coarser sediments such as gravel (Cccm facies) are observed, indicating an increase in energy flow that gradually decreases, intermediate sandy facies, until reaching slower levels marked by the deposition of fine sediments on the top. The presence of contraction cracks at the top of this sequence (Bsm facies) may indicate a time gap capable of providing a sub-area exposure of sediments. Geochemistry, mineralogy, and circularity index data resemble the sediments of Phase 3, corroborating to nearby sources despite the time interval of more than 100 Ka.

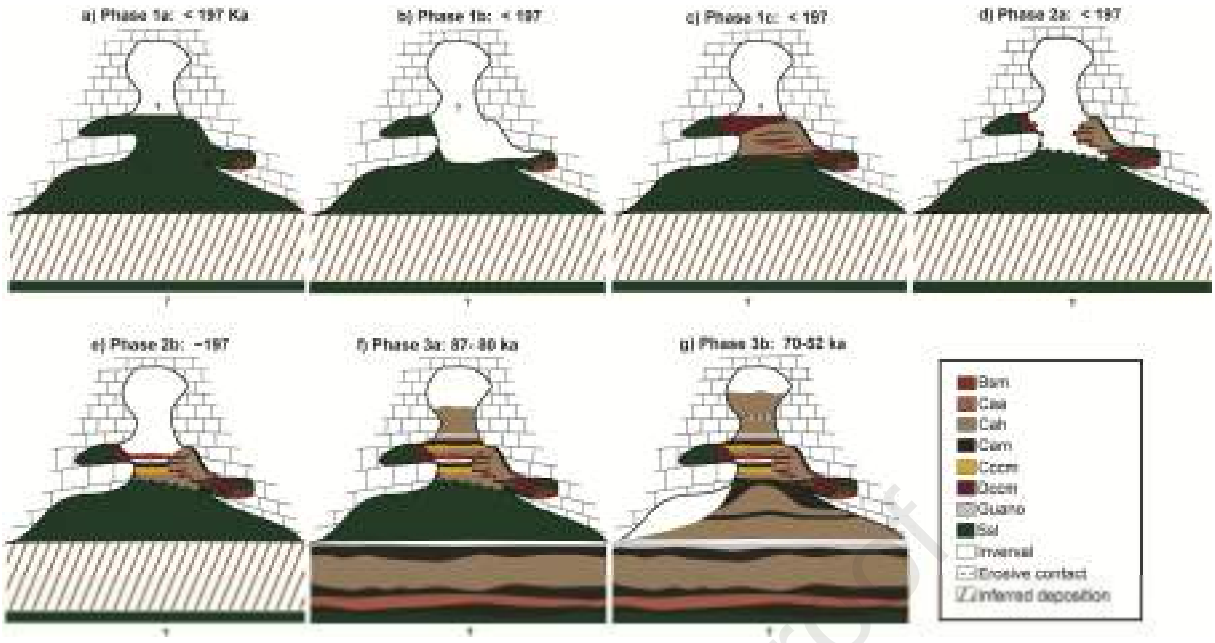

Fig. 11Sedimentary deposition evolution in Profile 1.

Phase 3 occurs during the Upper Pleistocene, corresponding to the range of 87 to 52 Ka (Units I, II, VI, VII, Fig. 5 and Fig. 6) marked by successive flows resulting from the oscillation of the water column in which recent sediments are transported through the upper passage of the profile, above the Bsm facies (Phase 2 thermal). This sequence results on the sediments spreading in the profile ground overlapping layers of phases 1 and 2, allowing to found chrono correlated sequences both in the base and top of the profile. (Fig. 11– f/g).

This correlation is observed in geochemistry, mineralogy, and grain size from the erosion surface that allows identifying a Phase 3a that involves an interval between 87 - 80 Ka (Unit II and base of unit I, Unit VII) and a Phase 3b between 70 - 52 Ka (Top of Unit I and Unit VI). Both phases have sandy sediments in which there are variations between the Channel facies and the presence of sedimentary structures reflects the change of the hydraulic behavior, which depending on the intensity, may even present levels with gravel (Cccm facies). At the top of the successions, a slight change in granulometry can be seen, with a decrease in the percentage of sand and an increase in finer sediments between 65-52 Ka old, which indicates a decrease in flow intensity. Finally, the Guano facies were deposited on the profile access floor from the stabilization of hydraulic conditions.

Profiles 2 and 3, used in a complementary way, have a similar depositional architecture ~~that is~~ not identified in P-1. This feature suggests that these sediments were not reached in P-1 or that they were removed during periods of more intense flow. Dating performed in P-3 are of little help in this case, given the saturation of the sediment, implying in the calculation of minimum ages (59.66 ± 5.01 Ka and 60.57 ± 5.06 Ka), and requiring future analysis to clarify it. Although there is an absence of

geochronological data, the association between facies allows us to infer that profiles 2 and 3 are contemporary because at least three phases can be identified (Fig. 12): Phase A - resulting from alternating hydraulic flows corresponding to the filling of the ducts by Backswamp and Channel facies; Phase B – sediment removal preserving the studied sequences and material on the cave walls, exposing the profiles used in the study; and Phase C formation of the paleofloor in P-3 after stabilization of the sedimentation, which demonstrates the existence of a relatively humid period.

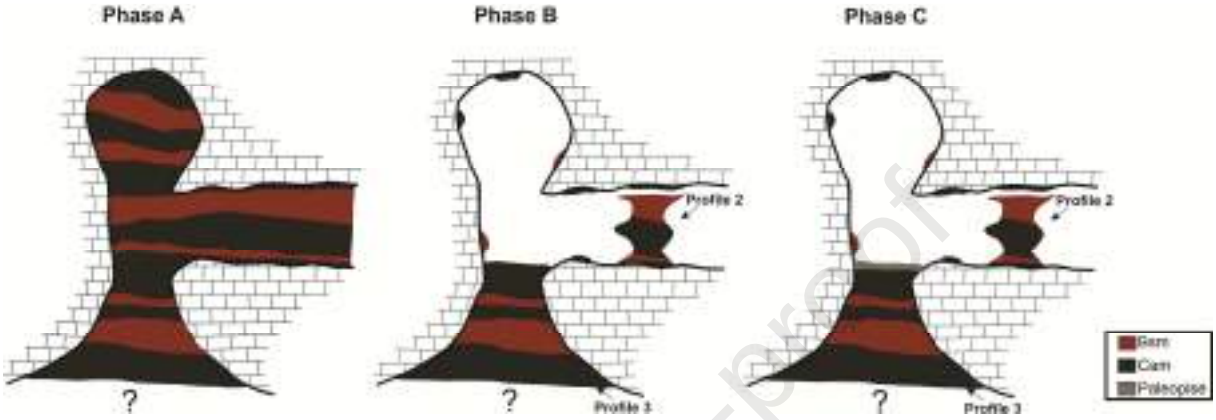

Fig. 12 Schematic section for depositional events that occurred in Profiles 2 and 3. ***Use color for printed pictures***

6.2 Surface landscape erosion, climate change and cave sediment deposition

The clastic deposits preserved in the Tarimba cave are derived from surface erosion, being product of the landscape evolution. The chronology of cave sedimentary deposits makes possible to constrain erosion and depositional events associated with the evolution of the relief over time, allowing the establishment of connections with environmental changes during the Quaternary. Studies with clastic sediments in the Brazilian caves have shown that the processes of erosion and deposition may be related to paleoclimatic variability. In dry climate settings, the entry of sediments in caves is controlled by episodic rainfall once that the absence of dense vegetation would increase soil erosion and sediment supply while in wet setting, the presence of a denser vegetation cover reduces erosive processes and sediment supply (Auler et al., 2002; 2009; Jaqueto et al., 2016; Haddad-Martim et al., 2017; Novello et al., 2019). However, this dynamics also depends of the fluvial processes and sediments temporary stored in river valleys (Herman et al., 2012; Laureano, 2014).

The absence of specific paleoclimatic records in the Tarimba region difficults the comparison between erosion-depositional phases and rainfall variations during the Late Quaternary. Then, we used weathering indexes (CPA) to deduce the erosion and deposition sedimentary dynamics of the landscape suppling sediment to the Tarimba cave. Furthermore, climatic conditions in the last 200 Ka

606 were inferred by comparing our geochronological data with paleoclimatic records from speleothems of
607 the Lapa Grande Cave, which represents climate conditions of Central Brazil (Stríkis, 2015). The
608 chemical weathering indexes reflect the intensity of the climate action on the relief according to the
609 exposure time, which will vary depending on the weathering material (Dinis et al., 2020). Although
610 there is no consensus on the interpretation of such indexes, the use of CPA proved to be a reliable
611 indicator of Quaternary climatic variability from sedimentary records inside the Mohui cave in China
612 (Cheng et al., 2020).

613 The CPA index was calculated using data from Profile 1, excluding the deposits where we obtained
614 only minimum OSL ages. The results show high weathering rates (79.22 to 98.58%) in which the
615 highest rates are correlated with warmer and wetter conditions (Dinis et al., 2020). However, even in
616 this scenario of high weathering rates, it is possible to infer three climatic situations that may have
617 influenced the erosion dynamics. The first situation is represented by the lower CPA index, compared
618 to the others (86.03%), which corresponds to the oldest depositional phase (Fig. 5) Such age can be
619 correlated with the Marine Isotope Stage (MIS) 7 period (Unit III, Fig. 13).

620

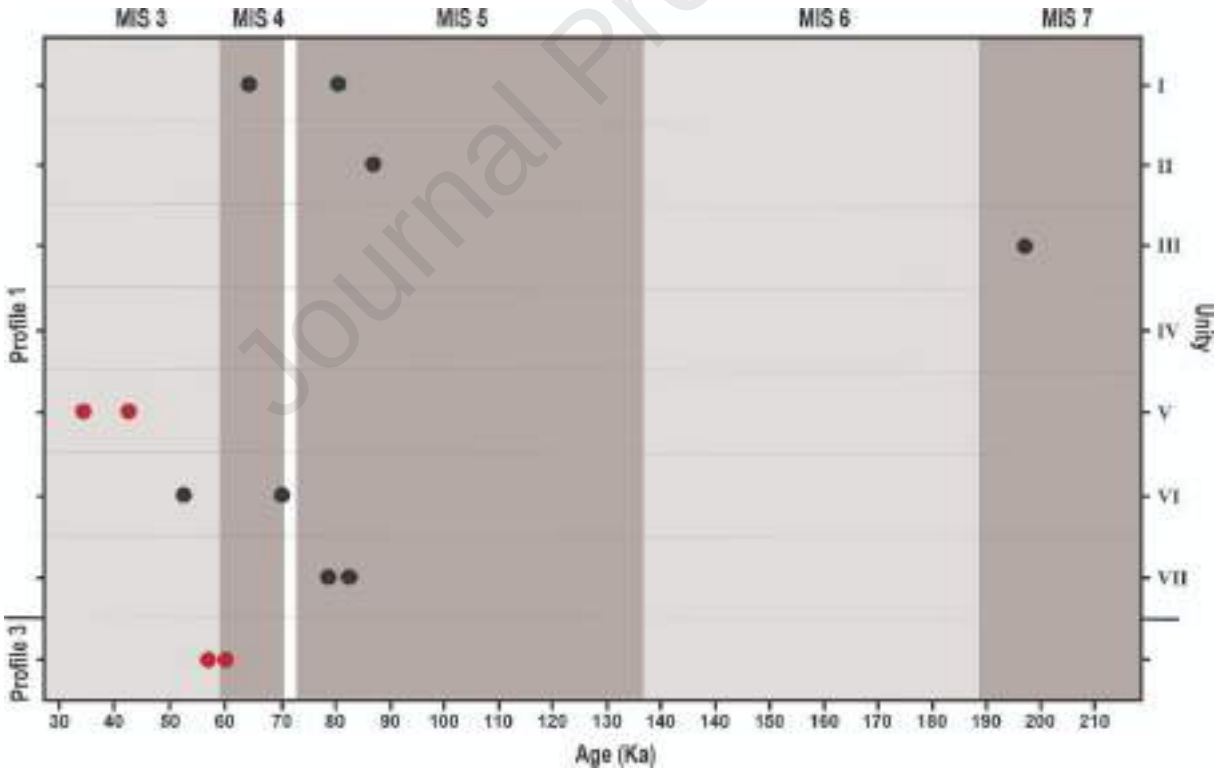

621

622 *Fig. 13 OSL ages obtained from Profile 1, with the corresponding Isotopic Marine Stages (MIS). Black dots*
623 *represent absolute ages, while red ones represent minimum ages.*

624

625 The interval in which the CPA reaches lower values between 79.22 and 89.17% is represented by
626 intermediate sediment layers with ages between 87 and 70 Ka, which are predominantly correlated

with the MIS 5 (130-75 Ka), (Unit I, II, VI and VII, Fig. 13). Isotopic analyses of $\delta^{18}O$ in speleothems from the Lapa Grande cave in the central-eastern region of Brazil showed that during the last glacial and Holocene period (60-85 Ka), the climate was predominantly drier with relatively low rainfall compared to the southernmost regions of Brazil (Stríkis, 2015).

In the last phase of sediment deposition (65-52 Ka), the weathering rate is higher (93.90 to 98.08%), suggesting wetter climate during the MIS 3 and MIS 4 (Unit I and VI,Fig. 13). Data on climatic conditions corresponding to the end of the MIS 3 period are absent. However, among the gaps identified throughout MIS 3 (between ~ 60 and ~ 27 Ka), the period between 49 and 40 Ka suggests the shift to a drier phase. It was also attributed to this period temperatures variations relate to stadial (cold) and interstadial (warm) phases (Stríkis, 2015).

Our survey shows that high weathering rates recorded by sediments preserved in the Tarimba cave indicate the predominance of warm and humid climates in the region during the last 200 Ka. However, according to the isotopic data from the Lapa Grande cave, the region was drier and with sporadic rainfall events. It must be highlighted that the clastic deposits can record only the major rainfall episodes while speleothems record average climatic conditions. Also, the sediment composition can represent long term weathering conditions for soil production, which can differ from the conditions prevailing during the phases of soil erosion and sediment transport to the cave. Thus, the deposition of clastic sediments inside the Tarimba cave occurred during drier periods, as showed by paleoclimate studies in central Brazil. As pointed out by Auler et al. (2009), past drier periods reduced the vegetation cover and exposed soil to erosion, increasing sedimentation rates during episodic rains. Considering the local character of the study setting, further studies will be necessary in order to test this explanation about how climate variations control the sedimentation in Brazilian cave systems.

7 FINAL CONSIDERATIONS

The deposition of clastic sediments in caves is associated with the climate dynamics of the surrounding environment. In the case of Tarimba cave, the geomorphological processes active in the retreat of the relief provides the sediments of the Urucuia (sandy) and Bambuí (silt-clay) groups that are transported and deposited inside the cave. The establishment of new base levels by regional rivers is responsible for the abandonment of galleries crammed with sediments in the upper levels, allowing the establishment of three major sedimentary deposition phases in Profile 1 and two in Profiles 2 and 3. In the last 200 Ka, the depositional architecture as well as the sedimentary facies analysis allowed the interpretation of flow conditions of sediment deposition, which are represented by eight facies corresponding to the features currently found in the cave.

The results found three depositional phases in the studied profiles. The first one is relative to the oldest sediments, prior to 200 Ka, whose configuration indicates alternation of water flow energy

transporting and forming a clast supported level. Contraction cracks indicate at least one period of sub-aerial exposure with an interruption in the deposition. The second phase begins after an erosive event and has at last one confirmed age of 197 Ka. Sandy sediments predominate, corresponding to the channel facies with oscillations in the energy and grain size gradation. The third phase is formed by channel facies as the second one, which comprises the interval between 87 to 52 Ka, subdivided into 87-80 Ka and 70-52 Ka, with alternation in the arrangement of sandy and silty facies that indicate an oscillation in the intensity of the hydraulic flow. The last phase establishing the current configuration visualized in the cave. The extensive amount of methodologies used offers important information for the development of future studies with a paleoenvironmental perspective in the Brazilian cave deposits.

8 FINANCING

This work is part of the project “Susceptibilidade e Hidro-geomorfologia Cárstica da APA Nascente do Rio Vermelho/GO” funded by CECAV / ICMBIO, process n.02667.000110 / 2017-10.

9 REFERENCES

Aitken, M.J., 1998. An Introduction to Optical Dating. Oxford University Press, New York.

Anderton, R., 1985. Clastic facies models and facies analysis. Geological Society, London, Special Publications 18, 31–47. doi:10.1144/GSL.SP.1985.018.01.03

Araujo, V.A. de, Moreton, L.C., 2008. Unidades Litoestratigráficas. In: Geologia Do Estado de Goiás e Distrito Federal. Goiânia, pp. 43–113.

Arriolabengoa, M., Iriarte, E., Aranburu, A., Arrizabalaga, A., 2015. Provenance study of endokarst fi ne sediments through mineralogical and geochemical data (Lezetxiki II cave , northern Iberia). Quaternary International journal 364, 231–243. doi:10.1016/j.quaint.2014.09.072

Auler, A.S.., Smart, P., Tarling, D.H.., Farrant, A.R., 2002. Fluvial incision rates derived from magnetotratigraphy.pdf. Zeitschrift für Geomorphologie 46, 391–403.

Auler, A.S., Piló, L.B., Smart, P.L., Wang, X., Hoffmann, D., Richards, D.A., Edwards, R.L., Neves, W.A., Cheng, H., 2006. U-series dating and taphonomy of Quaternary vertebrates from Brazilian caves. Palaeogeography, Palaeoclimatology, Palaeoecology 240, 508–522. doi:10.1016/j.palaeo.2006.03.002

Auler, A.S., Smart, P.L., Wang, X., Piló, L.B., Edwards, R.L., Cheng, H., 2009. Cyclic sedimentation in Brazilian caves: Mechanisms and palaeoenvironmental significance. Geomorphology 106, 142–153. doi:10.1016/j.geomorph.2008.09.020

Ballesteros, D., Giralt, S., García-Sansegundo, J., Jiménez-Sánchez, M., 2019. Quaternary regional evolution based on karst cave geomorphology in Picos de Europa (Atlantic Margin of the Iberian Peninsula). Geomorphology 336, 133–151. doi:10.1016/j.geomorph.2019.04.002

Buggle, B., Glaser, B., Hambach, U., Gerasimenko, N., Marković, S., 2011. An evaluation of

geochemical weathering indices in loess-paleosol studies. Quaternary International 240, 12–21. doi:10.1016/j.quaint.2010.07.019

Campaña, I., Benito-Calvo, A., Pérez-González, A., Bermúdez de Castro, J.M., Carbonell, E., 2016. Assessing automated image analysis of sand grain shape to identify sedimentary facies, Gran Dolina archaeological site (Burgos, Spain). Sedimentary Geology 346, 72–83. doi:10.1016/j.sedgeo.2016.09.010

Campaña, I., Benito-Calvo, A., Pérez-González, A., Ortega, A.I., Bermúdez de Castro, J.M., Carbonell, E., 2017. Pleistocene sedimentary facies of the Gran Dolina archaeo-paleoanthropological site (Sierra de Atapuerca, Burgos, Spain). Quaternary International 433, 68–84. doi:10.1016/j.quaint.2015.04.023

Campos, J.E.G., Dardenne, M.A., 1997. Estratigrafia E Sedimentação Da Bacia Sanfranciscana: Uma Revisão. Revista Brasileira de Geociências 27, 269–282. doi:10.25249/0375-7536.1997269282

Cheng, L., Bae, C.J., Hong, H., Huang, S., Wang, W., Yin, K., Wang, C., 2020. Environmental fluctuation impacted the evolution of Early Pleistocene non-human primates: Biomarker and geochemical evidence from Mohui Cave (Bubing, Guangxi, southern China). Quaternary International 563, 64–77. doi:10.1016/j.quaint.2020.02.035

Cherem, L.F.S., Varajão, C.A.C., 2014. O PAPEL DA LITO-ESTRUTURA DO CARSTE NA MORFODINÂMICA CENOZÓICA DA SERRA GERAL DE GOIÁS (GO/TO/BA): APROXIMAÇÕES INICIAIS. Geonorte 10, 180–184.

Constantin, S., Robu, M., Munteanu, C.M., Petculescu, A., Vlaicu, M., Mirea, I., Kenesz, M., Drăguşin, V., Hoffmann, D., Anechitei, V., Timar-Gabor, A., Roban, R.D., Panaiotu, C.G., 2014. Reconstructing the evolution of cave systems as a key to understanding the taphonomy of fossil accumulations: The case ofUrşilor Cave (Western Carpathians, Romania). Quaternary International 339–340, 25–40. doi:10.1016/j.quaint.2013.10.012

Cruz, A.B. da, 2012. Detalhamento da geologia das unidades carbonáticas do Grupo Bambuí na região de Alvorada do Norte, Goiás. Universidade de Brasilia.

Dardenne, M.A., 1981. Anais do Simpósio sobre o Cratón do São Francisco e suas faixas marginais. In: Os Grupos Paranoá e Bambuí Na Faixa Dobrada Brasília. Salvador, pp. 140–157.

Dardenne, M.A., Magalhaes, L.F., Soares, L.A., 1978. XXX Congresso Brasileiro de Geologia. In: Geologia Do Grupo Bambuí No Vale Do Rio Paranã (Goiás). Recife, pp. 611–621.

Darrénougué, N., Deckker, P. De, Fitzsimmons, K.E., Norman, M.D., Reed, L., Kaars, S. van der, Fallon, S., 2009. A late Pleistocene record of aeolian sedimentation in Blanche Cave, Naracoorte, South Australia. Quaternary Science Reviews 28, 2600–2615. doi:10.1016/j.quascirev.2009.05.021

Dinis, P.A., Garzanti, E., Hahn, A., Vermeesch, P., Cabral-Pinto, M., 2020. Weathering indices as climate proxies. A step forward based on Congo and SW African river muds. Earth-Science Reviews 201, 103039. doi:10.1016/j.earscirev.2019.103039

Farrant, A.R., Smart, P.L., 2011. Role of sediment in speleogenesis; sedimentation and paragenesis. Geomorphology 134, 79–93. doi:10.1016/j.geomorph.2011.06.006

Faure, M., Guérin, C., Parenti, F., 1999. Découverte d ’une mégafaune holocène do Serrote do Artur (aire archéologique de Sao Raimundo Nonato, Piauí, Brésil). C. R. Acad. Sci. Paris 443–448.

Ferreira, C.F., Uagoda, R.E.S., 2019. O uso de veículo aéreo não tripulado - VANT para construção de modelos digitais de terreno – MDT e identificação de dolinas na área da gruna da Tarimba-GO. In: ANAIS Do 35º Congresso Brasileiro de Espeleologia. Bonito/ MS, pp. 52–62.

Fontugne, M., 2013. New Radiocarbon Ages of Luzia Woman, Lapa Vermelha IV Site, Lagoa Santa, Minas Gerais, Brazil. Radiocarbon 55, 1187–1190. doi:10.2458/azu_js_rc.55.16253

Ford, D., Williams, P., 2007. Karst Hydrogeology and Geomorphology, Karst Hydrogeology and Geomorphology. Chichester, Wiley. doi:10.1002/9781118684986

Galbraith, R.F., Roberts, R.G., Laslett, G.M., Yoshida, H., Olley, J.M., 1999. Optical dating of single and multiple grains of quartz from Jinmium rock shelter, northern Australia: Part I, experimental design and statistical models. Archaeometry 41, 339–364. doi:10.1111/j.1475-4754.1999.tb00987.x

Garzanti, E., Resentini, A., 2016. Provenance control on chemical indices of weathering (Taiwan river sands). Sedimentary Geology 336, 81–95. doi:10.1016/j.sedgeo.2015.06.013

Gaspar, M.T.P., Campos, J.E.G., 2007. O Sistema Aqüífero Urucuia. Revista Brasileira de Geociências 37, 216–226. doi:10.25249/0375-7536.200737s4216226

Gillieson, D., 1996. Caves: Processes, Development and Management, 1º. ed. Blackwell, Massachusetts. doi:10.1002/9781444313680

Guérin, G., Mercier, N., Adamiec, G., 2011. Dose-rate conversion factors : Update Dose-rate conversion factors : update.

Haddad-Martim, P.M., Hubbe, A., Giannini, P.C.F., Auler, A.S., Piló, L.B., Hubbe, M., Mayer, E., Wang, X., Cheng, H., Edwards, R.L., Neves, W.A., 2017. Quaternary depositional facies in cave entrances and their relation to landscape evolution: The example of Cuvieri Cave, eastern Brazil. Catena 157, 372–387. doi:10.1016/j.catena.2017.05.029

Herman, E.K., Toran, L., White, W.B., 2012. Clastic sediment transport and storage in fluviokarst aquifers: An essential component of karst hydrogeology. Carbonates and Evaporites 27, 211–241. doi:10.1007/s13146-012-0112-7

Hubbe, A., Haddad-Martim, P.M., Hubbe, M., Mayer, E.L., Strauss, A., Auler, A.S., Piló, L.B., Neves, W.A., 2011. Identification and importance of critical depositional gaps in pitfall cave environments: The fossiliferous deposit of Cuvieri Cave, eastern Brazil. Palaeogeography, Palaeoclimatology, Palaeoecology 312, 66–78. doi:10.1016/j.palaeo.2011.09.010

Hussain, Y., Uagoda, R., Borges, W., Nunes, J., Hamza, O., Condori, C., Aslam, K., Dou, J., Cardenas-Soto, M., 2020. The potential use of geophysical methods to identify cavities, sinkholes and pathways for water infiltration: a case study from Mambaí, Brazil. Water 12, 1–19. doi:10.3390/w12082289

Hussain, Y. j, Uagoda, R., n.d. An introduction and GIS-based relief compartment mapping of fluvio-karst landscape in central Brazilian highlands. Unpublished results.

IBGE, 1995. Zoneamento Geoambiental e Agroecológico - Goiás/região nordeste, IBGE, Divi. ed. Rio de Janeiro.

ICMBio/CECAV, 2017. RELATÓRIO DE VISTORIA TÉCNICA EM CAVERNAS E SUAS ÁREAS DE INFLUÊNCIA NA ÁREA DE PROTEÇÃO AMBIENTAL DAS NASCENTES DO RIO VERMELHO.

ICMBio/CECAV, 2020. Relatório Estatístico - Cavidades por UF. Brasilia.

Iglesias, M., Uhlein, A., 2009. Estratigrafia do Grupo Bambuí e coberturas fanerozóicas no vale do rio São Francisco, norte de Minas Gerais. Revista Brasileira de Geociências 39, 256–266. doi:10.25249/0375-7536.2009392256266

Jacobs, Z., Meyer, M.C., Roberts, R.G., Aldeias, V., Dibble, H., Hajraoui, M.A. El, 2011. Single-grain OSL dating at La Grotte des Contrebandiers ("Smugglers" Cave'), Morocco: Improved age constraints for the Middle Paleolithic levels. Journal of Archaeological Science 38, 3631–3643. doi:10.1016/j.jas.2011.08.033

Jaqueto, P., Trindade, R.I.F., Hartmann, G.A., Novello, V.F., Cruz, F.W., Karmann, I., Strauss, B.E., Feinberg, J.M., 2016. Linking speleothem and soil magnetism in the Pau d'Alho cave (central South America). Journal of Geophysical Research: Solid Earth 121, 7024–7039. doi:10.1002/2016JB013541.Received

Kinoshita, A., Skinner, A.R., Guidon, N., Ignacio, E., Felice, G.D., Buco, C. de A., Tatumi, S., Yee, M., Figueiredo, A.M.G., Baffa, O., 2014. Dating human occupation at Toca do Serrote das Moendas, São Raimundo Nonato, Piauí-Brasil by electron spin resonance and optically stimulated luminescence. Journal of Human Evolution 77, 187–195. doi:10.1016/j.jhevol.2014.09.006

Laureano, F. V., Karmann, I., Granger, D.E., Auler, A.S., Almeida, R.P., Cruz, F.W., Strícks, N.M., Novello, V.F., 2016. Two million years of river and cave aggradation in NE Brazil: Implications for speleogenesis and landscape evolution. Geomorphology 273, 63–77. doi:10.1016/j.geomorph.2016.08.009

Laureano, F.V., 2014. Idades de Soterramento 26al/10 Be em grão de quartzo e o assoreamento de sistema de Cavernas Na Região Iraquara (Ba): 2 Milhões de anos de registro sedimentar Quaternário. Universidade de São Paulo, São Paulo.

Martini, I., 2011. Cave clastic sediments and implications for speleogenesis: New insights from the Mugnano Cave (Montagnola Senese, Northern Apennines, Italy). Geomorphology 134, 452–460. doi:10.1016/j.geomorph.2011.07.024

McAdams, C., Morley, M.W., Fu, X., Kandyba, A. V., Derevianko, A.P., Nguyen, D.T., Doi, N.G., Roberts, R.G., 2019. The Pleistocene geoarchaeology and geochronology of Con Moong Cave, North Vietnam: Site formation processes and hominin activity in the humid tropics. Geoarchaeology. doi:10.1002/gea.21758

Michab, M., Feathers, J.K., Joron, J.L., Mercier, N., Selo, M., Valladas, H., Valladas, G., Reyss, J.L., Roosevelt, A.C., 1998. Luminescence dates for the paleoindian site of Pedra Pintada, Brazil. Quaternary Science Reviews 17, 1041–1046. doi:10.1016/S0277-3791(97)00091-7

Motta, J.A.O. (org), 2003. Projeto cavernas de Mambaí: caracterização do ecossistema cárstico localizado no município de Mambaí e entorno. Brasília.

Murray, A.S., Wintle, A.G., 2000. Luminescence dating of quartz using an improved single- aliquot regenerative-dose protocol. Radiation Measurements 32, 57–73.

Novello, V.F., Cruz, F.W., McGlue, M.M., Wong, C.I., Ward, B.M., Vuille, M., Santos, R.A., Jaqueto, P., Pessenda, L.C.R., Atorre, T., Ribeiro, L.M.A.L., Karmann, I., Barreto, E.S., Cheng, H., Edwards, R.L., Paula, M.S., Scholz, D., 2019. Vegetation and environmental changes in tropical South America from the last glacial to the Holocene documented by multiple cave sediment proxies. Earth and Planetary Science Letters 524, 1–11. doi:10.1016/j.epsl.2019.115717

Nunes, J.G. da S., Uagoda, R., n.d. Mapeamento de solos em área cárstica, através do estudo da catena com auxílio de geotecnologias e descrições em campo: Um estudo de caso na APA Nascentes do Rio vermelho, Mambaí – GO. Unpublished results.

Oliveira, P. V., Ribeiro, A.M., Oliveira, É. V., Viana, M.S.S., 2014. The dasypodidae (mammalia, xenarthra) from the urso fóssil cave (quaternary), parque nacional de ubajara, state of ceará, Brazil: Paleoecological and taxonomic aspects. Anais da Academia Brasileira de Ciencias 86,

147–158. doi:10.1590/0001-3765201420120029

Osborne, R.A., 2005. Dating ancient caves and related palaeokarst. Acta Carsologica 34, 51–72.

Osborne, R.A.L., 1986. Sedimentation in caves- a review. Publications of the Geological Society of Australia 2, 189–217.

Peyre, E., Guérin, C., Guidon, N., Coppens, Y., 1998. Des restes humains pléistocènes dans la grotte du Garrincho, Piauí, Brésil. Comptes Rendus de l'Academie des Sciences, Serie II. Sciences de la Terre et des Planetes 327, 335–360.

Piló, L.B., Auler, A.S., Neves, W.A., Wang, X., Cheng, H., Edwards, R.L., 2005. Geochronology, sediment provenance, and fossil emplacement at Sumidouro Cave, a classic Late Pleistocene/Early Holocene paleoanthropological site in eastern Brazil. Geoarchaeology 20, 751–764. doi:10.1002/gea.20081

Plotnick, R.E., Kenig, F., Scott, A.C., 2015. Using the voids to fill the gaps: Caves, time, and stratigraphy. Geological Society Special Publication 404, 233–250. doi:10.1144/SP404.5

Prescott, J.R., Stephan, L.G., 1982. The contribution of cosmic radiation to the environmental dose for thermoluminescence dating. PACT 6, 17–25.

Rhodes, E.J., 2011. Optically Stimulated Luminescence Dating of Sediments over the Past 200,000 Years. Annual Review of Earth and Planetary Sciences 39, 461–488. doi:10.1146/annurev-earth-040610-133425

Rizzato, P.P., Bichuette, M.E., 2014. Ituglanis boticario, a new troglomorphic catfish (Teleostei: Siluriformes: Trichomycteridae) from Mambaí karst area, central Brazil. Zoologia (Curitiba) 31, 577–598. doi:10.1590/s1984-46702014000600006

Roosevelt, A.C., Costa, M.L., Machado, C.L., Michab, M., Mercier, N., Valladas, H., Feathers, J., Barnett, W., Silveira, M.I., Henderson, A., Sliva, J., Chernoff, B., Reese, D.S., Holman, J.A., Toth, N., Schick, K., 1996. Paleoindian Cave Dwellers in the Amazon : The Peopling of the Americas. Science 272, 373–384.

Santos, G.M., Bird, M.I., Parenti, F., Fifield, L.K., Guidon, N., Hausladen, P.A., 2003. A revised chronology of the lowest occupation layer of Pedra Furada Rock Shelter, Piauí, Brazil: The Pleistocene peopling of the Americas. Quaternary Science Reviews 22, 2303–2310. doi:10.1016/S0277-3791(03)00205-1

SBE, UPE, GREGO, UFSCar, LES, 2014. Caracterização ambiental e conservação do sistema cárstico da gruna da Tarimba – Mambaí, GO.

Springer, G.S., 2005. Clastic Sediments in Caves. In: Culver, David C; White, W.B. (Ed.), Encyclopedia of Caves. Elsevier Academic Press, San Diego, pp. 102–108.

Stríkis, N.M., 2015. Atividade do Sistema de Monção Sul-americana na porção central do Brasil durante o último período glacial a partir da aplicação de isótopos de oxigênio em espeleotemas.

Uagoda, R., Hussain, Y., Ferreira, C.F., Fonseca, M.R., Nogueira, A., Caldeira, D., Tavares, A., Nunes, J.G., Costa, B., 2019. Regional Conference of Geomorphology. In: Geomorphic Units Mapping of Fluviokarst Landscapes in Central Brazilian Higland. Athens, p. 212.

White, W.B., 2007. Cave sediments and paleoclimate. Journal of Cave and Karst Studies 69, 76–93.

Woodward, J.C., Goldberg, P., 2001. The Sedimentary Records in Mediterranean Rockshelters and Caves: Archives of Environmental Change. Geoarchaeology - An International Journal 16, 327–354. doi:10.1002/gea.1007

870

Declaration of interests

☒ The authors declare that they have no known competing financial interests or personal relationships that could have appeared to influence the work reported in this paper.

☐The authors declare the following financial interests/personal relationships which may be considered as potential competing interests:

Research Article

Yawar Hussain*, Welitom Borges, Rogerio Uagoda, Cristiane Moura, Susanne Maciel, Omar Hamza, and Hans-Balder Havenith

Estimation of total groundwater reserves and delineation of weathered/fault zones for aquifer potential: A case study from the Federal District of Brazil

https://doi.org/10.1515/geo-2020-0226
received September 04, 2020; accepted January 16, 2021

Abstract: In the Federal District of Brazil, groundwater extraction is challenged by fractured aquifers with difficulty in identification of hydraulic traps and significant uncertainty in the estimation of recharge potential. This study aims to optimize the demarcation of new locations of tubular wells by the aid of geophysical investigation. In the first stage of this study, the total exploitable amount of groundwater were calculated from the information of the physical environment and the existing wells. Second, electrical resistivity tomography (ERT) method was carried out on the selected sites – based on their surficial characteristics. The possible hydraulic traps (where groundwater might exist) were identified from the inversion of the resistivity measured by the dipole–dipole array and from the delineation of the resultant conducting zones (including the weathered rocks and fractures). Using this approach, we predicted the position and number of tubular wells required and ranked them according to their potential productivity. The study provides a promising framework for investigating groundwater in fractured aquifers.

Keywords: ERT, fracture, groundwater, environmental factor, tubular wells

*** Corresponding author: Yawar Hussain,** Geology Department, Liège University, Liège, 4000, Belgium, e-mail: yawar.pgn@gmail.com
Welitom Borges, Cristiane Moura: Institute of Geosciences, University of Brasilia, Brasilia, 70910-900, Brazil
Rogerio Uagoda: Department of Geography, University of Brasilia, Brasilia, 70910-900, Brazil
Susanne Maciel: Planaltina Campus, University of Brasilia, Brasilia, 73345-010, Brazil
Omar Hamza: College of Science and Engineering, University of Derby, Derby, DE22 3AW, Derbyshire, United Kingdom
Hans-Balder Havenith: Geology Department, Liège University, Liège, 4000, Belgium

1 Introduction

Worldwide water demand is on the increase because of the growing global population and the unplanned urban growth that exerts stress on the aquifers [1] and other water resources. This situation leads to the search for new locations of wells installed in productive aquifers. In the case of hard rock aquifers, groundwater can be found in weathered and fresh rock interface, where the presence of joints, fractures, and fault zones (which are created by different chemical or tectonic processes) are expected to enable groundwater storage and transport [2–7]. Such aquifers can exist at variable depth; if the aquifer is deep, groundwater is pumped out by installing deep tubular wells (100–200 m). However, it is essential to conduct adequate groundwater exploration before installing these wells.

Prospecting for groundwater seeks to locate suitable quality and quantity of groundwater for extraction from an aquifer. This process involves the assessment of the recharge potential of the site in relation to the natural settings of the aquifers e.g., discontinuities/fractures, lineament, and quartz veins, which are attributed to the presence of highly productive aquifer [8,9]. However, such natural settings represent complex hydrological characteristics of aquifers. Therefore, groundwater prospecting in such regions is a challenging task where the presence of fractures as well as the intrinsic properties and physical environment of the site can play essential roles.

In addition to the traditional approaches used for assessing the physical environment of the hydrogeological setting of aquifers, geophysical methods offer the opportunity to detect the variation in ground conditions and the delineation of the zones that may appear as possible traps for groundwater in complex environmental conditions [6]. In particular, direct current, electrical

resistivity tomography (ERT), which has been recognized as an economic and noninvasive geophysical technique with reasonable accuracy in the detection of hydrogeological features (fractures/weathered zones), can provide better structural information of highly heterogeneous geological features [10]. In ERT, a known value of current is passed through the earth, and a developed potential difference is observed which can be used for the subsurface analysis after inversion. ERT has been applied in many previous studies for the search of new groundwater prospects as well as for the monitoring of existing groundwater reservoirs [1,6].

These days, prospecting for groundwater is required more than ever. In the case of the Federal District of Brazil, unplanned urban growths in the surrounding regions of Brasilia are on the rise. In order to fulfill the rising water demands, new groundwater prospects are being investigated with consideration of the geology and the physical environment of the region. The city is constructed on a complex and heterogeneous groundwater flow system which constitutes both porous and fractured hydrological regimes having variable hydrogeological characteristics such as hydraulic conductivity and permeability.

This article presents a case study from the Federal District of Brazil, where ERT, as well as the existing geological and hydrogeological information of the study area, were utilized to optimize the demarcation of new tubular well locations. The study provided a description of the aquifer system of the area and then proposed and applied an integrated approach in which the recharge potential of the study area as well as the presence of fractures and weathered zones (conductive zones detected by ERT) were used as a criterion for the estimation of groundwater potential. The investigation was conducted on seven different sites in the *Condominio Solar da Serra*, Federal District of Brazil.

2 Description of the study area and methods

The study was conducted in *Condominio Solar da Serra*, located in the middle course of the *Taboca and Taboquinha Ribeirão* sub-basins (Figure 1). The area already has eight deep tubular wells installed, of which six of them are in

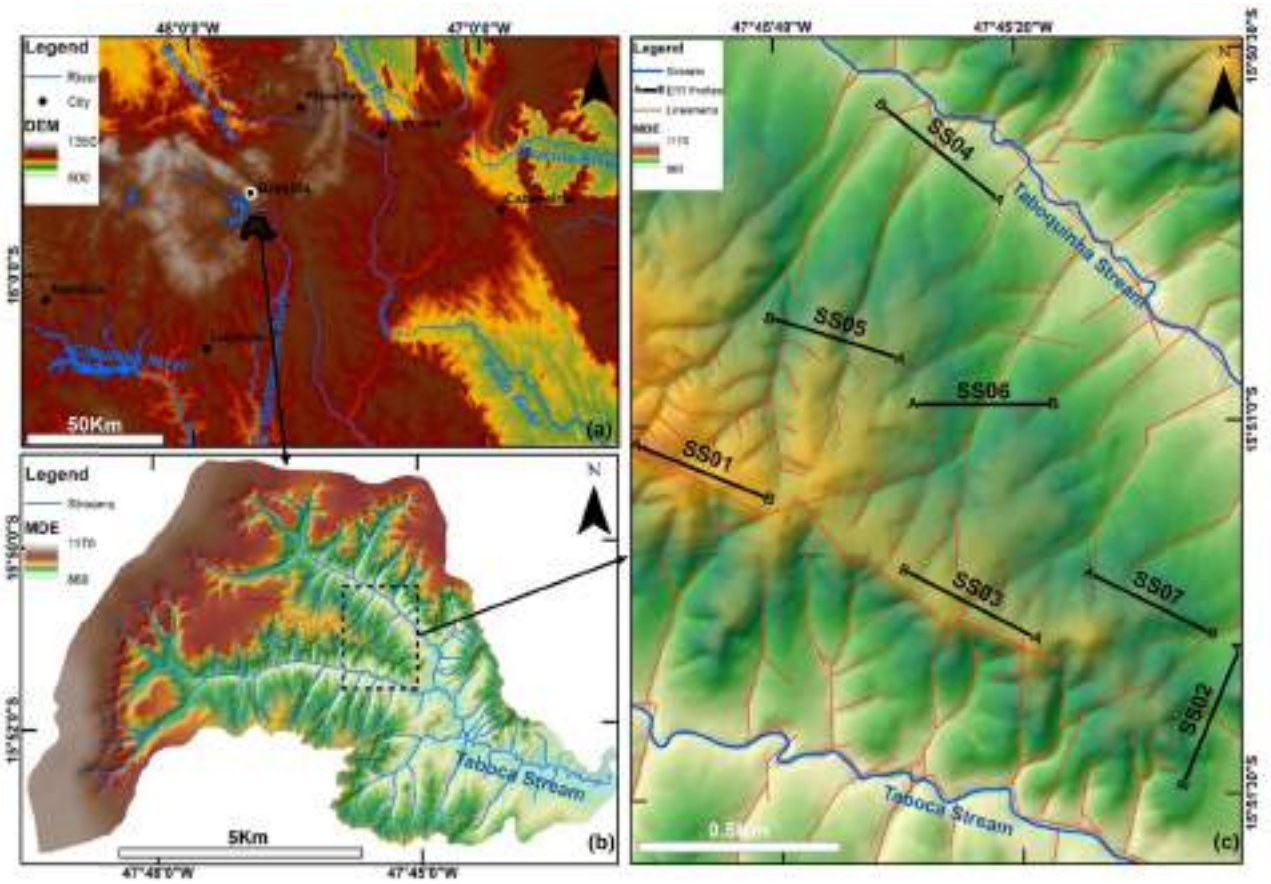

Figure 1: (a) Location of Brasilia on Brazil map, (b) location of *Condominio Solar da Serra* within the boundary Ribeirão Taboca-Taboquinha sub-basin, and (c) zoomed image of the study site along with the positions of ERT profiles and other hydrological features.

Table 1: Summary of the classification of domains, aquifer systems/sub-systems of the Federal District with respective mean flows [19]

Aquifer (system/subsystema)
Porous domain aquifer
Systems P1, P2, P3, and P4
Fracture domain aquifer
Paranoá system
Subsystem S/A
Subsystem A
Subsystem Q_3/R_3
Subsystem R_4
Subsystem PPC
Canastra system
Subsystem F
Subsystem F/Q/M
System Bambuí
System Araxá

operation. The region constitutes an aquifer system having moderate potential for production with an average flow rate of around 7.5 m^3/h (Table 1).

The Taboca and Taboquinha River sub-basins are located in the south and central portions of the Federal District and geologically constitute units of the *Paranoá* and *Canastra* groups. The Paranoá group is represented in the sub-basin by its *Ribeirão Contagem* (MNPparc) formation, which is further divided into two subunits as upper and lower (Figure 2). The lower subunit of Ribeirão formation consists of thin to medium-sized quartzites, white or light gray in color, well-sorted, mineralogically mature, usually very silicified, and having well-rounded grains. At the top, massive quartzites of the MNPparc superior formation found, characterized by the alternation of millimeter to centimeter levels of pure quartzites white to creamy color having millimeter to centimeter levels of ferruginous quartzites of medium particle size and gray in color. The MNPpacs *formation* is also divided into two subunits namely, upper and lower. The lower Sansão Stream formation subunit consists of homogeneous metarithmites with regular centimetric intercalations of metasilicates, metalamides, and fine quartzites that appear in different colors as gray, yellow, rose, or red. The Canastra group occupies about 70% of the area of the Taboca and Taboquinha Ribeirão sub-basins, which consists of phyllites, predominated by chlorite phyllites and quartz chlorite fengita filitos [11]. The lithosection and geological map of the area are presented in Figures 2 and 3, respectively.

Structurally, the area is located on the southeastern flank of the Brazilian structural dome. The NW–SE fracture-fault system controls the main drainage of the Taboca and

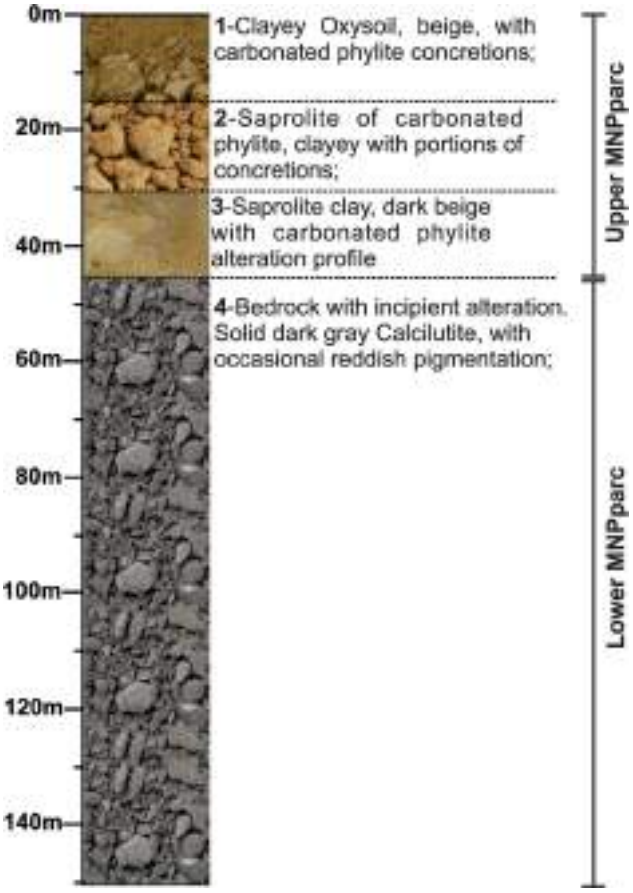

Figure 2: Lithosection of the area taken from the nearby tubular well. (1) Clayey oxisoil; (2) saprolite of carbonated phyllite; (3) fine yellow saprolite; and (4) bedrock [12].

Taboquinha streams that flow in the study area. The NE–SW system corresponds to the conjugate pair of the NW–SE system, which is in the predominant direction of the lineaments. The structural analysis of these systems, as well as the asymmetries of the drainage slopes shown on declivity map (Figure 3), were predominantly high angle fractures and faults with recessed blocks which are important features for the groundwater prospecting [13].

There are four large sets of residual soils in the Taboca and Taboquinha Ribeirões sub-basins [14]. These residual soils are deposited on the saprophytes of the Paranoá and Canastra groups. The soil of the area is divided as quartzarenic neosoils, latosols red-yellow, cambisols, and plintossolos (Figure 3). In the geomorphological context, the Taboca-Taboquinha sub-basin is located in the São Bartolomeu Rio Superior Course Unit. The Taboca-Taboquinha sub-basin is subdivided into seven geomorphological units as plateau plateau, elevated plateau, smooth section, dissection unit-high course, dissection unit-low course, dissection unit-lower middle course, dissection unit-middle higher course [15,16].

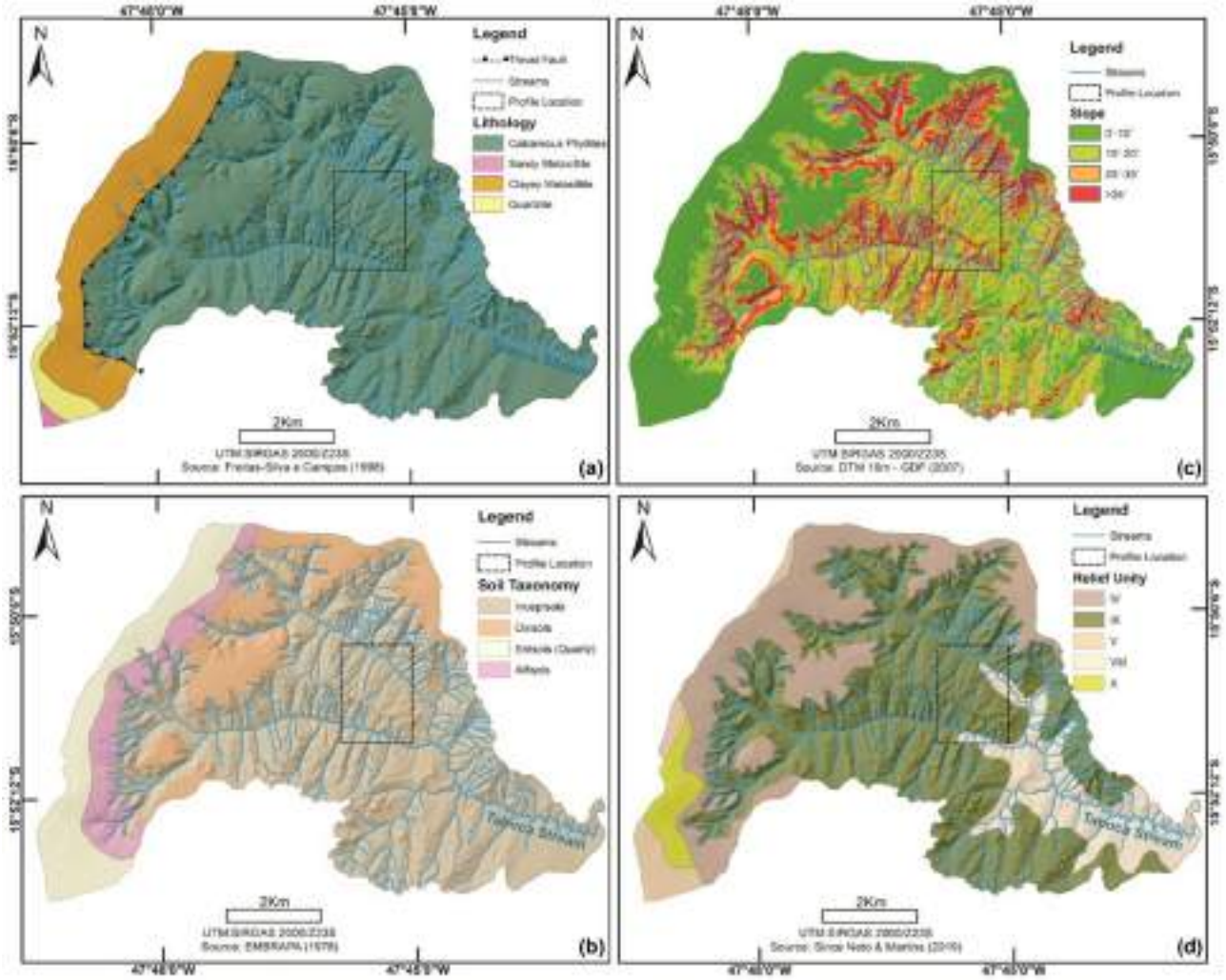

Figure 3: (a) Geology, (b) soil map, (c) declivity map, and (d) relief map of the Ribeirão Taboca-Taboquinha sub-basin.

The pioneering work on the hydrogeology of the Federal District was carried out by Romano and Rosas [17]. Subsequently, the contributions of Barros [18] were important for the assessment of groundwater in the region. After that, a succession of works has been developed in the region.

3 Aquifer domains

The Brazilian hydrogeological system is dominated by aquifers developed in fissures, covered by weathering layer of soils and altered rocks having variable hydrogeological characteristics (permeability and thickness). In Brasilia, two distinct aquifer domains are presented, namely: (i) Porous domain aquifers (PDA) and (ii) Fractured domain aquifers (FDA) (Table 1).

3.1 PDA

Since there are no sedimentary rocks with interstitial spaces, this domain consists of soils and the mantle of rock alteration (saprolite) in the area. Locally, the importance of aquifers in this domain is linked with several parameters, out of which only two are highlighted here: saturated thickness (b) and hydraulic conductivity (K), both are related with geology and geomorphology of their parent rocks. The domain is further subdivided into three systems: areas with latosols (Paranoá rocks), areas with structural soils (pelitic and carbonate rocks of the Paranoá group), and areas with cambisoils and neosoils (pelitic/claystone rocks of the Paranoá and Canastra groups). These sub-domains are named as P1, P2, P3, and P4, based on the "b" and "K" values (Table 1). The aquifers in the porous domain within the study area are of P3 and P4 subsystems with the argisoils/nitosoils and cambisoil/lithosoils,

respectively. The P3 has a large thickness (>5 m) and low hydraulic conductivity, while P4 has smaller thicknesses (usually less than 1 m, but it can reach 2.5 m) and low hydraulic conductivity. The P4 water flow is very restricted, generally smaller than 300 L/h and shallow wells are installed in this aquifer, not present in the studied area but are quite common in the surroundings.

3.2 FDA

The FDA is associated with groundwater stored in the discontinuities related to faults, fractures, and joints in the absence of residual primary porosity in the rocks of the Paranoá group. The recrystallization of minerals and cementation completely obliterated the primary porosity originated by the metamorphic processes. The domain is represented by the systems of unconfined or confined aquifers, of restricted lateral extension, with strong heterogeneity and anisotropy responsible for the storage and circulation of deep groundwater. The hydrodynamic characteristics are variable in the domain depending on the type of rock. The density of the discontinuity in the rock body controls the hydraulic conductivity of the aquifers [20]. Generally, the fractured aquifers are pumped by means of deep tubular wells with depth varying from 100 to 200 m in the Federal District. The recharge occurs by the percolation of rainfall water. Other important factors that control the recharge depend on soil conditions, type of vegetation cover, soil thickness, and percentage of urbanized areas. Figure 4 presents a conceptual groundwater model in the area.

4 Method – ERT

The visible structural lineaments were extracted from the satellite images and digital terrain model, at a scale of 1:10,000. This information was used for the planning of electrical resistivity survey in the area (terrain conditions, environmental restrictions, etc.). Based on the preliminary analysis, seven areas were selected for conducting electrical resistivity profiles (Figure 5).

The electrical resistivity measurements were taken with a four-electrode system, two of which are used to pass electric current (I) to the ground and the other two are used to measure the potential difference (V) between them. By obtaining the potential difference and the current flowing in the medium, the apparent electrical resistivity of the medium is calculated which depends on the geometric factor (K), a function of the configuration of the electrodes [4]. Depending on the research objective, the electrodes' configuration can be conducted in several ways such as Wenner, pole–pole, pole–dipole, dipole–dipole, Wenner–Schlumberger, and gradient. Each arrangement has specific characteristics such as spatial resolution (dipole–dipole and pole–dipole), depth of investigation (pole–pole), and signal-to-noise ratio [22–26]. In the present study, the dipole–dipole (DD) electrode arrangement was adopted. Based on the study objectives, DD array is the most common array adopted for the groundwater prospecting in hard rocks due to good depth range but low signal-to-noise ratio [27]. The widespread voltage and current cables may result in good image resolution capabilities and may decrease in electromagnetic inductive noise [28–30]. Other advantages of using DD include

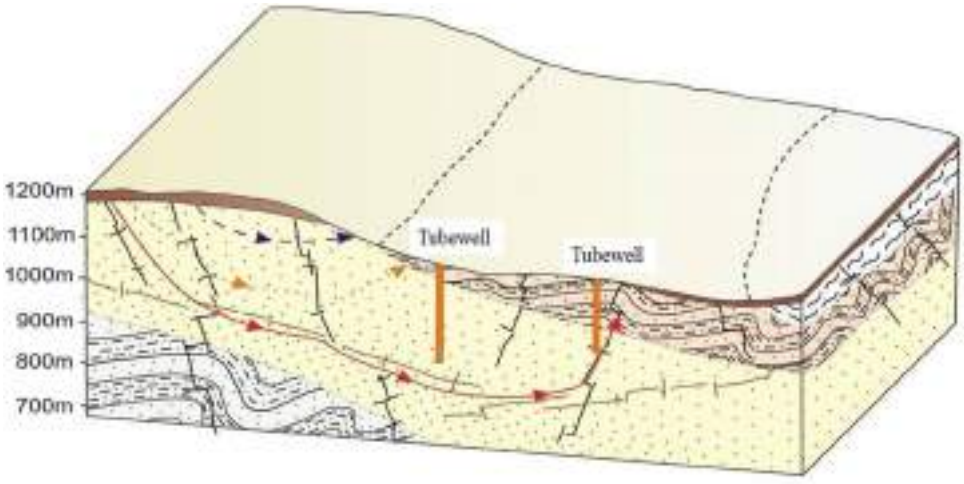

Figure 4: Schematic representation of the conceptual model of the aquifer system in the southern part of Brasilia [21].

Figure 5: Photographs illustrating the acquisition of ERT data on the selected sites in the study area.

delineation of lateral features and reciprocal measurements at shallow depth [31]. Data error and quality assessment can be made based on the reciprocal and forward measurements [32]. Okpoli [33] provided a detailed review of the advantages and disadvantages of the ERT arrays. Another approach was adopted in recent studies where multi-array configurations were used in the joint inversion [34,35].

The result of the acquisition is a set of electrical resistivity data obtained at various depths, forming a pseudo-section. This, in turn, reflects the behavior of the subsurface in response to the passage of electric currents. Each geological material shows a very broad range of resistivity, which depends mainly on the mineralogical composition of the rock, degree of weathering, the amount of fluids present in the pores of the rock, and the salinity of the fluid.

The acquisition of the geophysical data was executed along with eight profiles (Figure 5), each one of 350 m in length. One profile was not used because of poor signal-to-noise ration. In the field, the electrical resistivity data were collected with the electric roll-along technique, using the DD arrangement, with a spacing of 10 m between the electrodes. The data acquisition protocol with the multielectrode cables was elaborated in the software ELECTRE II, version 05.06.00, (IRIS Instruments) for acquisitions with 36 electrodes.

The measurements were taken in the dry season and salt water is poured to each electrode in order to increase the passage of current to the ground. The data were acquired with SYSCAL Pro 72 equipment (manufactured by IRIS Instruments), which consists of an interleaved acquisition module in multielectrode cables. Thirty-six stainless steel electrodes were used to inject current and measure the electric potential generated by the current flow in the subsurface.

ERT data were processed in a similar approach adopted by refs. [36,37]. The filtering and topographical correction on the dataset were performed in the PROSYS II software (IRIS Instruments). In order to determine the effective depth, the pseudo-sections of the electrical resistivity were inverted using the computer program RES2DINV (Geotomo Software). In our case, the resistivity values near the ground are high; therefore, a narrow model cell was used in RES2DINV program, where the width of the model block is kept as half of the electrode spacing for optimum result. The 2D model divides the subsurface into a series of blocks to determine the resistivity; its product is the apparent

resistivity pseudo-sections that fit with the field data, using an inversion process based on the variation of the least square method. The results obtained were presented in the form of 2D resistivity profiles.

5 Results and discussions

5.1 Estimation of groundwater reserves

The entire area of the *Condominio Solar da Serra* is mainly in the form of aquifer subsystem F of the Canastra aquifer system. The subsystem F is one of the lowest production aquifers in the Federal District with an average flow rate of around 6,500 L/h. The best flow rates are obtained in neotectonic fault/fracture zones, especially in the NW–SE, NE–SW, NS, and EW directions. In addition, the small soil thickness (porous subsystem P4) overlying the subsystem F and low permeability of the phyllites cause great difficulties in the implementation of infiltration induced systems (artificial recharge).

The physical environment and climatic (rainfall) information are used in the determination of the deeper aquifers' flow as well as the elements for their sustainable management and extraction. Taking this into account, the main parameters for the volume calculations and flow rate estimation and the outflows of groundwater extraction of the study area are calculated (Table 2).

The average climatic conditions of the Federal District, which are marked by the strong seasonality, with two contrasting seasons are considered for the study area. The period between May and September is evidenced by low precipitation rate, low cloudiness, high evaporation rate, and low relative air humidity. The period between October and April presents distinct patterns, and the months from December to March constitute 47% of the annual precipitation. The average annual precipitation of the Federal District is about 1,500 mm; however, for estimation of water reserves, an average rainfall of 1,450 mm was considered.

According to ref. [38], about 12% of the total precipitation infiltrates the vadose zone and effectively reaches the saturated zone. This is considered for the areas occupied by subsystem P1; however, for the subsystem P4, a value of 8–9% is determined based on the physical environment of the area.

The total area of the *Condominio Solar da Serra* is 250.99 ha (2,509,900 m^2), 63.2% of which is destined for residential, commercial lots, and institutional areas, and 36.8% is reserved for the green areas. Thus, for the calculation of the total exploitable reserve (TER) for the area, the green areas (923,500 m^2) plus 30% of the urbanized area (475,920 m^2) are used.

Table 2: Parameters used in the estimation of groundwater reserves of Condominio Solar da Serra

Average annual precipitation (AAP)	1,450 mm
Porous domain area P4 – 20 m thick	1,400,000 m^2
Area of fractured system-F	1,400,000 m^2
Effective recharge of the porous domain – P4 for the fractured system F (percentage)	8%
Percentage of the permanent reserve available (annual)	9%
Thickness of the shallow fractured domain	70 m
Index of fractures interconnected in the short interval of the fractured subsystem	1%
Pore spacing of lower zone	60 m
Index of interconnected fractures of the deep interval of the fractured subsystem deep interval	0.5%

In order to establish a sustainable exploitation rate, the following parameters for a conservative estimation are considered: (i) The whole area is covered by the porous system P4, represented by shallow changes; (ii) The entire area of the C*ondominio* is composed of the aquifer subsystem F; (iii) For the calculation of the renewable reserve of the subsystem F, the effective recharge rate of the porous system is 10% of the total annual precipitation.

Equation (1) is used to calculate the reserve renewed annually from the infiltration of rainwater through the unsaturated zone to the saturated zone of the porous system and from there to the saturated zone of the rocky fractured environment.

$$\mathrm{RrF} = A \times \mathrm{ERF} \times \mathrm{AAP}, \tag{1}$$

where RrF is the renewable reserve of subsystem F, A is the system area available for infiltration (green area + non-edificated area), ERF is the effective recharge percentage from the overlapping porous system, and AAP is the average annual precipitation. After substituting the values from Table 2 into the above equation (1), a numeric value of "RrF = 162,400 m^3/year" is obtained.

The water reservoir is permanently contained in the rock fracture systems of the Canastra aquifer subsystem. It is calculated for different depths as a function of the different interconnected fracture rates (IFr), which tend to decrease with depth due to the increase in the lithostatic pressure. Permanent reserve of system F (PrF) can

be calculated using equation (2). Substituting the values from Table 2 into equation (2) gives PrF = 1,400,000 m^3.

$$\begin{aligned} \mathrm{PrF} &= \mathrm{PrFs} + \mathrm{PrFi} \\ &= (A \times \mathrm{bs} \times I_{\mathrm{fii}}) + (A \times \mathrm{ps} \times I_{\mathrm{dif}}), \end{aligned} \tag{2}$$

where PrFs is the permanent reserve of system F, PrFi is the permanent reserve of system F inferior interval, A is the area of fractured domain, bs is the thickness of upper fracture zone, I_{fii} is the index of fractures having larger interconnection interval, ps is the pore spacing of lower zone, and I_{dif} is the index of deeper interconnected fractures.

For the location of the deep tubular wells in the investigated area, all the information regarding the physical environment as described above were obtained from the already installed seven wells in the considered area (Table 3). However, the assessment of the constructive and geological profiles of the wells are not available; the existing information mainly includes the well's depth and pumping rate as can be seen in Table 3.

5.2 Site selection by ERT

Based on the inverted resistivity, geological information of the ground was prepared along with each profile. Different resistivity zones such as low, medium, high, and very high resistivity are delineated on the inverted resistivity data. These resistivity zones are possibly associated with the soil, fine saprolite, coarse saprolite, and saturated saprolite (Figure 2). Along with these, on the inverted resistivity pseudo-sections, some features delineate having an opening on the ground and are labeled as the suspected fractured or weathered zones within the underlying bedrock. It is interesting to note that some of the profiles show the resistivity changes in the same geological layer as a function of depth which indicate the presence of heterogeneity. It is also found that on some of the profiles, that change from one layer to another is not abrupt and instead a progressive shift in resistivity values are shown indicating the absence of abrupt shift among the facies of weathered saprolite/rock. The detailed discussions on the delineated features of interests on the individual profiles are presented below.

The unprocessed apparent resistivity pseudo-section along with profile SS01 is shown in Figure 6a. It can be seen that there are very high resistivity values at the center, which are marked as an unknown anomaly. On profile SS01 (Figure 6b), two anomalous features of low resistivity were found which might be associated with the fractured structures in the subsurface with a possible presence of groundwater or clay. These clays might be associated with the fluvial deposition. This profile has three lithologies, namely dry soil, fine saprolite, and coarse saprolite, each having a different resistivity anomaly.

On profile SS02 (Figure 7a), two anomalous features of low resistivity were found which might be associated with the fractured structures in the subsurface as possible traps of groundwater accumulation. However, due to the inherent ambiguity of indirect investigation by geophysical methods, there are other possible explanations of the observed low resistivity zone. At the beginning of the profile, low resistivity vein is found. This zone may be associated with the presence of a fracture in saprolite – filled with the clay. This clay may be fluvial deposit by the water flow. This is also a potential recharge zone for the underlying deep aquifer depending on permeability of the material (proportion of coarse grained material). High resistivity saprolite (high permeability) is also found here.

Results of profile SS02 show a highly fractured subsurface flow system. Similar to SS01 profile, at the beginning of the profile filled fractured zone is observed, which present a potential area of aquifer recharge. Zones of different resistivity values can be seen; these variations in values may be created by differential degrees of weathering, the proportion of fine-grained, and the degree of saturation within the same saprolite layer. The migration of water may create the variations in saturation because of the pumping in the nearby tubular wells. This

Table 3: Data of existing wells in the area

Well	Name	UTM X	UTM Y	Time of operation (h)	Flow rate (m^3/h)	Depth (m)	Depth of pump (m)
1	Poço Solar 3	203908.87	8245181.94	18	2.9	150	70
2	Poço Praça B	205547.37	8245578.17	16	6.6	150	110
3	Poço Clube	205729.04	8244743.23	20	7.5	90	60
4	Poço Praça Colibri	205684.33	8245377.90	20	7.5	100	60
5	Poço do Trevo	204829.69	8245420.01	20	3.0	260	150
6	Poço da Portaria	203864.14	8245748.70	20	1.5	90	60
7	Poço Desativado	204549.00	8245907.00	20	2.4	150	90
Average					4.49		

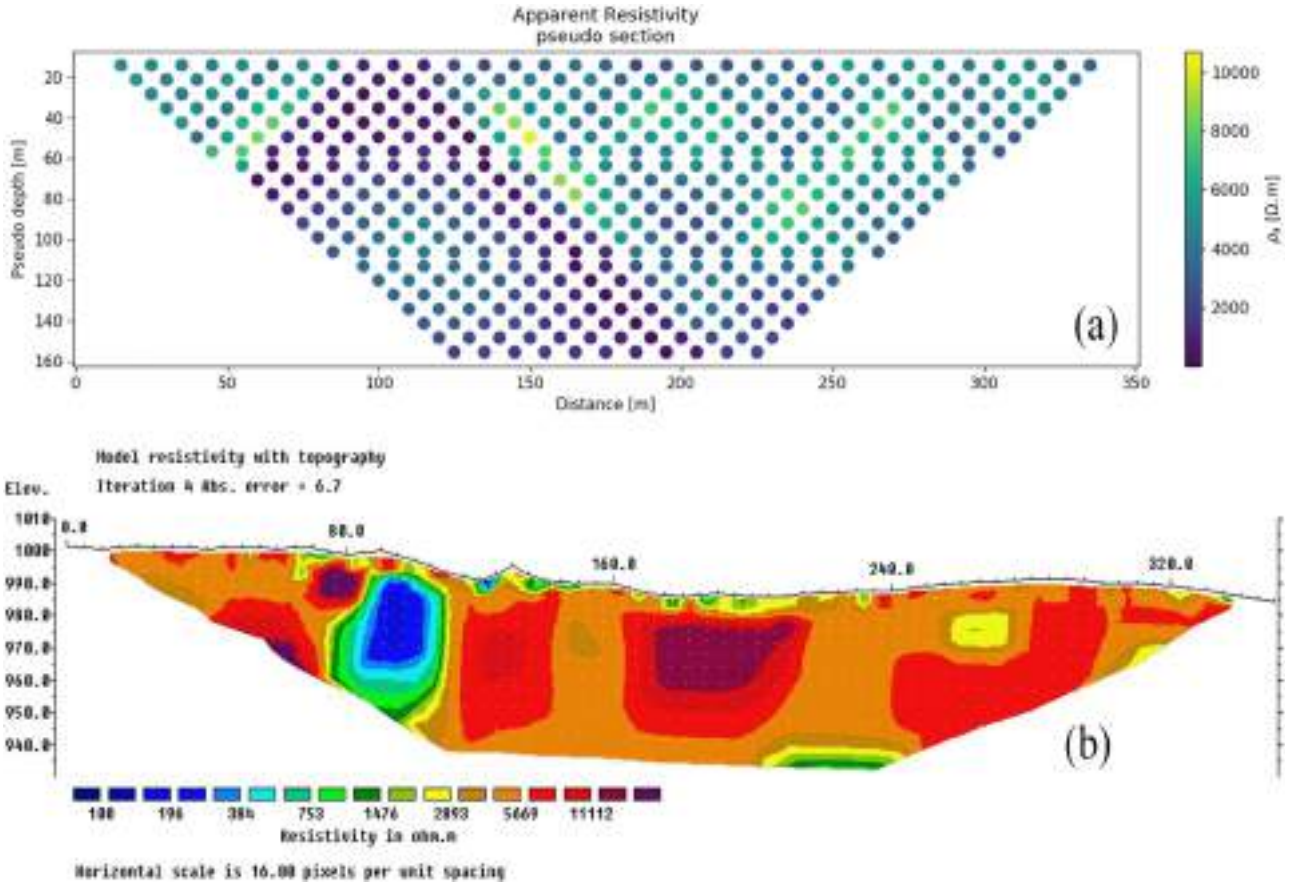

Figure 6: (a) Raw data record of profile SS01 and (b) the inverted resistivity cross-section.

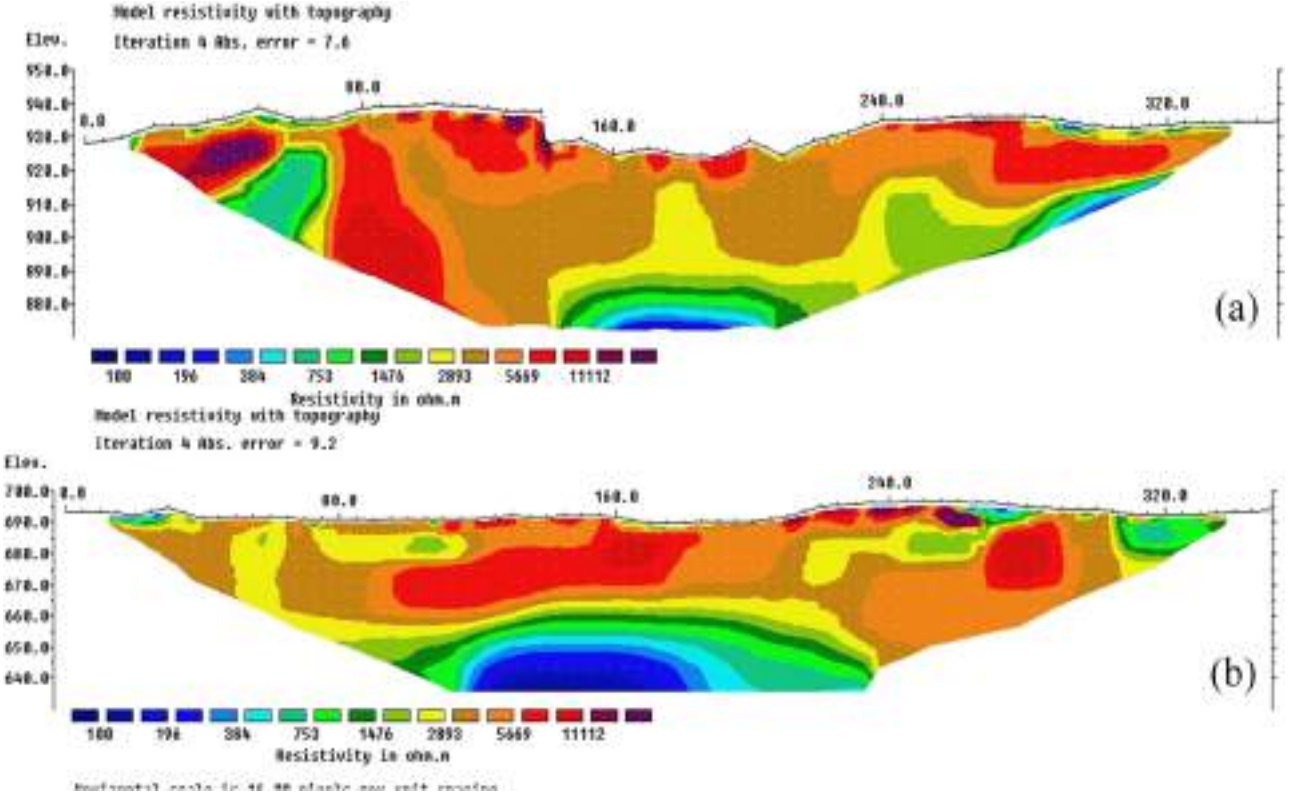

Figure 7: The inverted resistivity cross-sections of profiles: (a) SS02 and (b) SS03.

exploitation is further strengthened by the fact that ERT measurements were carried out in the dry season. On profile SS03 (Figure 7b), a medium to high resistivity anomaly was found which corresponds to a discontinuity coincident with relief lineage, which can store as well as recharge groundwater. Another possible explanation of the high resistivity anomaly near the end of the line may be related only to the presence of the coarse and dry material (saprolite). A contentious decrease in contour values within the same formation is observed on the middle to the right side of the profile SS03; this has also been reported in the literature by Soro et al. [39]. This may be related to seasonal aquifer which is pumped by the nearby well as explained above. In order to prove this hypothesis, measurement should be taken in the rainy seasons. Another possible reason for these resistivity variations may be linked with the variable degrees of weathering as explained above.

Profile SS03 (Figure 7b) shows very interesting results at the middle; there is a high resistivity propagating zone, below which there are layers with resistivity values showing that there is no abrupt change in the facies of same rock unit (saprolite). The high resistivity geoelectric anomaly corresponds to the presence of saprolite derived from phyllites, the layer below being interpreted as the presence of carbonaceous phyllites in the region. At a depth of 40 m there is a very low resistivity anomaly similar to the other profiles, which may be associated with the clayey saprolite – presenting a cap rock for the deeper deeper aquifer system. This profile shows a fractured opening at the ground at about 50 m from the start of the profile. The entire profile is horizontal, so it is not a favorable recharge site for the deeper aquifer.

Profile SS04 (Figure 8a) represents very similar favorable groundwater development conditions such as the presence of fractured opening at the surface, topographic depression, and the presence of clayey saprolite (cap rock) at shallow depth. These hydrogeological conditions are observed on profiles SS05, SS06, and SS07. Another possible explanation of the presence of such a low resistivity zone is the absorption of current by the layer above. In order to prove it drilling of borehole is recommended. It should be noted that the surface features of high resistivity, sometimes ellipsoidal, are associated with the presence of rainwater drainage network structures in the high resistivity geoelectric layer which may be associated with the presence of saprolite. Profile SS05 (Figure 8b) shows the presence of

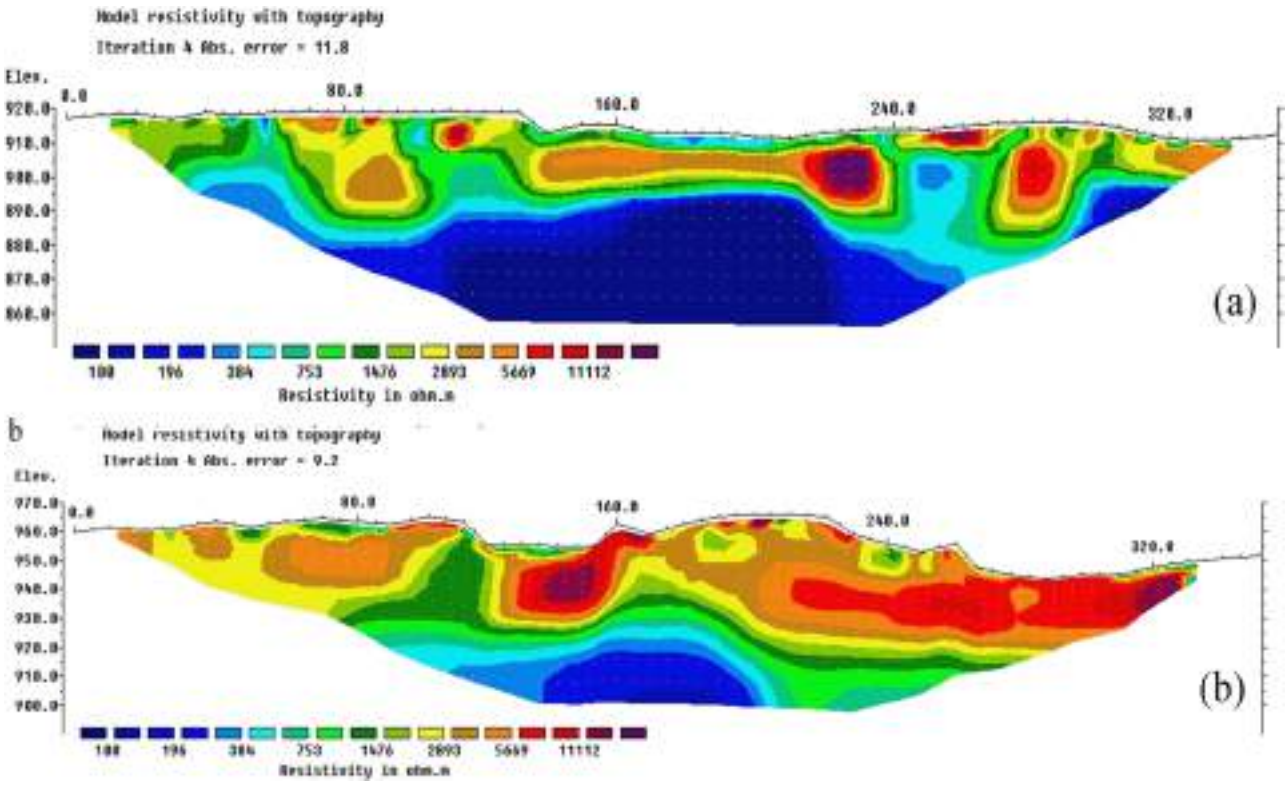

Figure 8: The inverted resistivity cross-sections: (a) SS04 and (b) SS05.

clayey saprolite associated with the domain of low resistivity. Therefore, this suggestion should be further confirmed by drilling (well) at the anomaly at 170 m away from the beginning of the profile SS06.

The discontinuities on profile SS07 suggest the presence of structures of interest, and this hypothesis can be investigated at a distance of 170 m from the beginning of profile SS06 (Figure 9b). This site presents a good topographic depression which can lead to holding of rainfall water which can infiltrate to the vadose zone and reach the saturated zone. Profile SS05 (Figure 8b) shows a very well defined and contentious soil layer. Below this soil layer is a coarse-grained dry saprolite layer (high permeability), which provides a pathway for the aquifer recharge. Below this layer comes a very low resistivity stratum which may be associated with the clayey saprolite – a potential cap rock at shallow depth for the deeper aquifer. At the beginning of the profile, similar to other sites, a fractured zone is delineated, which further enhances its suitability for the installation of the tubular well. From the beginning to the middle of the profile, there is very little topographic variation; however, from the middle to end, there is a considerable topographic variation.

From the results obtained by the adopted methodology, i.e., the application of 2D models of resistivity by inversion at seven locations, it was possible to identify the optimum distribution of the tubular wells. The wells' installation in the area is recommended based on the presence and ground opening of fractures, and presence of topographic depressions. These include the fractured or the conductive zones with possible recharge areas for the deeper aquifer, including any surficial features such as depression where rainfall water can accumulate. In total, seven tubular wells were suggested, and their proposed locations were prioritized as low, medium, and high depending on the analyzed data.

The profile SS01 has a high priority ranking based on the presence and surficial opening of the fracture; however, because of horizontal topography, an overall intermediate priority for the groundwater development is assigned to this site. The site of profile SS02 is ranked as high installation priority based on all the individual parameters (i.e., fracture, coarse saprolite, and depression).

Similar criteria were used to rank profiles SS03, SS04, SS05, SS06, and SS07, where the installation of two medium priority wells are recommended (based on the

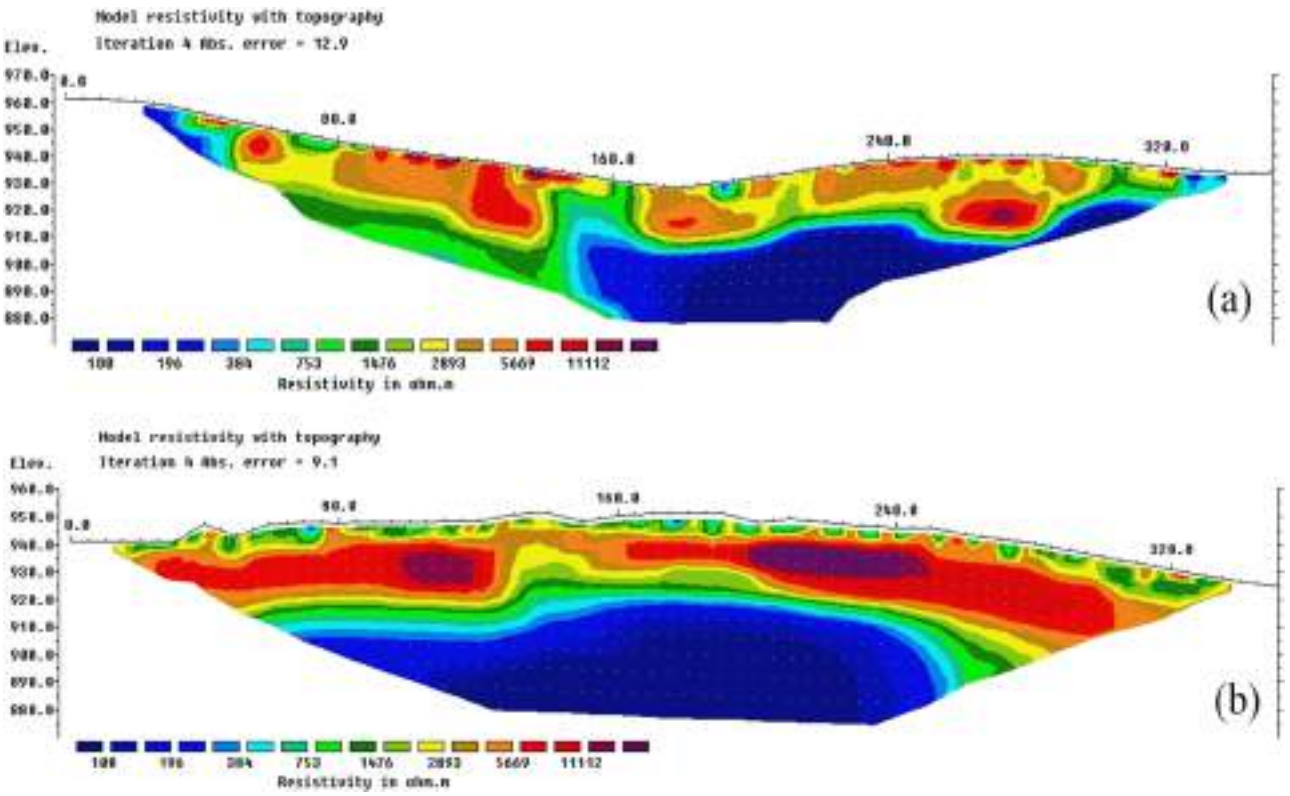

Figure 9: The inverted resistivity cross-sections: (a) SS06 and (b) SS07.

presence of the observed anomalous features). Accordingly, the location for the installation of a deep tubular well at 170 m from the beginning of the profile is suggested.

On the site of profile SS07, there are three lithologies interpreted as dry soil, dry saprolite, and clayey saprolite. In terms of the topographic and fractured zone, it is labeled as a high priority region. Profile SS07 also presents potential structures for surface water accumulation. Therefore, it is a recommended position for the installation of a tubular well in the region with lowest resistivity values, which is located at 150 m from the beginning of the ERT profile.

6 Conclusions and recommendations

In this paper, we presented a case study on the use of the geophysical approach (ERT) to identify new potential tubular wells and determined the recommended locations within the considered site (in the Federal District of Brazil).

The study demonstrated the ability to utilize the ERT inverted resistivity profiles accompanied with the geological information of the ground to conduct the following: (i) The development of site selection criteria (for potential tubular wells) based on the presence and surficial opening of the fracture; such prioritization criteria can increase the chances of success in the search for local groundwater. (ii) To exploit groundwater exclusively in the condominium tract and predict the maximum flow rate (e.g., in our case study, this was 39.5 m^3/h – considering 20 h of daily pumping). (iii) To estimate the optimum number of tubular wells required, based on the prediction of flow rate. For example, if the new wells reach the average flow rate of the aquifer subsystem F, 5–6 tubular wells (accurately constructed and operated) will be sufficient to reach the safe considered flow.

The approach presented in this study provides a promising framework for investigating and extracting groundwater in regions underlain by fractured aquifers. Overall, the study strengthens the idea that geophysical methods can aid groundwater exploration in challenging geological settings. Therefore, this approach is recommended to be carried out on any similar environments (hard rock), which would ensure that the use of ERT inverted resistivity profiles accompanied with the geological information optimizes both the position and production of tubular wells. For future work, coupled numerical modeling informed by geophysical, geological, hydrological, and meteorological data should be considered for more accurate estimation of wells' production.

Acknowledgments: The authors are most grateful to Dr. Eloi Campos of UnB and Regulatory Agency for Water, Energy, and Basic Sanitation of the Federal District of Brazil (ADASA) for providing the resistivity data and other related information.

Author contributions: Conceptualization, Y.H.; methodology, Y.H.; software, Y.H. and W.B.; writing-original draft preparation, Y.H.; writing-review and editing, Y.H., O.H., S.M., C.M., R.U., and H.-B.H. All authors have read and agreed to the published version of the manuscript.

Conflict of interest: Authors state no conflict of interest.

Data availability statement: Data is availbale on request to yawar.pgn@gmail.com.

Reference

[1] Hussain Y, Ullah S, Akhter G, Aslam AQ. Groundwater quality evaluation by electrical resistivity method for optimized tubewell site selection in an ago-stressed Thal Doab Aquifer in Pakistan. Model Earth Syst Environ. 2017;3(1):15.

[2] Xu S, Sirieix C, Riss J, Malaurent P. A clustering approach applied to time-lapse ERT interpretation – case study of Lascaux cave. J Appl Geophys. 2017;144:115–24.

[3] Watlet A, Kaufmann O, Triantafyllou A, Poulain A, Chambers JE, Meldrum PI, et al. Imaging groundwater infiltration dynamics in the karst vadose zone with long-term ERT monitoring. Hydrol Earth Syst Sci. 2018;22(2):1563–92.

[4] Guo W, Liu S, Liu Y, Chen S. Application of electrical resistivity imaging to detection of hidden geological structures in a single roadway. Open Geosci. 2020;12(1):1083–93.

[5] Rizzo E, Giampaolo V, Capozzoli L, Grimaldi S. Deep electrical resistivity tomography for the hydrogeological setting of Muro Lucano Mounts aquifer (Basilicata, Southern Italy). Geofluids. 2019:6594983.

[6] Hasan M, Shang Y, Jin W, Akhter G. Geophysical investigation of a weathered terrain for groundwater exploitation: a case study from Huidong County, China. Explor Geophys. Data 2020;52(3):273–93.

[7] Muzirafuti A, Boualoul M, Barreca G, Allaoui A, Bouikbane H, Lanza S, et al. Fusion of remote sensing and applied geophysics for sinkholes identification in Tabular Middle Atlas of Morocco (the Causse of El Hajeb): impact on the protection of water resource. Resources. 2020;9:51.

[8] Magowe M, Carr JR. Relationship between lineaments and ground water occurrence in western Botswana. Ground Water. 1999;37(2):282.

[9] Kuznetsov M, Viero AP, Sorek S, Roisenberg A, Ronen D. Modeling the flow pattern at the fractured granites in Porto Alegre, Brazil. Transp Porous Med. 2014;101(3):413–36.
[10] Redhaounia B, Ilondo BO, Gabtni H, Sami K, Bédir M. Electrical resistivity tomography (ERT) applied to Karst carbonate aquifers: case study from Amdoun, northwestern Tunisia. Pure Appl Geophys. 2016;173(4):1289–303.
[11] Campos JEG, Dardene MA, Freitas-Silva FH, Martins-Ferreira MAC. Geologia do Grupo Paranoá na Porção Externa da Faixa Brasília. Braz J Geol São Paulo. 2013;43(3):461–76.
[12] ADASA. Plano de Gerenciamento Integrado de recursos Hídricos do Distrito Federal – PGIRH. [Internet]; 2007. Available from: www.pgirh.df.gov.br
[13] Szűcs P, Szabó NP, Zubair M, Szalai S. Innovative hydrogeophysical approaches as aids to assess hungarian groundwater bodies. Appl Sci. 2021;11(5):2099.
[14] EMBRAPA. Brasilia: Empresa Brasileira de Pesquisa Agropecuária. Sistema brasileiro de classificação de solos; 2013. p. 353
[15] Novaes Pinto M. Caracterização geomorfológica do Distrito Federal. Novaes Pinto M (org). Cerrado: caracterização, ocupação e perspectivas. Brasília: Editora UnB; 1994. p. 285–320.
[16] Novaes Pinto M. Superfícies de aplainamento do Distrito Federal. Rev Bras Geogr. 1987;49(2):9–26.
[17] Romano O, Rosas JGC. Água subterrânea para fins de abastecimento de água e irrigação no Distrito Federal. Congresso Brasileiro Geologia, 24. Anais., Brasília: SBG; 1970. p. 313–33.
[18] Barros JGC. Caracterização geológica e hidrogeológica do Distrito Federal. Cerrado. 2a ed. UnB/SEMATEC; 1994. p. 265–83.
[19] Campos JEG, Freitas-Silva FH. Arcabouço hidrogeológico do Distrito Federal. In: Simp XII. Geol. Centro-Oeste. Boletim de Resumos. Brasília; 1999. p. 113.
[20] Campos JEG. Hidrogeologia do Distrito Federal: bases para a gestão dos recursos hídricos subterrâneos. Revista Brasileira de Geociências. 2004;34(1):41–8.
[21] Lousada EO, Campos JEG. Proposta de modelos hidrogeológicos conceituais aplicados aos aquíferos da região do Distrito Federal. Revista Brasileira de Geociências. 2005;35(3):407–14.
[22] Hussain Y, Hamza O, Cárdenas-Soto M, Borges WR, Dou J, Rebolledo JFR, et al. Characterization of Sobradinho landslide in fluvial valley using MASW and ERT methods. REM Int Eng J. 2020a;73(4):487–97.
[23] Park S, Yi M, Kim J, Shin SW. Electrical resistivity imaging (ERI) monitoring for groundwater contamination in an uncontrolled land fill, South Korea. J Appl Geophys. 2016;135:1–7.
[24] Martorana R, Capizzi P, D'Alessandro A, Luzio D. Comparison of different sets of array configurations for multichannel 2D ERT acquisition. J Appl Geophys. 2017;137:34–48.
[25] Samouëlian A, Cousin I, Tabbagh A, Bruand A, Richard G. Electrical resistivity survey in soil science: a review. Soil Tillage Res. 2005;83(2):173–93.
[26] Demirel S, Roubinet D, Irving J, Voytek E. Characterizing near-surface fractured-rock aquifers: insights provided by the numerical analysis of electrical resistivity experiments. Water. 2018;10(9):1117.
[27] Belle P, Lachassagne P, Mathieu F, Barbet C, Brisset N, Gourry JC. Characterization and location of the laminated layer within hard rock weathering profiles from electrical resistivity tomography: implications for water well siting. Geol Soc London Spec Publ. 2019;479(1):187–205.
[28] Dahlin T, Zhou B. A numerical comparison of 2-D resistivity imaging with 10 electrode arrays. Geophys Prospect. 2004;52:379–98.
[29] Fabregat I, Gutiérrez F, Roqué C, Comas X, Zarroca M, Carbonel D, et al. Reconstructing the internal structure and long-term evolution of hazardous sinkholes combining trenching, electrical resistivity imaging (ERI) and ground penetrating radar (GPR). Geomorphology. 2017;285:287–304.
[30] Pazzi V, Ceccatelli M, Ciani L, Patrizi G, Guidi G, Cappuccini L, et al. Analysis of the influence of the GPS errors occurred while collecting electrode coordinates on the electrical resistivity of Tumuli. Sensors. 2020;20(10):2966.
[31] Parasnis DS. Reciprocity theorems in geoelectric and geoelectromagnetic work. Geoexploration. 1988;25:177–98.
[32] Wilkinson PB, Loke MH, Meldrum PI, Chambers JE, Kuras O, Gunn DA, et al. Practical aspects of applied optimized survey design for electrical resistivity tomography. Geophys J Int. 2012;189:428–40.
[33] Okpoli CC. Sensitivity and resolution capacity of electrode configurations. Int J Geophys. 2013
[34] Bharti AK, Pal SK, Priyam P, Kumar S, Shalivahan PKY. Subsurface cavity detection over Patherdih colliery, Jharia Coalfield, India using electrical resistivity tomography. Environ Earth Sci. 2016;75(5):1–17.
[35] Bharti AK, Pal SK, Priyam P, Pathak VK, Kumar R. Detection of illegal mine voids using electrical resistivity tomography: the case-study of Raniganj coalfield (India). Eng Geol. 2016;213:120–32.
[36] Hussain Y, Uagoda R, Borges W, Nunes J, Hamza O, Condori C, et al. The potential use of geophysical methods to identify cavities, sinkholes and pathways for water infiltration. Water. 2020b;12:2289.
[37] Hussain Y, Uagoda R, Borges W, Prado R, Hamza O, Cárdenas-Soto M, et al. Detection of cover collapse doline and other epikarst features by multiple geophysical techniques: case study of Tarimba Cave, Brazil. Water. 2020c;12:2835.
[38] Carmelo AC. Caracterização de aquíferos fraturados por integração de informações geológicas e geofísicas. (PhD thesis). Brasília, DF, Brazil: Geociences Institut-University of Brasília; 2002. p. 179.
[39] Soro DD, Koïta M, Biaou CA, Outoumbe E, Vouillamoz JM, Yacouba H, et al. Geophysical demonstration of the absence of correlation between lineaments and hydrogeologically usefull fractures: case study of the Sanon hard rock aquifer (central northern Burkina Faso). J African Earth Sci. 2017;129:842–52.

Tavares, A.S.; Uagoda, R.E.S.; Spalevic, V.; Mincato, R.L. (2021): Analysis of the erosion potential and sediment yield using the IntErO model in an experimental watershed dominated by karst in Brazil. Agriculture and Forestry, 67 (2): 153-162.

DOI: 10.17707/AgricultForest.67.2.11

André Silva TAVARES[1], Rogério Elias Soares UAGODA[2], Velibor SPALEVIC[3,4], Ronaldo Luiz MINCATO[5]

ANALYSIS OF THE EROSION POTENTIAL AND SEDIMENT YIELD USING THE INTERO MODEL IN AN EXPERIMENTAL WATERSHED DOMINATED BY KARST IN BRAZIL

SUMMARY

Soil losses from water erosion jeopardize agricultural sustainability and food security for current and future generations. The research aimed to evaluate the application of the Erosion Potential Method by the Intensity of Erosion and Outflow – IntErO program in a karst watershed in a region with typical savanna climate in the northeast of the State of Goiás, Brazil. Input data were adapted according to the corresponding characteristics of tropical regions. The results indicated that the Extreme watershed has a value of 0.62 in the index (0 to 1) which defined the strength of the intensity of erosion. The river basin belongs to the category 3 of destruction with moderate erosion intensity, which indicates processes of surface erosion in the largest area of the hydrographic basin, and annual soil loss of 480.60 m^3 km^2 yr^{-1}. According to the IntErO model calculations 16% of the eroded material reaches the outflow of the hydrographic basin, and 84% of these sediments are deposited within the Basin, inside the surface and underground caves and galleries of the karst. Calculations by the IntErO model with the Erosion Potential Method in its algorithm proved to be valuable tool in evaluating the production of sediments in tropical soils, especially in evaluating different scenarios after establishing the inputs database for Brazil and will serve as a good starting point for future evaluations.

Key words: Karst Hydrology, Erosion Potential Method, IntErO model, Soil Conservation, Sedimentology.

[1] André Silva Tavares (corresponding author: andresttavares@gmail.com), Institute of Geosciences and Geodynamics, University of Brasília, Distrito Federal, BRAZIL;
[2] Rogério Elias Soares Uagoda, Department of Geography, University of Brasília, Distrito Federal, BRAZIL;
[3] Velibor Spalevic, University of Montenegro, Faculty of Philosophy Niksic, Department of Geography, MONTENEGRO;
[4] Velibor Spalevic, University of Montenegro, Biotechnical Faculty Podgorica, MONTENEGRO;
[5] Ronaldo Luiz Mincato, Institute of Natural Sciences, Federal University of Alfenas, Alfenas, Minas Gerais, BRAZIL;

Notes: The authors declare that they have no conflicts of interest. Authorship Form signed online.
Received:11/03/2021 *Accepted:22/05/2021*

INTRODUCTION

Soil is a finite natural resource that takes thousands of years to mature. Its sustainability is essential for the production of food and many other ecosystem goods and services, including climate regulation and nutrient cycling (Greiner *et al*., 2017). However, with the current developments in erosion, urbanization and climate change, impacts that promote the reduction of its surface layers (more fertile) become a risk for current and future generations (Parsipour *et al.*, 2019; Curovic *et al*., 2019; Spalevic *et al.*, 2020).

Water erosion is a natural process, subject to intensification according to the uses and managements adopted in agriculture. The process initiated by the impact of the raindrop breaks particles from the structure of the soil's surface layer, causing loss of arable soils and accumulation of sediments in the lower regions (EMBRAPA, 2013).

The erosion rate generally increases when the volume and velocity of surface water runoff occurs on steeper terrain with longer slope length. The adoption of conservation practices that ensure maximum vegetation cover and reduction in slope length, especially on steeper slopes and intensive cultivation, are essential to ensure the agricultural and environmental sustainability of terrestrial ecosystems (FAO, 2015). Hydrographic basins are ideal for evaluating the impacts of the intensification of water erosion processes, as it is a system with open water inlets and outlets for precipitated water, which can be drained or infiltrated. (Dyonisio, 2010).

In karst basins, Palmer (1984) draws attention to the importance of genetic aspects, especially in the hydrological bias, which shape the surface forms (lapias, canyons), the subsoil (porous medium), the vadose zone (free and gravitational flow), and the water table, with emphasis on recharge aspects (autochthonous, allochthonous). In groundwater systems, the transport of autochthonous and allochthonous sediments through conduits can imply high speeds and ascending water table, depending on the width of the underground channels (shape of the conduits), which can promote rapid flooding above the vadose or limited zone in confined flow networks (Caldeira *et al*., 2019). Among the fine suspended material (silt, clay and sand) the fine sand particles are more easily transported, which explains the presence of sandy sedimentary fans in caves dominated by mud and gravel (Gillieson, 1996).

In this aspect, Karst systems are sensitive to small changes in land use, such as activities that promote soil erosion, siltation of rivers and pollution of the karst aquifer, which must be mitigated in order not to increase the damage caused to karst systems. Thus, the present study aims to quantify and evaluate the application of the indirect model of Intensity of Erosion and Runoff - IntErO (Spalevic, 2011), which uses equations of the Erosion Potential Method of Gavrilovic (1962; 1972, 1988). This model has been applied in basins all over the world: Greece (Efthimiou *et al*, 2016), Iran (Mohammadi *et al*, 2021; Khaledi Darvishan *et al.*, 2019; Gholami *et al.*, 2016; Behzadfar *et al.*, 2014), Morocco (Ouallali *et al.*, 2020; El Mouatassime *et al.*, 2019), Montenegro (Spalevic *et al.*,

2020; Spalevic *et al.*, 2016; Spalevic *et al.*, 2014; Spalevic *et al.*, 2012), Nepal (Chalise *et al.*, 2019) but also in Brazil recently (Sakuno *et al*., 2020; Tavares *et al.*, 2019; Lense *et al.*, 2019).

Based on the characteristics of the hydrographic basin, the program estimates the production of annual sediments associated with the intensification of water erosion at the basin scale. Such results can be useful as an indication of areas with imminent potential risk of increasing rates of soil loss from arable areas, river siltation and aquifer and surface water pollution.

MATERIAL AND METHODS

Study Area

The karst river basin of the Extrema River has an area of 27.8 km², and a rainfall regime of 1,164 mm yr^{-1}, and is located in the northeast of Goiás State, Midwest Region, Brazil (Figure 1).

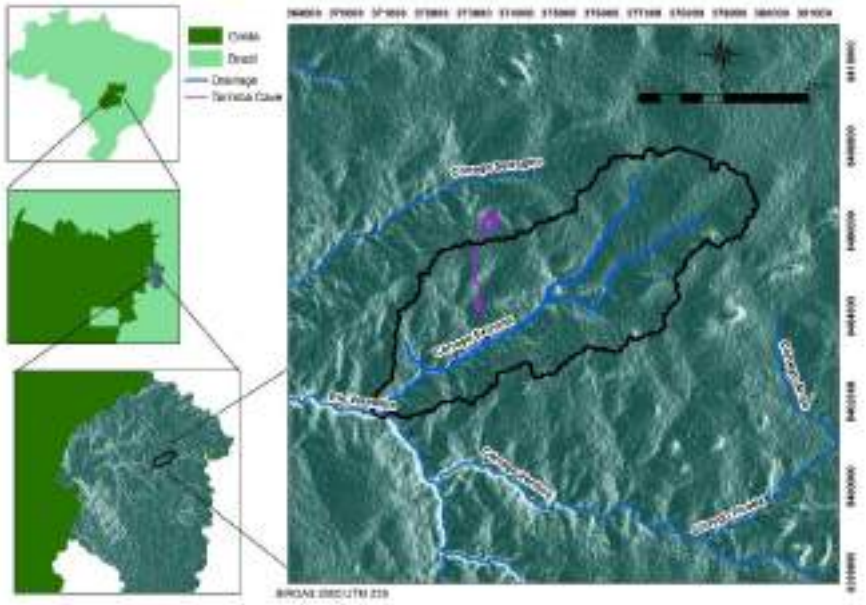

Figure 1: Location of the karstic watershed of the Extrema River with shaded relief effect.

The geomorphology surrounding the Extrema River basin is composed of the Central Chapadão (upper portion), originating from the South American surface that constitutes the Urucuia Group, formed by sandstones that present unconsolidated siliciclastic sediments, and the lower portion (Vão do Paranã) with intercalated pelitic rocks to the carbonates of the Lagoa do Jacaré Formation (Bambuí Group). In the "Lagoa do Jacaré" Formation clastochemical sediments (carbonate rocks) are favorable to karstification.

According to the Köppen-Geiger climatic classification, the climate is type tropical with dry winter (Aw) (Cardoso *et al*., 2014). Over the past few decades,

tropical savannas worldwide have been among the most affected biomes by the suppression of native vegetation. The dry season and the deficiency of phosphorus and other nutrient minerals in the very old soils do not favor forest development, giving rise to landscapes consisting mainly of grasslands with sparse or isolated trees (Walter and Breckle, 1986). Therefore, environmental changes resulting from human activities in these ecosystems pose threats to both biodiversity and climate.

With the increasing exchange of native vegetation for pastures, added to the natural savanna climate, erosion processes are intensified in rainfall events, resulting in surface runoff with a large volume of sediment that is transported to underground channels and galleries in the karst. As it represents the classical dynamics of the fluviocarstic system in the region, the Extrema River whatershed is an area with densification of karstic features that act as recharge areas through wide and distributed fractures and convections in sinks and underground flows.

In Strahler's (1957) hierarchical classification, the Extrema River configures a first-order level with a pattern of dendritic basin, with quick response to precipitation. At lower altitudes, between the domain of carbonates and siliciclastic sediments, karstic depressions occur with intensified erosive processes, from which there is capture of surface runoff by fractures and/or collapsed sinkholes, generating the accumulation of sediments in some caves above the level of base.

One hypothesis is that upper layers in adjacent caves contribute to the sediment carried by the underground flow in the Extrema cave. Possibly, the main source of sediment production in floods comes from the Tarimba cave (Figure 2), which has thick layers of preserved sedimentary rocks and a permanent flow in its interior. Another hypothesis is that the sediments originate from areas of upstream sinks, with the Tarimba cave acting as an underground stream that transports the sediments.

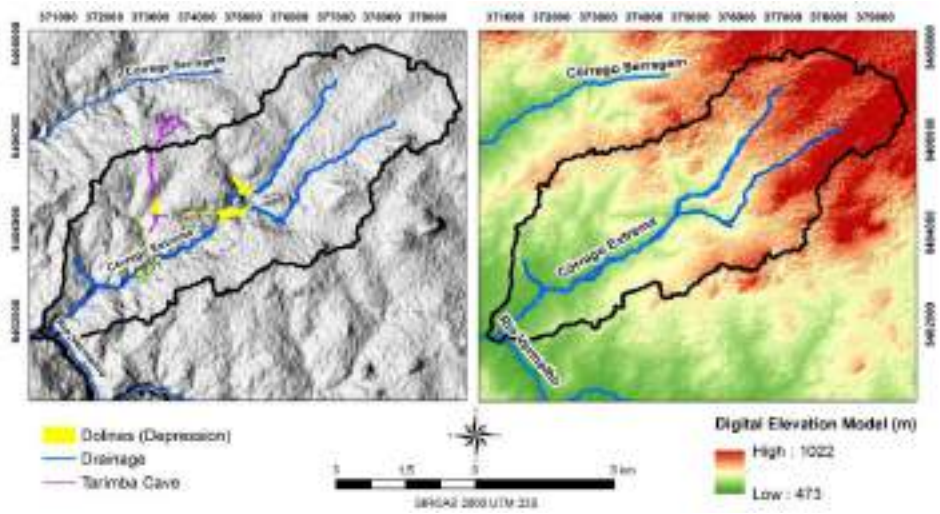

Figure 2: Depressions and connections of underground flows (Tarimba Cave) for the Extreme flow, and digital elevation model (m).

IntErO Model Application and EPM

The Intensity of Erosion and Outflow (IntErO) program package of Spalevic (2011) is based on Erosion Potential Method (EPM) of Gavrilovic (1962; 1972, 1988). The EPM is an empirically-based model that estimates soil loss and water erosion intensity determining factors that directly affect the rates of soil loss from water erosion at the scale of watersheds, such as land slope, soil resistance, field erosion, soil use and management, temperature and precipitation (Gavrilovic, 1988).

The calculations of the EPM model parameters are performed in an automatic form, in the compilation of the input data in the IntErO program. Spalevic (2011) proposed the creation of a database with twenty-six entries, including erosion, geometric, topographical, meteorological data, maximum flow and drainage system characteristics, integrating the EPM model parameters simultaneously (Table 1).

Table 1: Input data for the IntErO in Extrema watershed.

Inputs	**Amount and Unit**
River basin areas (F)	27.80 km²
The length of the watershed (O)	37.09 km
The area of the bigger river basin part (F_v)	14.08 km²
The area of the smaller river basin part (F_m)	13.72 km²
Natural length of the main watercourse (L_v)	7.57 km
Length of the contours/isohyets (L_{iz})	115.34 km
Altitude of the first contour line (h_0)	580 m
Incidence (Up)	100 yr
The lowest river basin elevation (H_{min})	579 m
The highest river basin elevation (H_{max})	854 m
River basin consisted of a very permeable product (f_p)	0.74
A part of the basin consisted of medium permeable rocks (f_{pp})	0.26
A part of the basin with poor water permeability rocks (f_0)	0
A part of the river basin under forests (f_s)	0.30
A part under grass, meadows, pastures, and orchards (f_t)	0.65
A part of the basin under plough-land, and without grass (f_g)	0.05
The length of the main watercourse with tributaries I & II class	9.91 km
The distance between the fountainhead and mouth (L_m)	6.79 km
The volume of the torrent rain (h_b)	50 mm
Average annual air temperature (t_0)	26° C
Average annual precipitation (H_{yr})	1,164 mm

Soil loss (W_{yr}) in the EPM model is estimated by Equation 1. Its algorithms are incorporated in the IntErO application (Spalevic, 2011), which calculates in an automated way, avoiding errors in manual modeling.

$$W_{yr} = T \cdot H_{yr} \cdot \pi \cdot \sqrt[3]{Z^2} \cdot R_a \quad \text{Equation 1}$$

Where: W_{yr} is total sediment production (m^3 yr^{-1}); T is temperature coefficient (dimensionless); H_{yr} is mean precipitation (mm yr^{-1}); π is the value of 3.14; Z is erosion coefficients (dimensionless); F is watershed area (km^2).

The temperature coefficient (T) is calculated according to Equation 2.

$$T = \sqrt[3]{\frac{t_0}{10}} + 0.1 \quad \text{Equation 2}$$

Where: T is temperature coefficient (dimensionless); t_0 is average air temperature (°C yr^{-1}).

The erosion coefficient (Z) is obtained by Equation 3:

$$Z = Y \cdot X_a \cdot (\varphi + \sqrt[3]{I_{sr}}) \quad \text{Equation 3}$$

Where: Y is soil resistance to water erosion (dimensionless); X_a is land use and management (dimensionless); φ is degree of erosion on the ground (dimensionless); I_{sr} is average slope of the watershed (%).

The values of the Z coefficient classified according to the degree of erosion intensity (Table 2)

Table 2: The degree of erosion intensity (Z)

Categories	Erosion intensity	Erosion Coefficient (Z)	Average of Z
I	Very severe	Z > 1.0	Z = 1.25
II	Severe	0.71 < Z < 1.00	Z = 0.85
III	Moderate	0.41 < Z < 0.70	Z = 0.55
IV	Weak	0.20 < Z < 0.40	Z = 0.30
V	Very weak	Z < 0.19	Z = 0.10

RESULTS AND DISCUSSION

Gavrilovic (1972) prepared tables with values that represent the attributes (Y, X_a, φ) needed to calculate the erosion coefficient Z (Dragicevic *et al*., 2016; 2017). However, the model was initially applied in temperate climate regions,

being necessary to adapt the values according to the characteristics of Brazilian tropical soils (Sakuno *et al.*, 2020) (Figure 3).

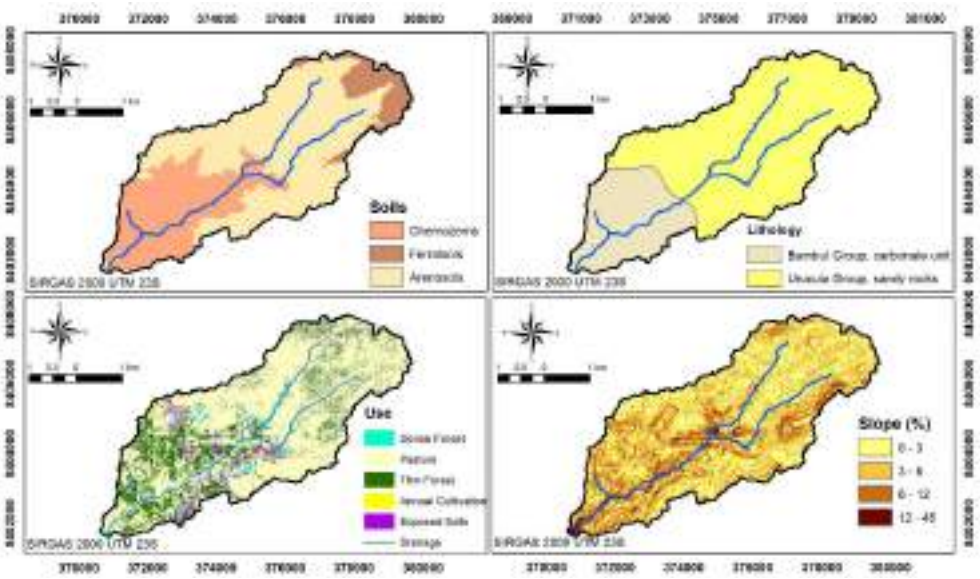

Figure 3: Cartographic base of soils, land use, lithology, and slope of the Extrema River watershed to obtain the Y, X_a and φ factors.

The coefficients of the river basin form (A), average river basin width (B) and watershed development (m) were calculated to be 0.95, 9.32 km, and 0.41, respectively. The value of peak discharge, with a return interval of 100 years (Q_{100}) and for a land use setup of 2021 resulted to 38.94 $m^3 s^{-1.}$

The drainage density of the study river basin (G) we calculated as 0.36, what indicates that there is a low density of the hydrographic network. The factor G is an important affecting the flood hydrograph and erosion process. The index of average decline to be 8.30% shown that in the studied watershed mild slopes prevail. The Z coefficient value of 0.626 indicates that the river basin belongs to destruction category III. The resistance to the erosion process is medium, where the surface erosion is predominant.

The production of erosion material (W yr^{-1}) in the Extrema watershed was calculated to be 81,927.2284 m^3 yr^{-1} and the coefficient of the deposit retention (Ru) resulted in 0.163. This means that 16% of the total eroded material reaches the exit point, while the remaining 84% é deposited in irregularities of the relief inside the watershed, in the hydrological drainage system, caves and underground galleries. Calculated real soil losses per year per square kilometer for the river basin amounts to 480.60 m^3 km^2 yr^{-1}, corresponds to the results obtained in 2021.The detailed report for the hydro morphological parameters is shown in Table 3.

Table 3: Outputs data for the IntErO in Extrema watershed.

Outputs		Amount and Unit
Coefficient of the river basin form	A	0.95
Coefficient of the watershed development	m	0.41
Average river basin width	B	9.32 km
(A)symmetry of the river basin	a	0.03
Density of the river network of the basin	G	0.36
Coefficient of the river basin tortuousness	K	1.12
Average river basin altitude	H_{sr}	634.36 m
Average elevation difference of the river basin	D	55.36 m
Average river basin decline	I_{sr}	8.30 %
The height of the local erosion base of the river basin	H_{leb}	275.00 m
Coefficient of the erosion energy of the river basin's relief	E_r	38.12
Coefficient of the region's permeability	S_1	0.48
Coefficient of the vegetation cover	S_2	0.75
Analytical presentation of the water retention in inflow	W	0.6537 m^{-3}
Energetic potential of water flow during torrent rains	$(2gDF)^{1/2}$	173.76 m km s^{-1}
Maximal outflow from the river basin	Q_{100}	38.94 m^3 s^{-1}
Temperature coefficient of the region	T	1.64
Coefficient of the river basin erosion	Z	0.626
Production of erosion material in the river basin	W yr^{-1}	81,927.2284 m^3 yr^{-1}
Coefficient of the sediment retention	Ru	0,163
Real soil losses	G yr^{-1}	13,360.31 m^3 yr^{-1}
Real soil losses per km^2	G yr^{-1} km^2	480.60 m^3 km^2 yr^{-1}

CONCLUSIONS

In the last three decades, the forest area has decreased with the replacement of native vegetation for the production of pastures in the northeast region of Goiás State, Brazil. This change in land cover increases the risks to water erosion, especially in sensitive areas of karstic watersheds. The accumulation of the annual production of sediments is demonstrated through deposits inside the caves of the watersheds in the region. Studies on the origin and fate of these sediments must be carefully monitored to understand the hydrosedimentological behavior of karst systems in tropical climates. This study analyzed some factors and processes that are associated with soil losses and the production of sediments by water erosion, serving as an important indicator of areas at risk of accelerated erosion, and must be constantly evaluated and monitored. The application of the IntErO model demonstrated that the removal of sediments by water erosion in the Extreme River watershed belongs to the 3rd category of destruction (Z = 0.62), which is classified as medium degree. Finally, it is important to emphasize that climate change can increase soil erosion and sediment production processes in extreme rainfall events, which are increasingly common in tropical regions, which requires such processes to be evaluated annually. It is strongly recommended that this approach be considered when planning public monitoring policies.

ACKNOWLEDGEMENTS

The authors thanks the Chico Mendes Institute for Biodiversity Conservation (ICMBio), National Water Agency (ANA), National Center for Research and Conservation of Caves (CECAV) and "Coordenação de Aperfeiçoamento de Pessoal de Nível Superior – Brasil" This study was financed in part by CAPES – Finance Code 001.

REFERENCES

Behzadfar, M.; Djurovic, N.; Simunic, I.; Filipovic, M. and Spalevic, V. Calculation of soil erosion intensity in the S1-6 Watershed of the Shirindareh River Basin, Iran. In Proceedings of the International Scientific Conference: Challenges in Modern Agricultural Production, Skopje, Macedonia, 11, 2014.

Caldeira, D.M.V.S.; Uagoda, R. and Nogueira, A.M. (2019): Dinâmica dos sedimentos clásticos cavernícolas: Potencialidade para estudo paleoambientes no Brasil. Espaço & Geografia, 22 (1), 153-189.

Cardoso, M.R.D.; Marcuzzo, F.F.N. and Barros, J.R. (2014). Classificação climática de Köppen-Geiger para o Estado de Goiás e o Distrito Federal. Acta Geográfica, 8(16), 40-55.

Chalise, D.; Kumar, L.; Spalevic, V. and Skataric, G. (2019): Estimation of Sediment Yield and Maximum Outflow Using the IntErO Model in the Sarada River Basin of Nepal. Water, 11, 952.

Curovic, Z.; Curovic, M.; Spalevic, V.; Janic, M.; Sestras, P. and Popovic, S.G. (2019): Identification and Evaluation of Landscape as a Precondition for Planning Revitalization and Development of Mediterranean Rural Settlements-Case Study: Mrkovi Village, Bay of Kotor, Montenegro. Sustainability, 11, 2039.

Dragicevic, N.; Karleusa, B.; and Ozanic, N. (2017): Erosion potential method (Gavrilovic Method) sensitivity analysis. Soil and Water Research, 12(1): 51-59

Dragicevic, N.; Karleusa, N. and Ozanic, N. (2016): A review of the Gavrilovic method (Erosion Potential Method) application. Gradevinar, 68(9); 715-725.

Dyonisio, H.A.F. (2010): Erosão hídrica: suscetibilidade do solo. Revista Eletrônica Thesis, 6 (13): 15-25.

El Mouatassime, S.; Boukdir, A.; Karaoui, I.; Skataric, G.; Nacka, M.; Khaledi Darvishan, A.; Sestras, P. and Spalevic, V. (2019): Modelling of soil erosion processes and runoff for sustainable watershed management: Case study Oued el Abid Watershed, Morocco. Agriculture and Forestry, 65(4), 241-250

Efthimiou, N. and Lykoudi, E. (2016) Soil erosion estimation using the EPM model. In Proceedings of the 14th International Conference of the Geological Society of Greece, Thessaloniki, Greece, 25–27 May; Volume L.

EMBRAPA - Empresa Brasileira de Pesquisa Agropecuária (2013): Sistema Brasileiro de Classificação de Solos. 4. ed. Brasília: EMBRAPA Solos, 376p.

Food and Agriculture Organization of the United Nations (2015): World Reference Base for Soil Resources (WRB): update 2015 International soil classification system for naming soils and creating legends for soil maps. Rome: FAO, n. 106, 203 p.

Gavrilovic, S. (1962): A method for estimating of the average annual quantity of sediments according to the potency of erosion. Bull. Fac. For, 26, 151–168.

Gavrilovic, S. (1972): Engineering of Torrential Flows and Erosion; Izgradnja: Belgrade, Serbia, 272p.

Gavrilovic, Z. (1988). The use of empirical method (erosion potential method) for calculating sediment production and transportation in unstudied or torrential streams. In: White, W.R. (ed.), International Conference on River Regime; 411–422. Chichester.

Gholami, L.; Batista, P.; Behzadfar, A., Khaledi Darvishan, A. and Behzadfar, M. Application of IntErO model for soil loss estimation case study: S7-1 Watershed of Shirindareh river basin, Iran. In Proceedings of the 7th International Agricultural Symposium "Agrosym 2016", Jahorina, Bosnia and Herzegovina, 6–9 October 2016; pp. 2169–2177.

Gillieson, D. (1986): Cave sedimentation in the New Guinea highlands. Earth Surface Processes and Landforms, 11: 533–543.

Greiner, L.; Kellera, A.; Grêt-Regameyb, A.; and Papritzc, A. (2017): Soil function assessment: review of methods for quantifying the contributions of soils to ecosystem services. Land Use Policy, 69: 224-237.

Khaledi Darvishan, A.; Mohammadi, M.; Skataric, G.; Popovic, S.; Behzadfar, M.; Rodolfo Ribeiro Sakuno, N.; Luiz Mincato, R. and Spalevic, V (2019): Assessment of soil erosion, sediment yield and maximum outflow, using IntErO model (Case study: S8-IntA Shirindarreh Watershed, Iran). Agriculture and Forestry, 65, 203–210.

Lense, GHE; Parreiras, T.C.; Moreira, R.S.; Avanzi, J.C. and Mincato, R.M. (2019) Estimativas de perdas de solo pelo método de erosão potencial em latossolos tropicais. Ciência e Agrotecnologia, Ciência e Agrotecnologia, 43:e012719.

Mohammadi, M.; Khaledi Darvishan, A.K.; Spalevic, V.; Dudic, B. and Billi, P. (2021): Analysis of the Impact of Land Use Changes on Soil Erosion Intensity and Sediment Yield Using the IntErO Model in the Talar Watershed of Iran. Water,13: 881. https://doi.org/10.3390/w13060881

Ouallali, A.; Aassoumi, H.; Moukhchane, M.; Moumou, A.; Houssni, M.; Spalevic, V. and Keesstra, S. (2020): Sediment mobilization study on Cretaceous, Tertiary and Quaternary lithological formations of an external Rif catchment, Morocco. Hydrology Sciences Journal, 65: 1568–1582.

Palmer, A.N. (1984): Geomorphic interpretation of karst features. In: Lafleur, R.G. Groundwater as a Geomorphic Agent. Boston: Allen and Unwin, pp.173-209.

Parsipour, H.; Popovic, S.; Behzadfar, M.; Skataric, G. and Spalevic, V. (2019): Cities expansion and land use changes of agricultural and garden lands in peri-urban villages (case study: Bojnurd). Agriculture and Forestry, 65(3): 173-187.

Sakuno, N.R.R.; Guiçardi, A.C.F.; Spalevic, V.; Silva, M.L.N. and Mincato, R.L. (2020). Adaptation and application of the erosion potential method for tropical soils. Revista Ciência Agronômica, 51, 1-10.

Spalevic, V. (2011): Impact of Land Use on Runoff and Soil Erosion in Polimlje. Ph.D. Thesis, Faculty of Agriculture, University of Belgrade, Serbia, 260p.

Spalevic, V.; Barovic, G.; Vujacic, D.; Curovic, M.; Behzadfar, M.; Djurovic, N.; Dudic, B. and Billi, P. (2020): The Impact of Land Use Changes on Soil Erosion in the River Basin of Miocki Potok, Montenegro. Water, 12, 2973.

Spalevic, V.; Barovic, G.; Fikfak, A.; Kosanovic, S.; Djurovic, M. and Popovic, S. (2016): Sediment yield and Land usechanges in the Northern Montenegrin Watersheds: Case study of Seocki Potok of the Polimlje Region. Journal of Environmental Protection Ecology, 17: 990–1002.

Spalevic, V.; Hübl, J.; Hasenauer, H. and Curovic, M. (2014). Calculation of soil erosion intensity in the Bosnjak Watershed, Polimlje River Basin, Montenegro. In Proceedings of the 5th International Agricultural Symposium "Agrosym 2014", Jahorina, Bosnia and Herzegovina, 23–26: 730–738.

Spalevic, V.; Curovic, M.; Borota, D. and Fustic, B. (2012): Soil erosion in the river basin Zeljeznica, area of Bar, Montenegro. Agriculture and Forestry, 54: 5–24.

Strahler, A.N. (1957) Quantitative analysis of watershed geomorphology. Transactions, American Geophysical Union, Washington, 38: 913-920.

Tavares, A.S.; Spalevic, V.; Avanzi, J.C.; Nogueira, D.A.; Silva, M.L.N. and Mincato, R.L. (2019): Modelling of water erosion by the erosion potential method in a pilot subbasin in southern Minas Gerais. Semina: Ciências Agrárias, 40: 555–572.

University of Montenegro
Biotechnical faculty
Univerzitet Crne Gore
Biotehnički fakultet

Agriculture and Forestry
Poljoprivreda i šumarstvo
2

Agriculture and Forestry, Vol.67. Issue 2: 1-272, Podgorica, 2021

ISSN 0554-5579; E-ISSN 1800-9492; DOI: 10.17707/AgricultForest
COBIS.CG-ID: 3758082 www.agricultforest.ac.me

Agriculture and Forestry - ***Poljoprivreda i šumarstvo***
PUBLISHER - ***IZDAVAČ***
University of Montenegro – Univerzitet Crne Gore
Biotechnical faculty (BTF), Podgorica - Biotehnički fakultet, Podgorica
Bul. M. Lalića 1, 81000 Podgorica, Crna Gora (Montenegro), P.Box 97,
Tel.: +382 20 268434; +382 20 268437; Fax: +382 20 268432
Web: www.agricultforest.ac.me; E-mail: agricultforest@ac.me

The journal "Agriculture and Forestry" is funded by the Biotechnical faculty, Co-funded by the Ministry of Science & the Ministry of Agriculture and Rural Development of Montenegro

CIP – Каталогизација у публикацији
Централна народна библиотека Црне Горе, Цетиње
ISSN 0554-5579
COBIS.CG-ID 3758082

CONTENT

Earth Surface Processes and Landforms

BSG British Society for Geomorphology

RESEARCH ARTICLE | Full Access

Rates, factors, and tolerances of water erosion in the Cerrado Biome (Brazil): A meta-analysis of runoff plot data

Maria Rita Souza Fonseca, Rogério Uagoda, Henrique Marinho Leite Chaves

First published: 22 October 2021 | https://doi.org/10.1002/esp.5273